Environmental Science

Joseph Awange

# GNSS Environmental Sensing

## Revolutionizing Environmental Monitoring

*Second Edition*

Springer

# Environmental Science and Engineering

## Environmental Science

More information about this series at http://www.springer.com/series/3234

Joseph Awange

# GNSS Environmental Sensing

## Revolutionizing Environmental Monitoring

Second Edition

Springer

Joseph Awange
Spatial Sciences
Curtin University
Perth, WA
Australia

ISSN 1863-5520 ISSN 1863-5539 (electronic)
Environmental Science and Engineering
ISSN 1431-6250
Environmental Science
ISBN 978-3-319-58417-1 ISBN 978-3-319-58418-8 (eBook)
DOI 10.1007/978-3-319-58418-8

Library of Congress Control Number: 2017945688


Originally published with the title/subtitle: Environmental Monitoring using GNSS/Global Navigation Satellite Systems.


Printed on acid-free paper

This Springer imprint is published by Springer Nature
The registered company is Springer International Publishing AG
The registered company address is: Gewerbestrasse 11, 6330 Cham, Switzerland

*The first edition of the book was dedicated to the first environmentalist to receive the Nobel Peace Prize honour, Prof. Wangari Maathai of Kenya (pictured above). The Nobel peace laureate led a sustained campaign for environmental conservation with her Green Belt Movement planting more than 40 million trees across Africa. This second edition of the book is dedicated to my past, present and future students of Satellite and Space Geodesy at Curtin University (Australia) as well as all Environmental students globally.*

Joseph Awange
Perth (Australia) and Pernambuco (Brazil)
April 2017


ALFRED NOBEL

# Foreword

Professor Awange has created a masterpiece in this work—cleverly combining *theoretical* with *practical* aspects of the Global Navigation Satellite Systems. The work provides invaluable insights into the theories behind Global Navigation Satellite Systems, and proceeds to discuss a plethora of possible applications of the technology. This work comes at a very crucial time when environment is universally acknowledged as the platform upon which human socio-economic endeavours take place. From the field of innovation economics, this work stands out because of its unrivalled attention to relevant applications of the technology in diverse areas ranging from urban infrastructure and pollution issues to monitoring of surface and underground water resources. Technologies only make sense when they can be cost-effectively applied to solving human problems and needs. Professor Awange makes a good case for Global Navigation Satellite Systems as one of those technologies that is quietly revolutionizing how solutions can be provided in almost all areas of human socio-economic activities.

In a nutshell, this is a comprehensive yet candid and compelling presentation of Global Navigation Satellite Systems and its application to environmental monitoring and a host of other socio-economic activities. This is an essential and new groundbreaking reading for all professional practitioners and even academics

seeking to study and become involved in using Global Navigation Satellite Systems in diverse fields ranging from environmental monitoring to economic activities such as monitoring *weather* and *climate* in order to design crop failure insurance.

October 2011

Nathaniel O. Agola
Professor of Business and Financial Economics
Ritsumeikan University
Kyoto, Japan

# Preface to the Second Edition

Never before has there been a tool that in its application spans all the four dimensions of relevance to mankind (position, navigation, timing and the environment). Global Navigation Satellite Systems (GNSS), a satellite microwave (L-band) technique, is such a tool that has widely been used for positioning (both by military and civilians), navigation, timing and is now revolutionizing the art of monitoring our environment in ways never fathomed before. In the first edition of the book, the theory and applications of GNSS to environmental monitoring was presented. Since then, however, so many things have changed both in the GNSS satellite development and applications. For instance, Galileo and Beidou satellites that were not operational during the writing of the first edition of the book are now operational. Furthermore, more long-term GNSS data collected from low earth orbiting satellites such as COSMIC (Constellation Observing System for Meteorology, Ionosphere, and Climate) have become available thereby enabling climate variability studies.

With all GNSS satellites (GPS, Galileo, GLONASS and Beidou) becoming operational, multi-signals are now available that are capable of remotely sensing the Earth's atmosphere and surface providing highly precise, continuous, all-weather and near real-time environmental monitoring data. In this regard, the refracted GNSS signals (i.e. occulted GNSS signals or GNSS-meteorology) are now emerging as sensors of climate variability while the reflected signals (i.e., GNSS-Reflectrometry or GNSS-R) are increasingly finding applications in determining, e.g. soil moisture content, ice and snow thickness, ocean heights and wind speed and direction of ocean surface among others. Furthermore, the increasing recognition and application of GNSS-supported unmanned aircraft vehicles (UAV)/drones in agriculture (e.g. through the determination of water holding capacity of soil) highlights the new challenges facing GNSS. Frank Veroustraete [1] puts it candidly:

> A lot is happening lately on the subject of drone applications in agriculture and precision farming. From the ability to image, recreate and analyze individual leaves on a corn plant from 120 meters height, to getting information on the water-holding capacity of soils to

variable-rate water applications, agricultural practices are changing due to drones delivering agricultural intelligence for both farmers and agricultural consultants.

In recognition to the developments above, it is necessary that the first edition of the book be updated. This has necessitated the writing of this second edition with a completely new title that captures its increasing applications to remotely sense the environment for changes. To this end, three new chapters have been added; GNSS reflectrometry and applications, GNSS sensing of climate variability and the applications to UAV/drones. In addition, various chapters of the first edition have been updated.

I am grateful to Dr. Richard Fischer, publisher of Inside GNSS/Inside Unmanned Systems for the permission to use Fig. 10 and to Dr. Volker Jenseen and Taylor & Francis Publishers for permission to use Figs. 19.7–19.9. Special thanks to my Ph.D. student Hu Kexiang (Frank), Curtin University, who contributed Chap. 20 and also helped with the preparation of the references as well as the figures in Chaps. 10 and 12.

Perth (Australia) and Recife (Brazil) Joseph Awange
April 2017

## Reference

1. Veroustraete F (2015). The rise of the drones in agriculture. EC Agric325–327. https://www.researchgate.net/publication/282093589.

# Preface to the First Edition

With ever increasing global population, intense pressure is being exerted on the Earth's resources, leading to severe changes in its land cover (e.g. forests giving way to settlements), diminishing biodiversity and natural habitats, dwindling fresh water supplies and the degradation in the quality of the little that is available, and changing weather and climatic patterns, especially global warming with its associated predicted catastrophes such as rising sea level and increased numbers of extreme weather events. These human-induced and natural impacts on the environment need to be well understood in order to develop informed policies, decisions and remedial measures to mitigate current and future negative impacts for the benefit of human society, and the natural world at large.

Such a situation calls for the continuous monitoring of the environment to acquire data that can be soundly and rigorously analyzed to provide information about the current state of the environment and its changing patterns, and to enable predictions of possible future impacts. Environmental monitoring techniques that may provide such information are under scrutiny from an increasingly environmentally conscious society that demands the efficient delivery of such information at a minimal cost. In addition, it is the nature of environmental changes that they vary both spatially and temporally, thereby putting pressure on traditional methods of data acquisition, some of which are very labour intensive, such as animal tracking for conservation purposes. With these challenges, conventional monitoring techniques, particularly those that record spatial changes, call for more sophisticated approaches that deliver the necessary information at an affordable cost. One direction being followed in the development of such techniques involves *satellite environmental monitoring*, which can act as stand-alone methods, or to complement traditional methods.

One of the most versatile means of using satellites for environmental monitoring involves global navigation satellite systems (GNSS), the general term for the US-based Global Positioning System (GPS), Russian's GLObal NAvigation Satellite System (GLONASS), China's Beidou or Compass and the European Galileo satellite systems. GNSS is a satellite tool with the capability of providing location (spatial) data, remote sensing of the Earth's atmosphere (temperature and

pressure) and surface, assisting in precise orbit determination of low earth orbiting environmental satellites, and supporting the tracking of elusive fresh underground and surface waters, among many other uses. Its spatial data are also integrable with other remote sensing, socio-economic and field survey data through geographical information systems (GIS) to provide highly continuous real-time spatio-temporal dataset that are of enormous benefit to the emerging field of *geosensor-network* environmental monitoring discussed in Sect. 17-12.

For example, *GNSS-based radio telemetry* is a modern method for observing animal movements, thereby moving the burden of making observations from the observer (i.e. researcher) to the observed (i.e. animal), and in so doing alleviating the difficulties associated with personal bias, animal reactions to human presence and animal habits that make most of them secretive and unseen [1]. This method provides large, continuous, high-frequency data about animal movement, data which, if complemented by other information dealing with animal behaviour, physiology and the environment itself, contributes significantly to our knowledge of the behaviour and ecological effects of animals, allowing the promotion of quantitative and mechanistic analysis [1]. Another very different example of the use of GNSS for environmental studies is its contribution to weather and climate change monitoring via the new field of *GNSS-meteorology*. Such methods are complimentary to traditional radiosonde techniques, which unfortunately inadequately cover the southern hemisphere and oceanic regions, while water vapor radiometers are adversely affected by clouds. In environmental impact assessment (EIA), strategic environmental assessment (SEA) and sustainability assessment (SA), GNSS methods provide maps, distances and locations that help in decision-making and also in the modelling of the impacts of policies. In epidemiology, GNSS is finding use in the study of the spread of infectious diseases and climate change effects on vector-borne diseases.

It is with this almost overwhelming variety of uses of GNSS for environmental monitoring in mind that this book is written, the purpose being to bring its theory and possible environmental monitoring applications together within one volume. It is hoped that environmentalists will be able to quickly find references to the theory of GNSS, while geodesists and others not specifically working in environmental fields will have numerous examples that could motivate further development of GNSS techniques for the benefit of environmental monitoring. For this reason, the book is divided into two parts. Part I deals with the basics of GNSS, while part II looks at its applications.

Thanks to C. Hirt, A. Elmowafy and J. Walker of Curtin University, C. Ogaja of California State University (Fresno) and G. Odhiambo of UAE University for their valuable comments on the initial chapters of the book. Special thanks to K. Fleming of GFZ-German Research Center for Geoscience (Germany) for sparing his time to proof read the book repeatedly without getting tired. Further thanks to him for providing many valuable comments and for preparing some figures of Chap. 11. Several figures in this book have been generously provided by various authors. In this regard, I would like to thank D. Rieser (Graz University of Technology), M. Motagh (GFZ), M. Jia (Geoscience Australia), F. Urbano (RICENRA, Edmund

Mach Foundation, Italy) and R. Mikosz (Federal University of Pernambuco, Brazil). Some figures and materials also came from the work undertaken jointly with my colleges B. Heck (Karlsruhe Institute of Technology, Germany), W. Featherstone, M. Kuhn, K. Fleming and I. Anjasmara (Curtin University), M. Sharifi (Tehran University), A. Hunegnaw (University of Edinburgh), O. Baur (Space Research Institute, Austrian Academy of Science), E. Forootan (Bonn University), J. Wickert, T. Schmidt (GFZ, Germany), JBK Kiema (University of Nairobi) and my students N. Wallace, Khandu, G. Schloderer, M. Bingham and T. Opande. To you all, "arigato gozaimasu" (Japanese for thank you very much). To all my Curtin University third year (Satellite and Space Geodesy unit), and second year (Civil Engineering) students who used materials from the draft book and provided feedback, I say "Danke sehr" (German for thank you very much).

I wish to express my sincere thanks to *Prof. B. Heck* of the Department of Physical Geodesy (Karlsruhe Institute of Technology, Germany) for hosting me during the period of my Alexander von Humboldt Fellowship (2008–2011) when part of this book was written. In particular, his ideas, suggestions and motivation on Chapters 9, 11 and 14 have enriched the book considerably. I am also grateful to *Prof. B. Veenendaal* (Head of Department, Spatial Sciences, Curtin University, Australia) and *Prof. F. N. Onyango* (former Vice Chancellor, Maseno University, Kenya) for the support and motivation that enabled the preparation of this edition. Last, but not least, I acknowledge the support of *Curtin Research Fellowship*, while my stay at Karlsruhe Institute of Technology (KIT) was supported by a *Alexander von Humboldt's Ludwig Leichhardt's Memorial Fellowship*. To all, I say, "ahsante sana" (Swahili for thank you very much). This is a TIGeR publication No 389.

Perth (Australia), Karlsruhe (Germany), and Maseno (Kenya)
October 2011

Joseph Awange

## Reference

1. Cagnacci F, Boitani L, Powell PA, Boyce MS (Eds) (2010). Challenges and opportunities of using GPS-based location data in animal ecology. Philosophical Transaction of the Royal Society B (365): 2155, doi:10.1098/rstb.2010.0098.

# Contents

# Chapter 1
# Environmental Monitoring

*If environmental monitoring is not carried out in a deep and exacting scientific manner, then it is likely that no action will be taken when needed for lack of firm evidence.*

Frank Burden

## 1.1 Monitoring

Environmental monitoring has been defined as the observation and study of the environment. This entails objective observations that produce sound data, which in turn provide valuable information that is useful, e.g., in supporting the protection of public water supplies, hazardous, non-hazardous, and radioactive waste management, natural resource protection and management, weather forecasting, and global climate change [1] studies. From such a definition, what exactly does the term "*monitoring*" mean within an environmental perspective? Is it synonymous to measuring or observing? A sound definition of monitoring is essential at this point so as to clearly understand the theme of this book, which intents to highlight the uses of GNSS (Global Navigation Satellite Systems) satellites, which have at times been largely regarded as military assets, to *monitor the environment*. This can be achieved by using GNSS signals to measure and observe changes in the environment.

*GNSS* is defined, e.g., in Hofman-Wellenhof et al. [2] as a space-based radio positioning system that includes one or more satellite constellations, augmented as necessary to support the intended operation, and that provides 24-h three-dimensional *position*, *velocity*, and *time* information to suitably equipped users anywhere on, or near the surface of the earth (and sometimes off Earth). Chapter 2 provides more discussion on the satellites that make up a GNSS, and as we shall see throughout the book, it is capable of providing other environmental monitoring indicators such as temperature and pressure.



J. Awange, *GNSS Environmental Sensing*, Environmental Science and Engineering, DOI 10.1007/978-3-319-58418-8_1

*Monitoring* has been defined by James et al. [3] as observing, detecting, or recording the operation of a system; watching closely for purposes of control; surveillance; keeping track of; checking continually; detecting change. They state that since monitoring implies change, and change implies time, monitoring then means *measuring those things that change in a system over time and space*. It is a process based on *surveying* and *surveillance*, but assumes that there is a specific reason for the collection of data [4].

A similar definition is provided by [5] who states that *monitoring is a systematic observation of parameters related to a specific problem, designed to provide information on the characteristics of the problem and their changes with time*. Surveying entails the *collection* of *quantitative* and *qualitative data* within a specified time frame without having a preconceived idea of what the results would be. Surveillance introduces the concept of time to surveying, leading to the systematic observation of variables and processes, with the aim of producing time series. Monitoring, therefore, is an extension of surveillance, but with a specific purpose in mind. It is thus a systematic observation of variables and processes for a specific purpose, such as ascertaining whether a given project is being undertaken according to predefined environmental standards [4, 6].

Spellerberg [4] provides examples of cases where people have categorized monitoring. In one example, Spellerberg [4] cites the Department of Conservation in New Zealand who recognizes three types of monitoring (results monitoring, outcome monitoring and surveillance monitoring). In another example, Spellerberg [4] provides four categories of environmental monitoring based on [7]:

- *Simple monitoring*, records the value of a single variable at one point over time.
- *Survey monitoring*, surveys the current state of environmental conditions in both affected and non-affected areas.
- *Surrogate or proxy monitoring*, which compensates for the lack of previous monitoring by using surrogate information to infer changes.
- *Integrated monitoring*, using detailed sets of ecological information.

Downes et al. [8] on the other hand classify monitoring into four categories that clarify the objectives of monitoring prior to a specific design. These are as follows:

- *Environmental monitoring*. This takes on many forms for many objectives, e.g., those undertaking environmental monitoring might be interested in gaining some indication of the state, as opposed to assessing human impacts upon the environment, of a particular place.
- *Long term monitoring* and *reference site monitoring*. These are forms of environmental state monitoring that are useful in providing a background measure for the long term dynamics of natural systems that may be used to indicate systematic, monotonic, or cyclical changes in the environment at large scales over long time periods. They are relevant in providing frameworks upon which shorter term or localized changes such as those arising from anthropogenic impacts could be measured against.

- *Compliance monitoring*. This seeks to ensure that a stipulated regulation is being followed, e.g., measuring the pollution level of effluent at a given location without bothering with neighbouring locations outside of the area of interest. The objective in compliance monitoring is usually to assess whether the level of particular compounds are below critical levels stipulated under some regulatory framework. Compliance monitoring could also be viewed as quality control measures.
- *Impact monitoring*. This is undertaken to assess the human impact upon the natural environment, with the objective of taking remedial measures to prevent or minimize such impacts. This type of monitoring is useful in compliance and impact assessment monitoring.

Within all these categories, a framework for designing a monitoring program, whose components may require support of GNSS satellites, is essential. For instance, Finlayson [6] presented a framework that consists of the identification of issues or problems, definition of objectives, formulation of hypothesis, choosing the desired methods and variables to observe, assessment of feasibility and cost effectiveness, conducting pilot studies, collecting samples, analyzing the collected samples, interpreting data and reporting the results, and implementing management actions.

A similar model is presented by Maher and Batley as reported in [9], who point out that good monitoring programs obtain information and are not just data collection exercise and as such should be cost effective, yet provide information and knowledge to inform those commissioning the data collection. Within this monitoring framework of Finlayson [6], GNSS satellites could play a key role of providing efficient methods for measuring *spatial environmental changes* at local, regional and global scales and over varying temporal scales. They could also be useful in conducting rapid pilot studies such as providing quick and accurate spatial coverage and in recording the locations of the collected samples. These satellite techniques could also play a vital role in implementing management actions and in auditing environmental plans. For coastal management plans, for example, they could be used to locate areas prone to erosion caused by variations in shoreline positions, thereby leading to preventive actions being taken. For auditing purposes, for example, they could be used to indicate the locations of effluent from a given factory. Such spatial information can then be used to study the ecosystem at that particular location.

With increasing development and technological advancement in the world, the task of monitoring the environment continues to become more important, as noted, e.g., by Burden et al. [9], who elucidates the role and practise of environmental monitoring. Burden et al. [9], in realizing the importance that underpins environmental monitoring, present a handbook that guides environmental monitoring of water, soil and sediments, and the atmosphere. Their work also considers chemical, physical and biological monitoring, all aimed at enhancing environmental management. An attempt to address environmental monitoring in an integrated manner is presented, e.g., in Wiersma [10], while Goldsmith [11] and Downes et al. [8] provide thorough overviews of ecological monitoring and conservation.

In most countries, environmental management requires development projects to undertake Environmental Impact Assessments (EIA), which brings with them the need for baseline survey data that are useful in assisting the prediction of the environmental impacts of proposed projects. The collection of baseline survey data therefore requires some form of monitoring. Downes et al. [8] put forward the BACI (Before-After-Control-Impact) model, which helps to assess whether a given activity has impacted upon the environment at a given location. GNSS could contribute significantly to the success of this model due to the fact that the model is *location-based* and thus operates within the GNSS areas of strength, i.e., the highly accurate determination of location (see Sect. 13.2).

Spellerberg [4] summarizes the relevance of environmental monitoring as (i) *adaptive management*, which provides a basis for managing data and provides a learning experience from outcomes of operational programs, (ii) *environmental planning* as a basis for the better use of land, (iii) *monitoring the state of the environment* using organism to monitor pollution and indicates the quality of the environment, (iv) *ecological sciences* monitoring as a way of advancing knowledge about the dynamics of the ecosystem, (v) *pest and diseases* monitoring for agriculture and forestry in order to establish effective means of controlling these, and (vi) *climate change* to monitor, for example, the effect of global warming. Owing to the increase in human population and the pressure it exerts on the Earth's resources, the planet's environment has been changing at an alarming rate which necessitates monitoring measures to be put in place [12]. In summary, therefore, environmental monitoring serves *to assess the effectiveness of an environmental legislation or policy*, *to monitor and assess compliance with regulatory statutes established to protect the environment, e.g., monitoring that the effluence from a given factory draining into a given river must be treated to a given standard*, and *for environmental change detection, e.g., vegetation change for the purpose of early warning*.

An example of change monitoring of agricultural land is shown in the photograph in Fig. 1.1, taken at Mt. Kokeby, Australia. In this figure, the vegetation (except salt tolerant fodders) are dying due to the effect of secondary salinity caused by vegetation clearing for farming purposes. This increased water recharge, which seeped into the ground and caused an upsurge of groundwater (rising to within 1 m of the top soil (i.e., root zone)), dissolve the salt trapped inside the soil and thereby causing secondary salinity. Monitoring the extent of salinity in this case enables comparisons to be made between the current state (Fig. 1.1) and the baseline data before the salinity effect had a noticeable impact. This can be done by comparing the spatial extent covered by the dying vegetation to that occupied by undisturbed vegetation (baseline data). A method of mapping the spatial boundaries is thus essential for monitoring changes in agricultural areas. GNSS satellites could provide a means for monitoring such spatial changes, as will be demonstrated in part II of this book.

**Fig. 1.1** Effect of secondary salinity at Mt. Kokeby, Australia. GNSS could be useful in mapping the spatial boundary of the affected vegetation

## 1.2 Satellite Monitoring

In 1997, the Kyoto protocol of the United Nation's framework convention on climate change spelt out measures that were to be taken to reduce the greenhouse gas emissions that are contributing to climate change, e.g., *global warming*. Global warming is but one of the many challenges facing our environment and as a consequence, human society, today. The rapid increase in *desertification* on the one hand and *flooding* on the other hand are environmental issues that are of increasing concern. For instance, the damage that arose from the torrential rains that caused havoc and destroyed properties in the USA in 1993 was estimated to have been $15 billion, with 50 people killed and thousands of people evacuated, some for several months [13].

Today, the threat from torrential rains and flooding still remains real, as was seen in the 1997 El Niño-Southern Oscillation (ENSO) rains that swept away roads and bridges in Kenya, the 2000 Mozambique floods, the 2002 Germany floods, Hurricane Isabel in the US coast in 2003, the flooding in Pakistan in 2010 that displaced millions of people, the 2011 eastern Australian floods that displaced thousand of people and destroyed properties estimated at billions of Australian dollars, and the Brazilian flush floods that killed more than 500 people in 2011.

Meanwhile, the melting of polar ice and the resulting raising sea level raises concerns for the submersion of beaches and cities surrounded by oceans and those already below sea level. In order to be able to predict and model these occurrences so as to minimize the negative consequences, such as those indicated by [13], atmospheric studies must be undertaken with the aim of improving current methods for providing *reliable*, *accurate* and *timely* data. These data are useful in Numerical Weather Prediction (NWP) models for weather forecasting, and climatic models for monitoring climatic changes. In addition, *accurate* and *reliable information* on weather is essential for other applications, such as agriculture, flight navigation, etc.

Data for NWP and climatic models are normally collected using balloon-borne radiosondes, satellites (polar and geostationary) and other sources, e.g., flight data from aeroplanes. Whereas [12, p. 94] point out that about 9500 land-based stations and 7000 merchant ships at any one time send up weather balloons, [14] noted that most of these data cover the northern hemisphere, with the southern hemisphere (especially Africa and South America) lacking adequate data due to financial constraints. The lack of radiosonde data is also noted in the oceanic areas, hence leading to a shortage of adequate data for NWP and climatic models. The shortage of radiosonde data, however, is partly compensated for by the availability of polar and geostationary satellite data. Polar orbiting satellites include the US-owned National Ocean and Atmospheric Administration NOAA-14 and NOAA-15 spacecrafts, while examples of geostationary satellites include the US-based Geostationary Operational Environmental Satellite (GEOS) and the European-owned METEOrological SATellite (METEOSAT).

Polar and geostationary satellites such as these, provide temperature and water vapour profile measurements. However, they have their own limitations. For high altitude winter conditions for instance, the use of passive Infra Red (IR) is difficult due to *very cold temperatures*, *common near-surface thermal inversion*, and a *high percentage of ice cloud* coverage that play a role in limiting IR soundings [15]. In volcanic areas, remote sensing satellite measurements are also affected by the presence of dust and aerosol. Large-scale volcanic eruptions normally inject large amounts of aerosols into the lower stratosphere, thus limiting the IR observation of the stratosphere and lower regions.

In-order therefore to enhance global weather and climatic predictions, current systems have to be complemented by a system that will provide global coverage, and whose signals will be able to penetrate clouds and dust to remote sense the atmosphere. Such a system, already proposed as early as 1965 by Fischbach [16], and which is currently an active area of research, is the new field of ***GNSS-meteorology***. This involves the use of GPS satellites to obtain atmospheric profiles of *temperature*, *pressure* and *water vapour/humidity*. More recently, the reflected GNSS signals are increasingly being used to provide change in the reflecting surfaces, thereby enabling monitoring of these features in what is known as GNSS-reflectometry. Its applications include, e.g., monitoring changes in soil moisture, vegetation and snow level (see, e.g., [17]).

GPS was developed by the US for its military purposes. It is an all weather tool capable of providing three-dimensional positions at any time [18]. At the time of its conception, fewer civilian uses were envisaged. In recent years, however, its use has widened to include, e.g., meteorological and environmental applications, e.g., monitoring of sea level and variation in stored fresh water [19]. This wide increase in GPS usage has led to the establishment of other equivalent systems by various nations/group of nations in the interest of their national security.

For example, the European Union (EU) is launching the Galileo satellites (30 satellites expected), the Chinese are developing BeiDou (BDS) that is expected to have 35 satellites, and the Russians are improving upon their GLONASS system by having smaller and more manageable satellites (30 expected). These constellations of satellites, collectively termed Global Navigation Satellite Systems (GNSS), will provide more than 100 satellites in space that will be very useful tools for monitoring the environment. In Chap. 2 we will present a brief overview of the GNSS systems and their future.

## 1.3 Integration of GNSS with Remote Sensing Satellites

The broad nature of environmental monitoring calls for the integration of various multi-disciplinary skills and the materials presented in this book looks at the contribution to environmental monitoring from the field of Geodesy, which engages mainly with the generation of spatial (location/position) based data. These data alone are insufficient for environmental monitoring, and will often be integrated with data from other techniques. One such area that complements GNSS is remote sensing.

Remote sensing is a rapidly advancing field of study that aims at the gathering of environmental data using a wide range of satellite and airborne platforms. When combined with location-based GNSS data, remote sensing contributes enormously to spatio-temporal Earth surface monitoring with a spatial resolution approaching GPS data precision [20]. Various forms of remote sensing approaches, e.g., optical (passive), thermal (passive), LiDAR (Light Detection And Ranging) (active) and microwave (active), see e.g., [21, 22] are available for environmental monitoring.

The importance of remote sensing for environmental applications has been demonstrated through NASA's launch of the Earth Observation Satellites (EOS) 'Terra' and 'Aqua' in 1999 and 2002, respectively, among many others. The objective of the EOS program was to develop the ability to monitor and predict environmental changes that occur both naturally and as a result of human activities through measurements of global and seasonally distributed Earth surface and atmospheric parameters such as land use, land cover, surface wetness, snow and ice cover, surface temperature, clouds, aerosols, fire occurrence, volcanic effects and trace gases [23].

Coupled with such information are geographical information system (GIS), which refers to a georeferenced computer-based mapping of features. It is comprised of hardware (computers and accessories), software (e.g., ArcGIS or ArcView), human resource (e.g., data analysts), data (which forms the primary component of GIS), and end users (clients). Spatial maps are produced together with attributes describing the information. For example, in contrast to the traditional map where the location of a road would be indicated on a sheet of paper, GIS would provide additional information, e.g., the number of accidents that occurred on that road in an attribute table, which can store more information than would normally be included on a paper map.

GIS, therefore, is simply made up of a database of information about a given location and hardware with cartographic (geocoordinates) display capability that is used to create maps from a database [24]. Gibson and McKenzie [25] define it in an even simpler way, that is, it is a tool for combining, manipulating, and displaying spatial information captured in a variety of ways, including through GNSS. The locations upon which the database are related are obtained from maps, field observations (e.g., surveying or GNSS), and airborne photogrammetry (e.g., orthophoto and LiDAR). The georeferenced database and the hardware/software system are linked such that when the database is updated, the maps are also automatically updated, unlike the traditional static paper maps that often take years to update.

Until recently, GIS and related technologies such as GPS and remote sensing were largely the domain of a few researchers. Things, however, are changing with the exploitation of these systems for environmental monitoring. For instance, GIS is finding use in environmental applications because [24]:

- Environmental issues are subject to widespread interest and heated debate,
- GIS can handle a large amount of different kinds of data and organize these data into topics or themes that represent the multiple aspect of complex environmental issues, and
- GIS serves as a collaborative tool that promotes interaction.

The important feature of GIS that separates it from other database management systems, e.g., those used in the financial world that need not or cannot make use of spatial or location-based attributes of the data set, is its capability to make use of its data bases to reference spatial features to locations (longitude, latitude, and altitude), relate these spatial attributes to maps of the region, and to offer spatial integration with other pertinent data bases for the region, e.g., Taylor et al. [26]. It is in providing these cost effective location-based data for creating and updating GIS that GNSS plays a major role. GNSS also provides ground control points for remote sensing techniques that supply attribute data to GIS, and the provision of a field mapping tool that enables attributes or features to be directly captured together with positions.

In most text books, e.g., [4], the most common satellite technique mentioned for environmental monitoring is remote sensing. Several applications have, however, directly reported the direct combination of GIS and GNSS for environmental monitoring, see e.g., [27]. As an example of the integration of GNSS and GIS, Taylor et al. [26] discuss the case of monitoring traffic congestion, which has the environmental impact of emitting $CO_2$ in the atmosphere, contributing to global warming and increasing fuel consumption. They demonstrate how a GIS-GNSS system can be integrated to provide useful monitoring information, where GNSS provides locations for both static and dynamic recordings of vehicles' positions over time. GIS on the other hand plays the role of data base integrator by super-positioning separate map layers of the data base, e.g., maps of topography and land use, transport networks, infrastructure, socio-economic and demographic data, traffic flow data, pollution, and environmental impact data [26].

Kitron [28] discusses the relevance of spatial tools and landscape ecology to emerging infectious diseases and to studies of global change effects on vector-borne diseases, while Bonner et al. [29] consider the combination of GNSS and GIS geocoding in epidemiologic research. Barbari [30] examined the potential of combining GNSS and GIS to support studies on livestock behaviour in pastures. They illustrated the potential to acquire information useful for cases such as breeding and good environmental management.

In another animal behaviour study, Hebblewhite and Haydon [31] found that the populations of most wide-ranging species move over areas orders of magnitude larger in scope than could be revealed by traditional methods such as very high frequency (VHF) radio telemetry, and that the advent of GNSS-based radio telemetry offered the possibility of conservation benefits such as harvest management, habitat and movement corridor protection, and trans-boundary collaboration. They present the example of the Serengeti in East Africa where simple GNSS-based locations over different jurisdictions with different levels of protection highlighted the precarious state of the Serengeti wildebeest migration [31, 32].

A combination of GNSS and Argos collars have been used by Durner et al. [33] to contribute to understanding the impact of climate change on polar bears. This is achieved, thanks to GNSS' all-weather continuous observations that permitted year-round observations, revealing the circumpolar nature of polar bear movements, and the details of how sea ice thickness and structure influences polar bear success in hunting their main prey, seals [31]. The possibility of integrating GNSS spatial data with other data, e.g., from remote sensing satellites, and socio-economic studies could potentially create a spatial database (e.g., Fig. 1.2), which is of valuable use to environmental monitoring and management.

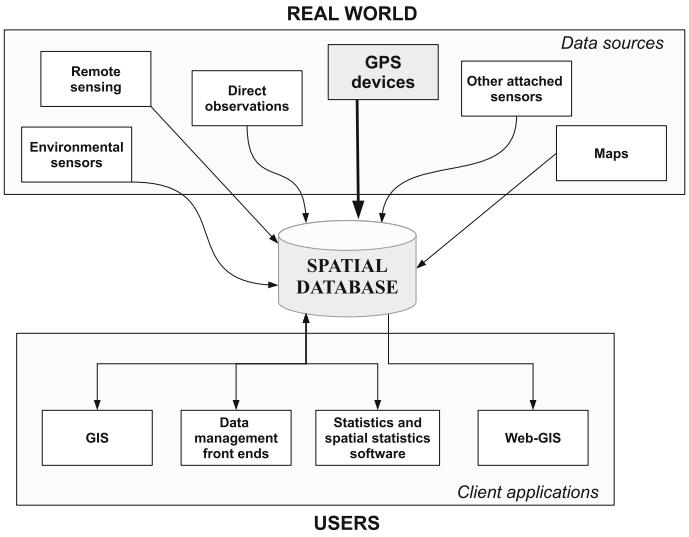


**Fig. 1.2** Schema of a possible client/server software system that combines information from several data sources, including core GNSS data (i.e., GPS), into the central spatial database where it is accessed, locally or remotely, by client applications for manipulation, visualization and analysis. Outputs are stored back in the database. *Source* Urbano et al. [20]

## 1.4 Objectives and Aims of the Book

This book is intended to be of use to two main groups of readers; those who deal with GNSS related theory, and those who apply it for environmental related tasks. It is aimed at realizing two main objectives:

(1) To the geodesist, who deals with modelling GNSS related errors and those in the hardware-software development, the book aims at presenting examples of the possible applications of GNSS to environmental monitoring and management. Whereas GNSS is widely used as a tool for spatial data collection for position determination, its role in environmental monitoring has not been well documented. Examples are presented of possible applications to support monitoring of tsunamis, earthquakes, e.g., [34], rising sea level, flash floods, global warming, conservation measures of endangered species, and many other environmental phenomena that can be monitored with the help of GNSS satellites. It is hoped that these examples will stimulate further research in the areas of GNSS in an attempt to meet the needs of environmental monitoring. Indeed, this is now being realized in geosensor networks where they are now contributing to real-time, sensor-rich event detection and monitoring that is fundamental to environmental monitoring applications [35].
(2) To those in environmental monitoring and management related fields, the book aims at presenting the concepts of GNSS in a simplified format, moving away

from the mathematical formulations found in many GNSS books, which often intimidate those whose aim is to simply understand the basics. Where only absolutely necessary are the mathematical details presented with such usage limited to the understanding of particular topics. Besides the basics of GNSS, the book attempts to highlight the possibility for integrating GNSS-based location data with other spatial data derived from, for example remote sensing of the environment and socio-economic data for the further enhancement of environmental monitoring and management through the generation of spatial databases (e.g., Fig. 1.2). This is shown, e.g., in environmental impact assessments (EIA), which integrate GNSS-based locational data with GIS to enhance the community participation during the implementation of environmental impact statements (EIS), where graphic presentations are employed. This second edition adds Chapters that showcase its application to monitoring climate variability, expands on its application through the use of reflected signals (GNSS-R), and reports on its support of the emerging use of unmanned aircraft vehicle (UAV)/drones in, e.g., precise agriculture for crop and soil moisture condition monitoring. This edition also updates the state of GNSS satellites. Hopefully, this book adds to the list of environmental measuring/sensing tools at your disposal.

In recognition of the first objective above, Europe is currently engaged in the deployment of Galileo, which are hoped to contribute towards environmental monitoring of global warming and sea level changes (see Chap. 7). With the future commissioning of the Galileo system, there exists a wide window of opportunity for environmentalists to further refine their tools and monitoring programs. It is with this in mind that this second edition of the book is written, to exploit the potentials of GNSS, and to prepare environmentalists for more GNSS satellites and systems, such as Galileo, BeiDou and modernised GPS and GLONASS.

In Part I of this book, the basic operational principles of GNSS satellites (specifically GPS) are presented, hopefully in a manner that would be easily understood by environmentalists. Part II of the book presents practical applications of GNSS in monitoring the environmental.

## References

1. Artiola J, Pepper IL, Brusseau ML (eds) (2004) Environmental monitoring and characterization. Elsevier Academic Press, USA
2. Hofman-Wellenhof B, Lichtenegger H, Wasle E (2008) GNSS global navigation satellite system: GPS. GLONASS; Galileo and more, Springer, Wien
3. James LF, Young JA, Sanders K (2003) A new approach to monitoring rangelands. Arid Land Res Manag 17:319–328. doi:10.1080/15324980390225467
4. Spellerberg IF (2005) Monitoring ecological change, 2nd edn. Cambridge University Press, Cambridge
5. Study of Critical Environmental Problems (1970) Man's impact on the global environment. MIT Press, Cambridge

6. Finlayson CM (1996) Framework for designing a monitoring program. In: Tomas Vives P (ed) Monitoring mediterranean wetlands: a methodological guide. MedWet Publication, Wetlands International, Slimbridge, UK and ICN, Lisbon
7. Vaughan H, Brydges T, Fenech A, Lumb A (2001) Monitoring long-term ecological changes through the ecological monitoring and assessment network: science-based and policy relevant. Environ Monit Assess 67(1–2):3–28. doi:10.1023/A:1006423432114
8. Downes BJ, Barmuta LA, Fairweather PG, Faith DP, Keough MJ, Lake PS, Mapstone BD, Quinn GP (2002) Monitoring ecological impacts: conceipts and practise in flowing waters. Cambridge University Press, Cambridge
9. Burden FR, McKelvie I, Förstner U, Guenther A (2002) Environmental monitoring handbook. McGraw-Hill, New York
10. Wiersma GB (ed) (2004) Environmental monitoring. CRC Press, Boca Raton
11. Goldsmith FB (ed) (1995) Monitoring for conservation and ecology. Chapman and Hall, London
12. Mackenzie FT (2003) Our changing planet; an introduction to Earth system science and global environmental change, 3rd edn. Prentice Hall, New Jersey
13. Larson LW (1996) Destructive water: water-caused natural disasters, their abetment and control. IAHS conference, Anaheim California, June 24–28
14. Wickert J (2002) Das CHAMP-Radiookkultationsexperiment: Algorithmen, Prozessierungs system und erste Ergebnisse. Dissertation. Scientific Technical Report STR02/07, GFZ Potsdam
15. Melbourne WG, Davis ES, Duncan CB, Hajj GA, Hardy K, Kursinski R, Mechan TK, Young LE, Yunck TP (1994) The application of spaceborne GPS to atmospheric limb sounding and global change monitoring. JPL Publication, Pasadena, pp 94–18
16. Fischbach FF (1965) A satellite method for pressure and temperature below 24 km. Bull Am Meteorol Soc 46:528–532
17. Jin S, Cardellach E, Xie F (2014) GNSS remote sensing. Theory, methods, and applications. Springer, New York
18. Hofman-Wellenhof B, Lichtenegger H, Collins J (2001) Global positioning system: theory and practice, 5th edn. Springer, Wien
19. Awange JL, Sharifi M, Ogonda G, Wickert J, Grafarend EW, Omulo M (2008) The falling lake victoria water level: GRACE, TRIMM and CHAMP satellite analysis. Water Res Manag 22:775–796. doi:10.1007/s11269-007-9191-y
20. Urbano F, Cagnacci F, Clement C, Dettki H, Cameron A, Neteler M (2010) Wildlife tracking data management: a new vision. Philos Trans R Soc B 365:2177–2185. doi:10.1098/rstb.2010.0081
21. Lillesand TM, Kiefer RW, Chipman JW (2008) Remote sensing and image interpretation, 6th edn. Wiley, New York
22. Awange JL, Kiema JBK (2013) Environmental geoinformatics. Monitoring and management, Springer, Berlin
23. Huete AR (2004) Remote sensing for environmental monitoring. In: Artiola J, Pepper IL, Brusseau ML (eds) Environmental monitoring and characterization. Elsevier Academic Press, USA
24. Macarthur R (2004) Geographical information systems and their use for environmental monitoring. In: Artiola J, Pepper IL, Brusseau ML (eds) Environmental monitoring and characterization. Elsevier Academic Press, USA
25. Gibson J, MacKenzie D (2007) Using global positioning systems in household surveys for better economics and better policy. World Bank Res Obs 22(2):217–241. doi:10.1093/wbro/lkm009
26. Taylor MAP, Woolley JE, Zito R (2000) Integration of the global positioning system and geographical information systems for traffic congestion studies. Trans Res Part C 8(1–6):257–285. doi:10.1016/S0968-090X(00)00015-2
27. Steede-Terry K (2000) Integrating GIS and the global positioning system. ESRI Press, California

28. Kitron U (1998) Landscape ecology and epidemiology of vector-borne diseases: tools for spatial analysis. J Med Entomol 35(4):435–445
29. Bonner MR, Han D, Nie J, Rogerson P, Vena JE, Freudenheim Jo L (2003) Positional accuracy of geocoded addresses in epidemiologic research. Epidemiology 14:408–412. doi:10.1097/01.EDE.0000073121.63254.c5
30. Barbari M, Conti L, Koostra BK, Masi G, Sorbetti Guerri F, Workman SR (2006) The use of global positioning and geographical information systems in the management of extensive cattle grazing. Biosyst Eng 95(2):271–280. doi:10.1016/j.biosystemseng.2006.06.012
31. Hebblewhite M, Haydon DT (2010) Distinguishing technology from biology: a critical review of the use of GPS telemetry data in ecology. Philos Trans R Soc B 365:2303–2312. doi:10.1098/rstb.2010.0087
32. Thirgood S, Mosser A, Tham S, Hopcraft G, Mwangomo E, Mlengeya T, Kilewo M, Fryxell J, Sinclair ARE, Borner M (2004) Can parks protect migratory ungulates? The case of the Serengeti wildebeest. Animal Conserv 7:113–120. doi:10.1017/S1367943004001404
33. Durner GM et al (2009) Predicting 21st-century polar bear habitat distribution from global climate models. Ecol Monogr 79:25–58. doi:10.1890/07-2089.1
34. Segall P, Davis JL (1997) GPS applications for geodynamics and earthquake studies. Annu Rev Earth Planet Sci 25:301–336. doi:10.1146/annurev.earth.25.1.301
35. Nittel S, Labrinidis A, Stefanidis A (eds) (2008) Geosensor networks. Lecture notes in computer science, vol 4540, pp. 1–6. Springer, Berlin

# Part I
# Global Navigation Satellite Systems (GNSS)

# Chapter 2
# Modernization of GNSS

*With four Global Navigation Satellite Systems fully operational by the end of the decade, users on Earth can enjoy signals, at multiple frequencies in the L-band of the Electro-Magnetic (EM) spectrum, from 1.1 to 1.6 GHz, from over 110 satellites. There should then be, on average, about 30 satellites in view above a 10 degrees elevation, anywhere on Earth.*

Christian Tiberius [1]

## 2.1 Introductory Remarks

Throughout history, position (location) determination has been one of the fundamental tasks undertaken by humans on a daily basis. Each day, one deals with positioning, be it going to work, the market, sports, church, mosque, temple, school or college, one has to start from a known location and move towards a known destination. Usually the start and end locations are known, since the surrounding physical features form a reference upon which we navigate ourselves. In the absence of these reference features, for instance in the desert or at sea, one then requires some tool that can provide knowledge of one's position.

To mountaineers, pilots, sailors, etc., knowledge of position is of great importance. The traditional way of locating one's position has been the use of maps or compasses to determine directions. In modern times, however, the entry into the game by Global Navigation Satellite Systems (GNSS) have revolutionized the art of positioning, see e.g., [2]. The use of GNSS satellites can be best illustrated by a case where someone is lost in the middle of the desert or ocean and is seeking to know his or her exact location (Fig. 2.1). In such a case, one requires a GNSS receiver to be able to locate one's own position. Assuming one has access to a hand-held GNSS receiver (Fig. 2.1), a mobile phone or a watch fitted with a GNSS receiver, one needs only to press a button and the position will be displayed in terms of geographical longitude and latitude $(\phi, \lambda)$. One then needs to locate these values on a given map or press a



J. Awange, *GNSS Environmental Sensing*, Environmental Science and Engineering, DOI 10.1007/978-3-319-58418-8_2

button to send his/her position as a short message service (sms) on a mobile phone as is the case for search and rescue missions. Other areas where GNSS find use are geodetic surveying (positioning) where accuracies are required to mm level, GIS (Geographical Information System) data capture, car, ship and aircraft navigation, geophysical surveying and recreational uses.

The increase in civilian use has led to the desire of autonomy by different nations who have in turn embarked on designing and developing their own systems. In this regard, the European nations are developing the Galileo system (discussed in Chap. 7), the Russians are modernizing their GLONASS system, while the Chinese are lalready having 21 out of the 30 BeiDou navigation satellite system (abbreviated as BDS) in space. All of these systems form GNSS with desirable positional capability suitable for environmental monitoring. GNSS are:

1. Global: This enables the monitoring of global environmental phenomena, e.g., global warming, sea level rise, etc.
2. All weather: This feature makes GNSS useful during cloudy and rainy periods, which are still stumbling blocks to radar systems and low Earth orbiting satellites.
3. Able to provide 24 h coverage: This enables both day and night observations and can thus enable the continuous monitoring of events such as the spread of oil from a maritime disaster.
4. Cheaper: Although the initial expense and maintenance of the satellites and ground support are very high, from the user's point of view, they are cheaper as compared to other terrestrial observation techniques such as photogrammetry or Very Long Baseline Interferometry (VLBI) [3]. GNSS are economical due to the fact that only a few operators are needed to operate the receivers and process data. Less time is therefore required to undertake a GNSS survey to obtain a solution.
5. Able to use a common global reference frame (e.g., WGS-84 Coordinate System for the GPS system).

## 2.2 GNSS Family and the Future

Besides GPS, GNSS comprise GLONASS (Russian), Galileo (European Union), and BeiDou (Chinese). GLONASS, first launched in 1982, has been in operation after attaining full operational capability in 1995. The full constellation of GLONASS was designed to have 24 satellites (21 satellites in 3 orbits plus 3 spares) orbiting at 25,000 km above the Earth's surface. By 2001, however, only 6 satellites were in orbit due to funding limitations that led to its near demise [1]. Currently, fewer than originally planned satellites are operating (i.e., 23 satellites as of January, 2017, with a total of 27 in orbit, see.[1]

[1] https://www.glonass-iac.ru/en/GLONASS/.

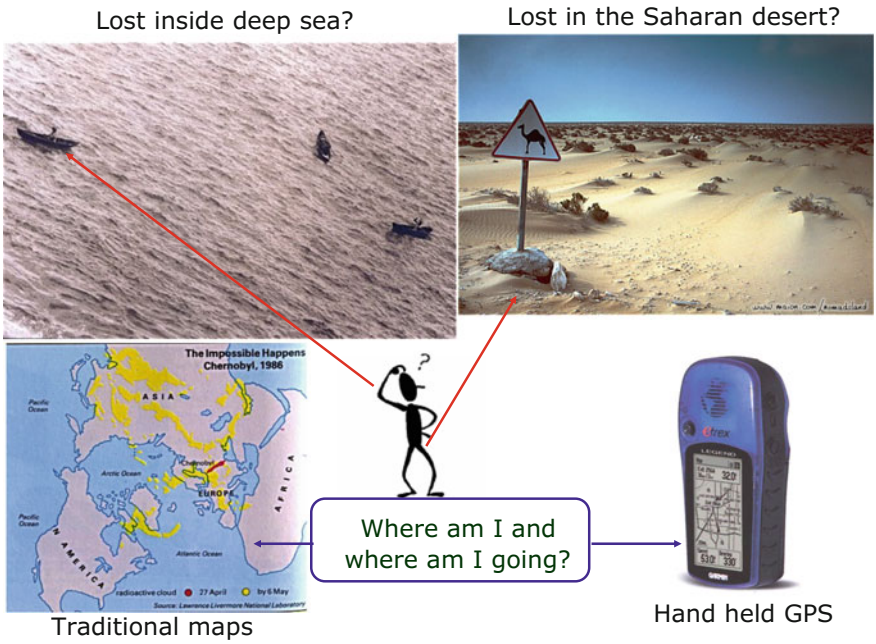


**Fig. 2.1** Use of GNSS to position oneself. In case one is in deep sea or desert and wants to know his or her position, pressing a button on a hand-held GNSS receiver will provide the position

The Russian government has, however, embarked on a modernization program which will see the deployment of second generation GLONASS-M and the new third generation GLONASS-K satellites that will have improved features, e.g., reduced weight, more stable clocks, longer lifespan and improved navigation messages, and allow much simpler integration with other GNSS system such as GPS [1]. Table 2.1 provides a comparison between the GLONASS and GPS. On 25th of September 2008, the Space Forces successfully launched three GLONASS-M satellites (launched since 2003) into orbit from the Baykonur launch site in Kazakhstan bringing the number of GLONASS-M satellites to about 18. The launch of the GLONASS-K satellites with three civilian frequencies, which are supposed to have a longer lifetime than the GLONASS-M satellites (i.e., 10 years), and with added integrity components took place on 26th of February 2011, having been delayed from its planned date in December 2010 following the crash of the three GLONASS-M type satellites into the Pacific ocean. From 2025, Russia is planning the launch of GLONASS-KM satellites with comparable frequencies and formats as GPS's L5 and L1C signals, and corresponding to Galileo/BeiDou's E1, E5a and E5b signals (see Chaps. 3 and 7 for more details on the signal structure). GLONASS, like GPS, reserves more highly accurate signals for military use, while providing free standard signals for civilian use.

However, the satellites mentioned in Sect. 2.1 are not the only satellites within the GNSS system where new satellites are continuously being launched. Due to the

**Table 2.1** Comparison between GPS and GLONASS as of January 2017

| | GPS | GLONASS |
|---|---|---|
| Number of satellites | 31 | 27 |
| Number of orbital planes | 6 | 3 |
| Orbital radius | 26,000 km | 25,000 km |
| Orbital period | 11 h 58 m | 11 h 15 m |
| Geodetic datum | WGS84 | SGS84 |
| Time reference | UTC(USNO) | UTC(SU) |
| Selective availability | Yes | No |
| Antispoofing | Yes | Possible |
| Carrier | L1:1575.42 MHz | 1602.56–1615.5 MHz |
| | L2:1227.60 MHz | 246.43–1256.5 MHz |
| C/A code (L1) | 1.023 MHz | 0.511 MHz |
| P-code (L1,L2) | 10.23 MHz | 5.11 MHz |

global nature of the GNSS satellites, ensuring sufficient number of a given satellite (e.g., GPS) in other parts of the world or for applications in specific areas (e.g., urban or forested areas) can be challenging. For this reason, other systems have been developed that include satellite based augmentation systems (SBAS) such as US's WAAS (Wide Area Augmentation System), European's EGNOS (European Geostationary Navigation Overlay Service), Japan's MTSAT Space-based Augmentation System (MSAS) and India's GPS-Aided GEO-Augmented Navigation (GAGAN) system.

Local augmentation systems include the Indian Regional Navigation Satellite System (IRNSS) consisting of seven satellites, with the first satellite launched on the 1st of July 2013. As of January 2017, four IRNSS satellites had been launched. IRNSS is an independent regional navigation satellite system being developed by India. It is designed to provide accurate position information service to users in India as well as the region extending up to 1500 km from its boundary, and is expected to provide Standard Positioning Service (SPS) to all the users and Restricted Service (RS) to the authorised users with a positioning accuracy of better than 20 m.[2] The Japanese Quasi-Zenith Satellite System (QZSS) is expected to consists of four satellites by 2018, with 3 satellites visible at all times from locations in Asia-Oceanic regions. The first satellite 'Michibiki' was launched on 11 September 2010, and QZSS is expected to reach full operational capability by 2018 with a total of 7 satellites envisioned by 2024 to improve on stability that will enable positioning in urban and mountainous regions, see.[3]

EGNOS, which is briefly discussed in Chap. 7 is a stand alone system that seeks to augment the existing GPS and GLONASS systems to improve satellite positioning accuracy within Europe. It has its own ground, space, and user segments with

[2] http://www.isro.gov.in/irnss-programme.

[3] http://qzss.go.jp/en/.

support facilities. The ground segment is made up of GNSS (GPS, GLONASS) Geostationary Earth Orbiting satellites-GEO, Ranging and Integrity Monitoring Stations (called RIMS) connected to a set of redundant control, and processing facilities called Mission Control Centre (MCC) that determine the *integrity*, *pseudorange differential corrections* for each monitored satellite, *ionospheric delays* and generates GEO satellite ephemeris [4]. This information is uplinked to the GEO satellites from the Navigation Land Earth Station (NLES). The GEO satellites then send the correction information to individual users (user segment) who use them to correct their positions. For discussions on other GNSS systems, such as DORIS, PRARE, etc., the reader is referred to [2, 5].

China launched the first BeiDou navigation satellite system (BDS) in 2007 and as per January 2017, 21 satellites were in orbit providing regional services for the Asia-Pacific region [1]. BDS constellation is expected to comprise more than 30 satellites orbiting at an altitude of about 21,150 km (i.e., 30 non-geostationary and 5 stationary), see e.g., [2, p. 402] for more details. It will provide positioning (accuracy of 10 m), navigation (velocity accuracy of 0.2 m/s) and timing services (accuracy of 10 nanoseconds) globally based on open and restricted services.[4] BeiDou has already been tested in areas such as communication and transportation, forest fire prevention, disaster forecast, public security and the Wenchuan earthquake, environmental areas where BeiDou will play an important role, see, e.g.[5] By 2020, BeiDou is expected to provide global coverage.

## 2.3 Benefits of the Expanding GNSS Family

With the receivers undergoing significant improvement to enhance their reliability and the quality of signals tracked, the world is already inundated with various kinds of receivers that are able to track several or all GNSS satellites. The monitoring and management of environmental aspects should therefore benefit enormously from these enhanced and improved GNSS satellites, where the possibilities of combining some of the main GNSS satellite systems is possible. For example, a receiver capable of trucking both GLONASS and GPS satellites such as Sokkia's GSR2700-ISX receiver has the possibility of receiving signals from a total constellation of more than 50 satellites. Similarly, the design of Galileo is being tailored towards an interoperability with other systems, thereby necessitating compatibility with GPS and GLONASS and potentially leading to a constellation of nearly 80 satellites. Adding the Chinese BeiDou puts the number to nearly 110 when all the system will be complete.

This combination of systems will further provide more visible satellites as illustrated by the proposed Australian CORS stations shown in Fig. 5.15, which could be useful in monitoring the future expected rise in sea level, submergence of land due

[4] http://en.beidou.gov.cn/introduction.html.

[5] http://en.beidou.gov.cn/introduction.html.

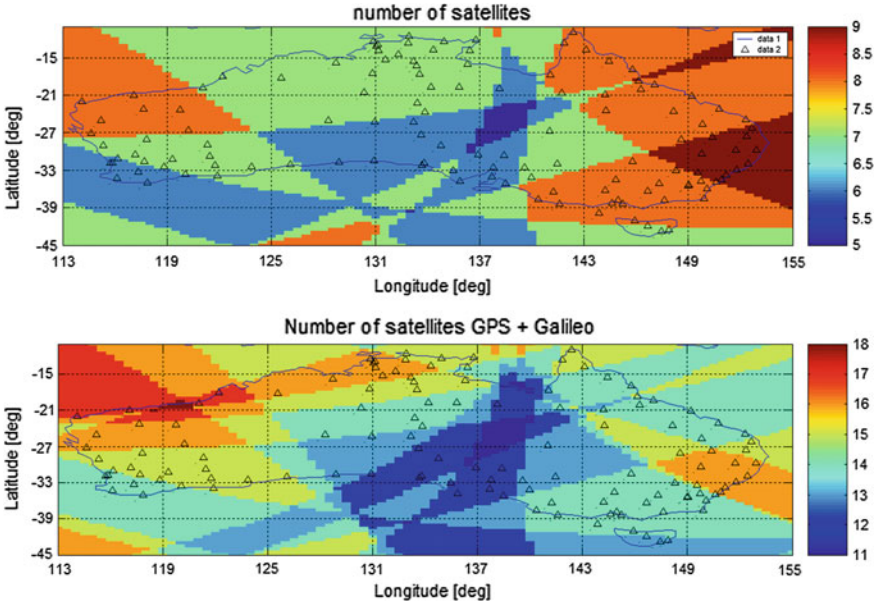


**Fig. 2.2** *Top* Number of visible GPS satellites over Australia on 15.03.2007. *Bottom* Number of visible GPS+Galileo satellites over Australia on 15.03.2007. *Source* [6]

to groundwater abstraction and other environmental phenomenon. As an example, Fig. 2.2 presents the number of GPS satellites that were visible on the 15th of March 2007 compared to the situation that would have been if the Galileo system was fully operational on this day. As can be seen, the lowest number of satellites visible at any station on this day was 6. When Galileo satellites are included, the minimum number of visible satellites doubles to 12. Thus, anywhere on the Australian continent at the aforementioned "snapshot" of time, there could have been enough visible satellites for the proposed CORS network since the addition of GALILEO greatly improves satellite visibility. Table 2.2 presents the total number of visible Galileo and GPS satellites as reported by the definition phase of Galileo, see [4].

This increase in the number of visible satellites ensures a better geometry and improved resolution of unknown ambiguity, thereby increasing the positioning accuracies discussed in Sect. 5.3. The advantages of combining GNSS systems listed by the European Union (EU) and European Space Agency (ESA) [4] include:

- Availability: For example, a combination of Galileo, GLONASS and GPS will result in more than 60 operational satellites, resulting in the increased availability of the minimum required number of 4 satellites from 40% to more than 90% in normal urban environments worldwide.
- Position accuracy: Allied to an increased availability in restricted environments (urban) is a better geometry of spacecraft and enhanced positioning performance.

**Table 2.2** Maximum number of visible satellites for various masking angles. *Source* [4]

| Receiver elevation masking angle | Number of visible Galileo satellites | Number of visible GPS satellites | Total |
|---|---|---|---|
| 5° | 13 | 12 | 25 |
| 10° | 11 | 10 | 21 |
| 15° | 9 | 8 | 17 |

- Integrity: In addition to generating ranging signals, augmentation of GNSS with SBAS discussed in Sect. 5.4.4.2 will enhance the provision of integrity information.
- Redundancy: The combination of services from separate and fully independent systems will lead to redundant observations.

Increased satellite availability from 40% to more than 90% in urban environments would benefit environmental monitoring measurements undertaken in urban areas, where the effect of multipath and signal reflection from buildings and other features are rampant. Redundant observations will also be beneficial to environmental monitoring projects that may need continuous measurements (e.g., in animal telemetry).

GNSS systems can be combined with non-GNSS systems such as conventional surveying, Long Range Aid to Navigation (LORAN-C) and Inertial Navigation Systems (INS) to assist where GNSS systems fail, such as inside forests and tunnels. Other benefits that would be accrued through the combination of GNSS with conventional methods have been listed, e.g., by the EU and ESA [4] as offering improved signal strength, which provides better indoor penetration and resistance to jamming; offering a limited communication capability, and complementary positioning capability to users in satellite critical environments through mobile communication networks; and the provision of a means for transferring additional GNSS data through communication systems to enable enhanced positioning performances (e.g., accuracy) as well as better communication capabilities (e.g., higher data rates and bi-directional data links).

## 2.4 Concluding Remarks

With the continuing expansion of the GNSS systems, environmental monitoring tasks requiring space observations will benefit greatly. Some of the advantages arising from the increased number of satellites as opposed to the current regime include additional frequencies which will enable more accurate and better resolved modelling of ionospheric and atmospheric errors, and additional signals that will benefit wider range of environmental monitoring tasks. GNSS will offer much improved accuracy, integrity and efficiency performances for all kinds of user communities over the world. In the Chaps. 3–7, two of the GNSS systems (GPS and Galileo) are discussed in great detail, with the oldest, GPS, given more coverage.

## References

1. Tiberius C (2011) Global navigation satellite systems. A status update. Hydro Int. 15(2):23–27
2. Hofman-Wellenhof B, Lichtenegger H, Wasle E (2008) GNSS global navigation satellite system: GPS. GLONASS; Galileo and more, Springer, Wien
3. Takahashi F, Kondo T, Takahashi Y, Koyama Y (2000) Very long baseline interferometer. IOS press, Amsterdam, Netherlands
4. European Commission and European Space Agency (2002) Galileo mission high level definition, 3rd edn. http://ec.europa.eu/dgs/energy_transport/Galileo/doc/Galileo_hld_v3_23_09_02.pdf. Accessed 11 Nov 2008
5. Prasad R, Ruggieri M (2005) Applied satellite navigation using GPS. GALILEO and augmentation systems, Artech House, Boston/London
6. Wallace N (2007) CORS simulation for Australia. Curtin University of Technology, Final year project (unpublished)

# Chapter 3
# The Global Positioning System

*The number of GPS units and sensors is growing fast, and if georeferencing was a specialist's work a few years ago, it is a mainstream one click matter today. Software in smart-phones and alike makes it incredibly easy to create geo-referenced data. Location-based services are a fast growing business accordingly and all kinds of geo-related social networking here I am applications invade our daily lives.*

Erik Kjems

## 3.1 Introductory Remarks

The Global Positioning System (GPS) is the oldest and most widely used GNSS system, and as such will be extensively discussed in the first part of this book. The development of GPS satellites dates from the 1960s [1, 2]. By 1973, the US military had embarked on a program that would culminate into the NAVSTAR GPS, which became fully operational in 1995. The overall aim was to develop a tool that could be used to locate points on the Earth without using terrestrial targets, some of which could have been based in domains hostile to the US. GPS satellites were therefore primarily designed for the use of the US military operating anywhere in the world, with the aim of providing passive real-time three-dimensional (3D) positioning, navigation, and velocity data. The civilian applications and time transfer, though the predominant use of GPS, is in fact, a secondary role.[1]

## 3.2 GPS Design and Operation

In general, GPS is comprised of *space*, *control*, and *user segments*.

[1]The world of geographically referenced information is facing a paradigm shift. Source: http://www.vector1media.com/.



J. Awange, *GNSS Environmental Sensing*, Environmental Science and Engineering, DOI 10.1007/978-3-319-58418-8_3

### 3.2.1 Space Segment

This segment is designed to be made up of 24 satellites plus 4 spares orbiting in a near circular orbit at a height of about 20, 200 km above the Earth's surface. As of January 2017, there were 31 operational GPS satellites in space (e.g., Table 2.1). Each satellite takes about 11 h 58 min to orbit around the Earth (i.e., orbits the Earth twice a day [3]). The constellation consists of 6 orbital planes inclined at 55° from the equator, each orbit containing 4 satellites (Fig. 3.1). With this setup, and an elevation of above 15°, about 4–8 satellites can be observed anywhere on the Earth at anytime [1, 2]. This is important to obtain 3D positioning in real-time but becomes crucial in urban and mountainous regions where the number of visible GPS satellites might be low necessitating augmentations with regional satellites as discussed in Sects. 2.2 and 5.4.4.2. The satellites themselves are made up of solar panels, internal components (atomic clock and radio transmitters), and external components such as antennas. The orientation of the satellite in space is such that the solar panels face the sun so as to receive energy to power the satellite while the antennas face the Earth to transmit and receive radio signals.

The launch of GPS satellites has undergone several stages since inception. First launched were Block I prototype satellites, from 1978 to 1985. Powered by solar panels, they weighed 845 kg and were designed with a lifespan of 4.5 years. They, however, exceeded this time span with some operating for more than 10 years. These satellites are now not operational, having been replaced by Block II satellites launched in 1989 and weighing 1500 kg. They operated until 1996, by which time 27 satellites of Blocks II and IIA ("A" stands for Advanced) had been launched. The last of the Block IIA satellites was launched in 2001. Their lifespan was designed to be 7.5 years, but some were still operational even after 10 years. By April 1995, GPS had been declared fully operational with the third generation satellites, Block IIR ("R" stands for Replacement), designed to replace the early Block II satellites, being deployed in July 1997.

On 26th September 2005, the first satellite of Block IIR-M ("M" standing for modernized) was successfully launched. The last of the Block IIR-M satellites was launched on 17/08/2009. The first of the Block IIF ("F" standing for Follow-on) series was launched on 27th May 2010 from Cape Canaveral, Florida, USA. Finally, the launch of Block III satellites scheduled for 2018 is expected to improve the capability of the GPS positioning and is expected to operate up to 2030 and beyond [4, p. 324]. This would provide a wider window of opportunity for important applications such as *environmental monitoring* and *management*. As of January 2017, 12 Block IIR, 7 Block IIR-M and 12 Block IIF were operational bringing the number of GPS satellites to 31.[2] With the final launch of Block IIF on 5th February 2016, the addition of these Block IIF satellites to the constellation enabled the system to reach its best performance day ever on May 11, 2016, achieving 36.5-cm accuracy in average user range error.[3]

[2] http://www.gps.gov/systems/gps/space/.

[3] Col. Steven Whitney: http://gpsworld.com/2016-in-review-gps-navigates-the-future/.

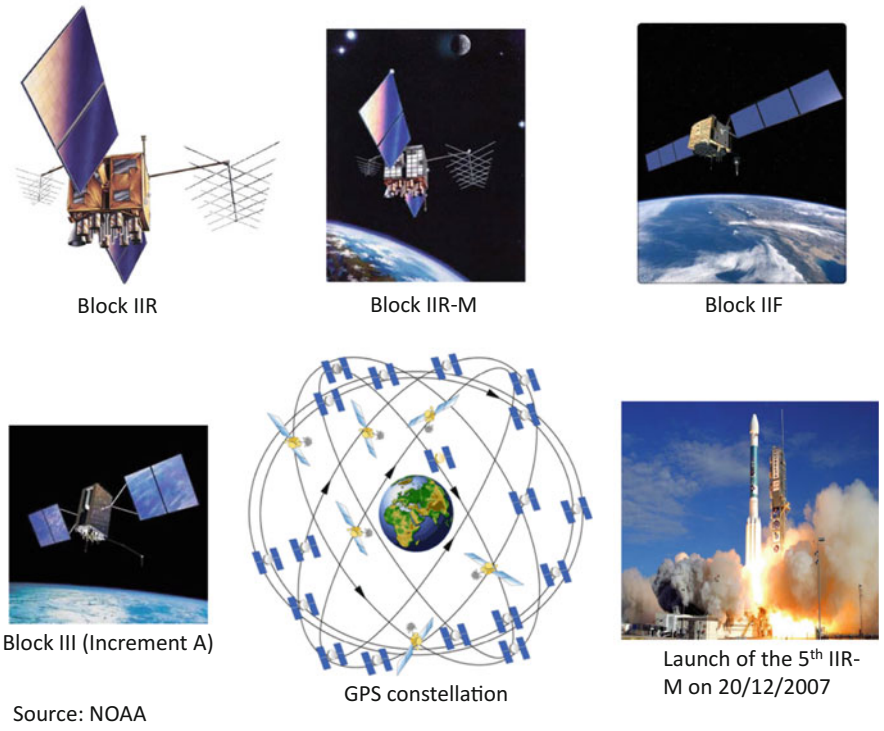


**Fig. 3.1** A schematic showing the configuration of the GPS satellites in orbit and the various GPS-blocks

Figure 3.1 shows some of these GPS Blocks and the pattern they take in their constellation.

### *3.2.2 Control Segment*

The GPS control segment consists of *master*, *monitor*, and *ground* stations. The master control station is located at Colorado Springs (Schriever Air Force Base, Colorado) with a backup station at Gaithersburg, Maryland. The monitor stations are made up of five stations located at *Colorado Springs*, *Ascension Island* in the Atlantic Ocean, *Hawaii*, *Diego Garcia* in the Indian Ocean, and *Kwajalein Island* in the Pacific Ocean. In September 2005, six more monitoring stations of the NGA (National Geospatial-Intelligence Agency) were added to the network, enabling every satellite to be seen by at least two monitoring stations and thus improve the accuracy of the computed satellite orbital parameters (known as ephemeris) (Fig. 3.2).[4]

[4]Source: http://www.gps.gov/multimedia/images/GPS-control-segment-map.pdf.

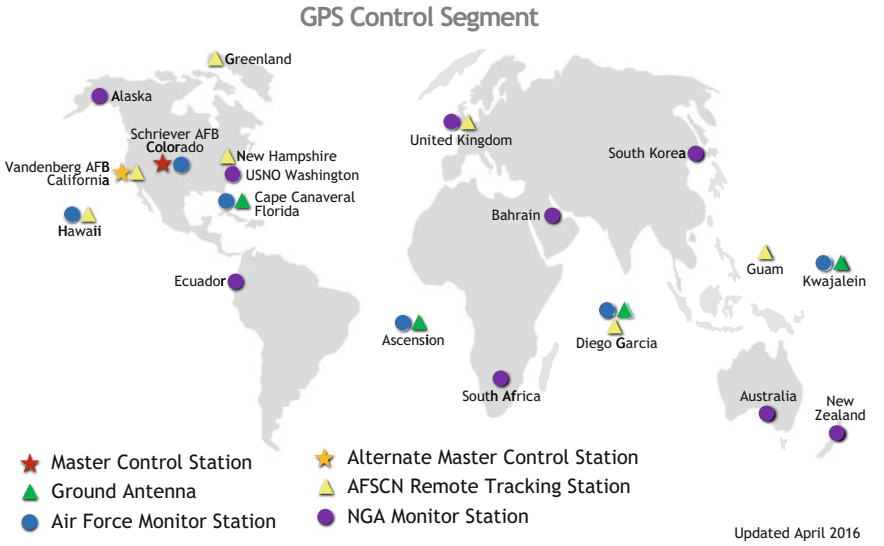


**Fig. 3.2** GPS monitoring stations. *Source* http://www.gps.gov/multimedia/images/GPS-control-segment-map.pdf

The satellite's *ephemeris* consists of the satellite's positions and velocities predicted at given times. These ephemeris records are valid for a maximum of 4 h and are updated every hour, hence fresh ephemeris records should be used [5]. The computed satellite coordinates at the time of signal transmission are with respect to the World Geodetic System (WGS 84), see Sect. 5.6.2. These stations monitor the orbital parameters and send the information to the master station at Colorado Springs. The information obtained from these monitoring stations tracking the satellites are in turn used to control the satellites and predict their orbits. This is done through the processing and analysis of the information by the master station, which computes the satellite ephemeris and clock parameters and transmits them to the satellites.

There are several ground stations distributed across the world that augment the control system by monitoring and tracking the satellites in space and transmitting correction information to individual satellites through ground antennas. These stations form the International GNSS Service (IGS) network. The ground control network is therefore responsible for tracking and maintaining the satellite constellation by monitoring satellite health and signal integrity, and maintaining the satellite orbital configuration.

### *3.2.3 User Segment*

The user segment consists of receivers (most of which consist of 12 channels or more), which are either hand-held (also available in wrist watches, mobile phones, etc.) or mountable receivers, e.g., in vehicles, or permanently positioned. The availability of

12 channels enables receivers to track and process data from 12 satellites in parallel given that the constellation enables 24 satellites to cover the globe and as such, up to 12 satellites can be seen in each hemisphere. The acquisition of 12 satellites thus improves on the positioning accuracy (see accuracies for various applications in Chap. 5). These receivers are employed by a wide range of users to meet their daily needs. So wide and varied are the uses of GPS that Awange and Grafarend [6] termed it the Global Problem Solver (GPS). For military purposes, it is useful in guiding fighter planes, bombers and missiles, as well as naval and ground units.

Civilian use covers a wide range of applications, such as mining, where it is used to guide heavy machinery or locating positions, to agriculture in what has become known as "*precision farming*". Using GPS and GIS, farmers can integrate location, amount of fertilizer and yield expected, and analyze the three for optimum output. Modern car tracking companies use GPS to locate stolen vehicles, while in the aviation sector, GPS can be used in both aircrafts and airports to guide landings and take offs. GPS is also widely used in sports such as mountaineering. The list of uses is therefore only limited to our imaginations.

For *environment monitoring*, the main subject of this book, GPS as one of the GNSS plays a key role as will be discussed in detail in part II. For example, GPS plays a vital role in earthquake monitoring and as such is useful for environmental disaster mitigation. It can also map post disaster areas and monitor events such as forest fires and oil spills, and how fast they are spreading [7]. Its application to environmental phenomena such as El Niño, tsunami warning, weather, climate change, and global warming, in what is known as GNSS-meteorology promises more benefits to humanity. In recent studies, GPS has contributed to the monitoring of variations in fresh water resources and has together with other satellites established the cause of the recent rapid fall in Lake Victoria, see e.g., [8]. Its entry into reflectometry discussed in Chap. 10, climate variability in Chap. 12 and support of the unmanned aircraft vehicle (UAV)/drones discussed in Chap. 20 motivated the writing of this current edition of the book.

## 3.3 GPS Observation Principles

In this section, the basic principles upon which GPS operates are presented. More detailed expositions of the operational principles can be obtained in more advanced text books such as [1, 2, 9]. We begin the section by looking at the structure of the GPS signals.

### *3.3.1 GPS Signals*

Earlier GPS satellites (Blocks II, IIA and IIR) sent microwave radio signals to receivers that are comprised of

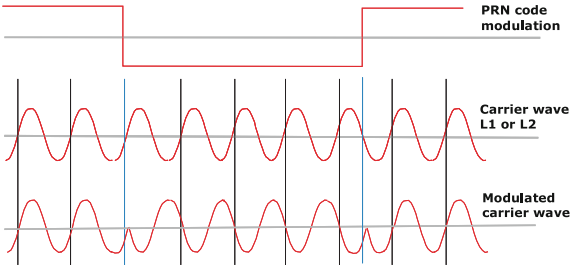


**Fig. 3.3** Code modulation in the GPS carrier frequencies

- L1 and L2 carrier frequencies,
- *coarse acquisition* ($C/A-code$) and *precise acquisition* ($P-code$), and
- the navigation messages.

The precise atomic clocks onboard the GPS satellites generate a fundamental clock rate or frequency $f_0$ of 10.23 MHz, which is used to generate the two L-band carrier frequencies L1 and L2 through integer multiplication (i.e., $L1 = 154\,f_0$ and $L2 = 120\,f_0$). This leads to the frequency of L1 to be 1575.42 MHz with a wavelength of 19 cm and that of L2 as 1227.60 MHz, with a wavelength of 24.4 cm. The ranging binary codes $C/A-code$ and $P-code$ are then modulated onto the carrier frequencies (e.g., Fig. 3.3). Each of these ranging codes consists of a stream of binary digits, zeros and ones, known as bits or chips [5, p. 14]. Due to the noisy nature of these codes, they are known as Pseudo Random Noise (PRN) but are normally generated using a mathematical algorithm, see e.g., [1]. The L1 frequency carries both the $C/A-code$ and $P-code$, while the L2 frequency carries only the $P-code$. The $C/A-code$ modulates at 1 MHz and repeats every 1023 bits while the $P-code$ modulates at 10 MHz and repeats every 7 days with a wavelength of 29.3 m, and is reserved for the US militarily and its allies and thus not accessible to civilian users.

Each satellite has a specific $C/A-code$ that enables a GPS receiver to identify it. For example, a GPS satellite with an ID of PRN 20 refers to a GPS satellite that is assigned to the twentieth week segment of the PRN $P-code$ [5, p. 14]. $C/A-code$ is less precise compared to $P-code$ and is reserved for civilian use. The reservation of the $P-code$ code for military use is realized through the addition of an unknown $W-code$ to the $P-code$ to generate a $P(Y)-code$. This process is called antispoofing (AS).

Besides the *ranging* $C/A-code$ and $P-codes$, a GPS satellite will also broadcast *navigation* messages to its users. The navigation message contains information on the *health of the satellite*, *orbital parameters* (satellites broadcast their ephemeris as a function of time), generic *ionospheric corrections*, *satellite clock correction parameters*, satellite almanac and some information on other satellites. The GPS almanac is less accurate compared to ephemeris and are updated every 6 days or less and are used to predict satellite visibility at a particular location and time, as discussed in Sect. 5.3. Each message has a 50 Hz frequency and consists of 25 pages (also known as frames) and 5 subframes of data. Subframe 1 contains GPS week number, satellite accuracy and health, and satellite clock correction terms. Subframes 2 and 3 carry

the satellite ephemeris, while subframe 4 contains ionospheric corrections, satellite health and almanac data for satellites 25–32, special messages, satellite configuration flags, ionospheric and UTC (Coordinated Universal Time) data. Subframe 5 contains the satellite health and almanac data for satellites 1–24, almanac reference time and week number. Each subframe is made up of 10 words, and each word is made up of 30 bits. The total message length is therefore 1500 bits.

The advantage of using dual frequencies (L1 and L2) is the ability to mitigate ionospheric errors as will be discussed in detail in Sect. 3.4.3. The setback with the traditional GPS signal structure is that the user is only accessible to the L1 carrier frequency. Positioning with L1 alone has the limitation of not being able to use the differencing techniques that combine both L1 and L2 frequencies to minimize *ionospheric errors*. To circumvent this problem, most geodetic high precision GPS receivers adopt techniques such as cross-correlation that do not require the $Y-code$ to recover the L2 signal [5, p. 20]. These techniques, however, recover L2 signals which are noisier than the original signals. For long baselines, i.e., distances of 100 s of km between receivers, use of such L2 signals provides some relief against the effect of the ionosphere. For very short baselines, e.g., $<5$ km, the ionospheric effects cancel out between the receivers as the atmospheric conditions are almost identical between these receivers. Use of L2 signals could thus be omitted without significant effects.

Modernized GPS satellites (Block IIR-M and Block IIF) address this problem through the introduction of a second civilian *ranging code L2C* that will be modulated on the L2 carrier frequency. The L2C signal is already being transmitted by Block IIR-M satellites currently in orbit. This provides civilians with the capability of combining the two frequencies L1 and L2C to mitigate ionospheric errors and boost accuracy. For civilian users with dual-frequency GPS receivers on the one hand, use of L2C signal will enable them to achieve the same or better accuracy as those in the military. For professional users with existing dual-frequency operations on the other hand, using L2C signal will delivers faster signal acquisition, enhanced reliability, and greater operating range.[5] Furthermore, the fact that L2C broadcasts at a higher effective power than the legacy L1 C/A signal, makes it easier to receive under trees and even indoors.[6] This attribute will make it attractive for monitoring changing environmental phenomenon in forested or urban regions.

In addition to this civilian frequency, Block IIR-M satellites also have a new military signal with a new code (M-code on L1M and L2M) for enhanced jam resistance. Although this is expected to improve autonomous positioning (stand-alone GPS), the additional of the second civil code is found to be insufficient for use in civil safety-of-life transportation and other high performance applications, mainly due to the potential interference of ground radars that operate near the L2 band [5, p. 17]. Therefore, in order to meet the needs of safety-of-life in aviation, a third civil code L5 is incorporated in Block IIF and planned for inclusion in future Block III satellites, in addition to the L2C and the new robust and higher power

[5] http://www.gps.gov/systems/gps/modernization/civilsignals/.

[6] http://www.gps.gov/systems/gps/modernization/civilsignals/.

military M-codes. They will be modulated into the L1 and L2 carrier frequencies. The L5 signals currently in Block IIF satellites and whose pre-operational signal were broadcasting from 12 GPS satellites as of 31st October 2016 is broadcast in a radio band reserved exclusively for aviation safety services. It is expected to be available on 24 satellites in 2024.[7] It features higher power, greater bandwidth, and an advanced signal design, and its combination with L1 C/A-code is expected to correct for the ionospheric errors thereby improving accuracy on the one hand, while on the other hand, its signal redundancy will enhance the robustness of the solution. In addition to enhancing safety, and for environmental benefits, use of L5 signals will increase capacity and fuel efficiency within U.S. airspace, railroads, waterways, and highways. Furthermore, its use will provide users worldwide with the most advanced civilian GPS signal that when used in combination with L1 C/A and L2C, the three GPS frequencies could enable sub-meter accuracy without augmentations, and very long range operations with augmentations discussed in Sects. 2.2 and 5.4.4.2.[8] These additional civilian signals are expected to improve positioning accuracy, see e.g., Fig. 5.7 on p. 69.

### *3.3.2 Measuring Principle*

The starting point is the basic principle of physics that relates the travel time $t$, distance travelled $d$, and speed of light $c$, namely:

$$Distance(d) = Speed(c) \times Time(t). \tag{3.1}$$

If time $t$ can be accurately measured in (3.1), and the speed $c$ is known, then it is possible to obtain the distance $d$. This basic expression forms the foundation of GPS satellite positioning. GPS receivers situated on the ground or in space accurately measure the time $t$ taken by a signal to travel from the satellites to the receivers. Knowing the speed of light (i.e., $c = 3 \times 10^5$ km/s), the distance from the satellites to the receivers, known as "*pseudoranges*", can be measured. Since the GPS satellites orbit at about 20,200 km above the Earth, it takes around 0.07 s for the signal to travel from the satellite to the receivers.

The satellites generate binary codes ($C/A$ and $P$) that are send to the receiver, which generates identical binary codes. The receiver generated codes are then compared to those received from the satellites, which lag behind those generated by the receivers. By comparing the two signals (from the satellite and the receiver), the receivers are able to compute the travel time of the signal. A binary code generated by the satellite takes the form of $+1/-1$ (see Fig. 3.3).

In order to measure the time travelled by the signal accurately, the receiver and satellite clocks must be synchronized and be error free. The clocks, however, normally

[7] http://www.gps.gov/systems/gps/modernization/civilsignals/.

[8] http://www.gps.gov/systems/gps/modernization/civilsignals/.

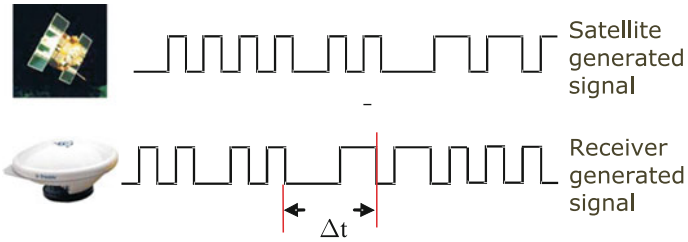


**Fig. 3.4** The time difference between the receiver and GPS code signals

have errors that are propagated to the measured ranges. Furthermore, clock errors are not the only ones that degrade the measured ranges. The atmosphere, orbital errors, multipath, and other types of errors discussed in Sect. 3.4 also contribute to the degradation of the measured ranges, hence the term *pseudoranges*. Because the receiver's position is given by the three Cartesian coordinates $X$, $Y$, $Z$, one solution of Eq. (3.1) would not suffice, with three such equations being required. This would essentially mean simultaneously observing three satellites in space to obtain position for one epoch. Due to clock errors, however, there is an additional *receiver clock* unknown bias $\Delta t$ which takes the number of unknowns to four, i.e., $X$, $Y$, $Z$, $\Delta t$. Hence a fourth satellite is needed to determine the receiver clock error $\Delta t$, while the satellite clock errors are modelled. This topic will be treated in more detail in Chap. 4.

There are two ways by which the distances from the receivers to the satellites are measured. These are:

(i) Code ranging.
(ii) Carrier-phase ranging.

*Code-pseudorange* involves measuring the time lag between the satellite and receiver generated signals using either $C/A-code$ or $P-code$ (Fig. 3.4). The receiver locks onto the signal and synchronizes a matching code, thereby measuring the delay of the signal, as illustrated in Fig. 3.4. The measured time delay, $\Delta t$, is then multiplied by the speed of light $c$ in Eq. 3.1 to generate the pseudorange $p$. Code-pseudoranges can achieve an accuracy of about 5–15 m for C/A-code and therefore may suffice for those environmental applications that do not require higher accuracies such as locating a waste dumping site. For accuracies at cm and mm-levels, i.e., those required for monitoring environmental phenomenon such as rising sea level or the movement of tectonic plates, one has to use the carrier-phase measurements (Fig. 3.5). For *Carrier-phase pseudorange*, *phase lag* instead of time lag is measured. The measuring principle is similar to that used in an EDM (electronic distance measurement), see e.g., [10, 11]. By measuring carrier-phase, more precise positioning is possible.

As seen in Fig. 3.5, the complete number of cycles plus the fractional portion (phase) are used in the case of GPS carrier phase pseudorange measurements from the satellites to the receiver. Since the initial *complete number of cycles* are not normally known at the time the receiver is switched on, there exists an unknown

*integer ambiguity* $N$. The accurate determination of this integer ambiguity underpins the accuracy of the final position derived from the carrier-phase measurements. For GPS phase measurements, the one way distance equation becomes

$$pseudorange(p_p) = N\lambda + \phi, \tag{3.2}$$

where $N$ is the unknown number of complete cycles (i.e., integer ambiguity), $\lambda$ is the wavelength of the signal, and $\phi$ the measured phase. Clearly, if $N$ is known, then the orangeade $p_p$ will be accurately determined.

Example 3.1 (Carrier-phase measurements).

As an illustration, let us consider carrier-phase measurements made from the satellite to the receiver for a duration of 1 min (Fig. 3.5). At the time the receiver is switched on (i.e., $t = 0$s), it generates a random integer number such as (565730) since it does not know the complete number of cycles of the signal from the satellite. As the measurement progresses, the number of cycles increases and the complete number of cycles are accurately counted (if no cycle slips occur, i.e., loss of lock to the satellites). After $t = 60$s, the total number of cycles counted is recorded as 816543.9534. The complete number of cycles measured in 1 min is thus $816543 - 565730 = 250813$ together with the fractional portion of the cycle 0.9534. If 1 cycle of the L2 signal has a wavelength of $\lambda = 0.244$ m, the measured pseudorange $P_p$ will be given by

$$\left.\begin{aligned} P_p &= 250813\lambda + 0.9534\lambda + N\lambda \\ P_p &= 61198.60463 + N\lambda \end{aligned}\right], \tag{3.3}$$

where $N$ is the unknown integer ambiguity. If its value is known, then the phase pseudorange could be determined. Since this value is often unknown, it is determined independently or together with the unknown coordinates $X, Y, Z$ and clock parameters as discussed in Chap. 4.

♣ End of Example 3.1.

In Sect. 4.2, we show how the pseudoranges discussed above are used in the observation equations to generate positions. Detailed discussion of the signal structure and how they are processed can be found, e.g., in [1, 2, pp. 71–85].

## 3.4 Errors in GPS Measurements

Just like any other measurement, the accuracy derived from GPS measurements are subject to errors that degrade the quality of the derived parameters, including those of environmental interest. This section considers some of the most significant errors that undermine GPS observations and discusses the means by which these errors could be minimized and/or avoided. As already pointed out in Sect. 3.3.2, these errors lead to pseudorange rather than an accurate range between the satellite and the receiver.

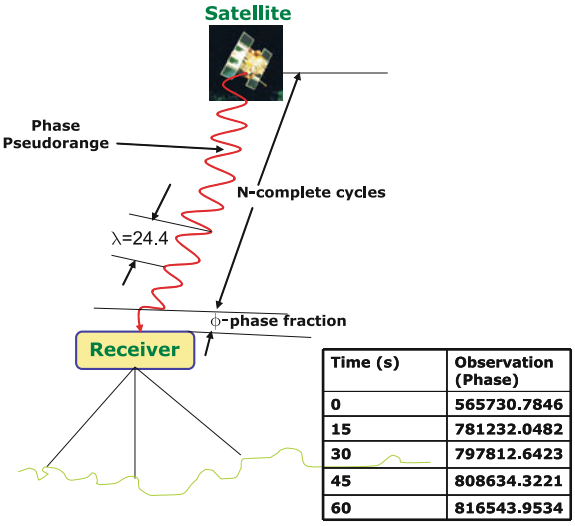


**Fig. 3.5** Carrier-phase pseudorange measurement. At the time the receiver is switched on, the complete number of cycles $N$ is unknown, and what the receiver measures is the fractional phase $\phi$

We will present some modelling techniques by which these errors are eliminated or minimized in Chap. 4.

### *3.4.1 Ephemeris Errors*

As the satellites move along their orbits, they are influenced by external forces such as solar and lunar (moon) gravitational attraction, as well as periodic solar flares [10, p. 180].

For shorter baselines (i.e., distances less than 30 km between two receivers on Earth), orbital errors tend to cancel through differencing techniques discussed in Chap. 4 (pp. 54–55). Over long baselines however, e.g., over 1000 km, orbital errors no longer cancel owing to different receivers sensing different components of the error due to significant changes in the vector directions.

As pointed out in Sect. 3.2.2, ground monitoring stations are used to continuously measure the positions of the satellites. Techniques such as satellite laser ranging (SLR), lunar laser ranging (LLR), and Very Long Baseline Interferometry (VLBI) are used to locate these ground control stations to a very high accuracy. Using the data from the monitoring stations, the master control station predicts satellite positions (broadcast ephemeris), which are transmitted to the user as part of the navigation message together with the data signals during positioning. The accuracy of the broadcast ephemeris has improved tremendously, i.e., from 20 to 80 m in 1987 to 2 m, see e.g., [5, p. 16]. El-Rabbany [5, p. 16] attributes this improvement to superior operational software, and improved orbital modelling.

*Broadcast ephemeris* are useful for real-time positioning (i.e., if the GPS receiver is expected to deliver results while collecting measurements in the field). *Precise ephemeris* on the other hand are useful for post-processing tasks, which are required at a later date. In such cases, the post-processed positions of the satellites by other global tracking stations are available 17 h to 2 weeks later with accuracies of 0.02–0.2 m.

### 3.4.2 Clock Errors

Satellite clocks are precise atomic clocks (i.e., rubidium and cesium time standards). In contrast, the receivers cannot include atomic clocks since the cost would be too high for users to afford and for safety concerns. Clocks within the receivers are thus less precise, and as such, subject to errors. This is not to say that the satellite clocks are error free, but that the magnitude of the receiver errors are much higher.

The satellite and receiver clocks also have to be synchronized in order to measure the time taken by the signal to travel from the satellites to the receiver. Since the synchronization is normally not perfect, errors are likely to occur. This error is also known as time offset, i.e., the difference between the time as recorded by the satellite and that recorded by the receiver, see e.g., [9]. The measured range error is then given by

$$R_e = c\delta t, \tag{3.4}$$

where $c$ is the speed of light and $\delta t$ is the time offset. From (3.4), considering that $c = 3 \times 10^5$ km/s, a clock error of 0.000001 s, for instance, would cause the measured range to be erroneous by 300 m, while an error of 0.001 s would result in a range error of 300 km. Such errors in the measured pseudorange eventually propagates into the determined receiver's position, thereby degrading its accuracy.

Satellite clock errors are small in magnitude and easily corrected due to the fact that the ground control stations closely monitor the time drift and are able to determine second order polynomials, which accurately model the time drift [9]. These second order polynomials are included in the broadcast message. The receiver clock error is determined as a nuisance unknown along with the required coordinate parameters in the observation Eq. (4.17) and this explains the need of the fourth satellite as discussed in Sect. 3.3.2.

### 3.4.3 Atmospheric Errors

The atmosphere is the medium above the Earth by which the GPS signal passes before it reaches the receiver. *Charged particles* in the ionosphere (50–1000 km) and *water vapour* in the troposphere (1–8 km) affect the speed of the GPS signals, leading to an optical path length between the satellite and the receiver and a delay

in the corresponding time the GPS signal takes to reach the receiver, see e.g., [12]. One of the key tasks of geodetic GNSS processing software therefore is to "correct" the ranges between the satellite and the receiver so as to remove the effects of the Earth's atmosphere, thereby reducing all optical path lengths to straight-line path lengths [12].

The *ionosphere* is made of *negatively charged electrons*, *positively charged atoms* and *molecules* called *ions*. The charged particles are a result of free electrons that occur high in the atmosphere and are caused by solar activity and geomagnetic storms. The number of free electrons in the column of a unit area along which the signal travels between the sending satellite and the receiver make up what is known in GPS literatures as the Total Electron Content (TEC). Free electrons in the ionosphere delay the GPS code measurements, thus making the measured ranges too long on the one-hand while advancing the GPS phase measurements, making the measured ranges too short on the other hand, thus resulting in incorrect ranges (i.e., errors in the measured ranges) [1, pp. 99–108], [2, p. 191]. The size of the delay or advance (which can amount to tens of meters) depends on the TEC and carrier frequency, i.e., the ionosphere is a dispersive medium [2, p. 191].

The error effect of the ionospheric refraction on the GPS range value depend on sunspot activity, time of the day, satellite geometry, geographical location and the season. Ionospheric delay can vary from 40 to 60 m during the day to 6–12 m at night [9]. GPS operations conducted during periods of high sunspot activity or with satellites near the horizon produce range results with the highest errors, whereas GPS observations conducted during low sunspot activity, during the night, or with satellites near the zenith produce range results with the smallest ionospheric errors. Ionospheric effects are prominent over longer baselines (>30–50 km) although high ionospheric activity can affect shorter distances. Ionospheric errors can be significantly reduced through:

1. *Use of dual frequency*. Since signal speed through the ionosphere is dependent on frequency (dispersive medium), ionospheric effects, which cause a delay of about 2–80 m can be modelled using frequency combination. They are removed mostly by comparing the signal delays of the $L1$ and $L2$ frequencies and exploiting the known dispersion relations for the atmosphere [13, 14], i.e.,

$$\rho_{IF} = \frac{f_{L1}^2}{(f_{L1}^2 - f_{L2}^2)}\rho_{L1} - \frac{f_{L2}^2}{(f_{L1}^2 - f_{L2}^2)}\rho_{L2} \tag{3.5}$$

and

$$\Phi_{IF} = \frac{f_{L1}^2}{(f_{L1}^2 - f_{L2}^2)}\Phi_{L1} - \frac{f_{L2}^2}{(f_{L1}^2 - f_{L2}^2)}\Phi_{L2}, \tag{3.6}$$

where $\rho_{IF}$ and $\Phi_{IF}$ are the *ionosphere-free* code-pseudorange and phase-pseudorange, respectively. $\rho_{L1}$ and $\rho_{L2}$ are measured code-pseudoranges while $\Phi_{L1}$ and $\Phi_{L2}$ are phase-pseudoranges measurements at L1 and L2 carrier frequencies. The resulting observations in (3.5) and (3.6) are known as

ionosphere free observations and hence explain the main reason why GPS uses two frequencies. It should be pointed out that the L2 signal is not accessible to users and as such, users can obtain it through e.g., cross-correlation technique. The disadvantage with using dual frequencies as illustrated above where L2 is obtained through cross-correlation is the increased noise and as such, this approach is useful mainly for longer baselines. For very short baseline (<5 km), where the atmosphere is assumed uniform, the ionosphere error is minimized once differencing techniques are used (see Chap. 4). Lack of L2 for civilian users has necessitated the introduction of L2C and L5 signals as was discussed in Sect. 3.3.1, which are used in Eqs. 3.5 and 3.6 above in place of L2.

2. *Modelling*. GPS navigation messages contain ionospheric correction parameters that are used in correction models during data processing. Several ionospheric correction models, such as the Klobuchar model, are available in commercial software and can be used to reduce ionospheric errors. However, this only gives an approximate value that usually does not remove more than 50% of the error. Moreover, modelling is generally inefficient in handling short-term variations in the ionospheric error.

The second medium, the *troposphere*, also known as the neutral atmosphere, consists of 75% of the total molecular mass of the atmosphere, as well as all of the water vapour and aerosols. The troposphere is a non-dispersive medium, i.e., the refraction is independent of the frequency of the signal passing through it. Tropospheric errors vary significantly with *latitude* and *height* and are dependent on *climatic zone*. The neutral atmosphere is therefore a mixture of *dry gases* and *water vapour*.

Water vapour is unique in this mixture because it is the only constituent that possesses a dipole moment contribution to its refractivity, thus leading to separate treatment between the dipole and non-dipole contribution to refractivity by the water vapour and other constituents in the atmosphere [12]. The tropospheric errors thus comprise two parts (see Fig. 9.1, p. 145): the "*hydrostatic part*", commonly referred to in various GPS text as "dry part", and the dipole component known as the "*wet part*". Belvis et al. [12], while citing Saastamoinen [15] and Davis et al. [16], state that the *hydrostatic delay* is generally erroneously referred to as "*dry delay*" in the literature, meaning that they are due to the contribution of dry air. In actual fact, according to Belvis et al. [12], the dry air contributes mostly to the hydrostatic delay, but there is also the contribution of the non-dipole component of water vapour. They propose the use of the term hydrostatic delay instead of dry delay. In this book, the term hydrostatic delay therefore is adopted.

According to Belvis et al. [12], both hydrostatic and wet delays are smallest for paths oriented along the zenith direction and increase approximately inversely with the sine of the elevation angle, i.e., either delay will tend to increase by about a factor of 4 from zenith to an elevation of about 15°. Consequently, Belvis et al. [12] point out that most expressions for the delay along a path of arbitrary elevation consist of the zenith delay multiplied by a mapping function. This mapping function has been shown, e.g., by Davis et al. [16] to describe the dependence of the delay on elevation angle.

The *hydrostatic part* contributes 90% of the tropospheric error. It is easily modelled out to few millimeter or better given surface pressure. The remaining 10% occurs from the wet part, resulting from the *water vapour*, which depends on the refractivity of the air through which the signal is travelling. The refractivity of air depends on (1) the *density of air molecules* (dry component) and (2) the *density of the water vapour* (wet component). Above 50 km altitude, the density of molecules is very low and hence its effect is small. Although the wet delay is always much smaller than the hydrostatic delay, it is usually far *more variable* and *more difficult to remove* [12].

The tropospheric delay therefore depends on *temperature*, *pressure* and *humidity* and affects signals from satellites at lower elevations more than those at higher elevation. For example, El-Rabbany [5, p. 55] and [12] indicate that tropospheric delay results in pseudorange errors of about 2.3 m for satellites at the zenith (i.e., satellites directly overhead), 9.3 m at 15° elevation, and 20–28 m for 5° elevation. Therefore, the lower the elevation angle of the incoming GPS signal, the greater the tropospheric effect because the signal travels a longer path through the troposphere.

Tropospheric delay can be problematic, especially when stations are widely distributed at different altitudes. For example, cold (dense) air can accumulate in mountain basins on clear calm nights whilst mountain tops may be considerably warmer. Tropospheric delay can also exhibit short-term variations, e.g., due to the passing of *weather fronts*. The *hydrostatic part* can be modelled by employing surface meteorological data or by acquiring them from external sources such as the European Center for Medium Weather Forecast (ECMWF) and the National Center for Environmental Prediction (NCEP).

Whereas the hydrostatic delay can be modelled from the surface meteorological data, the wet component cannot be accurately determined in the same manner, but is instead measured from water vapour radiometers (WVR) [17–19] or by directly estimating the time varying *zenith wet delay* (ZWD) as unknowns from the GPS observations [20, 21]. These estimation techniques usually assume azimuthal symmetry of the atmosphere, and they exploit the form of the elevation dependence of the delay (i.e., the mapping function) and the fact that the delay changes little over short periods of time [12]. These analyzes typically constrain the variations in the *zenith wet delay* to between 1 and 20 mm per hour, depending on location and time of year, leading to the recovery of ZWD from GPS data with an accuracy between 5 and 20 mm [12].

In most processing software, ZWD is estimated using Integrated Precipitate Water Vapour (IPWV) models. Many models, e.g., Saastamoinen, Hopfield, and Magnet, have been proposed to model tropospheric errors, see e.g., [1]. Some of these models depend on real meteorological data input. However, the best observational principle is to keep the baselines as short as possible.

The discussions in this section have focused on eliminating the effects of atmospheric delay in order to improve the accuracy of positioning. In Chap. 9, we will see that such noise, as geodesist are keen on positioning, are actually valuable environmental monitoring parameters. In essence, *one person's poison is another person's meat!*

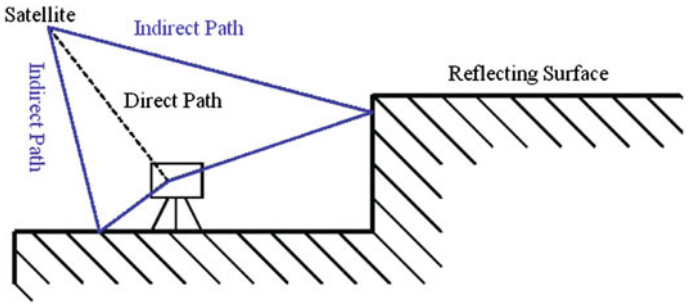


**Fig. 3.6** Multipath effect

### *3.4.4 Multipath*

Consider now a satellite signal that is meant to travel straight to the receiver being reflected by a surface, as shown in Fig. 3.6. The measured pseudorange reaching the receiver ends up being longer than the actual pseudorange, had the signal travelled directly. In urban areas, the presence of buildings contribute greatly to the multipath effect. Multipath errors can be avoided by placing the receiver in a place without reflective or refractive surfaces. The best practise is to place the receiver at least 3 m from reflecting walls and in addition use GPS antennas with ground panels which discard indirect reflected signals (which are of a lower power). A choke ring antenna also provides a means of reducing multipath while other receivers have in-built filtering mechanisms. Good mission planning (see Sect. 5.3) also helps to reduce the effect of multipath. In Chap. 10, it will be seen how this geodetic nuisance, i.e., reflected signal becomes a vital observable for monitoring changes in the environment, e.g., soil moisture changes through the emerging technique of GNSS-reflectometry (GNSS-R),

### *3.4.5 Satellite Constellation "Geometry"*

Dilution of precision (DOP) depends on the distribution of the satellites in space (see Fig. 5.1 on p. 62). With clear visibility and a large number of satellites, the value of DOP is low, indicating a good geometry. With obstructions and fewer satellites, however, the DOP values becomes high, indicating poor geometry, which may negatively affect positioning accuracy.

Also used to measure the geometric strength is the Position Dilution of Precision (PDOP), which can be used essentially as an expression of the quality of the satellites' geometry, which is essential for ambiguity resolution. Usually, a PDOP value of less than 6 but greater than 1 is desirable. For a detailed discussion of this topic, we refer to Sect. 5.3.

### *3.4.6 Other Sources of Errors*

Other sources of errors which may degrade accuracy include hardware errors due to variations in the antenna phase centers with satellite altitude. This error is greater at elevations below 15° but less between 15 and 60°. In addition, there is receiver noise (e.g., signal processing, clock synchronization, receiver resolution, signal noise, etc.) and cycle slips, which results when the receivers lose lock on a satellite due to, for example, signal blockage by buildings. Radio interference, severe ionospheric disturbance, and high receiver dynamics can also cause signal loss [5, p. 25].

## 3.5 Concluding Remarks

In summary, this chapter has presented the basics of GPS satellites by looking at the satellites, signal structure and measurement principle used to obtain position. Position is calculated by accurately measuring the distance of a receiver from the satellite by determining the delay in the radio signal transmitted by the satellite. This delay is measured by matching and comparing the received signals to an equivalent receiver generated signal. More precise measurements use phase instead of timing code measurements. The signals, however, are subject to various sources of errors, which have been discussed in this chapter.

In general, the measuring principle and the errors discussed in this chapter are also valid for all the other GNSS systems (GLONASS, Galileo and BeiDou). They only differ in design, signal structure and coordinate systems (see Sect. 5.6).

## References

1. Hofman-Wellenhof B, Lichtenegger H, Collins J (2001) Global positioning system: theory and practice, 5th edn. Springer, Wien
2. Leick A (2004) GPS satellite surveying, 3rd edn. Wiley, New York
3. Agnew DC, Larson KM (2007) Finding the repeat times of the GPS constellation. GPS Solution 11:71–76. doi:10.1007/s10291-006-0038-4
4. Hofman-Wellenhof B, Lichtenegger H, Wasle E (2008) GNSS global navigation satellite system: GPS. GLONASS, Galileo and more, Springer, Wien
5. El-Rabbany A (2006) Introduction to GPS global positioning system, 2nd edn. Artech House

6. Awange JL, Grafarend EW (2005) Solving algebraic computational problems in geodesy and geoinformatics. Springer, Berlin
7. Steede-Terry K (2000) Integrating GIS and the global positioning system. ESRI Press, California
8. Awange JL, Sharifi M, Ogonda G, Wickert J, Grafarend EW, Omulo M (2008) The falling lake Victoria water level: GRACE, TRIMM and CHAMP satellite analysis. Water Resour Manag 22:775–796. doi:10.1007/s11269-007-9191-y
9. US Army Corps of Engineers (2007) NAVSTAR global positioning system surveying. Engineering and design manual, EM 1110-1-1003
10. Irvine W, Maclennan F (2006) Surveying for construction, 5th edn. McGraw-Hill, Berkshire
11. Walker J, Awange JL (2017) Surveying for civil and mining engineers - theory, workshops and practicals. Springer, Heidelberg
12. Bevis M, Businger S, Herring TA, Rocken C, Anthes RA, Ware RH (1992) GPS meteorology: remote sensing of water vapour using global positioning system. J Geophys Res 97:15787–15801
13. Brunner FK, Gu M (1991) An improved model for the dual frequency ionospheric correction of GPS observations. Manuscripta Geod 16:205–214
14. Spilker JJ (1980) GPS signal structure and performance characteristics, in global positioning system, vol 1. The Institute of Navigation, Washington, D.C
15. Saastamoinen J (1972) Atmospheric correction for the troposphere and stratosphere in radio ranging of satellites, in the use of artificial satellites for geodesy, geophys. Monogr. In: Henriksen SW et al (eds) vol 15. AGU, Washington D.C., pp 247–251
16. Davis JL, Herring TA, Shapiro II, Rogers AE, Elgered G (1985) Geodesy by radio interferometry: effects of atmospheric modelling errors on estimates of baseline length. Radio Sci 20:1593–1607
17. Elgered G, Davis JL, Herring TA, Shapiro II (1991) Geodesy by radio interferometry: water vapor radiometry for estimation of the wet delay. J Geophys Res 96:6541–6555
18. Resch GM (1984) Water vapor radiometry in geodetic applications. In: Brunner FK (ed) Geodetic refraction. Springer, New York, pp 53–84
19. Ware R, Rocken C, Hurst KJ (1986) A GPS baseline determination including bias fixing and water vapor radiometer corrections. J Geophys Res 91:9183–9192
20. Herring T, Davis JL, Shapiro II (1990) Geodesy by radio interferometry: the application of Kalman filtering to the analysis of very long baseline interferometry data. J Geophys Res 95:12,561-12,581
21. Tralli DM, Dixon TH, Stephens SA (1988) Effect of wet tropospheric path delays on estimation of geodetic baselines in the Gulf of California using the global positioning system. J Geophys Res 93(B6):6545–6557. doi:10.1029/JB093iB06p06545

# Chapter 4
# Mathematical Modelling

*If I were again beginning my studies, I would follow the advice of Plato and start with mathematics.*

Galileo Galilei

## 4.1 Introductory Remarks

When talking about mathematical models, most readers normally associate this concept with a very complex notion. In this chapter, the GPS mathematical models are presented in very simple terms that will allow the reader to understand how errors are managed and positions finally extracted from the observations discussed in Sect. 3.3. In addition, it will be shown how errors can be eliminated or avoided through the design of a GNSS survey. The intended outcomes of this chapter are to assist the reader to:

(i) Know and understand the nature of code- and phase-pseudorange observation equations (derived from Sect. 3.3) and their uses.
(ii) Know how various GPS observational errors can be modelled through simple observation techniques.
(iii) Understand the basic concepts of static, kinematic, Differential GPS (DGPS), and relative positioning modes and their uses.

More detailed discussions can be found, e.g., in [1, pp. 107–116], [2, pp. 181–201], and [3, pp. 170–187, 250–261]. Here, the focus is on the observations, models, and the subsequent configurations that enable the solution of positions and other parameters required for environmental monitoring.

Before looking at the mathematical formulations that underpin the GPS observations, let us briefly examine how these satellites orbit in space (i.e., space segments discussed in Sect. 3.2.1). In general, the motions of planets in space obey the three Johannes Kepler's laws:



J. Awange, *GNSS Environmental Sensing*, Environmental Science and Engineering, DOI 10.1007/978-3-319-58418-8_4

(i) The orbital path of a planet takes the shape of an ellipse, with the sun located at one of its focal points.
(ii) The (imaginary) line connecting the sun to any of the planet sweeps equal areas of the orbital ellipse over equal time intervals.
(iii) The ratio of the square of the planets orbital period and the cube of the mean distance from the sun is constant.

These Keplerian laws apply not only to the planets, but also to artificial satellites (e.g., GNSS) orbiting the Earth. The orbital path takes the shape of an ellipse, with the Earth located at one of its focal points. Satellite orbits are characterized by their altitudes, i.e., Low Earth Orbiting (LEO) satellites (up to 2000 km), e.g., GRACE (Gravity Recovery And Climate Experiment) and COSMIC (Constellation Observing System for Meteorology, Ionosphere, and Climate), which together with GNSS satellites provide useful tools for environmental monitoring at continental scales as we shall see in part II of the book. Besides LEO satellites, we have Medium Earth Orbiting (MEO) satellites (5000–20,000 km) in which GNSS satellites fall, and Geostationary Earth Orbiting (GEO) satellites, orbiting at about 36,000 km, and which comprise communication satellites.

In a perfect situation, a satellite orbit should ideally follow the ideal *Keplerian laws* in which all forces except the Earth's gravitational force are neglected, the Earth's gravitational field is radially symmetric, and there exists no atmospheric drag. In reality, however, the *central* and *non-central* gravitational forces act on the satellites. In addition, other forces acting on the satellites include *gravitational attraction* of the Sun, Moon and planets; solar radiation pressure; and magnetic forces. All the other forces other than the central gravitational force are normally grouped under *perturbing forces*.

Modelling of GPS observations makes use of satellite positions broadcast through navigation messages (see e.g., Sect. 3.3.1). This is of particular importance in instantaneous positioning (i.e., in real-time positioning). Understanding how to model the orbital errors of GNSS satellites is therefore a good starting point towards achieving more accurate positions and other environmental monitoring parameters. For other applications that require post-processing of GNSS data, and which the results may not be immediately required, such as those of long term monitoring of environmental changes (e.g., sea level), *precise ephemeris* (see Sect. 3.4.1) should be used.

## 4.2 Observation Equations

For *code ranging*, let us consider that a signal is send by a satellite at time $t^s$ and received by a ground-based receiver at time $t_r$ (see e.g., Sect. 3.3.2). The time taken by the signal to travel from the satellite to the receiver would therefore be

$$\Delta t = t_r - t^s. \tag{4.1}$$

Due to clock errors (see e.g., Sect. 3.4.2) in the transmitting satellite (i.e., $\delta^s$) and the receiving receiver (i.e., $\delta_r$), Eq. (4.1) becomes

$$\Delta t = \{t_r + \delta_r\} - \{t^s + \delta^s\} = \Delta t + \Delta\delta, \tag{4.2}$$

which when multiplied by the speed of light $c$ (e.g., Eq. 3.1) gives the distance between the satellite and the receiver. Since *time difference* is used, the derived distance between the satellite and the receiver, i.e., code-pseudorange (e.g., Sect. 3.3.2) is obtained from (4.2) by

$$\boxed{R(t) = c\Delta t = c(\Delta t + \Delta\delta) = \varrho(t) + c\Delta\delta(t)}, \tag{4.3}$$

where $R(t)$ is the measured pseudorange, $\varrho(t)$ the geometric (true) unknown distance between the satellite and the receiver, and $c\Delta\delta(t)$ is the range bias.

For precise GPS measurements, *carrier-phase measurements* are often used to obtain ranges. Consider the phase $\varphi^s(t)$ (cycles) with a frequency $f^s$ (cycles per second) to have been sent by a satellite. At the receiver, a phase $\varphi_r(t)$ with a frequency $f_r$ is generated. Taking the start time of the signal as $t_0$, the time passed in the GPS system from when the signal was sent from the satellite to the receiver will be $t_{sr}$. The relationship between frequency and phase is such that the frequency is the derivative of phase, see e.g., [2, p. 72]

$$f = \frac{d\varphi}{dt}. \tag{4.4}$$

From (4.4), phase can be obtained by integrating the frequency from the initial time $t_0$ to $t$ as

$$\varphi = \int_{t_0}^{t} f\,dt, \tag{4.5}$$

which leads to

$$\varphi = f(t - t_0). \tag{4.6}$$

For the initial time $t_0 = 0$, (4.6) yields $\varphi(t_0) = 0$. When the satellite signal reaches the receiver, it is

- reconstructed with phase $\varphi^s = f^s(t - t_{sr})$, and
- compared with the receiver generated signal with phase $\varphi_r = f_r(t)$

Using Eq. (3.1) relating speed, distance and time, $t_{sr}$ is given as $\varrho/c$, which when substituted for $t_{sr}$ in $\varphi^s = f^s(t - t_{sr})$ leads to

$$\varphi^s = f^s(t - \frac{\varrho}{c}). \tag{4.7}$$

The reconstructed signal is then written as

$$\varphi^s(t) = f^s t - f^s \frac{\varrho}{c} - \varphi_{0s}, \tag{4.8}$$

while for the receiver generated signal, (4.7) becomes

$$\varphi_r(t) = f_r t - \varphi_{0r}. \tag{4.9}$$

In (4.8) and (4.9), $\varphi_{0s}$ and $\varphi_{0r}$ arise from the satellite and receiver clock errors. Considering the clock errors to be $\delta^s$ and $\delta_r$ for the satellite and receiver, respectively, from (4.2) and using $\varphi_{0s} = -f^s\delta^s$ and $\varphi_{0r} = -f_r\delta_r$, the phase measured at a time $t$ is given by

$$\varphi_r^s(t) = \varphi^s(t) - \varphi_r(t) = -f^s\frac{\varrho}{c} + f^s\delta^s - f_r\delta_r + (f^s - f_r)t. \tag{4.10}$$

Expressing the receiver-satellite clock bias term as $\Delta\delta = \delta_r - \delta^s$ and using the frequency-wavelength relation $f = c/\lambda$, assuming the satellite frequency $f^s$ and receiver frequency $f_r$ to be equal to the nominal frequency $f$, (4.10) is rewritten as

$$\Delta\varphi(t) = -\frac{\varrho}{\lambda}(t) - c\frac{\Delta\delta}{\lambda}(t), \tag{4.11}$$

where $\Delta\varphi$ is the measured phase expressed in terms of the measured pseudorange $\varrho$, wavelength $\lambda$, and the speed of light $c$.

Besides expressing the phase in terms of pseudorange as in (4.11), it can also be expressed in terms of the initial instantaneous fractional measurement immediately when the receiver is switched on at time $t_0$. At this stage, the receiver still does not know the integer number $N$ of cycles between it and the satellite, i.e., the integer ambiguity (cf. Eq. 3.2). If a satellite is tracked by the receiver without loosing lock, this integer number remains the same (see e.g., Fig. 4.1). The phase at time $t$ can therefore be expressed in-terms of the *measured value* at time $t$ plus the unknown *integer number of cycles* $N$ since the initial time $t_0$ as [2, p. 89]

$$\Delta\varphi(t) = \Delta\varphi_0(t) + N, \tag{4.12}$$

Comparing Eqs. (4.11) and (4.12), one obtains

$$\boxed{\lambda\Delta\varphi_m(t) = \varrho(t) + c\Delta\delta(t) + \lambda N}, \tag{4.13}$$

where $\Delta\varphi_m(t) = -\Delta\varphi_0(\mathrm{t})$ is the measurable phase at epoch $t$. Note that (4.13) is similar to (4.3), only that it has the ambiguity term $N$ added. Hence, the difference between code-pseudorange and phase-pseudorange in positioning with GPS satellites is that the former is only concerned with the position $X, Y, Z$ of a receiver while the later is concerned with determining the receiver's position plus the unknown

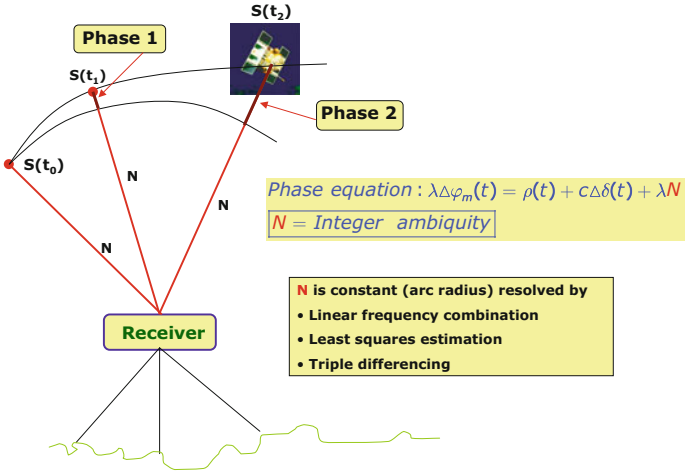


**Fig. 4.1** How does the integer ambiguity arises? When a receiver is switched on, the number of complete cycles, known as integer ambiguity $N$, is unknown. The receiver measures the phase, i.e., fraction of a cycle shown in the figure. As subsequent measurements are taken, it is possible to determine the $N$ whose value remains constant as shown in the figure

ambiguity term $N$. Note that the phase observation in (4.13) has been multiplied by the wavelength $\lambda$ to convert it into a distance measurement. In Sect. 6.2.2.2 on p. 99, the ambiguity solution is discussed in more detail.

## 4.3 Models

The word "*model*" has about 8 meanings,[1] ranging from a small object that is built to represent in detail another, often larger, object, to an animal whose appearance is copied by a mimic in Zoology. Model is a term that we often meet in daily life. For example, it is common for architects to work with models as a representation of the real world, or for people to display clothing as we see on the TV. It is also often common to hear people speak of role models, i.e., people they would like to emulate.

Mathematical models can also be seen as a representation of ideas using formulae as objects. An encyclopedic definition of a mathematical model is given as follows[2]:

> *A mathematical model is an abstract model that uses mathematical language to describe the behaviour of a system. Mathematical models are used particularly in the natural sciences and engineering disciplines (such as physics, biology, and electrical engineering) but also in the social sciences (such as economics, sociology and political science); physicists, engineers, computer scientists, and economists use mathematical models most extensively.*

[1] http://www.thefreedictionary.com/model.

[2] http://encyclopedia.thefreedictionary.com/Mathematical+model.

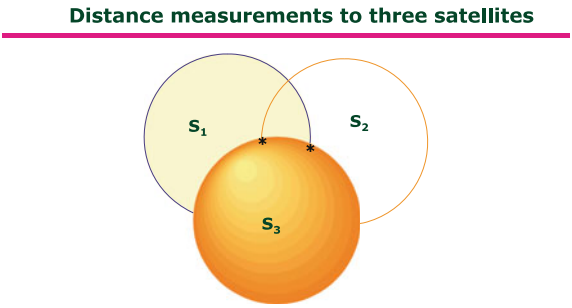


**Fig. 4.2** GPS positioning geometry. Normally two positions of the receiver's position indicated by the *star* (*) in the figure will be given, one of which will be on the Earth's surface while the other in space (outside the Earth's surface)

An abstract model (or conceptual model) in the definition above is a theoretical construction that represents physical, biological or social processes, with a set of variables and a set of logical and quantitative relationships between them. In what follows, mathematical models are used to relate the measured GPS pseudoranges to their geometrical equivalent, and to model the observational errors discussed in Sect. 3.4.

A simple way to conceptualize a mathematical model in GPS operations involves distance measurements from a ground-based receiver to GPS satellites. In this case, the distance, which is a measurable quantity is geometrically represented by an equation that relates it to the position of the ground receiver and those of the satellites. The geometrical (true) distance $S$ between the satellite and the receiver is represented by the model

$$S = \sqrt{(X^j - X_r)^2 + (Y^j - Y_r)^2 + (Z^j - Z_r)^2}, \tag{4.14}$$

where $\{X^j, Y^j, Z^j\}$ is the position of a satellite $j$ and $\{X_r, Y_r, Z_r\}$ is the receiver's position. Since the distance from the satellite to the receiver $S$ is measured, and the satellite's position $\{X^j, Y^j, Z^j\}$ is known from the transmitted ephemeris (e.g., Sect. 3.3.1), only the receiver's position $\{X_r, Y_r, Z_r\}$ needs to be determined from Eq. (4.14). Geometrically, to determine the three coordinates $\{X_r, Y_r, Z_r\}$ of the receiver's position, an intersection of three spherical cones, each representing a distance $S_i | i = 1, 2, 3$ is performed (see e.g., Fig. 4.2). Distance measurements to only one satellite puts the user's position anywhere within the sphere defined by distance $S_1$. Measurements to two satellites narrows the solution to the intersection of the two spheres $S_1$ and $S_2$. A third satellite is therefore required to definitely fix the user's position. This is achieved by the intersection of the third sphere $S_3$ with the other two (Fig. 4.2).

If direct distance measurements to the satellites were possible, Eq. (4.14) would suffice to provide the user's position. However, as already stated earlier, distance measurements to satellites are not *direct* owing to the satellites' and receivers' clock errors, errors in the satellites' positions, atmospheric delays, and receiver related errors such as phase centering and multipath discussed in Sect. 3.4. The distance Eq. (4.14), therefore, converts to the *pseudorange* equation

$$\boxed{\varrho_i^j = \sqrt{(X^j - X_r)^2 + (Y^j - Y_r)^2 + (Z^j - Z_r)^2}}, \tag{4.15}$$

where $\varrho_i^j$ has now replaced $S_i$ and contains the error uncertainties (cf. Eq. 6.7 on p. 109). Since the satellites' clock errors can be modeled while the receiver's clock errors must be determined as unknowns, the code pseudorange Eq. (4.3) then becomes

$$\boxed{R(t) + c\delta^j(t) = \varrho(t) + c\delta_i(t)}, \tag{4.16}$$

where at time $t$, $R(t)$ is the measured range, $\delta^j(t)$ and $\delta_i(t)$ are the satellite and receiver clock errors, $\varrho(t)$ the geometrical pseudorange from Eq. (4.15) and $c$ is the velocity of propagation (i.e., speed of light). In Eq. 4.16, the addition of $c\delta_i(t)$ as an unknown to the receiver's position $\{X_r, Y_r, Z_r\}$ leads to four unknowns to be determined. This means, therefore, that instead of three satellites required to determine the receiver's position (e.g., Fig. 4.2), four satellites are required (Fig. 4.4). The fourth satellite is used to determine the receiver clock bias $c\delta_i(t)$.

When four satellites are observed as required for positioning, four pseudorange equations are formed from (4.16) and (4.15) as

$$\begin{aligned} R_1 &= [(X^1 - X_r)^2 + (Y^1 - Y_r)^2 + (Z^1 - Z_r)^2]^{1/2} + c\delta \\ R_2 &= [(X^2 - X_r)^2 + (Y^2 - Y_r)^2 + (Z^2 - Z_r)^2]^{1/2} + c\delta \\ R_3 &= [(X^3 - X_r)^2 + (Y^3 - Y_r)^2 + (Z^3 - Z_r)^2]^{1/2} + c\delta \\ R_4 &= [(X^4 - X_r)^2 + (Y^4 - Y_r)^2 + (Z^4 - Z_r)^2]^{1/2} + c\delta \end{aligned}, \tag{4.17}$$

with the four unknowns being the receiver's 3D position $(X_r, Y_r, Z_r)$ and the receiver clock bias $c\delta$. With the observations of more satellites, Eq. (4.17) retains the four unknown with increased number of equations thereby necessitating the use of least squares solutions discussed in Sect. 6.3. Examples of algebraic methods for solving Eq. (4.17) are presented in Awange et al. [1, 4, 5]. It should be mention here that the accuracy of the obtained receiver's position from Eq. (4.17) depends upon the accuracies of *range measurements*, the accuracy of each satellite's position, the accuracy by which the atmospheric parameters are modeled, the accuracy upon which the receiver measures time (i.e., clock synchronization, signals processing, signal noise, etc.), the geometry of the satellite and the length of time taken to observe [6]. For practical use, the determined receiver's geocentric coordinates $(X_r, Y_r, Z_r)$ in the GPS's WGS-84 system can then be transformed to the user's local reference datum (see e.g., Sect. 5.6.1). This is often done automatically by the processing software.

For the *phase-pseudorange*, in addition to the receiver's position and receiver clock uncertainties, the integer ambiguity $N$ which corresponds to the unknown number of complete cycles the signal has travelled from the satellite to the receiver must be added as an unknown. Equation (4.13) is then modeled by

$$\boxed{\lambda\Delta\varphi_m(t) + c\delta^j(t) = \varrho(t) + c\delta_i(t) + \lambda N}. \tag{4.18}$$

Similarly to Eqs. (4.3) and (4.13), comparison between Eqs. (4.16) and (4.18) reveal similarities, with (4.18) having the additional term of $\lambda N$ on the right-hand side. The solution of the right-hand side of (4.16), when inserted into the right-hand side of (4.18), leads to the solution of $N$. For this reason, code-pseudorange finds use in the linear combination of code and phase approaches for solving the integer ambiguity unknown $N$ (e.g., Sect. 6.2.2.2).

The models (4.16) and (4.18) only become valid once other errors associated with the ionospheric effect $I$, tropospheric effect $T$ and multipath $m$ have been modeled.

### 4.3.1 Static and Kinematic Positioning

*Static positioning* is where a receiver is set up on top of a tripod or pillar at some point of interest and measurements are taken, see e.g., Fig. 4.3. The stationary receiver takes observations from a minimum of four satellites (e.g., Fig. 4.4) for example every 10 s (or as set by the user) for up to one hour or more to achieve a more precise position than is possible by a stand-alone instantaneous reading. During this period, it is hoped that the number of satellites either remains at the minimum of 4, or more, with an adequate PDOP (see Sect. 3.4.5). This would potentially lead to a better solution for the unknown ambiguity $N$, and better solutions of position $X_r$, $Y_r$, $Z_r$. It should be pointed out, however, that the occupation time being recommended by some receiver manufactures, e.g., Sokkia, is currently less than 30 min. This decrease in occupation time is attributed to improved receiver technology and modernization of the satellites as discussed in the preceding chapters.

Consider, for example, the code-pseudorange model (4.16). For a stationary receiver, 3 unknown receiver position $\{X_r, Y_r, Z_r\}$ and 1 unknown receiver clock bias have to be determined. For each observational epoch, we have an additional receiver clock bias as an unknown. If $n$ is the number of satellites that can be observed in static mode and $m$ the number of epochs, the following relation can be written [2, p. 185]

$$nm \geq 3 + m, \tag{4.19}$$

which gives

$$m \geq \frac{3}{n-1}. \tag{4.20}$$

Therefore, for static point positioning, for $n = 4$, $m \geq 1$, gives the minimum number of satellites and epoch needed to solve the three receiver coordinates and the receiver clock bias (see, e.g., Fig. 4.4). Exact solutions of these 4 equations to obtain point positions with GPS have been presented e.g., in [1, pp. 107–116], [7–10] and [11].

For *kinematic positioning*, the antenna is moving onboard a pole, boat or vehicle. In this mode of point positioning, there exist more unknown points since the receiver is in motion. The unknown coordinates now change from the static mode of 3 to $3m$, i.e., for each epoch of measurement while in motion. The addition of the receiver

**Fig. 4.3** A static receiver stationed on a tripod at point G2 of Curtin University (Bentley Campus), Australia

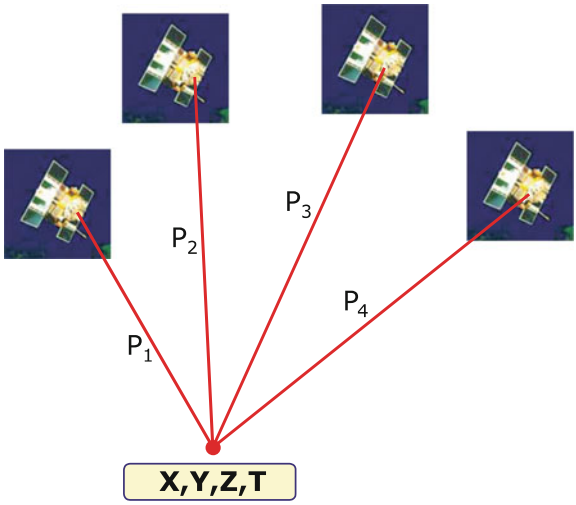


**Fig. 4.4** Absolute point positioning using GPS satellites (see, e.g., Fig. 4.3)

clock bias $m$ gives a total of $4m$ unknowns leading to

$$nm \geq 4m, \tag{4.21}$$

which leads to

$$n \geq 4. \tag{4.22}$$

The position of the receiver in motion can therefore be determined at any epoch $t$ as long as a minimum of 4 satellites are visible.

### *4.3.2 Differential GPS (DGPS)*

Absolute point in Sect. 4.3.1 (i.e., Fig. 4.4) is not suitable for applications requiring high accuracies such as the provision of controls for monitoring deformation, e.g., of dams. The reason for this is largely due to the errors discussed in Sect. 3.4. In order to minimize these errors and obtain higher accuracies, GPS can be used in relative or differential positioning mode [6]. The *differential positioning method*, also known as Differential GPS (DGPS) is one of the techniques most commonly used to model positioning errors in order to improve the accuracy of the final solutions. In this approach, code-pseudoranges are simultaneously measured by two receivers with one receiver occupying a *known reference station* (see Figs. 4.5 and 5.5). The reference station calculates the geometric pseudorange by making use of the satellite's position through $\rho_g^j = \|\mathbf{X}_r - \mathbf{X}^s\|$, where $\mathbf{X}_r$ are the coordinates of the reference station and $\mathbf{X}^s$ those of the satellite (from the received ephemeris). Since the positions of the satellite $\mathbf{X}^s = \{X^j(t), Y^j(t), Z^j(t)\}$ and that of the receiver $\mathbf{X}_r = \{X_A, Y_A, Z_A\}$ at a reference station are both known, the geometrical distance $\varrho_g^j$ is computed from (4.15) as

$$\varrho_g^j = \|\mathbf{X}_r - \mathbf{X}^s\| = \sqrt{(X^j(t) - X_A)^2 + (Y^j(t) - Y_A)^2 + (Z^j(t) - Z_A)^2}. \tag{4.23}$$

If $\varrho_{ma}^j$ is the measured pseudorange at the reference station A, then the pseudorange corrections (PRC) $\Delta\varrho_A$ for point A are given by

$$PRC = \Delta\varrho_A = \varrho_g^j - \varrho_{ma}^j, \tag{4.24}$$

where the correction term $PRC = \Delta\varrho_A$ comprises the range, satellite, and receiver bias terms corresponding to station A and the range rate correction. $PRC$ are due to errors discussed in Sect. 3.4, which are assumed to be similar at both stations (A and B) due to their close proximity. $PRCs$ are transmitted to the roving receiver at location B in real-time using communication link (e.g., radio, satellite, or cell phone

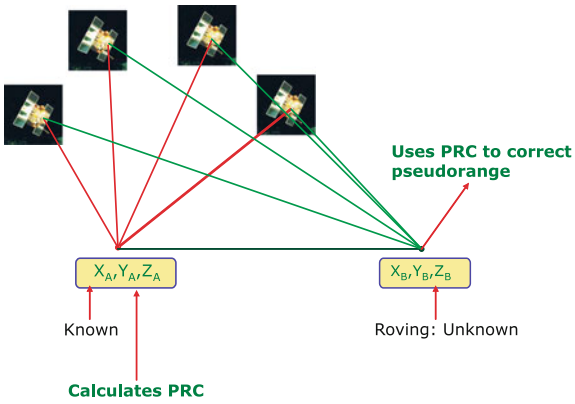


**Fig. 4.5** DGPS positioning. One receiver is placed at a known reference station (e.g., A) and the other at a location B whose position is desired. The measured pseudoranges at station A are compared to the actual values computed from the satellites' and receivers' positions using Eq. 4.23. The difference between the measured and the computed values give the pseudoranges corrections $PRC$, which are send from receiver A to receiver B via a communication link to correct the measured pseudoranges of station B, assuming that the stations are close enough such that the same errors affecting A also affect B. If the stations are close the atmospheric conditions are largely the same for both stations. DGPS positions are obtained in real-time at decimeter level accuracy

links) to correct its measured pseudoranges, which are then used to derive its position. For example, the measured pseudorange $\varrho^j_{mb}$ at station B would be corrected by

$$\varrho^j_{Bcorr} = \varrho^j_{mb} + \Delta\varrho_A. \tag{4.25}$$

As an example (see, e.g., [6]), consider that the computed range, i.e., the distance between the satellite antenna and the receiver antenna $\varrho^j_g$ for station A is 20,000,000 m and the measured code-pseudorange $\varrho^j_{ma}$ is 19,999,990. Then, $\Delta\varrho_A = 20,000,000 - 19,999,990$ gives 10 as the pseudorange correction, which is transmitted to correct the pseudorange measured by the satellite at B using (4.25) as $\varrho^j_{Bcorr} = \varrho^j_{mb} + 10$. Pseudorange measurements to each satellite at location B is corrected in the same manner and the resulting corrected pseudoranges used to determine the position of B using Eq. (4.17). The coordinates of B will be relative to those of A, hence they belong to the same datum. If more than one reference station is used to obtain the pseudorange corrections, then the corrections may further be refined using the network of reference stations. A network of stations transmitting differential GPS corrections are termed "*augmented GPS*", which are discussed in Sect. 5.4.4.2.

Improvements to the positioning accuracy depend on the accuracy of the known station's location, the accuracy of the satellite positions, and the mode of operation (i.e., whether code or phase). For phase pseudorange, (4.25) becomes

$$\lambda\varphi^j_{Bcorr} = \varrho^j_{MB} + \Delta\varrho_A + \lambda N^j_{AB}. \tag{4.26}$$

Several countries have service providers who operate DGPS. The user only needs to have one receiver and use nearby DGPS station to obtain the corrections at some cost. In Australia, for example, DGPS services are provided by the Australian Maritime Safety Authority (AMSA), as well as private companies, e.g., FUGRO. DGPS with carrier-phase ranges is applicable for real-time kinematic operations where the ambiguity is resolved using a technique known as On-The-Fly (OTF) as discussed in Sect. 5.4.6.

### 4.3.3 Relative Positioning

In the DGPS technique discussed above, pseudorange corrections and range-rate changes computed from a known station are transmitted via communication link and used to correct those of the unknown station. In relative positioning, instead, the baseline vector is computed and added to the coordinates of the reference station to obtain those of the unknown station (see, e.g., Fig. 4.6). Also, in contrast to DGPS, which is performed in real-time, relative positioning requires post-processing of data, where simultaneous *carrier-phase observations* from both reference and rover stations are processed.

If one considers the positions of the known reference station A (Fig. 4.6) as

$$\mathbf{X}_A = \begin{bmatrix} X \\ Y \\ Z \end{bmatrix}, \tag{4.27}$$

and the computed baseline vector as

$$\Delta\mathbf{X}_{AB} = \begin{bmatrix} \Delta X \\ \Delta Y \\ \Delta Z \end{bmatrix}, \tag{4.28}$$

then the position $\mathbf{X}_B$ of the rover station B is given by

$$\mathbf{X}_B = \mathbf{X}_A + \Delta\mathbf{X}_{AB}. \tag{4.29}$$

Relative positioning can be performed through *single-*, *double-*, and *triple* differencing in both static and kinematic modes (see Sect. 4.3.1).

1. In *single differencing*, ***two ground receivers*** occupying the reference station A and a rover station B simultaneously observe ***one satellite*** $j$ (see, e.g., Fig. 4.7). Using Eq. (4.18), the two phase range equations are differenced (subtracting one from the other) as

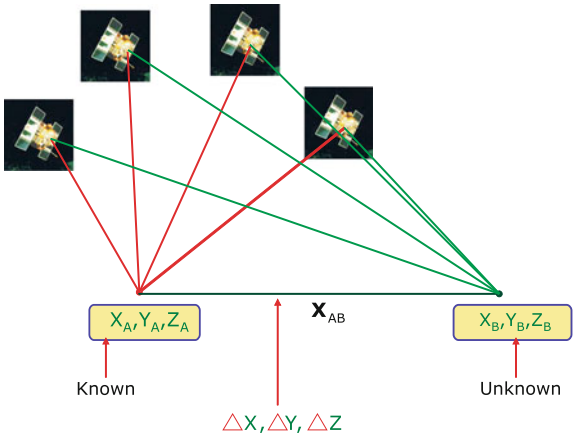


**Fig. 4.6** Relative positioning. One receiver is placed at a reference station A whose position is known and the other at a rover location B whose position is sought. Baseline vectors are computed during post-processing of the data and added to the coordinates of A to obtain those of B. No radio link is required as in the case of DGPS (Fig. 4.5), and post-processing of the data is necessary hence positions are not obtained in real-time

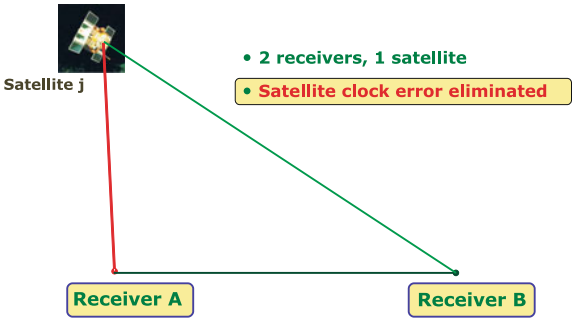


**Fig. 4.7** Single differencing. Two receivers A and B simultaneously observing the same satellite j. This technique eliminates the satellite clock errors (e.g., Eq. 4.30)

$$\begin{array}{c} \lambda\Delta\varphi_A^j(t) + c\delta^j(t) = \varrho_A^j(t) + c\delta_A(t) + \lambda N_A^j \\ \lambda\Delta\varphi_B^j(t) + c\delta^j(t) = \varrho_B^j(t) + c\delta_B(t) + \lambda N_B^j \\ \hline \lambda\left[\Delta\varphi_B^j - \Delta\varphi_A^j\right](t) = \left[\varrho_B^j - \varrho_A^j\right](t) + c\left[\delta_B - \delta_A\right](t) + \lambda\left[N_B^j - N_A^j\right] \end{array}, \tag{4.30}$$

which simplifies to

$$\lambda\Delta\varphi_{AB}^j(t) = \varrho_{AB}^j(t) + c\delta_{AB}(t) + \lambda N_{AB}^j. \tag{4.31}$$

The significance of the results from Eq. (4.31) is that the *satellite clock bias* term $c\delta^j(t)$ is eliminated.

2. *Double differencing* refers to the case where, again, ***two ground receivers*** occupy the reference station A and rover station B, but now simultaneously observe ***two satellites, j and k*** (see, e.g., Fig. 4.8). In this case, (4.31) is written for the second satellite $k$ as

$$\lambda\Delta\varphi_{AB}^k(t) = \varrho_{AB}^k(t) + c\delta_{AB}(t) + \lambda N_{AB}^k. \tag{4.32}$$

Differencing (4.31) and (4.32) leads to

$$\begin{array}{c} \lambda\Delta\varphi^{j}_{AB}(t) = \varrho^{j}_{AB}(t) + c\delta_{AB}(t) + \lambda N^{j}_{AB} \\ \lambda\Delta\varphi^{k}_{AB}(t) = \varrho^{k}_{AB}(t) + c\delta_{AB}(t) + \lambda N^{k}_{AB} \\ \hline \lambda\left[\Delta\varphi^{k}_{AB} - \Delta\varphi^{j}_{AB}\right](t) = \left[\varrho^{k}_{AB} - \varrho^{j}_{AB}\right](t) + \lambda\left[N^{k}_{AB} - N^{k}_{AB}\right] \end{array}, \tag{4.33}$$

which simplifies to

$$\lambda\Delta\varphi^{jk}_{AB}(t) = \varrho^{jk}_{AB}(t) + \lambda N^{jk}_{AB}. \tag{4.34}$$

Equation (4.34), known as the *double differencing equation*, is the most commonly used equation in processing GPS data. The importance of this equation is that both the satellite and receiver clock errors are eliminated.

3. Finally, double differencing can be done at two epochs, $t_1$ and $t_2$, to give a *triple difference* (see, e.g., Fig. 4.9). In this case, Eq. (4.34) will be written for both epochs and differenced to give

$$\begin{array}{c} \lambda\Delta\varphi^{jk}_{AB}(t_1) = \varrho^{jk}_{AB}(t_1) + \lambda N^{jk}_{AB} \\ \lambda\Delta\varphi^{jk}_{AB}(t_2) = \varrho^{jk}_{AB}(t_2) + \lambda N^{jk}_{AB} \\ \hline \lambda\left[\Delta\varphi^{jk}_{AB}(t_2) - \Delta\varphi^{jk}_{AB}(t_1)\right] = \varrho^{jk}_{AB}(t_2) - \varrho^{jk}_{AB}(t_1) \end{array}, \tag{4.35}$$

which simplifies to

$$\lambda\Delta\varphi^{jk}_{AB}(t_{12}) = \varrho^{jk}_{AB}(t_{12}), \tag{4.36}$$

where the *unknown ambiguity* term $\lambda N^{jk}_{AB}$ corresponding to ambiguities $\lambda N_A$ and $\lambda N_B$ for satellites $j$ and $k$ have been eliminated. Triple differencing is relevant to GPS positioning in that clock errors and the unknown integer ambiguity term $N$ have been eliminated. Triple differencing is useful as an alternative approach for solving the unknown integer ambiguity term $N$ and is often used to obtain the initial solutions of station coordinates in what is known as a *float solution*. These initial solutions are then used in the double differencing models to obtain a rigorous solution in what is termed the *fixed solution*. Section 6.2.3.1 presents detailed discussion on float and fixed solutions.

## 4.4 Concluding Remarks

In summary, this chapter has introduced the codes and phase GPS observation equations and has highlighted the similarities and differences between these equations. The differences occur in terms of the measured quantities (i.e., time and phase) and

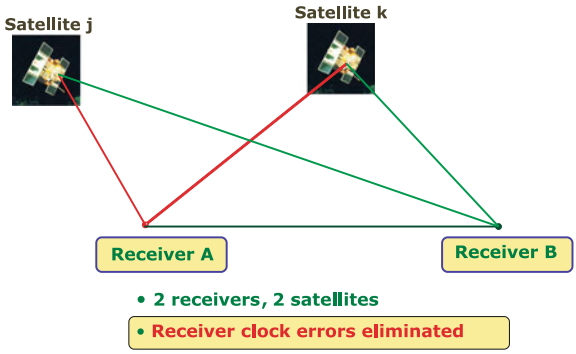


**Fig. 4.8** Double differencing. Two receivers, A and B, simultaneously observe the same satellites j and k. This is the most commonly used Eq. (4.34) to process GPS data during post-processing

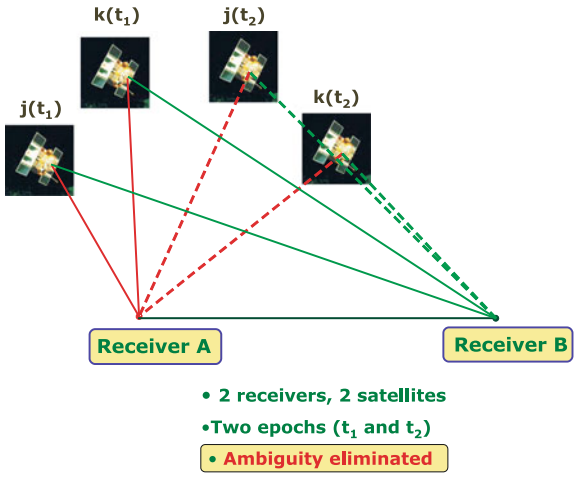


**Fig. 4.9** Triple differencing. Two receivers, A and B, simultaneously observe the same satellites, j and k, at times $t_1$ and $t_2$. The advantage of this differenced solution is the capability of eliminating the unknown ambiguity term $N$ leading to float solutions needed to obtain more accurate fixed solutions (see e.g., Sect. 6.2.3.1)

the addition of the unknown integer ambiguity term $N$ on the phase equation. In general, the configurations confirm the well-known practise of using more than four satellites for positioning in both static and kinematic modes. Positioning accuracies can be improved by using DGPS or relative positioning techniques, which model errors associated with the atmosphere and clock errors. In particular, *single*, *double* and *triple differencing* eliminates satellite, receiver and ambiguity error terms, respectively.

It should be emphasized that the accuracies of phase observations are in the cm-mm level range, while those of code are in meters. Code-pseudorange observations are, however, relevant since they do not suffer from the unknown integer ambiguity and can thus be used to offer quick (or even instantaneous) environmental solutions that do not require higher accuracy, e.g., locating a waste damping site. They could also be used (similarly to triple differencing solutions) to provide the initial solutions required in the double differencing to resolve the integer ambiguity $N$ in order to

obtain fixed solutions. This could be of benefit in environmental monitoring tasks that require accurate observations. In the next chapter, we will provide a more in-depth discussion of the field procedures of the techniques discussed in this chapter.

## References

1. Awange JL, Grafarend EW (2005) Solving algebraic computational problems in geodesy and geoinformatics. Springer, Berlin
2. Hofman-Wellenhof B, Lichtenegger H, Collins J (2001) Global positioning system: theory and practice, 5th edn. Springer, Wien
3. Leick A (2004) GPS satellite surveying, 3rd edn. Wiley, New York
4. Awange JL, Grafarend EW, Paláncz B, Zaletnyik P (2010) Algebraic geodesy and geoinformatics, 2nd edn. Springer, Berlin
5. Awange JL, Palancz Bela (2016) Geospatial algebraic computations: theory and application. Springer, Berlin
6. US Army Corps of Engineers (2007) NAVSTAR global positioning system surveying. Engineering and design manual, EM 1110-1-1003
7. Awange JL, Ong'ang'a O (2006) Lake Victoria-ecology, resources, environment. Springer, Berlin
8. Bancroft S (1985) An algebraic solution of the GPS equations. IEEE Trans Aerosp Electron Syst 21:56–59
9. Kleusberg A (1994) Die direkte Lösung des räumlichen Hyperbelschnitts. Zeitschrift für Vermessungswesen 119:188–192
10. Lichtenegger H (1995) Eine direkte Lösung des räumlichen Bogenschnitts. Österreichische Zeitschrift für Vermessung und Geoinformation 83:224–226
11. Singer P, Ströbel D, Hördt R, Bahndorf J, Linkwitz K (1993) Direkte Lösung des räümlichen Bogenschnitts. Zeitschrift für Vermessungswesen 118:20–24

# Chapter 5
# Environmental Surveying and Surveillance

*Any measurement must take into account the position of the observer. There is no such thing as measurement absolute, there is only measurement relative.*

Jeanette Winterson

In that case, *Measure what is measurable, and make measurable what is not so.*

Galileo Galilei

## 5.1 Environmental Monitoring Parameters

In this section, we discuss the *quantitative* and *qualitative data* that could be collected using GNSS satellites, and in so doing, attempt to answer the question "what can GNSS satellites deliver that are of use to environmental monitoring?" The observed parameters necessary for environmental monitoring vary, depending upon the indicators being assessed. Some are *physical variables* such as changes in soil patterns, vegetation, rainfall, water levels, temperature, deforestation, solar and UV radiation. Others are *chemical variables*, e.g., pH, salinity, nutrients, metals, pesticides, while others are *biological variables*, e.g., species types, ecosystem health, and indicator species.

GNSS satellites are useful in measuring physical variables such as atmospheric temperature, pressure, and tropopause heights needed for weather and climate change monitoring, as we will see in Chap. 11. The emergence of GNSS-reflectometry (GNSS-R) discussed in Chap. 10 provide GNSS satellites with the opportunity to measure the physical changes of the reflecting surfaces, e.g., soil moisture and vegetation. For chemical and biological variables, the main environmental monitoring parameter provided by GNSS satellites are the *positions* of the respective variables (i.e., sampled locations). Positions are useful not only in providing physical locations, but also in measuring spatial variation in the variables being monitored. For example, monitoring coastal erosion can be undertaken by the constant monitoring of



J. Awange, *GNSS Environmental Sensing*, Environmental Science and Engineering, DOI 10.1007/978-3-319-58418-8_5

shoreline's positions at various times using GNSS satellites. In other environmental monitoring examples, satellite derived positions could complement other systems to enhance monitoring. For example, GNSS satellites complement low-flying satellites such as the Gravity Recovery And Climate Experiment (GRACE) to allow more detailed and accurate monitoring of mass redistribution on the Earth's surface. Such mass distribution include, e.g., changes in surface and groundwater at local, regional and global scales, as will be discussed in Chap. 9. For dynamic environmental phenomena, such as variations in deforestation, GNSS satellites could provide efficient tools for measuring such changes by providing time series of their variations in position and also the biomass changes through GNSS-R techniques discussed in Chap. 10.

## 5.2 Design of GNSS Monitoring Survey

In order to achieve maximum benefit from the use of GNSS satellites for environmental monitoring, it is essential that proper measurement procedures be undertaken with clear aims and objectives. As in all measurements, the quality of the observations will be determined by the purpose and objectives and, to a greater extend, the client's requirements. These objectives and needs will dictate the methods chosen for *data collection*, the *frequency of data collection*, and *temporal* and *spatial* extent. A monitoring design should therefore specify the monitoring variables desired from GNSS satellites, where, when and by whom the data shall be collected. Like other environmental monitoring techniques, GNSS satellite monitoring also requires some *baseline survey* or information upon which any change in the environment could be referred to. In the case of positions, permanent reference stations whose positions are accurately known normally provide such baseline data. Any spatial change (i.e., change in the environmental variable being monitored with respect to its position at a given time) will then be referred to these points. Measurements can be repeatedly taken at given time intervals (temporal resolution) depending on the monitoring budget and the desired accuracy.

The final accuracy of the collected data will depend on how the errors are handled. For GNSS satellite monitoring, these errors (discussed in Sect. 3.4) could be external (i.e., outside the user's control) or internal (i.e., during the actual measurements). In this chapter, GNSS measurement procedures that may help minimize errors and achieve meaningful results relevant for environmental monitoring are presented. GNSS surveys can be divided into three components:

- *Planning and reconnaissance*: This is an essential part of any monitoring campaign. For a GNSS survey, it is essential to plan the measuring campaign in such a manner that the errors discussed in Sect. 3.4 are minimized. For example, it is important that the sky visibility and satellite paths are plotted in a skyplot for the survey area and the desired survey period. The advantage of having sky plots is that the number of satellite visible during the planned observation period and features

blocking the satellite are determined in advance. The main objective is to ensure unobstructed view of at least four satellites with a good geometric distribution in the sky. As already indicated in Sect. 3.4.5 (p. 40), satellite geometry is indicated by the dilution of precision (DOP) factor. Reconnaissance provides the opportunity of visiting the survey site prior to the actual GNSS survey and assessing the availability and accessibility to the existing reference stations, while at the same time looking out for potential sources of errors such as buildings and trees that can cause multipath. The advantage of undertaking reconnaissance and planning prior to a satellite survey is that it can significantly reduce some logistical problems such as setting up a receiver in an area where the signals would be blocked.

- *Undertaking the monitoring survey*: Once the aims and objectives of the environmental monitoring project have been identified and the reconnaissance done, the survey task can be executed through proper *choice of GNSS positioning method*, *undertaking care in the actual survey procedures*, and *avoiding or minimizing errors where possible* (e.g., setting the receiver in an open space that is not very close to buildings to reduce the likelihood of multipath errors).
- *Processing of the data*: In order to obtain the monitoring parameters or baseline information from the GNSS observations, data can be processed in real-time or post-processed. Chapter 6 treats this topic in more detail.

## 5.3 Mission Planning and Reconnaissance

In Sect. 3.3.1, satellite signals were introduced as the measurable quantities that are needed to generate monitoring information. GNSS signals are microwaves that penetrate cloud cover and travel under all weather conditions, but unfortunately cannot penetrate dense *vegetation* canopies or buildings. Because of this, and in order to reduce the detrimental effects of atmospheric refraction and multipath signals, it is desirable that the antenna has as clear view of the sky as possible. An elevation angle of above 15° is often considered suitable to enable a clear sky view, although this could at times be as low as 10°. Some antennas are equipped with a groundplane that blocks unwanted multipath signals from reaching the antenna. Nearby metallic objects, such as fences and power lines, should be avoided where possible in order to prevent imaging, i.e., when metallic objects act as secondary antennas, thereby distorting the positions derived from GNSS satellites. It is therefore recommended that the GNSS observation sites be selected in open areas away from potential sources of multipath and imaging where possible.

As already pointed out in Sect. 3.4.5, the geometrical strength of the satellite constellations will contribute to the quality (accuracy) of the positions obtained. A weaker geometry from satellites close together in the sky as illustrated in Fig. 5.1 (right) will contribute to geometrically weaker solutions while those computed from evenly distributed satellites in the sky (e.g., Fig. 5.1, left) will lead to geometrically stronger solutions. Both geometric dilution of precision (GDOP) and position dilution of precision (PDOP) are useful in measuring the geometrical strength of a satellite

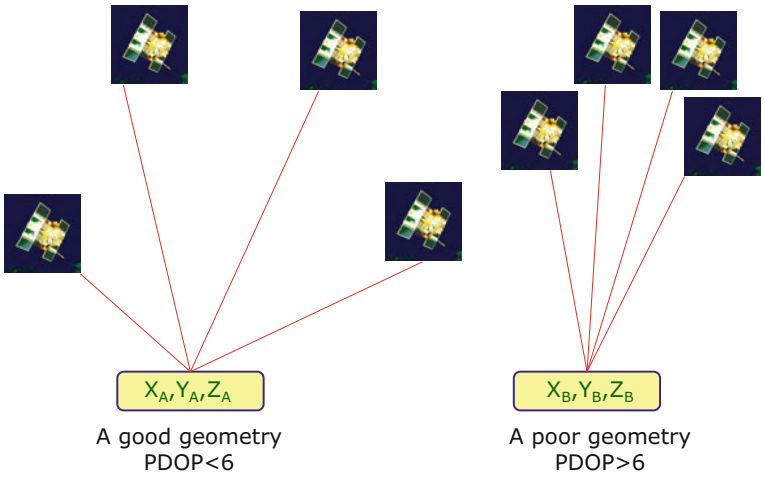


**Fig. 5.1** Satellite geometry: *Left* (good geometry); *Right* (poor geometry)

constellation, but PDOP is the most commonly used. PDOP is computed from the positions of the satellites in relation to the receiver and takes a single value, see e.g., [1, pp. 262–266]. It is a measure based solely on the geometry of the satellites and therefore can be computed prior to any observation being taken. A higher PDOP value (i.e., >6) indicates a poor satellite geometry for computing a position. In mission planning therefore, PDOP values are computed and used to indicate the observation window where the satellite constellation is adequate.

Satellite geometry becomes more crucial when one is observing over short occupation times, as is often the case in real-time kinematic (RTK) surveys discussed in Sect. 5.4.6. Whereas satellite geometry can be improved by longer observation period, poor sky visibility combined with a low number of satellites above the horizon can severely compromise static solutions. This essentially means that before a successful GNSS environmental monitoring campaign is undertaken, it is essential to know when bad situations are likely to occur so that they can either be avoided or the survey team prepares itself for a significantly longer period of observation. This knowledge can only be made possible through careful reconnaissance and well executed *mission planning*. Mission planning is thus a very vital component of any GNSS environmental monitoring campaign.

If the only possible observation window gives a PDOP between 6 and 10, it is recommended that the observation time frame be between 30 and 45 min. For PDOPs greater than 10, it might be necessary to postpone the observations. If, for whatever reason, postponing is not feasible, then the observation period should be made as long as possible, assuming of course that the effects of other errors such as multipath are minimal. If this is not possible, then it may not be possible to achieve an accurate position for this point using satellite positioning as one may wish, regardless of the length of the observation time.

Finally, a word of caution is necessary. PDOP values only indicate when satellites are likely to produce good or bad results and should therefore not be considered as a measure of the actual quality of the positions. Chapter 6 will discuss the quality estimation during the post-processing of the satellite data.

The basic stages for planning a GNSS survey are generally as follows:

1. Locate points of interest (i.e., those to be positioned) and update reference marks information if necessary.
2. Assess the suitability of these points for GNSS positioning and check for multipath sources in the vicinity.
3. If necessary, construct a visibility diagram using a compass and a clinometer (see, e.g., Fig. 5.2). The compass will provide an approximate position from the true North, while the clinometer will give the elevation of features such as buildings and vegetation. This will indicate the satellites likely to be blocked by tall buildings and trees. Such a diagram should also contain information on potential multipath sources.
4. Locate local reference stations. This will provide baseline positioning information.
5. Assess the suitability of these reference stations for satellite surveying and check for multipath sources in the vicinity.

Example 5.1 (Mission planning).

In order to decide on the appropriate time to carry out GNSS observations, any mission planning software such as those of Sokkia or Trimble could be used. Most receivers will come with software, which are capable of conducting mission planning that can be used to indicate the position of the satellites during the desired observation time. The software provides DOPs, which are useful in indicating the geometrical strength of the satellite constellation as already discussed. The following example illustrates how mission planning can be undertaken using any available commercial software. In general, the operational steps of most mission planning software are similar and will tend to give similar results. Using any planning software, one would generally proceed as follows:

- *Step 1 (Running the software)*: Within the appropriate user window of the software, start by inserting the *dates* over which you wish to undertake the GNSS survey and the *approximate coordinates* of the point for which the receiver will be stationed during the selected day. Approximate coordinates of this station can be entered in terms of latitude and longitude since the satellite constellation varies slowly with distance. One may enter the latitudes and longitudes of the local area, for example, by selecting the city from an option list which is often provided.
- *Step 2 (Setting the time zone)*: It is convenient when planning the survey to work in local standard time, thus, ensure the time zone is correct.
- *Step 3 (Loading the almanac)*: The almanac contains information about the satellites' positions in their orbits and are normally send as part of the navigation message (see Sect. 3.3.1). For mission planning, one can use ephemerides to predict satellite orbits over a period of about a month. Note that the more recent

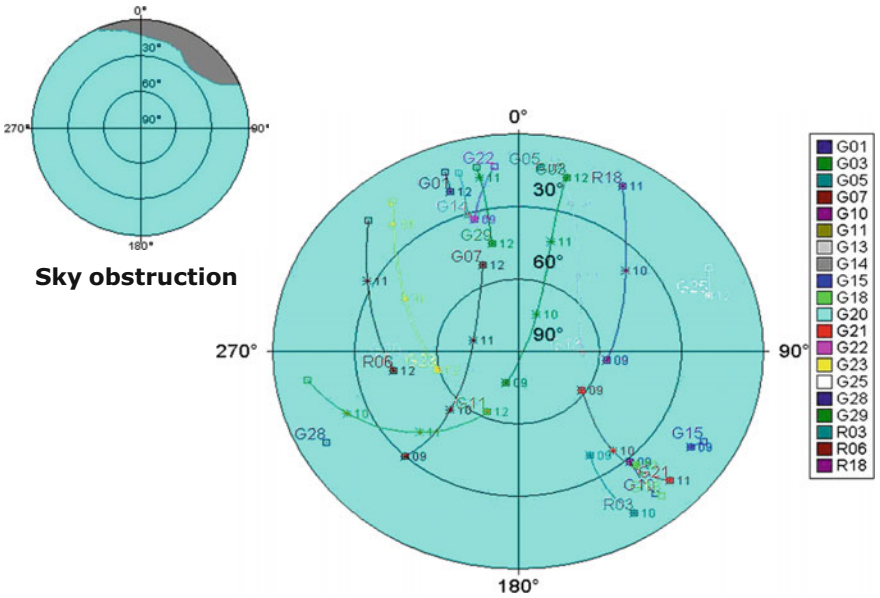


**Fig. 5.2** Satellite visibility diagram of Astro deck 8 located at one of the buildings of Curtin University (Bentley Campus, Australia) on the 16th of May 2008. *Left* Obstructed sky is noted at elevation 28° and azimuth between 0° and 60°. *Right* Satellite travel paths. The colours indicate the individual satellites. From these figures, one notices that satellite number R18 would be obstructed

the ephemeris are, the more precise are the planning mission results. Most GNSS receivers automatically acquire almanac data during regular operations. One way of accessing the current almanac data is to carry out quick observations (e.g., about 15 min) without necessarily setting up the antenna to survey specifications. The almanac can also be obtained on the internet.[1]

- *Step 4 (Planning graphs)*: Within the mission planning software, graphs giving various types of information for the day specified can be viewed. These graphs will indicate *satellite elevations plotted against time*, *satellite azimuths plotted against time*, *number of available satellites plotted against time*, representation of the *visibility time spans* of individual satellites, separate displays plotting the respective types of *dilution of precision (DOP) against time*, and *satellite tracks* through the time interval being plotted, showing elevations and azimuths in polar coordinates. Figure 5.3 presents an example of visibility time spans of individual satellites for station Astro deck 8 at Curtin University, Bentley Campus, Australia. A plot of the number of visible satellites and the related DOP is given in Fig. 5.4. Together with the skyplot in Fig. 5.2, these four diagrams can be used to obtain an indication of the state of the satellite constellation during the period planned for the GNSS environmental monitoring survey.

[1] E.g., typing YUMA+GPS leads to http://celestrak.com/GPS/almanac/Yuma/.

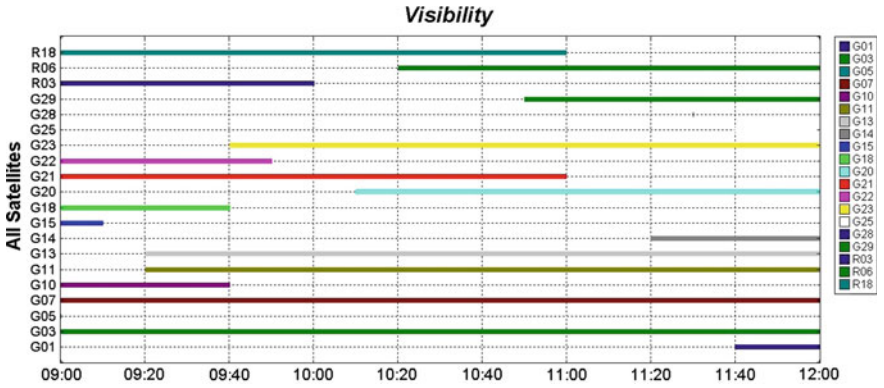


**Fig. 5.3** Time spans of the visibility of individual satellites at Astro deck 8 of Curtin University, Bentley Campus, Australia

For instance, looking at the skyplot Fig. 5.2 (left), one notices that the sky is blocked at an elevation of 28° and an azimuth between 0° and 60°. The corresponding plot of satellite visibility (right) shows that this obstruction would most likely affect satellite R18. At this stage, the planning software assumes a perfect satellite coverage, i.e., that no satellite is unhealthy and no obstructions exist above a given cutoff elevation angle (usually 15°). In reality, obstructions will exist at some sites and some satellites may be known to be malfunctioning. Therefore, the planning software must be modified to give a more realistic situation. For example, if a satellite is known to have problems, the software would allow it to be excluded from the planning.

Figure 5.3 shows the visible satellite for a whole day while Fig. 5.4 present the corresponding DOP values. The greater the number of visible satellites and the better the geometry, the lower the DOP values. In this example, done for the 16th May 2008, it can be seen that the time between 11:00 and 11:20 had the least number of satellites and the corresponding DOP values were higher. The maximum DOP value in this example was 4, which meant that the satellite observations could be undertaken at anytime before 12:00. The period after 9:40 had more than 10 satellites in view and as can be seen, the corresponding values of DOP were lower. It should be pointed out, however, that in this example, both GPS and GLONASS satellites were used, hence the larger number of satellites and lower DOP.

♣ End of Example 5.1.

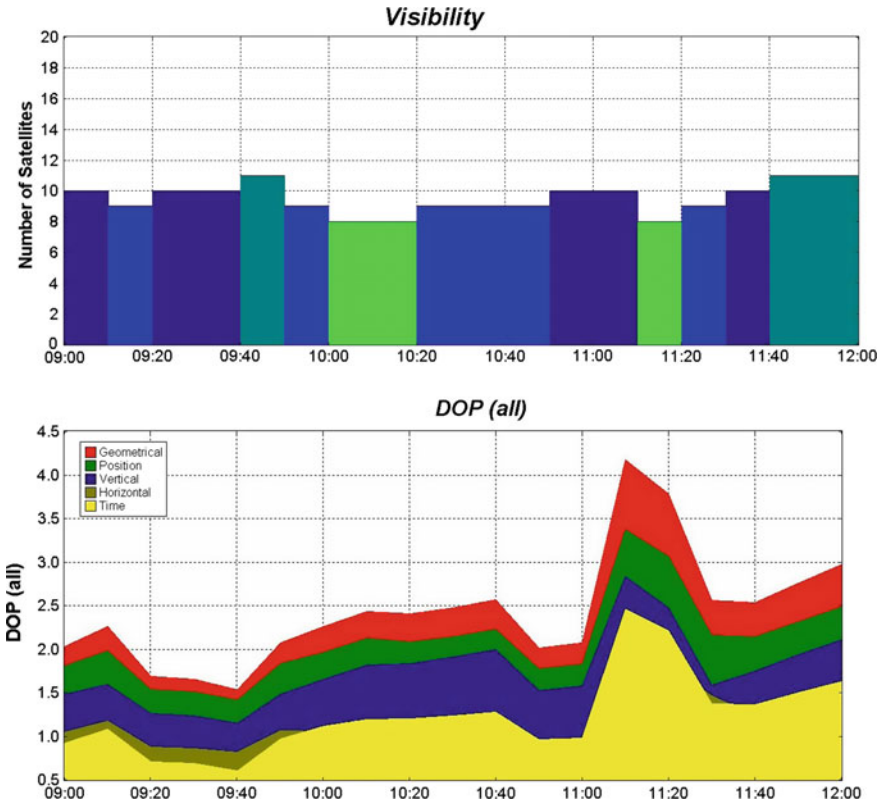


**Fig. 5.4** Number of visible satellites (*top*) and the related DOP (*bottom*)

## 5.4 GNSS Field Procedures

Having done the planning, the next step involves the actual procedure for the field measurements. The objective of a given monitoring environmental task will dictate the types of equipment required. If the objectives call for more precise and accurate work, e.g., monitoring rise in sea level (Sect. 17.2), then the correct receivers and field procedure must be adopted. One of the tasks undertaken during a GNSS survey is the setting up of the antenna over some mark. These marks consist of pillars upon which the GNSS receiver is set (e.g., Fig. 5.5) or some marks on the ground, in which case a tripod has to be used (e.g., Fig. 5.6). In older GNSS equipment, the receivers and antennas were separate components but modern equipment such as Sokkia or Trimble incorporate both receivers and antennas in one unit.

Setting up the antenna over a mark should be done as accurately as possible in order to reduce centering errors. The receiver must be *levelled*, *aligned over each point*, and the *height of its geometrical center above the point recorded*. Antenna heights are normally measured to the phase center. Sometimes, this phase center does not

**Fig. 5.5** Reference station, pillar 18 at Curtin University, Bentley Campus, Australia

coincide with the geometrical center of the antenna leading to antenna phase center variation (see Sect. 3.4.6). In high precision satellite measurements, this phase center variation can lead to errors in the range of millimeters to a centimeter. Most precise (geodetic) receivers posses antenna phase center models, which can reduce this effect during the post-processing of the measurements. In relative positioning (Sect. 5.4.2), the error due to phase center variation can be eliminated through the matching of the antennas by aligning both to North.

The most common source of error during the setting up of the antenna is the incorrect measurement of the antenna height. Since GNSS provides three-dimensional positions (recall Sect. 3.3), any error in height determination will propagate to contaminate the lateral position, and vice versa. As a standard practise, comprehensive field notes should be kept, which should include the *station and surveyor's name*, *start and end times of the survey*, *type of receivers and antennae used*, *data file names*, *satellites used*, *details of reference marks*, *potential sources of errors and obstructions* and *most importantly, the antenna height*.

### *5.4.1 Single Point Positioning*

In Sect. 4.3.1 we introduced the concept of *static surveying*. Here, it is demonstrate how the field survey is performed. Depending on the environmental monitoring task at hand, the single point positioning operation can take the form of *absolute point positioning*, also called autonomous positioning in some books, *relative positioning* or *differential positioning*. For absolute point positioning, pseudoranges have to be

**Fig. 5.6** Setting up a GNSS antenna and measuring its height at Station John Walker (JW) at Curtin University, Bentley Campus, Australia

measured to the satellites whose positions are known. The accuracy of the positioned point will therefore rely on how well the pseudoranges are measured and how good the satellite positions are known. It should be pointed out that repeated measurements leading to redundant observations will generally improve range accuracy [2].

If the task just requires a simple location of a station, e.g., the location of a *soil analysis pit*, with an accuracy of several meters, then a low-cost, hand-held GNSS receiver such as that in Fig. 18.1 on p. 389 will suffice. These kinds of receivers use *code-pseudoranges* and are the ones commonly used for personal navigation in cars, boats, low-accuracy GIS data capture, etc. Hand-held receivers provide absolute positioning to a horizontal accuracy of about 5–15 m (95% of the time). Decimeter accuracy can be achieved by stationing a receiver over a station of interest and taking observations for 30–45 min. Modernized GNSS satellites discussed in Chap. 2 are already improving the positioning accuracy by an order of magnitude (see Fig. 5.7). This improvement comes as a result of improved satellite orbit determination, improved receiver technology, additional user signals L2C and L5 that are assisting in modelling ionospheric errors, and additional ground monitoring stations.

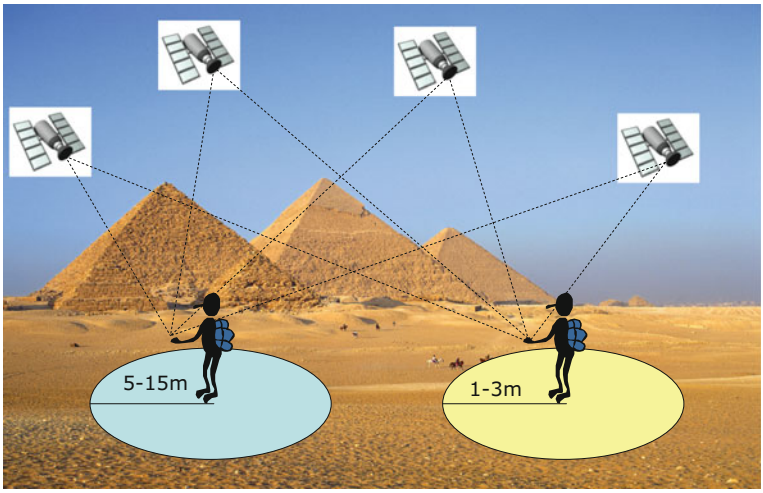


**Fig. 5.7** Improved point positioning accuracy following modernization of GNSS satellites and receiver technology

### *5.4.2 Static Relative Positioning*

Where a reference station (i.e., of known position) exist (e.g., Fig. 5.5), the static *relative positioning* (see Sect. 4.3.3) method is recommended for higher positioning accuracy. In this mode of operation, *two GNSS receivers* or more are required in order to observe the same satellites simultaneously. Although additional cost is incurred in providing more equipment, the advantage over absolute (autonomous) point positioning is the capability of eliminating or minimizing errors associated with the atmosphere and satellite orbits (see Sect. 3.4) through differencing techniques (see Sect. 4.3.3).

The method is more effective over short baselines of less than 20 km where the atmospheric errors are assumed to be the same. Using this method, one receiver is set at a reference (control) station (Fig. 5.5) while the other receiver is set at a station whose position is desired (e.g., Fig. 5.6). Tracking of satellites must then be simultaneous and synchronized. The observation time would normally take 20 min to 1 h with data being sampled at intervals of 10–15 s (or as set in the receiver). Longer durations of observation benefit from improved satellite geometry leading to better solution of the unknown integer ambiguities $\{N\}$. When the settings are properly done, and errors minimized through proper prior planning, the method is capable of giving coordinate differences $(\triangle X, \triangle Y, \triangle Z)$ to a centimeter to millimeter level accuracy. The method is useful in the establishment of higher precision control

networks (baseline reference networks) useful for providing baseline environmental monitoring data.

The static relative positioning approach is potentially extremely useful for monitoring *environmental spatial variations*, e.g., deformation or land subsidence (e.g., Fig. 5.8). In this case, the control (reference) stations that provide the baseline monitoring data are set on a permanent non-deforming surface far from the deforming site being monitored, while the stations to be monitored are set on the boundary of the deforming surface. Relative positioning using *carrier-phase* provides more accurate results to a few cm, depending on the accuracy of the control stations and on how the other errors are managed. If the observations are undertaken for a longer period of say 1 h, depending on baseline lengths, the improved satellite geometry will enable the calculation of integer ambiguity and also reduce satellite geometry errors leading to more accurate results.

Post-processing can also permit the use of *precise ephemeris* obtained within one to two weeks after the actual survey to give very accurate results. For example, the temporal monitoring (i.e., surveillance) of the position of a dam's wall will indicate any spatial change such as horizontal or vertical shift with respect to the baseline data (Fig. 5.8, red triangles), which can be analyzed to see whether the dam is deforming and posing a potential danger. The static relative positioning method is

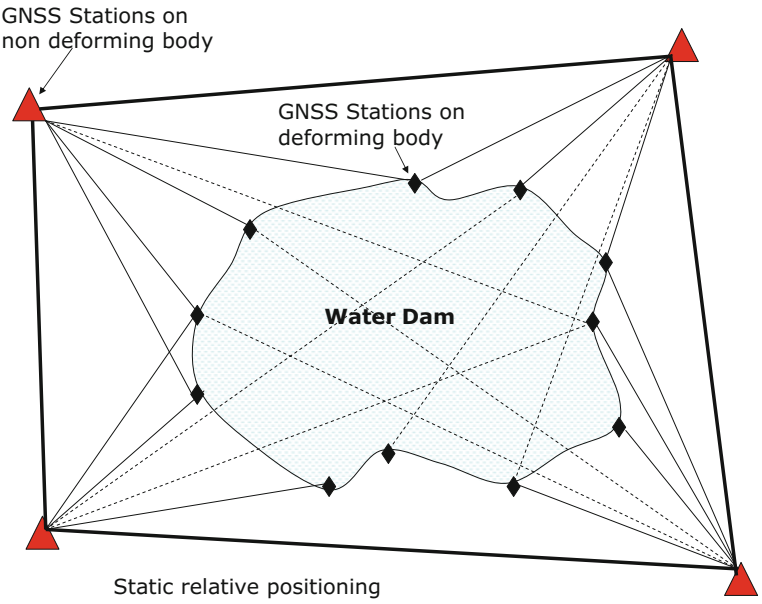


**Fig. 5.8** Monitoring of deformation of a dam using static relative positioning. The *red triangles* indicate control stations on the non-deforming surface that provide baseline monitoring data. The *black diamonds* indicate GNSS stations around the dam, which are being monitored for horizontal and vertical motion (shift) relative to the *red triangles*

further useful for densification of existing control networks, monitoring earthquakes through measuring plate movements in crustal dynamics and oil rig monitoring [3, p. 339].

### 5.4.3 Real-Time GNSS (RTGNSS)

In Sect. 5.4.1, a decimeter accuracy for a stand alone receiver was said to be achievable by taking observations for 30–45 min using code observations. It was also pointed out that future modernized GNSS satellites (see Fig. 5.7) are expected to improve positioning accuracy as a results of improved satellite orbit determination, receiver technology, additional user signals L2C and L5, which would assist in modelling ionospheric errors, and additional ground monitoring stations. Although higher accuracies can be realized through post-processing of data, i.e., as done for precise point positioning, e.g., [4, p. 68], more and more users want these higher accuracies to be achieved in real-time. With such demands, receiver manufacturers are responding by coming up with receivers capable of delivering cm-level accuracy in real-time. More recently, position solution accuracy and speed have advanced to the point where cm-level coordinates are available within seconds, while mm-level are available for daily solutions [5].

An example is the NASA's Global Differential GPS (GDGPS) System, which is fully operational since 2000. It is a complete, highly accurate, and extremely robust real-time GPS monitoring and augmentation system that uses a large ground network of regional and global real-time GNSS reference receivers, innovative network architecture, and award-winning real-time data processing software to give decimeter-level (10 cm) positioning accuracy and sub-nanosecond time transfer accuracy anywhere in the world, on the ground, in the air, and in space, independent of local infrastructure.[2] It supports the GREAT (GPS real-time Earthquake and Tsunami) Alert Project, which is a NASA-sponsored endeavor to develop an advanced Earthquake and Tsunami alert system (see Sect. 17.3) benefiting from the availability of the real-time GNSS infrastructure.[3]

Another example is the hand-held Mobile Mapper 100 from Ashtech that combines internal high-grade antenna and processing capability to achieve decimeter-level accuracy.[4] This hand-held receiver is suitable in monitoring changes in perimeters and areas of environmental features with spatial changes.

Besides the requirement of real-time GNSS data, other environmental applications such as earthquake monitoring would prefer that such data be delivered at a higher sampling rate (e.g., 1 Hz or higher), and at a low-latency (e.g., an order of seconds or less, e.g., [6]. Real-time data allow for real-time science and have a place in an increasingly real-time society. For example, today, it is possible for anyone to receive

[2] http://www.gdgps.net/.

[3] http://www.gdgps.net/products/great-alert.html.

[4] Mobile Mapper 100. White paper: A break through in hand-held accuracy.

notification of hypocentral and moment tensor information for earthquakes, placed into geographic and tectonic context, within minutes of their occurrence [6].

Hammond et al. [6] provide an illustration of the benefit of low-latency information as exemplified by people who live in the path of natural hazards and require information about catastrophic events to be delivered as quickly as possible. The ability to detect and characterize events rapidly can make all the difference in the critical minutes to hours that follow an event, as was the case in the catastrophic 2004 Sumatra and the 11th of March 2011 Tohoku-oki earthquakes and tsunamis where many lives were lost [5, 6].

## *5.4.4 Differential and Augmented GNSS*

### 5.4.4.1 Differential GNSS (DGPS)

In this approach, which was introduced in Sect. 4.3.2, the procedure is theoretically identical to post-processed static relative positioning using *code-pseudoranges*, except that everything happens in real-time. Due to the fact that the user obtains real-time results, in addition to the two receivers, a *real-time data link, e.g., radio or mobile* is required. The purpose of the data link is to transmit the "*pseudorange corrections PRC*" from the reference station to the roving receiver for it to correct its own measured pseudoranges (see Sect. 4.3.2; Fig. 4.5).

In general, a DGPS system will comprise of the *reference sites* whose coordinates are already well known to a higher accuracy, having been previously surveyed using GPS carrier-phase; a receiver measuring code or carrier-phase pseudo-ranges, computing and transmitting the corrections; and a data link for transmitting the differential corrections using different radio frequencies. The reference station also monitors the integrity of the system and is often a permanent site with continuous power supply and automated equipment. There can be several reference sites whose coordinates are known in a DGPS system, of which there are two types:

1. The user's own independent reference station, which essentially means that the user has to purchase an additional receiver, thereby incurring additional costs;
2. Commercially owned reference stations, which charges users to access transmitted signals, e.g., Fugro in Australia.

Users of commercially owned DGPS only require one receiver, a communication link, and the cost of accessing the data. Japan's GEONET (GPS Earth Observation Network System) is comprised of more than 1500 receivers dedicated to GNSS-meteorology. In Australia, the National Collaborative Research Infrastructure Strategy (NCRIS) is establishing a nation-wide geodetic continuous operating reference stations (CORS) network that will consist of 126 stations. These commercially owned systems are discussed in detail in Sect. 5.5.

The *user's station* is comprised of a receiver, with a data link software to apply corrections to its measured pseudoranges. Fax, telephones or mobile phones are also

applicable in addition to the radio as data links, and are range dependent. Some communication link systems are also line of sight dependent. Data link frequency bands vary depending on the baseline range while the data is transmitted from the reference to a roving station using a standard format called Radio Technical Commission for Maritime Services Special Committee 104 (RTCM SC-104) Format.

With DGPS positioning method, the achievable accuracy is in the range 3–5 m [2]. This accuracy, however, is dependent on the closeness between the user's (rover) and the reference stations. The separation distance should ideally be below 50 km in order to assume that the satellite signals at both the rover and the reference stations are affected by the same errors. Users also have to be aware of data latency (i.e., time-lag in the reception of the corrections by the rover, which is about 0.25–2 s). This time-lag latency reduces the accuracy of the method.

#### 5.4.4.2 Augmented GNSS

For applications that are more than 50 km from a reference station, the DGPS approach discussed above is limited, thus paving way to the *Wide Area Differential GPS (WADGPS)*. WADGPS has a global or regional coverage of reference stations required to model *atmospheric* and *orbital errors* that suffices for long baselines, and are classified into either *Ground-Based Augmented Systems (GBAS)* or *Satellite-Based Augmented Systems (SBAS)*. GBAS, which uses ground-based stations, are useful for real-time applications. For multiple reference stations, RTCM SC-104 pseudorange corrections are received onboard the roving receiver from $n$ reference stations (up to approximately 400 km).

The pseudorange observations at the roving receiver are combined with each set of corrections to provide $n$ independent solutions that are then combined in a conventional 3D adjustment to provide an additional estimate of the roving receiver's position. The accuracy of the roving receiver, similar to that of the DGPS method will depend on its distance from the reference station. For Government provided GBAS, the services are free to the users while subscription is required for privately delivered GBAS. Examples of GBAS are the Australian Maritime Safety Authority (AMSA) that has been operational since 2002 and offers maritime services to users; and the Nationwide Differential GPS (NDGPS) that is being expanded to cover all surface areas of the United States to meet the requirement of surface users.

SBAS send corrections to remote areas (e.g., areas out of reach of ordinary DGPS or GBAS, such as oceans). Unlike a DGPS system where the data is transmitted via radio links, SBAS transmits data via geostationary communication satellites. These corrections are transmitted on a similar frequency to GPS satellites, thereby alleviating the need for additional software from the users. In Europe, the EGNOS geostationary satellites discussed in Sects. 2.2 and 7.1 augment the GPS and GLONASS systems to provide wide area differential corrections. In US, the Federal Aviation Authority (FAA) developed the Wide Area Augmentation System (WAAS) to improve on the accuracy, integrity and availability of GPS so that it can be a primary means of navigation for aircraft enroute, and for non-precision approaches, thereby improving the

real-time civil accuracy of GPS to 7 m [3, p. 362]. WAAS is also used in many other civil applications.

Examples of DGPS/WADGPS Companies include FUGRO, who operates the Omnistar and Starfix systems, Racal who operates Landstar and Skyfix, and Western Geophysical who operate SARGAS. Other WADGPS systems are as discussed in Sect. 5.5.

### 5.4.5 *Rapid Positioning Methods*

Rapid GNSS positioning using carrier-phase pseudorange includes techniques such as *rapid-static or fast-static surveys*, *stop-and-go surveys*, and *kinematic surveys*. Rapid or fast-static survey are usually post-processed while stop-and-go and kinematic survey can be used in post-processing or in real-time modes of operation. Whereas the static surveying discussed in Sect. 5.4.2 resolves ambiguity through long-term averaging and a simple geometric calibration principle resulting in the solution of the linear equations that produces a resultant position, a variety of physical and mathematical techniques have been developed for rapid methods [2]. These include:

- Static occupation of a known point (e.g., previously positioned points, i.e., known baselines) for over 30 s.
- Static measurement at another known point on the baseline.
- Static occupation of an unknown baseline (e.g., fast-static occupation time).
- Static occupation of an unknown baseline and swapping of reference-rover receivers for 2–4 min (i.e., between known and unknown points).

A mathematical approach adopted by most GPS systems used today is the ambiguity resolution *on-the-fly* (while moving). This technique is common for most real-time kinematic (RTK) applications (Sect. 5.4.6). *Rapid-static* or *fast-static surveys* are essentially the same as static surveys but make use of shorter station occupation times. In this approach, one or more roving GPS receivers occupies all *unknown stations* while at least one receiver (reference station) is stationary at a known control station all the time (Fig. 5.9). The rapid nature of this type of survey compared to static surveys is due to the rapid solution of the integer ambiguities, making use of *all observable satellites*, *single or both dual-frequency L1/L2*, and *carrier-phase data*. Although fast-static relative positioning is accurate and economical where there are many points to be surveyed and offers more efficient positioning than conventional static relative positioning, the accuracy is usually slightly lower at the cm-level. It is, however, suitable for short baselines where systematic errors such as atmospheric and orbital factors are considered identical and can be differenced.

Due to the special processing algorithm used for solving the integer ambiguities, at least four satellites need to be tracked continuously. The technique is only effective over short ($<$10–20 km) baselines and the observation occupation time depends on the number and geometry of the satellites visible. Station occupation time vary between

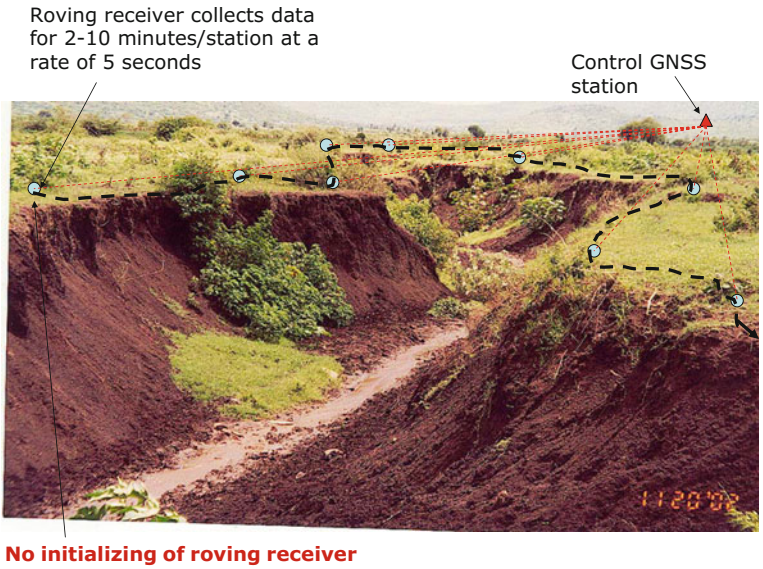


**Fig. 5.9** Monitoring of the extent of erosion using fast-static positioning. The *triangle* indicates the control station while the *circles* indicate the positions occupied by the roving receiver (cf. the method of stop-and-go in Fig. 5.10)

2 and 10 min with a data sampling rate every 5 s, depending on the distance to the base as well as the satellite geometry, see e.g., El-Rabbany [4, p. 74] and [2]. Redundant observations to more than four satellites with good geometry help improve the solution of the ambiguities and reduce the time required to achieve a sufficiently accurate position. While moving from one station to another, the receiver can also be switched off to conserve power. For static and fast-static satellite surveying, the effect of high PDOPs because of poor geometry is less significant since the observation time is normally longer (2–60 min), thereby guaranteeing a better or improved satellite geometry. For environmental monitoring, e.g., of land degradation due to erosion (Fig. 5.9), fast-static method can be used.

The *stop-and-go* method is a mixture of pure kinematic and static positioning. A series of points are positioned with respect to the reference receiver by moving the roving receiver sequentially to the points (Fig. 5.10). To initialize the survey, the roving receiver has to remain static (e.g., at the first station to be positioned) for a certain time to allow for a solution of the integer ambiguities. The slightly longer period required for the initialization is to enable the satellite geometry to improve. Essentially, the initial static time is the same as that required for a fast-static survey. However, the initialization time can be greatly reduced by the occupation of a known station.

After initialization, the roving receiver is moved to the next station while continuously tracking the common (same) satellite signals. Initialization can also be achieved through reference-rover antenna swapping, by observing static data at another known

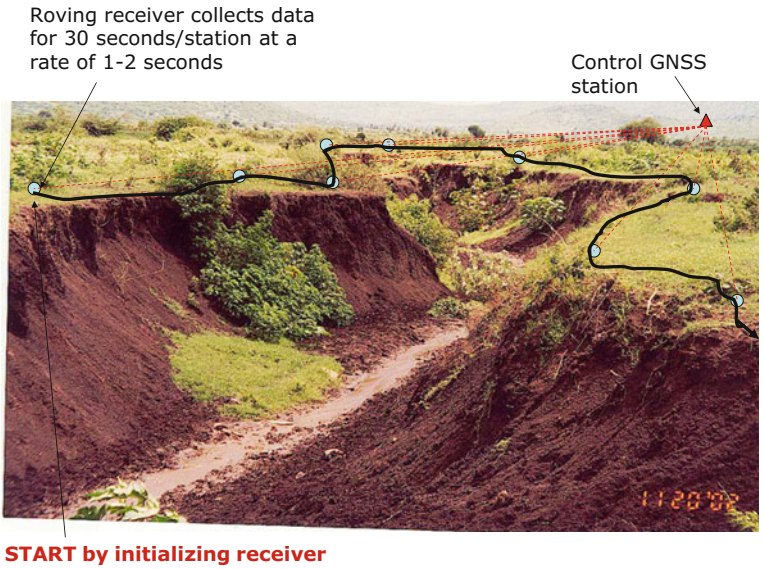


**Fig. 5.10** Monitoring of the extent of erosion using the stop-and-go positioning method. The *triangle* indicate the control station while the *circles* indicate the positions occupied by the roving receiver. Initialization has to be done at the first station and a lock on four or more common satellites maintained. The advantage over the fast-static approach in Fig. 5.9 is the shorter occupation time (e.g., 30 s compared to 2–10 min). The disadvantage is the loss of lock to the satellite and having to re-initialize

point on the network, or by observing on a known baseline. At a given station, an observation time of only one or a few epochs (period of observations) is necessary to obtain a precise position as the integer ambiguities are already solved during the initialization phase. The rover typically collects data for a period of 30 s at a sampling rate of 1–2 s before moving to the next station [4, p. 75]. In this way, by moving the roving receiver, a series of stations can be coordinated sequentially. Similar to the fast-static survey, the stop-and-go survey technique requires at least four satellites to be continuously tracked. If lock to one of the minimum four satellites is lost, the roving antenna must be re-initialized by *returning the roving receiver to a previously surveyed point*, or *preferably to a known station*.

With the availability of fast ambiguity resolution techniques, the stop-and-go survey technique is best suited to coordinate a large number of stations (e.g., survey grid or precise mapping). However, there must be open sky in order to avoid frequent loss-of-lock of the satellite signal. It is essential for this technique that the satellites' signals can be continuously tracked throughout the survey. This method has an advantage over static positioning since it reduces observation time and is ideal for topographic surveys (see e.g., Chap. 8), such as the mapping of habitats, since it offers an accuracy of 2–3 cm for a baseline of 10–15 km (real-time or post-processed). The

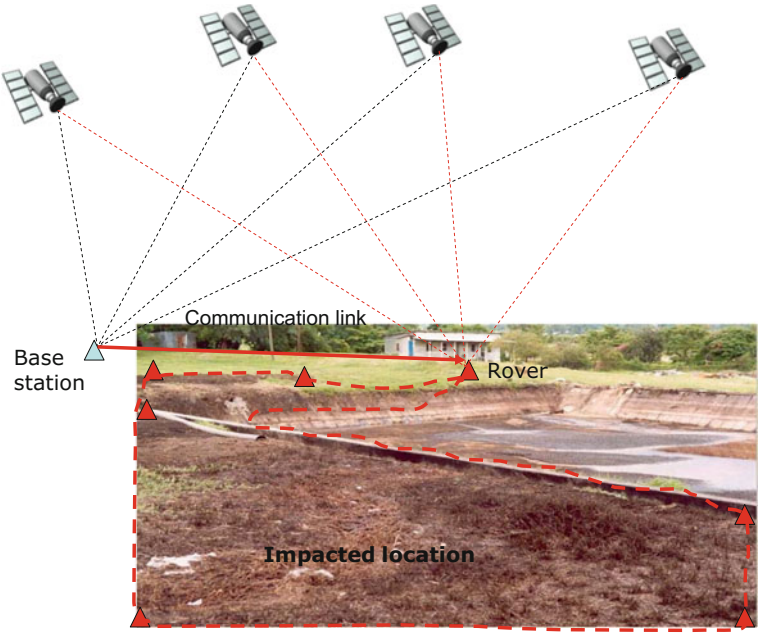


**Fig. 5.11** RTK mapping of the boundary of an impacted location to monitor its spatial extent. The base receiver remains stationary and transmits raw data together with its position via the communication link to the roving receiver

disadvantage of the method is the reliance on locked satellites (i.e., the satellites detected by the receiver) and having to re-initialize once loss of lock occurs.

*Kinematic surveying* operates with the same principle as the stop-and-go method, only that in this case, there is no stopping but the roving receiver is in continuous motion. Unlike fast-static approach, the receiver is not switched off while in motion. In Fig. 5.11 the use of kinematic survey, particularly when a linear feature is being mapped is shown. The accuracy of kinematic surveys is, however, lower than that of stop-and-go, since some of the common errors encountered cancel with improved satellite geometry in stop-and-go.

### *5.4.6 Real-Time Kinematic (RTK)*

As the name suggests, RTK is capable of delivering real-time positions in the field. Similar to the other rapid positioning techniques discussed above, RTK also requires more than two receivers, with one being placed at a reference (base station) station. Unlike the fast-static and stop-and-go methods, it uses a similar principle to that of DGPS discussed in Sect. 5.4.4; only that instead of code-pseudorange, carrier-phase

measurements are used. The base receiver remains stationary and has a transmitting radio link while the roving receiver is in motion and has a receiving radio link (Fig. 5.11).

The base receiver samples data every second and transmits these raw data together with its position via the communications link (e.g., satellites, mobiles or radio) to the roving receiver. Using its radio receiver, the rover receives the transmitted data from the base receiver and uses in-built software to combine and process the GNSS measurements obtained at both the base and roving receivers to obtain its position [4, p. 78]. Some GPS manufacturers provide a hand-held controller that can be used to operate both the roving and the base receivers. Normally, the user carries the roving receiver attached to the radio link in a back pack. The method requires the fixing of the integer ambiguity at the start of the survey (initialization) before undertaking the survey. Ambiguities can be initialized through the methods discussed in Sect. 5.4.5. Once the initial ambiguity has been fixed, the roving receiver can be moved. Any loss-of-lock due to obstructions makes a re-initialization necessary.

Most kinematic survey algorithms use the ambiguity resolution on-the-fly as it allows integer resolution while the antenna is moving. With this approach, no initial *static initialization* is required. Once the integer ambiguities have been fixed, all previous measurements can be calculated back to obtain precise coordinates for all positions. This surveying technique, which requires dual frequency observations (L1/L2), makes it possible to perform certain precise environmental monitoring tasks in a kinematic mode, e.g., monitoring the proposed construction of linear features such as roads for the purpose of assisting environmental impact assessment (EIA) discussed in Chap. 13. The integer ambiguity is fixed and preserved for at least four (preferably five) satellites during the motion of the roving receiver. The accuracy of this method is about 2–5 cm with a possibility of improvement if a longer period of station observation (i.e., 30 s) is adopted [4, p. 78]. Compared to the kinematic survey, which allows post-processing (i.e., post processed kinematic, PPK), the accuracy of RTK is a bit lower. This is due to the time-lag in the transmitted data reaching the rover, whereas post-processing enables the matching of data, correcting it for some errors, and also allows the use of precise ephemeris.

In order not to confuse real-time DGPS and RTK, it should be remembered that DGPS uses code-pseudorange corrections, improving the positioning accuracy from 15 to 5 m or less, while RTK uses raw carrier-phases and codes.[5] RTK facilitates the efficient establishment of a series of points in open areas, and even in areas of some overhead obstructions due to the advent of fast ambiguity resolution techniques. Unlike DGPS, the fundamental principle of RTK is that the carrier-phase and code data from the reference station are transmitted to the roving receiver, which then uses the data from both the roving and reference receivers to form double difference observations and compute the position of the rover.

Telemetry links form a critical component of RTK systems, over which the data from the reference receiver are transmitted to the rover. High baud rates and high radio

[5] Some providers, such as FUGRO in Australia, have started using carrier-phase pseudorange corrections to deliver sub-centimeter accuracy.

frequencies are required, which limit the extent of the surveys. Reference (control) stations can normally be obtained from local surveying offices or the appropriate government agencies. The accuracies of the control points will contribute to the accuracies of the user's derived position, particularly when using relative, DGPS or RTK methods.

*Network-RTK*: Since most RTK systems require the roving receiver to be within 10 km of the base station (assuming similar atmospheric conditions), use of multiple base stations, i.e., network-RTK, provides an alternative for baselines more than 10 km long. Ambiguities must still be resolvable within seconds or instantaneously, up to baselines of 50–100 km in length, which requires the consideration of the orbital and atmospheric (tropospheric and ionospheric) errors. An approach currently receiving wide attention around the world uses the virtual reference station. In this approach, the roving receiver is located within the bounds of three or more reference stations and the observation errors modelled according to the approximate position of the rover (i.e., AUSPOS and OPUS online processing operational principles discussed in Sect. 6.4). Rizos et al. [7] identified some advantages of network RTK over single-baseline RTK as:

1. Rapid-static and kinematic GPS techniques that could be used over baselines many tens of kilometers in length.
2. Instantaneous (i.e., single-epoch) on-the-fly ambiguity resolution algorithms could be used for GPS positioning, at the same time ensuring high accuracy, availability and reliability for critical applications.
3. Rapid-static positioning is possible using lower-cost, single-frequency GPS receivers, even over baselines tens of kilometers in length.

### *5.4.7 Precise Point Positioning (PPP)*

Unlike DGPS and RTK positioning approaches that require users to have access to at least two receivers, precise point positioning (PPP) uses only a single receiver to achieve cm-level positioning accuracy. The key to this success is its capability to exploit precise GNSS orbit and clock products during post-processing. The precise orbit and clock data are provided, e.g., by the International GNSS Service (IGS), Jet Propulsion Laboratory (JPL), and other commercial sources.

Positioning with PPP has widely been based on using precise orbit and clock products at cm-level accuracy to process the ionospheric-free combinations of undifferenced code and phase observation Eqs. (3.5) and (3.6) on p. 37 to estimate positions, integer ambiguity $N$, receiver clock bias $c\delta_i(t)$, and the tropospheric effect. It also requires a number of unconventional corrections such as satellite antenna offset to mitigate systematic effect that can cause cm-level variation in Eqs. (3.5) and (3.6) [8]. Furthermore, integer ambiguity resolution-enabled precise point positioning (PPP) are emerging, see e.g., [9, and the reference therein].

Its advantages compared to DGPS and RTK are [8]:

1. It uses only a single receiver to achieve cm-level accuracy hence removes the requirement of a reference station and simultaneous observations to the same satellites from both rover and reference stations. Further, operating range limit is not an issue.
2. Its use of a global reference frame gives it a global outlook enabling it to provide much greater consistency than the DGPS whose position are relative to a local reference station.
3. Its use of a single receiver reduces equipment cost and also makes the approach less labour intensive.
4. Besides the provision of location-based data, PPP needs to estimate clock and tropospheric parameters from Eqs. (3.5) and (3.6) thereby providing a new way for precise time transfer and water vapour estimation using a single GNSS receiver. The use of water vapour for weather forecasting is discussed in Sect. 11.4.1.

For environmental monitoring applications, besides the provision of location-based data and water vapour, it could also assist in airborne mapping where ground-based station are not available. Its limitations, however, include long initialization time (e.g., 20 min) limiting its use in real-time applications, non integer nature of the ambiguity terms following the solution of Eqs. (3.5) and (3.6) since they are corrupted by the satellite and receiver initial phase biases, and the need to access precise orbit and clock products that may be of concern to some users [8].

## 5.5 Environmental Surveillance: CORS Monitoring

In Sect. 1.1, *surveillance* was introduced as the systematic observation of variables and processes with the aim of producing *time series*. Indeed, most environmental events require *continuous monitoring* in order to analyze time series maps. Such environmental processes are those that result in changes with time, such as *plate tectonic motion*, *land submergence* or *changes in sea levels*. As an example, let us consider a locality like Perth (Australia), which uses groundwater for its domestic and industrial activities. In order to monitor the environmental impacts of groundwater extraction, i.e., whether there are some land submergence due to water extraction, continuous observation of locations of known heights can provide time series maps which can be analyzed to show any sinking of land. Currently, GPS stations provide such capability in what is known as a Continuous Operating Reference Station (CORS).

CORS data support high-accuracy three-dimensional positioning activities useful in environmental monitoring of spatial motions in time. Its data are also used by geophysicists, meteorologists, atmospheric and ionospheric scientists, and others in support of a wide variety of applications [10]. For example,l [11–13] undertook surveillance monitoring of land subsidence in northeast Iran using both GPS and InSAR

(interferometric synthetic aperture radar) and obtained a 19 cm/year subsidence using both methods (see Sect. 17.4 for more details).

A CORS station is a stationary GNSS receiver, which is continually collecting data from visible GNSS satellites on a 24 h basis in order to produce its three-dimensional coordinates (e.g., Fig. 5.12). CORS networks vary in size ranging from regional, national, to global scales (e.g., the International Global Navigation Satellite System Service (IGS)). Each individual CORS station is positioned to a very high degree of accuracy using precise GNSS, satellite laser ranging (SLR), and very long baseline interferometry (VLBI), thereby enabling them to be used as reference stations to position other points, besides continuously providing their own positions. Individual users can also benefit from CORS networks by acquiring data from the CORS stations within their vicinity to achieve more accurate results (see, Sect. 5.4.4). Perhaps of importance to environmentalists is the question posed by Rizos [7]:

> *What if, instead of broadcasting RTK corrections and placing the onus of obtaining a final solution on users and their equipment, users' coordinates are determined by a service provider?*

**Fig. 5.12** A GEONET GNSS-based CORS station in Japan. *Source* Geospatial Information Authority of Japan

This is the client-server approach envisaged by Rizos [7] who then states:

> *Final (position) solutions for all real-time (logged) users could be simply computed as a by-product of the continuous network processes, all the time satisfying the quality and integrity criteria implemented at the network administrator level. Note that improved accuracy and reliability of the user coordinates can be expected if GPS data is processed in the network mode, rather than as individual baselines as is the case for standard RTK-type techniques. In addition, precise ultra-rapid IGS ephemerides can be used in the network computations instead of the broadcast ephemeris.*

The feasibility of Rizos' proposed model (see e.g., Sect. 6.4) will enormously benefit environmentalists who would then have to only send their data to a central processing unit and receive their final products in the form of their receiver positions.

Examples of CORS-type networks include the Japanese GEONET (e.g., Fig. 5.14), Germany's Satellite Positioning Service (SAPOS), and the US's National Spatial Reference System (NSRS; Fig. 5.13), which comprised a network of over 1,350 sites in 2008 and is growing at a rate of about 15 sites per month [10]. Two scenarios of CORS made up of 1450 stations (as of May 2010) are presented: the National CORS system made up of over 988 stations and run by the National Geodetic Survey

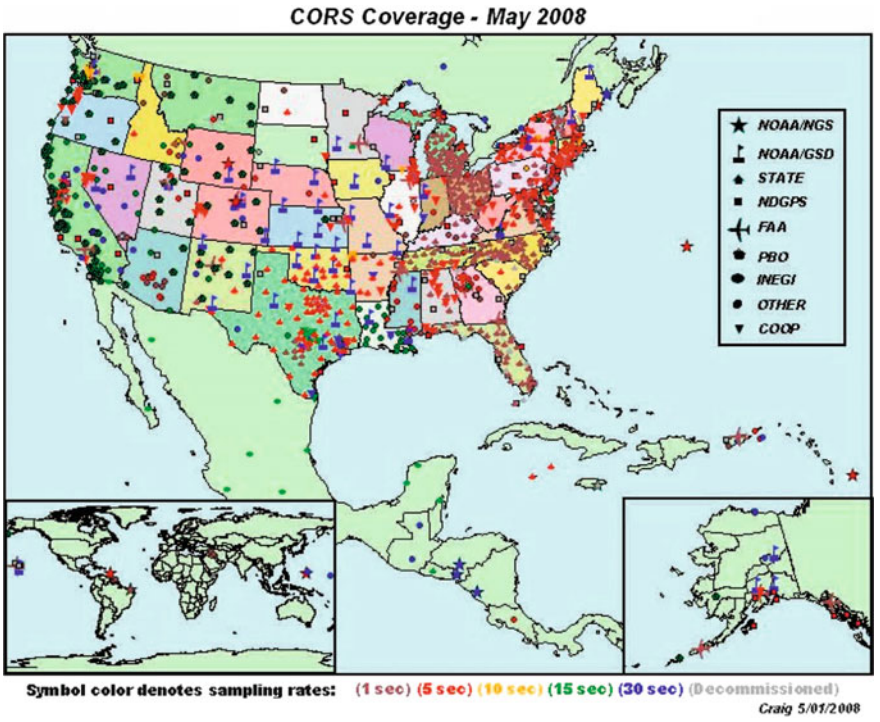


**Fig. 5.13** NSRS CORS stations as of May 2008. *Source* Snay and Soler [10]

(NGS), and a collaborative network comprising more than 200 organizations.[6] CORS observational data are freely provided to the user community via the Internet and are capable of supporting high-accuracy positioning requirements. In addition to enhancing geospatial positioning, applications using CORS data include the following [14];

- a critical role in defining the nation's geodetic reference system,
- *the ability to characterize the free electron content of the ionosphere*, and
- an important *source of precipitable water vapor input to meteorological forecasts*.

The last two are environmental monitoring related tasks. Snay and Soler [10] summarize the history, applications, and future prospects of the NSRS-CORS network by describing the more important contributions of the CORS system to the scientific community. Some of the uses of CORS documented e.g., by Snay and Soler [10], which may be of benefit to environmental monitoring tasks include;

- Upgrading national geodetic reference systems (e.g., Sect. 5.6). Snay and Soler [10] report on the upgrading of the US based national geodetic system with the help of CORS coordinates that were held fixed in the adjustment process.
- Assessing GNSS observational accuracies. With a well-established network of CORS stations, it is possible to design experiments that are aimed at improving GNSS positioning methodologies within a relative positioning framework, e.g., [10].
- Multipath studies. In this regard, the CORS network could be used for instance to investigate further possibilities of minimizing positioning errors resulting from multipath discussed in Sect. 3.4.4. Snay and Soler [10] report on how CORS stations were used to evaluate the amount of multipath occurring at each of the more than 390 sites, where the most and least affected sites were identified in the network, different receiver/antenna combinations compared, and those sites that appeared to be severely affected by multipath more closely investigated.
- Crustal motion monitoring. This could be the most visible environmental monitoring application of CORS stations where the horizontal and vertical motion of the Earth's surface is monitored to mitigate, e.g., the impacts of earthquakes, tsunamis and other disasters resulting from plate motions, as we will see in Chap. 17. For this, many CORS stations provide velocities that are useful in indicating plate motions and time information.
- Sea level change monitoring. The variations of vertical crustal velocities at CORS sites near tide gauge stations may be used to determine the "absolute" sea level change with respect to the International Terrestrial Reference Frame (ITRF). This type of analysis was impossible to conduct before the proliferation of CORS in coastal areas [10]. This application is discussed further in Sect. 17.2.3.
- Atmospheric monitoring. CORS are currently contributing to the new field of GNSS-meteorology (see Sect. 9.2.1). Besides their application to GNSS-meteorology, CORS stations could be useful in ionospheric studies as discussed, e.g., by [10].

[6] http://www.ngs.noaa.gov/CORS/.

- Support of remote sensing applications. CORS stations have been used to support remote sensing applications such as the accurate positioning of aircraft employed in aerial mapping in order to improve the reliability of photogrammetric restitution, especially for large-scale aerial surveys over remote or inaccessible terrain. It may then be implemented for georeferencing landmarks from the air with digital cameras, as well as being applied to a broad range of mapping technologies, such as scanning radar, light detection and ranging (LiDAR), inertial systems, interferometric synthetic aperture radar (InSAR), and/or sonar [10].

To date, Japan's distribution of CORS stations is the most numerous and densest in the world. This network, known as *GEONET* (Fig. 5.14), is used mainly for geodynamic/geophysical monitoring around Japan where four tectonic plates are interacting with each other, i.e., the monitoring of earthquakes and volcanic hazards [15, 16].

Matsuzaka [15] points to the fact that 1200 GEONET CORS stations with an average spacing of 20–30 km between stations are operational in order to realize the system's desired use. This network has been operational since 1994 under the control of the Geospatial Information Authority of Japan (GSI), providing precise daily coordinates of all stations, with which displacement and strain rates are calculated nationwide, thereby revealing the various characteristics of tectonic deformation in the Japanese islands [17]. Japan has also undertaken several measures to improve the quality of data collected, including creating a double cylindrical structure of observation pillar to reduce thermal effects (see Fig. 5.12), unification of antenna types to reduce multipath and a better analysis strategy to obtain more reliable and accurate solutions [15]. A typical GEONET station consists of a 5 m pillar, chokering antenna, 24 h observations, 1 Hz sampling rate and real-time data transfer (e.g., Fig. 5.12). These attributes enable Japan to measure *tectonic plate movements* and "slips" occurring along fault lines to a high degree of accuracy (post-processed ±2 mm) [15].

*SAPOS* comprises a network of more than 250 CORS stations[7] run by the German State Survey for the purpose of supporting cadastral surveying, engineering surveying, private industry sector applications (e.g., transport fleet management), emergency guidance systems (e.g., police, fire and radio) and deformation measurements [18]. The average spacing between the stations is 50 km. Various quality control measures carried out allow a precision of the order of 1 cm to 5 m in real-time positioning, see e.g., [19].

*CORS Networks in Australia* are at the development stage. Australia-wide, there are several CORS networks in place. The Australian Fiducial Network (AFN) consists of 8 CORS stations, which together with a further 8 CORS stations, both on the Australian continent and offshore, form the Australian Regional GPS Network (ARGN) [20]. The network has reached a global accuracy of a few centimeters which is sufficient for the designed purpose. Besides this, several Australian states and cities have begun installing their own CORS networks, e.g., Victoria's VICPOS. Some of

[7] http://www.sapos.de/pdf/Flyer/2004Flyer_e.pdf.

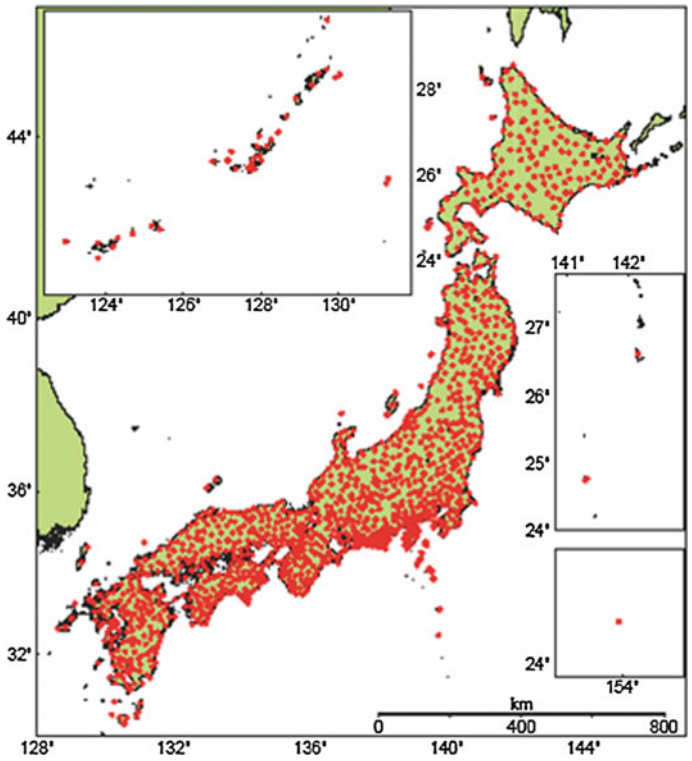


**Fig. 5.14** GEONET CORS stations. GEONET data are used in various disaster related meetings and geophysical model estimation of crustal activities and thus are reflected in the decision making process to cope with the disaster as well as the scientific researches. *Source* Matsuzaka [15]

the CORS stations in VICPOS are also incorporated in MELBPOS, a CORS network specifically for Melbourne. Sydney also has a specific CORS network named SYDNET.

Densification of the Australian CORS network is currently ongoing, as indicated in Fig. 5.15 which shows the proposed Australian CORS network that is designed to cater for the needs of most of the populated areas of the country. This network would allow a maximum baseline length of 200 km spatial coverage. To be able to position with the online based AUSPOS discussed in Sect. 6.4, the number of stations that a user can access within the proposed baseline length of 200 km are illustrated in Fig. 5.16.

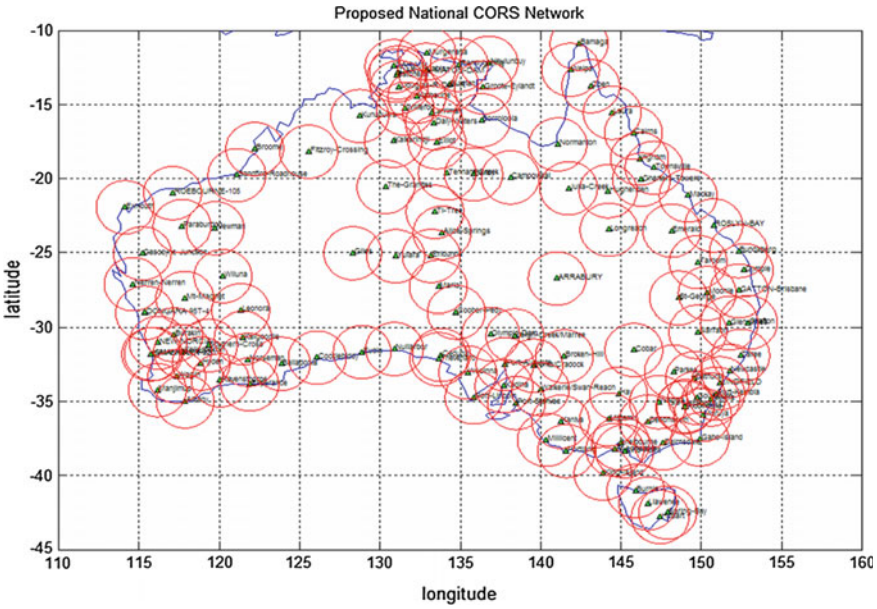


**Fig. 5.15** Coverage by the proposed Australian national CORS network (baseline length 200 km). *Source* Wallace [21]

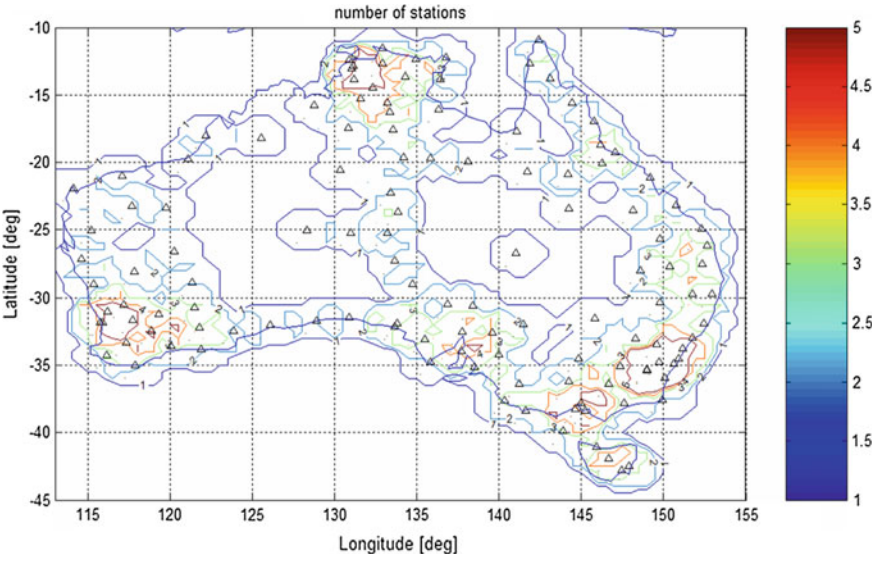


**Fig. 5.16** Station overlap for 200 km baseline. *Source* Wallace [21]

## 5.6 Coordinate Reference System

The preceding sections have dwelt with the measurement techniques and variables used with GNSS. What has not been discussed at length is that these measurements have to refer to some coordinate system. From a social perspective, human beings have names that identify them, as do places and biological species. When we talk of GNSS providing locations, how therefore do we refer to them? The answer lies in the concept of a Coordinate Reference System, which is comprised of a *datum*, *coordinate system* and *map projection* .

### *5.6.1 Datum*

A datum, a *mathematical figure* (ellipsoid) that enables measurements and computations to be undertaken on the surface of the Earth, is defined by its size, shape, location and orientation, and its relation to the geoid by means of geoid undulation and deflection of the vertical [22, p. 29]. This is necessitated by the fact that the topographical surface of the Earth is irregular and unfit to be used for computations. For simple tasks, a sphere is normally used to approximate the Earth. In more precise work, such as GNSS measurements and computations, however, an *ellipsoid of revolutions* (e.g., Fig. 5.17) is normally used. An ellipsoid of revolution is simply a bi-axial ellipsoid defined by the axes $\{a, b\}$ rotated around the minor axes $\{b\}$. Besides these axes, the ellipsoid has to have an origin. For the case where this origin coincides with the center of mass of the Earth, it is called a geocentric ellipsoid. The ellipsoid thus becomes a reference surface for horizontal positioning. A well-positioned reference ellipsoid has two axes defining the dimensions of the ellipsoid, three parameters defining its origin, and three parameters defining the orientation in space. All together, these form a *geodetic datum* [4, p. 48] or simply a *reference ellipsoid*. A geodetic datum as defined above will therefore give the horizontal position (two-dimensional) of any location on Earth.

Some environmental monitoring tasks, such as land subsidence, change in sea level, or the amount of siltation in a lake, require information on heights with respect to some reference. This reference is often known as the *vertical datum*, whose definition uses the sea level. If sea level in a coastal area is measured by tide gauges and averaged over a period of time (i.e., several years), a *mean sea level* MSL is obtained. Now, let us project this MSL through the Earth such that it passes through the continents (e.g., Fig. 5.18), as if there were canals all the way through the continents. The obtained surface is called a *geoid*, and is defined as an equipotential surface approximating mean sea level, and is the *vertical datum*. Height measurements in local systems are normally measured with respect to this datum or simply the MSL, hence it is common to give readings above MSL.

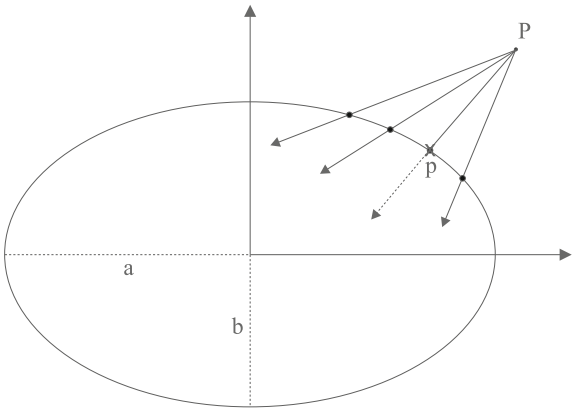


**Fig. 5.17** Reference ellipsoid: Point *P* on the Earth's topographic surface and its corresponding point *p* on the *Reference ellipsoid of revolution* with semi-major axis *a* and semi-minor axis *b*. *Source* Awange and Grafarend [23]

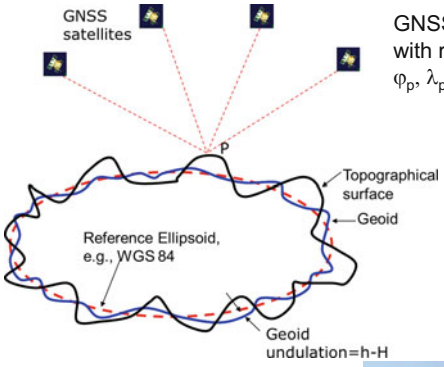


GNSS position of point P is given with reference to the ellipsoid, i.e., $\varphi_p$, $\lambda_p$, $h_p$.

GNSS heights (h) have to be converted to orthometric heights ($H_p$) using the geoid undulations (N).

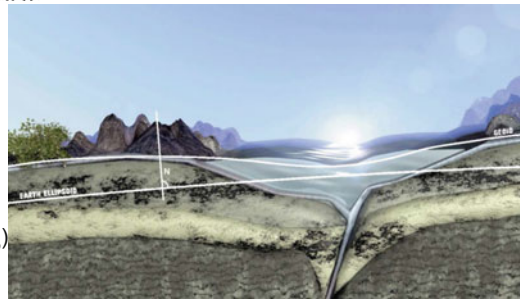

**Fig. 5.18** *Top* Vertical datum–the geoid (the *blue line*). The *black continuous line* gives the topographical surface while the *red dotted line* gives the ellipsoid (i.e., a mathematical approximation of the geoid) upon which the GNSS heights are referred, hence known as ellipsoidal heights. *Bottom* The geoid and reference ellipsoid (©ESA, figure modified by D. Rieser [24]). For practical use, these measured ellipsoidal heights have to be converted to orthometric (i.e., heights measured with respect to the geoid)

Unlike the traditionally used heights (orthometric heights), which are normally referred to MSL as a reference, GNSS heights are normally measured with respect to the reference ellipsoid. The shape of the geoid is complex, determined by the Earth's gravity field. Therefore, when using GNSS for vertical positioning, knowledge of the geoid-ellipsoid separation (i.e., $(h - H)$ in Fig. 5.18), is highly desirable, if not essential. For surveys over small areas (e.g., up to 10 km), it is often acceptable to use an approximation to the geoid. This method makes use of the fact that the geoid height does not vary that much over these distances.

In traditional surveying methods, the horizontal and vertical positions are determined separately. With GNSS positioning, however, both the vertical and horizontal positions are obtained from the same set of measurements. For instance, the position of point $P$ in Fig. 5.18 would be given by GNSS as $\{\phi, \lambda, h\}$. The height $h$ is, however, measured with respect to the reference ellipsoid. Of interest is the height with respect to the geoid, i.e., $H$. In this case, we have to subtract the geoid undulation from the measured ellipsoidal GNSS height $h$ to obtain the physical height $H$ above the MSL (geoid).

In Australia, for example, the AUSgeoid98 model developed by Featherstone et al. [25] gives this geoid undulation, and is incorporated in most commercial GNSS processing software. During post-processing of GNSS data in Australia, the measured GNSS ellipsoidal heights are converted to orthometric heights using AUSgeoid09, which is an updated version of Ausgeoid98 model. A new version of Ausgeoid09, i.e., Ausgeoid20 is planned for 2020.

### *5.6.2 Coordinate Systems*

A *coordinate system* is a set of rules that state the correspondence between coordinates and points; a *coordinate* is one of the set of the $N$ numbers individuating the location of a point in an $N$-dimensional space. A coordinate system is defined once a point of known *origin*, a set of $N$ lines, known as *axes*, all passing through the origin and having a well-known relationship to each other, and *a unit length* are established [26, p. 17]. A coordinate system is thus a set of rules that specify the locations (also called the coordinates of points), see e.g., Fig. 5.19 [4, p. 49]. Coordinate systems are normally:

- One-dimension (e.g., the 1D heights or sea level tide gauge readings); two-dimensions (e.g., the 2D position of points in Easting and Northing); or three-dimensions (e.g., the 3D position of points in latitude $\phi$, longitude $\lambda$, and height $h$). GNSS positioning will always give 3D coordinates of points either in geographical form $(\phi, \lambda, h)$ or Cartesian form $(X, Y, Z)$. Transformation between geographical and Cartesian are documented, e.g., in [23, 27].

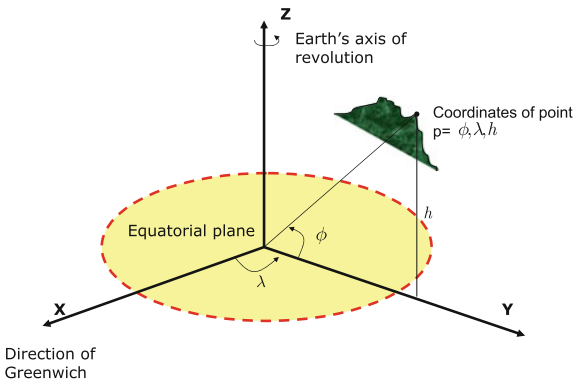


**Fig. 5.19** A coordinate system

- Refer to reference surfaces. Many countries have their own local reference surfaces (i.e., their own origins and axes parameters). For GNSS positioning, the reference surface is always an ellipsoid of revolution known as the World Geodetic System 84 (WGS-84).

A *reference system* is the conceptual idea of a particular coordinate system, whereas a *reference frame* is the practical realization of a reference system through observations and measurements (affected by errors), which means that a reference frame is a list of coordinates and velocities of stations (related to tectonic plate motion) placed in the area of interest, together with the estimated level of errors in those values [26, p. 18]. An example of a 3D geocentric coordinate system is the *Conventional Terrestrial Reference System (CTRS)* whose origin coincides with the center of the Earth. The $z$-axis points towards the conventional terrestrial reference pole (i.e., mean of the pole during the period 1900–1905), the $x$-axis points in the direction of the Greenwich meridian and the $y$-axis is perpendicular to the $x - z$-plane, thus completing a right-handed system (Fig. 5.19). To be of use, the CTRS must be positioned with respect to the Earth, a task often undertaken by assigning coordinates to selected points (stations) on the Earth's surface. The assignment of coordinates, i.e., realization, is often achieved using accurate geodetic techniques such as GNSS, VLBI and SLR.

*The International Terrestrial Reference Frame (ITRF)* is one of the CTRS commonly used and is realized through GPS and other geodetic measurements of globally distributed stations. It is maintained by the IERS (International Earth Rotation Service) under the auspices of the IAG (International Association of Geodesy) and is updated every 1–3 years to achieve the highest level of accuracy and, often refers to the particular time of updating, e.g., ITRF2005 as per 2005. This therefore means that ITRFs are dynamic in nature with the coordinates changing due to plate tectonic motions. They are only valid for a specific period (epoch) and incorporate velocity information to update other epochs.

The *WGS-84* established in 1984 is a 3D system that is used in an Earth-Centered Earth-fixed (ECEF) reference frame. It is defined as [26, p. 22]:

- Its origin is at the center of mass, the $Z$ axis points towards the direction of the International Earth Rotation Service (IERS) reference pole (IRP), which corresponds to the direction of the BIH (Bureau International de l'Heure) Conventional Terrestrial Pole (CTP) at the epoch 1984.0 with uncertainty of 0.005".
- The $X$ axis is defined by the intersection of the IERS reference meridian and the plane passing through the origin and normal to the $Z$ axis.
- The $Y$ axis completes a right-handed, ECEF orthogonal coordinate system.

The satellite positions sent via the navigation message discussed in Sect. 3.3.1, i.e., the broadcast ephemeris, are with respect to the WGS-84 system. Any user whose positions values are based on broadcast ephemeris will thus obtain the receiver's position in the WGS-84 system [4, p. 52]. The WGS-84 system was originally established using a number of Doppler stations and has since been updated to bring it to ITRF as close as possible [4, p. 49]. This has since seen the WGS-84 system evolve to being a dynamic system. If users work with the precise ephemeris obtained from the IGS (International GNSS Service), see e.g., [28], then their coordinates will be in the ITRF reference system.

Datum transformations are the conversion of coordinates from one form to another, i.e., WGS-84 to local systems. This is necessitated by the fact that old maps in most countries were done in local systems (e.g., separate horizontal and vertical datums). Normally, there exists transformation parameters that are used for these transformations, see e.g., Awange and Grafarend [23] and Awange and Palancz [29]. Most GNSS processing software have in-built transformation algorithms that undertakes this task.

### *5.6.3 Map Projection*

Finally, once the datum (ellipsoid of revolution) and the coordinate system for referencing the locations have been chosen, an appropriate mathematical method of transferring locations from the idealized Earth model to the chosen planar coordinate system must be chosen, a procedure known as *map projection*. Map projections are thus the representation of objects and information on a curved surface in a plane using mathematical and geometric relations (see Fig. 5.20). Detailed discussion on map projection can be found, e.g., in Grafarend and Krumm [30].

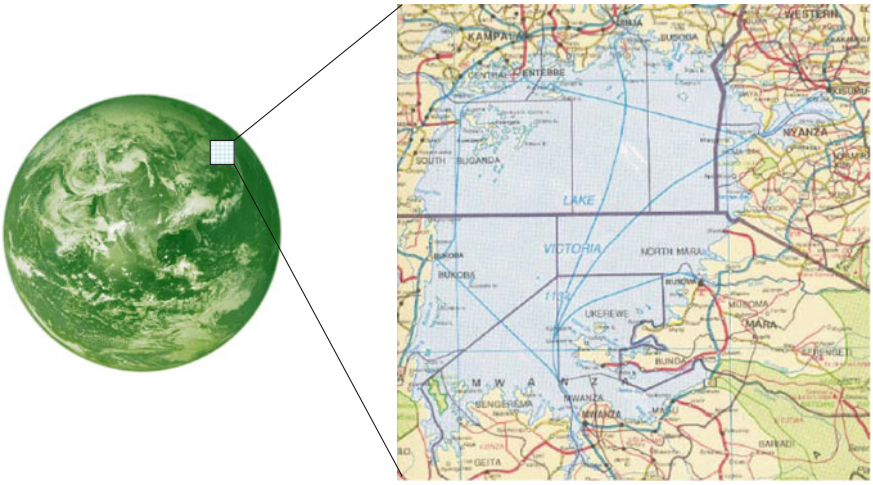


**Fig. 5.20** Map projection, i.e., representation of the information of a curved surface such as a sphere on a plane

## 5.7 Concluding Remarks

This chapter has presented some of the GNSS field techniques that are essential for measuring key indicators for environmental monitoring, e.g., the precise point positioning, which will likely benefit from increased satellites that will provide more orbital and clock products. Essentially, kinematic GNSS surveying refers to taking measurements while the receivers are 'on the move' and can be operated either in *single point positioning mode* or *continuous positioning mode*. In single point positioning mode the user holds the antenna stationary over a point for a set period of time, normally between 10 s and 5 min, depending on the satellite geometry and the number of satellites visible. Over baselines of less than 5 km, this mode will generally deliver coordinate accuracies similar to fast-static methods, although the antenna height errors are magnified due to the fact that the antenna is in motion and not fixed.

In continuous positioning mode, the user may move around an area of interest logging data at time intervals suitable for the needs of the survey. This mode is good for topographic mapping discussed in Chap. 8, boundary definition (e.g., Fig. 5.8), and other types of survey that may require rapid data collection within points surrounding a reference station. Over short baselines (<5 km), horizontal point accuracy is at the 1–3 cm level, depending on satellite geometry, number of satellites and the multipath environment. As with all GNSS observation techniques, height accuracy is slightly worse.

Kinematic data can be post-processed (e.g., post-processing kinematics; PPK) or have results given in real-time (real-time kinematic; RTK). PPK differs from RTK in the following ways:

- PPK surveys logs raw GNSS code and carrier-phase data on the hard disks at their base and roving receivers. For RTK, base stations do not log data, but the roving receivers log the *coordinates* of the points visited and receives data from reference station via communication link.
- A communication link is required for RTK systems between the reference station and rover receivers to transmit the raw phase data from the base to the rover, while for PPK, this is not required.
- Once the raw data has been received by the roving receivers in RTK, all data processing and analysis are done 'on board' whilst in the field, while PPK processing is performed back in the office using proprietary processing software.
- With a communications link comes additional hardware and firmware, which makes RTK systems more expensive compared to PPK systems.
- Post-processing in PPK enables the use of precise ephemeris from the IGS and the possibility of removing cycle slip errors, thereby giving more accurate results compared to RTK, which uses broadcast ephemeris.
- Advantages of RTK for environmental monitoring include rapid and efficient data collection that provide results in real-time.

In summary, real-time satellite positioning can be achieved at three levels of accuracy for navigation.

1. Low-accuracy, real-time positions are given by any stand-alone receiver.
2. DGPS uses telemetry of C/A-code pseudorange corrections to give improved 2–5 m-level positioning and 0.1 m/s velocity accuracies of the roving receiver. This is of use in applications such as airborne magnetic surveying or remote sensing. Real-time DGPS is robust due to its use of the unambiguous codes, which are not as susceptible to loss of satellite lock as the carrier-phases.
3. The highest accuracy real-time requirements, 10 cm positioning and 0.01 m/s velocity are offered by real-time pure kinematic relative GPS. Its applications include accurate marine and airborne navigation and precise hydrographic surveying. On land, detailed survey grids can be established in the field to better than 5 cm. This is an example of RTK, where the real-time capability requires only one visit to the field.
4. Kinematic surveys (Sect. 4.3.1) using carrier-phases can position the roving receiver with respect to the stationary reference receiver to better than 10 cm.
5. GPS positioning accuracy depending on position mode and measurement types used are listed below:

    - Kinematic point positioning (code) ~15–20 m.
    - Static (autonomous) point positioning (code) 5–15 m.
    - Kinematic relative positioning (DGPS) 3–5 m.
    - Kinematic relative positioning (carrier-phase) < 10 cm.
    - Static relative positioning (code) 0.5–1 m.
    - Static relative positioning (carrier-phase) mm-cm level.
    - RTK surveying 10 cm.
    - WADGPS has accuracy of about 7 m.

## References


1. Hofman-Wellenhof B, Lichtenegger H, Wasle E (2008) GNSS global navigation satellite system: GPS. GLONASS; Galileo and more, Springer, Wien
2. US Army Corps of Engineers (2007) NAVSTAR global positioning system surveying. Engineering and design manual, EM 1110-1-1003
3. Schofield W, Breach M (2007) Engineering surveying, 6th edn. Elsevier, Amsterdam
4. El-Rabbany A (2006) Introduction to GPS global positioning system, 2nd edn. Artech House, Boston
5. Hammond WC, Brooks BA, Bürgmann R, Heaton T, Jackson M, Lowry AR, Anandakrishnan S (2011) Scientific value of real-time global positioning system data. Eos 92(15):125–126. doi:10.1029/2011EO150001
6. Hammond WC, Brooks BA, Bürgmann R, Heaton T, Jackson M, Lowry AR, Anandakrishnan S (2010) The scientific value of high-rate, low-latency GPS data, a white paper. http://www.unavco.org/community_science/science_highlights/2010/realtimeGPSWhitePaper2010.pdf. Accessed 06 June 2011
7. Rizos C (2001) Alternatives to current GPS-RTK services and some implications for CORS infrastructure and operations. GPS Solut 11(3):151–158. doi:10.1007/s10291-007-0056-x
8. Gao Y (2006) Precise point positioning and its challenges. Inside GNSS, November/December issue, pp 16–18
9. Khodabandeh A, Teunissen PJG (2016) PPP-RTK and inter-system biases: the ISB look-up table as a means to support multi-system PPP-RTK. J Geod. doi:10.1007/s00190-016-0914-9
10. Snay R, Soler T (2008) Continuously operating reference station (CORS): History, applications, and future enhancements. J Surv Eng 134(4):95–104. doi:10.1061/(ASCE)0733-9453(2008)134:4(95)
11. Anderssohn J, Wetzel H, Walter TR, Motagh M, Djamour Y, Kaufmann H (2008) Land subsidence pattern controlled by old alpine basement faults in the Kashmar Valley, northeast Iran: results from InSAR and levelling. Geophys J Int 174:287–294. doi:10.1111/j.1365-246X.2008.03805.x
12. Maryam D, Zoej V, Javad M, Iman E, Ali M, Sassan S (2009) InSAR monitoring of progressive land subsidence in Neyshabour, northeast Iran. Geophys J Int 186(1):382. doi:10.1111/j.1365-246X.2009.04135.x
13. Motagh M, Djamour Y, Walter TR, Wetze H, Zschau J, Arabi S (2007) Land subsidence in Mashhad Valley, northeast Iran: results from InSAR, levelling and GPS. Geophys J Int 168:518–526. doi:10.1111/j.1365-246X.2006.03246.x
14. Stone W (2006) The evolution of the national geodetic survey's continuously operating reference station network and online positioning user service. http://www.ngs.noaa.gov/PUBS_LIB/Evolution_of_CORS_and_OPUS.pdf
15. Matsuzaka S (2006) GPS network experience in Japan and its usefulness. In: Seventeenth united nations regional cartographic conference for Asia and the Pacific. Geographical Survey Institute, 18–22 September 2006, Bangkok, Thailand
16. Westerhaus M, Welle W (2002) Environmental effects on tilt measurements at Merapi volcano. Bulletin d'Information des Maré's Terrestres 137:10917–10926
17. Sagiya T (2005) A decade of GEONET: 1994-2003 he continuous GPS observation in Japan and its impact on earthquake studies? Earth Planets Space (56): xxix–xli
18. SAPOS (2009) Satellitenpositionierungsdienst der deutschen Landesvermessung. http://www.sapos.de/. Accessed 16 May 2009
19. Wolfgang D (2005) Funktion und Nutzung des SAPOS - Deutschland-Netzes, Flächenmanagement und Bodenordnung (FuB). http://www.sapos.de/pdf/SAPOS_Deutschland_Netz_klein.pdf
20. Geoscience Australia (2009) Australian regional GPS network. http://www.ga.gov.au/geodesy/argn/. Accessed 16 May 2009
21. Wallace N (2007) CORS simulation for Australia. Curtin University of Technology, Final year project (unpublished)

22. Leick A (2004) GPS satellite surveying, 3rd edn. Wiley, New York
23. Awange JL, Grafarend EW (2005) Solving algebraic computational problems in geodesy and geoinformatics. Springer, Berlin
24. Rieser D (2008) Comparison of GRACE-derived monthly surface mass variations with rainfall data in Australia. MSc Thesis. Graz University of Technology
25. Featherstone WE, Kirby JF, Kearsley AHW, Gilliland JR, Johnston GM, Steed J (2001) The AUSGeoid98 geoid model of Australia: data treatment, computations and comparisons with GPS-levelling data. J. Geod. 75(5–6):313–330. doi:10.1007/s001900100177
26. Prasad R, Ruggieri M (2005) Applied satellite navigation using GPS. GALILEO and augmentation systems, Artech House, Boston
27. Awange JL, Grafarend EW, Paláncz B, Zaletnyik P (2010) Algebraic geodesy and geoinformatics, 2nd edn. Springer, Berlin
28. IGS (2009) International GNSS service http://igscb.jpl.nasa.gov/
29. Awange JL, Palancz B (2016) Geospatial algebraic computations. Springer, Berlin, Heidelberg
30. Grafarend EW, Krum FW (2006) Map projections - cartographic information systems. Springer, Berlin

# Chapter 6
# Data Processing and Adjustment

*Pauca des Matura –a few but ripe –*
C. F. Gauss

## 6.1 Introductory Remarks

In this chapter, the necessary data processing or post-processing following field measurements is presented. First, the general procedures undertaken to process baseline data are considered, followed by the adjustment of network observations. Network observations, as was illustrated in Fig. 5.8 on 70, play an important role in monitoring the spatial motion of the land surface, and as such, an understanding of their adjustment is essential. Besides showing how the observed GPS data are processed, the chapter also presents the basics of least squares solutions, which facilitates the adjustment of the observations, and looks at the quality assessment factors that need to be considered after an adjustment. In general, most commercial processing software will generate solutions once approximate positions of the occupied points, and observational data are available.

## 6.2 Processing of Observations

### *6.2.1 Data*

Satellite observations will be useless unless they can be properly processed in a form that can lead to some meaningful solutions relevant to environmental monitoring. Data processing generally proceeds in three steps (Fig. 6.1, left). The first step involves transferring the data from the GNSS receiver or data collection device to the computer for processing and archiving. Most commercial software are automated and have user interactive options for transferring the data. As we have already seen, there exist several types of GNSS receivers that can be used for data collection. With



J. Awange, *GNSS Environmental Sensing*, Environmental Science and Engineering, DOI 10.1007/978-3-319-58418-8_6

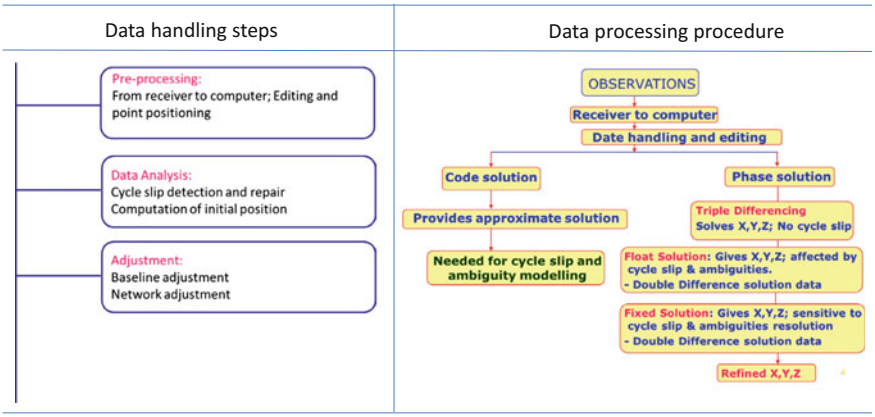


**Fig. 6.1** *Left* GNSS data handling steps. *Right* data processing steps

the full operational capability of additional GNSS satellites (see Chap. 2), there will certainly be more receivers on the market for civilian use. These receivers normally come with their own commercial vendor processing software. For example, Trimble receivers come with the Trimble Business Center (TBC) for processing the data.

Where multiple receivers of different types are employed in a GNSS campaign, data from all these receivers should first be converted into a format that can be understood independent of the source receiver. This format is the RINEX (Receiver INdependent EXchange Format), which can be automatically performed by most vendor software. For example, Trimble receivers will save GNSS data with an extension 'file.dat', while Sokkia receivers will save their data with an extension 'file.PDC', both of which are in binary, which must then be converted into RINEX format, an ASCII (American Standard Code for Information Interchange) type of data before processing. Once the data are in RINEX format, they can then be processed using any software.

Once the data has been transferred to a computer, the next step is preprocessing, which is dependent upon the type of the data collected, e.g., static, and the type of initialization (see Sect. 5.4.5). Preprocessing consists of editing the data to ensure data quality, and determining the ephemeris, where one has to choose between broadcast and precise ephemeris (see Sect. 3.4.1) when post-processing baseline carrier-phase observations. Autonomous hand-held receivers that use code measurements require no post-processing, since this is automatically recorded during field operations. Editing activities done include the identification and elimination of cycle slips, editing gaps in information, and checking station names and antenna heights. In addition, elevation mask angles should be set during this phase, along with options to select tropospheric and ionospheric models [1].

## 6.2.2 *Baseline Processing*

### 6.2.2.1 Cycle Slips: Detection and Repair

When collecting data by GNSS methods, cycle slip is said to occur when a receiver loses it's 'grip' or 'lock' on a satellite. Hoffman–Wellenhof [2] define cycle slip as a discontinuity or a jump in the GNSS carrier-phase measurement by an integer number of cycles caused by temporary loss of signal. Signal loss can occur as a result of one of the following factors:

- Obstruction from trees, buildings, etc.
- Low signal to noise ratio due to ionospheric effects, multipath or low GNSS satellite elevation.
- Software failure in the receiver.
- Severe ionospheric disturbances, radio interference, and high receiver dynamics.

Once cycle slip occur during a GNSS survey, the integer count has to be re-initialized by an equivalent "jump" Cycle. Cycle slips occur independently in L1 and L2 carriers. All observations thereafter have to be shifted by the same integer number of cycles.

During data processing, editing and correcting for cycle slip errors is one of the major tasks that has to be undertaken to achieve quality output. In general, the detection and correction of cycle slips becomes easy when using dual frequencies and differenced data in a static mode. This is due to the fact that dual frequencies provide the possibility of linear combinations that give residuals that can be analyzed to diagnose cycle slip errors. Short baselines are preferable as the effect of atmospheric errors (ionospheric) easily cancel, thus isolating cycle slip errors. When the data is post-processed, the detection becomes much easier as opposed to real-time positioning since cycle slips are always indicated by gaps in the data. Such gaps have to be deleted before the data is fully processed.

Cycle slips could also be detected and corrected using the Kalman Filtering approach [2]. Correction of cycle slips ensures that the observations to be used in baseline and network adjustments are free from signals gaps. Automated procedures for correcting cycle slips exist in commercial software.

### 6.2.2.2 Ambiguity Resolution

In Sect. 4.2, the concept of integer ambiguity was introduced (e.g., Fig. 4.1, p. 47). In this section, it is considered in more detail. When measuring pseudoranges using carrier-phases, when the receiver is first switched on, what is measured is the *carrier 'beat' phase*, which is the difference between the satellite-sent phase and the receiver-generated phase. The initial integer number of cycles between the satellite and receiver's antenna, i.e., the *integer cycle ambiguity* $N$, is not known. For each satellite-receiver observation, as long as the receiver maintains phase-lock to the

satellite during observations, there exist one integer ambiguity value. Its determination is essential to ensure high quality in the estimated parameters (e.g., positions, temperatures and pressures), which are required for high accuracy environmental tasks (e.g., monitoring sea level changes and global warming).

Generally, there are *three steps* to ambiguity resolution. From the *float solution* discussed in Sect. 6.2.3, potential integers values of $N$ are generated. This can be achieved if the coordinates of one station (i.e., the reference station) are known so as to give an approximate baseline length, or by differencing code- and phase-pseudorange equations. For static positioning, float solutions are used, whereas for the kinematic approach, code-pseudorange solutions can be adopted. Once the integer candidates of $N$ have been generated in the first step, the correct integer combinations are then selected in the second step such that the sum of the squares of the residual is a minimum. This is done by inserting the selected integers in the initial equations, and assessing in the third step whether the obtained residuals are the smallest. Approaches for ambiguity determination can generally be grouped into four types; geometrical approach, code-phase combinations, search approach, and a combination of these approaches. The most commonly used search method is known as the LAMBDA method developed by Teunissen [3]. For detailed discussion on these approaches, we refer to [4].

## *6.2.3 Solution Types*

### 6.2.3.1 Float and Fixed Solutions

Integer ambiguity $N$ resolution determines whether a *float* or *fixed* solution has been achieved during data processing (Fig. 6.2). A *float solution* is where the ambiguity is determined together with other unknowns $\{X, Y, Z, c\delta t\}$ (Eq. 6.17, p. 111) and is normally a *real number*. Because of this, the term *ambiguity free solution* is sometimes used. The estimated parameters will, however, be of a lower accuracy compared to those of the *fixed solution*, but at least better than those from triple differencing (e.g., Fig. 4.9 on p. 57). Ambiguity-free solutions are, however, useful for obtaining fixed solutions. The resultant solution (baseline vector) produced when differenced carrier-phase observations resolve the cycle ambiguity is thus called a "fixed" solution, with the exact cycle ambiguity no longer needed to be known to produce a solution [1]. In fixed solutions, also known as *ambiguity-fixed solutions*, the actual integer values are first determined, fixed, and then used in the adjustment (Eq. 6.17, p. 111). This leaves only the position parameters $\{X, Y, Z\}$ and the receiver clock bias term $c\delta t$ to be determined. Fixed solutions normally lead to more accurate position. However, when the cycle ambiguities cannot be resolved, which sometimes occurs when a baseline distance is greater than 75 km in length, a float solution may actually be the best option [1].

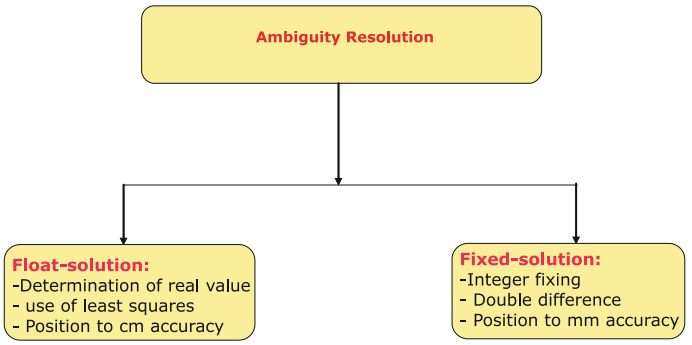


**Fig. 6.2** Float and fixed GNSS solutions

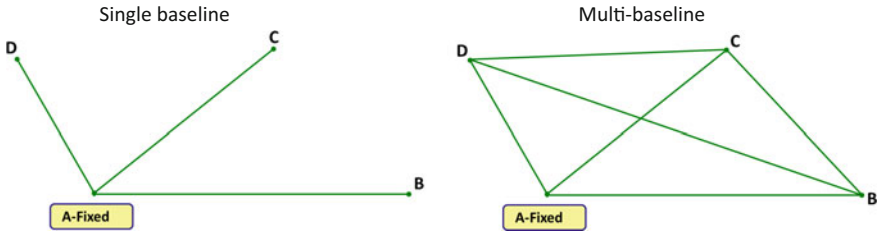


**Fig. 6.3** *Left* Single baseline. *Right* Multi-baselines. The coordinates of a station A are known and fixed, while those of B, C, and D are unknown

#### 6.2.3.2 Baseline Solutions

For single baselines (e.g., Fig. 6.3, left), the processing (see Fig. 6.1, left) deals with each baseline individually, or processes all baselines through a joint adjustment. The final results depends on how well the ambiguities and other errors are handled. Commercial baseline reduction software have a variety of options that are automatically (or manually) set to determine the most "optimum" solution where, after an initial code solution is performed, a triple differencing is carried out followed by a double differencing (e.g., Figs. 4.8 and 4.9 on p. 57) leading to a fixed solution in the event that the integer ambiguities are successfully resolved [1]. Correlations between the baselines are not necessarily taken into consideration except for network adjustment, where they provide weight information (see Sect. 6.2.5).

If $n$ GNSS satellites are observed, $n(n-1)/2$ baselines will be adjusted with the double-differencing offering the best solutions due to the fact that the integer nature of the ambiguities are preserved. Most commercial software offer baseline processing capabilities and normally provide different types of solutions, e.g., L1 Fixed (only the L1 signal is used to derive the solution), Ionospheric-Free Fixed (both the L1 and L2 signals are used to remove ionospheric errors (e.g. Sect. 3.4.3)), and float (see Sect. 6.2.3.1). In addition, the packages attempt to perform the most accurate fixed solution for short lines (e.g., less than 15 km for single-frequency and less than

30 km for dual-frequency receivers) [1]. As was discussed in Sect. 3.4, positioning accuracy will depend on how well the errors are managed. In general triple difference accuracies are less than those of fixed and float solutions.

For baselines longer than 30–50 km, if the fixed solution is not deemed to be reliable (based on various quality indicators discussed below), then the default float solution may be used. Although it is not as accurate as the fixed solution, if the session time is long enough (e.g., 1 to 2 h), it will still be fairly accurate, e.g., 20–50 mm for lines less than 75 km [1]. After the baseline solutions, users can then assess the reliability of the obtained solution from numerous statistical and graphical displays by the commercial software.

### *6.2.4 Quality Assessment*

The output of data processing from most commercial software will often consist of positions (whose accuracy is a function of the items in Fig. 6.4), covariances and residuals. Covariances are often provided in the dispersion matrix (Eq. 6.18), which enables the analysis of the quality of the estimated positions. The square roots of the diagonals of the dispersion matrices give the standard deviations (discussed below). The dispersion matrix can also be used to construct error ellipses useful for the analysis of the estimates (e.g., Fig. 6.5), and also to generate the dilution of precision. Commercial software have set criteria upon which they base any decision to reject bad observations or output. The software compare solutions from triple, float, fixed, single baseline and multi-baselines to obtain the most optimum solution. The

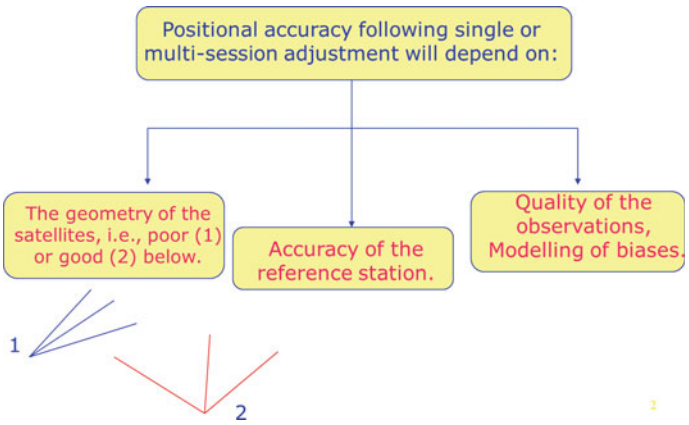


**Fig. 6.4** The accuracy of the derived values are dependent upon the geometry of the satellites, the accuracy of the position of the reference stations, the quality of the observations, and how well the errors have been managed. In this figure, for example, satellite geometry no. 2 is better than 1

following quality assessment factors are what various software base their acceptance criteria upon [1]:

- *Variance ratio*: A fixed solution indicates that the integer ambiguity has been successfully resolved. Most software will compute the variance of each integer ambiguity solution and compares the solution with the lowest variance to the next higher variance solution. The software then impose a minimum value of the ratio that must be exceeded, else the processor reverts to the float solution.
- *Reference variance*: Also known as the *variance of unit weight*, this value indicates how well the computed errors in the solution compare with the a priori values for a typical baseline. A value of 1.0 indicates a good solution. Values over 1.0 indicate that the observed data were worse. Baselines with higher reference variances and lower variance ratios need to be checked for possible problems (e.g., cycle slips discussed in Sect. 6.2.2.1).
- *Root-mean-square* (RMS): This is a quality factor that helps the user determine which vector solution (triple, float or fixed) to use in the adjustment and is usually stated at a 95% confidence level. It is dependent on baseline length, the time over which the baseline was observed, as well as ionospheric, tropospheric and multipath errors. A lower RMS may not always indicate a good result, but will provide a judgement on the quality of the data used in the post-processed baseline vector.
- *Repeatability*: Redundant lines should agree to a level of accuracy that GNSS is capable of measuring to. Residual plots depict the data quality of individual satellite signals and typically vary $\pm 5$ mm from the mean, with those exceeding $\pm 15$ mm being suspect. If the quality assessment above are not met, one may consider removing some or all of the baselines of a session, changing the elevation mask, removing one or more satellites solutions and/or, if necessary, re-observe the baseline.
- *Accuracy*: Indicates how close a measure or group of measures are from the "true" value.
- *Precision*: This is how close a group or sample of measurements are to each other or to their mean. A low standard deviation will indicate a high precision. Measurements can have high precision, but a low accuracy.
- *Standard deviation*: This is a range of how close the measured values are from the arithmetic average. It is obtained by taking the square root of the variance, and is sometimes known as the "standard error", though the two are slightly different. A lower standard deviation indicate that the observation measurements are close together.

### 6.2.5 Adjustment of GNSS Network Surveys

Network adjustment often follows baseline processing, which provide the covariance matrices used as weights in the adjustment. Where the correlations between

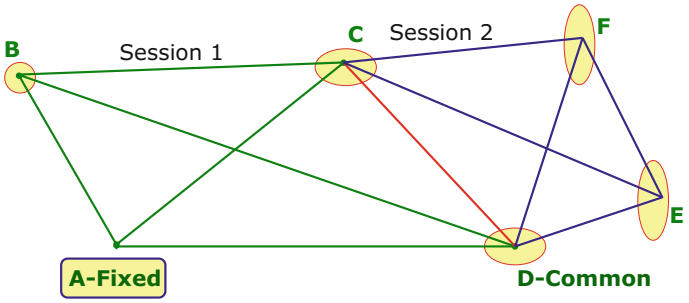


**Fig. 6.5** Accuracy control through error ellipses, where the smaller the ellipse the more accurate the solution. Stations near the control points have smaller ellipses. Session 1 entails observing network A, B, C and D, while session 2 entails network C, D, E, and F

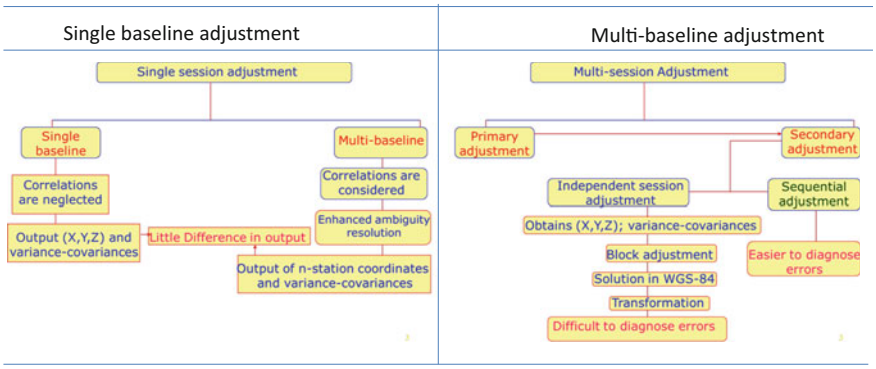


**Fig. 6.6** *Left* Single session solution. *Right* Multi-session solution. See, Fig. 6.5 for definition of a session

baselines are considered, processing is performed first using *primary*, and then *secondary* adjustments steps. The primary adjustment step consists of baseline processing, while the secondary adjustment step utilizes the raw baseline distances and variance-covariance information obtained from the primary adjustment to improve on the results. Processing can be done for a single session that comprises a single baseline where one station is fixed (i.e., the coordinates are known) while the coordinates of the other stations are unknown (Fig. 6.3, left), or multi-baselines where the baselines are interconnected (Fig. 6.3, right). Figure 6.6 provides a summary of single session processing.

In practise, it may happen for one reason or another that a session survey (e.g., A, B, C, and D in Fig. 6.5) is not completed, necessitating continuing the survey to C, D, E and F at another time. In this case, two sessions are involved and a multi-session processing is adopted. Both adjustment procedures are treated, e.g., in [5, 6]. Similarly to the single session adjustment, the positions obtained from the primary adjustment provide the weights used in the secondary adjustment. The only

exception is that the double differencing functional model used requires at least 1 common station between the sessions.

Two types of adjustment are presented in [1] as *free* and *constrained* (fixed) network adjustment. A *Free network adjustment* fixes one point and for this reason, is known also as *minimally constrained*. It is useful for assessing the internal accuracy of the observed network. If the fixed point is given arbitrary values and a GNSS loop survey is carried out with respect to it (i,e., starting from point A, through to B, C, D, and then back to A in Fig. 6.5), the sum of the vector parameters should be zero. Any misclose of the loop (i.e., the non-zero sum of vectors) will indicate internal reliability. A Free network, therefore, is vital for removing poor quality observations. *Constrained (fixed) adjustment* on its part fixes two or more points and assesses external reliability with respect to these external fixed (reference) control points (e.g., point A in Fig. 6.5). Care must be taken since these external control points also come with their own accuracies (i.e., they are not absolute-error free), which may be lower than those of GNSS. For adjustment, it is recommended first to process the baseline, then the free network adjustment and finally the constrained adjustment. Baseline data provides input data plus weights (from the standard deviations).

In undertaking GNSS surveys, it is advisable that they be adjusted and analyzed relative to their internal consistency and external fit with existing control points. The internal consistency adjustment (i.e., free or minimally constrained adjustment) is important from a contract compliance standpoint, while the final, or constrained, adjustment fits the GNSS survey to the existing network. This is not always easily accomplished since existing networks often have lower relative accuracies than the GNSS observations being fitted. An evaluation of a survey's adequacy should therefore not be based solely on the results of a constrained adjustment [1].

## 6.3 Least Squares Solution

In Chap. 4, various ways of modelling GNSS observations with the aim of eliminating or minimizing errors were discussed. Although systematic biases can be eliminated or corrected, random errors associated with observations normally remain and have to be taken care of through an adjustment procedure. Through such adjustment, coordinates and receiver clock parameters can be estimated. In this section, we present the basics of the "*least squares*" estimation method used in most commercial GNSS processing software.

In this chapter, the term estimation has been repeatedly used. But what exactly is estimation? In environmental monitoring, observations are normally collected with the aim of finding or measuring changes in some desired environmental parameters to assess specific tasks, e.g., compliance with a given legislation or policy, spatial or temporal changes, or predicting the environmental impact of a proposed project. If we take the case of surface displacement due to earthquakes for example, GNSS measurements would be undertaken with the aim of determining the extent of the surface movement. As was pointed out in Sect. 5.4.2, the desired environmental parameters

for monitoring spatial changes are the relative motion of positions ($\Delta X$, $\Delta Y$, $\Delta Z$) with respect to some fixed network of *controls* (reference) points established before the event of concern using the BACI (Before-After-Control-Impact) monitoring model (1-1 in p. 1). In general, these relative change in position would be the "*unknown parameters*" and the process of obtaining them through an adjustment criteria is known as the "*estimation of parameters*".

With improvement in instrumentation, more observations are often collected than the unknowns. For deformable surfaces being monitored, such as is the case in mining areas, or structures (e.g., bridges), several observation points will normally be marked on the surface of the body being monitored. These points would then be observed from a network of *control* points set up on a non-deformable stable surface (e.g. Fig. 5.8 on p. 70). Measurements taken between the control points and the points being monitored (see Sect. 5.4.2) will generally lead to an overdetermined system, i.e., more observations than unknowns, see e.g., [7–9].

The procedures that are often used to estimate the unknown parameters from the measured values will depend on the nature of the equations relating the observations to the unknowns. These equations are normally referred to as the "*functional model*". If these equations are linear, then the task is much simpler. In such cases, any procedure that can invert the normal equation matrix, such as least squares, would suffice. Procedures for estimating parameters in linear models have been documented, e.g., in [9–12]. If the equations relating the observations to the unknowns are nonlinear, they are first linearized and the unknown parameters estimated iteratively using the least squares method. The operation of these numerical methods require some approximate starting values. At each iteration step, the preceding estimated values of the unknowns are improved. The iteration steps are repeated until the difference between two consecutive estimates satisfy a specified threshold. Awange and Grafarend [7, 8] present algebraic-based procedures that avoid linearization and iteration in order to estimate the unknown parameters from nonlinear models. Linear and nonlinear models are treated in more detail e.g., in Grafarend and Awange [8, 9, 14].

**Method of Least Squares**

The least squares approach traces its roots to the work of *C.F. Gauss* (1777–855). Since GNSS operates by measuring the distances between the receiver and the satellites (as discussed in Sect. 3.3.2), let us consider a simple example where two distances $\{S_1, S_2\}$ are measured from an unknown station $P_0$ to two known stations $P_1$ and $P_2$ as shown in Fig. 6.7, (left). From these measured distances $\{S_1, S_2\}$ and the known positions $\{X_1, Y_1\}_{P_1}$ of station $P_1$ and $\{X_2, Y_2\}_{P_2}$ of station $P_2$, the position $\{X_0, Y_0\}_{P_0}$ of the unknown station $P_0$ can be obtained.

The nonlinear distance equations relating the measured distances to the coordinates of the unknown station are expressed as

$$\begin{bmatrix} S_1^2 = (X_1 - X_0)^2 + (Y_1 - Y_0)^2 \\ S_2^2 = (X_2 - X_0)^2 + (Y_2 - Y_0)^2, \end{bmatrix} \tag{6.1}$$

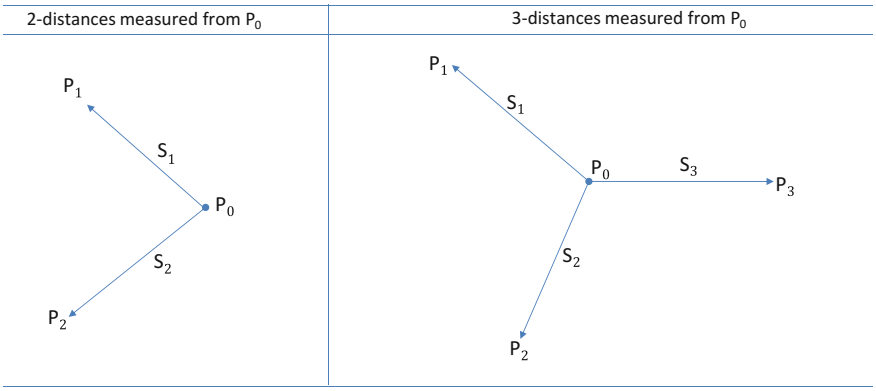


**Fig. 6.7** *Left* Distance measurements ($S_1$, $S_2$) to two known stations ($P_1$, $P_2$) from an unknown point $P_0$ whose position is to be determined. *Right* distance measurements to three known stations ($P_1$, $P_2$, $P_3$)

which leads to the two possible solutions presented in Fig. 6.8. Now, let us consider a case where a third station $P_3$, is also measured, as indicated in Fig. 6.7, (right). This gives rise to an overdetermined system of three equations with two unknowns, expressed as

$$\begin{bmatrix} S_1^2 = (X_1 - X_0)^2 + (Y_1 - Y_0)^2 \\ S_2^2 = (X_2 - X_0)^2 + (Y_2 - Y_0)^2 \\ S_3^2 = (X_3 - X_0)^2 + (Y_3 - Y_0)^2, \end{bmatrix} \tag{6.2}$$

which must be used to solve the unknown coordinates $X_0, Y_0$ of station $P_0$. In (6.2), we have more equations than unknowns, thus necessitating the need for least squares techniques. The equations have to be first linearized, otherwise one must use *nonlinear* methods, such as those presented in [7, 8, 14]. *Linear* models commonly used for parameter estimation are elaborately presented in [9, 11]. We will limit our discussion to the simple least squares model and refer interested readers who desire a more thorough coverage of parameter estimation methods to the works of [7–9, 11].

Least squares consist of *functional* and *stochastic* models, where a functional model, also known as the observation equations, can be viewed as an equation relating what has been measured (known) to what is to be estimated (unknown parameters). In the case of a stochastic model, the weight matrix $\mathbf{W}$ is related to the variance-covariance matrix $\mathbf{Q}$ of the observations (Eq. 6.3). The variance-covariance matrix shows the relationship between the observations and the unknown parameters. In general, the weight matrix is a measure of the random errors of the observations and arises from the fact that no observation can be error free. It is related to the variance-covariance matrix through

$$\mathbf{W} = \mathbf{Q}^{-1}. \tag{6.3}$$

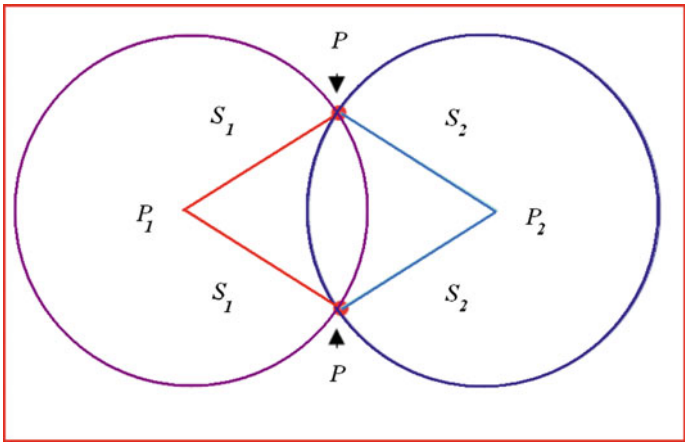


**Fig. 6.8** Exact solution of the distance problem described in Fig. 6.7. $P$ indicates the two possible solution points based on $S_1$, $S_2$ from two known stations $P_1$, $P_2$

The diagonal elements of the matrix **Q** are termed variances while the off diagonal elements are known as covariances.

In least squares terms, the equation

$$\mathbf{y} = \mathbf{A}\xi + \epsilon, \tag{6.4}$$

is a functional model relating the observation vector **y** to the vector of unknown parameters $\xi$, with $\epsilon = \mathbf{y} - \mathbf{A}\xi$ being the vector of discrepancies (or error vector). The vector **y** is comprised of the observations (measured quantities) or the differences between the measured values and those computed from the functional model part $\mathbf{A}\xi$. **A** is the design matrix which normally consists of the coefficients of the unknown terms. For linear terms, the matrix **A** are the direct coefficients.

Example 6.1 (Design Matrix **A**).

Consider two simultaneous equation given as

$$\begin{aligned} 2x + y &= 4 \\ 3x - 2y &= 6. \end{aligned} \tag{6.5}$$

In (6.5), the design matrix **A**, vector **y** of observation and vector $\xi$ of unknowns will therefore be

$$\mathbf{A} = \begin{bmatrix} 2 & 1 \\ 3 & -2 \end{bmatrix}, \ \mathbf{y} = \begin{bmatrix} 4 \\ 6 \end{bmatrix}, \ \xi = \begin{bmatrix} x \\ y \end{bmatrix}. \tag{6.6}$$

♣ End of Example 6.1.

In GNSS satellite observations, there exist two groups of parameters namely;

1. parameters related to the geometrical range $\varrho$, and
2. parameters related to biases, e.g., clock biases.

These are related by a functional model (pseudorange equation) described by Eq. (4.15) on p.49. Let us re-write the pseudorange equation (4.15) for a satellite 1 as

$$\boxed{F := \varrho^1 = \sqrt{(X^S - X_R)^2 + (Y^S - Y_R)^2 + (Z^S - Z_R)^2} + c\triangle t}, \tag{6.7}$$

where $X^S$, $Y^S$, $Z^S$ is the satellite's position and $X_R$, $Y_R$, $Z_R$ is the receiver's position. The receiver clock error term is designated $\Delta t$ and $c$ is the speed of light in a vacuum. All the other biases and errors that were discussed in Chap. 4 are assumed to have been modelled. In comparison to (6.5), (6.7) is nonlinear and cannot be expressed directly in the form (6.4) and therefore has to be linearized. This is achieved through the Taylor series expansion about approximate values of the unknown parameters. If the unknown receiver coordinates $X_R$, $Y_R$, $Z_R$ are approximated by $X_0$, $Y_0$, $Z_0$, such that

$$\left[\begin{array}{l} X_R = X_0 + \Delta X \\ Y_R = Y_0 + \Delta Y \\ Z_R = Z_0 + \Delta Z, \end{array}\right. \tag{6.8}$$

the Taylor series expansion of (6.7) about these approximate coordinates become

$$\begin{aligned} F := F(X_0, Y_0, Z_0) + \frac{\partial F(X_0, Y_0, Z_0)}{\partial X_0}\Delta X + \frac{\partial F(X_0, Y_0, Z_0)}{\partial Y_0}\Delta Y + \\ \frac{\partial F(X_0, Y_0, Z_0)}{\partial Z_0}\Delta Z, \end{aligned} \tag{6.9}$$

where higher order terms have been neglected. This leads to the linearized pseudorange equation (6.7) being written as

$$\varrho^1 = \varrho^0 + \frac{X_0 - X^S}{\varrho^0}\Delta X + \frac{Y_0 - Y^S}{\varrho^0}\Delta Y + \frac{Z_0 - Z^S}{\varrho^0}\Delta Z + c\Delta t, \tag{6.10}$$

with the partial derivatives being

$$\begin{bmatrix} \dfrac{\partial F_1}{\partial X_0} = \dfrac{X_0 - X^S}{\sqrt{(X_0 - X^S)^2 + (Y_0 - Y^S)^2 + (Z_0 - Z^S)^2}} = \dfrac{X_0 - X^S}{\varrho^0} \\ \dfrac{\partial F_1}{\partial Y_0} = \dfrac{Y_0 - Y^S}{\varrho^0} \\ \dfrac{\partial F_1}{\partial Z_0} = \dfrac{Z_0 - Z^S}{\varrho^0} \\ \dfrac{\partial F_1}{\partial c\triangle t} = 1. \end{bmatrix} \tag{6.11}$$

In order to express this equation in the functional model form (6.4), the design matrix **A**, vector **y** of observation for $n$ satellites observed by a receiver, and the vector $\xi$ of the unknowns are expressed as:

$$\mathbf{A} = \begin{bmatrix} \dfrac{\partial F_1}{\partial X_R} & \dfrac{\partial F_1}{\partial Y_R} & \dfrac{\partial F_1}{\partial Z_R} & 1 \\ \dfrac{\partial F_2}{\partial X_R} & \dfrac{\partial F_2}{\partial Y_R} & \dfrac{\partial F_2}{\partial Z_R} & 1 \\ . & . & . & . \\ \dfrac{\partial F_n}{\partial X_R} & \dfrac{\partial F_n}{\partial Y_R} & \dfrac{\partial F_n}{\partial Z_R} & 1 \end{bmatrix}, \quad \mathbf{y} = \begin{bmatrix} \varrho^1 - \varrho^{01} \\ \varrho^2 - \varrho^{02} \\ . \\ \varrho^3 - \varrho^{0n} \end{bmatrix}, \quad \xi = \begin{bmatrix} \Delta X_R \\ \Delta Y_R \\ \Delta Z_R \\ c\Delta t \end{bmatrix}, \tag{6.12}$$

where the values of **y** are pseudorange differences (measured-computed) using approximate coordinates. Exact solutions of (6.7) are presented e.g., in Awange and Grafarend [7, 8, 14, 15].

The requirement of least squares solution is simply that the sum of the squares of errors $\epsilon = \mathbf{y} - \mathbf{A}\xi$ be minimized through

$$\varepsilon^T \epsilon \rightarrow min. \tag{6.13}$$

If we now incorporate the weights **W** of the observations from the stochastic model, (6.13) becomes

$$\epsilon^T \mathbf{W} \epsilon \rightarrow min. \tag{6.14}$$

The minimum requirement in (6.14) is subject to the functional model (6.4).

Rewriting (6.4) as

$$\epsilon = \mathbf{y} - \mathbf{A}\xi, \tag{6.15}$$

and inserting it in (6.14) leads to

$$f := \epsilon^T \mathbf{W} \epsilon = (\mathbf{y} - \mathbf{A}\xi)^T \mathbf{W} (\mathbf{y} - \mathbf{A}\xi) \rightarrow min. \tag{6.16}$$

In the expansion of (6.16), setting the condition $\frac{df}{dx} = 0$ leads to the solution of unknown vector $\xi$ in (6.12) as

$$\hat{\xi} = (\mathbf{A}^T\mathbf{W}\mathbf{A})^{-1}(\mathbf{A}^T\mathbf{W}\mathbf{y}), \tag{6.17}$$

with a variance-covariance matrix of the estimated parameters (receiver coordinates and clock parameter) given by

$$\mathbf{Q}_{\hat{\mathbf{x}}} = (\mathbf{A}^T\mathbf{W}\mathbf{A})^{-1} = \begin{bmatrix} \sigma_x^2 & \sigma_{xY} & \sigma_{xZ} & \sigma_{xct} \\ \sigma_{yx} & \sigma_y^2 & \sigma_{yZ} & \sigma_{yct} \\ \sigma_{zx} & \sigma_{zy} & \sigma_z^2 & \sigma_{zct} \\ \sigma_{ctx} & \sigma_{cty} & \sigma_{ctz} & \sigma_{ct}^2 \end{bmatrix}. \tag{6.18}$$

The square root of the diagonal matrix in (6.18) gives the standard deviations of the estimated parameters in (6.17). Equations (6.17) and (6.18) are the ones mainly used in GNSS processing software to generate the final products. For more details, the reader is referred to [4, 16].

## 6.4 Online Processing

Several internet based GNSS processing software systems are freely available to users to process their baselines online. In Australia for example, AUSPOS (Australian online GPS processing service) enables users to send their data to a central processing unit at Geoscience Australia via the Internet [17]. The processing software thereafter, chooses three or more CORS stations that are near the user's observing station and employs them to process the user's position. The results are then send back to the user via email. In the US, the OPUS (Online Positioning User Service) has performed similar functions as AUSPOS since March 2001 [18].

The Australian Surveying and Land Information Group (AUSLIG), which is now part of Geoscience Australia, is Australia's national mapping agency, providing fundamental geographic information to support the mining, agricultural, transport, tourism, and communications industries, as well as defence, education, surveillance and emergency services activities [19]. OPUS is a US-based service that provides baseline reduction and position adjustment relative to three nearby national CORS reference stations. It is ideal for establishing accurate horizontal control relative to the National Geodetic Reference System (NGRS), and can also be used as a quality control check on previously established control points [1].

To use such services, for a single GNSS receiver, an AUSPOS user for example needs to upload the dual-frequency static data in RINEX format (see discussion in Sect. 6.2.1) as well as the antenna type and height information to a web site which processes the data using the service provider's software (e.g., Fig. 6.9). The antenna type should be as defined by the International GNSS Service (IGS) and the input

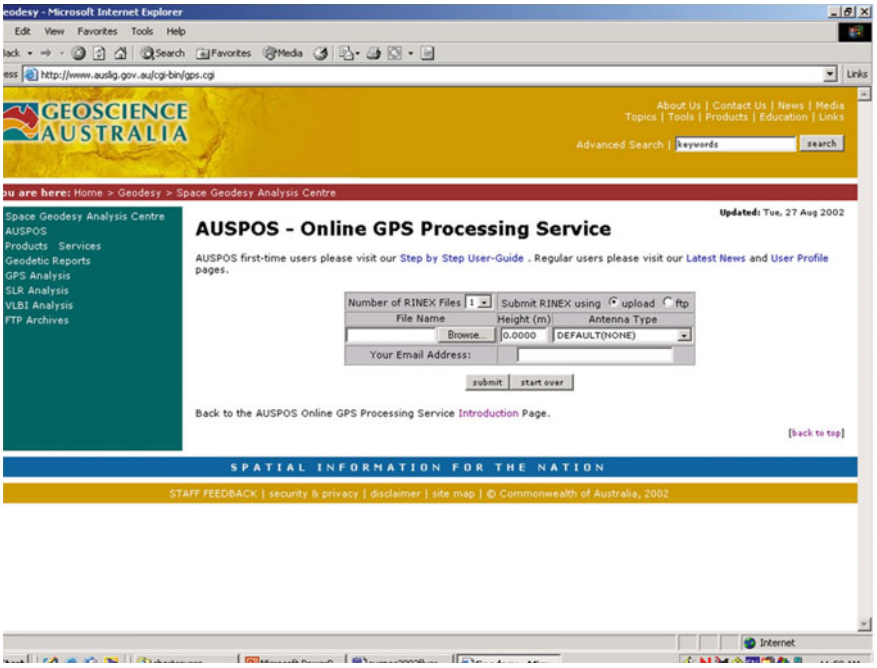


**Fig. 6.9** AUSPOS - online GPS processing service. *Source* Geoscience Australia

antenna heights should be with respect to the IGS defined Antenna Reference Point (ARP).

Once the data is received by the AUSPOS system, the format is checked, an approximate user position computed from the submitted RINEX file, and data files from the three or more nearest IGS stations acquired. The best available IGS ephemeris and earth rotation parameters (ERPs) are then acquired, dependent upon the observation latency. The international terrestrial reference frame (ITRF) coordinates are then computed for the selected IGS stations at the observational epoch. The user station plus the three or more selected IGS stations thus form a network of 4 stations that is adjusted through a network adjustment procedure. Cycle slips from the user data are removed by double differencing the carrier-phase data for each baseline. In the network adjustment, a constrained framework (see Sect. 6.2.5) is adopted where the three or more IGS stations are held fixed to ITRF coordinates. When the processing is completed, a pdf file is generated and emailed to the user.

Similarly to AUSPOS, OPUS computes an average solution from the three baselines and the output positions are provided with an overall RMS (95%) confidence level, along with the maximum coordinate spreads between the three CORS stations for both the ITRF and North American Datum (NAD) 83 positions [1]. However, OPUS users need to enter at least two hours of static, dual-frequency GNSS observation.

## 6.5 Concluding Remarks

This chapter has simply presented some of the aspects of data processing. For detailed exposition, we refer the reader to [1, 2, 7–9, 13, 14, 16], as well as, the various user manuals for the assorted instruments.

## References


1. US Army Corps of Engineers (2007) NAVSTAR global positioning system surveying. Engineering and design manual, EM 1110-1-1003
2. Hofman-Wellenhof B, Lichtenegger H, Wasle E (2008) GNSS global navigation satellite system: GPS. GLONASS; Galileo and more, Springer, Wien
3. Teunissen PJG, PJ de Jonge, Tiberius CCJM (1995) The LAMBDA method for fast GPS surveying. In Proceedings of International Symposium 'GPS technology applications', Bucharest, Romania, September 26–29, pp 203-210
4. Hofman-Wellenhof B, Lichtenegger H, Collins J (2001) Global positioning system: theory and practice, 5th edn. Springer, Wien
5. Craymer MR, Beck N (1992) Session versus single-baseline GPS processing. In Proceedings of the 5th international technical meeting of the satellite division of the US Institute of Navigation, Sept .16–18,1992, 995–1004
6. Han S, Rizos C (1995) Selection and scaling of simultaneous baselines for GPS network adjustment, or correct procedures for processing trivial baselines. Geomat Res Australas 63:51–66
7. Awange JL, Grafarend EW (2005) Solving algebraic computational problems in geodesy and geoinformatics. Springer, Berlin
8. Awange JL, Grafarend EW, Paláncz B, Zaletnyik P (2010) Algebraic geodesy and geoinformatics, 2nd edn. Springer, Berlin
9. Grafarend EW, Awange JL (2012) Linear and nonlinear models - fixed effects, random effects, and total least squares. Springer, Berlin
10. Heck B (1987) Rechenverfahren und Auswertemodelle der Landesvermessung. Wichmann Verlag, Karlsruhe, Germany
11. Koch KR (1999) Parameter estimation and hypothesis testing in linear models. Springer, Berlin
12. Press WH, Teukolsky SA, Vetterling WT, Flannery BP (1992) Numerical recipes in Fortran 77: The art of scientific computing, 2nd edn. Cambridge University Press
13. Awange J, Paláncz B, Lewis R, Völgyesi L (2018) Mathematical geosciences. Hybrid symbolic-numeric methods. Springer International Publishing
14. Awange JL, Bela Palancz (2016) Geospatial algebraic computations. Theory and application, Springer, Berlin
15. Awange JL, Grafarend EW (2002) Algebraic solution of GPS pseudo-ranging equations. J GPS Solut 4:20–32
16. Leick A (2004) GPS satellite surveying, 3rd edn. John Wiley & Sons, New York
17. AUSPOS (2006) Australian online GPS processing service. http://www.ga.gov.au/bin/gps.pl. Accessed on 14 May 2009
18. National Geodetic Survey (2006) Guidelines for new and existing continuously operating reference stations (CORS). Silver Spring, MD, NOAA
19. Dawson J, Govind R, Manning J (2010) The AUSLIG online gps processing system (AUSPOS). http://www.ga.gov.au/image_cache/GA5057.pdf or http://www.ga.gov.au/geodesy/sgc/wwwgps/auspos_system_summary.jsp. Accessed 8 Oct 2010

# Chapter 7
# Basics of Galileo Satellites

*Europe early recognized the strategic, economic, social, and technological importance of satellite-based navigation. In 1999, they contributed to satellite navigation through Galileo, a satellite system named after the Scientist and Astronomer, Galileo Galilei.* Wellenhof et al. [1, p. 366] *With the Declaration of Galileo Initial Services, Galileo officially moves from a testing phase to the provision of live services. For the first time ever, users around the world can be guided using the positioning, navigation and timing information provided by Galileos global satellite constellation.*

## 7.1 Introductory Remarks

Since their inception,[1] GPS satellites have been the primary GNSS (see Chap. 2), and in doing so, have attracted global usage. The Russian GLONASS has to a lesser extent been used, but it has faced maintenance problems and as such, has not been able to compete effectively with GPS. Both systems, however, have one thing in common, and that is, they are controlled by the military of their respective countries. Users from other countries have been at the mercies of the two providers and therefore do not have autonomous control or a say in the *integrity* of the systems. Integrity is the capability of a system to provide a timely alert to the user when it fails to meet the thresholds of accuracy for which it is designed. Similar to the two satellite providers above, the Chinese BeiDou is also to a large extent designed for military purposes.

Realizing the value of GNSS and the importance of autonomous control and integrity issues, plans to have a GNSS under European civilian control were initiated as early as the 1990 s and announced in May 2003. For the first time, the world was going to have a civilian-operated system, whose design was based on the users' needs. Hence, future civil navigation and other applications would no longer be dependant

[1] https://www.gsa.europa.eu/galileo/services/initial-services.



J. Awange, *GNSS Environmental Sensing*, Environmental Science and Engineering, DOI 10.1007/978-3-319-58418-8_7

on the military controlled GPS and GLONASS system. A joint venture between the European Commission (EU) and the European Space Agency (ESA) adopted a two-way approach towards realizing a European autonomy in global satellite navigation, e.g., EC and ESA [2]. This Chapter therefore gives this first civilian-owned GNSS a more in-depth coverage.

*First*, the European Geostationary Navigation Overlay Service (EGNOS), a satellite-based augmentation system SBAS (see e.g., Sect. 5.4.4.2), was developed by the European Space Agency (ESA) under a tripartite agreement between the EC, the European Organization for the Safety of Air Navigation (Eurocontrol) and ESA to augment the existing satellite missions of GPS and GLONASS with the aim of complementing them. EGNOS is made up of three geostationary satellites and a network of more than forty elements all over Europe that collect, record, correct and improve data from GPS and GLONASS satellites. The modified signals are then relayed via the geostationary satellites to users' receivers, offering a positional accuracy of better than 2 m, compared to the 15 – 20 m for a stand alone GPS.

In addition, EGNOS gives a guarantee of quality for these signals that GPS does not provide [3]. EGNOS entered its pre-operational phase in 2006 and by October 2009, the open service (e.g., personal navigation, goods tracking and precision farming) where human lifes are not at risk become available.[2] On 2/3/2011, the European Satellite Service Provider (ESSP) declared the safety-of-life (SoL) signal officially available for aviation (guiding aircrafts on landing). Its coverage area includes all European states and extend to include other regions, e.g., South America, Africa, and parts of Asia and Australia, within the coverage of the three geostationary satellites being used. EGNOS is used foremost for safety-critical transport applications, e.g., in the aviation and maritime sectors. Environmental monitoring tasks requiring m-level accuracy such as monitoring changes in perimeters and areas of wetlands are potential areas of applications of the system.

*Second*, Europe has ventured towards the development of a state-of-the-art global navigation satellite system that will provide highly accurate global positioning services to users, but which unlike GPS, will be purely under civilian control. From its conception, Europe did not intend to compete with established systems such as GPS and GLONASS, but rather, have a system under its complete control that would enhance inter-operability with GPS, GLONASS and other GNSS systems discussed in Chap. 2. As such, the system is envisioned where a user with a GNSS receiver will be able to receive either GPS, GLONASS, Galileo, BeiDou or a combination of all signals, thereby improving positional accuracy (Sect. 5.3).

The name *Galileo* was chosen in honour of the famous Italian scientist and astronomer Galileo Galilei (1564–1642) who discovered four satellites of the planet Jupiter and described how the regular movement of the four satellites could be used for longitude determination by observing their eclipses [1, p. 366]. The Galileo satellite implementation went through four phases: *definition*, *development and in-orbit validation*, *deployment*, and *operational*. The system is anticipated to become fully

[2] http://www.esa.int/Our_Activities/Navigation/The_story_so_far.

operational by 2020 with the complete deployment of the 30 satellites (24 operational and 6 spares) in orbit. As per January 2017, 18 of the 30 satellites had been deployed.

## 7.2 Galileo Design and Operation

Unlike the GPS system, which is comprised of a *space segment*, *control segment*, and *user segment*, the Galileo system is divided into four principle components: the *global component*, the *regional component*, the *local component*, and the user component, remembering that it is the user's needs that dictates the design of the system. The global component forms the main element of the system and is subdivided into *space* and *ground* components. The regional component consists of a network of integrity monitoring stations and an integrity control center, which determines regionally valid integrity information and directly sends this information to the Galileo satellites via a dedicated and secured channel. The local component enhances the Galileo global service by providing locally assisted services that increase navigation performance in order to meet special application requirements, see e.g., [1, pp. 373–374].

So far, the definition phase of Galileo, which included a cost benefit analysis, was completed and the main issues documented in EU and ESA reports [4]. The development and in-orbit phase that entailed the detailed design, manufacture and testing of the system components leading to the validation of Galileo satellite system is also complete. Two prototype test satellites Galileo In-Orbit Validation Element - GIOVE A and GIOVE B were launched in 2006 and 2008, respectively, and transmitted signals that were analyzed to validate the performance of the system in space with regards to whether the signals met the predefined specifications. With the system successfully undergoing validation, the deployment phase gradually involved deploying the space segment and ensuring the full deployment of the ground-based infrastructure on 21/10/2011, with two more on 12/10/2012. The operations phase will then cover the operation of the system (ground facilities and satellites) and the replenishment of satellites for an indefinite period [4]. On 15th December 2016, the EU announced the start of Galileo Initial Service, the first step towards full operational capacity expected in 2019. The complete deployment of the 30 satellites is expected in 2020.[3]

### *7.2.1 User Component*

The Galileo users range from public, private, and commercial sectors to governments. These users can choose the services they want and as such the Galileo receivers designed and built during the development phase are slightly different from those of GPS. Galileo receivers have different capabilities of using the Galileo signals

[3] http://www.esa.int/Our_Activities/Navigation/Galileo_begins_serving_the_globe.

to satisfy various user needs. The EU and ESA [4] have suggested that in order to fully benefit from all of the Galileo services (global, local, combined), users must be equipped with adequate multi-functional terminals capable of receiving directly the Galileo signal, having access to the services provided by the regional and local components, and being inter-operable with other GNSS systems.

In general, four navigation services and one service to support search and rescue (SAR) operations were identified in the definition phase as offering the widest range of coverage of users' needs, see, e.g., [4]. These are:

- *Open service* (OS), freely provided to users, are similar to the normal operations of GPS. Users will receive unrestricted signals which they could use to derive positions, velocities and timing information. With a single frequency, open service will provide horizontal positions to an accuracy of 15 m and vertical positions to an accuracy of 35 m, similar to what is achieved by autonomous (stand alone) GPS without selective availability.[4] If dual frequencies are used, then the horizontal and vertical positioning accuracies are expected to be 4 and 8 m, respectively.
- *Safety-of-life (SoL) service*, which adds the integrity component to the services provided by the open service, thereby providing timely warnings to users in case of system failure to meet certain margins of accuracy. Its three frequencies will achieve horizontal and vertical positioning accuracies of 4 and 8 m, respectively. Users of safety-of-life will include safety critical users such as maritime, aviation, and train services, whose applications or operations require stringent performance levels [4].
- *Commercial service* (CS) will enable users to have access to two additional signals that will facilitate higher data transmission (i.e., 500 bps) and an improvement in accuracy. The two signals will facilitate advanced applications such as the integration of Galileo positioning applications with wireless communications networks, high accuracy positioning, and indoor navigation [4].
- *Public regulated service* (PRS) will provide position and timing information to specific users requiring a high continuity of service, with controlled access. Its dual frequencies will achieve horizontal and vertical positioning accuracies of 4 and 8 m, respectively. Two PRS navigation signals will be encrypted to protect against threats to Galileo signals by economic terrorists, malcontents, subversives or hostile agencies as opposed to the open services (OS, CS and SoL) through the use of appropriate interference mitigation technologies [4]. According to EU and ESA [4], the objective of the PRS is to improve the probability of continuous availability of the signal, in the presence of interfering threats, to those users with needs such as law enforcement (EUROPOL, Customs, European Anti-Fraud Office - OLAF), security services (Maritime Safety Agency) or emergency services (peace keeping forces or humanitarian interventions), and intelligence services.
- Search and rescue (SAR) will receive distress signals and broadcast them to the alert stations globally, thereby assisting in humanitarian search and rescue activities.

[4] Selective availability was switched off in 2000.

Galileo receivers therefore are designed and developed in such a manner that they meet the requirement of a wide range of users. Galileo high level definition specifies that the receiver will have three main functions. The *first* function will constitute the baseline activity or receiving the signals for open service. The other two functions will be optional and depend on application needs, e.g., commercial or SAR.

### *7.2.2 Global Component*

**Space Segment**

When fully operational, the Galileo space segment is envisaged to be comprised of a constellation of 30 (24 operational plus 6 active spare) satellites at an altitude of 23,222 km arranged in 3 near-circular Medium Earth Orbit (MEO) planes inclined at 56° to the Earth's equatorial plane. Eight operational satellites equally distributed at 40°, plus two spare satellite (also transmitting) will occupy each orbital plane with an orbital period of about 14 h, guaranteeing a visibility of at least four satellites anywhere on Earth approximately 90% of the time.[5] This space design is expected to provide continual satellite availability to enable single point instantaneous positioning in all but the highest latitudes (> 75degrees). The satellites are expected to transmit 10 signals (see Sect. 7.3). Similarly to GPS satellites, each Galileo satellite will broadcast precise *time signals*, *clock synchronization*, *orbit ephemeris* and *other data*. The constellation is further expected to provide better coverage at high latitudes than GPS, which is one of the intentions of the system, since GPS coverage is not particularly good over northern Europe.

**Ground Segment**

Galileo ground segment differs from the GPS system owing to the user specification design discussed in Sect. 7.2.1. The high level definition envisaged the basic functions of the ground segment to be the control of satellites (i.e., constellation) and the mission (i.e., navigation and integrity issues). The ground segment will be comprised of the following [4]:

(i) *Control center*, which includes all control and processing facilities responsible for the determination of satellite orbits and time synchronization, determination of global satellite integrity, maintenance of Galileo system time, monitoring and controlling of the satellites and their services, and various off-line maintenance tasks. Galileo control centres (GCC) are located in Fucino (Italy) and Oberpfaffenhofen (Germany).

(ii) *Galileo sensor stations*, which will collect navigation data from the Galileo satellites, meteorological and other required environmental information and transmits the information to the control center for processing.

[5] http://www.esa.int/Our_Activities/Navigation/Galileo/Galileo_a_constellation_of_navigation_satellites.

(iii) *Galileo up-link stations*, that will transmit the processed information to the Galileo satellites.
(iv) A global network of *mission uplink stations* installed at five sites to support the communication between Galileo mission segment (GMS) and Galileo satellites.
(v) Global area network, to provide a communication network linking all system elements around the world.

### *7.2.3 Regional Component*

The main task of the regional component is the provision of a regionally-based network consisting of ground segments dedicated to Galileo integrity determination and the dissemination of the same to the ground stations for up-linking to the satellites. Another part of the regional component is the search and rescue (SAR) systems made up of the user segment responsible for transmitting distress calls, the space segment that detects this distress call and then broadcast them globally, and the ground segment that receives and processes the alert signals transmitted from the space segment. The processed information is finally validated by the mission control centers before being dispatched to rescue services.

### *7.2.4 Local Component*

Galileo local component is made up of local elements and is responsible for enhancing the system performance and enabling the possibility of combining Galileo with other GNSS and terrestrial based positioning and communication systems on a local basis. Areas of enhancement envisaged for the local component are a local precision navigation element expected to provide local differential corrections (see Sect. 4.3.2) to improve positioning accuracy and also enhance the quality of integrity information, a local high precision navigation element which will incorporate ambiguity resolution and provide further improvements in accuracy, locally assisted navigation elements that will assist users in positioning in difficult environments, and local augmented-availability navigation elements that will supplement Galileo satellites by providing pseudolite transmissions that mimic the Galileo satellites and provide signals that have not been corrupted by the atmosphere, as occurs with the Galileo signals. The advantage of these local elements, as outlined by the EU and ESA, is [4]:

With local elements being globally proliferated, the potential will also exist to use the quality of the received SIS (signal-in-space) at the local elements to aid in the identification and isolation of interference sources to the Galileo SIS. This additional functionality could be of great benefit to Galileo and indeed GNSS, as the SIS are very weak and as such are particularly susceptible to many forms of interference that at best degrade performance and at worst completely deny it, and as such deserves further investigation.

## 7.3 Galileo Signals

According to the high level definition, Galileo satellites are expected to transmit signals in the frequency ranges of 1164–1215, 1215–1300 and 1559–1592 MHz in the radio navigation satellite services allocated frequency bands. *Four signals* are anticipated in the 1164–1215 MHz range, i.e., a pair of E5A transmitting at 1176.450 MHz and another pair of E5B transmitting at 1207.140 MHz. For each pair, one signal will contain a navigation message while the other will be a dataless signal mainly for tracking purposes. Both E5A and E5B will enable correcting for effects such as ionospheric influence, thereby enhancing the positioning accuracies. These signals will be freely available to users, similar to the C/A-code for GPS signals (see Sect. 3.3.1).

In the range 1215–1300 MHz (E6), *three signals* are expected to be used. One signal will be controlled through government approved encryption and is specifically designed for government applications that need continuity of service even during a crisis period. The other pair of signals is protected through commercial encryption and is designed for commercial use with a high capability for resolving ambiguity to deliver more accurate positions. For this pair, one signal contains navigation data that can be transmitted at a higher rate of 500 bps while the other signal is a dataless, again signal mainly for tracking purposes.

Finally, three signals are anticipated in the last range of 1559–1592 MHz (E2-L1-E1). One signal will be controlled through government approved encryption and is specifically designed for government applications that again need continuity of service during crises. This signal will be more flexible than the one for E6 mentioned above. The remaining pair will have one signal loaded with navigation messages that will support integrity and search-and-rescue, while the remaining signal, again will be without data to increase tracking.

In total, 10 signals will be transmitted with each navigation signal being made up of a ranging code and data. As pointed out above, three types of ranging codes can be distinguished for Galileo, i.e., the open access ranging codes (e.g., E5A, E5B), government restricted codes (e.g., single signal of E6) and commercial control code (e.g., the pair signal of E6). There are five types of data; *basic navigation data*, *integrity data*, *commercial data*, *PRS data*, and *SAR data*. These data are either open access data (navigation data, integrity data, search and rescue - SAR data) or protected data (commercial data using commercial encryption, public regulated services (PRS) data using governmental encryption) [4].

## 7.4 Concluding Remarks

This chapter has presented Galileo satellites in a nutshell. The design and development phase and the validation of test-satellites GIOVE-A and GIOVE-B are complete. The deployment stage is currently (2017) underway with 18 satellites already launched and 12 remaining to complete the anticipated 30 satellites. One main distinction that separates Galileo from other GNSS satellites is its being the first civilian owned and operated GNSS in the world, with the added advantage of integrity monitoring. Users will therefore be alerted in the shortest possible time in case of system failure, information which will benefit applications where safety is crucial, e.g., running trains, guiding cars and landing aircraft. Its provision of dual frequencies that will be accessible to users free of charge will greatly improve positioning accuracies, what has now been addressed in GPS satellites through the introduction of the new civilian code L2C.

Environmental monitoring applications will especially benefit from the wide range of choices offered by the Galileo system. For the case of land management, for example, precise farming will benefit from the commercial service that will provide differential corrections for local areas. Improved land management is an essential component of environmental conservation and management (see, e.g., Chap. 16) and Galileo will definitely play a leading role in this venture. Other environmental monitoring activities that do not require very high accuracies such as locating a waste dumping site will be able to benefit from the free open service that will provide accuracies of up to 4 and 8 m in horizontal and vertical positioning, respectively.

## References

1. Hofman-Wellenhof B, Lichtenegger H, Wasle E (2008) GNSS global navigation satellite system: GPS. GLONASS; Galileo and more, Springer, Wien
2. European Commission and European Space Agency (2002) Galileo mission high level definition, 3rd issue. http://ec.europa.eu/dgs/energy_transport/Galileo/doc/Galileo_hld_v3_23_09_02.pdf Accessed 11 Nov 2008
3. European Space Agency (2008) What is EGNOS? http://www.esa.int/esaNA/SEM1AG3CXCF_egnos_0.html. Accessed 10 Nov 2008
4. EU and ESA (European Union and European Space Agency) (2002) Galileo: Mission high level definition, 3rd issue

# Part II
# Applications to Environmental Monitoring

# Chapter 8
# GNSS Maps in Environmental Monitoring

*The science of map making, known as cartography, is now intimately related to environmental monitoring because maps are generated from remote sensing, including aerial photography and satellites, as well as from field surveying and observations.*

–D. M. Hendricks [1]

## 8.1 Maps and Their Environmental Applications

Traditionally, maps have been produced by plotting features on paper at a given scale, calling upon a variety of cartographic skills. The advent of computers, satellite data, and geographical information system (GIS), however, has revolutionized the art of map production, with the modern day cartographer required to master computer skills for the purpose of not only the production, but also the management of digital maps.

This revolution in map production has in turn had a significant impact on environmental monitoring in that maps that took years to be updated can now be updated within minutes, hence permitting the monitoring of spatial features that are changing at a higher temporal rate, e.g., the BP oil spillage in the Gulf of Mexico in 2010. So great are the changes such that the science of map making, i.e., cartography, is now intimately related to environmental monitoring due to the fact that maps can now be generated from remote sensing data (i.e., aerial photographs and satellites), in addition to field observation techniques such as surveying and GNSS [1].

Applications of maps often dictate the scales at which they are produced. A scale is a relationship between the distance on a map and the equivalent distance on the ground and is often expressed as a ratio $1{:}x$ or fraction $1/x$, where $x$ is a numerical value. The smaller the value of $x$, the larger the value of the fraction $1/x$, leading to a large scale map that, while covering a smaller area contains a great deal of detail. In contrast, the larger the value of $x$, the smaller the fraction $1/x$, leading to a small scale map that often covers large areas, but with lesser detail since many features become lumped together.



J. Awange, *GNSS Environmental Sensing*, Environmental Science and Engineering, DOI 10.1007/978-3-319-58418-8_8

A map at a scale 1/1,000 (1:1000) would be a large scale map, typical of most engineering related maps (also called plans) that depict features such as dams, buildings, pipelines, etc. Small scale maps would typically be at ratio of 1:50,000 and are normally topographic maps covering almost a whole country or sections thereof. Environmental monitoring applications would typically take on both large and small scale maps, depending on the application at hand, as will be discussed in various sections of the book.

There are various types of maps, ranging from engineering plans, which could be useful in environmental monitoring tasks, e.g., in dam monitoring to avoid environmental disasters such as that which was witnessed in 2010 in Hungary, where there was a dam burst and sludge outflow with severe environmental consequences, to topographical maps that show the form and elevation of terrain at various scales. Land provides the base upon which *social*, *cultural* and *economic* activities are undertaken.

In environmental monitoring, environmental impact assessments (EIA) and audits (EA), topographical maps play an essential role in providing a means by which the locations of sampling sites may be selected, in assisting with the interpretation of physical features, and in indicating the impact or potential impact on an area due to changes in the system being monitored (e.g., spatially changing features such as wetlands). GNSS is hereby presented as a rapid method for monitoring spatial changes in the environment through its map generating capability thereby supporting decisions and policies.

## 8.2 Types of Maps

### *8.2.1 Thematic Maps*

A category of maps that finds use in environmental monitoring are *special purpose maps*, also known as *thematic maps*, which are theme specific, e.g., vegetation maps that show the distribution of plant communities, flood control maps that are used to depict areas prone to floods, soil maps that show the soil types and locations, and climate maps that show the climatic indicators of temperature and precipitation. Therefore, in addition to the application of GNSS to the generation of topographic maps discussed below, they are also useful in the production of thematic maps as demonstrated in the work of Rutchey and Vilcheck [2]. Rutchey and Vilcheck [2] use SPOT multispectral imagery, ERDAS image processing software, GNSS, and error analysis techniques to develop a baseline vegetation map of water conservation area, which is an impounded portion of the remnant Everglades managed for flood control and water supply.

### 8.2.2 Topographical Maps

Topographic maps have long been used in some form or another to define the cultural and natural features of a landscape. They require the carrying out of topographic surveys, whose purpose is to gather data about the natural and man-made features of an area of interest, in particular the spatial distribution of elevation, to give a three-dimensional representation of the area. Topographical maps are used for a variety of situations, including cadastre, e.g., [3], engineering, e.g., [4], earthworks, e.g., [5], archaeology, e.g., [6], land-deformation monitoring, e.g., [7], basic landscape and geological mapping, e.g., [8, 9], while such information in a digital database serves as a fundamental layer for geographic information systems (GIS), e.g., [10, 11].

The role of topographic maps in supporting environmental monitoring has been highlighted, e.g., by Hendricks [1], who identifies the use of topographical maps as the provision of a means for determining the nature of landforms, hydrology and, in some cases, the vegetation of an area. Topographic maps also find use in environmental monitoring that support EIA or EA legislations. Most of the environmental monitoring of spatially changing features such as small water bodies required in support of EIA and EA may not require very high accuracies and as such, topographic maps with horizontal accuracies of up to 3 m could suffice, see, e.g., [4, Table 4.3b].

In Germany, for example, deep hard-coal mining activities by the company "Deutsche SteinkohleAG" (DSK) resulted in subsidence movements, thereby necessitating high demands on planning and monitoring since such effects entailed lasting changes and influences on the environment [12]. To minimize possible effects, extensive environmental compatibility studies were performed and detailed prognosis carried out to satisfy EIA legal requirements. In these studies, topographic maps were used to make a prognosis and to forecast the effect of mining excavations [12].

Fischer and Spreckels [12] report on the limitations of the photogrammetric measurements and high-resolution digital terrain models (DTMs) that described the topographic situation, information on biotopes and the actual land-cover, and propose a multi-temporal satellite data set. They suggest that for environmental changes occurring over wider spatial areas (e.g., 1,500 $km^2$), topographical maps generated from such multitemporal remote sensing methods are advantageous compared to those from photogrammetry methods. In another example, Ji et al. [13] show how thematic maps generated using remote sensing were useful in monitoring urban expansion, which contributes to the loss of productive farmlands in China. Similarly, Shalaby and Tateishi [14] applied remote sensing and GIS generated maps to monitor land-cover and land-use changes in the north-western coastal zone of Egypt. Their results indicated that a very pronounced land cover change took place as a result of tourism and development projects during the study period.

For monitoring environmental changes occurring over smaller areas (e.g., Jack Finney Lake discussed in Sect. 8.2.4 has an area of only 12,000 $m^2$), the use of remote sensing and photogrammetry techniques to generate topographical maps is quite expensive and as such, the use of conventional methods such as total station or GNSS-generated topographical maps may be a more feasible approach. This is

demonstrated, e.g., in the work of Fischer and Spreckels [12] who show how a GNSS system provided results whose accuracy in height was nearly identical and within the precision of remote sensing methods, and thus could be useful in detecting mining-induced subsidence, enabling the updating of monitoring data at regular intervals.

Another example is presented, e.g., in Gili et al. [7] where GNSS-generated topographical maps are shown to have the capability to support environmental monitoring of the Vallcebre landslide in the Eastern Pyrenees (Spain), which had been periodically monitored using terrestrial photogrammetry and total station methods since 1987. Gili et al. [7] found that the GNSS generated topographic maps allowed greater coverage and productivity with similar accuracies (i.e., 12–16 mm in the horizontal, and 18–24 mm in elevation) as obtained by classical surveying methods.

The examples given above illustrate the major influence on topographic surveys that has resulted from the development of GNSS systems. The possibility of incorporating all the information that may be made available from such an increase in satellite coverage has the potential to deliver much greater accuracies (e.g., below 1–3 m autonomous positioning level accuracy or up to mm level accuracies for relative positioning approaches), and increased reliability and availability to the spatial information industry. This could in turn support environmental monitoring tasks, most of which require accuracies no greater than the cm-level. In the next section, the applicability of GNSS real-time kinematic (RTK) method presented in Sect. 5.4.6 to small-scale topographic surveys that may be necessary for supporting environmental monitoring will be discussed.

Compared to conventional methods for generating topographical maps, GNSS has the advantages of being less expensive in terms of time and labor and can provide adequate accuracies for most types of topographical surveys. These advantages are only evident, however, as long as the user has the skills and knowledge to use the system, and satellite visibility is adequate. In particular, knowledge of possible error sources is important in successfully applying GNSS.

### *8.2.3 GNSS-Derived Topographical Maps*

Although topographical maps have vital uses as discussed above, new areas of application requiring the rapid continuous generation of topographical maps continue to emerge, thanks to the use of GNSS in the production of such maps. One of these areas includes land management (e.g., *precision farming*, and *soil erosion modelling and assessment*), where, for example Bakhsh et al. [15] uses soil attributes and topographical maps to establish field yield variability. These applications require substantial and accurate topographic data in order to deliver meaningful results that will inform decision makers on *soil* and *water conservation* practices. To be able to monitor yield variation with respect to topographical features, traditional surveying methods for generating topographic maps, such as the use of total stations instruments, are not sufficient to rapidly generate the substantial amounts of data (horizontal position and elevation), required hence the attraction of GNSS.

Surveys using Differential GPS (DGPS) and RTK modes of GNSS to map *topographic attributes* of two fields in Northeast Kansas were performed by Schmidt et al. [16] to compare the two systems. The two fields selected for the study were 24 ha in area and 31 ha with a relief of 19–23 m. Elevation data was obtained using RTK with 3–50 m intervals with the relatively uniform areas having greater intervals. Elevation was also obtained using DGPS at 4–14 m intervals. The elevation data was then interpolated to a 5 m grid. A Trimble MS750 GPS receiver that was used for the RTK survey had a typical vertical accuracy of 1–2 cm. A reference station was established in each field prior to logging elevation data using an AgGPS 170 Field Computer. Digital elevation models (DEMs) were then created from the RTK and DGPS data using the Spatial Analyst Extension in ArcView GIS 3.2. Topographic maps with 10-m cells developed with the DGPS elevation were nearly identical to those developed from the RTK, except for depicting small topographic features such as terraces. Therefore, the RTK system was found to be suitable for producing *topographic maps* of the fields as the depiction of smaller topographic features was not necessary.

As well as the use of topographical maps to provide tagging of site-specific information to a unique location $(x, y)$ in *precision farming*, the elevation data $(z)$ derived from these topographic maps has the potential to be used for topographic analysis such as the delineation of *flow paths*, *channels*, and *watershed boundaries* [17]. For instance, Fraisse et al. [18] applied topographical maps to delineate subfield management zones using the statistical method of Principal Component Analysis (PCA). Renschler et al. [17] provide an analysis of the impact of the accuracy of six alternative topographic data sources on watershed topography and delineation in comparison to GNSS measurements using a survey-grade cm-accuracy.

Tokmakidis et al. [19] produced a GNSS-topographic map and digital terrain model (DTM) for Kilkis, Northern Greece, for land management purposes using RTK technique. The produced topographic maps and DTM were compared with existing topographical maps that were obtained from conventional photogrammetry techniques, with differences of a few centimeters up to a meter being noted. They also compared heights of contour lines crossed by the GNSS measuring lines where differences of 0.6 m were observed. They concluded that the magnitude of the differences could be considered to be realistic, keeping in mind that changes in the landscape over a period of 25 years could be greater than the difference in the values they obtained, due to farming activities, constructions, etc. The photogrammetry DTM showed sufficient reliability for accuracies of the order of one meter, while the GNSS technique proved to be a very efficient method of capturing data with an accuracy of a few centimeters in order to produce a reliable DTM.

GNSS topographical maps generated by rapid methods such as stop-and-go and RTK (see Sect. 5.4.5) could also be used for monitoring environmental changes resulting from the implementation of projects following EIA approvals. Resource conservation and disaster management are other possible areas of the application of GNSS to land management [20]. These applications require topographical maps that can rapidly be generated, see e.g., [21]. It is apparent from the examples mentioned

above that GNSS can be used for a variety of topographic surveys sufficient for environmental monitoring.

Since topographical maps provide different information and accuracies depending on the specific client or end-user, their generation will vary in *size* and *scale*. Typically, these maps are characterized by a quantitative representation of *relief*, usually using contour lines. The accuracy required for survey data is such that there be no potable error. For instance, Hall [22] states that a hand drawn line on a sheet of paper should be within 0.25 mm. Consequently, if a survey is to be undertaken at a scale of 1: 1000, all measurements must be sufficiently accurate to ensure that the relative positions of any point with respect to any other point in the survey can be stated to an accuracy within 0.25 mm at survey scale, which for a 1: 1000 map scale would represent 25 cm.

GNSS topographical maps with such accuracies could be rapidly produced using the RTK approach discussed in Sect. 5.4.6. El Mowafy [23] noted that the horizontal positions using the RTK method can be achieved to the cm-level of accuracy. The determination of the heights compared to the horizontal measurements, however, is inherently less precise and less accurate. GNSS derived ellipsoidal heights must be transformed into a local vertical datum (e.g., the Australian Height Datum (AHD) for Australia, see e.g., Featherstone and Stewart [24]).

**Example of a GNSS-Generated Topographic Map**

GNSS has been presented, e.g., by Schloderer et al. [25] as a rapid method for monitoring spatial changes to support environmental monitoring decisions and policies. In what follows, a brief discussion of their work is presented to highlight the capabilities of GNSS to generate topographical maps. In their work, Schloderer et al. [25] set the *base receiver* on a pillar (see Fig. 5.5, p. 67) due to its central location within the survey site (Fig. 8.1) and open unobstructed sky view.

To validate the GNSS-based method, a comparison was made of results from a small-scale topographic survey using RTK and total station survey methods at Jack Finney Lake, Perth, Australia. The accuracies achieved by the total station in their study were 2 cm horizontally and 6 cm vertically, while RTK also achieved an accuracy of 2 cm horizontally, but only 28 cm vertically. While the RTK measurements were less accurate in the height component compared to those from the total station method, they were still capable of achieving accuracies sufficient for a topographic map at a scale of 1: 1750 (Fig. 8.2) that could support environmental monitoring tasks such as identifying spatial changes in small water bodies or wetlands. The time taken to perform the GNSS survey, however, was much shorter compared to the total station method, thereby making it quite suitable for monitoring spatial changes within an environmental context, e.g., dynamic mining activities that require rapid surveys and the updating of the monitored data at regular intervals.

The resulting 3D Digital Terrain Model (DTM) is presented in Fig. 8.3. Such DTM find use in flood forecasting as discussed in Sect. 17.6.1. Some discrepancies between the contour maps can be noticed for areas covered with trees (Fig. 8.2). This is due to the inability of the GNSS system to take observations under dense tree cover. The contours displayed on the total station map would therefore be more reliable in these areas.


**Fig. 8.1** Edinburgh Oval, Curtin University's study area with control peg network. *Source* http://maps.google.com/maps


**(a) GNSS topographical map** **(b) Total Station topographical map**

**Fig. 8.2** Topographical maps of Edinburgh Oval, Curtin University, Perth, Australia

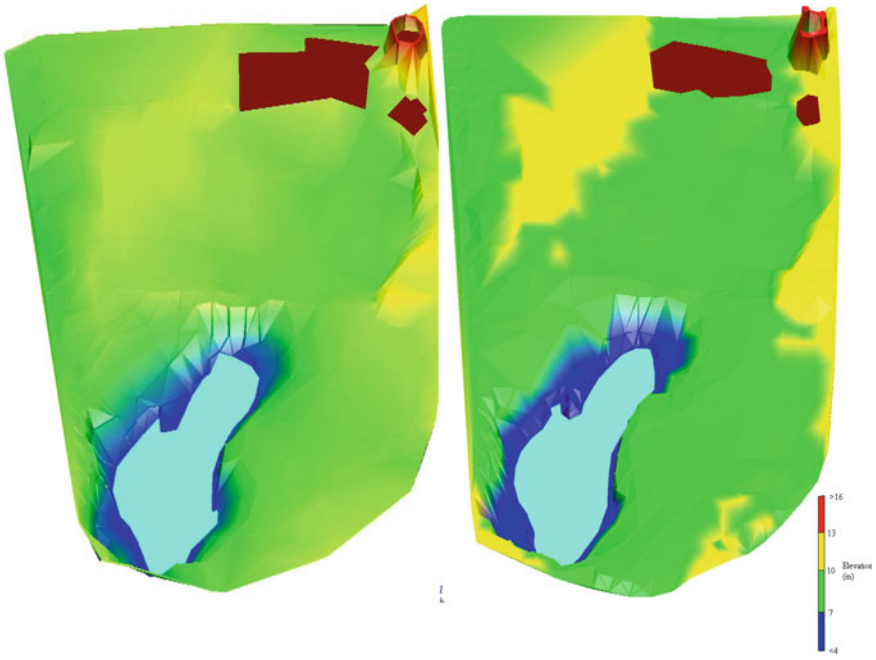


**Fig. 8.3** Digital Terrain Models (DTM) of Edinburgh Oval, Curtin University. DTM finds use, e.g., in flood forecasting as discussed in Sect. 17.6.1

Lengths of some chosen features were measured on the maps in Fig. 8.2 and compared to the actual ground measurements. The deviations from the actual distances are plotted in Fig. 8.4. The results highlight the fact that GNSS can be used to achieve accuracies suitable for a topographic map at a scale of 1:1750. For example, a difference in the length measured between the two techniques of the sports pavilion wall of 1.61 m measured on the ground corresponds to a 1 mm difference on the topographic maps. The largest differences were found when measuring the faces of buildings due to the fact that the GNSS receiver cannot be directly positioned on the building corner due to multipath errors. GNSS observations could only be taken some distance from the building at a point with adequate satellite visibility. However, the building was still positioned on the 1:1750 topographic map with sufficient accuracy.

Figure 8.4a indicates that both the GNSS and total station techniques have similar accuracies in the horizontal dimension. However, the largest variabilities in the RTK measured distances (Fig. 8.4b) occurred where observations were taken in the proximity of areas of dense tree cover, which would have reduced satellite visibility and introduced multipath errors (see Sect. 3.4.4, p. 40). The results of Fig. 8.4c show the expected outcome of lower accuracies and precisions of the GNSS elevations compared to those of the total station. Multipath could have been one of the more

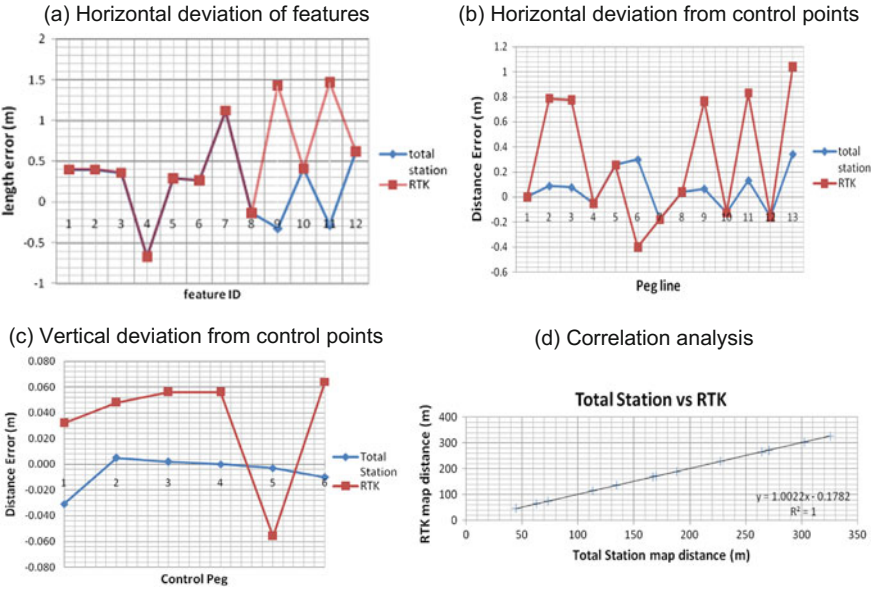


**Fig. 8.4** **a** Error distribution for lengths of features measured on the total station and RTK topographic maps. **b** Error distribution for distances between control pegs interpreted from total station and RTK topographic maps compared with ground control distances. **c** Comparison of vertical heights. **d** Regression analysis of distances interpreted from 1:1750 topographic maps produced from the total station and RTK surveys

significant sources of errors due to the presence of large obstructions within the survey area. For example, control point 5 was located near tall pine trees to the west and point 6 was located near a building to the north. Figure 8.4d shows that the distances measured from each of the topographic maps are strongly correlated with $r^2 = 1$, where $r$ is the fraction of the variance in the total station or RTK measurements that is accounted for by a linear fit of the total station to RTK measurements. More than 99% of the variability in RTK was accounted for by the total station horizontal distances with the coefficient of determinant $r^2$ value equal to 1.

### *8.2.4 Application to the Monitoring of Lake Jack Finney*

The area of the Lake Jack Finney was determined from the RTK survey and compared with areas determined from Google Earth Pro imagery for the years 2000, 2005, and 2009 (Fig. 8.5) [25]. The trend shown by the Google images suggests that the lake is gradually shrinking over time, as indicated by the decreasing lake areas from 2000 to 2008 (Fig. 8.6). The data obtained from the RTK survey in 2009 follows this trend with a smaller area compared with 2008.

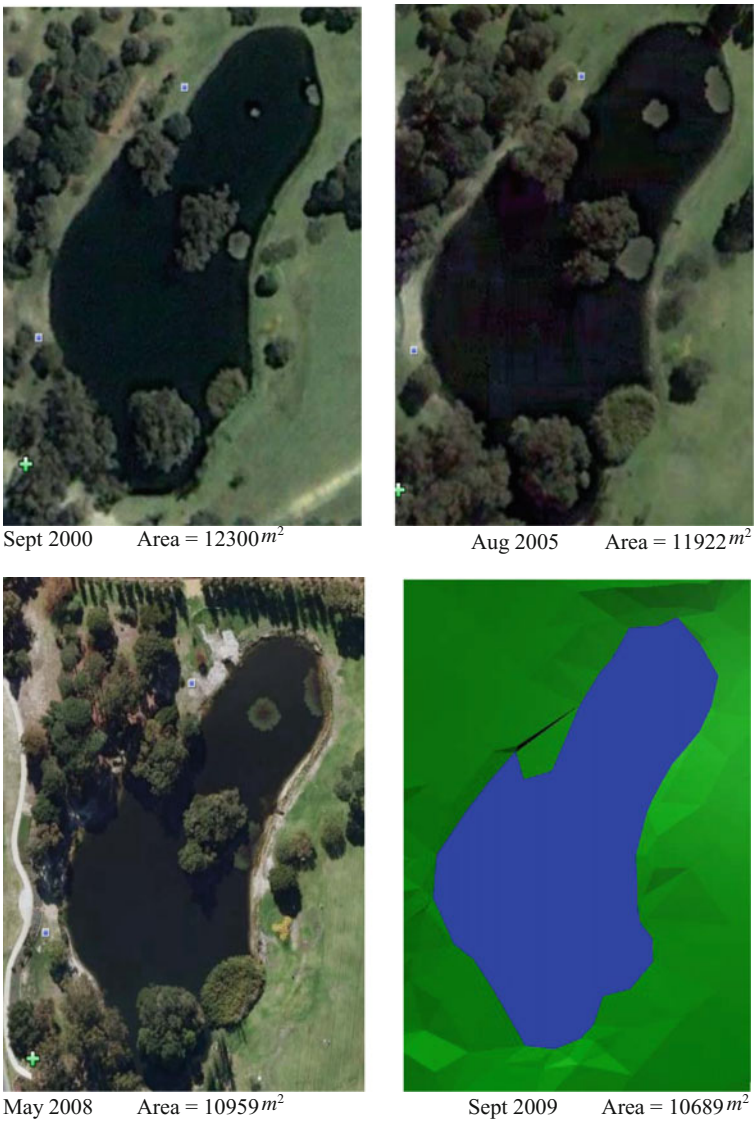


**Fig. 8.5** Comparison of the area of Jack Finney Lake during the years 2000, 2005, and 2008 as measured from Google Earth satellite imagery, and from the RTK generated model. *Source* Google Earth Pro

Figure 8.6 describes the decrease in the surface area of the lake found from the GNSS measurements at a rate of 194 $m^2$ a year, with a correlation of 0.9. Although ideally more data would have been accessible, making for a more accurate and meaningful model to quantify the shrinking size of the lake, the usefulness of the

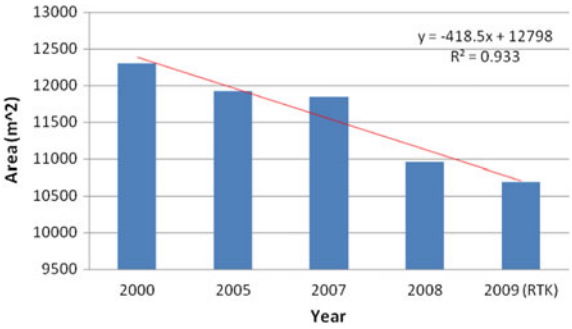


**Fig. 8.6** Spatial variation of Jack Finney Lake over time. By March 2011, the lake had dried up

GNSS method is apparent. Since Google Maps are normally not updated frequently enough to be suitable for such monitoring tasks, this again emphasizes the need for rapid and reliable GNSS methods.

As a check on the area obtained from GNSS measurements, Fig. 8.7 compares the GNSS generated surface area to that measured by the total station, with the GNSS-derived area being 148 $m^2$ greater. This difference comes from the GNSS recording of fewer points around the lake due to the heavy tree cover, while the total station recorded all necessary points to accurately define the edge of the lake. A further comparison of the lake area found by GNSS (Fig. 8.7, left) with that from the total station (Fig. 8.7, right) shows additional differences. Points A, B, C and D are shown on Fig. (8.7, left) as specific points of difference. Point A represents a spot where the GNSS could not measure the necessary point due to dense tree coverage to complete the curve of the lake, hence the lake appears to dip back whereas the total station (on the right) located the required point and completed the curve. Point B is perhaps the most significant point where the GNSS image demonstrates a poor definition of the edge of the lake. As before, this was due to large trees blocking the satellite signal. Comparing the GNSS image to the total station image, it is clear that the total station performed a much better job of mapping the area than the GNSS. The same situation applies to point C with large trees blocking the satellite signals, again leading to a poor definition of the edge of the lake. Point D is an area where the opposite of above happens. There were tall reeds that prevented the line of sight to the prism even when set at the maximum pole height of 2.1 m. However, with the RTK system, an observation was possible.

With the changing surface area of the lake over time and the effectiveness of each method to define these changes, this is just one area of application that is possible for GNSS.

This example shows that GNSS can be used for the surveys needed for environmental applications such as wetland management. Instead of using expensive satellite imagery to monitor water bodies over time, GNSS can be used to map waterlines quickly and accurately to monitor the growth or recession of water bodies over time.

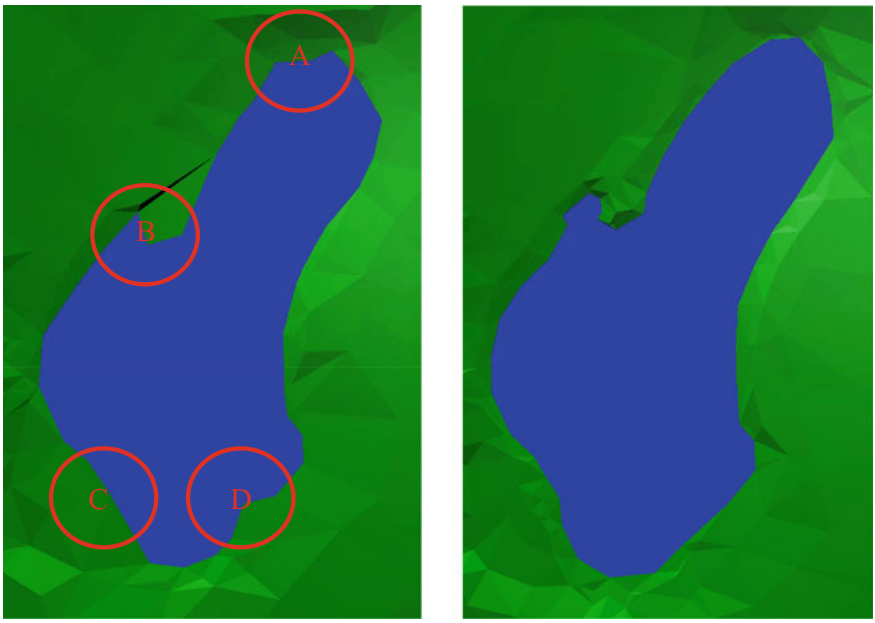


**Fig. 8.7** Lake Jack Finney (September 2009). *Left* GNSS. *Right* Total station. The points marked on the *left*-hand figure are discussed in the text

## 8.3 Concluding Remarks

Attributes that are important to topographic maps can be successfully identified and represented by GNSS techniques. The example of Schloderer et al. [25] indicates that the GNSS technique is capable of achieving a level of accuracy sufficient to develop a reliable topographic map at a scale of 1:1750, which suffices for most environmental monitoring purposes. At this scale, given that the GNSS generated topographical map achieved a horizontal accuracy of 2 cm and a vertical accuracy of 28 cm, it would be useful for most types of environmental monitoring, except where heights need to be more accurate than 28 cm, such as land subsidence monitoring.

It should be pointed out, however, that this is not the absolute achievable value, since GNSS accuracy depends on many factors, which include satellite availability and visibility, signal blockage from trees and buildings, the effects of multipath errors, and the experience of the observers, to name just a few. These error sources could have contributed to the relatively low accuracy achieved. The results, however, still indicate the potential of GNSS to generate topographical maps capable of supporting the environmental applications listed in [25, Table 3], although we must point out that this is not conclusive, given the problems of error sources and limited data.

In the example presented, the time taken to perform the survey was much shorter using GNSS compared with the total station method, where the need for multiple

setups and a traverse to establish control on the multiple stations greatly increased the time taken to perform the survey. The GNSS accuracies achieved, when compared against typical accuracies desired for particular survey tasks were found not to meet the required accuracies for cadastral work, utility surveys, land deformation surveys, or archaeological surveys that require cm to mm-level accuracies, but was sufficient for environmental monitoring tasks that does not require such high accuracies, such as the mapping the spatial changes in small water bodies, e.g., Jack Finney Lake.

Therefore, for environmental monitoring of areas with adequate satellite visibility throughout the survey area, and fewer obstructions introducing multipath errors, the generation of topographic surveys that serve as a preliminary reconnaissance for environmental studies, or to quickly examine the changing spatial dimensions of a feature, such as a small water body during an environmental audit, GNSS is recommended. It should be noted, however, that GNSS is capable of providing higher accuracies as discussed in Chap. 5.

## References


1. Hendricks DM (2004) Maps in environmental monitoring. In: Artiola J, Pepper IL, Brusseau ML (eds) Environmental monitoring and characterization. Elsevier Academic Press, USA
2. Rutchey K, Vilcheck L (1994) Development of an Everglades vegetation map using a SPOT image and the global positioning system. Photogram Eng Remote Sens 60(6):767–775
3. Jacobs PG (2005) Assessing RTK GPS for a suburban survey practice, University of Southern Queensland, Faculty of Engineering and Surveying. http://eprints.usq.edu.au/546/1/PeterJACOBS-2005.pdf Accessed 28 Jan 2010
4. US Army Corps of Engineers (2007) Control and topographic surveying. engineering and design manual, EM 1110-1-1005
5. Garget D (2005) Testing of robotic total station for dynamic tracking. University of Southern Queensland. http://eprints.usq.edu.au/ Accessed 20 Aug 2009
6. Kvamme K, Ernenwein E, Markussen C (2006) Robotic total station for microtopographic mapping: an example from the Northern great plains. In: Archaeological prospection, vol 13, pp 91–102. Wiley Interscience, New Jersey. www.interscience.wiley.com. Accessed 18 Aug 2009
7. Gili JA, Corominas J, Rius J (2000) Using global positioning techniques in landslide monitoring. Eng Geol 155(3):167–192. doi:10.1016/S0013-7952(99)00127-1
8. Reynolds W, Young F, Gibbings P (2005) A Comparison of methods for mapping golf greens. In: Spatial Science Queensland, vol 4 2007, pp 33–36. ISSN 1032-3848
9. Lavine A, Gardner J, Reneau S (2003) Total station geologic mapping: an innovative approach to annalyzing surface-faulting hazards. Eng Geol 70:71–91. doi:10.1016/S0013-7952(03)00083-8
10. Awange JL, Kiema JBK (2013) Environmental geoinformatics. Monitoring and management, Springer, Berlin
11. Braun M, Simões JC, Vogt S, Bremer UF, Blindow N, Pfender M, Saurer H, Aquino FE, Ferron FA (2001) An improved topographic database for King George Island: compilation, application and outlook. Antarct Sci 13(1):41–52. doi:10.1017/S0954102001000074
12. Fischer C, Spreckels V (1999) Environmental monitoring of coal mining subsidences by airborne high resolution scanner. In: IEEE 1999 international geoscience and remote sensing symposium, 1999. IGARSS '99 Proceedings. pp 897–899. doi:10.1109/IGARSS.1999.774478
13. Ji CY, Liu Q, Sun D, Wang S, Lin P, Li X (2001) Monitoring urban expansion with remote sensing in China. Int J Remote Sens 22(8):1441–1455. doi:10.1080/01431160117207

14. Shalaby A, Tateishi R (2007) Remote sensing and GIS for mapping and monitoring land cover and land-use changes in the Northwestern coastal zone of Egypt. Appl Geogr 27:28–41. doi:10.1016/j.apgeog.2006.09.004
15. Bakhsh A, Jaynes DB, Colvin TS, Kanwar RS (2000) Spatio-temporal analysis of yield variability for a corn-soybean field in Iowa. Trans ASAE 43(1):31–38
16. Schmidt JP, Taylor RK, Gehl RJ (2003) Developing topographic maps using a sub-meter accuracy global positioning system. Appl Eng Agric 19(3):291–300
17. Renschler CS, Flanagan DC, Engel BA, Kramer LA, Sudduth KA (2002) Site specific decision-making based on RTK GPS survey and six alternative data sources: watershed topography and delineation. Trans ASAE 45(6):1883–1895
18. Fraisse CW, Sudduth KA, Kitchen NR (2001) Delineation of site-specific management zones by use of unsupervised classification of topographic attributes and soil electrical conductivity. Trans ASAE 44(1):155–166
19. Tokmakidis K, Spatalas S, Pikridas C (2003) A comparison of a digital terrain model obtained from GPS and classical data. In: Proceedings of international symposium on modern technologies, education and professional practice in the Globalizing World, November, Sofia, Bulgaria, pp 30–35
20. Monico JFG (2004) United nations office for outer space affairs GNSS web pages. GPS Sol 8(2):112–114. doi:10.1007/s10291-004-0096-4
21. Clark RL, Lee R (1998) Development of topographic maps for precision farming with kinematic GPS. Trans ASAE 41(4):909–916
22. Hall B (1994) Environmental mapping systems - locationally linked databases. riversinfo. Precision info. http://www.precisioninfo.com/rivers_org/au/archive/?doc_id=1. Accessed 20 Aug 2009
23. El-Mowafy A (2000) Performance analysis of the RTK technique in an urban environment. Aust Surv 45(1):47–54
24. Featherstone WE, Stewart MP (2001) Combined analysis of real-time kinematic GPS and its users for height determination. J Surv Eng 127(2):31–51. doi:10.1061/(ASCE)0733-9453(2001)127:2(31)
25. Schloderer G, Bingham M, Awange JL, Fleming KM (2010) Application of GNSS-RTK derived topographical maps for rapid environmental monitoring: a case study of Jack Finney Lake (Perth, Australia). Environ Monit Assess 180(1–4):147–161. doi:10.1007/s10661-010-1778-8

# Chapter 9
# GNSS Remote Sensing of the Environment

*GNSS data provide the opportunity to observe Earth system processes with greater accuracy and detail, as they occur.*
W.C. Hammond et al. [1]

## 9.1 Introductory Remarks

GNSS satellites such as GPS are playing an increasingly crucial role in tracking low earth orbiting (LEO) remote sensing satellites at altitudes below 3000 km with accuracies of better than 10 cm [2]. These remote sensing satellites employ a precise global network of GNSS ground receivers operating in concert with receivers onboard the LEO satellites, with all estimating the satellites' orbits, GPS orbits, and selected ground locations simultaneously [2]. In this chapter, we illustrate the role played by GNSS satellites in measuring changes in the Earth's atmosphere, its gravity field, and mass redistribution (e.g., changes in terrestrial water storage). These changes are found by measuring *refractivity* and *inter-satellite distances*.

The last two decades has seen the emergence of GNSS remote sensing techniques that are capable of monitoring changes in the global tropopause height and in so doing, contribute to monitoring *global warming* as we shall see in Chap. 11. GNSS satellites in conjunction, with LEO satellites, e.g., the GRACE (Gravity Recovery And Climate Experiment), have been used to derive vertical atmospheric profiles of, e.g., *temperature*, *height*, and *pressure*, in what is known as GNSS radio occultation (RO) or GNSS-Meteorology [3]. Foelsche et al. [4] point to its potential to overcome problems associated with traditional data sources (e.g., radiosondes) due to their unique combination of *high accuracy* and *vertical resolution*, *long-term stability* and *all-weather global coverage* that is not feasible with other systems.

Indeed, Schmidt et al. [5] compared RO data from CHAMP (CHAllenging Mini-satellite Payload) with radiosonde measurements and found an agreement within less than 0.5 K (i.e., in the measured temperature profiles). In another study of global tropopause height changes over a period of 7 years (2001–2007) using CHAMP and



J. Awange, *GNSS Environmental Sensing*, Environmental Science and Engineering, DOI 10.1007/978-3-319-58418-8_9

GRACE, Schmidt et al. [6], found a trend of +(23–44) m/decade, which is consistent with the results published by [7] based on radiosonde data. The six operational COSMIC (Constellation Observing System for Meteorology, Ionosphere, and Climate) satellites, launched in 2006, have significantly increased the availability of GNSS-RO data for climate studies, see e.g., Anthes et al. [8].

In the next section, a brief look at the basics of GNSS remote sensing of the atmosphere is presented. In Chap. 11, it will be demonstrated how it could be used to enhance tropopause monitoring and in doing so, contribute towards monitoring climatic change. Chapters 11 and 12 will further look at its applicability to climate variability studies. In Sect. 9.2, GNSS remote sensing of the atmosphere for weather forecasting and climatic modelling is presented. Section 9.3 then presents GNSS applications for supporting LEO satellite remote sensing of variations to the gravity field caused by mass changes. The other GNSS remote sensing application of altimetry, which makes use of the measurement of the delay time between the signals that reach the LEO satellite receiver directly from the GNSS transmitter and those that are reflected, e.g., by the sea surface, will be treated in Sect. 9.4.

## 9.2 GNSS Remote Sensing of the Atmosphere

As stated in part I of the book, some GNSS satellites, such as GPS and GLONASS, were primarily designed to be used by the military with the primary objective of obtaining accurate *positions* of points on the Earth from space. In order to obtain these positions, we saw that the signals emitted by GNSS satellites have to traverse the ionosphere and neutral atmosphere to be received by ground-based GNSS receivers. One of the major obstacles to positioning with GNSS discussed in Sect. 3.4.3 was the *signal delay* caused by atmospheric refraction.

As opposed to geodesists whose interest is to estimate *ionospheric* and *tropospheric* delays only to eliminate them to obtain accurate positions, *meteorologists* and *environmentalists* use these ionospheric and tropospheric delays for *weather forecasting*, *climate studies* (e.g., sea, land, and ice level changes), *hazard predictions* and *early warning systems* (see e.g., Fig. 17.13 on p. 373). Belvis et al. [9] presents a win-win situation for professionals in both geodesy and environmental studies; for a geodesist, accurate knowledge of the atmospheric delay will improve the vertical accuracy, which in turn is of great interest to environmental scientists studying *global climate change*, which may be reflected in changes in the atmospheric delay. Or to put it another way, "one scientist's noise is another scientist's signal".

Currently, the NASA Deep Space Network (DSN) uses near-real-time tropospheric delay estimates based on real-time global differential GNSS (GDGPS discussed in Sect. 5.4.3) to calibrate the radio signals from spacecraft in support of deep space navigation. Real-time global ionospheric total electron content (TEC) maps are derived at JPL and by the Air Force Weather Agency (AFWA) based on

GDGPS tracking data.[1] Hammond et al. [10] point out that GNSS measurements have the potential to contribute to tropospheric weather and climatic modelling, and/or weather forecasting in up to four different ways; (i) integrative measurement of atmospheric water vapor in GPS signal delays, (ii) localized sensing of soil moisture and snow depth from satellite to antenna multipaths, (iii) large-scale sensing of water mass from elastic deformation signals, and (iv) imaging of hydrometeor scattering.

For the ionosphere, where almost all aspects of ionospheric research uses GNSS observations (i.e., the measured *total electronic content* (TEC) from the differential delay of the two L1 and L2 signals), higher sampling rates of real-time GNSS will benefit studies of travelling ionospheric disturbances and other wave phenomena, including disturbances from *earthquakes* and *tsunamis*, while lower latency will aid in the development of operational forecasting for space weather, with significant implications for global communications systems and satellite maintenance [1].

This section examines how GNSS satellites could be used to remote sense various atmospheric parameters as their signals pass through the different portions of the atmosphere. The goal is to show how atmospheric parameters such as the TEC and electron density profile in the ionosphere, tropospheric *temperatures*, *pressures* and *water vapour* could be measured by GNSS satellites, and related to meteorological (weather and climatological) applications, and hence to develop the field of *GNSS-meteorology*. In what follows, we start by presenting the background to GNSS-meteorology before discussing the environmental parameters that could be derived from it. The measuring techniques and the potential applications to environmental monitoring are also discussed.

### *9.2.1 Background to GNSS-Meteorology*

Melbourne [11] suggested that the complicating effect of the atmosphere on GNSS signals could be inverted to remote sense the atmosphere using space-borne techniques. He proposed that LEO satellites be fitted with GNSS receivers and be used to track the signals of rising or setting GNSS satellites (occulting satellites).

The proposed technology is currently playing a major role in complementing existing techniques, e.g., radiosondes. Atmospheric profiles from GNSS remote sensing have been tested in numerical weather prediction (NWP) models and the results were found to be promising [13]. Indeed, Kuo et al. [14] demonstrated using GPS/MET (GPS/meteorology space trial mission) data that the accuracy of global and regional analysis of weather prediction could be significantly improved. Also encouraging were the results of Steiner et al. [15] who showed that highly accurate measurements and fine vertical resolution around the tropopause would be employed to monitor climatic change over the next decades.

[1] http://www.gdgps.net/applications/index.html.

Several atmospheric sounding missions have been launched aboard LEO satellites, e.g., CHAMP, which is no longer active, but whose data are available, GRACE, and COSMIC [8]. The latest entry is the European owned EUropean organization for the exploitation of METeorological SATellites (EUMETSAT), which is installed with a GNSS occultation receivers GRAS (GNSS Receiver for Atmospheric Sounding). Combined, these missions provide more than 5000 occultation data daily. Future possibilities for atmospheric sounding missions may have satellites the size of a laptop with GNSS receivers the size of a credit card, see e.g., Yunck [16]. The planned LEO satellite missions, together with the increasing number of GNSS satellites, promises a bright future for atmospheric studies, which would in turn benefit environmental monitoring. Indeed, such atmospheric sounding missions promise to provide daily global coverage of thousands of remotely sensed data that will be vital for weather, climatic and atmospheric studies.

Space-borne GNSS-meteorology, which we discuss in detail in Sect. 9.2.3.1 is just one part of this new technique. The other component is the ground-based GNSS-meteorology, which will be discussed in Sect. 9.2.3.3. Overviews of this new technique have been presented, for instance, in [17, 18]. In ground-based GNSS-meteorology, a dense GNSS network (e.g., GEONET, Fig. 5.14 on p. 85) is used to measure precisely GNSS path delays caused by the ionosphere and the neutral troposphere traversed by the GNSS signals. These path delays are then converted into TEC and integrated precipitable water vapour (IPWV) values. Conversion to IPWV requires prior information of surface pressure or estimates along the GNSS ray path. These create a continuous, accurate, all weather, real-time lower and upper atmospheric data set with a variety of opportunities for atmospheric research [19].

Use of the GNSS-derived atmospheric precipitate water vapour (PWV) in real-time weather forecasting has, however, been slow due to the fact that forecasters preferred high-rate and low-latency measurements. However, increased availability of high-rate sampling and low-latency GNSS products, e.g., those discussed in Sect. 5.4.3, together with greater station densities, is posed to change the forecasters' perception and lead towards future GNSS water vapor sensing using high-rate, low-latency data from GNSS receivers [10].

### *9.2.2 GNSS-Derived Atmospheric Parameters*

What exactly are the parameters in the atmosphere measurable by GNSS that are of interest to environmental monitoring?

This section attempts to answer this question by examining the effect of the atmosphere on the GNSS signals as they pass through it from the satellites to the receivers. Understanding these effects would in turn enable us know exactly the parameters that could be remotely sensed by GNSS signals. The key to understanding the atmospheric signals of interest is to look at the GNSS signal delays.

The atmosphere acts as a medium through which the GNSS signals travel from the satellites to the receivers. If the atmosphere was a vacuum, the GNSS signal would travel in a straight line. But since the atmosphere is made up of various layers of different densities, the GNSS signal instead curves before reaching the receiver. Hence, the distance increases and the velocity of the radiowaves decreases, thus delaying the signal. In 1992, when GPS attained full operational capability, Ware [20] suggested the possibility of using its delayed signals to remotely sense the atmosphere in what is known as GPS atmospheric sounding. By 1996, the potential of using GPS satellites for atmospheric sounding were already recognised as reported, e.g., by Businger et al., [21, 22]. This GNSS signal delay is what is measured, as will be discussed in the next section. Once the delay has been measured, it is converted into the required atmospheric parameters; *refractivity*, *bending angles*, *temperatures*, *pressures*, *water vapour* and *geopotential heights*. In measuring these atmospheric signals, GNSS-meteorology has the advantages of;

(a) being *global, highly precise and continuous*,
(b) *stable*, owing to the stable GNSS oscillators, and
(c) use of radio frequencies (microwave L-band signals) that can *penetrate* clouds and dust, unlike other remote sensing techniques such as radar-based whose signals are blocked by clouds.

Next, the relationship between the GNSS signals and refractivity as it traverses the troposphere from an altitude of 40 km to the antenna is presented. This will enhance our understanding of how GNSS satellites remotely sense these environmental attributes. Belvis et al. [9] classify the effects of the atmosphere on GNSS signal into two parts:

- *First*, there is a reduction in the speed of propagation of the GNSS signals in a region of finite density compared to that in a vacuum, leading to an increase in the time taken by the signal to reach the receiver. This increase in time can be expressed in terms of *excess path length*, leading to an *optical delay*.
- *Second*, the signals travel in a curved path instead of a straight line due to the refractive effects of the atmosphere's changing density (Snell's laws) (see, Fig. 9.2) leading to a *geometrical delay*.

Both the *optical* and *geometrical delays* are attributed to variations in the *index of refraction n* along the path taken by the signals. The excess path length $\Delta L$ is given by [9]

$$\Delta L = \int_L n(s)ds - G, \tag{9.1}$$

where $n(s)$ is the refractive index as a function of position $s$ along the curved path $L$, and $G$ is the straight-line geometrical path length through the atmosphere (i.e., the path that would be taken by the signal in a vacuum). Equation (9.1) can be expressed as

$$\Delta L = \int_L [n(s) - 1]ds - [S - G], \tag{9.2}$$

where $S$ is the path length along $L$. In Eq. (9.2), $\int_L [n(s) - 1]ds$ represents the reduction in speed, i.e., optic delay while $[S - G]$ is due to the bending effect, i.e., geometric delay. The bending term $[S - G]$ is smaller, about 1 cm or less, for paths with elevations greater than about 15° [9]. In addition, rather than the refractive index in $n$ above, which is numerically close to unity, refractivity, given by

$$N = (n - 1)10^6 \tag{9.3}$$

is usually used, leading to

$$\boxed{N = 77.6\frac{P}{T} + \left(3.73 \times 10^5 \frac{P_w}{T^2}\right) - \left(40.3 \times 10^6 \frac{n_e}{f^2}\right) + 1.4w}, \tag{9.4}$$

where $P$ denotes the total atmospheric pressure in {mbar}, $T$ is the atmospheric temperature in K, $P_w$ is the partial pressure of water vapour in {mbar}, $n_e$ is the number of electron density per cubic meter {number of electron/$m^3$}, $f$ is the transmitter frequency in Hz, and $w$ is the liquid water content in $g/m^3$. The three main contributors to *refractivity*, as was discussed in Sect. 3.4.3, are:

- The *dry neutral atmosphere* (called the hydrostatic component, i.e., the first component on the right-hand-side of Eq. (9.4), dependent mainly on *dry air* and also the *non-dipole component of water vapour*). From this component, GNSS-derived vertical profiles of temperatures and pressures used for global warming monitoring are obtained.
- *Water vapour* (also called the wet or moist component, i.e., the second component on the right-hand-side of Eq. (9.4), dependent on the *dipole component of water vapour*). GNSS are used to measure water vapour through the estimated zenith wet delay (ZWD) as discussed below. The GNSS-derived water vapour are useful both for weather forecasting in numerical weather prediction (NWP) models and also in climate change studies.
- The *free electrons* in the ionosphere (i.e., the third component on the right-hand-side of Eq. (9.4)). GNSS plays a key role in providing slant TEC[2] derived through the differencing of the L1 and L2 frequency phase delay. GPS estimates of slant TEC are by far the most plentiful observations of ionospheric processes and provide the bulk of global spatial sampling, so global models necessarily rely on them heavily [10]. Furthermore, both space-borne and ground-based GPS observations provide information related to various activities and states in the atmosphere, e.g., solar flare and geomagnetic storm [23].

[2]Total electronic contents.

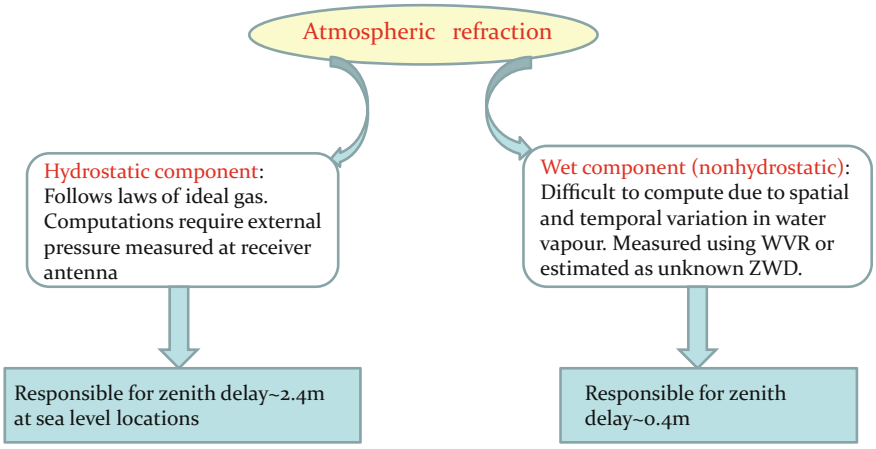


**Fig. 9.1** Components of tropospheric refractivity. WVR (water vapour radiometers) and ZWD (zenith wet delay) help in determining the wet component

### GNSS Measurement of Water Vapour

The first two items of Eq. (9.4) are summarized in Fig. 9.1. The contribution of the *free electrons* leading to refraction effects on the signals in the ionosphere are corrected for using signals at two frequencies for which these effects are substantially different, taking advantage of the dispersive nature of the ionosphere. This leaves the last term of Eq. (9.4), which is normally very small and is often neglected, see e.g., [9]. The first two terms of Eq. (9.4) are indicated by Resch [24] to be accurate to about 0.5% under normal atmospheric conditions. Thayer [25] provided an improved version [9] of Eq. (9.4), expressed as [26, p. 195]

$$N = k_1 \frac{P_d}{T} Z_d^{-1} + k_2 \frac{P_{wv}}{T} Z_{wv}^{-1} + k_3 \frac{P_{wv}}{T^2} Z_{wv}^{-1}, \tag{9.5}$$

where

- $k_1 = (77.60)\,\mathrm{K\,mbar^{-1}}$, $k_2 = (69.5)\,\mathrm{K\,mbar^{-1}}$, $k_3 = (370100)\,\mathrm{K^2\,mbar^{-1}}$,
- $P_d$ is the *partial pressure of dry air* (in mbar), with the dry gases of the atmosphere in decreasing percentage of volume being $N_2, O_2, Ar, CO_2, Ne, He, Kr, Xe, CH_4, H_2,$ *and* $N_2O$, representing 99.96% of the total volume,
- $P_{wv}$ is the partial pressure of water vapour (water vapour content is highly variable, but rarely exceeds 1% of the mass of the atmosphere),
- $T$ is the absolute temperature in degrees Kelvin (K),
- $Z_d^{-1}$ and $Z_{wv}^{-1}$ are the *inverse compressibility factors* for dry air and water vapor, respectively, that account for small departures in the behaviour of moist atmosphere from an ideal gas.

Thayer's [25] modified Eq. (9.5) leads to the retrieval of refraction with an accuracy of about 0.02% [27]. Leick [26, p. 196] provides an explanation of Eq. (9.5) as follows: the first term is the sum of the *distortion* of the electron charges of the dry gas molecules under the influence of a magnetic field, the second term expresses the same effect, but for water vapour, while the third term describes the permanent dipole moment of the water vapour, i.e., it is a direct result of the geometry of water vapour's molecular structure. The *first term* of Eq. (9.5) is then divided into two parts to give [26, p. 196]:

1. the refractivity of an ideal gas in hydrostatic equilibrium, i.e., *hydrostatic refractivity*, which is the larger component and can be accurately computed if the surface total pressure is available, and
2. a function of *partial water vapour pressure*. This is the smaller component of the two and has to be either measured or estimated (e.g., Fig. 9.1).

The division is achieved using the equation of the state of a gas

$$p_i = Z_i \rho_i R_i T, \; for \; i = \{d, wv\}, \tag{9.6}$$

with $\rho_i$ being the mass density and $R_i$ the specific gas constant. In Eq. (9.6), the subscripts $d$, and $wv$ represent dry gas and water vapour, respectively. Using this equation in (9.5), it is immediately noticeable that the term $P_d$ in the first part can be replaced. This introduces the density term $\rho_d$, which can then be replaced by the total density $\rho$ and partial density of water vapour $\rho_{wv}$. Replacing this partial density of water vapour $\rho_{wv}$ by Eq. (9.6) leads to the division of the first term as [26, p. 196]

$$k_1 \frac{P_d}{T} Z_d^{-1} = k_1 R_d \rho - k_1 \frac{R_d}{R_{wv}} \frac{P_{wv}}{T} Z_{wv}^{-1}, \tag{9.7}$$

which clearly indicates that the refractivity of the hydrostatic term is due to both dry gas and partial water vapour, as had been previously stated, e.g., by [9]. When (9.7) is substituted into Eq. (9.5) and combined with the second term of (9.5), one obtains

$$N = k_1 R_d \rho + k_2^{'} \frac{P_{wv}}{T} Z_{wv}^{-1} + k_3 \frac{P_{wv}}{T^2} Z_{wv}^{-1}, \tag{9.8}$$

and

$$k_2^{'} = k_2 - k_1 \frac{R_d}{R_{wv}} = k_2 - k_1 \frac{M_{wv}}{M_d}, \tag{9.9}$$

with $M_i$, $i = \{d, wv\}$ being the molar mass. Equation (9.8) essentially provides the *hydrostatic* ($N_d$) and *wet refractivity* ($N_{wv}$) terms, respectively, as

$$N_d = k_1 \frac{P}{T}, \tag{9.10}$$

and

$$N_{wv} = k_2^{'} \frac{P_{wv}}{T} Z_{wv}^{-1} + k_3 \frac{P_{wv}}{T^2} Z_{wv}^{-1}. \tag{9.11}$$

Integrating (9.5) along the zenith direction using (9.10) and (9.11) gives the zenith hydrostatic delay (ZHD) and the zenith wet delay (ZWD), respectively, as [26, p. 197]

$$ZHD = 10^6 \int_{antenna}^{\infty} N_d(h) \mathrm{d}h, \tag{9.12}$$

$$\boxed{ZWD = 10^6 \int_{antenna}^{\infty} N_{wv}(h) \mathrm{d}h}. \tag{9.13}$$

For satellites that are not vertically overhead, i.e., not in the direction of the zenith, the hydrostatic and wet delays in (9.12) and (9.13) have to be converted into the equivalent slant delays through

$$\begin{aligned} SHD &= ZHD.mf_h(\alpha) \\ SWD &= ZWD.mf_{wv}(\alpha), \end{aligned} \tag{9.14}$$

leading to the slant total delay (STD) expressed as

$$STD = SHD + SWD, \tag{9.15}$$

where $mf_h$ and $mf_{wv}$ are mapping functions and $\alpha$ is the elevation angle. Note that the zenith angle $(90 - \alpha)$ could also be used. The simplest relation between the wet delay (SWD) along a line of elevation angle $\alpha$ and the ZWD is given through the simple pythagorean

$$\boxed{SWD = \frac{ZWD}{sin(\alpha)}}. \tag{9.16}$$

The most commonly used mapping function is Niell's [28]. Using the zenith angle $z$, Niell's mapping functions $mf_h(z)$ and $mf_{wv}(z)$ are given by [28]

$$mf_h = \frac{1 + f_1}{cos(z) + f_2} + h\left(\frac{1}{cos(z)} - \frac{1 + f_3}{cos(z) + f_4}\right), \tag{9.17}$$

and

$$mf_{wv}(z) = \frac{1 + f_5}{cos(z) + f_6}, \tag{9.18}$$

where

$$f_1 = \frac{a}{1 + \left(\frac{b}{1+c}\right)}$$

$$f_2 = \frac{a}{cos(z) + \left(\frac{b}{cos(z)+c}\right)}$$

$$f_3 = \frac{a_h}{1 + \left(\frac{b_h}{1+c_h}\right)}$$

$$f_4 = \frac{a_h}{cos(z) + \left(\frac{b_h}{cos(z)+c_h}\right)}$$

$$f_5 = \frac{\tilde{a}}{1 + \left(\frac{\tilde{b}}{1+\tilde{c}}\right)}$$

$$f_6 = \frac{\tilde{a}}{cos(z) + \left(\frac{\tilde{b}}{cos(z)+\tilde{c}}\right)},$$

where $a$, $b$, and $c$ are the coefficients of the hydrostatic mapping function given in Niell [28, Table 3], while $\tilde{a}$, $\tilde{b}$, and $\tilde{c}$ are the coefficients of the wet mapping function in Niell [28, Table 4]. Tropospheric delay is thus shortest in the zenith direction where the elevation angle $\alpha = 90°$, but increases as the elevation angle decreases.

From the STD, which can be estimated from GPS observations, the measurable signals of interest to environmental monitoring are the *precipitable water* (PW) and the *integrated water vapour* (IWV). Let us now consider that for each receiver of the continuous operating reference stations (CORS; see Sect. 5.5), Eq. 4.18 from p. 49 applies. For a known station, the range between the satellite and the receiver will be accurately known. If the other errors discussed in Sect. 3.4 are properly modelled, the remaining residual errors of the observations will be due to STD, see e.g., [26]. These STD could then be used to estimate ZWD given a proper mapping function and assuming that the ZHD has been accurately obtained from surface meteorological measurements. The estimation of ZWD from GNSS observation equations can take on the form of [29, 30]:

(i) *Least squares solution* (see Sect. 6.3) where the ZWDs are obtained as unknowns, i.e., the deterministic approach from which one parameter is estimated per station per specified time interval. This approach involves constraining the value of the ZWD and perhaps its rate of change, to keep it within a reasonable set of bounds [29].

(ii) Estimation as a *stochastic process* using a Kalman filter [31], where the temporal variation of ZWD is assumed not to change by a large amount over a short period of time. The stochastic filter estimation of ZWD requires a proper choice of the

stochastic process that represents its fluctuation. One common choice is the first-order Gauss–Markov process and the stochastic noise is chosen so as to constrain the variation of the ZWD to between 1 and 20 mm per hour, depending on location and the time of the year [29].

As we shall see in Sect. 11.3.2, NWP models require precipitable water and as such the conversion of the GNSS measured ZWD to precipitable water vapour (PWV) and integrated water vapour (IWV) is necessary. Askne and Nordius [32] have shown that it is possible to relate IWV and the measured ZWD. The relationship is presented by Belvis et al. [29] as

$$IWV \approx \zeta ZWD \tag{9.19}$$

and

$$\boxed{PWV = \frac{\zeta ZWD}{\rho}}, \tag{9.20}$$

where $\rho$ is the total density. In (9.19) and (9.20), the value of the constant $\zeta$, i.e., the ratio IWV/ZWD, varies between 5.9 and 6.6 and is given by [26, p. 201] as

$$\frac{1}{\zeta} = 10^{-6}\left(\frac{k_3}{T_m} + k_2'\right) R_{wv}, \tag{9.21}$$

where $T_m$ is the weighted mean temperature of the atmosphere given by

$$T_m = \frac{\int \frac{P_{wv}}{T} Z_{wv}^{-1} dh}{\int \frac{P_{wv}}{T^2} Z_{wv}^{-1} dh}. \tag{9.22}$$

In estimating PWV from (9.20), the largest source of error is attributed to the mean temperature $T_m$, which varies with *location*, *height*, *season*, and *weather*. Belvis et al. [29] provided a total error budget of the estimated ZWD of $\sim 10$ mm random error and $\sim 10$ mm long-term bias. This was based on the comparison of the results of Very Long Baseline Interferometry (VLBI), GPS, and WVR (water vapour radiometers), with the error component divided as follows [29]:

(a) 5% error due to the inversion from path delay to IWV in non-arid areas.
(b) Errors of less than 10 mm in path delay arising from carrier-phase measurements and propagated through the Kalman filtering estimation method.
(c) Errors of the order of 3 mm in ZWD under normal ionospheric conditions arising from the use of dual-frequency signals for range correction (i.e., ionospheric correction).
(d) Less than 1% (23 mm) errors in hydrostatic delay as a result of atmospheric dynamics. Proper station calibration, however, can potentially reduce this error to less than 1 mm.

(e) Multipath errors will depend on the type of antenna, elevation angle of the satellites and the environment in which the antenna is located. Belvis et al. [29] suggest that since this error is normally less than 100 mm for elevation angles of 15°, it is likely to perturb the zenith delay measurement by less than 20 mm.
(f) The contribution of ionospheric effects on the signal will generally be below the total error budget.

### *9.2.3 GNSS Remote Sensing Techniques*

Over the years, research efforts have been dedicated to modelling atmospheric refraction in order to improve on GNSS positioning accuracy by accounting for the excess path delay in Eq. (9.2). As we discussed in Sect. 3.4.3, modelling of the propagation delay is done separately for the *ionosphere* and *troposphere*. For the ionosphere, Eqs. (3.5) and (3.6) on p. 37 are applied to eliminate most of the ionospheric delay. For the tropospheric delay on the other hand, we saw that the troposphere is a non-dispersive medium and that its delay could not be eliminated by the linear combination of dual-frequency observations, but must instead be measured or estimated. In the next sections, we present both space and ground based GNSS remote sensing methods and related missions, which are essential in measuring the atmospheric parameters discussed in Sect. 9.2.2.

#### 9.2.3.1 Space-Borne GNSS Remote Sensing

GNSS radio occultation (GNSS-RO) takes place when a transmitting satellite, setting or rising behind the Earth's limb, is viewed by a LEO satellite as illustrated in Fig. 9.2. GNSS satellites send radio signals that pass through successively deeper layer of the

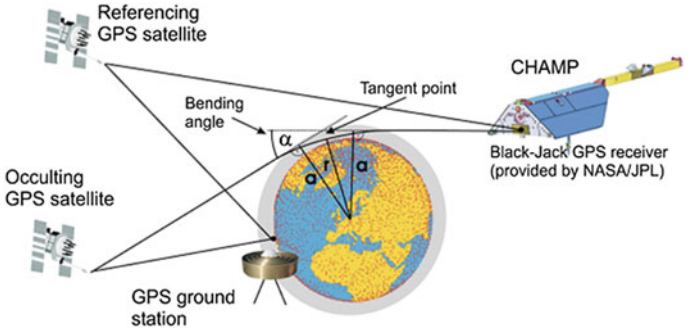


**Fig. 9.2** GNSS radio occultation. Use is made of (i) an occulting satellite, (ii) a non-occulting GNSS satellite and (iii) a ground-based GNSS station to determine the bending angle $\alpha$ from which the vertical profiles of temperature and pressure are determined, e.g., from Eq. 9.4 on p. 144. *Source* Wickert [3]

Earth's atmosphere and are received by LEO satellites. These signals are bent and retarded, causing a delay in their arrival at the LEO.

Figure 9.2 shows the occultation geometry where the signal transmitted from a GNSS to a LEO satellite passes through dispersive layers of the ionosphere and atmosphere, and in so doing senses them. As the signal is bent, the total bending angle, $\alpha$, an impact parameter, $a$, and a tangent radius, $r_t$, define the ray passing through the atmosphere. The *refraction angle* is accurately measured and related to the atmospheric parameters; temperature, pressure and water vapour via the refractive index in Eq. 9.4. Use is made of radio waves where a GNSS receiver onboard a LEO satellite measures, at the required sampling rate, the dual-band carrier-phases (L1 and L2), the C/A-code and P-code group delay (see Sect. 3.3.1) [11, 12]. The data is then processed to remove errors arising from short-term oscillator and instabilities in the satellites and receivers. This is achieved by using at least one ground station and one satellite that is not being occulted, leading to a doppler shift (see Fig. 9.2). Once the observations have been corrected for possible sources of errors, the resulting *Doppler shift* is used to determine the refraction angle $\alpha$.

The variation of $\alpha$ with $a$ during an occultation depends primarily on the vertical profile of the atmospheric refractive index, which is determined globally by *Fermat's principle* of least time and locally by *Snell's law*

$$n \times sin\phi = constant, \tag{9.23}$$

where $\phi$ denotes the angle between the gradient of refraction and the ray path. The doppler shift is determined by projecting spacecraft velocities onto the ray paths at the transmitter and receiver so that atmospheric bending contributes to its measured value. Data from several GNSS transmitters and post-processing ground stations are used to establish the precise positions and velocities of the GNSS transmitters and LEO satellites. These derived positions and velocities are used to calculate the Doppler shift expected in the absence of atmospheric bending (i.e., were the signal to travel in a straight line). By subtracting the *expected* shift from the measured shift, one obtains the excess Doppler shift. Assuming local symmetry and with Snell's law, the excess Doppler shift, together with satellites' *positions* and *velocities*, are used to compute the values of the bending angles $\alpha$ with respect to the impact parameters $a$. Once computed, these bending (refraction) angles are related to the refractive index by

$$\alpha(a) = 2a \int_{r=r_0}^{r=\infty} \frac{1}{\sqrt{n^2 r^2 - a^2}} \frac{\mathrm{d}In(n)}{\mathrm{d}r} \mathrm{d}r, \tag{9.24}$$

which is then inverted using Abel's transformation to give the desired refractive index

$$n(r_0) = \exp\left[\frac{1}{\pi} \int_{a=a_0}^{a=\infty} \frac{\alpha(a)}{\sqrt{a^2 - a_0^2}} da\right]. \tag{9.25}$$

If the atmospheric temperature $T$ and pressure $P$ are provided from external source, e.g., from models and synoptic meteorological data, then the vertical water vapour density could be recovered from GNSS remote sensing data using Eq. (9.4) [11].

To demonstrate the capability of the method, the following examples show that the temperature profiles measured by GNSS around the tropopause region (8–17 km) gives accurate results comparable to the traditional radiosonde method.

Example 9.1 (Validating GNSS derived atmospheric parameters [33]).

In Fig. 9.3, GNSS-derived temperature profiles from LEO missions (COSMIC, CHAMP and GRACE) are compared with the profiles of the closest radiosondes in Australia. The radiosonde launched from Learmonth Airport (22.24°S, 114.09°E) on 14th June 2005 was within 70 km and 40 min from the CHAMP measurement, whereas the radiosonde launched from Hobart Airport (42.84°S, 147.50°E) on 20th December 2006 was within 12 km and 1.25 h from the COSMIC measurement. The radiosonde from Weipa Aero location and the GRACE RO profile were located within 92 km, with time difference of 1.25 h from each other.

A visual examination of Fig. 9.3 indicates that the COSMIC RO temperature profile agrees very well with its corresponding radiosonde profile with almost no deviation from the radiosonde data. The temperature profiles from the CHAMP satellite have been shown, e.g., by Schmidt et al. [34] to agree well in the upper troposphere and lower stratosphere. However, looking at Fig. 9.3, below 5 km, the CHAMP profiles do not fit the radiosonde data as well as those for the COSMIC profiles due to the effect of water vapour. The GRACE temperature profile agrees well with the corresponding radiosonde measurement above 8 km, while below 8 km it is also affected by water vapour like the CHAMP profiles.

♣ End of Example 9.1.

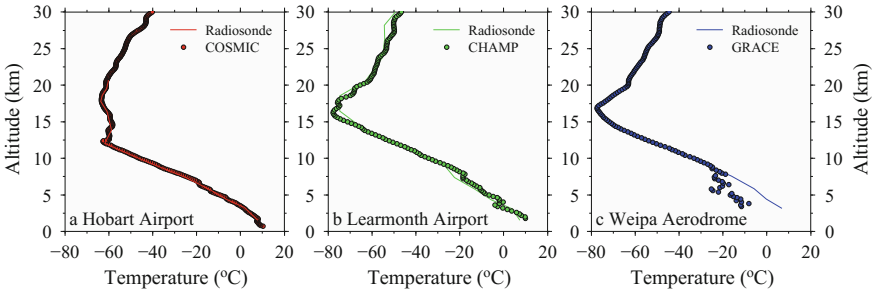


**Fig. 9.3** GNSS-RO soundings observed on **a** 20 December 2006 over Hobart Airport [42.84°S, 147.50°E] using COSMIC RO data, **b** 14 June 2005 over Learmonth Airport in Western Australia [22.24°S, 114.09°E] using CHAMP RO data and **c** on 8 September 2006 over Weipa Aero using GRACE data [12.68°S, 141.92°E]. *Source* [33]

Example 9.2 (Comparison of profiles between 7–30 km height [33]).

GNSS-derived temperature profiles between 7–30 km were then compared to those from the radiosonde observations between 2001 and 2006. The comparison method was based on a maximum spatial separation of 100 km and a temporal difference of 3 h between the GNSS-RO measurements and the radiosonde (e.g., Schmidt et al. [34] use values between 3 h and a distance of 300 km, which they state would mean near constant weather). A distance of 100 km was chosen to account for the spatial drift of the radiosondes, which can reach as far as 200 km from its initial position [35]. Temperatures are compared at 14 standard pressure levels $l$ of the radiosonde data files between 850 and 20 hPa.

The mean temperature deviation at each pressure level $\overline{\Delta T(l)}$ and its standard deviation $\sigma_{\Delta T}(l)$ are calculated according to Eqs. (9.26) and (9.27) [36].

$$\overline{\Delta T(l)} = \frac{\sum_{i=1}^{M(l)} T_{D(LEO)}(i,l) - T_{Radiosonde}(i,l)}{M(l) - 1} \tag{9.26}$$

$$\sigma_{\Delta T}(l) = \sqrt{\frac{1}{M(l) - 1} \sum_{i=1}^{M(l)} \left(T_{D(LEO)}(i,l) - T_{Radiosonde}(i,l)\right)^2}, \tag{9.27}$$

where $M(l)$ denotes the number of data points at each pressure level. The index $i$ indicates the individual pairs of LEO satellite and radiosonde data, $T_{D(LEO)}$ is the dry temperature derived from the LEO data while $T_{Radiosonde}$ is the temperature given by radiosonde measurements. Temperature deviations exhibiting more than 20 K were ignored to eliminate the influence of outliers.

Figure 9.4 compares the deviation between the radiosonde and CHAMP, GRACE and COSMIC profiles, as well as the number of profiles. 80 CHAMP profiles from September 2001 to December 2006 were found to occur within 100 km and a time delay of less than 3 h of a radiosonde profile. The results of the comparisons indicate a temperature bias of less than 1 k for the complete height interval between 9 and 26 km, with a standard deviation of less than 2 K. Between 11 and 26 km the bias is less than 0.5 K with a standard deviation of 1–2 K. The bias of the CHAMP temperature in the lower troposphere (altitude $< 7.5$ km) is largely due to the presence of water vapour, see also [4, 36, 37]. The larger bias between CHAMP and radiosonde data is less than 0.5 k in the upper troposphere and lower stratosphere where there is little or no water vapour. Biases between CHAMP RO data and radiosonde data are all negative for all the altitude levels between 1.5 and 26 km.

Only 18 profiles from GRACE RO data from January 2006 to October 2007 were found within the defined spatial and temporal limits. Nevertheless, the bias is less than 3 K between the altitude range of 9 and 20 km, showing that GRACE RO data agrees well over this range with the radiosonde measurements. Below 9 km, like the CHAMP data, the GRACE temperature profiles are also affected by the presence of

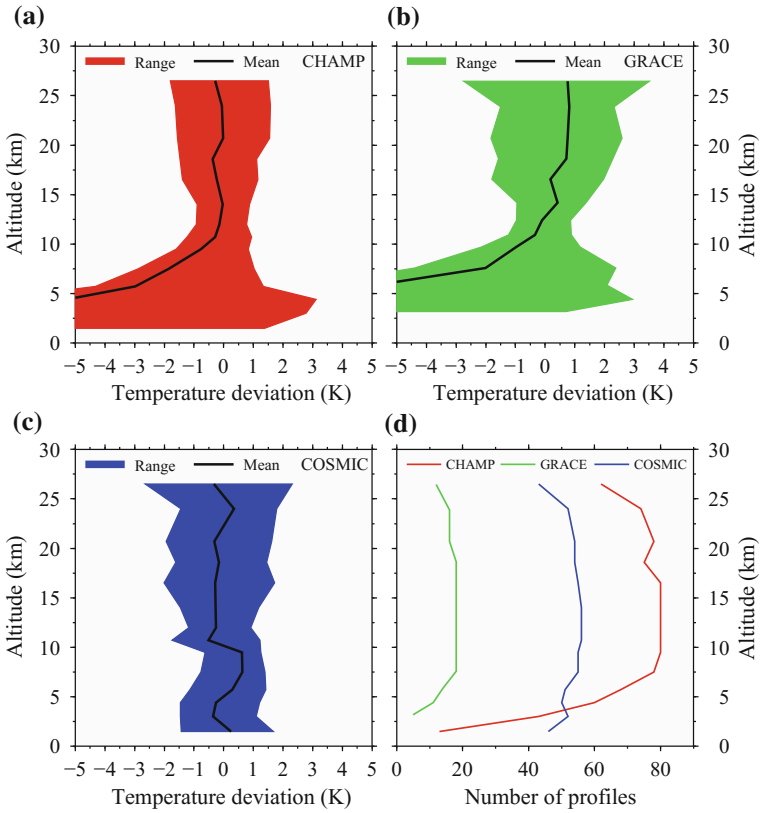


**Fig. 9.4** Comparison of the deviations between GNSS-RO profiles **a** CHAMP, **b** GRACE, and **c** COSMIC profiles. **d** Number of profiles from each satellite. *Source* [33]

water vapour. However, the bias in the GRACE temperatures could be due to the lower number of GRACE profiles meeting the selection criteria.

COSMIC RO data from April 2006 to December 2006 were also used for these comparisons, with 54 COSMIC RO profiles meeting the criteria. From Fig. 9.4, it can be seen that the bias between CHAMP and COSMIC RO data agree well between 10.7 and 25 km, with the difference in the bias over this altitude range being less than 0.5 K. CHAMP RO data displays a lower standard deviation than COSMIC data between 10 and 18 km, with a standard deviation of less than 1.5 K. Below 7.5 km, CHAMP temperatures show a large negative bias whereas the bias from the COSMIC temperature remains constant.

From these three GNSS-RO data sets, the COSMIC temperature data provided a good correlation of data with much smaller standard deviations, with CHAMP and GRACE having higher standard deviations below 10 km. This example highlights the possibility of GNSS satellites being used to remote sense the atmosphere at the heights between 7–25 km with accuracies that will suffice for the environmental

monitoring of the atmosphere, specifically the tropopause, an issue that will be discussed in detail in the next chapters.

♣ End of Example 9.2.

Next, we look at the LEO satellite missions that make the GNSS space borne remote sensing possible. Several missions are currently operational, but we will present only the three most commonly discussed.

#### 9.2.3.2 GNSS Radio Occultation Missions

The three LEO missions covered in this work; CHAMP, GRACE, and COSMIC, jointly contributed a total of 2 478 829 profiles between 2001 and 2008 that were analysed [38]. The German CHAMP (Fig. 9.9, left) satellite was launched on July 15, 2000 into an almost circular and near polar orbit (with an inclination of 87°) at an altitude of about 454 km [39]. The GNSS radio occultation on board CHAMP was activated on Febraury 11, 2001, and from then nearly 541,527 occultations were recorded worldwide by 2008 [38]. Having been in operation for more than a decade, CHAMP ended its mission on 19th of September 2010. CHAMP data can however still be obtained from GFZ (German Research Centre for Geosciences), the Jet Propulsion Laboratory (JPL) or the University Corporation for Atmospheric Research (UCAR).[3]

CHAMP Level 3 data (version 005) from GFZ data contains Abel inverted profiles of refractivity derived from the vertical profiles of bending angles. They also contain the environmental monitoring indicators of air temperature, air density, air pressure, bending angles, positions (latitudes, longitudes), heights above mean sea level, impact parameters, and signal to noise ratios (SNR) up to 30 km above mean sea level with a vertical resolution of 200 m.

Radio occultation measurements by GRACE satellites (Fig. 9.9, right), discussed in detail in Sect. 9.3.3, were first recorded during a 25 h period on July 28/29, 2004 [36, 40]. Atmospheric profiles derived from GRACE show nearly identical characteristics as those from the ECMWF (European Center for Medium-Range Weather Forecasts) [41]. The GRACE satellites had recorded over 141,987 occultations worldwide as of 2008 [38]. The BlackJack GNSS receiver present in the GRACE satellites enables deep atmospheric sounding into the lower troposphere. The GRACE level 2 data, obtainable from GFZ, is equivalent to that from CHAMP, with the same vertical resolution of 200 m.

GNSS limb sounding reached new heights after the launch of the COSMIC mission (see, Fig. 9.5) into a near circular orbit on April 15, 2006, e.g., [8, 42]. COSMIC, a constellation of six identical micro-satellites, is a joint mission between the National Space Organisation (NSPO) of Taiwan and UCAR in the United States, with the main goal of obtaining vertical profiles in near-real time of temperature,

[3] via http://www.cosmic.ucar.edu.

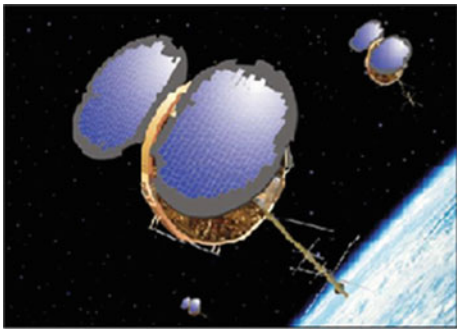

**Fig. 9.5** The COSMIC-1 satellites. Cosmic-2 satellites are planned for launch in 2017 (6 satellites) and in 2020 (6 more satellites). *Source* http://www.cosmic.ucar.edu

pressure, and water vapour in the neutral atmosphere and electron density in the ionosphere [42]. One major change in the COSMIC data compared to CHAMP and GRACE is the improved data quality, with higher yields in the lower troposphere (below 7 km; cf. Figs. 9.3 and 9.4). This is made possible by the use of the Open-Loop (OL) signal tracking technique by the Black Jack GNSS receiver [41]. OL signal tracking, which was not available in previous missions, allows for the tracking of rising occultation and deeper penetration into the lower troposphere.

The COSMIC mission provides about 2200 profiles per day on average and by 2008, it had recorded about 1,796,315 [38, 41] and by 20th January 2017, it had recorded 4,436,178.[4] Level 2 COSMIC data can be obtained from both UCAR[5] and NSPO.[6] It contains the environmental monitoring indicators of refractivity, air temperature, water vapour, air pressure, height above mean sea level, and the position (latitude and longitude) from mean sea level to 400 km. The tropopause region from COSMIC (like CHAMP Level 3 data) contains temperatures, in which the water vapour is neglected. Level 2 COSMIC atmospheric profiles are provided with a vertical resolution of 100 m. In the following example, the number and distribution of GNSS-RO measured over Australia by 2008 from these missions are presented. Due to the success of COSMIC satellite mission that has operated for more than a decade, U.S. agencies and Taiwan have decided to move forward with a follow-on RO mission (called FORMOSAT-7/COSMIC-2) that will launch six satellites into low-inclination orbits in 2017, and another six satellites into high-inclination orbits in 2020.[7]

Example 9.3 (Distribution of GNSS-RO over Australia by 2008 [33]).

The distribution of the GNSS-RO events depends on the geometry of the orbits of the LEO satellites and the transmitting GNSS satellites. CHAMP RO events occured

[4] http://www.cosmic.ucar.edu/index.html.

[5] via http://www.cosmic.ucar.edu.

[6] via http://www.tacc.cwb.gov.tw.

[7] http://www.cosmic.ucar.edu/cosmic2/index.html.

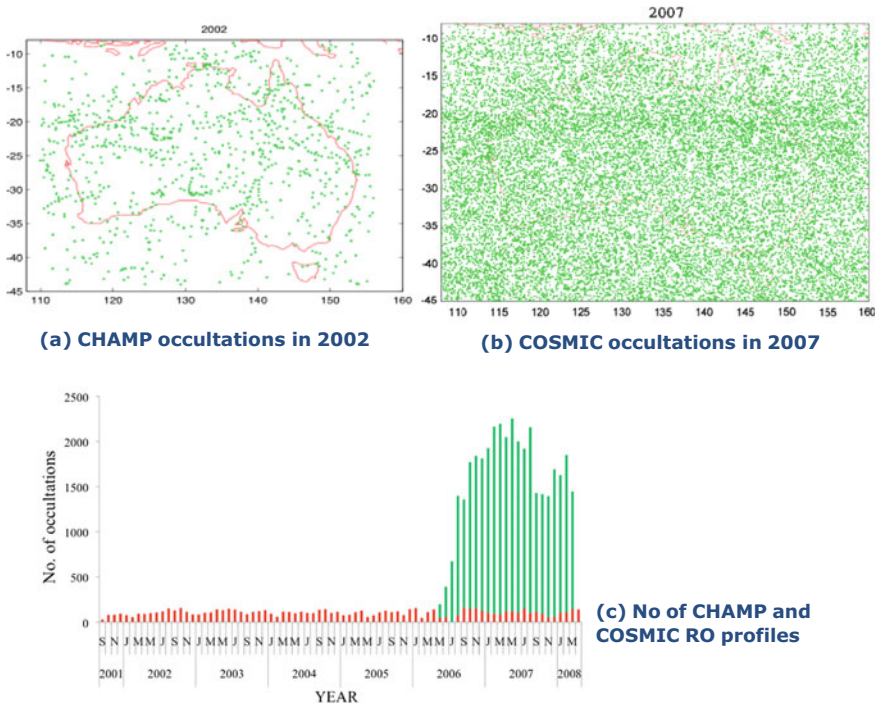


**Fig. 9.6** Number of radio occultations over Australia from **a** CHAMP in 2002, **b** COSMIC in 2007, and **c** total number of occultations for CHAMP and COSMIC from 2001 to 2008. It can be seen that COSMIC provided a very dense coverage within its two years of existence. *Source* [33]

more commonly in high latitudes, with the exception of the poles, with a relatively low distribution in the equatorial regions, e.g., [4, 43]. From the start of September 2001 to April 2008 for example, Australia was covered by 8,472 CHAMP RO profiles, averaging about 108 occultations per month, except for July 2006 (Fig. 9.6). Figure 9.6 indicates that the occultations are well distributed over Australia, although with fewer data in the far north, a fact already pointed out by [43]. It can be seen from Fig. 9.6 that the COSMIC occultations are also well distributed across the region. Like CHAMP RO data, the COSMIC RO profiles are also fewer nearer to the equator (8–15°S).

♣ End of Example 9.3.

#### 9.2.3.3 Ground-Based GNSS Remote Sensing

Whereas GNSS receivers are onboard LEO satellites (e.g., CHAMP and GRACE) in space-borne GNSS remote sensing, they are fixed to ground stations in the case

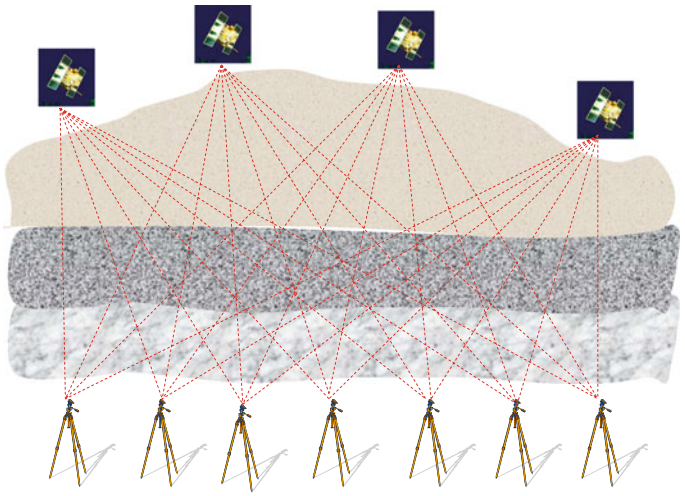

**Fig. 9.7** Schematic diagram showing the remote sensing of water vapour via ground-based GNSS receivers. Figure 5.12 on p. 81 presents an example of a GEONET ground-based station

of ground-based GNSS remote sensing (Fig. 9.7). As we indicated in Sect. 3.4.3, the contribution of the *hydrostatic part*, which can be modeled and eliminated very accurately using surface pressure data or three-dimensional numerical models, is about 90% of the total delay, while that of the wet delay is highly variable with little correlation to surface meteorological measurements, see also [27, 44].

Assuming that the *wet delay* can be accurately derived from GNSS data as discussed in Sect. 9.2.2, and that reliable surface temperature data are available, the wet delay can be converted into an estimate of the total atmospheric water vapour $P_w$ present along the GNSS ray path, as suggested by Belvis et al. [29]. This atmospheric water vapour $P_w$, termed *precipitable water* in GNSS-meteorology, is obtained using Eq. (9.20) on p. 149.

Using several receivers to track several satellites (see Fig. 9.7), a three-dimensional distribution of water vapour and its temporal variation can be quantified. For example, the Japanese GEONET CORS network (Fig. 5.14 on p. 85) is dedicated to ground-based GNSS meteorology, e.g., [17, 45]. The dense network of GNSS receivers is capable of delivering information about atmospheric water vapour content, which is useful to meteorological monitoring (e.g., climate studies and weather forecasting discussed in Sect. 11.4). Hanssen et al. [46] point out that maps of the water vapor distribution associated with, for example, a precipitating cloud, a partly precipitating cold front, or horizontal convective rolls, reveal quantitative measurements that are not observable with conventional methods.

Example 9.4 (Global validation of GNSS-derived water vapor [47]).

Heise et al. [47] provides an overview of the *data processing* and *retrieval* of vertical refractivity, temperature and water vapor profiles from GNSS radio occultation observations. They also undertook a global validation of CHAMP water vapor profiles with radiosonde data and obtain a bias of about 0.2 g/kg and a standard deviation of less than 1 g/kg specific humidity in the lower troposphere, thus demonstrating the potentials of GNSS-derived CHAMP retrievals for monitoring the mean tropospheric water vapor distribution on a global scale.

♣ End of Example 9.4.

## 9.3 GNSS Contribution to Remote Sensing of Gravity Variations

In the subsections that follow, it is explained how GNSS satellites (particularly GPS) support LEO satellites used to monitor variations in gravity field, which are in turn used to remote sense the changes in stored water at continental scales. The most significant success of a LEO satellite is evidenced in the GRACE satellites discussed in Sect. 9.3.3. A possible use of GNSS satellites to measure variations in water mass is illustrated by Tregoning et al. [48] whose predictions derived from GRACE measured fields show a correlation with GNSS measured deformations, suggesting the possible use of such deformations to infer changes in stored water potential on much shorter temporal and spatial scales than GRACE provides (and with low-latency), while averaging over much larger spatial scales than afforded by multipath amplitude measurements [10].

### *9.3.1 Mass Variation and Gravity*

Two types of gravity field variation exists. The *first* is the long-term, also known as mean gravity field, which is due to the static part of the gravity field. The variation is constant over a very long time interval. Its study is useful in understanding the solid structure of the Earth, ocean circulation, and in achieving a universal height measuring system. In this respect, GNSS satellites are used to position LEO satellites such as GOCE (Gravity field and the steady state-of-the ocean circulation explorer, Fig. 9.8), which maps changes in gravity using state-of-the-art gradiometer with improved accuracy, see e.g., Hirt [49]. GOCE data is expected to benefit other studies such as those concerned with earthquakes, changes in sea level, and volcanoes.[8]

[8] See, e.g., http://www.esa.int/esaCP/SEMV3FO4KKF_Germany_0.html.

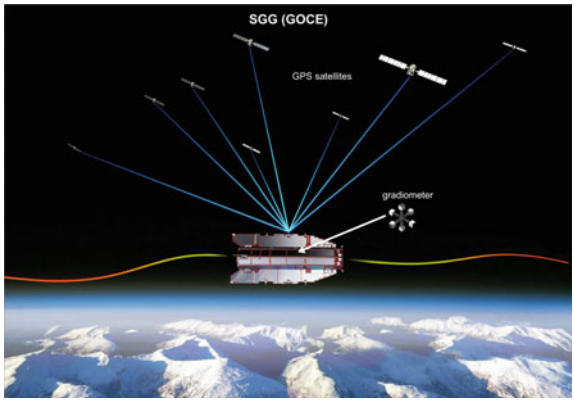


**Fig. 9.8** GNSS satellites track the GOCE satellite in space, thus contributing to the determination of its position (©ESA). The GOCE satellite's accurate determination of the static gravity field is expected to contribute towards studies of changes in sea level, earthquakes, and volcanoes. Figure modified by D. Rieser [50]

The *second* type of variation of the Earth's gravity field is associated with those processes that occur over shorter time scales, such as atmospheric circulation or the hydrological cycle. This is known as the *time-varying gravity field* and is the component which enables the monitoring of, for example, variations in water resources and the melting of the polar ice.

By removing the effects of the other processes that cause changes in the gravity field, changes in *terrestrial water storage* can thus be inferred from the observed temporal changes in the terrestrial gravity field. By assuming the density of water as 1.00 g/cm$^3$, and following the relation of [51], Ellet et al. [52] present the relationship between changes in stored water and gravity as

$$\Delta S = 0.419 \Delta g, \tag{9.28}$$

where water storage change $\Delta S$ is given in units of cm of water and gravity change $\Delta g$ is in units of microGal ($10^{-6}$ cm/s$^2$). From Eq. (9.28), it is seen therefore, that monitoring variations in the gravity field can enable hydrological changes to be monitored.

### 9.3.2 High and Low Earth Orbiting Satellites

At the broadest conceptual level, LEO satellites' gravity field missions observe (either directly or indirectly) gradients in the Earth's external gravitational field. This is essentially done through differential measurements between two or more points, thus largely eliminating spatially correlated errors (cf. differential GPS in Chap. 5). When done from space, two approaches can be used, e.g., [53, 54]:

1. Satellite-to-satellite tracking (SST), or
2. A dedicated gravity gradiometer on board a satellite, coupled with SST.

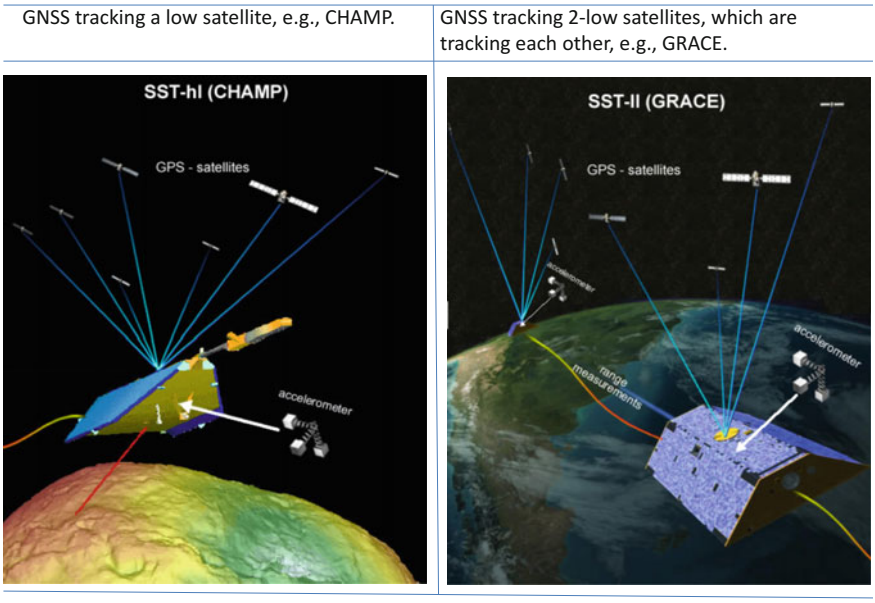


**Fig. 9.9** *Left* SST-hl realized with CHAMP (©GFZ Potsdam ([2.2]). *Right* A combination of ll-SST and hl-SST realized with GRACE and GNSS satellites(©GRACE - CSR Texas ([2.2]). Figures modified by D. Rieser [50]). GNSS satellites are used in determining the positions of these satellites in space. For the GRACE satellites (*right*) inter-satellite distances can be computed from these positions and compared to the measured K-band distances, thus providing additional independent information

The SST methods can use either low-low inter-satellite tracking (ll-SST, see Fig. 9.9, right), where two LEO satellites track one another and additional observations in terms of high precision ranges and range rates between the two satellites are taken, or high-low inter-satellite tracking (hl-SST, see Fig. 9.9), where high-Earth orbiting satellites (notably GPS) track a LEO satellite. The low-low mode, compared to the high-low mode, has the advantage of signal amplification leading to a higher resolution of the obtained gravity variations, up to the medium wavelength spectrum of a few hundred km in spatial extent [53]. Taking this further, a combination of ll-SST and hl-SST is conceptually better still, as is currently demonstrated by the GRACE mission (Fig. 9.9, right) with a baseline length between the two satellites of about 220 km. This is treated in detail in the next section.

In order to detect temporal gravity field variations at smaller spatial scales, the satellite(s) being tracked must be in as-low-as-possible orbits (close to the mass source), with the satellites being as free as possible from the perturbing effects of atmospheric drag [53]. In addition, so-called de-aliasing models (for correcting short-term - 6 h - variations due to atmosphere and ocean mass variations) have to be used to mitigate the propagation of unwanted signals (e.g., leakage from the oceans) into the derived gravity solutions, e.g., [55].

### 9.3.3 Gravity Recovery and Climate Experiment

The GRACE mission, launched on 17th of March 2002, consists of two near-identical satellites following one another in nearly the same orbital plane (about 400 km altitude) separated by a distance of 220 km; the so-called tandem formation (see Fig. 9.9, right). The ll-SST is measured using K-band ranging, coupled with hl-SST tracking of both satellites by GNSS (GPS; Fig. 9.9, right). GNSS receivers are placed on GRACE satellites to measure occulted signals (see Sect. 9.2.3.1), and also to determine the orbital parameters of GRACE satellites required in order to determine gravity changes. On-board accelerometers monitor orbital perturbations of non-gravitational origin (see, e.g., Sect. 4.1).

GRACE mission processes GNSS data to contribute to the recovery of long-wavelength gravity field, remove errors due to long-term onboard oscillator drift, and aligns measurements between the two spacecraft [56, p. 200]. The timing function of GNSS for precision orbit determination, in terms of position and velocity as a function of time, enable orbits to be determined within an accuracy better than 2 cm in each coordinate [56, p. 200]. These precise locations of the two satellites in orbit allows for the creation of gravity maps approximately once a month.[9] These gravity maps, when converted to total water storage maps, are useful for monitoring changes in stored water potential as demonstrated in Chap. 14.

The Earth's gravity field is mapped by making accurate measurements of changes in the distance between the satellites, using GNSS and a microwave ranging system. These changes in the distances between the two satellites occur due to the effect of the gravity (mass concentration) of the Earth. As the lead satellite passes through a region of mass concentration, it is pulled away from the trailing satellite (Fig. 9.9, right). As the trailing satellite passes over the same point, it is pulled towards the lead satellite thus changing the distance between the satellites.

Time-variable gravity field solutions are obtained by the exploitation of GRACE observation data over certain time intervals, i.e., every month [57, 58], or less, e.g., [59, 60]. There are a number of institutions delivering GRACE products, each applying their own processing methodologies and, often, different background models. The mission is currently providing scientists with an efficient and cost-effective way to monitor time-varying component of the gravity field with unprecedented accuracy and in the process yield crucial information about the distribution and flow of mass within the Earth system. The process causing gravity variations that are currently being studied by GRACE include [61];

- changes due to surface and deep currents in the ocean leading to more information about ocean circulation, e.g., [62, 63],
- changes in groundwater storage on land masses, relevant to water resource managers, e.g., [61, 64–66, see also Chap. 14],

[9] http://www.csr.utexas.edu/grace/publications/brochure/page11.html.

- exchanges between ice sheets or glaciers and the oceans, needed for constraining the mass balance of the global ice regime and sea level change, e.g., [67, 68, see also Sect. 11.4.4],
- air and water vapour mass change within the atmosphere, vital for atmospheric studies, e.g., [69, 70], and
- variations of mass distribution within the Earth arising from, e.g., on-going glacial-isostatic adjustments and earthquakes, e.g., [71, 72].

Currently, river basins of the order of 200,000 km$^2$ and above in area can be successfully studied using the GRACE products [73]. In general, to understand how the GRACE satellites monitor changes in fresh water (all groundwater, soil moisture, snow, ice, and surface waters), first, the larger effect of the mass of the Earth, i.e., the static gravity field discussed in Sect. 9.3.1, which is always a constant $G_0$ corresponding to nearly 99% of the total field, is computed from a static model (e.g., *GGSM01S* [58]) and removed by subtracting it from the monthly gravity field ($G(t)$) measured by GRACE at a time $t$ [74], i.e.,

$$\Delta G(t) = G(t) - G_0, \tag{9.29}$$

to give the monthly time-variable gravity field $\Delta G(t)$. Changes mostly related to the atmosphere and ocean, which occur over timescales shorter than one month, are then removed using models, see e.g., Wahr et al. [75]. Remnant atmospheric and oceanographic effects that last for more than one month can be removed using atmospheric and ocean circulation models before water storage change can be analyzed. The resulting difference in Eq. (9.29), which is called the gravity field anomaly is usually due to changes in stored water. If we consider $\overline{\Delta C}_{nm}(t)$ and $\overline{\Delta S}_{nm}(t)$ to be the normalized Stokes coefficients expressed in terms of millimeters of geoid height, with $n$ and $m$ being degree and order respectively, the time-variable geoid in (9.29) is then expanded in-terms of spherical harmonic coefficients (see [76]) as

$$\Delta G(t) = \sum_{n=1}^{N} \sum_{m=0}^{n} (\overline{\Delta C}_{nm}(t) cos(m\lambda) + \overline{\Delta S}_{nm}(t) sin(m\lambda)) \overline{P}_{nm}\,(cos(\theta))\,, \tag{9.30}$$

where $N$ is the maximum degree of expansion, $\theta$ is the co-latitude, $\lambda$ the longitude and $\overline{P}_{nm}$ the fully normalized Legendre polynomial [76]. From the gravitational spherical harmonic coefficients (9.30), the equivalent water thickness is computed using the following steps:

1. The gravitational residual coefficients are converted into the surface density coefficient differences by [75]

$$\begin{pmatrix} \Delta \check{C}_{lm}(\mathrm{M}_j) \\ \Delta \check{S}_{lm}(\mathrm{M}_j) \end{pmatrix} = \frac{\rho_{\mathrm{avg}}}{3\rho_{\mathrm{w}}} \frac{2l+1}{1+k'_l} \begin{pmatrix} \Delta \bar{C}_{lm}(\mathrm{M}_j) \\ \Delta \bar{S}_{lm}(\mathrm{M}_j) \end{pmatrix}, \tag{9.31}$$

where $k'_l$ is the *load Love* number of degree $l$, $\rho_{\text{avg}} = 5517\,\text{kg/m}^3$ the average density of the Earth, and $\rho_{\text{w}} = 1000\,\text{kg/m}^3$ the density of water.

2. The spatial variation of the surface density is then computed through

$$\Delta\sigma(\theta, \lambda, \text{M}_j) = R\rho_{\text{w}} \sum_{l=1}^{l_{\max}} \sum_{m=0}^{l} [\Delta\check{C}_{lm}(\text{M}_j) \cos m\lambda + \Delta\check{S}_{lm}(\text{M}_j) \sin m\lambda] \bar{P}_{lm}(\cos\theta), \tag{9.32}$$

where $R = 6378137\,\text{m}$ is the radius of the Earth and $\Delta\sigma$ is in $kg/m^2$.

3. Finally, the changes in total water storage (TWS) are calculated by

$$\text{TWS}(\phi, \lambda, \text{M}_j) = \frac{\Delta\sigma(\theta, \lambda, \text{M}_j)}{\rho_{\text{w}}} = \frac{\Delta\sigma(\theta, \lambda, \text{M}_j)}{1000} \quad \text{[meters]}. \tag{9.33}$$

The first steps in the analysis of GRACE data would provide an estimate of the changes in total water storage. In the second step, the changes can then be separated into their various components as discussed, e.g., in [61, 74] to obtain changes in the respective components (e.g., groundwater, surface water, soil moisture, and ice).

The GRACE satellites have now well exceeded their planned 5 year life-span, however, plans are underway to launch a GRACE follow-on mission (GRACE-FO) around 2017 given the excellent results that have been delivered so far, see e.g., [38]. Although GRACE-FO satellites, like their predecessor, will use the same kind of microwave ranging system giving a similar level of precision, they will also test an experimental instrument using lasers instead of microwaves, which promises to make the measurement of their separation distance at least 20 times more precise[10]. In Yang [77], GRACE products are used to constrain recent freshwater flux from Greenland where the data show that Arctic freshwater flux started to increase rapidly in the mid-late 1990s, coincident with a decrease in the formation of dense Labrador Sea Water, a key component of the deep southward return flow of the Atlantic Meridional Overturning Circulation (AMOC). Recent freshening of the polar oceans may be reducing formation of Labrador Sea Water and hence may be weakening the AMOC [77].

## 9.4 Satellite Altimetry

### *9.4.1 Remote Sensing with Satellite Altimetry*

Satellites altimetry (Fig. 9.10) operates in two steps:

- *First*, the precise orbit of the satellite, i.e., its position, is determined. Through this, its *height* above the Earth is obtained.

[10] http://gracefo.jpl.nasa.gov/mission/.

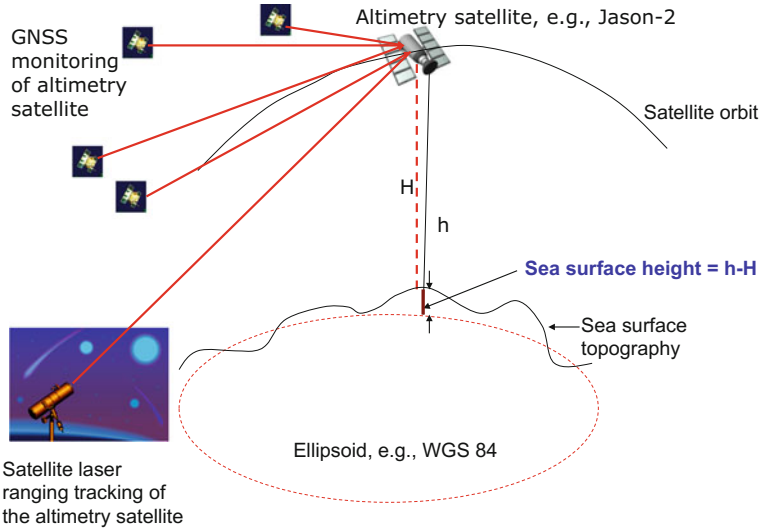


**Fig. 9.10** GNSS in support of monitoring changes in sea level through the determination of the altimetry satellites' precise orbit. From the precise orbital parameters, the height component $h$ is useful in determining changes in sea level through the difference $\{h - H\}$, where $H$ is measured by multiplying the speed of light with the time taken by the signals to travel from and to the satellite divided by 2, since the same distance is covered twice

- *Second*, range measurements are made by obtaining the time an emitted signal (radar or laser) travels to the Earth's surface and reflected back to the satellite.

GNSS contributes to the *first step* where height is determined. This is achieved through GNSS receiver onboard the space satellites that enables monitoring of ranges and timing signals from GNSS satellites (see Sect. 4.2). The observed GNSS ranges provide precise and continuous tracking of the spacecraft, thereby delivering its position $\{\phi, \lambda, h\}$ at any time. The height component $h$ is useful in determining the measured height (see Fig. 9.10). Besides GNSS tracking, other approaches such as satellite laser ranging (SLR) and DORIS (Doppler Orbitography and Radio positioning Integrated by Satellite) are also used to ensure that precise orbit determination is achieved.

In the *second step*, the Earth's surface heights (e.g., ocean surface, glaciers, and ice sheets) are measured using ranges from the space altimetry satellite to the surface of interest. Radar altimeters send microwave signals to the Earth's surface and measures the time taken by the reflected signals to travel back. Using Eq. (3.1), the distance from the satellite to the Earth's surface is derived. Since the signals pass through the atmosphere from and to the satellites, they are affected by the atmosphere (see Sect. 3.4.3) and as such, atmospheric corrections again have to be made. The sea surface height is then obtained by subtracting the measured ranges in step 2 from the GNSS-derived satellite heights in step 1 (Fig. 9.10).

### 9.4.2 Satellite Altimetry Missions

Direct use of GNSS to measure the annual changes in mass loss of the Greenland ice sheet is demonstrated in the work of Yang [77] who uses coastal uplift observed by GPS whose results show both spatial and temporal variations of coastal ice mass loss and suggest that a combination of warm atmospheric and oceanic condition drove the variations. Changes in ice sheet have been monitored using satellite altimetry among other methods. The first true altimetry mission was TOPEX/Poseidon, developed by NASA and the Centre National d'Etudes Spatiales (CNES) and launched on 10 August 1992. Its mission ended in 2006 after 13 years of operation, providing 11 years of data. It was followed by Jason-series (Jason-1 was launched on 07/12/2001 and Jason-2 on 20/06/2008). Both TOPEX/Poseidon and Jason-1 were dedicated to measuring global mean sea level from space. TOPEX/Poseidon orbited at 1336 km above the Earth and covered the global oceans every 10 days, measuring the heights of the ocean surface directly underneath the satellite with an accuracy of 2–4 cm or better when averaging over several measurements [78]. Jason-2 is expected to be replaced by Jason-3 launched on 17th of January 2016, and subsequently Sentinel-6. Sentinel-6 will continue high precision ocean altimetry measurements in the 2020–2030 time-frame using two successive, identical satellites (Jason-Continuity of Service): Jason-CS-A and Jason-CS-B, and as a secondary objective, collect high resolution vertical profiles of temperature using the GNSS Radio-Occultation sounding technique discussed in Sect. 9.2.3.1.[11] Combined, all these satellites will provide long-term series of data capable of undertaking *climatological studies* resulting from changes in sea level.

ICESat (launched on January 12, 2003) uses a 1064 nm-laser operating at 40 Hz to make measurements at 172-m intervals over ice, ocean, and land [79]. It combines state-of-the-art laser ranging capabilities with precise orbit and attitude control and knowledge to provide very accurate measurements of ice sheet topography and elevation changes along track. It has the specific objective of measuring changes in polar ice as part of NASA's Earth Observing System.

By observing changes in ice sheet elevation, it is possible to quantify the growth and shrinkage of parts of the ice sheets with great spatial detail, thus enabling an assessment of ice sheet mass balance and contributions to sea level. Moreover, because the mechanisms that control ice sheet mass loss and gain in accumulation, surface ablation, and discharge presumably have distinct topographic expressions, ice sheet elevation changes also provide important insights into the processes causing the observed changes [79]. ICESat-2 schedule for launch in 2017 is expected to be a follow-on mission to ICESat (Fig. 9.11) with improved laser capability compared to ICESat and will have the objectives of measuring ice sheet changes, sea ice thickness, and vegetation biomass. Achieving these objectives will contribute to the following [79]:

[11] https://eospso.nasa.gov/missions/sentinel-6.

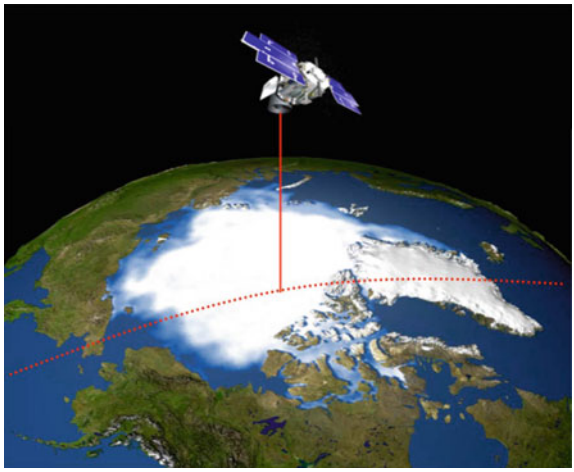

**Fig. 9.11** Schematic diagram of ICESat on a transect over the Arctic. ICESat uses a 1064 nm-laser operating at 40 Hz to make measurements at 172-m intervals over ice, oceans, and land. *Source* Abdalati et al. [79]

- Contribute to the development of predictive models that capture both dynamic and surface processes.
- Since the thickness distribution of sea ice controls energy and mass exchanges between the ocean and atmosphere at the surface, and the fresh water fluxes associated with melting ice serve as stabilizing elements in the circulation of the North Atlantic waters, basin-scale fields of ice thickness are therefore essential to improve our estimates of the seasonal and interannual variability in regional mass balance, the freshwater budget of the polar oceans, and the representation of these processes in regional and climate models.
- Its capability of producing a vegetation height surface with 3-m accuracy at 1-km spatial resolution, assuming that off-nadir pointing can be used to increase the spatial distribution of observations over terrestrial surfaces. This sampling, combined with a smaller footprint of 50 m or less, would allow characterization of vegetation at a higher spatial resolution than ICESat, and is expected to provide a new set of global ecosystem applications.
- In addition, the atmospheric measurement capability of ICESat-2, even at near-IR wavelengths, will enable global measurements of cloud and aerosol structure to extend the record of these observations beyond those provided by the current lasers onboard ICESat.

## 9.5 Concluding Remarks

GNSS remote sensing and its application to environmental monitoring is a new and active area of research. The data that has been collected so far has provided several environmental (atmospheric) properties that were hitherto difficult to fathom. The

new technique clearly promises to contribute significantly to environmental studies. When the life span of the various missions (e.g., GRACE) is reached, thousands of data sets will have been collected that will help to unravel some of the complex nature of atmospheric and environmental phenomenon. From the analysis of water vapour trapped in the atmosphere and tropopause temperature, climate change studies will be significantly enhanced. This will be discussed further in Chaps. 11 and 12.

## References


1. Hammond WC, Brooks BA, Bürgmann R, Heaton T, Jackson M, Lowry AR, Anandakrishnan S (2011) Scientific value of real-time Global Positioning System data. Eos 92(15):125–126. doi:10.1029/2011EO150001
2. Yunck TP, Wu SC, Wu JT, Thornton CL (1990) Precise tracking of remote sensing satellites with the global positioning system. IEEE Transactions on Geoscience and Remote Sensing 28:108–116
3. Wickert J (2002) Das CHAMP-Radiookkultationsexperiment: Algorithmen, Prozessierungssystem und erste Ergebnisse. Dissertation. Scientific Technical Report STR02/07, GFZ Potsdam
4. Foelsche U, Borsche M, Steiner AK, Gobiet M, Pirscher B, Kirchengast G, Wickert J, Schmidt T (2008) Observing upper troposphere-lower stratosphere climate with radio occultation from the CHAMP satellite. Climate Dynamics 31:49–65. doi:10.1007/s00382-007-0337-7
5. Schmidt T, Heise S, Wickert J, Beyerle G, Reigber C (2005) GPS radio occultation with CHAMP and SAC-C: global monitoring of thermal tropopause parameters. Atmospheric Chemistry and Physics 5:1473–1488
6. Schmidt T, Wickert J, Beyerle G, Heise S (2008) Global tropopause height trends estimated from GPS radio occultation data. Geophysical Research Letters 35:L11806. doi:10.1029/2008GL034012
7. Seidel DJ, Randel WJ (2006) Variability and trends in the global tropopause estimated from radiosonde data. Journal of Geophysical Research 111:D21101. doi:10.1029/2006JD007363
8. Anthes RA, Bernhardt PA, Chen Y, Cucurull L, Dymond KF, Ector D, Healy SB, Ho SP, Hunt DC, Kuo YH, Liu H, Manning K, McCormick C, Meehan TK, Randel WJ, Rocken C, Schreiner WS, Sokolovskiy SV, Syndergaard S, Thompson DC, Trenberth KE, Wee TK, Yen NL, Zeng Z (2008) The COSMIC/FORMOSAT-3 mission: early results. Bulletin of the American Meteorological Society 89(3):313–333. doi:10.1175/BAMS-89-3-313
9. Bevis M, Businger S, Herring TA, Rocken C, Anthes RA, Ware RH (1992) GPS Meteorology: remote sensing of water vapour using global positioning system. Journal of Geophysical Research 97:15787–15801
10. Hammond WC, Brooks BA, Bürgmann R, Heaton T, Jackson M, Lowry AR, Anandakrishnan S (2010) The scientific value of high-rate, low-latency GPS data, a white paper. http://www.unavco.org/community_science/science_highlights/2010/realtimeGPSWhitePaper2010.pdf. Accessed 06 June 2011
11. Melbourne WG, Davis ES, Duncan CB, Hajj GA, Hardy K, Kursinski R, Mechan TK, Young LE, Yunck TP (1994) The application of spaceborne GPS to atmospheric limb sounding and global change monitoring. JPL Publication 94-18
12. Awange, JL, Fukuda Y, Takemoto S, Wickert J, Aoyama A (2004) Analytic solution of GPS atmospheric sounding refraction angles. Earth, Planet and Space 56: 573–587. doi:10.1186/BF03352518
13. Healey S, Jupp A, Offiler D, Eyre J (2003) The assimilation of radio occultation measurements. In: Reigber C, Lühr H, Schwintzer P (eds) First CHAMP mission results for gravity, magnetic and atmospheric studies. Springer, Heidelberg

14. Kuo Y-H, Sokolovski SV, Anthens RA, Vandenberghe F (2000) Assimilation of the GPS radio occultation data for numerical weather prediction. Terrestrial, Atmospheric and Oceanic Science 11:157–186
15. Steiner AK, Kirchengast G, Foelsche U, Kornblueh L, Manzini E, Bengtsson L (2001) GNSS occultation sounding for climate monitoring. Physics and Chemistry of the Earth (A) 26(3):113–124. doi:10.1016/S1464-1895(01)00034-5
16. Yunck TP (2003) The promise of spaceborne GPS for Earth remote sensing. In: International workshop on GPS meteorology, 14th-17th January 2003, Tsukuba, Japan
17. Anthes RA et al (2004) Application of GPS remote sensing to meteorology and related fields. Journal of Meteorological Society of Japan 82(1B):259–596
18. Foelsche U, Kirchengast G, Steiner AK (2006) Atmosphere and climate. Studies by occultation methods, Springer, Berlin
19. Ware H, Fulker D, Stein S, Anderson D, Avery S, Clerk R, Droegmeier K, Kuettner J, Minster B, Sorooshian S (2000a) SuomiNet: a real-time national GPS network for atmospheric research and education. Bulletin of the American Meteorological Society 81:677–694
20. Ware R (1992) GPS sounding of the earth's atmosphere. GPS World 3:56–57
21. Businger S, Chiswell SR, Bevis M, Duan J, Anthes RA, Rocken C, Ware RH, Exner M, VanHove T, Solheim FS (1996) The promise of GPS in atmospheric monitoring. Bulletin of the American Meteorological Society 77:5–18
22. Ware R, Exner M, Schreiner W, Anthes R, Feng D, Herman B, Gorbunov M, Sokolovskiy S, Hardy K, Kuo Y, Zou X, Trenberth K, Meehan T, Melbourne W, Businger S (1996) GPS sounding of atmosphere from low earth orbit: preliminary results. Bulletin of the American Meteorological Society 77:19–40. doi:10.1175/1520-0477(1996)077<0019:GSOTAF>2.0.CO;2
23. Jin S, Komjathy A (2010) GNSS reflectometry and remote sensing: a new objectives and results. Advances in Space Research 46:111–117
24. Resch GM (1984) Water vapor radiometry in geodetic applications. In: Geodetic Refraction (ed) Brunner FK. Springer, New York, pp 53–84
25. Thayer GD (1974) An improved equation for the radio refractive index of air. Radio Science 9(10):803–807. doi:10.1029/RS009i010p00803
26. Leick A (2004) GPS satellite surveying, 3rd edn. Wiley, New York
27. Davis JL, Herring TA, Shapiro II, Rogers AE, Elgered G (1985) Geodesy by radio interferometry: effects of atmospheric modelling errors on estimates of baseline length. Radio Science 20:1593–1607
28. Niell AE (1996) Global mapping functions for the atmosphere delay at radio wavelengths. Journal of Geophysical Research 101(B2):3227–3246. doi:10.1029/95JB03048
29. Bevis M, Businger S, Chiswell S, Herring TA, Anthes RA, Rocken C, Ware RH (1994) GPS Meteorology: mapping zenith wet delays onto precipitable water. Journal of Applied Meteorology 33:379–386
30. Rocken C, Ware R, Hove TV, Solheim F, Alber C, Johnson J, Bevis M, Businger S (1993) Sensing atmospheric water vapour with the Global Positioning System. Geophysical Research Letters 20(23):2631–2634. doi:10.1029/93GL02935
31. Tralli DM, Lichten SM (1990) Stochastic estimation of tropospheric path delays in global positioning system geodetic measurements. Journal of Geodesy 64:127–159. doi:10.1007/BF02520642
32. Askne J, Nordius H (1987) Estimation of tropospheric delay for microwaves from surface weather data. Radio Science 22:379–386
33. Khandu Awange JL, Wickert J, Schmidt T, Sharifi MA, Heck B, Fleming K (2011) GNSS remote sensing of the Australian tropopause. Climatic Change 105(3–4):597–618. doi:10.1007/s10584-010-9894-6
34. Schmidt T, Wickert J, Beyerle G, Reigber C (2004) Tropical tropopause parameters derived from GPS radio occultation measurements with CHAMP. Journal of Geophysical Research 109:D13105. doi:10.1029/2004JD004566
35. McGrat R, Semmler T, Sweeney C, Wang S (2006) Impact of balloon drift errors in radiosonde data on climate statistics. Journal of climate 19(14):3430–3442. doi:10.1175/JCLI3804.1

36. Wickert J (2004) Comparison of vertical refractivity and temperature profiles from CHAMP with radiosonde measurements. Danish Meteorological Institute, Copenhagen
37. Kuo Y-H, Schreiner WS, Wang J, Rossiter DL, Zhang Y (2005) Comparison of GPS Radio occultation soundings with radiosonde. Geophysical Research Letters 32:L05817. doi:10.1029/2004GL021443
38. Arras C, Jacobi C, Wickert J, Heise S, Schmidt T (2010) Sporadic E signatures revealed from multi-satellite radio occultation measurements. Advances in Radio Science 8:225–230. doi:10.5194/ars-8-225-2010
39. Wickert J, Beyerle G, Hajj GA, Schwieger V, Reigber C (2002) GPS radio occultation with CHAMP: atmospheric profiling utilizing the space-based single differencing technique. Geophysical Research Letters 29(8):1187. doi:10.1029/2001GL013982
40. Beyerle G, Schmidt T, Michalak G, Heise S, Wickert J, Reigber C (2005) GPS radio occultation with GRACE: atmospheric profiling utilizing the zero difference technique. Geophysical Research Letters 32(L13806): doi:10.1029/2005GL023109
41. Wickert J, Michalak G, Schmidt T, Beyerle G, Cheng C, Healy S, Heise S, Huang C, Jakowski N, Köhler W, Mayer C, Offiler D, Ozawa E, Pavelyev A, Rothacher M, Tapley B, Arras C (2009) GPS radio occultation: results from CHAMP, GRACE and FORMOSAT-3/COSMIC. Terrestrial, Atmospheric and Oceanic Sciences 20:35–50. doi:10.3319/TAO.2007.12.26.01(F3C)
42. Cheng CZ, Kuo Y-H, Anthes RA, Wu L (2006) Satellite constellation monitors global and space weather. EOS, Transactions American Geophysical Union 87(17):166. doi:10.1029/2006EO170003
43. Tsuda T, Hocke K (2004) Application of GPS occultation for studies of atmospheric waves in the Middle Atmosphere and Ionosphere. In: Anthens et al (eds) Application of GPS remote sensing to meteorology and related fields. Journal of Meteorological Society of Japan, vol 82, No. 1B, pp 419–426
44. Chen G, Herring TA (1997) Effects of atmospheric azimuthal asymmetry on the analysis of apace geodetic data. Journal of Geophysical Research 102(B9):20489–20502
45. Tsuda T, Heki K, Miyazaki S, Aonashi K, Hirahara K, Tobita M, Kimata F, Tabei T, Matsushima T, Kimura F, Satomura M, Kato T, Naito I (1998) GPS meteorology project of Japan - Exploring frontiers of geodesy - Earth Planets Space, 50(10): i–v
46. Hanssen RF, Weckwerth TM, Zebker HA, Klees R (1999) High-Resolution water vapor mapping from interferometric radar measurements. Science 283:1297–1299. doi:10.1126/science.283.5406.1297
47. Heise S, Wickert J, Beyerle G, Schmidt T, Reigber C (2006) Global monitoring of tropospheric water vapor with GPS radio occultation aboard CHAMP. Advances in Space Research 37(12):2222–2227. doi:10.1016/j.asr.2005.06.066
48. Tregoning P, Watson C, Ramillien G, McQueen H, Zhang J (2009) Detecting hydrologic deformation using GRACE and GPS. Geophysical Research Letters 36:L15401. doi:10.1029/2009GL038718
49. Hirt C, Gruber T, Featherstone WE (2011) Evaluation of the first GOCE static gravity field models using terrestrial gravity, vertical deflections and EGM2008. quasigeoid heights. Journal of Geodesy 85:723–740. doi:10.1007/s00190-011-0482-y
50. Rieser D (2008) Comparison of GRACE-derived monthly Surface Mass Variations with Rainfall Data in Australia. MSc thesis. Graz University of Technology
51. Pool DR, Eychaner JH (1995) Measurements of aquifer-storage change and specific yield using gravity surveys. Groundwater 33(3):425–432. doi:10.1111/j.1745-6584.1995.tb00299.x
52. Ellett KM, Walker JP, Western AW, Rodell M (2006) A framework for assessing the potential of remote sensed gravity to provide new insight on the hydrology of the Murray–Darling Basin. Australian Journal of Water Resources 10(2):89–101
53. Awange JL, Sharifi MA, Baur O, Keller W, Featherstone WE, Kuhn M (2009) GRACE hydrological monitoring of Australia. Current limitations and future prospects. Journal of Spatial Science 54(1):23–36. doi:10.1080/14498596.2009.9635164
54. Rummel R, Balmino G, Johannessen J, Visser P, Woodworth P (2002) Dedicated gravity field missions - principles and aims. Journal of Geodynamics 33(1):3–20. doi:10.1016/S0264-3707(01)00050-3

55. Schrama EJO, Visser PNAM (2007) Accuracy assessment of the monthly GRACE geoids based upon a simulation. Journal of Geodesy 81(1):67–80. doi:10.1007/s00190-006-0085-1
56. Prasad R, Ruggieri M (2005) Applied satellite navigation using GPS. GALILEO and augmentation systems, Artech House, Boston/London
57. Luthcke S, Rowlands D, Lemoine F, Klosko S, Chinn D, McCarthy J (2006) Monthly spherical harmonic gravity field solutions determined from GRACE inter-satellite range-rate data alone. Geophysical Research Letters 33:L02402. doi:10.1029/2005GL024846
58. Tapley BD, Bettadpur S, Ries JC, Thompson PF, Watkins MM (2004) GRACE measurements of mass variability in the Earth system. Science 305:503–505. doi:10.1126/science.1099192
59. Bruinsma S, Lemoine J, Biancale R, Valès N (2010) CNES/GRGS 10-day gravity field models (release 2) and their evaluation. Advances in Space Research 45(4):587–601. doi:10.1016/j.asr.2009.10.012
60. Lemoine F, Luthcke S, Rowlands D, Chinn D, Klosko S, Cox C (2007) The use of mascons to resolve time-variable gravity from GRACE. In: Tregoning P, Rizos C (eds) Dynamic planet. Springer, Berlin, pp 231–236
61. Ramillien G, Cazenave A, Brunau O (2004) Global time variations of hydrological signals from GRACE satellite gravimetry. Geophysical Journal International 158(3):813–826. doi:10.1111/j.1365-246X.2004.02328.x
62. Chambers D, Wahr J, Nerem R (2004) Preliminary observations of global ocean mass variations with GRACE. Geophysical Research Letters 31(L13310): doi:10.1029/2004GL020461
63. Wahr J, Jayne S, Bryan F (2002) A method of inferring changes in deep ocean currents from satellite measurements of time-variable gravity. Journal of Geophysical Research 107(C12):3218. doi:10.1029/2002JC001274
64. Rodell M, Famiglietti JS (1999) Detectability of variations in continental water storage from satellite observations of the time dependent gravity field. Water Resources Research 35(9):2705–2724. doi:10.1029/1999WR900141
65. Tiwari V, Wahr J, Swenson S (2009) Dwindling groundwater resources in northern India, from satellite gravity observations. Geophysical Research Letters 36:L18401. doi:10.1029/2009GL039401
66. Werth S, Güntner A, Petrovic S, Schmidt R (2009) Integration of GRACE mass variations into a global hydrological model. Earth and Planetary Science Letters 27(1–2):166–173. doi:10.1016/j.epsl.2008.10.021
67. Baur O, Kuhn M, Featherstone W (2009) GRACE-derived ice-mass variations over Greenland by acocunting for leakage effects. Journal of Geophysical Research 114(B06407). doi:10.1029/2008JB006239
68. Velicogna I (2009) Increasing rates of ice mass loss from the Greenland and Antarctic ice sheets revealed by GRACE. Geophysical Research Letters 36:L19503. doi:10.1029/2009GL040222
69. Boy J-P, Chao B (2005) Precise evaluation of atmospheric loading effects on Earth's time-variable gravity field. Journal of Geophysical Research 110:B08412. doi:10.1029/2002JB002333
70. Swenson S, Wahr J (2002) Estimated effects of the vertical structure of atmospheric mass on the time-variable geoid. Journal of Geophysical Research 107(B9):2194. doi:10.1029/2000JB000024
71. Barletta V, Sabadini R, Bordoni A (2008) Isolating the PGR signal in the GRACE data: impact on mass balance estimates in Antarctica and Greenland. Geophysical Journal International 172(1):18–30. doi:10.1111/j.1365-246X.2007.03630.x
72. Tregoning P, Ramillien G, McQueen H, Zwartz D (2009) Glacial isostatic adjustment and nonstationary signals observed by GRACE. Journal of Geophysical Research 114:B06406. doi:10.1029/2008JB006161
73. Swenson S, Wahr J, Milly PCD (2003) Estimated accuracies of regional water storage variations inferred from the Gravity Recovery and Climate Experiment (GRACE). Water Resources Research 39(8):1223. doi:10.1029/2002WR001736
74. Ramillien G, Frappart F, Cazenave A, Gutner A (2005) Time variations of land water storage from an inversion of two years of GRACE geoids [rapid communication]. Earth and Planetary Science Letters 235(1–2):283–301. doi:10.1016/j.epsl.2005.04.005

75. Wahr J, Molenaar M, Bryan F (1998) Time variability of the Earth's gravity field: hydrological and oceanic effects and their possible detection using GRACE. Journal of Geophysical Research (Solid Earth) 103(B12):30205–30230. doi:10.1029/98JB02844
76. Heiskanen WA, Moritz H (1967) Physical geodesy. W.H, Freeman and Company, San Francisco
77. Yang Q (2016) Applications of Satellite Geodesy in Environmental and Climate Change. Graduate Theses and Dissertations. http://scholarcommons.usf.edu/etd/6440. Accessed 26 Jan 2017
78. Pugh D (2004) Changing sea levels. Effect of tides, weather and climate. Cambridge Univeristy Press
79. Abdalati W, Zwally HJ, Bindschadler B, Csatho B, Farrell SL, Fricker HA, Harding D, Kwok R, Lefsky M, Markus T, Marshak A, Neumann T, Palm S, Schutz B, Smith B, Spinhirne J, Webb C (2010) The ICESat-2 laser altimetry mission. Proceedings of the IEEE 98(5):735–751. doi:10.1109/JPROC.2009.2034765

# Chapter 10
# GNSS Reflectometry and Applications

*Increasing sophisticated uses of GNSS observables have led to a new era in remote sensing. Geodesists, geophysicists, and surveyors have all established large GNSS networks. Nearly all of them have open data policies and encourage broad usage of their data. The vast majority of GNSS data users focus on positioning, although the timing and atmospheric communities also value data from GNSS networks. Here, we have shown how to further extend the value of ground GNSS networks by describing how to routinely measure soil moisture, snow depth, and vegetation growth. These data are valuable both to scientists and water managers and a cost effective use of existing infrastructure.*

–K.M. Larson [1]

## 10.1 Remote Sensing Using GNSS Reflectometry

### *10.1.1 Background*

When positioning with GNSS, multipath signal is a reflected GNSS signal that is a nuisance and as such needs to be eliminated. Whereas this reflected signal on the one hand is a nuisance for positioning, for environmental monitoring purposes, it could be useful in monitoring sea-wind retrieval, seawater salinity detection, ice-layer density measurements and other remote sensing applications (e.g., topography, soil moisture and vegetation), see, e.g., [2].

In this approach, also known as the GNSS-reflectometry (GNSS-R) remote sensing, which works as a bi-static radar (i.e., where the transmitter and receiver are separated by a significant distance, [3], the microwave signals reflected from various surfaces are received and processed to extract useful environmental information about those surfaces. As can be seen in Fig. 10.1, GNSS satellites (GPS, Galileo, GLONASS and Beidou) transmit signals to the receiver onboard low earth orbiting (LEO) satellites, but some signals are reflected by nearby surfaces. In this example, the reflected signals are received by the receivers, placed on LEO satellites such



J. Awange, *GNSS Environmental Sensing*, Environmental Science and Engineering, DOI 10.1007/978-3-319-58418-8_10

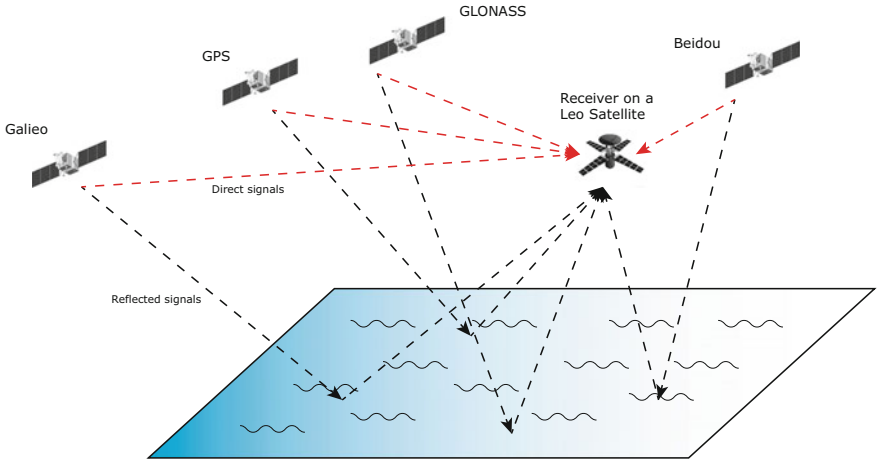


**Fig. 10.1** Remote sensing using GNSS reflected signals

as GRACE, as discussed in Sect. 9.2.3.2. These reflected microwave signals, which could also be received by receivers situated on land, are processed in GNSS-R remote sensing to provide geophysical characteristics of the reflecting/scattering surface and in so doing give environmental monitoring parameters as we shall see in Sect. 10.1.2.

The possibility of using GNSS reflected signals for remote sensing sea surface heights was proposed by Martín-Neira [4], who used fixed-platform experiments to demonstrate that GNSS-reflection altimetry performed to an accuracy of ∼20 m over the ocean, 450 m above Crater Lake, and 10 m over a pond, see e.g., [5, and the references therein]. In this pioneering work, Martín-Neira [4] suggested the use of delayed signals between the direct and reflected signals (e.g., Fig. 10.1) in what is known as passive reflectometry and interferometry system (PARIS), [3]. According to Lowe et al. [5], such GNSS altimetry would involve an orbiting receiver that obtains position and timing information from the GNSS constellation as usual, but measures ocean height using the arrival time of GNSS signals reflected from the surface. The advantage over mono-static radar altimeters is that the receiver could produce about 25 simultaneous measurements (∼55 GNSS satellites are fully operational) [3], distributed over an area thousands of km across-track [5]. Such high number of independent observations obtained from GNSS over the same scene has the advantage of increasing the coverage of the area and providing more reliability of the estimated environmental monitoring parameter. Egido [6] points to two reasons why GNSS-R has gained increasing interest, i.e., (i) global availability and stability of GNSS signals, and (ii), the use of L-band radiation that makes it highly interactive with the natural scattering medium. Studies of GNSS-reflections from space include, e.g., [5, 7]. The advantages of GNSS-R remote sensing over traditional satellite scatterometry and radar altimetry are given, e.g., by Yang et al. [2, 3] as follows:

- provision of long term stable signals that are free without any need for additional transmitter,
- attractive of GNSS-R receivers that are small in size, light-weight, with low power consumption,
- plenty of signal sources, which now include GPS, Galileo, GLONASS, and Beidou/Compass, all which will contribute to improved spatial and temporal resolution,
- unlike radiometers, GNSS-R signals are not affected by background temperature.
- works at L-band range that is suitable for soil moisture monitoring
- use of spread-spectrum communication technology to enable the receiver to receive weak signals, and
- wide range of uses for such things as sea-wind retrieval, seawater salinity detection, ice-layer density measurement, humidity measurement of land, and the detection of moving objects.

### *10.1.2 Geometry and Observations*

Jin et al. [3] provides good reading on GNSS-R geometry and observables. In this section, a brief outlook is provided to simplify the understanding of the GNSS-R concept. When waves originating from a single direction are reflected towards a given (single) direction, i.e., assuming a flat surface where the incident and the reflected angles are equal (Fig. 10.2), specular scattering is said to have occurred. If on the other hand the waves from a single direction are reflected into different directions, diffuse scattering is said to have occurred. Looking at Fig. 10.2, the *specular point* is the point with minimum (shortest) distance from the reflecting surface to the

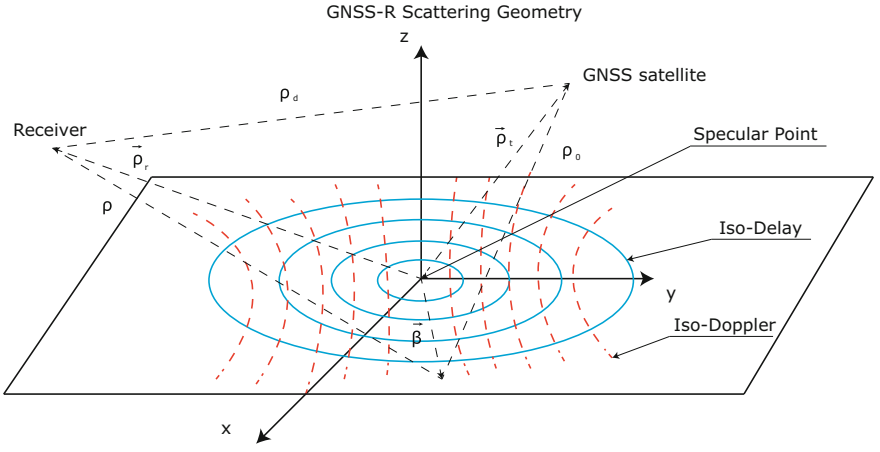


**Fig. 10.2** GNSS-R geometry and observations

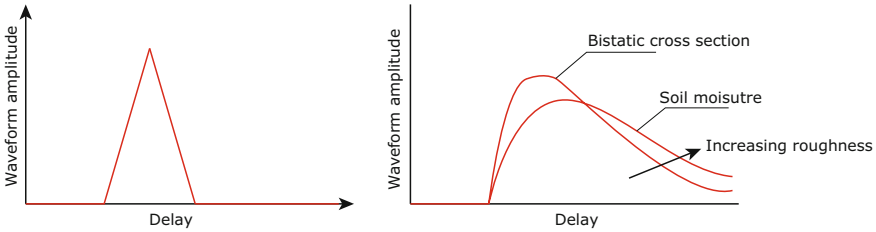


**Fig. 10.3** GNSS reflectometry: Direct and reflected waveforms. Modified after Egido [6]

receiver. Away from the specular point, as the surface becomes rough, other points will also redirect the reflected signals towards the receiver, thus contributing towards the final reflected signals. The area occupied by these reflecting points is known as the *glistening zone* [3, 6].

Assuming the specular point to be the center of origin of a cartesian coordinate system with the YZ plane being the reflection plane (Fig. 10.2), the distance $\beta$ of any point to the specular point within the glistening zone can be calculated from the transmitted vector $\rho_t$ and receiver vector $\rho_r$, see Edigo [6]. This distance to the specular point form the delay distance or iso-delay (blue lines in Fig. 10.2). Points with the same delay can be joined by lines forming ellipse with semi-major and semi-minor axes. Besides the iso-delay, points in the glistening zone have different doppler shift due to the transmitter - surface - receiver geometry, which can be computed from respective velocities, $\mu_t$, $\mu_r$ [6]. Similarly, points with equal doppler shift can be joined by a line to form iso-Doppler (red lines in Fig. 10.2). The intersection of the iso-delay and iso-doppler form the *delay doppler map* (DDM), which forms the first observable of GNSS-R signal that accounts for the average GNSS scattered power on the surface as a function of delay and frequency.

The second type of GNSS-R observations is obtained from performing cross correlation between the direct and the reflected signals with a pseudo random noise PRN replica code (for delay) and frequency shift with carrier frequency to obtain a *complex waveform*. By selecting the doppler shift of the specular point, the reflected cross correlation waveform can be obtained [8] and are depicted, e.g., in Fig. 10.3.

In general, there are two ways in which GNSS-R technique could be used to sense changes in environmental features such as soil moisture, snow depth and vegetation:

(a) using a second receiver to measure the reflected signals as performed by the GNSS reflectometry group that uses two receivers, or
(b) using a single receiver such as that used by geodesists, surveyors and geophysicists, see Fig. 10.1.

In (b), we saw in Sect. 3.4.4 that the geodesists view the reflected signal from multipath as a nuisance and attempt to model it during data processing. Using the vendor software such as Trimble Business Center (TBC), this is achieved through the scrutinization of the least squares generated residuals. For environmentalists,

however, this reflected signal is exactly what they need to decipher changes in the environmental surfaces such as snow/ice and vegetation. Larson et al. [1] postulate that if one thinks on how best to measure multipath reflection rather that to model multipath corrections for carrier phase data, then one is better off using signal power, which is similar to the data used by the GNSS-reflectometry community in (a). GNSS-R receivers will slightly differ from those used by geodesist, surveyors and geophysicist to obtain positions. Geodesist GNSS receivers are tuned to measure the direct signals and suppress the reflected signals, while those of GNSS-R measure both direct and reflected signals. In addition to the direct signals, however, the geodesists receiver measures the interference of the direct and reflected signals through the signal power.

Geodetic GNSS receivers generate carrier-to-noise density data stored in Receiver Independent Exchange (RINEX) data format as signal-to-noise ratio (SNR). SNR are functions of satellite elevation angles and manifest themselves in lower elevation satellites (i.e., those setting or rising, 25° and below). GNSS-R on the other hand will receive both right hand circularly polarized (RHCP) and left hand circularly polarised (LHCP) components of the reflected signal. RHCP include the direct signal while LHCP measures the indirect (reflected) signal, see e.g., Fig. 10.3. Larson et al. [1] used both RHCP and LHCP to generate signal-to-noise ratio (SNR) as a function of the reflecting surface and the elevation angle. For a planar horizontal reflection (e.g., Fig. 10.1), the frequency of the interference of the direct and reflected signal observed in SNR data is constant as a function of the sine of the elevation angle [1]. Larson et al. [1] called this dominant frequency that can be estimated from the spectral density of the signal or extracted using periodogram as the *effective reflector height* and analysed its changes to derive the ice-depth and soil moisture changes. In essence, change in the effective reflector height implies change in the surface around the antenna [1]. Also, by analysing the amplitude of the multipath reflected signals at a GNSS site, soil moisture can be estimated [3]. In general, the measuring principle from remote sensing satellites is largely based on the dielectric properties of the reflecting surface (e.g.,wet and dry soils have different dielectric constants). Larson et al. [1] employ the amplitude of the reflection observed in the SNR data, which depend on the dielectric constant of the surface material (e.g., vegetation with high water content has much smaller SNR than vegetation with very low water content) to monitor changes in snow, soil moisture and vegetation.

## 10.2 Environmental Applications

Such GNSS remote sensing using reflected signals find use, e.g., in the provision of altimetric precision and spatial resolution necessary to map mesoscale eddies, which has been the most prominent limitation of conventional radar altimeters [5]. Other applications of GNSS-R remote sensing include water reservoir level and ocean monitoring [8, 9]. In addition, over the last few years, there has been increasing interest in this technique for applications such as soil moisture monitoring, where the

observations relating to the flux of water to- and from- the land surface can be gleaned from GNSS multipath measurements of, e.g., snow depth and soil moisture [10, 11]. These measurements derive changes in the properties of a site's environment from changes in the amplitude and frequency of the multipath interference (relating, respectively, to attenuation properties and position of reflective surfaces) [12]. These developments have led to the establishment of new research themes targeting the measurement of land bio-geophysical parameters [8].

### *10.2.1 Sensing Changes in Soil Moisture*

Soil moisture plays a crucial role in several fields that include agriculture [13], hydrology [14, 15], engineering (i.e., flood prediction, modelling surface runoffs and soil erosion) [16], drought monitoring [13], surface runoff after rainfall events [6], among others. In agriculture, it is well known that vegetation (crop) water content originates from soil moisture, which plays a double role of providing the essential water needed to support plant growth on the one hand while on the other hand, it is used to monitor changes in vegetation water contents. Monitoring of vegetation water content is vital for informing the impacts of climate change on crops. Soil moisture also finds use in regulating the energy balance during land-atmosphere interaction through evapotranspiration. Its accurate monitoring is therefor essential in informing, e.g., the impacts of climate change besides playing an active role in food production.

Traditionally, it has been monitored using passive radiometers that are less sensitive to surface characteristics but influenced more by background temperature. In use are also the active sensors such as radars that are less sensitive to soil moisture but are affected by surface characteristics, see e.g., [3]. Both the passive and the active methods are, however, expensive. Its monitoring can also be through in-situ sensors, e.g., portable sensors that can be pushed directly into the ground or buried sensors that are connected either to a fixed meter or a central monitoring station [6]. In-situ methods, however, suffer from their limited coverage that does not encompass regional or global scales. Owing to this spatial inadequacy of the in-situ sensors, remote sensing techniques (i.e., passive, e.g., optical spectrometers and microwave radiometers) and active (e.g., microwave radars)) have been employed to measure the scattering characteristics of the soil. These scattering characteristics are in turn used to provide information of the soil moisture content.

Radiometers, which measures surface temperature (i.e., from the sun or natural bodies) are endowed with high temporal resolution but poor spatial resolution. Instruments include optical that sense the top soil layer due to their short wavelength to microwave that have the advantage of being all-weather, day and night operational capability, and cloud penetration. For sensing soil moisture, the P-band (50 cm) and L-band (20 cm) are good [3]. GNSS reflectometry (GNSS-R) works within the L-band, i.e., GNSS' band (see Chap. 4). As opposed to the passive radiometers that measures the sun's radiation scattered off the Earth's surface or the natural radiation

from bodies, active radars generate their own source of energy to illuminate and measure reflected signals back to the instrument (i.e., monostatic) or a separate receiver (i.e., bi-static, to which GNSS-R belong), see e.g., [6]. Radars can be classified as imaging (e.g., real and synthetic aperture radars (SAR)) and non-imaging (e.g., satellite altimetry discussed in Sect. 9.4.1 and scatterometers used to measure cryosphere), e.g., [6]. To maximize on the advantages of both passive and active instruments, a combination of both has been used, e.g., in the soil moisture active and passive (SMAP) mission launched on 31st January 2015, and whose mission ended with data at kilometer spatial resolution valuable for scientific study. Another soil moisture satellite mission with kilometer spatial resolution is the soil moisture and ocean salinity (SMOS) launched on the 2nd of November 2009 with a three year life span, which has been extended to 2017. GNSS-R could be useful in calibrating and validating soil moisture products from these two missions as it can provide soil moisture (similar to SMAP and SMOS) to 0–5 cm depth [3, 10].

At a GNSS station at San Jose, California, Larson et al. [1] obtained GNSS-R measurements of volumetric soil moisture using the amplitude of SNR discussed in

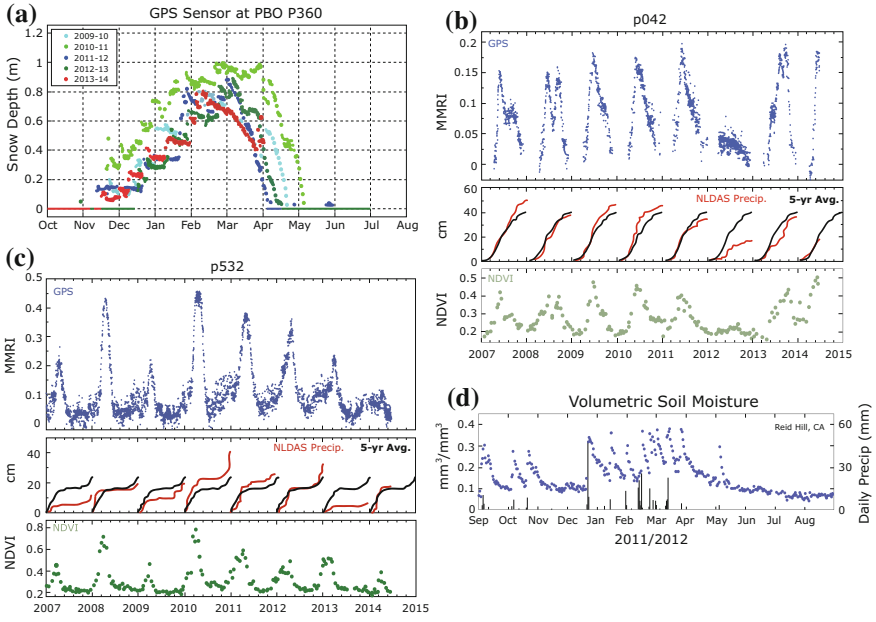


**Fig. 10.4** GNSS reflectometry test results of Larson [1]; **a** Five years of snow depth time series of GPS site at P360 in southern Idaho **b** GPS site at Wheatland, Wyoming (*top*), GPS vegetation measurement (also called normalised microwave reflection index - NMRI) compared with normalised difference vegetation index (*middle*) and the cumulative precipitation from the North America Land Data Assimilation System (NLDAS) **c** GPS vegetation growth index compared with NDVI and accumulated NLDAS at site P532 located northwest of Santa Barbara, California, and **d** daily measurement of volumetric soil moisture measured with GNSS (*Blue*) and daily precipitation from NLDAS. *Source* Larson [1]

Sect. 10.1.2 and compared them with daily precipitation and found a strong correlation between the two products at 0–5 cm depth (Fig. 10.4d). They caution, however, that the use of GNSS-R is challenged by the presence of snow on top of the soil and also when the soil is covered by vegetation with very high water content.

### *10.2.2 Sensing Changes in Vegetation*

Vegetation, like soil moisture, plays a crucial role in agriculture, hydrology, drought monitoring through, e.g., normalised difference vegetation index (NDVI) and carbon cycle, among others, see e.g., [3, 6, 13, 17]. For climate change, for instance, carbon dioxide ($CO_2$) is known to be a component of the greenhouse gas that contribute to global warming. Vegetation contributes to regulating the carbon dioxide in the atmosphere through photosynthesis process and as such, is vital for regulating global change. In-situ methods adopted for monitoring of vegetation changes measures vegetation parameters such as above ground biomass, vegetation water content and plant heights, see e.g., [6]. Similar to the case of soil moisture, the spatial inadequacy of the in-situ vegetation measuring methods necessitate the use of remote sensing techniques with regional and global coverage.

Satellite methods employed to measure vegetation changes use the scattering and attenuation of the electromagnetic waves. Sensors include optical (e.g., light detection and ranging - LIDAR) and microwave (e.g., synthetic aperture radar - SAR), both which are active sensors. Passive sensors of vegetation include multispectral and hyper-spectral optical sensors such as MODIS (moderate resolution imaging spectroradiometer) and NDVI (normalized difference vegetation index).

Using signal to noise ratio (SNR), see Sect. 10.1.2, Larson et al. [1] defined the GNSS-R derived vegetation changes based on the changes in the reflection amplitude as normalised microwave reflection index (NMRI), where a value of zero is assigned to vegetation with the lowest water content. Using two test sites (eastern Wyoming and California), they compared the NMRI vegetation water content generated from GNSS-R and those obtained from NDVI data generated at 16 days interval using MODIS sensor with a spatial resolution of 250 m. Their study revealed a close correlation between the GNSS-R derived NMRI and NDVI (i.e., a correlation of 0.86) in Wyoming, with both products capturing the 2012 drought that impacted on the vegetation (Fig. 10.4b). Just like in Wyoming, both NMRI and NDVI captured the 2014 drought in California (Fig. 10.4c). Larson et al. [1] point out that the GNSS-R sensing of vegetation has a shorter seasonal length compared to NDVI that has consistently longer growth season. They conclude that given that GNSS-R is sensitive to vegetation water content while NDVI is correlated to chlorophyl production, combining both products could provide better constraints to penologists studying the influence of climate variations on periodic plant life cycle. Further applications of GNSS satellites to sense vegetation are discussed in Sect. 19.3.

### 10.2.3 Sensing Changes in Cryosphere

In Sect. 9.4.2, ICESat was presented as an altimetry satellite that is useful for monitoring changes in ice sheet. GNSS-R provide an alternative to sensing snow and ice, two components of climate system and total water storage (surface water, groundwater, soil moisture, biomass, ice and snow, see Sect. 9.3.3). Monitoring them is therefore essential in understanding how ice respond to climate change, predicting the size of ice in the polar regions, and for hydrological studies. In-situ methods for monitoring snow and ice are sparse on the one hand while the remote sensing methods are imprecise with poor spatial resolution, e.g., [3].

Jin et al. [3] present GNSS-R sensing of snow and ice in two-fold (i) relating the thickness of the amplitude of the reflected signal as a function of the incident angle or relative amplitude between polarization, and (ii) the use of multipath modulated signal. Larson et al. [1] made their first snow depth measurements in 2009 at a flat mesa site south of Boulder (USA) and reported the success of the method in retrieving the snow depths. They repeated the experiment over 5 year time period in two sites; Niwot Ridge Colorado (due to its topographical variability, extreme cold and very high wind) and Island Park, Idaho (USA). From the time series of the 5 year period, they concluded that the method was robust with very few data outages and when compared to in-situ measurements taken every two weeks, the method proved to be very accurate (Fig. 10.4a).

### 10.2.4 Sensing Changes in Lakes and Oceans

For sensing lakes or oceans level changes, satellite altimetry techniques discussed in Sect. 9.4 would be preferable to GNSS-R method. However, the cross-track distance of satellite altimetry method is usually large with low spatial resolution making the method unsuitable for monitoring changes in smaller lakes. It is in such instances that the GNSS-R method becomes attractive, see e.g., [16].

For oceans, the GNSS-R method offers the capability of sensing surface toughness (wind) besides the sea surface altimetry. Due to its temporal and spatial resolution, it could therefore complement the traditional satellite altimetry approach and assist in detecting, e.g., tsunami among others, see [3]. It should be mentioned that GNSS satellites can be used to obtain sea surface heights directly using buoys fitted with GNSS receivers (see Fig. 17.3 in p. 360). In contrast, GNSS-R uses a second receiver that receives the reflected signals from the sea surface and then computes the time delay that is multiplied by the speed of light to give the equivalent range delay. Knowing the position of the GNSS satellites accurately as well as that of the receiver measuring time delay, the obtained range delay is exploited to give the instantaneous sea surface heights after the atmospheric, instrumental and other errors have been accounted for, see e.g., Jin et al. [3] for more elaboration on the techniques and the applications of GNSS-R to measure ocean surface roughness.

## 10.3 Concluding Remarks

This chapter has presented in a nutshell the concepts of GNSS reflectometry (GNSS-R) and their applications to sensing the environment (e.g., soil moisture, snow/ice and hydrology). Details of the techniques are not elaborately covered here since they have been treated in other works such as [3, 8, and the references therein]. Here, the focus was to present the basics of GNSS-R method and showcase its potentials for environmental sensing. With the proliferation of GNSS continuous operating reference stations discussed in Sect. 5.5, there exists the potential of using their signal power through the signal-to-noise ratio (SNR) to remote sense the environment as demonstrated, e.g., by Larson et al. [1]. The development of the new L2C GPS signal (see Sect. 3.3) and the freely available Galileo signals (see Chap. 7) further adds weight to the potentials of GNSS-R for sensing the environment. However, even with such praise of the GNSS-R method, limitations do exist. Two such limitations are presented by Larson et al. [1] as (i) changes in environmental features of interest such as soil moisture, snow depth and vegetation cannot be measured in all GNSS sites since some are situated on top of buildings while others are near car parks where the reflected signals will be contaminated, and (ii), not all the receiver independent exchange (RINEX) data contain the desired observable, i.e., SNR or where they are available, they could have been degraded.

## References

1. Larson KM, Small EE, Braun JJ, Zavorotny VU (2014) Environmental sensing. A revolution in GNSS applications. Inside GNSS. 36–46 July/Aug 2014
2. Yang D, Zhou Y, Wang Y (2009) Remote sensing with reflected signals. GNSS-R data processing software and test analysis. Inside GNSS, Sept/Oct 2009:40–45
3. Jin S, Cardellach E, Xie F (2014) GNSS remote sensing. Theory, methods, and applications. Springer, Dordrecht
4. Martín-Neira M (1993) A passive reflectometry and interferometry system (PARIS): application to Ocean altimetry. ESA J 17(4):331–335
5. Lowe ST, Zuffada C, Chao Y, Kroger P, Young LE, LaBrecque JL (2002) 5-cm-precision aircraft ocean altimetry using GPS reflections. Geophys Res Lett 29(10):1375. doi:10.1029/2002GL014759
6. Egido AE (2013) GNSS reflectometry for land remote sensing applications. PhD thesis Dissertation, Starlabs, Barcelona. https://www.researchgate.net/publication/280732466_GNSS_Reflectometry_for_Land_Remote_Sensing_Applications. Accessed 25 Jan 2017
7. Lowe ST, LaBrecque JL, Zuffada C, Romans LJ, Young L, Hajj GA (2002) First spaceborne observation of an earth-reflected GPS signal. Radio Sci 37(1):7-1–7-28
8. Egido AE, Delas M, Garcia M, Caparrini M (2009) Non-space applications of GNSS-R: from research to operational services. Examples of water and land monitoring systems. In: IEEE international geoscience and remote sensing symposium, IGARSS, Cape Town, pp II-170–II-173
9. Gleason S, Hodgart S, Sun Y, Gommenginger C, Mackin S, Adjrad M, Unwin M (2005) Detection and processing of bistatically reflected GPS signals from low Earth orbit for the purpose of ocean remote sensing. IEEE Trans Geosci Remote Sens 43(6):1229–1241. doi:10.1109/TGRS.2005.845643

10. Larson KM, Small EE, Gutmann ED, Bilich AL, Braun JJ, Zavorotny VU (2008) Use of GPS receivers as a soil moisture network for water cycle studies. Geophys Res Lett 35(24):L24405. doi:10.1029/2008GL036013
11. Larson KM, Gutmann ED, Zavorotny VU, Braun JJ, Williams MW, Nievinski FG (2009) Can we measure snow depth with GPS receivers? Geophys Res Lett 36(17):L17502. doi:10.1029/2009GL039430
12. Hammond WC, Brooks BA, Bürgmann R, Heaton T, Jackson M, Lowry AR, Anandakrishnan S (2010) The scientific value of high-rate, low-latency GPS data, a white paper. http://www.unavco.org/community_science/science_highlights/2010/realtimeGPSWhitePaper2010.pdf. Accessed 06 June 2011
13. Agutu N, Awange JL, Zerihun A, Ndehedehe C, Kuhn M, Fukuda Y (2017) Assessing multi-satellite remote sensing, reanalysis, and land surface models' products in characterizing agricultural drought in East Africa. Remote Sens Environ 194:287–302. doi:10.1016/j.rse.2017.03.041
14. Awange LJ, Gebremichael M, Forootan E, Wakbulcho G, Anyah R, Ferreira CG, Alemayehu T (2014) Characterization of Ethiopian mega hydrogeological regimes using GRACE, TRMM and GLDAS datasets. Adv Water Resour 74:64–78. doi:10.1016/j.advwatres.2014.07.012
15. Ndehedehe CE, Awange JL, Corner RJ, Kuhn M, Okwuashi O (2016) On the potentials of multiple climate variables in assessing the spatio-temporal characteristics of hydrological droughts over the Volta Basin. Sci Total Environ 557–558(3–4):819–837. doi:10.1016/j.scitotenv.2016.03.004
16. Jin S, Komjathy A (2010) GNSS reflectometry and remote sensing: a new objectives and results. Adv Sp Res 46:111–117
17. Omute P, Corner R, Awange J (2012) (submitted) NDVI monitoring of Lake Victoria water level and drought. Water Resour Manag 26(6):1591–1613

# Chapter 11
# Climate Change and Weather Related Impacts

*Real-time GNSS measurements have the potential to contribute to climate modeling and weather forecasting through integrative measurement of atmospheric water vapor in GNSS signal delays and measurements of soil moisture flux.*

–W.C. Hammond et al. [1]

## 11.1 Weather, Climate, and Global Warming

In order to address the contributions of GNSS to monitor climate change caused by increase in temperature, a distinction between *weather* and *climate* on one hand, and *climate variability* and *climate change* on the other hand is essential. Burroughs [2] points out that weather is what is happening to the atmosphere at any given time (i.e., what one gets) whereas climate is what would be expected to occur at any given time of the year based on statistics built up over many years (i.e., what one expects). From these definitions, it follows that *changes in the climate* constitute shifts in meteorological conditions lasting a few years or longer, and may involve a single parameter, e.g., temperature or rainfall, but usually accompany more shift in weather patterns that might result in a shift to, say, colder, wetter, cloudier and windier conditions [2]. If meteorological observations, e.g., of temperature are taken over time, a series of its annual averages could be developed. This series would indicate that over the period of measurements, the average value remains effectively constant but fluctuates considerably from observation to observation. This fluctuation about the mean is a measure of *climate variability* [2]. Now, if a linear or cyclic trend is fitted onto the variability, the effect of climate change could be analysed.

Human activities of all kinds contribute to increased emission of quantities of gases to the atmosphere. Of particular importance is *carbon dioxide* ($CO_2$), a greenhouse gas that is said to contribute about seven thousand million tones to the carbon already present in the atmosphere [3]. Greenhouse gases, such as carbon dioxide and *water*



J. Awange, *GNSS Environmental Sensing*, Environmental Science and Engineering, DOI 10.1007/978-3-319-58418-8_11

*vapour,* play a key role in naturally warming the surface of the planet by acting as a blanket that shields the Earth by trapping, in the atmosphere, direct heat radiated by the sun. Whereas this maintains the Earth's temperature balance, the downside is that the energy radiated back into space from the Earth is also trapped by the same greenhouse gases, thereby further warming the Earth. In fact, increase in carbon dioxide contributes to increased temperature, which in turn leads to increased water vapour in the atmosphere thereby providing more blanketing and causing the Earth to be even warmer.

Increase in greenhouse gas concentration in the Earth's atmosphere, particularly carbon dioxide, caused by burning fossil fuels such as oil and coal, and by clearing forests, are believed to be the primary cause of the rise in the Earth's temperature. With rapid industrialization in the world and in the absence of efforts to curb the rise in emission of carbon dioxide, the global average temperature is expected to rise by about 3° in a century (i.e., 0.03° annually) [3]. Such a change would potentially lead to the melting of ice masses [4], which may also lead to increased rates of flow in the ice streams [5], dislocation of plants and animals from their habitats, and the spread of diseases such as malaria [6–8]. There is therefore a wider agreement that continuous *increases* in greenhouse gas concentrations in the lower atmosphere is well known to intensify the warming effect, which in turn has a serious impact on the *global climate change*.

While there is little doubt that the Earth's surface temperature has risen by 0.74 K over the past century, see e.g., [9], our understanding of the upper atmosphere's temperature evolution is still not clear. In an effort to understand the impact of increasing greenhouse gas concentrations in the atmosphere, the tropopause has seen intense monitoring over the last 30 years using weather-balloons (i.e., radiosondes) and reanalyses (e.g., European Center for Medium range Weather Forecasting, ECMWF). For instance [10–12] have shown that changes in tropopause height is a useful and sensitive indicator of human effects on climate. The heights of the tropopause rise with increased temperature in the troposphere due to global warming [4]. Santer et al. [13] estimated that nearly 80% of the rise in tropopause height between the period 1979 and 1999 is attributed to human-induced greenhouse concentrations in the atmosphere.

The importance of the troposphere and lower stratospheric temperature evolution in understanding the cause of the climate change was further highlight in the IPCC's assessment report [4]. This chapter examines the contribution of GNSS satellites to monitor the tropopause and in so doing contribute to monitoring of global warming. In Sect. 11.4.4, its contribution to monitoring cryospheric changes resulting from global warming is discussed.

## 11.2 Impacts of Weather and the Changing Climate

### *11.2.1 Weather Related Impacts*

The unpredictability of weather and its socio-economic dimensions is a major factor in the destruction of properties, which in many cases leads to, or enhances poverty, see e.g., Agola and Awange [14]. Extreme weather events affects food security in households and as such proper weather forecasts are necessary to ensure food production as it may help to determine what crops to plant in a particular season. However, food production is not the only aspect that suffers from adverse weather. For example, some diseases are weather dependent, see e.g., [15].

Some of the seasonal variations and extreme weather and climatic anomalies have been associated with phenomenon and the Indian Ocean Dipole (IOD), e.g., [16], which lead to anomalous rainfall that results in large losses in the economy. Other weather-related impacts include hailstorm destruction of crops, lightning strikes, thunderstorms, seasonal floods, frost damage, and strong winds. These impacts also often result in the loss of lives and properties, and the mass displacement of people, as witnessed in the floods that ravaged Pakistan and Eastern parts of Australia in 2010–2011. Also common as a result of extreme weather events are erosion, siltation and increase in water-borne diseases.

To reduce the impacts of these factors, considerable research, awareness, monitoring and finance for the mitigation of weather and climate hazards is needed to implement sustainable climate and weather mitigation initiatives. The simplest and cheapest methods of addressing these problems almost solely takes into account public awareness and information about weather and climate and their roles in life quality. The awareness and information gap is better filled by following the weather *forecasts* issued by meteorological departments and climate-based organizations [17].

Weather and climate forecast information generated by various models has the potential to assist in the fight against poverty by allowing early planning for the mitigation of the adverse effects of droughts and persistent floods [18]. The desire to reduce the negative impacts of weather necessitates that forecasters work together with the general population and provide them with timely warnings. In order for the forecasters to provide sufficiently accurate predictions, they would need not only to understand and be familiar with *prediction models*, but also the *long-term* trends in weather and climate. These would in turn lead to forecasting conditions that influence our behaviour and livelihoods. GNSS satellites have started playing a major role in *numerical weather prediction* (NWP) models, as will be discussed in Sect. 11.3.2.

### *11.2.2 Climate Related Impacts*

Though climate change is one of the greatest challenges facing humanity, not all the climate change ends up being adverse. While some parts of the world experience more frequent and more severe droughts, floods, or significant sea level rise, in other

**Fig. 11.1** Severe drought in Australia (2007): Sheep wondering what to eat! *Source* http://en.wikipedia.org/wiki/File:Riverina_Sheep_(during_drought).jpg

places, crop yield may increase due to the fertilization effect of carbon dioxide [3]. That said, it is the adverse effects that are of great concern to mankind today. In the last decade alone, we have witnessed the melting of glaciers and polar ice caps (e.g., Sect. 11.4.4), increased numbers of severe storms, hurricanes and typhoons wrecking havoc [19], and severe wide spread droughts threatening farming and water resources, see e.g., [20]. For example, in its January 2007 monthly statement on the Australian drought, the Bureau of Meteorology (BoM) reported the year 2006 as having been one of the driest on record for most parts of southern Australia. The drought, see e.g., Fig. 11.1, which persisted in many parts of Australia until 2011, had been made worse by increased temperature, e.g., Ummenhofer et al. [21]. Two widely felt consequences of the drought are:

- A drop in farming output, leading to a reduction in the nation's overall economic growth, and
- a decline in stored fresh water (surface and ground) suitable for human consumption, see e.g., [22], industrial and mining applications, as seen from media interest. For instance, on the dwindling water resource in Australia, Philips [23] wrote: "*With a growing population and a drying climate, Australia - like many rich nations - is running out of water. Solutions are not easy nor cheap ... and may require cities to tap their sewers*".

The Intergovernmental Panel on Climate Change [4] assessment report points to the fact that the rate of global average warming over the past 50 years (i.e., $0.13 \pm 0.03$ K per decade) was almost double compared to the past 100 years ($0.07 \pm 0.02$ K per decade). This findings further paints a gloomy picture for countries such as Australia where the impact of global warming is already being felt. In fact, in 2005, Steffen [9] already issued an alert that Australia would be faced with the impact of climate change on its water quantity due to decreased precipitation over parts of the continent. More astonishing for Australia was the IPCC [4] projection of an increase in drought over the continent and a further decline in fresh water resources over the next two decades.

These impacts of climate change could be monitored through various proxy indicators such as tree rings, ice cores, ocean sediments, pollen records, boreholes, speleothems and corals, see e.g., [2]. Global sea level is an indicator of climate change, as it is sensitive to both the *thermal expansion* of the oceans and a reduction in the volume of land-based *ice* [24]. The influence of climate change on terrestrial water supply has already been noticed, e.g., by Magadza [25] who analyzed the sensitivity of major African rivers to climate change. Magadza [25] examined changes in Zimbabwe's main water storage facilities during the 1991–1992 drought cycles, and established that storage had dwindled to less than 10% of its installed capacity. Jallow et al. [26] and Li [27] also studied the impact of climate change on water supplies. In their study of the flow of the Gambian river, Jallow et al. [26] found that the Gambia river flow was very sensitive to climate change. Based on the results of river flow responses and vulnerability analysis, climate variables alone were found to cause a 50% change in runoff in the Gambia river catchments [26]. Li et al. [27] noted that the primary climate indicators of precipitation and temperature influenced the fluctuation of Lake Qinghai water levels.

In general, Manneh [28] points out that a 1% change in rainfall results in a 3% change in runoff, which in-turn reduces the lake's recharge. Since lake level fluctuations have been shown to track drought episodes, e.g., [29], Mistry and Conway [30] investigated the climatological factors responsible for the rise in the lake level, and found that there was a significant correlation between the lake's rainfall series and its levels. They also pointed out that there was a time lag of 1–2 years between rainfall episodes and the water level peaks of the lake. Since the rainfall time series are based on land-based observations, and the lake itself is roughly one quarter of the whole basin, the lake level variability is partially explained by the over-lake rainfall. Awange [31] investigated whether the fall in Lake Victoria water levels were attributed to climate change. In Chap. 14, the use of GNSS to monitor changes in fresh water levels will be discussed, while Chap. 17 will look at how changing sea levels can be monitored using GNSS to mitigate potential disasters associated with rising sea levels.

## 11.3 Water Vapour

### *11.3.1 Significance*

Section 3.4.3 discussed the effects of atmospheric delay on the measured GNSS signals, the desire by the geodesist to eliminate it in order to improve their positioning accuracies, and ended by stating that *one person's poison is another person's meat!* In this section and subsequent ones, we demonstrate how this geodesist's *poison* becomes an environmentalist's *meat*. We start by looking at water vapour.

Atmospheric *water vapour* is the gaseous state of water once evaporation takes place and plays a key role in weather forecasting. Its significant role in weather forecasting was pointed out by Bevis et al. [32] who noted that the limitations in the analysis of water vapour are the major source of error in short-term (0–24 h) forecasts of precipitation. The global composition of water vapour in air is on average roughly equivalent to a layer of liquid water covering the Earth to a thickness of around 25 mm [33, p. 23]. The thickness of this layer provides the total liquid equivalent of water vapour in an atmospheric column at a given location and is often referred to as *precipitable water* [33, p. 23]. The spatial distribution of water vapor in the atmosphere varies with latitude as well as vertical elevation. Water vapour concentrations vary until an elevation of 9 km at the poles, and until more than 16 km at the equator, decreasing rapidly with elevation [34], with 50% found within the lowest 1–2 km [33, p. 23]. According to Brutsaert [33, p. 23], current data indicates that the amount of precipitable water vapour near the poles is less than 5 mm, and close to 50 mm at the equator.

Water vapor plays a key role in environmental phenomena since it provides the means by which *moisture* and *latent heat* are transported. This makes it a key environmental monitoring parameter since knowing its spatial and temporal distribution accurately could significantly enhance weather analysis and forecasting at local, regional and global scales. This could provide early warning systems with adequate information to mitigate the effects of *hurricanes* and *typhoons*. Unfortunately, water vapour fields are inadequately defined, thereby contributing immensely towards hampering the accurate *prediction of weather* and *modelling of climatic change*. Trenberth and Guillemot [35] attribute this inadequacy to *sparsity of water vapour observations*, combined with the high spatial and temporal variability of water vapour fields.

The critical role played by *water vapour* in the global climate system are listed, e.g., by Brutsaert [33, p. 23] as *first*, it is a vital component of the hydrological cycle, enabling the movement of evaporated water from the oceans to land where it falls as rain. *Second*, it provides the medium for energy transfer during evaporation (i.e., from Earth to the atmosphere) and during condensation, thus providing the energy required for atmospheric circulation. *Third*, it plays a significant role in controlling the amount and type of cloud cover due to its concentration and spatial distribution. These clouds then play a role in the distribution of solar radiation. *Fourth*, it is a greenhouse gas and contributes to global warming by trapping the radiated energy from the Earth. Ware et al. [36, p. 23] adds the role of water vapour in the chemistry

of the lower atmosphere to the list, while the vital role of water vapour in atmospheric processes ranging from global climate change to micrometeorology are pointed out, e.g., by Rocken et al. [37].

Traditional techniques for monitoring water vapour include *radiosondes*, *surface based humidity sensors*, *surface and satellite based radiometers*, and *research aircraft* [36, p. 23]. According to Elliot and Gaffen [38], radiosondes measure temperature and humidity with an accuracy of about 0.2 °C and 3.5%, respectively, and that the performance deteriorates in cold-dry regions. Surface-based radiometers are comprised of upward-looking water vapor radiometers (WVR) that measure the microwave energy emitted by the atmosphere (i.e., microwave radiation produced by water vapour) against the cold background of space and uses it to estimate the zenithal integrated water vapour (IWV) along a given line of sight using retrieval coefficients. These coefficients are derived from the *regression analysis* of *radiosonde data* and are functions of location and climate variations [32, 37]. Space-based WVR are downward-looking and measure microwave emissions from the atmosphere against the background of the underlying Earth's hot surface. Because of the hot surface, the derived IWV are greatly affected by the large variability in the surface brightness temperature, leading to the method being inefficient for land since the temperatures of the hot background are quite variable and difficult to determine [32].

Belvis et al. [32] further state that satellite-based WVR are affected by clouds and as such may be more useful over the ocean. In fact, they reckon that both systems complement each other, with the ground-based WVR providing good temporal, but poor spatial coverage while space-based WVR provide good spatial, but poor temporal coverage. Operating both systems could therefore be of significant benefit to environmental monitoring since it could lead to improved short-term weather forecasting (1–12 h) with the benefit of mitigating environmental catastrophes caused by episodic events such as *flash floods*. The shortcomings of the methods, however, are that both are affected by rain which absorbs and scatters the emitted microwaves. Also, like the radiosonde method, they too are expensive to operate, and are limited in high-latitude areas like the Arctic [34]. GNSS monitoring of water vapour discussed in Sect. 9.2 promises to provide more data, that hopefully will lead to enhanced monitoring of potential environmental catastrophes as well as the prediction of longer-term climatic change.

### *11.3.2 Numerical Weather Prediction*

In order to understand the role that could be played by GNSS satellites in weather forecasting, it is essential at this point to introduce the concept of mathematically predicting the weather using supercomputers. Prediction of weather, referred to as *numerical weather prediction* (NWP) can be traced back to the work of *Vilhelm Bjerknes* in 1904 [39] who proposed the representation of weather as a problem in mechanics and physics. NWP is an initial/boundary value problem, i.e., the future state of the atmosphere is determinable through model simulations (forecasts) if its

present state (*initial conditions*), and appropriate and lateral *boundary conditions* are known [40, p. 136].

In this approach, Bjerknes [39] identified a nonlinear system of equations consisting of seven variables as necessary to characterize weather at any given location $\{x, y, z\}$ and time $t$ in the Earth's atmosphere. These nonlinear equations make up *models* that seek to employ the current state of the weather to produce meteorological information for future times at a given *location*. Before the advent of the computers, the solution of this system of equations was extremely difficult, as evident by the works of Charney [41], Charney et al. [42], and Richardson [43]. With the increased powers of modern supercomputers, however, the solution of these numerical weather prediction models have become a routine task. Besides improved computing power, other factors that have enhanced NWP include [40]:

- The improved representation of small-scale physical processes within the models. These include clouds, precipitation, turbulent transfer of heat, moisture and radiation.
- The use of more accurate methods of data assimilation, which results in improved initial conditions for the models.
- The increased availability of data, especially satellite and aircraft data, over the oceans and the Southern Hemisphere.

One common characteristic of nonlinear systems of equations is that they can fail to have exact solutions, thereby necessitating alternative solutions, see e.g., Awange et al. [44–46]. For NWP models, these systems of nonlinear equations are solved numerically through *global* or *regional circulation models* (GCM). Global models are useful in forecasting weather changes for 2 days or more (i.e., *medium range forecasts*). At the National Center for Environmental Protection (NCEP), for example, global models are run through 16 days everyday [40, p. 11]. Due to the fact that global models cover the entire Earth, the resulting solution is generally poor, thus necessitating the use of more focused high resolution regional models for *short-range forecasts* (1–3 days).

Both global and regional circulation models require some *initial tortology values* (present state of the atmosphere) in order to simulate (forecast) the future state of the weather. Methods for determining these initial starting values are presented in details, e.g., in [40, 47]. Here, a summary of one of these methods, the 3D-Var, is presented. Generally, initial values obtained from $\pm 3$ h *observations* (e.g., radiosonde data, weather satellites, surface weather or radiance, etc.) are normally of few orders, e.g., $10^5$ compared to $10^7$ for the degree of freedom of the circulation models. Clearly, they are insufficient to initialize the models. This necessitates the use of additional information known as *first guesses* to generate the *initial conditions* for the forecast. According to Bergthorsson and Döös [48], these first guesses provide the *first estimate* of the state of the atmosphere at all grid points. The initial approach adopted for obtaining the first guesses use *climatology* data, which are obtained by averaging observational data ranging over a long period of time from a variety of observing systems [48, 49]. These first guesses are later complemented by a short range forecast obtained numerically by running a model from an old set of initial

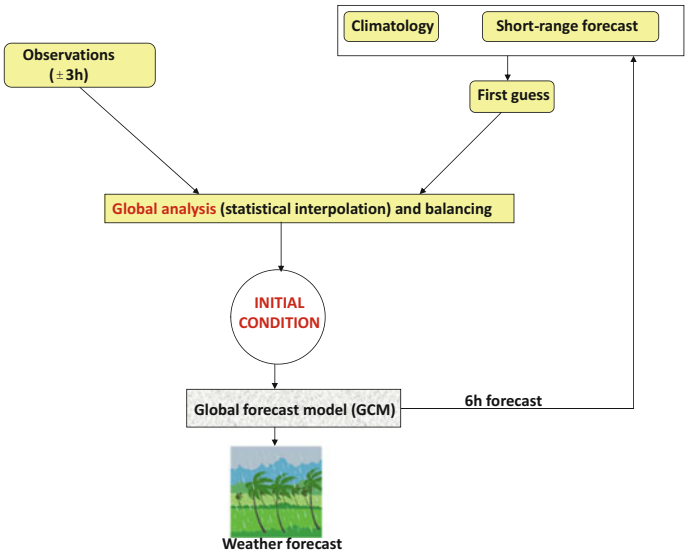


**Fig. 11.2** Global data assimilation with 6-h forecast. A global 6-h cycle is performed at 00, 06, 12, and 18 UTC. For regional models, the observation times change from ±3 h to ± 30 min, while the forecast data changes from 6 to 1 h

conditions [48]. With improved weather forecasting, the use of short-range weather forecasting as a first guess is universally adopted in operation systems called the *analysis cycle* (Fig. 11.2) [40, p. 138].

The *observations*, *climatology* and short-range forecasts are then combined through some method of *data assimilation* to produce the '*best estimate*' of the current state of the weather (initial values) called the *analysis*, which are used in the NWP models as illustrated in Fig. 11.2. In atmospheric science therefore, an analysis is a detailed representation of the state of the atmosphere that is based on observations [50]. More generally, Dole et al. [50] state that an analysis may also be performed for other parts of the climate system, such as the oceans or land surface, and is often displayed as a map depicting the values of a single variable, such as air temperature, wind speed, or precipitation, or of multiple variables for a specific time period, level, and region. The daily weather maps that are presented in newspapers, television, and numerous other sources are familiar examples of this form of analysis [50]. Analyzes are also performed at levels above the Earth's surface in order to provide a complete depiction of atmospheric conditions throughout the depth of the atmosphere. This type of analysis enables atmospheric scientists to locate key atmospheric features, such as the jet stream, and plays a crucial role in weather forecasting by providing initial conditions required for models used for weather prediction [50]. Currently, operational NWP centers produce initial conditions through a statistical combination of observations and short-range forecasts [40].

Data assimilation, as illustrated by Fig. 11.2, and whose purpose is to use all available information to determine as accurately as possible the state of the atmospheric flow [51], can be achieved in several ways, see e.g., [40]. One approach that operates in a statistical way is the 3D-Var, which minimizes the cost function $J_0[\xi]$ constructed as the sum of [40, p. 15]

$$J_0[\xi] = \frac{1}{2}\{(\mathbf{y} - f(\boldsymbol{\xi}))^T \boldsymbol{\Sigma}_y^{-1}(\mathbf{y} - f(\boldsymbol{\xi})) + (\boldsymbol{\xi} - \tilde{\boldsymbol{\xi}})^T \boldsymbol{\Sigma}_\xi^{-1}(\boldsymbol{\xi} - \tilde{\boldsymbol{\xi}})\}, \tag{11.1}$$

where the first term of $J_0$ measures the distance between the newly created initial conditions $\boldsymbol{\xi}$ and the assimilated observations $\mathbf{y}$ (i.e., the first term on the right-hand-side). The second term on the right-hand-side measures the distance between the newly created initial conditions (analysis) and the first guess and is essential for constraining the initial conditions to ensure that they are close to the first guess [49]. The observation operator $f$ maps the initial conditions $\xi$ through interpolation and transformation into the observation space $\mathbf{y}$. The variance-covariance matrices $\boldsymbol{\Sigma}_y^{-1}$ and $\boldsymbol{\Sigma}_\xi^{-1}$ perform the function of adjusting observational errors and first-guess errors, respectively. Assimilating new data types requires accurate knowledge of the variance-covariance matrices, and an accurate, yet computationally efficient, mapping operator $f$, whose tangential linear model is also required in order to minimize the total cost function [49].

In Eq. (11.1) only two terms have been presented for the cost function $J_0$. Other formulations of $J_0$ may include an optional *third term* which is added to balance the initial conditions. An extension to the 3D-Var model is the 4D-Var model, which includes within its cost function, the distance to the observation over the time window. For detailed discussions about this model and others, plus a wealth of references on NWP and data assimilation, we refer the reader to [40, 47].

## 11.4 Environmental Monitoring Applications

In the next subsections, areas of possible applications of GNSS to weather and climate that can contribute to environmental monitoring are presented.

### *11.4.1 GNSS Applications to Weather Monitoring*

GNSS remote sensing data that are capable of being used for assimilation discussed in Sect. 11.3.2 include; *water vapour*, *raw amplitude and phase*, *bending angles*, *refractivity*, *temperature* and *humidity* [49, 52, 53]. Discussions on the possible assimilation of GNSS data into NWP models are presented, e.g., in [49, 54, 55]. Poli et al. [56] discuss the effect of GNSS-derived data on NWPs by looking at the influence of European ground-based GNSS-derived zenith total delay (ZTD) data (e.g., summation of Eqs. (9.12) and (9.13) on p. xxx) introduced into the Météo-France global forecasting and assimilation system. They report that over three different sea-

sons, the benefits of including such data was most apparent in *improved predictions of temperature and wind*, and especially, in superior quantitative *precipitation forecasts* over France. For space-based GNSS remote sensing (Sect. 9.2.3.1), they report some positive impact on the analysis of the Southern Hemisphere's tropopause. They conclude that these demonstrated benefits has resulted in Météo-France using ZTD-derived from European ground-based GNSS networks and GNSS space-based remote sensing data since September 2006 and September 2007, respectively, to update its operational weather prediction analysis.

Furthermore, the success of GNSS data assimilation for stratospheric temperature forecasts and the advantages of GNSS remote sensing data in comparison to other satellite data for assimilation into NWP models are presented by Poli [49] as:

1. Being all-weather, though the lower 5 km of the atmosphere is generally affected by the presence of water vapour that limits the application of GNSS,
2. the ability to monitor the Earth from an angle, thus providing higher vertical resolution (less than 1 km). The disadvantage with this, though, is the provision of horizontal resolution elongated in the direction of the ray that makes it difficult to use in models such as ECMWF[1] and Météo France 4DVAR, which assumes vertically-averaged observations,
3. yielding observations that are independent of surface type, and
4. providing data that relates to altitude as opposed to pressure, as in other techniques.

The potential of water vapour being used for meteorological forecasting have been outlined, e.g., in [57]. For environmental monitoring of weather-related hazards, GNSS remote sensing may potentially play the following roles [58]:

1. *Derive water vapour*: Precise analysis of water vapour content will contribute to the data required by hydrologists to enhance their predictions of local torrential rains that normally cause damage and havoc, see e.g., [59]. Knowledge of water vapour density in the lower troposphere will also be useful for the following:
   - Providing data that could be directly assimilated into meteorological models (NWP) to enhance the predictability and forecasting of weather. The increase in the number of CORS networks (See Sect. 5.5) is already providing the possibility of regional monitoring of IWV. This is achievable by estimating the ZWD in the vicinity of CORS stations and converting them to IWV by means of Eq. (9.19). This unprecedented monitoring of IWV will provide useful data for operational *weather forecasting*, and studies in *atmospheric storm systems*, *atmospheric chemistry* and the *hydrological cycle*.
   - Resolving the distribution of water vapour via tomographic techniques, e.g., [60].
   - Correcting the wet delay component for both Synthetic Aperture Radar (SAR) and GNSS positioning, thus benefiting applications requiring precise positioning such as crustal deformation monitoring.

[1] European Centre for Medium-Range Weather Forecasts.

- Monitoring global warming by determining the latent heat suspended in the atmosphere, since water vapour is one of the most important greenhouse gases. Whereas Randall and Tjemkes [61] indicated that long-term measurements of global IWV could provide a source of information for global and regional *climate change studies*, Belvis et al. [62] pointed to the theorists' belief that global warming will cause changes in the total water vapour content of the atmosphere, a change which would be easily detectable as compared to the associated changes of atmospheric temperatures.
- The radiative forcing due to water vapour and clouds inferred from humidity estimates.
- Improved inputs for weather forecasting, climate and hydrology. Water vapour is essential for short-term (0–24 h) forecasting of precipitation. Currently, the lack of up-to-date atmospheric water vapour content is the major source of error in short-term weather forecasting [63].

2. Enhance disaster mitigation measures, in that the provided data will contribute to the much-needed information required to improve the forecasting of catastrophic weather around the world.

### *11.4.2 GNSS Applications to Climate Change Monitoring*

The provision of *accurate*, *long-term*, and *consistent* data to sustain and expand the observational foundation for climate studies is one of the high-priority areas for action to improve the ability to detect, attribute and understand *climate variability and changes* [64, 65]. GNSS remote sensing is fast emerging as a promising climate monitoring tool capable of meeting the requirements above due to the following properties [66]:

- *Global coverage of radio occultation (RO) data*. GNSS-RO observations (e.g., Sect. 9.2.3.1; Fig. 9.2 on p. xxx) have a fairly uniform distribution around the world, both over land and ocean, in contrast to radiosondes and aircraft measurements. This is true for longer averaging periods (as is required for climate monitoring), whereas for shorter, e.g., daily periods, observations tend to cluster due to the sun-synchronous orbits of the LEO satellites.
- *Self-calibrated nature*. GNSS-RO observations are free of instrumental biases since the observations depend on the measurement of time, not of radiation intensities. If double-differencing (e.g., Fig. 4.8 on p. xxx) is applied, the measurements are also essentially self-calibrating. These long-term stability properties imply that it is possible to compare two data sets separated by several years and taken by different sensors, which is not at all straight forward for current microwave sounders.
- *All weather capability*. They can be used in all weather conditions, in particular in cloudy areas, which will not be covered adequately, even by future advanced infrared sounders. Furthermore, the observational quality and sampling characteristics are virtually the same over all geographical regions and at all times.

- They have a relatively high vertical resolution (1 km or better) compared to existing and planned passive infrared and microwave sounders, and thus addressing the main limitation of these systems. This is true for both temperature and water vapour measurements.
- Quantities that are key observable for climate change, such as near tropopause geopotential heights [67] or refractivity itself can be obtained almost totally independent of conventional measuring systems. Only surface pressure needs to be taken from other sources.
- The unprecedented time stability, accuracy and resolution of GNSS-RO data offers a new possibility to identify spurious trends in radiosonde, Microwave Sounding Units (MSU)/Advanced Microwave Sounding Units (AMSU) and reanalysis data sets discussed in Sect. 11.4.3.1.

The possibilities of using GNSS remote sensing as a tool for monitoring climate change is documented, e.g., in the works of [58, 68, 69]. Recognizing the advantages of *global coverage of RO data*, *self-calibrated nature*, *high accuracy*, and *all-weather capability* listed above, recent studies have centered on the possibilities of utilizing it for climate studies, see e.g., [64, 70]. For example, the use of refractivity and geopotentail heights as global warming parameters have been suggested by [66, 67, 71]. Leroy et al. [70] states that a good climate monitoring tool must help address the physics of a climate model so as to make it better able to predict future climates, and suggest that GNSS remote sensing be used to provide benchmark for climate models. In Shum [72], GNSS observed climate variables are validated over the Tibetan plateau.

Poli et al. [56], however, caution that though the potential for using GNSS observations for climate studies is significant, detailed sensitivity studies are required in order to evaluate the effects of possible sources of interruption in measurements as well as trends in the stability in the time-series measurements being collected. They reckon that since the atmospheric observations are capable of being used for climate change monitoring, they should be highly accurate and have long-term stability. According to Poli et al. [56], although the signal delay measured by GNSS offers unmatched meteorological calibration, thanks to the atomic clocks onboard the satellites, the measured GNSS atmospheric delays are not usable directly for climate change monitoring, as they must be converted to other quantities, as was discussed in Sect. 9.2.3.1. Each stage of the conversion could introduce errors that may degrade the atomic calibration aspect.

If successful, however, GNSS remote sensing could benefit climate change monitoring in the following ways [58]:

1. *Precisely derive vertical temperature and pressure profiles*: These will be useful in the following ways:

   (a) By combining them with other observations of ozone densities and dynamic models, our understanding of the conditions that lead to the formation of polar stratosphere clouds will be improved. It will also help us to be able to understand the chemical reactions that lead to ozone loss.

(b) The precisely measured *temperature* will enable the monitoring of *global warming* and the *effect of greenhouse gases*. This is made possible as the change in surface temperatures caused by an increase in greenhouse gas concentration is generally predicted to be largest and therefore most apparent at high latitudes. Precise temperatures can therefore be used to map the structure of the stratosphere, particularly in the polar regions where temperature is believed to be an important factor in the minimum levels of ozone observed in spring.
(c) Accurate high-vertical resolution *temperature* reconstructions for the upper troposphere will increase our understanding of the conditions under which cirrus clouds form. Cirrus clouds will generate a positive feedback effect if *global warming* displaces a given cloud layer to a higher and colder region. The colder cloud will then emit less radiation, forcing the troposphere to warm in order to compensate for the decrease.
(d) Accurate temperature retrievals from GNSS meteorological measurements combined with high-horizontal resolution temperatures derived from the nadir-viewing microwave radiometers will provide a powerful data set for climate studies of the Earth's lower atmosphere. This can be achieved by using the derived profiles to monitor trends in the upper troposphere and lower stratosphere where the GNSS meteorological technique yields its most accurate results.
(e) The measured *pressure* is expected to contribute to the monitoring of *global warming*. This is because pressure versus geometrical height is potentially an interesting diagnostic of the troposphere's climatic change since the height of any pressure surface is a function of the integrated temperature below.
(f) The *temperature* in the upper troposphere/tropopause influences the amount of energy radiated out to space. In Sect. 11.4.3, the GNSS monitoring of the tropopause to support the monitoring of climate change will be pursued further.
(g) Contribute towards *climatic studies*: By comparing the observed temperatures against the predicted model values, a method for detecting and characterizing stratospheric climatic variations as well as a means for evaluating the performance of model behaviour at stratospheric altitudes will be developed and the existing ones tested.

2. Enhance geodynamic studies: The study of the gravitation effects of atmospheric pressure, water vapour and other phenomena will contribute towards the determination of high-resolution local geoids (see Sect. 5.6.1), which are vital for monitoring crustal deformation. The transient drift that occurs over time in the estimation of crustal deformation from GNSS measurement will therefore be corrected for.
3. With an abundance of GNSS remote sensing data, accuracies better than 1–2 K in temperature given by GNSS meteorological missions (e.g., COSMIC, GRACE, etc.) will be realized.

### 11.4.3 Monitoring of Global Warming

The layer separating the troposphere and stratosphere is known as the *tropopause*. It is vital to the gaseous exchange between the two layers due to its different characterization with respect to chemical composition and stability. Its height above the Earth's surface normally varies from about 17 km at the equator to about 8 km above the poles, and is influenced by the variation in temperature between the two layers [4, 10]. When the stratosphere warms because of, for example, the absorption of radiation by volcanic aerosols, a lowering of the tropopause height occurs. If the troposphere warms due to, say increases in greenhouse gas concentrations (e.g., carbon dioxide) and stratospheric ozone depletion, the tropopause height increases [4, 12]. Indeed, IPCC [4] noted that most of the observed warming over the last 50 years is likely to have been due to the increase in greenhouse gas concentrations in the lower troposphere.

Evidence of tropospheric warming has been reported, e.g., in Christy et al. [73, 74], Mears et al. [75], and Vinnikov and Grody [76]. For instance, Christy et al. [73] estimated a global trend of $+0.09$ K/decade from satellite-based Microwave Soundings Unit (MSU) over a 25-year period. Vinnikov and Grody [76] on the other hand showed a trend of $+0.22 \pm 0.26$ K/decade, which is much higher than the findings of Christy et al. [73] and Mears et al. [75], although because of large uncertainty, one cannot definitively say that there is an upward trend.

Santer et al. [10] identified two different factors that play a key role in the change of tropopause heights, namely *natural forcing* and *anthropogenic forcing*. The anthropogenic forcing include increased greenhouse gas concentration (mainly carbon dioxide), direct scattering of sulphate aerosols, and stratospheric ozone. The natural forcings are the changes in solar irradiance and volcanic aerosols. Santer et al. [10] estimated that human-induced changes in ozone and greenhouse gases accounted for 80% of the rise in tropopause height during the period 1979–1999. Radiosonde observations over the past 50 years, e.g., [77], indicate a strong link between climate change and tropopause variability. Global tropopause height indicates an upward trend with decreasing temperature and pressure [12, 78]. During the period 1979–2001, Santer et al. [11] observed a global increase in tropopause height of 200 m in ECMWF reanalysis, which was mostly caused by tropospheric warming. Similarly, Seidel and Randel [77] observed a global tropopause trend of $64 \pm 21$ m/decade using 25 years of radiosonde measurements (1980–2004).

There are many definitions and concepts that are available to identify the tropopause region, e.g., Pan et al. [79], depending on its latitudinal position and the availability of atmospheric data (such as temperature, pressure, water vapour). Currently, five different definitions are accepted and widely used for identifying the tropopause. These are: *the lapse-rate tropopause* (LRT); *cold point tropopause* (CPT); *the ozone tropopause* (OT); *the isentropic potential vorticity* (IPV) tropopause; and *the* 100 hPa *pressure level* (PLT). Of these, the LRT has been identified as a key indicator of climate change, see, e.g., Santer et al. [10]. Previous investigations, e.g., [10–12], based on LRT height trends, indicate significant increases in the

tropopause's height, which is consistent with model prediction used to estimate the impact of increasing greenhouse gases. The definition of the LRT has been outlined by the World Meteorological Organization [80] as "*the lowest level at which the lapse rate decreases to* 2 K/km *or less, provided also the average lapse rate between this level and all higher levels within* 2 km *does not exceed* 2 K/km". This definition has the advantage of being applicable globally and can easily be calculated from the vertical profiles of the atmospheric temperature [81].

Whereas surface temperature observations are necessary to monitor daily temperature trends, *monitoring tropopause parameters* (such as temperature and height) is vital for studying changes in the atmosphere as a result of global temperature rise.

#### 11.4.3.1 Traditional Tropopause Monitoring Techniques

Various traditional techniques (e.g., radiosondes, weather analyzes) have been applied by different countries to monitor the tropopause parameters (such as temperatures and heights) over the past 100 years. A brief overview of the existing methods used and their limitations are provided below.

*Radiosondes*: This is a balloon-borne instrument, also called weather balloon that is traditionally used for collecting weather information along a vertical profile. The Bureau of Meteorology of the United States used radiosondes as early as the 1930s to monitor upper air conditions. A global radiosonde network had been established by 1940s and more than 1000 radiosonde stations had been installed by 1991 by 92 nations [82]. Radiosonde can be launched in any type of weather, but severe thunderstorms and heavy precipitation can lead to system failure. Under ideal conditions and careful calibration, radiosondes are found to provide temperature observations accurately to about 0.5 K [81]. Although radiosondes provide soundings with high vertical resolution, global coverage is not feasible with sparse to non-existent data over the oceans and the Southern Hemisphere [78, 83]. With fairly low temporal resolution (12-h frequency), the accuracy of the data obtained from this system is affected by instrumental changes, see e.g., [82].

Although several investigations using radiosonde data sets have been done for a few regions [84–89], no studies were performed with regards to global tropopause trends using radiosonde data until 2006. Seidel and Randel [77] used radiosonde data sets to study global tropopause changes during the period 1980–2004. They divided the globe into seven 29.7° bands to study tropopause trends based on 100 stations around the world. Their findings indicated highly significant tropopause changes during the study period, where the height of the LRT increased by $64 \pm 21$ m/decade, which is 160 m over 25 years of observations. The increase in tropopause height was associated with a temperature decrease of $0.46 \pm 0.09$ K/decade and these changes were accompanied by a slight tropospheric warming ($+0.036 \pm 0.066$ K/decade) and strong stratospheric cooling ($-0.77 \pm 0.21$ K/decade). However, this study was based on a fairly low number of stations which may not provide reliable trends due to instrumental differences across the globe and limited redundancy [4, 82]. Moreover,

the stratospheric cooling indicated by Seidel and Randel [77] appears to contradict the findings of Santer et al. [11].

The problem with tropopause analysis using radiosondes is that when global estimates based solely on radiosondes are presented, considerable uncertainties exist, see e.g., [90]. Having a denser network of radiosonde stations encompassing even the oceans would be desirable to yield a more reliable global trend, but unfortunately this does not exist nor is it practical.

*Satellite-borne Microwave Sounding Units* (MSU): These units (e.g., NOAA-N[2]) have played an important role in providing meteorological information since their first launch in the early 1960s [82]. The first satellite capable of producing temperature and water vapour soundings was Nimbus III, launched in 1969, followed by NOAA-2 in 1972. Later, these were superseded by Advanced Microwave Sounding Units (AMSU), which began operating in mid 1998 [4]. Details of MSU data can be found, e.g., in [91, 92].

Satellite-borne microwave sounders emit microwaves into the atmosphere, which are then measured and inverted into temperature profiles (and water vapour). These are important sources of data for the lower atmosphere (stratosphere and troposphere) and have been used in several studies of global atmospheric change, see e.g., [73–76, 93]. The global atmospheric temperature data sets constructed from the satellite MSU measurements of NOAA were used by Christy et al. [73, 74] and Mears et al. [75] to monitor stratosphere-troposphere temperature changes from 1979–1988. A comparison of satellite data with those from radiosondes show reliable trends and have proved to be an important tool for global climate change monitoring. Global time series constructed from MSU records show a global cooling of the stratosphere of $-0.32$ to $-0.47$ K per decade and a global warming of the troposphere of 0.04–0.20 K per decade for the period 1979–2004 [4].

Satellite-based MSUs and AMSUs are designed to measure short-term temperature changes in the atmosphere and are not suited for the detection of long-term changes, since MSU and AMSU data are contaminated by instrumental and orbital drift and coarse vertical resolutions [94]. The vertical profiles obtained from the satellite data often *miss* the tropopause region due to insufficient vertical resolution [82]. Hence, the use of data sets from MSU and AMSU for long-term climate change monitoring has been under considerable scrutiny and debate, see e.g., [73, 76]. Nonetheless, satellite data sets serve as an important data source for weather models and analyzes (e.g., ECMWF).

*Reanalyses*: In Sect. 11.3.2, we introduced the concept of analysis and its role in weather prediction and forecasting. Reanalysis, therefore, is an objective, quantitative method for producing a high-quality sequence of analyzes that extends over a sufficiently long-term period to have values for climate research applications, as well as, for other purposes [50]. An important goal of most reanalysis efforts to date has been to provide an accurate and consistent long-term data record of the global atmosphere [50]. In certain cases, a reanalysis may be performed for a single variable, such as precipitation or surface temperature, however, in many modern atmospheric

[2]See e.g., http://www.nasa.gov/mission_pages/noaa-n/main/index.html.

reanalyses, the goal is to develop an accurate and physically consistent representation of an extensive set of variables (e.g., wind, temperatures, pressures, etc.) required to provide a comprehensive, detailed depiction of how the atmosphere has evolved over an extended period of time, typically, decades [50].

Weather models and reanalyses data are consistently used by researchers to investigate global tropopause changes, e.g., [4, 12]. They can also be used to validate data sets from radiosondes and satellites, e.g., [11, 95]. Global reanalysis such as ERA-40 (ECMWF) provides comprehensive information about climate. The vertical profiles of temperature, pressure, etc. retrieved from the reanalysis models can be used to infer tropopause parameters, as shown in the works of Santer et al. [10, 11]. Sausen and Santer [12] and Santer et al. [10] estimated a tropopause pressure trend of −1.82 hPa/decade for 1979–1997 and −2.16 hPa/decade during the period 1979–2000 in the NCEP/NCAR reanalysis, indicating an increase in the height of the tropopause. Santer et al. [10] also reported a global mean trend of −1.13 hPa/decade over 1979–1993 in the ECMWF reanalysis. Santer et al. [11] observed a tropopause height increase of 200 m in the ERA-40 (provided by ECMWF) reanalysis during the observation period 1979–2001.

However, the drawbacks of reanalysis data are that the change in the estimated climate trends may be affected by changes in the observation system over time, and that climate trends proposed by different reanalysis may vary due to differences in the underlying processing techniques.

#### 11.4.3.2 GNSS Tropopause Monitoring

The application of GNSS remote sensing to the monitor the tropopause, as presented in Chap. 9, is sure to improve global monitoring of climate change resulting from global warming, especially with more GNSS satellites being planned (see Chap. 2) and with the vertical resolution of the profiles acquired from LEO satellites continuously improving. For example, CHAMP improved its vertical resolution from 200 to 100 m and its horizontal resolution too [96]. Although a long-term study of global tropopause trend using GNSS-RO (e.g.. GRACE and COSMIC) data is still not possible due to their short lifespan, Schmidt et al. [78] estimated a global trend based on the CHAMP satellite's profiles during the period May 2001–December 2007 (80 months). They obtained a trend of 26–44 m/decade with trend errors varying between 19–21 m, a value which is in good agreement with the radiosonde observations, between 1980 and 2004, both of which indicate a maximum trend around 30°S and between 30°–50°N, e.g., [77]. However, discrepancies occur in the tropics, which may be associated with the poor RO data distribution [97] and fewer radiosonde stations due to oceanic areas [98].

***GNSS tropopause data sources***: RO measurements obtained from LEO satellites are processed at various institutions (e.g., GFZ, UCAR) into different products for various uses. Level 3 CHAMP data, Level 2 COSMIC data and GRACE data are essential for tropopause analysis. These data and their sources are discussed in Sect. 9.2.3.2.

Example 11.1 (GNSS monitoring of the Australian tropopause [99]).

Australia is a large relatively flat region extending from the tropics to mid-latitudes [8°–46°S; 108°–160°E]. The total land area of Australia is 7.7 million square kilometers [100]. Its climate is characterized by varying rainfalls (seasonal, annual and decadal time series) and worsening drought conditions. Australia's climate is strongly influenced by the surrounding oceans, which includes tropical cyclones and monsoon rains in northern Australia, mid-latitude storms in the south causing floods, and prolonged droughts and bushfire outbreaks notably in the mid-latitude zones [100]. The population distribution is fairly uneven with more than 80% of the settlements being near the coastal areas [100]. The average surface temperature of Australia has warmed by 0.9 K since 1950, with significant regional variations [101]. The mean annual temperature anomaly follows an upward trend showing a warming of 1 K over the last 100 years.

In the recent years, Australia, like many other countries in the world, has begun to feel the effects of increasing greenhouse gases leading to regional warming. The rising temperature in Australia thus speeds up the rate of evaporation, enhancing the effect of drought.

Khandu et al. [99] demonstrated the significance of GNSS remote sensing of the Australian tropopause through their study of changes in the tropopause heights and temperatures (Fig. 11.3). Since the latitude of Australia ranges from 8°–46°S, the tropopause height also varies, ranging from around 8 km (mid-latitude) to 17 km (equatorial region) [96]. Khandu et al. [99] applied 80 months (September 2001–April 2008) of CHAMP and 23 months (May 2006–March 2008) of COSMIC satellite RO data to analyze the Australian tropopause structure (height and temperature trends) as shown in Figs. 11.4, 11.5, and 11.6. Their analysis of tropopause height and temperature anomalies indicated a height increase over Australia as a whole of approximately $4.8 \pm 1.3$ m between September 2001 and April 2008 for CHAMP, with a corresponding temperature decrease of $-0.019 \pm 0.007$ K. They observed a similar pattern of increasing height/decreasing temperature when determining the spatial distribution of the tropopause height and temperature rate of change over Australia.

Although only a short period of data was considered in [99], a function of the operating time of these satellites, their results nonetheless were consistent with those of Schmidt et al. [78] and Seidel and Randel [77], and showed an increase in the heights of the tropopause over Australia during that period, and thus may indicate regional warming. Several mechanisms could be responsible for these changes, such as an increase in the concentration of greenhouse gases in the atmosphere, and lower stratospheric cooling due to ozone loss, both of which have been observed during the last decades.

How these rates vary over all of Australia is illustrated in Fig. 11.6 that shows the rate of change of (a) tropopause heights and (b) tropopause temperatures derived from the combined CHAMP and COSMIC data sets between September 2001 and April 2008. There is a general autocorrelation between the two sets of results as one

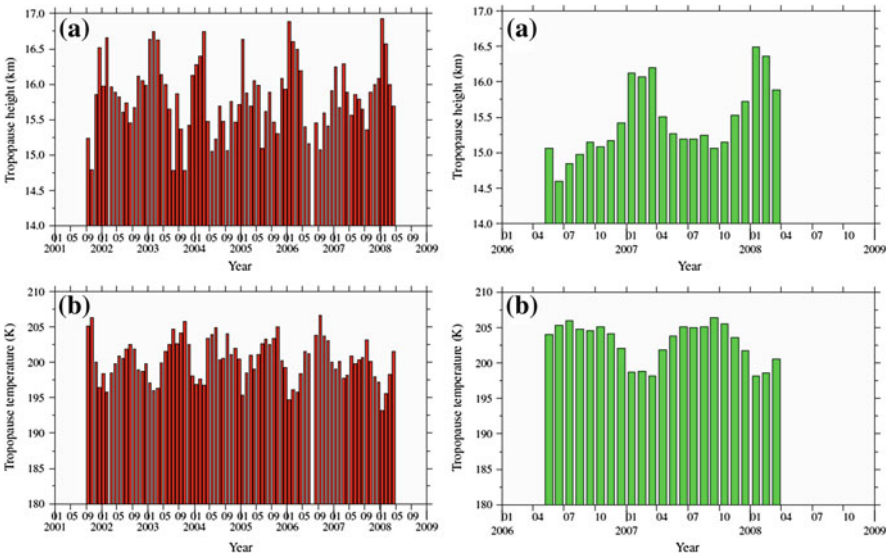


**Fig. 11.3** *Left panel* **a** Tropopause heights and **b** tropopause temperatures for Australia from CHAMP RO data for the period between 2001 and 2008. *Right panel* **a** Tropopause heights and **b** temperatures for Australia from COSMIC RO data for the period between 2006 and 2008. *Source* Khandu et al. [99]

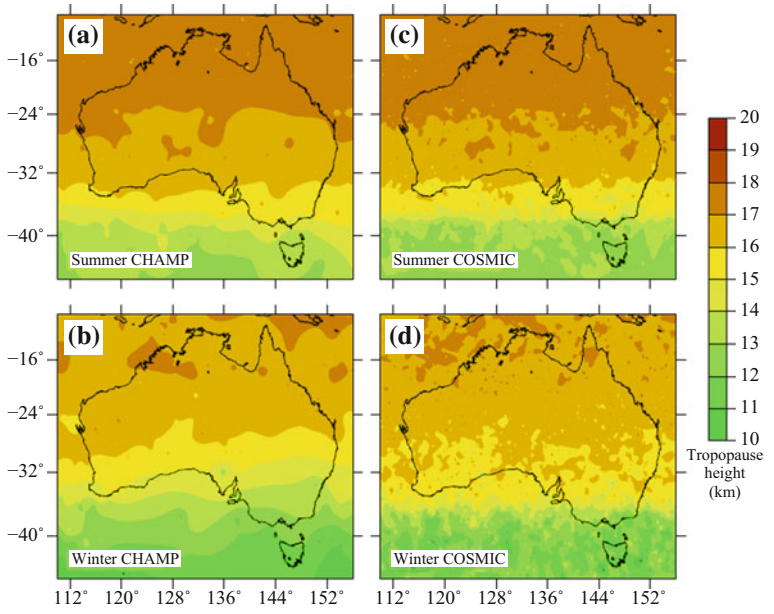


**Fig. 11.4** Tropopause heights (in km) derived from CHAMP and COSMIC RO data from between 2006–2007. **a** CHAMP results for summer, **b** CHAMP results for winter, **c** COSMIC results for summer, and **d** COSMIC results for winter. *Source* Khandu et al. [99]

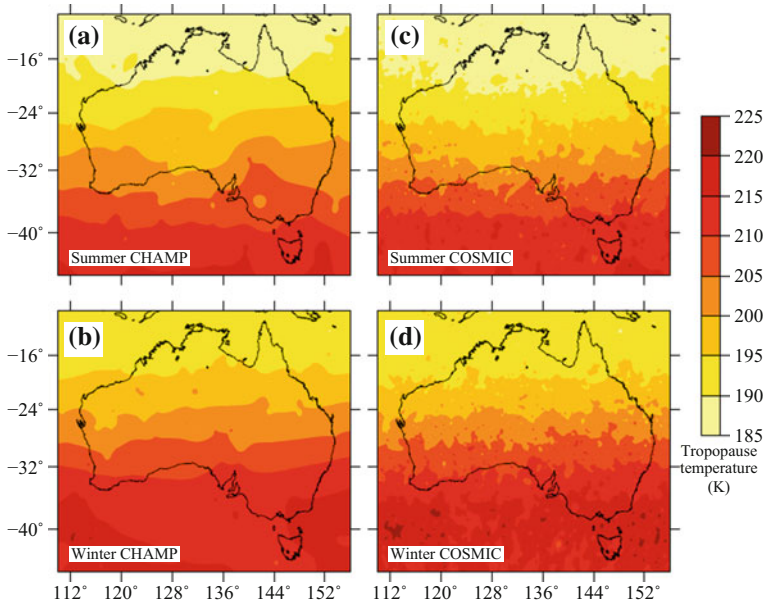


**Fig. 11.5** Tropopause temperatures (in K) derived from CHAMP and COSMIC RO data from between 2006–2007. **a** CHAMP results for summer, **b** CHAMP results for winter, **c** COSMIC results for summer, and **d** COSMIC results for winter. *Source* Khandu et al. [99]

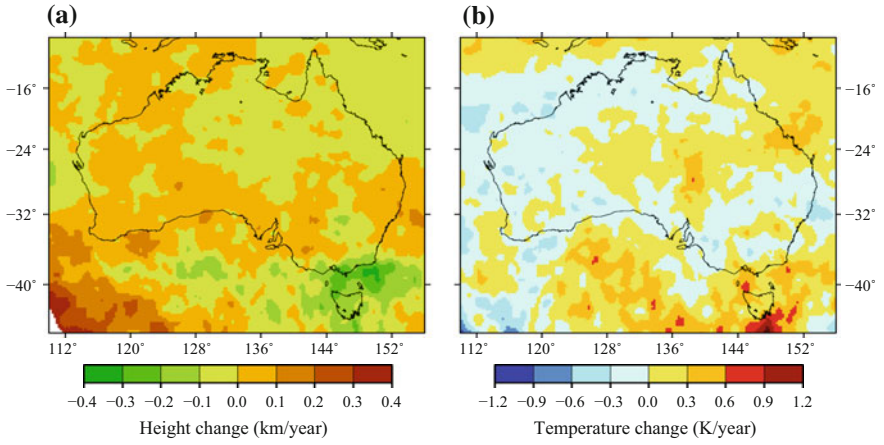


**Fig. 11.6** Rate of change in **a** the tropopause heights and **b** tropopause temperatures between September 2001 and April 2008. *Source* Khandu et al. [99]

would expect (e.g. increasing height/decreasing temperature). Much of Australia displays trends of 0–0.1 km/year of increasing tropopause height, with a corresponding temperature decrease of 0 to −0.3 K/year. These values are much higher than those presented earlier (see further discussions in Khandu et al. [99]).

♣ End of Example 11.1.

### *11.4.4 Monitoring Cryospheric Changes*

The cyrosphere, the subsystem of the Earth characterized by the presence of snow, ice, and permafrost, is fundamental to changes occurring in the Earth's environment, e.g., global warming as a result of the melting snow cover, glaciers, and sea ice that produces more warming due to decreased albedo associated with the greater extent and duration of the dark surface [102]. Some of the occurrences in the Earth's polar region (Greenland and Antarctic) could have far reaching consequences on the environment and as such require constant monitoring, which can be achieved through remote sensing using of satellite altimetry such as NASA's ICESat-2 (ice, cloud, and land elevation satellite) discussed in Sect. 9.4.1 and GRACE satellites, e.g., [103, 104, see also Sect. 9.3.3].

For instance, the Greenland and Antarctic ice sheets are reported to be losing mass at an increasing rate. Fast flowing outlet glaciers and ice streams carrying most of the mass flux from the interiors of the vast Greenland and Antarctic ice sheets toward the ocean have accelerated dramatically, the sea ice that covers the Arctic Ocean has decreased in areal extent far more rapidly than climate models have predicted and has thinned substantially, some of the thick and ancient ice shelves that fringe the Antarctic Peninsula have disintegrated, triggering the acceleration of the outlet glaciers that feed them, see [105, and the references therein].

Abdalati et al. [105] list the following consequences as the possible likely outcome of the behavior of ice sheets and sea ice changes to society:

- The melting ice sheets from Greenland and Antarctic are thought to contain enough ice to raise sea level by about 7 and 60 m, respectively, see [105, and the references therein].
- Sea ice exhibits a major influence on the Earth's planetary energy budget, influencing global weather and climate; and the Arctic ice cover is especially sensitive to and a strong driver of climate change, in large part due to the positive albedo feedbacks associated with melting ice [105].

ICESat-2, through the use of precise laser measurements of surface elevation, is specifically intended to quantify the rate of change of ice sheets and sea ice and provide key insights into the processes that drive those changes, and in addition will also provide important information on other components of the Earth system, in particular, vegetation biomass through the measurement of vegetation canopy height [105].

GNSS contributes to glaciology measurements as evidenced by the performance of GPS where it has had a remarkable impact on the study of glacier volume, flow, and history in the last few years, leading to improvements in measurements of gross flow velocities, rates of surface snowfall, and isostatic adjustment associated with glacial mass change. In particular, real-time GPS (RTGPS; Sect. 5.4.3) can contribute to a better understanding of the dynamics of glaciers by allowing researchers to collect and analyze glacier flow data along with the ocean and atmospheric data [106].

## *11.4.5 Possible Contributions of GNSS to International Protocols*

### 11.4.5.1 Background to the Kyoto Protocol

The United Nations Framework Convention on Climate Change (UNFCCC) became operational on 21st March 1994 in response to scientific evidence that the Earth was warming due to increased atmospheric content of $CO_2$ and other greenhouse gases. In 1997, the *Kyoto Protocol*, an extension of UNFCCC but with more legal binding powers, was passed [107].

In Article 3 of the protocol, quantifiable legal binding commitments are imposed on member countries to the treaty to limit or reduce their greenhouse gas emissions by at least 5% below the 1990 level during the commitment period 2008–2012 [107, 108]. Section 11.3 states that the balance between carbon emission and carbon sinks resulting from direct human-induced, land-use change and forestry activities, limited to afforestation, reforestation and deforestation since 1990, *measured as verifiable changes in carbon stocks in each commitment period*, shall be used to meet the commitments under the Article of each Party included in the protocol. The greenhouse gas emissions by sources and removal by sinks associated with those activities shall be reported in a transparent and verifiable manner and reviewed in accordance with Articles 7 and 8 [107]. Article 5 states that methods to be used to ensure compliance should be those approved by the *Intergovernmental Panel on Climate Change (IPCC)*. Vegetation is listed in the Article as a measured variable, thereby requiring techniques with the capacity to provide regional as well as global, spatial coverage. Remote sensing, GIS and GNSS satellite methods offer such capabilities.

### 11.4.5.2 Application of GNSS, Remote Sensing, and GIS

On 20–22 October 1999, two working groups of the International Society of Photogrammetry and Remote Sensing (ISPRS), together with the University of Michigan, convened to discuss possible areas in which remote sensing technique could be used to support the Kyoto protocol [109]. The groups identified 5 areas where remote sensing technology could be used. In these areas, GNSS georeferencing will be required

to validate the data and support the remote sensing efforts. Remote sensing data has the potential to provide information about certain features (e.g., forests), which can be georeferenced using, e.g., GNSS. This information can then be processed and stored in a GIS (see Sect. 1.3), which benefits monitoring compliance with the Articles of the protocol. The 5 identified areas are:

*Provision of systematic observation of relevant land cover (Articles 5 and 10)*: Rosenqvist et al. [109] observed that multi-spectral systems, in particularly sensors that include mid-infrared bands such as Landsat TM,[3] ETM+[4] and SPOT HRVIR,[5] are suited for the mapping of vegetation. The delineation of fragmented forest lands and smaller patches of forest being used to map vegetation would require high resolution data. To provide mapping of larger spatial coverage (e.g., Australia), higher-resolution data could be complemented by coarse resolution sensors, e.g., NOAA AVHRR[6] [110]. For countries within the tropics, high resolution mapping of vegetation will have to reckon with limitations imposed by cloud cover, smoke and haze. In such situations, coarser resolution sensors with higher temporal repeat cycles or a combination of optical and active microwave data could be adopted. Regional and local scales could also benefit from multi-band/polarimetric and interferometric radar systems that have the advantage of being all weather and achieve spatial resolutions of about 50–100 m [109]. Radar systems, however, suffer from sensitivity to terrain undulation and hydrological conditions on the ground. Another potential technique for mapping vegetation and its potential to absorb $CO_2$ is LIDAR (Laser Infrared Detection And Ranging).

*Support to the establishment of the 1990 carbon stock baseline (Article 3)*: Since 1990 was chosen as a baseline, Landsat TM and SPOT HRV[7] sensors, in operation in 1990, are useful. High resolution data for compiling national coverage maps to support the establishment of the carbon stock baseline is possible, though expensive [109]. Rosenqvist et al. [109] suggests the use of SAR[8] data for the quantification of component biomass (leaves, branches, stems) of the extensive areas of woodlands that occur throughout parts of Australia, Africa and South America, for which the establishment of a 1990 baseline could be supported.

*Detection and spatial quantification of changes in land cover (Articles 3 and 12)*: Article 3.3 focuses on the detection and spatial quantification of afforestation, reforestation and deforestation during the commitment period of 2008–2012, while Article 3.4 (to be implemented in coming phases) focuses on greenhouse gas balances in agriculture, soils, land-use changes and forestry [107]. Article 12 concerns a clean development mechanism that allows trading in $CO_2$. To support Article 3.3, repetitive collection of data is required, preferably annually, at specific seasons and

[3] Thematic mapper.

[4] http://landsat.gsfc.nasa.gov/about/L7_td.html.

[5] High-Resolution Visible and Infrared (imaging instrument). See http://www.cnes.fr/web/CNES-en/7114-home-cnes.php.

[6] Advanced Very High Resolution Radiometer.

[7] High Resolution Visible.

[8] Synthetic Aperture Radar.

at a spatial resolution of the minimum area of interest [109]. Panchromatic and multi-spectral remote sensing data can detect and spatially quantify deforestation activities. Partial deforestation resulting from logging will require higher spatial resolution data. Reforestation (characterizing developmental phase in forests, i.e., from non-forest to forest) and afforestation events (characterized by small patches outside forests) both require high-resolution repetitive multi-spectral measurements. Fire events could be detected using coarse resolution optical sensors that provide daily coverage. Long-wavelength active microwave systems are also useful since they interact with forests at the branch and trunk level and are essential in separating the contributions from the ground and forests [109]. The presence of cloud cover will, however, remain an impediment in some areas. The application of LIDAR to repeatedly characterize structural attributes at specific location could also be valuable, see e.g., Blair [111]. Trading in $CO_2$, for instance, could be supported by the use of passive remote sensing. Under such a system, sensors could be placed within the emission source to transmit the collected digital data. The locations of such emission source could be obtained using GNSS, which also helps in mapping forest fires as discussed in Sect. 17.1.2.

*Quantification of above ground vegetation biomass stocks and associated changes therein (Articles 3 and 12)*: ICESat and its follow on ICESat-2 are expected to contribute in this regard by measuring tree heights (see Sect. 19.3, Fig. 19.11, p. xxx). Indirect estimation using vegetation indices based on photosynthetically active radiation (PAR) is proposed by [109]. The use of multispectral sensors to measure PAR for the prediction of net primary production (NPP) presented as units of Carbon is demonstrated, e.g., by Prince and Goward [112]. The use of active microwave systems and LIDAR to support this Article is still an active area of research. Ranson et al. [113] demonstrated that aircraft based radar sensors having full multi-band, polammetric, and interferometric capabilities are capable of detecting biomass above the ground. In Chap. 10, we discuss how GNSS-reflectometry (GNSS-R) could be used to monitor changes in vegetation biomass.

*Mapping and monitoring of sources of anthropogenic Methane $CH_4$ (Articles 3, 5 and 10)*: Although 6 greenhouse gases are listed in the protocol, see e.g., [107], $CH_4$ was considered by the working groups to be second in importance after $CO_2$. Sources of $CH_4$ include irrigated rice paddies, aquaculture and hydroelectric reservoirs. High-resolution optic sensors could be used to detect and spatial-quantify open water bodies while repetitive measurements could be employed in the irrigated rice paddies. However, repetitive measurements will be affected by clouds, thereby necessitating the use of SAR [114]. The physical locations of these sources, i.e., their boundaries could be mapped using rapid GNSS positioning methods discussed in Chap. 5, Sect. 5.4.5.

## 11.5 Concluding Remarks

The chapter has highlighted the potential of GNSS measurements to contribute to weather forecasting and climate change monitoring through integrative measurement of atmospheric parameters (temperature, pressure and water vapour) in GPS signal delays as discussed in Chap. 9. The success is largely due to the sensitivity of the microwave frequencies used in GNSS in the presence of water vapor whose estimation along GNSS signal propagation paths is discussed in Sect. 11.3. Because water vapor is key to energy transport and buoyancy, assimilation of water vapor measurements is vital to weather modeling. Operational weather forecasts routinely assimilate observations of relative humidity along with pressure and temperature collected using radiosondes, rocketsondes and surface meteorological sensors. In most continental regions, such measurements sample adequately to prevent significant aliasing of pressure and temperature fields (which co-vary on large spatial and temporal scales) but can undersample the relatively short temporal and small spatial-scale variability of humidity [106]. GNSS-derived water vapor data will thus become more useful for weather and climate applications as RTGPS networks (see Sect. 5.4.3) provide data with low latency and high reliability [1].

The rising troposphere temperature due to global warming increases the height of the tropopause. Therefore, information on tropopause height trend is vital for monitoring global warming. This Chapter has explained how GNSS remote sensing of signal delays discussed in Chap. 9 are useful in monitoring global warming. Its atmospheric profiles match those from radiosonde measurements (i.e., temperature accurate to $1 \pm 1.5$ K in the tropopause region), and are suitable for use in the analysis of the tropopause for the studies of climate change. The tropopause, analysed in [77, 78, 99], provided examples of the capability of the method. Furthermore, GNSS-reflectometry (GNSS-R) discussed in Chap. 10 are now being used to monitor changes in soil moisture, vegetation and snow/ice, thereby supporting GNSS sensing of climate change impacts. In Chap. 12, we extend the materials covered in this Chapter by looking at the climate variability of the tropopause. This is now made possible by over a decade of GNSS radio occultation data.

## References

1. Hammond WC, Brooks BA, Bürgmann R, Heaton T, Jackson M, Lowry AR, Anandakrishnan S (2011) Scientific value of real-time Global Positioning System data. Eos 92(15):125–126. doi:10.1029/2011EO150001
2. Burroughs WJ (2007) Climate change: a multidisciplinary approach, 2nd edn. Cambridge University Press, Cambridge
3. Houghton J (2004) Global warming, 3rd edn. Cambridge University Press, Cambridge
4. IPCC (Intergovernmental Panel on Climate Change) (2007), Contribution of Working Group I to the Fourth Assessment Report

5. Krabill W, Hanna E, Huybrechts P, Abdalati W, Cappelen J, Csatho B, Frefick E, Manizade S, Martin C, Sonntag J, Swift R, Thomas R, Yungel J (2004) Greenland ice sheet: increased coastal thinning. Geophysical Research Letters 31(24):L24402. doi:10.1029/2004GL021533
6. Martens WJ, Niessen LW, Rotmans J, Jetten TH, McMichael AJ (1995) Potential impact of global climate change on malaria risk. Environmental Health Perspectives 103(5):458–464
7. Martens WJ (1998) Health impacts of climate change and ozone depletion: an ecoepidemiologic modelling approach. Health Perspect 106:241–251
8. Kitron U (1998) Landscape ecology and epidemiology of vector-borne diseases: tools for spatial analysis. Journal of Medical Entomology 35(4):435–445
9. Steffen W, Sanderson A, Tyson PD, Jäger J, Matson PA, Moore BIII, Oldfield F, Richardson K, Schellnhuber HJ, Turner BLII, Wasson RJ (2005) Global Change and the Earth System: A Planet Under Pressure. Springer, Berlin
10. Santer BD, Sausen Wigley, Wigley TML, Boyle JS, Doutriaux C, AchutaRao K, Hansen JE, Meehl GA, Roeckner E, Ruedy R, Schmidt G, Taylor KE (2003b) Behavior of tropopause height and atmospheric temperature in models, reanalyses, and observations: Decadal changes. Journal of Geophysical Research 108:ACL 1-1–ACL 1-22. doi:10.1029/2002JD00225
11. Santer BD, Wigley TML, Simmons AJ, Kallberg PW, Kelly GA, Uppala SM, Ammann C, Boyle JS, Bruggemann W, Doutriaux C, Fiorino M, Mears C, Meehl GA, Sausen R, Taylor KE, Washington WM, Wehner MF, Wentz FJ (2004) Identification of anthropogenic climate change using a second-generation reanalysis. Journal of Geophysical Research 109:D21104. doi:10.1029/2004JD005075
12. Sausen R, Santer BD (2003) Use of changes in tropopause height to detect influences on climate. Meteorologische Zeitschrift 12(3):131–136. doi:10.1127/0941-2948/2003/0012-0131
13. Santer BD, Wehner MF, Wigley TML, Sausen R, Meehl GA, Taylor KE, Ammann C, Arblaster J, Washington WM, Boyle JS, Bruggemann W (2003) Contributions of anthropogenic and natural forcing to recent tropopause height changes. Science 301:479–483. doi:10.1126/science.1084123
14. Agola NO, Awange JL (2014) Globalized poverty and environment. Springer, Berlin
15. Nyakwada W (2000) The use of weather and climate forecasts by rural people to enhance food production. In: Akunda E, Mango C, Oteng'l SBB et al (eds) Sustainable environmental management for poverty alleviationin the Lake Victoria Basin. KMFRI, pp 38–42
16. Atheru ZKK, Ogallo LA, Ambenje PG (2000) Regional climate forecasts for enhanced food production to alleviate rural poverty around the Lake Victoria region. KMFRI, pp. 28–30
17. Otengi SBB (2000) Weather and climate hazards that affect food production in the Lake Victoria Basin. In: Akunda E, Mango C, Oteng'i SBB et al (eds) Sustainable environmental management for poverty alleviation in the Lake Victoria Basin. KMFRI, Kisii, 3–5 October 1995, pp. 24–27
18. Okoola RE (2000) Climate change as related to food production for the alleviation of rural poverty in the Lake basin region. In: Akunda E, Mango C, Oteng'i SBB et al (eds) Sustainable environmental management for poverty alleviation in the Lake Victoria Basin. KMFRI, pp 43–45
19. Emanuel K (2005) Increasing destructiveness of tropical cyclones over the past 30 years. Nature 436:686–688. doi:10.1038/nature03906
20. Awange JL, Mpelasoka F, Goncalves R (2016) When every drop counts: analysis of droughts in Brazil for the 1901–2013 period. Science of the Total Environment 566–567:1472–1488. doi:10.1016/j.scitotenv.2016.06.031
21. Ummenhofer C, England M, McIntosh P, Meyers G, Pook M, Risbey J, Gupta A, Taschetto A (2009) What causes southeast Australia worst droughts? Geophysical Research Letters 36:L04706. doi:10.1029/2008GL036801
22. Awange JL, Khandu Forootan E, Schumacher M, Heck B (2016) Exploring hydrometeorological drought patterns over the Greater Horn of Africa (1979–2014) using remote sensing and reanalysis products. Advances in Water Resources. doi:10.1016/j.advwatres.2016.04.005

23. Phillips S (2006) Water Crisis. COSMOS, issue 9. http://www.cosmosmagazine.com/issues/2006/9/
24. Mitrovica JX, Gomez N, Clark PU (2009) The Sea-Level Fingerprint of West Antarctic collapse. Science 323(5915):753. doi:10.1126/science.1166510
25. Magadza CHD (1996) Climate change: some likely multiple impacts in southern Africa. In: Downing TE (ed) Climate change and world food security. Springer, Heidelberg, pp 449–483
26. Jallow BP, Barrow MKA, Leatherman SP (1996) Vulnerability of the coastal zone of the Gambia to sea level rise and development of response options. Climate Research 6:165–177
27. Li XY, Xu HY, Sun YL, Zhang DS, Yang ZP (2007) Lake-level change and water balance analysis at Lake Qinghai, West China during recent decades. Water Resource Management 21:1505–1516. doi:10.1007/s11269-006-9096-1
28. Manneh A (1997 Vulnerability of the water resources sector of the Gambia to climate change. In: Republic of the Gambia: Final report of the Gambia/U.S. Country study program project on assessment of the vulnerability of the major economic sectors of the Gambia to the projected climate change. Banjul, The Gambia (unpublished)
29. Beaudoin AB (2002) On the identification and characterization of drought and aridity in postglacial paleoenvironmental records from the northern great plains. Ggraphie physique et Quaternaire 56(2-3): 229–246. E-SCAPE Contribution 3. Note: Volume dated 2002, but published in 2004
30. Mistry VV, Conway D (2003) Remote forcing of East African rainfall and relationships with fluctuations in levels of Lake Victoria. International Journal of Climatology 23:67–89. doi:10.1002/joc.861
31. Awange JL, Ogallo L, Kwang-Ho B, Were P, Omondi P, Omute P, Omulo M (2008) Falling lake victoria water levels: is climate a contribution factor? Journal Climatic Change 89:287–297. doi:10.1007/s10584-008-9409-x
32. Bevis M, Businger S, Herring TA, Rocken C, Anthes RA, Ware RH (1992) GPS Meteorology: Remote sensing of water vapour using global positioning system. Journal of Geophysical Research 97:15787–15801
33. Brutsaert W (2005) Hydrology. An introduction, Fourth edn, Cambridge University Press, New York
34. Tao W (2008) Near real-time GPS PPP-inferred water vapour system development and evaluation. MSc. thesis, UCGE Reports No. 20275. http://www.geomatics.ucalgary.ca/research/publications. Accessed on 26 Aug 2009
35. Trenberth K, Guillemot C (1996) Evaluation of the atmospheric moisture and hydrological cycle in the NCEP Reanalyses. NCAR Technical Note TN-430
36. Ware RH, Fulker DW, Stein SA, Anderson DN, Avery SK, Clerk RD, Droegmeier KK, Kuettner JP, Minster JB, Sorooshian S (2000) Real-time national GPS networks: opportunities for atmospheric sesning. Earth Planet Space 52:901–905
37. Rocken C, Ware R, Hove TV, Solheim F, Alber C, Johnson J, Bevis M, Businger S (1993) Sensing atmospheric water vapour with the Global Positioning System. Geophysical Research Letters 20(23):2631–2634. doi:10.1029/93GL02935
38. Elliot WP, Gaffen DJ (1991) On the utility of radiosonde humidity archives for climate studies. Bulletin of the American Meteorological Society 72:1507–1520
39. Bjerknes V (1904) Das Problem der Wettervorhersage, betrachtet vom Stanpunkt der Mechanik und der Physik. Meteorologische Zeitschrift 21:1–7
40. Kalnay E (2003) Atmospheric modelling, data assimilation and predictability. Cambridge University Press, UK
41. Charney JG (1955) The use of primitive equations of motion in numerical prediction. Tellus 7:22–26
42. Charney JG, Fjørtoft R, von Neuman J (1950) Numerical integration of the barotropic vorticity equation. Tellus 2:237–254
43. Richardson LF (2007) Weather prediction by numerical process, 2nd edn. Cambridge Mathematical Library (the first edition appeared in 1922)

44. Awange JL, Bela Palancz (2016) Geospatial algebraic computations. Theory and application, Springer, Berlin
45. Awange JL, Grafarend EW (2005) Solving algebraic computational problems in geodesy and geoinformatics, 2nd edn. Springer, Berlin
46. Awange JL, Grafarend EW, Paláncz B, Zaletnyik P (2010) Algebraic geodesy and geoinformatics, 2nd edn. Springer, Berlin
47. Daley R (1991) Atmospheric data analysis. Cambridge University Press, Cambridge
48. Bergthorsson P, Döös B (1955) Numerical weather map analysis. Tellus 7:329–340
49. Poli P (2006) Assimilation of GNSS radio occultation data into numerical weather prediction. In: Foelsche U, Kirchengast G, Steiner A (eds) Atmosphere and climate studies by occultation methods. Springer, Berlin, pp 195–204
50. U.S. Climate Change Science Program (CCSP), (2008) Reanalysis of historical climate data for key atmospheric features: Implications for attribution of causes of observed change. A report by the U.S. Climate Change Science Program and the Subcommittee on Global Change Research. In: Dole RM, Hoerling M, Schubert S (eds) National Oceanic and Atmospheric Administration. National Climatic Data Center, Asheville, NC, p 156
51. Talagrand O (1997) Assimilation of observations, an introduction. Journal of the Meteorological Society of Japan. Special Issue 75(1B): 191-209
52. Kuo Y-H, Sokolovski SV, Anthens RA, Vandenberghe F (2000) Assimilation of the GPS radio occultation data for numerical weather prediction. Terrestrial, Atmospheric and Oceanic Science 11:157–186
53. Syndergaard S, Kuo Y-H, Lohmann MS (2006) Observation operators for the assimilation of occultation data into atmospheric models: a review. In: Foelsche U, Kirchengast G, Steiner A (eds) Atmosphere and climate studies by occultation methods. Springer, Berlin, pp 205–224
54. Healy SB, Thépaut JN (2006) Assimilation experiment with CHAMP GPS radio occultation measurements. Quarterly Journal of the Royal Meteorological Society 132:605–623. doi:10.1256/qj.04.182
55. Healey SB, Jupp AM, Marquardt C (2005) Forecast impact experiment with GPS radio occultation measurements. Geophysical Research Letters 32: L03804.1–L03804.4
56. Poli P, Pailleux J, Ducrocq V, Moll P, Rabier F, Mauprivez M, Dufour S, Grondin M, Lechat-Carvalho F, De Latour A, Issler J, Ries L (2008) Weather report. Meteorological Applications of GNSS from Space and on the Ground. InsideGNSS 3(8): 30-39
57. Baker HC, Dodson AH, Penna NT, Higgins M, Offiler D (2001) Ground-based GPS water vapour estimation: potential for meteorological forecasting. Journal of Atmospheric and Solar-Terrestrial Physics 63(12):1305–1314. doi:10.1016/S1364-6826(00)00249-2
58. Melbourne WG, Davis ES, Duncan CB, Hajj GA, Hardy K, Kursinski R, Mechan TK, Young LE, Yunck TP (1994) The application of spaceborne GPS to atmospheric limb sounding and global change monitoring. JPL Publication 94-18
59. Awange JL, Fukuda Y (2003) On possible use of GPS-LEO satellite for flood forecasting. The International Civil Engineering Conference on Sustainable Development in the 21st Century "The Civil Engineer in Development", 12-16 August 2003, Nairobi, Kenya
60. Flores A, Ruffini G, Rius A (2000) 4D Tropospheric tomography using GPS slant wet delay. Annales Geophysicae 18(2):223–234. doi:10.1007/s00585-000-0223-7
61. Randall DA, Tjemkes S (1991) Clouds, the Earth's radiation budget and the hydrological cycle. Global and Planetary Change 4(1–3):3–9. doi:10.1016/0921-8181(91)90063-3
62. Bevis M, Businger S, Chiswell S, Herring TA, Anthes RA, Rocken C, Ware RH (1994) GPS Meteorology: mapping zenith wet delays onto precipitable water. Journal of Applied Meteorology 33:379–386
63. Hanssen RF, Weckwerth TM, Zebker HA, Klees R (1999) High-Resolution water vapor mapping from interferometric radar measurements. Science 283:1297–1299. doi:10.1126/science.283.5406.1297
64. Foelsche U, Gobiet A, Steiner AK, Borsche M, Wickert J, Schmidt T, Kirchengast G (2006) Global Climatologies Based on Radio Occultation
65. IPCC (2001) Climate change 2001: The scientific basis. Cambridge University Press, 881 pp

66. Stendel M (2006) Monitoring climate variability and change by means of GNSS data. In: Foelsche U, Kirchengast G, Steiner A (eds) Atmosphere and climate studies by occultation methods. Springer, Berlin, pp 275–285
67. Schröder T, Leroy S, Stendel M, Kaas E (2003) Stratospheric temperatures probed by Microwave Sounding Units or by occultation of the Global Positioning System. Geophysical Research Letters 30(14):1734. doi:10.1029/2003GL017588
68. Kursinski ER, Hajj GA, Schofield JT, Linfield RP, Hardy KR (1997) Observing Earth' atmosphere with radio occultation measurements using Global Positioning System. Journal of Geophysical Research 102(D19):23429–23465
69. Yuan LL, Anthes RA, Ware RH, Rocken C, Bonner WD, Bevis MG, Businger S (1993) Sensing climate-change using the Global Positioning System. Journal of Geophyisical Research 98(D8):14925–14937. doi:10.1029/93JD00948
70. Leroy SS, Dykema JA, Anderson JG (2006) Climate benchmarking using GNSS occultation. In: Foelsche U, Kirchengast G, Steiner A (eds) Atmosphere and climate studies by occultation methods. Springer, Berlin, pp 287–301
71. Leroy SS (1997) Measurements of geopotential heights by GPS radio occultation. Journal of Geophysical Research 102(D6):6971–6986
72. Shum C, Tseng K, Kuo C, Cheng K, Dai C, Duan J, Huang Z, Lee H, Song S, Yang M (2011) Validation of GNSS-Observed climate variables over Tibetan Plateau. Journal of Aeronautics, Astronautics and Aviation 43(1):009–016
73. Christy JR, Spencer RW, Norris WB, Braswell WD, Parker DE (2003) Error estimates of version 5.0 of MSU-AMSU bulk atmospheric temperatures. Journal of Atmospheric and Oceanic Technology 20(5):613–629
74. Christy JR, Spencer RW, Braswell WD (2000) MSU tropospheric temperatures: dataset construction and radiosonde comparisons. Journal of Atmospheric and Oceanic Technology 17:1153–1170
75. Mears CA, Schabel MC, Wents FJ (2003) A reanalysis of MSU channel 2 tropospheric temperature trend. Journal of Climate 16(22):3560–3664. doi:10.1175/1520-0442(2003)016<3650:AROTMC>2.0.CO;2
76. Vinnikov KY, Grody NC (2003) Global warming trend of mean tropospheric temperature observed by satellites. Science 302(5643):269–272. doi:10.1126/science.1087910
77. Seidel DJ, Randel WJ (2006) Variability and trends in the global tropopause estimated from radiosonde data. Journal of Geophysical Research 111:D21101. doi:10.1029/2006JD007363
78. Schmidt T, Wickert J, Beyerle G, Heise S (2008) Global tropopause height trends estimated from GPS radio occultation data. Geophysical Research Letters 35:L11806. doi:10.1029/2008GL034012
79. Pan LL, Randel WJ, Gary BL, Mahony MJ, Hintsa EJ (2004) Definitions and sharpness of the extratropical tropopause: a trace gas perspective. Journal of Geophysical Research 109:D23103. doi:10.1029/2004JD004982
80. WMO (1957) Definition of Tropopause. Geneva. World Meteorological Organisation, Geneva
81. Shea DJ, Wifley SJ, Stern IR, Hoar TJ (1994) An introduction to atmospheric and oceanographic data. NCAR Tech, Note
82. Ware R, Exner M, Schreiner W, Anthes R, Feng D, Herman B, Gorbunov M, Sokolovskiy S, Hardy K, Kuo Y, Zou X, Trenberth K, Meehan T, Melbourne W, Businger S (1996) GPS sounding of atmosphere from low earth orbit: Preliminary Results. Bulletin of the American Meteorological Society 77:19–40. doi:10.1175/1520-0477(1996)077<0019:GSOTAF>2.0.CO;2
83. Rocken C, Anthes R, Exner M, Hunt D, Sokolovski S, Ware R, Gorbunov M, Schreiner S, Feng D, Hermann B, Kuo Y-H, Zou X (1997) Analysis and validation of GPS/MET data in the neutral atmosphere. Journal of Geophysical Research 102(D25):29849–29866. doi:10.1029/97JD02400
84. Añel JA, Gimeno L, de la Torre L, Nieto R (2006) Changes in the tropopause height for the Eurasian region from CARDS radiosonde data. Naturwissenchaften 93:603–609. doi:10.1007/s00114-006-0147-5.doi10.1007/S00114-006-0147-5

85. Highwood EJ, Hoskins BJ, Berrisforde P (2000) Properties of the Arctic tropopause. Quarterly Journal of the Royal Meteorological Society 126:1515–1532. doi:10.1002/qj.49712656515
86. Nagurny AP (1998) Climatic characteristics of the tropopause over the Arctic Basin. Annales Geophysicae 16:110–115
87. Randel WJ, Wu F, Gaffen DJ (2000) Interannual variability of the tropical tropopause derived from radiosonde data and NCEP reanalyses. Journal of Geophysical Research 105(D12):15509–15523. doi:10.1029/2000JD900155
88. Seidel JD, Ross RJ, Angell JK, Reid GC (2001) Climatological characteristics of the tropical tropopause as revealed by radiosondes. Journal of Geophysical Research 106(D8):7857–7878. doi:10.1029/2000JD900837
89. Varotsos C, Cartalis C, Vlamakis A, Tzanis C, Keramitsoglou I (2004) The long-term coupling between column ozone and tropopause properties. Journal of Climate 17:3843–3854. doi:10.1175/1520-0442(2004)017<3843:TLCBCO>2.0.CO;2
90. Agudelo PA, Curry JA (2004) Analysis of spatial distribution in tropospheric temperature trends. Geophysical Research Letters 31(L22207): doi:10.1029/2004GL02818
91. Christy JR, Spencer RW, Lobl ES (1998) Analysis of the merging procedure for the MSU daily temeperature series. Journal of Climate 11:2016–2041
92. Spencer RW, Christy JR, Grody NC (1990) Global atmospheric temperature monitoring with satellite microwave measurements: Methods and results 1979–84. Journal of Climate 3(10):1111–1128. doi:10.1175/1520-0442(1990)003<1111:GATMWS>2.0.CO;2
93. Parker DE, Gorden M, Cullum DPN, Sexton DMH, Folland CK, Rayner N (1997) A new global gridded radiosonde temperature database and recent temperature trends. Geophysical Research Letters 24(12):1499–1502. doi:10.1029/97GL01186
94. Anthes RA, Rocken C, Kuo YH (2000) Applications of COSMIC to meteorology and climate. Terrestrial, Atmospheric and Oceanic Sciences 11:115–156
95. Schmidt T, Heise S, Wickert J, Beyerle G, Reigber C (2005) GPS radio occultation with CHAMP and SAC-C: global monitoring of thermal tropopause parameters. Atmospheric Chemistry and Physics 5:1473–1488
96. Wickert J, Michalak G, Schmidt T, Beyerle G, Cheng C, Healy S, Heise S, Huang C, Jakowski N, Köhler W, Mayer C, Offiler D, Ozawa E, Pavelyev A, Rothacher M, Tapley B, Arras C (2009) GPS radio occultation: results from CHAMP, GRACE and FORMOSAT-3/COSMIC. Terrestrial, Atmospheric and Oceanic Sciences. 20:35–50. doi:10.3319/TAO.2007.12.26.01(F3C)
97. Wickert J, Beyerle G, Konig K, Heise S, Grunwaldt L, Michalak G, Reigber C, Schmidt T (2005) GPS radio ocultation with CHAMP and GRACE: a first look at a new and promising satellite configuration for global atmospheric sounding. Annales Geophysicae 23:653–657. doi:10.5194/angeo-23-653-2005
98. Free M, Seidel DJ (2005) Causes of differing temperature trends in radiosonde upper air data sets. Journal of Geophysical Research 110:D07101. doi:10.1029/2004JD005481
99. Khandu Awange JL, Wickert J, Schmidt T, Sharifi MA, Heck B, Fleming K (2011) GNSS remote sensing of the Australian tropopause. Climatic Change 105(3–4):597–618. doi:10.1007/s10584-010-9894-6
100. Pittcock B (2003) Climate change: An Australian guide to the science and potential impacts. Climate Change, Australian Greenhouse Office, Canberra
101. Bureau of Meteorology, Australia (2009) Australia's climate change and variability. http://www.bom.gov.au/silo/products/cli_chg/. Accessed 25 Dec 2009
102. Slaymaker O, Kelly REJ (2007) The cryosphere and global environmental change (environmental systems and global change series), 1st edn. Wiley-Blackwell, Victoria
103. Baur O, Kuhn M, Featherstone W (2009) GRACE-derived ice-mass variations over Greenland by acocunting for leakage effects. Journal of Geophysical Research 114(B06407): doi:10.1029/2008JB006239
104. Velicogna I (2009) Increasing rates of ice mass loss from the Greenland and Antarctic ice sheets revealed by GRACE. Geophysical Research Letters 36:L19503. doi:10.1029/2009GL040222

105. Abdalati W, Zwally HJ, Bindschadler B, Csatho B, Farrell SL, Fricker HA, Harding D, Kwok R, Lefsky M, Markus T, Marshak A, Neumann T, Palm S, Schutz B, Smith B, Spinhirne J, Webb C (2010) The ICESat-2 laser altimetry mission. Proceedings of the IEEE 98(5):735–751. doi:10.1109/JPROC.2009.2034765
106. Hammond WC, Brooks BA, Bürgmann R, Heaton T, Jackson M, Lowry AR, Anandakrishnan S (2010) The scientific value of high-rate, low-latency GPS data, a white paper. http://www.unavco.org/community_science/science_highlights/2010/realtimeGPSWhitePaper2010.pdf. Accessed 06 June 2011
107. UN (1998) Kyoto protocol to the United Nations framework convention on climate change. http://unfccc.int/resource/docs/convkp/kpeng.pdf. Accessed 26 Sept 2011
108. UNFCCC (2007) Kyoto Protocol Reference Manual on Accounting of Emissions and Assigned Amounts. Framework Convention on Climate Change. http://unfccc.int/kyoto_protocol/items/2830.php
109. Rosenqvist Å, Imhoff M, Milne A, Dobson C (eds.) (1999) Remote sensing and the Kyoto Protocol: a review of available and future technology for monitoring treaty compliance. Ann Arbor, Michigan, USA, 20–22 October
110. Richards TS, Gallego J, Achard F (2000) Sampling for forest cover change assessment at the pantropical scale. International Journal of Remote Sensing 21(6–7):1473–1490. doi:10.1080/014311600210272
111. Blair JB, Rabine D, Hofton M (1999) The laser vegetation imaging sensor (LVIS): a medium-altitude, digitization only, airborne laser altimeter for mapping. ISPRS 54:115–122
112. Prince SD, Goward S (1995) Global primary production: a remote sensing approach. Journal of Biogeography 22:815–835
113. Ranson KJ, Sun G, Weishampel JF, Knox RG (1997) Forest biomass from combined ecosystem and radar backscatter. Remote Sensing of Environment 59(1):118–133. doi:10.1016/S0034-4257(96)00114-9
114. Le Toan T, Ribbes F, Floury N, Wang LF, Ding KH, Kong JA, Kurosu Fujita M, Kurosu T (1997) Rice crop mapping and monitoring using ERS-1 data based on experiment and modelling results. IEEE Transactions on Geoscience and Remote Sensing 35:41–56. doi:10.1109/36.551933

# Chapter 12
# GNSS Sensing of Climate Variability

*Real-time GNSS measurements have the potential to contribute to climate modeling and weather forecasting through integrative measurement of atmospheric water vapor in GNSS signal delays and measurements of soil moisture flux.*

-W.C. Hammond et al. [1]

## 12.1 Introductory Remarks

Poor reliability of radiosonde records across most developing countries in the southern hemisphere imposes serious challenges in understanding the structure of upper-tropospheric and lower-stratospheric (UTLS) region, i.e., the tropopause. The Constellation Observing System for Meteorology, Ionosphere, and Climate (COSMIC) mission launched in April 2006 has overcome many observational limitations inherent in conventional atmospheric sounding instruments. This chapter presents the study undertaken by Khandu et al. [2] that examined the interannual variability of UTLS temperature over the Ganges-Brahmaputra-Meghna (GBM) River Basin in South Asia using monthly averaged COSMIC radio occultation (RO) data, together with two global reanalyses. Comparisons between August 2006 and December 2013 indicated that MERRA (Modern-Era Retrospective Analysis for Research Application) and ERA-Interim (European Centre for Medium-Range Weather Forecasts reanalysis) were found to be warmer than COSMIC RO data by 2 °C between 200 and 50 hPa levels but these warm biases with respect to COSMIC RO data were found to be consistent over time. The UTLS temperature showed considerable inter-annual variability from 2006 to 2013 in addition to warming (cooling) trends in the troposphere (stratosphere). The cold (warm) anomalies in the upper troposphere (tropopause region) were found to be associated with warm ENSO (El Niño Southern Oscillation) phase, while quasi-biennial oscillation (QBO) is negatively (positively) correlated with temperature anomalies at 70 hPa (50 hPa) level. PCA (Principal Component Analysis) decomposition of tropopause temperatures and heights over the basin indicated that ENSO accounts for 73% of the interannual variability with a correlation of 0.77 with Niño3.4 index whereas the quasi-biennial oscillation (QBO)



J. Awange, *GNSS Environmental Sensing*, Environmental Science and Engineering, DOI 10.1007/978-3-319-58418-8_12

explains about 10% of the variability. The largest tropopause anomaly associated with ENSO occurs during the winter, when ENSO reaches its peak. The tropopause temperature (height) increased (decreased) by about 1.5 °C (300 m) during the last major El Niño event of 2009/2010. In general, a decreasing (increasing) trend in tropopause temperature (height) between 2006 and 2013 was noticed.

## 12.2 Variability of the Tropopause

The upper troposphere-lower stratosphere (UTLS) region (400–30 hPa) is characterised by steep changes in static stability (temperature lapse rate) with large gradients in a number of radiatively active trace gases, including ozone and water vapour [3, 4]. The variability and changes in UTLS temperature play an important role in regulating the exchange of water vapour, ozone, and other trace gases between the troposphere and the stratosphere. Observational evidence suggests that the troposphere has warmed considerably over the past decades with substantial cooling in the lower stratosphere [5–7]. Much of these temperature changes has been attributed to the increasing concentration of the greenhouse gases, and are consistent with trends from climate model simulations, e.g., [6, 8]. The *tropopause*, which marks the separation between the troposphere and the stratosphere in the UTLS region is of special importance for understanding the transport of water vapour into the stratosphere and exchange of ozone between the two layers [4]. The height of the tropopause is affected by the heat balance of both the troposphere (e.g., warming as a result of increasing greenhouse gas concentration) and the stratosphere (e.g., warming as a result of absorbtion of aerosols) [8–10].

Many studies have analyzed the seasonal and inter-annual variations of UTLS temperature using observations from global network of radiosondes, satellite-based measurements, and global reanalyses, e.g., [3, 4, 6, 9–12]. Large-scale variation of the tropopause is dominated by an annual cycle and longer-term interannual variability associated with the El Niño Southern Oscillation (ENSO) [13] and the quasi-biennial oscillation (QBO) [14]. While the global characteristics of UTLS temperature is widely studied, much remains to be known in terms of its regional behaviour and how it influences the regional climate (e.g., rainfall). Large observational uncertainties still exist over South Asia, specifically over the Ganges-Brahmaputra-Meghna (GBM) River Basin due to poor quality of radiosonde networks, e.g., [15–18]. Some stations have been recently updated by the Indian Meteorological Department (IMD) with Global Navigation Satellite Systems (GNSS)-based radiosondes to improve their accuracies, see, [15, 18]. The analysis over the GBM Basin between August 2006 and December 2013 showed that GPS-based radiosondes indicate significant improvement over the previous versions and exhibit negligible bias against the highly-accurate Constellation Observing System for Meteorology, Ionosphere, and Climate (COSMIC) [19] radio occultation (RO) data sets.

## 12.3 GNSS Monitoring of Tropopause Variability

Since the launch of GPS/Meteorology (GPS/MET) mission in 1995 [20], Global Navigation Satellite Systems (GNSS) RO has demonstrated immense potential to provide improved spatio-temporal (and vertical) resolution in the probing of Earth's atmospheric including pressure, temperature, and water vapour [21, 22]. Several studies have demonstrated the usefulness of GNSS RO in improving numerical weather prediction (NWP) forecasts, e.g., [23–26], climate studies [22, 27, 28] and space weather/ionospheric research and operations, e.g., [29, 30] over the past two decades. The number of RO profiles has increased substantially over the past years with the launch of several GNSS RO missions enabling wider applications in regional studies, see, e.g., [21]. For instance, the joint Taiwan-US six-satellite mission, COSMIC/FORMOSA Satellite Mission 3 (COSMIC/FORMOSAT-3, hereafter, COSMIC) [19] has provided about 1500–2000 RO soundings per day globally with 70–90% of the soundings since August 2006. It is now possible to infer decadal temperature trends in the UTLS and the tropopause with a structural uncertainty of less than 0.06 °C in the tropics and mid-latitudes [28]. Using ∼9 years of RO data from CHAllenging Minisatellite Payload (CHAMP, 2001–2008) [31], Gravity Recovery And Climate Experiment (GRACE, 2006–2009) [32] and COSMIC (2006–2009), [22] found an increase of global tropopause height (5–9 m/yr), which is consistent with the current global warming trends.

In the context of growing RO mission and its ability to provide high spatio-temporal (and vertical) resolution vertical profiles, this chapter examines the inter-annual variability of temperature in the UTLS over the GBM River Basin using ∼8 years of monthly accumulated COSMIC RO data from August 2006 to December 2013. Two global reanalysis fields from European Centre for Medium-Range Weather Forecasts reanalysis (ERA-Interim) [33] and Modern-Era Retrospective Analysis for Research Application (MERRA) [34] are also used in conjunction with COSMIC RO data to examine their accuracies over the region. Reanalyses have proven to be useful in understanding the thermodynamics of the lower atmosphere as well as the tropospheric-stratospheric exchange process. Both ERA-Interim and MERRA were developed primarily to improve on various aspects of the hydrological cycle that were not adequately represented in previous generations of reanalyses [33, 34]. ERA-Interim also assimilates refractivity profiles from various GNSS RO missions from 2001 to reduce temperature biases [26, 33]. Thus, modern reanalysis such as MERRA and ERA-Interim are expected to accurately capture the interannual variability of temperature in the UTLS for the most recent decade.

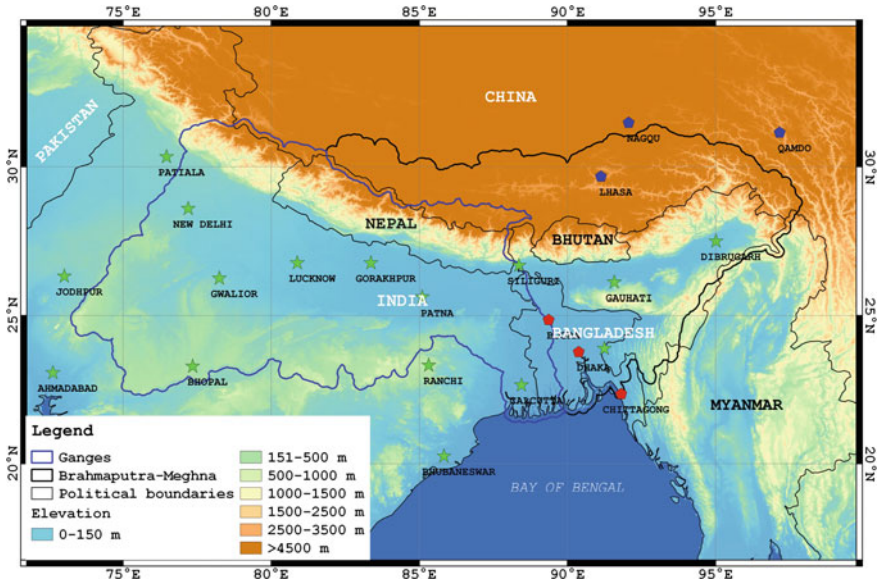


**Fig. 12.1** Overview of the GBM Basin in South Asia. The digital elevation model displayed is derived from the Shuttle Radar Topography mission (SRTM, http://srtm.csi.cgiar.org). The locations of the radiosonde stations are shown in different colors, *green* for those over India (IMD/MK4), *red* for those over Bangladesh (unknown), and *blue* for those over China (ShangE/M). *Source* Khandu et al. [2]

## 12.4 Example: Ganges-Brahmaputra-Meghna (GBM) River Basin

## 12.5 The GBM River Basin

The GBM River Basin in South Asia is a combination of three large river basins, namely, Ganges basin (907,000 km$^2$), Brahmaputra basin (583,000 km$^2$) and the Meghna basin (65,000 km$^2$) [35]. Figure 12.1 shows an overview of the GBM River basin, which is being shared by 5 countries (India (64%), China (18%), Nepal (9%), Bangladesh (7%) and Bhutan (3%). The GBM River Basin with a total surface area of approximately 1.75 million km$^2$, and with an elevation range of about 8,000 m, features distinct climatic characteristics owing to factors such as high topographic variations and the Indian Monsoon, and its interaction with large-scale circulations, e.g., [36]. For example, Ganges Basin is generally characterised by low precipitation whereas the Brahmaputra and Meghna Basins are characterised by high rainfall amount [37] during the summer. The Himalayan fronts (e.g., Meghalayan Plateau) act as a barrier to the monsoon flow and are usually characterized by pronounced rainfall especially during the summer.

The atmospheric conditions over the basin are largely controlled by the monsoon circulation during the summer, which is often modulated by global and regional large-scale climate variabilities such as ENSO and IOD, e.g., [36, 38]. The impact of global warming, increasing population and rapid industrial and agricultural activities, and land use changes across the basin may have contributed significantly to the recent tropospheric warming [39, 40].

### *12.5.1 COSMIC GNSS-Meteorological Data*

COSMIC is a highly successful RO mission that has demonstrated wide scientific applications in operational weather forecasts, see e.g., [19, 21, 41] and global atmospheric studies, see e.g., [22, 27]. In the RO data retrieval process, the bending angle ($\alpha$) derived from Doppler shift measurements onboard Low Earth Orbiting (LEO) satellites can be inverted to recover refractivity ($N$) based on the Abel transform, which is related to total pressure ($P$), temperature ($T$) and water vapour pressure ($P_w$) [42]. In a dry atmosphere (with $P_w = 0$), density profiles are obtained from the known relationship between refractivity and density, while pressure and dry temperature can be derived using the hydrostatic equation and equation of state for ideal gas, see, [42, 43]. In the presence of water vapour (especially in the lower troposphere), humidity and temperature profiles should be complemented with a priori information (e.g., numerical weather forecasts).

Alternatively, wet profiles can be generated using a one-dimensional Variational (1D-Var) method implemented at the COSMIC Data Analysis and Archive Center (CDAAC) at the University Corporation for Atmospheric Research (UCAR). These atmospheric profiles are provided as Level 2 RO data by various data retrieval centres including CDAAC.[1] In Khandu [2], COSMIC Level 2 RO data (both wet and dry profiles) covering the GBM River Basin between April 2006 and December 2013 were used. The wet and dry profiles mainly differ in the lower troposphere due to the presence of water vapour but are similar and highly accurate between 8 and 20 km, see, [19].The wet profiles are used for evaluating the accuracy of radiosonde observations (see details in [2]) while the dry profiles (i.e., temperature only) are used for examining the interannual variations of UTLS over the GBM River Basin. The GBM River Basin received 59,419 COSMIC profiles from April 2006 to December 2013, out of which ~14% were found to be of bad quality. Figure 12.2a shows the number of monthly accumulated COSMIC RO data retrieved during the period, which indicated an average of ~576 profiles per month. The number of profiles decreased considerably between late 2010 and 2012 (Fig. 12.2a) due to problems in some COSMIC satellites.[2] Figure 12.2b shows the distribution of RO data points at various pressure (altitude) levels indicating that many COSMIC data penetrate deep into the lower troposphere with more than 56% of the profiles reaching at least

[1] http://cdaac-www.cosmic.ucar.edu/cdaac/status.html.

[2] http://cdaac-www.cosmic.ucar.edu/cdaac/status.html.

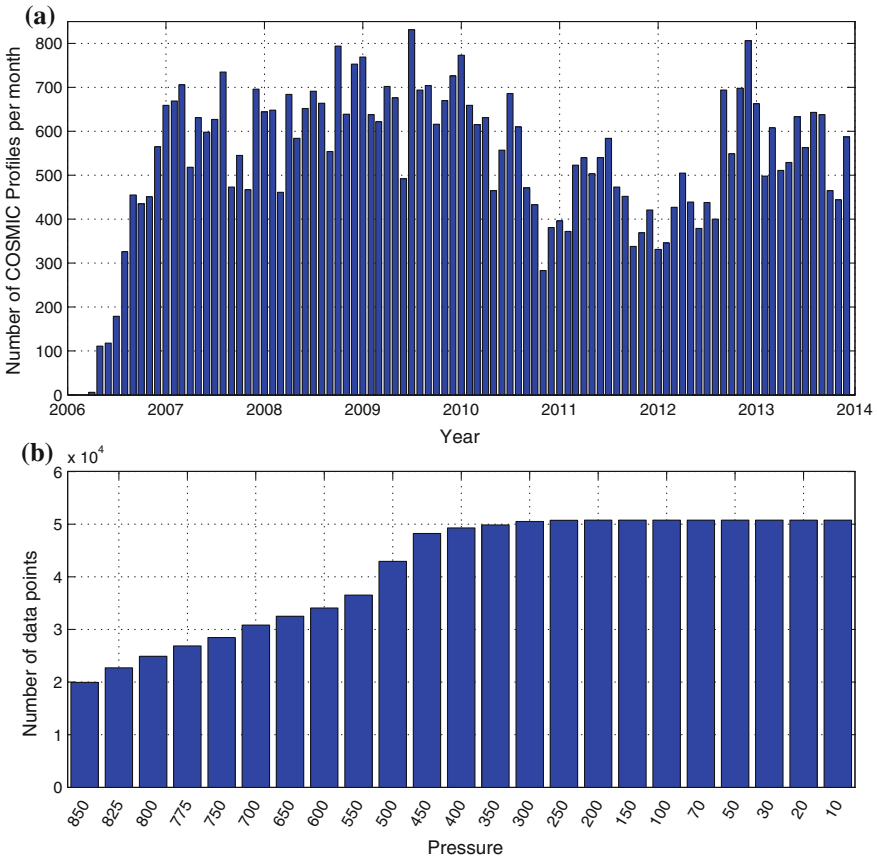


**Fig. 12.2** **a** Total number of monthly COSMIC RO profiles reported in and around the GBM River Basin between April 2006 and December 2013, and **b** the corresponding number of data points at each pressure levels 850–30 hPa (1.5–24.0 km). *Source* Khandu et al. [2]

850 hPa (∼1.5 km above MSL). The geographical distribution of COSMIC profiles at 850 hPa (∼1.5 km), 700 hPa (∼3.1 km), 500 hPa (∼6.0 km), and 400 hPa (∼7.5 km) levels in Fig. 12.3a, b, c, d indicates the effect of high topography over the region (Fig. 12.1), which blocks the GNSS radiowaves. A near-complete coverage of the RO data can be seen at 400 hPa (∼7.5 km) corresponding to the highest altitude of the Himalayas.

### *12.5.2 Reanalysis Products*

COSMIC temperature profiles over the GBM region are compared with two high-resolution modern reanalysis products, (a) MERRA [44] and (b) ERA-Interim [33]. MERRA is produced by the state-of-art Goddard Earth Observing System Data

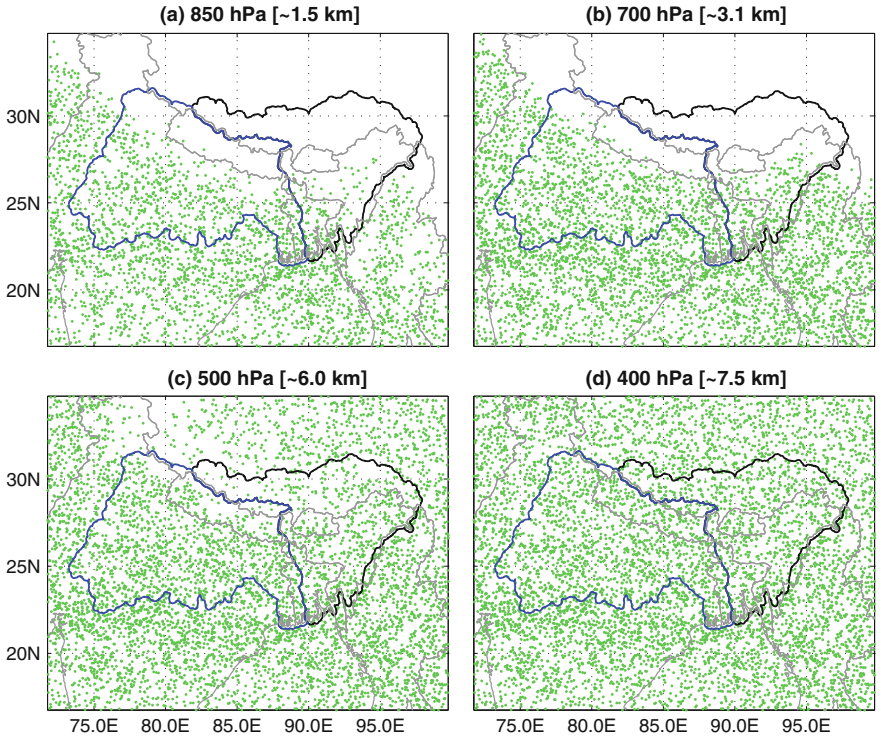


**Fig. 12.3** **a** Spatial distribution of COSMIC data points in the lower troposphere for the year 2012: **a** 850 hPa (∼1.5 km), **b** 700 hPa (∼3.1 km), **c** 500 hPa (∼5.8 km), and **d** 400h Pa (∼7.5 km). *Source* Khandu et al. [2]

Assimilation System, version 5 (GOES-5) at National Aeronautic and Space Administration (NASA), US. GEOS-5 assimilates data from a wide variety of observing systems (e.g., in-situ, satellites, etc.) to produce a consistent set of spatio-temporal meteorological and climatic variables since the beginning of the satellite-era (i.e., 1979). GEOS-5 is run on a $1/2^\circ \times 2/3^\circ$ (or $\sim 50 \times 70$ km) grid with 72 vertical layers extending from the surface through to the stratosphere. Atmospheric variables (e.g., temperature, humidity) are produced at various temporal scales ranging from 3-hourly at $1.5^\circ \times 1.5^\circ$ (or $\sim 150 \times 150$ km grid), to monthly scales at the nominal horizontal resolution.

ERA-Interim is the latest global atmospheric reanalysis produced by ECMWF covering the period 1979 to present [33]. ERA-interim builds on the previous generation of reanalyses (e.g., ERA-15 and ERA-40) with improved model aspects, more advanced assimilation techniques (e.g., 4D Variational Schemes) and better land surface model, and assimilates atmospheric profiles retrieved from the GNSS RO data. The atmospheric variables (e.g., temperature and water vapour) are simulated at 6-hourly time-scales over 60 vertical levels at a $\sim 79 \times \sim 79$ km grid. Because

ERA-Interim assimilates GNSS RO data, ERA-Interim and COSMIC RO data are not completely independent. Reference [26] found that GNSS RO data help to reduce temperature bias of ERA-Interim in the UTLS but are found to produce drying effects in the tropics. Monthly mean temperatures at 14 pressure levels from 500 to 10 hPa are obtained for both MERRA[3] and ERA-Interim[4] to assess UTLS temperature over the GBM River Basin.

### *12.5.3 Climate Variability Indices*

Three climate variability indices are used in this study, namely, (a) El Niño Southern Oscillation Index (ENSO), (b) Indian Ocean Dipole (IOD), and (c) quasi-biennial oscillation (QBO) that are commonly associated with significant fluctuations in UTLS temperatures. ENSO is commonly defined by sea surface temperature (SST) anomalies in the equatorial Pacific ocean, typically over (5°N–5°S, 120°–170°W), which is also known as Niño3.4, see, [13]. ENSO events are said to occur if SST anomalies exceed 4 °C for 6 months or more. Warm and cold ENSO phases are referred to as El Niño and La Niña events, respectively, which are represented by anomalous warming of the central and eastern tropical Pacific (warm phase), and vice versa. Niño3.4 index is obtained from the National Oceanic and Atmospheric Administration (NOAA).[5]

IOD is measured by difference of SST anomalies between the western (50–70°E and 10°S–10°N) and eastern (90–110°E and 10–0°S) equatorial Indian ocean, also referred to as Dipole Mode Index (DMI). Positive IOD events are identified by cooler than normal water in the tropical eastern Indian Ocean and warmer than normal water in the tropical western Indian Ocean and are associated with a shift of active convection from eastern Indian Ocean to the west leading to potentially higher than normal rainfall over parts of the Indian subcontinent. DMI index is obtained from.[6] QBO is stratospheric phenomenon characterized by an eastwest oscillation in stratospheric winds over a period of approximately 28 months [14]. The QBO dominates variability of the equatorial stratosphere and is easily identified as downward propagating easterly (negative) and westerly (negative) wind regimes. It is commonly characterized by an index derived based on zonal winds at 30 hPa or 50 hPa. Here, the QBO index at 30 hPa level covering the period 2006–2013 is obtained from NOAA. Further details on ENSO and IOD are presented in Sect. 17.6.4.

[3] http://disc.sci.gsfc.nasa.gov/daac-bin/FTPSubset.pl.

[4] http://apps.ecmwf.int/datasets/data/interim-full-daily/levtype=sfc/.

[5] http://www.esrl.noaa.gov/psd/data/climateindices/list/.

[6] http://www.jamstec.go.jp/frsgc/research/d1/iod/.

### 12.5.4 GBM Tropopause Temperatures and Heights

Various methods have been used to define the tropopause, such as *lapse-rate tropopause* (LRT), *cold point tropopause* (CPT), *dynamical tropopause* (IPV or isentropic potential vorticity), *ozone tropopause* (OT), and *100 hPa pressure level*, see, [45]. Khandu [2] focused on the changes and interannual variations of the "LRT" given that it is an important indicator of climate change, see, [9, 46]. Based on [47], the LRT (hereinafter as tropopause) is defined as "the lowest level at which the lapse rate decreases to 2 °C/km or less, provided also the average lapse rate between this level and all higher levels within 2 km does not exceed 2 °C/km." COSMIC RO data obtained from CDAAC already contain the derived tropopause parameters (heights and temperatures), while MERRA also provides tropopause temperatures and pressures based on the [47] definition. The tropopause heights, $h_{LRT}$ (in km) for MERRA was approximated from the tropopause pressures, $P$ (in Pa) using the following relationship [48]:

$$h_{LRT} \equiv 44330.8 - 4946.54 \times P^{0.1902632}. \tag{12.1}$$

### 12.5.5 Principal Component Analysis (PCA)

Monthly COSMIC RO data are interpolated to a $0.5° \times 0.5°$ grid over 14 standard pressure levels from 500 to 10 hPa (or 7.5–31 km) and the tropopause using the kriging technique (see details in the [2]). Geostatistical kriging methods have been shown to be more robust and spatially more reliable than other existing methods such as inverse-distance-weighting, Thiessen Polygons, see, e.g., [49]. To study the interannual variations of temperature at various pressure levels, Principal Component Analysis (PCA) [50] was applied to the deseasonalized (annual cycle removed) tropopause heights and temperatures. PCA is a well-known data exploratory tool used in atmospheric/oceanic science since it allows for a space-time display of geophysical data (e.g., temperature), in very few modes, see, [4, 11]. The idea of PCA is to find a set of orthogonal spatial patterns (or Empirical Orthogonal Functions, EOFs) along with a set of associated uncorrelated time-series or principal components (PCs) that captures most of the observed variance (expressed in %) from the available spatio-temporal data (e.g., temperature). In summary, the EOF decomposition can be written as $\mathbf{X}_{(\mathbf{t},\mathbf{s})} = \mathbf{P}_{(\mathbf{t},\mathbf{n})}\mathbf{E}^{\mathrm{T}}_{(\mathbf{s},\mathbf{n})}$, where $\mathbf{X}_{(\mathbf{t},\mathbf{s})}$ is the space ($s$)-time ($t$) data with its time-mean or annual cycle removed, $\mathbf{E}_{(\mathbf{s},\mathbf{n})}$ contains the EOFs with $n$ number of retained modes, and $\mathbf{P}_{(\mathbf{t},\mathbf{n})}$ are the PCs obtained by projecting the original data ($\mathbf{X}_{(\mathbf{t},\mathbf{s})}$) on the orthogonal base-functions $\mathbf{E}_{(\mathbf{s},\mathbf{n})}$, i.e., $\mathbf{P}_{(\mathbf{t},\mathbf{n})} = \mathbf{X}_{(\mathbf{t},\mathbf{s})}\mathbf{E}_{(\mathbf{s},\mathbf{n})}$, see e.g., [51] for details.

## 12.6 Variability of the GBM Tropopause

### *12.6.1 Seasonal and Interannual Variability of Temperature*

First, we compared COSMIC profiles (both dry and wet profiles) with temperature, water vapour pressure, and refractivity profiles from 24 radiosonde stations across the GBM River Basin from August 2006 to December 2013. The results, see, [2] confirmed those of the previous studies, e.g., [15, 17, 18] with radiosondes over India (referred as IMD/MK4) and Bangladesh indicating substantial bias in the UTLS. The results from three recently upgraded radiosondes (over India) showed significantly reduced bias in the UTLS with respect to the COSMIC RO data suggesting that incorporating GPS receivers in conventional radiosondes helps to provide better estimates of temperature and water vapour profiles through more accurate measurement of pressure at various altitude levels, see [2]. This highlights the importance of RO data in providing state-of-art data for calibrating existing radiosondes.

Figure 12.4 shows the regional mean temporal evolution of UTLS (dry) temperature anomalies (time mean removed). For COSMIC, dry temperature anomalies are plotted in Fig. 12.4a. The temperature anomalies range between ±6 °C, indicating largest values above 50 hPa level (lower stratosphere) and below 200 hPa (troposphere). A strong seasonal cycle is evident in the troposphere below 200 hPa level and the stratosphere (above 70 hPa level). The three data sets (COSMIC, MERRA, and ERA-Interim) agree very well above 200 hPa where water vapour is negligible. Below 200 hPa level, however, COSMIC data (Fig. 12.4a) is found to be colder than the two reanalyses (Fig. 12.4b, c) as the effect of water vapour becomes more significant. Both MERRA and ERA-Interim show quantitatively similar biases with respect to the COSMIC RO data, indicating a bias of 1.23 °C and 1.22 °C, respectively, when averaged over 200–70 hPa level whereas the differences between MERRA and ERA-Interim was found to be ±0.5 °C over the same layer during the last 89 months. The annual cycle of temperature at (a) 200 hPa, (b) 100 hPa, (c) 70 hPa, and (d) 50 hPa levels are shown in Fig. 12.5 to estimate the absolute bias (against COSMIC RO data) in reanalysis temperature data. Both MERRA and ERA-Interim indicate warm bias at all the levels with varying magnitudes over different seasons. Both reanalysis products are found to be warmer by ∼ 1°C in June at 200 hPa level (Fig. 12.5a), ∼ 1.5°C at 100 hPa level (Fig. 12.5b), and by up to 2 °C at 70 hPa level from November to May (Fig. 12.5c).

Figure 12.6 shows the detrended (as well as deseasonalized) time-series of temperature anomalies at four pressure levels mentioned above. The temperature anomalies show considerable interannual variability from 2006 to 2013, indicating large negative anomalies in the troposphere during 2009/2010 winter and early 2013, and the low stratosphere during 2007/2008, 2008/2009, and 2012/2013 winters. The 100 hPa level was warmer by ∼1.5 °C during the period 2006/2007, 2009/2010, and 2012/2013, and this is consistent in all the three data sets (Fig. 12.6a, b, c). The warm anomalies at the 100 hPa level for all three periods coincide with warm (i.e., El Niño) ENSO phase, while anomalously cold temperatures at 50 hPa level during

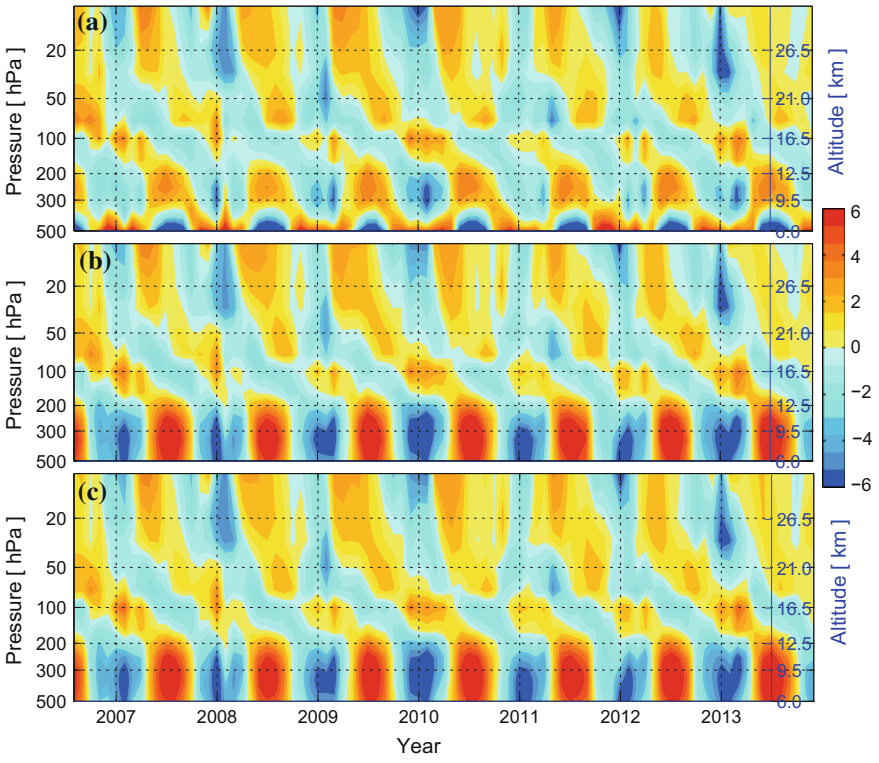


**Fig. 12.4** Temporal evolution of temperature(°C) with the time mean removed at each pressure level (500–10 hPa) based on **a** COSMIC RO, **b** MERRA, and **c** ERA-Interim. Data spans between August 2006 and December 2013 and contains area-average over the region (16°N-35°N, 71°E-100°E) covering the GBM River Basin. *Source* Khandu et al. [2]

2009/2010 and 2010/2011 coincides with the recent stratospheric sudden warming (SSW) events. The stratospheric planetary waves in the northern winter hemisphere can become so intense that they can rapidly disrupt the northern polar vortex, replacing the westerly winds with easterly winds at high latitudes, leading to a dramatically warm polar stratosphere. This phenomenon is called SSW [14], and has a tendency to cool the stratosphere in the tropics and subtropics (e.g., 50 hPa level in Fig. 12.6). The temperature decreased by about 5 °C during the 2008/2009 SSW event at 50 hPa level, see also, [52]. The SSW events can occur during both westerly and easterly phase of the QBO, in which both 2008/2009 and 2010/2011 events occurred during the westerly phase. The warm temperatures during 2006–2007 at the UTLS are associated with the combined impacts of ENSO and IOD, whereas positive temperature anomalies above 50 hPa possibly indicate a weak SSW.

In order to relate them to the three ocean-atmospheric indices described in Sect. 12.5.3, the temperature anomalies at (a) 200 hPa, (b) 100 hPa, (c) 70 hPa, and (d) 50 hPa are plotted in Fig. 12.7a, b, c, d together with the three indices in

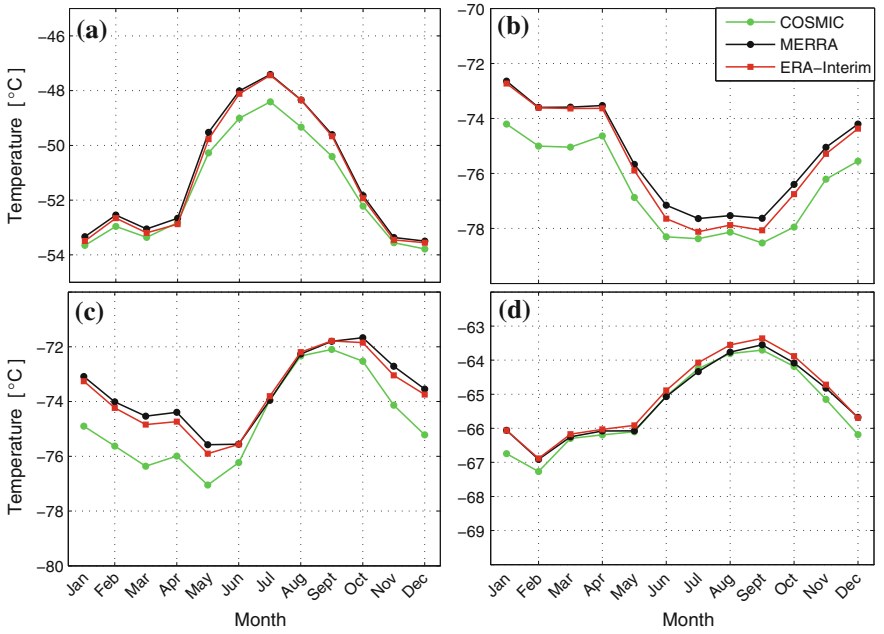


**Fig. 12.5** Seasonal cycle of temperature(°C) at **a** 200 hPa, **b** 100 hPa, **c** 70 hPa, and **d** 50 hPa from August 2006 to December 2013 based on COSMIC RO, MERRA, and ERA-Interim averaged over the GBM River Basin. *Source* Khandu et al. [2]

Fig. 12.7e. The 200 hPa level temperature anomalies clearly indicate the influence of 2009/2010 El Niño event (Fig. 12.7a) where temperature decreased by ∼1.5 °C when El Niño was at its peak in January 2010 (Fig. 12.7a). The 200 hPa level temperatures are negatively correlated with ENSO (Fig. 12.7e). The 100 hPa level, whose temperatures are highly correlated with ENSO, also appears to closely associated with the QBO anomalies especially during 2008/2009 and 2010/2011 (Fig. 12.7b). The temperature anomalies at 70 and 50 hPa levels (Fig. 12.7c, d) primarily depicts the structure of recent major SSW events (see also, Fig. 12.6), both of which occurred during the westerly phase of the QBO cycle. Correlation coefficients between temperature anomalies at these four pressure levels and three atmospheric/ocean indices are given in Table 12.1. Significance of the correlations are tested at 95% confidence level using a reduced degree of freedom, which was obtained by dividing the total number of months ($n = 89$) by 4 months that are used to smooth the time series.

As shown in Fig. 12.7, ENSO is highly correlated (0.82 at 1 month time-lag) with temperatures at 100 hPa level, and tend to be insignificant above 70 hPa level. Warmer (colder) SST leads to stronger (weaker) convection resulting in colder (warmer) tropopause temperatures and are also negatively correlated with temperatures at 200 hPa level. Both MERRA and ERA-Interim show similar correlation coefficients (results not shown). Since the IOD phenomenon is closely associated with the ENSO events between 2006 and 2013 (with a correlation coefficient of 0.42), it is found to be

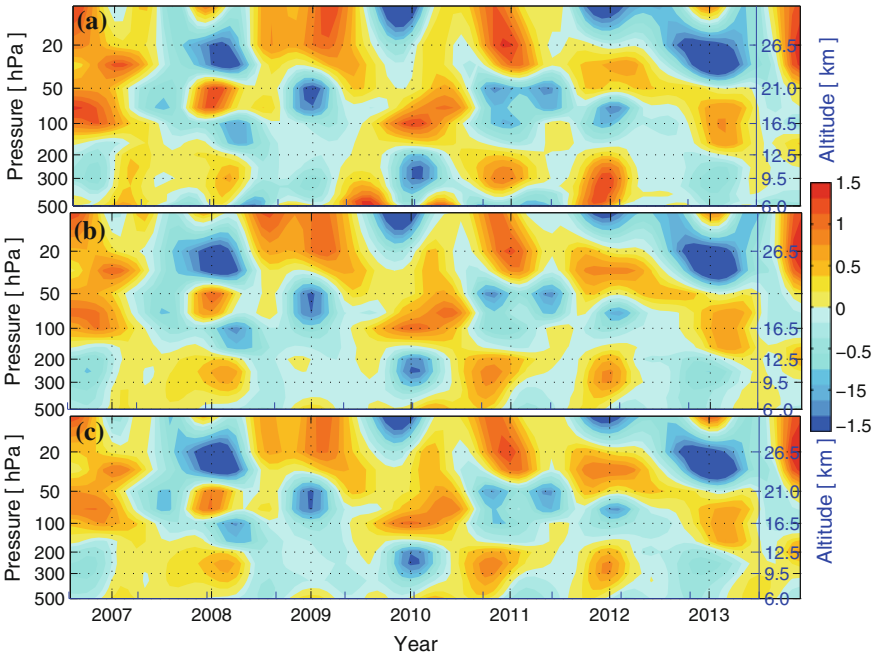


**Fig. 12.6** Interannual variability of temperature (°C) in the UTLS region based on **a** COSMIC RO, **b** MERRA, and **c** ERA-Interim from August 2006 to December 2013. *Source* Khandu et al. [2]

significantly correlated with temperatures in the lower troposphere with a correlation of −0.53 at 400 hPa level (see, Table 12.1). At the 200 hPa level, its correlation decreased to −0.42 (see, Table 12.1) but are still significant at 95% confidence level. Temperatures at 100 hPa level over the tropics has been shown as a approximation of the QBO signal in [53] due their very high correlation (0.86) between 2004 and 2010. However, their relationship did not hold steady (with a correlation of 0.47 at 100 hPa level) as the QBO westerly phase slowed dramatically lasting for about 21 months (i.e., 1 and 1/2 cycle) from June 2008 to January 2010 followed by a step easterly phase in June 2010.

Temperature changes estimated at the four pressure levels (Fig. 12.6) from 2006 to 2013 are given in Table 12.2. The linear trends were estimated from the deseasonalized temperature anomalies using non-parametric Sen's slope estimator [54]. Significance of trends were tested at 95% confidence level based on the Mann-Kendall's non-parametric test [55, 56]. Consistent with Fig. 12.6a, there is a slight increase (but not significant) in temperature (0.02±0.02 °C/yr based on COSMIC RO) at 200 hPa level, and decrease in temperature (−0.04±0.05 °C/yr based on COSMIC RO) at the 100 hPa level. It also confirms the recent stratospheric cooling trends [57], indicating a temperature decrease at the rate of 0.07±0.05 °C/yr based on COSMIC RO at 70 hPa level during the past 8 years. These trends are also consistently estimated by the two reanalysis products (MERRA and ERA-Interim) except at 100 hPa level where

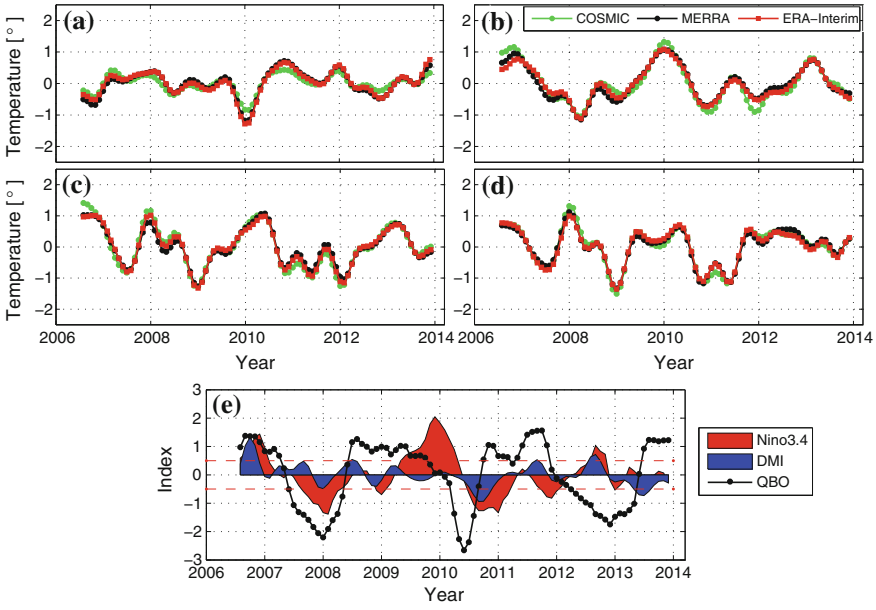


**Fig. 12.7** Interannual variability of temperature (°C) at **a** 200 hPa, **b** 100 hPa, **c** 70 hPa, and **d** 50 hPa from August 2006 to December 2013 based on COSMIC RO, MERRA, and ERA-Interim. **e** Ocean-atmospheric indices: Niño3.4, DMI, and QBO are also plotted for reference. *Source* Khandu et al. [2]

MERRA data did not show any trend (see, Table 12.2). The uncertainties in trend estimates were relatively larger than the trends themselves due to the short time-span but nevertheless the trends are clearly visible at different levels (see Fig. 12.7).

### *12.6.2 Trends and Variability of Tropopause Heights and Temperatures*

The annual mean and standard deviation of tropopause temperatures and heights are plotted in Figs. 12.8 and 12.9. The tropopause is generally colder (higher) in south (closer to the equator) reaching a minimum (maximum) of −81.5 °C (16.9 km) over southern Myanmar (Figs. 12.8a and 12.9a). While the temperature gradually increases from south to north (from −81.5 °C to −69.5 °C, based on COSMIC RO in Fig. 12.8a), its heights are more or less homogenous at around 16.8 km below 29°N with its boundary roughly falling on the northern boundaries of Bhutan. However, its height changes steeply by around 2 km from 29°N to 35°N, which also showed the largest standard deviation (∼1.8 km, Fig. 12.9b). The standard deviations of temper-

**Table 12.1** Correlation coefficients between ocean-atmospheric climate indices and temperature anomalies at 200, 100, 70, and 50 hPa for the period August 2006 to December 2013. The values that are significant at 95% confidence level based on the reduced degree of freedom are bolded. *Source* Khandu et al. [2]

| Pressure levels(hPa) | ENSO | | IOD | | QBO | |
|---|---|---|---|---|---|---|
| | Correlation | Lag (months) | Correlation | Lag (months) | Correlation | Lag (months) |
| 200 | **−0.70** | 0 | **−0.42** | 0 | 0.39 | 26 |
| 100 | **0.82** | 1 | 0.27 | 2 | **0.47** | 27 |
| 70 | **0.40** | 3 | −0.35 | −4 | **−0.45** | 25 |
| 50 | 0.27 | 1 | 0.34 | 2 | **0.53** | 12 |

**Table 12.2** Trends in temperature (°C/yr) at 200, 100, 70, and 50 hPa for the period August 2006 to December 2013. Uncertainties in trend estimates are reported at 95% confidence interval. *Source* Khandu et al. [2]

| Pressure levels(hPa) | COSMIC | MERRA | ERA-Interim |
|---|---|---|---|
| 200 | 0.02±0.02 | 0.03±0.03 | 0.03±0.05 |
| 100 | −0.04±0.05 | 0.00±0.00 | −0.02±0.04 |
| 70 | −0.07±0.05 | −0.04±0.05 | −0.05±0.05 |
| 50 | −0.02±0.04 | −0.01±0.01 | −0.01±0.02 |

atures reaches up to ±6 °C based on COSMIC RO data (Fig. 12.8b) over the same region.

The tropopause over the GBM River Basin often reaches as high as 18 km in response to the Indian summer monsoon when intense convective activities occur, and as low as 10 Km during winter. The spatial patterns of tropopause shown by MERRA were consistent with those from COSMIC RO but are found to be more zonally homogenous, warmer (by up to 4 °C in the north) and lower (by ∼1 km) over the region. This warm bias (against COSMIC RO data) is also observed in ERA-Interim at 100 hPa level(see Fig. 12.5b) but are relatively lower than MERRA, especially during the monsoon. The annual cycle of area-averaged (over the spatial domain covering [71.5°E-99.5°E, 16.5°N-34.5°N]) tropopause temperatures and heights of COSMIC RO and MERRA are shown in Fig. 12.10. The area-averaged temperatures (heights) of COSMIC RO reach minimum (maximum) in June but are warmer (lower) in MERRA by 1.0–2.5 °C (∼1.2 km from May to December). MERRA also shows the tropopause temperature minimum in July instead of June (Fig. 12.10a). The large differences in MERRA could partly be related to the approximation in Eq. 12.1, but it should be noted that errors in tropopause heights may cause large errors in temperature due to the lapse-rate criterion. The warm bias (against COSMIC RO data) observed in reanalysis products were thought to mainly stem from assimilation of radiance observations from aircrafts and satellites, see e.g., [33,

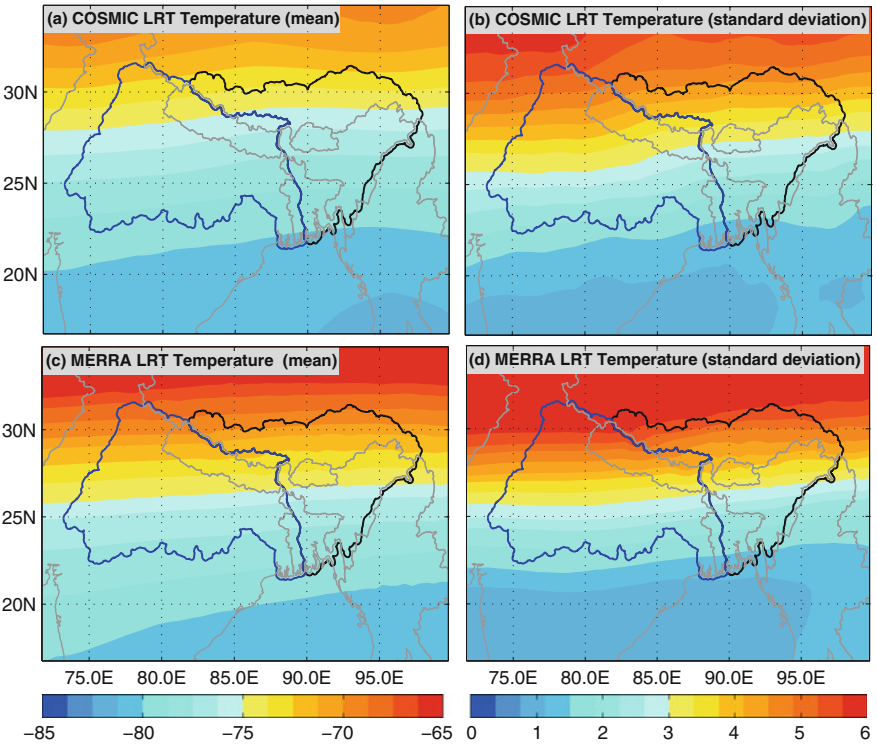


**Fig. 12.8** Spatial variation of mean and standard deviation of tropopause temperatures (°C) derived from COSMIC RO and MERRA product based on 89 months from August 2006 to December 2013. **a** Mean and **b** standard deviation of tropopause temperatures (°C) from COSMIC RO, **c** mean and **d** standard deviation of tropopause temperatures (°C) from MERRA product. *Source* Khandu et al. [2]

and references therein]. Large variations in tropopause temperatures and heights in Fig. 12.10 (indicated by error bars) during winter and spring could be related to high diurnal temperature variations [58].

The annual cycle was removed from each grid cell to examine the interannual variability of tropopause temperatures and heights, and to estimate linear trends over the period August 2006 to December 2013. The area-averaged linear trends and their uncertainties are given in Table 12.3. In general, based on the COSMIC RO data, the tropopause appears to be cooling (increasing in height) at a rate of $-0.039 \pm 0.05$ ° C/yr ($6.01 \pm 5.02$ m/yr) during the period (see Table 12.3), which to some degree is also estimated by MERRA. However, MERRA shows negligible cooling compared to COSMIC RO while its height increase is not consistent with its temperature decline. The increasing (decreasing) tropopause heights (temperatures) has been consistently observed in GNSS RO data over the years at both global and

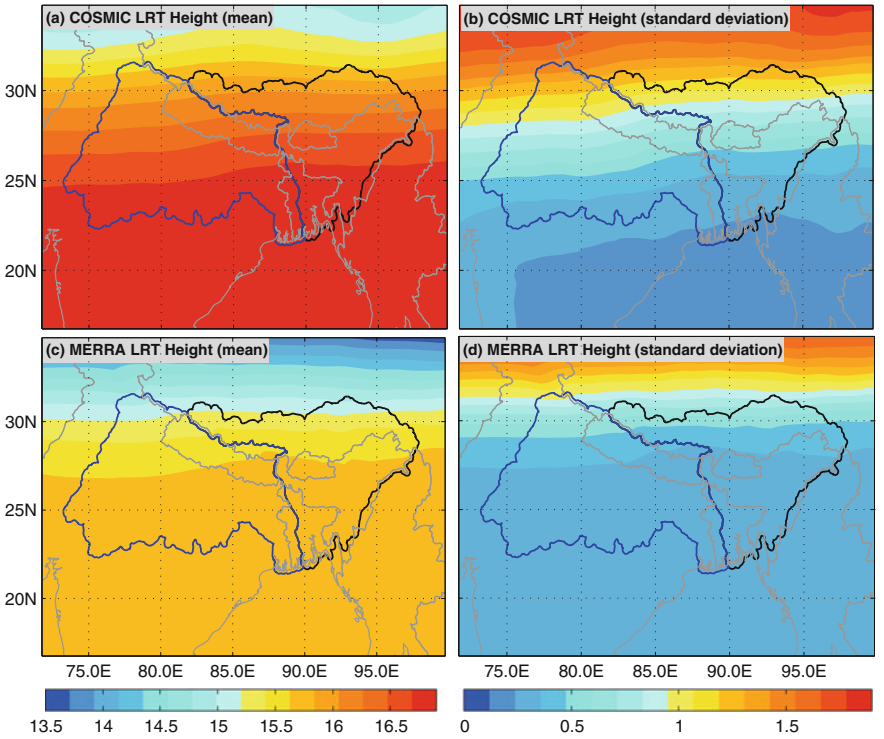


**Fig. 12.9** Spatial variation of mean and standard deviation of tropopause heights (km) derived from COSMIC RO and MERRA product based on 89 months from August 2006 to December 2013. **a** Mean and **b** standard deviation of tropopause heights (km) from COSMIC RO, **c** mean and **d** standard deviation of tropopause heights (km) from MERRA product. *Source* Khandu et al. [2]

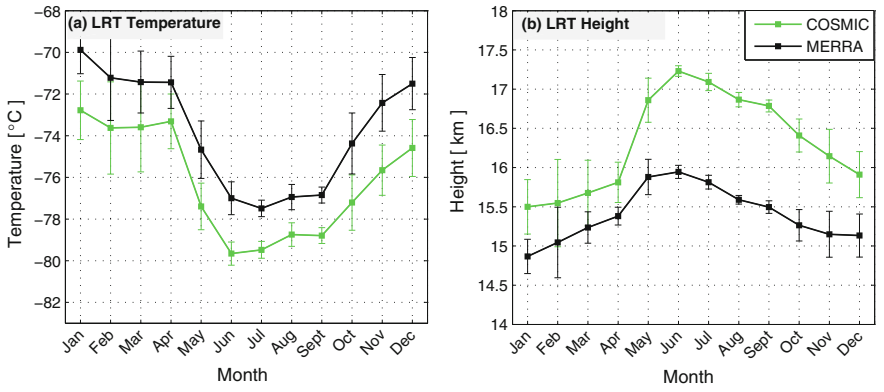


**Fig. 12.10** Annual cycle of tropopause over the GBM River Basin computed from MERRA and COSMIC RO data for the period between August 2006 and December 2013: **a** tropopause temperatures, and **b** tropopause heights. *Source* Khandu et al. [2]

**Table 12.3** Trends in tropopause temperatures (°C/yr) and heights (m/yr) based on the area-averaged time-series anomalies derived from COSMIC RO and MERRA. Data span between August 2006 and December 2013. Uncertainties in trend estimates are reported at 95% confidence interval. *Source* Khandu et al. [2]

| Data | Temperature (°C/yr) | Height (m/yr) |
|---|---|---|
| COSMIC RO | −0.039±0.05 | 6.01±5.02 |
| MERRA | −0.005±0.03 | 17.00±10.20 |

**Table 12.4** Correlation coefficients between tropopause parameters (temperature and height) derived from COSMIC RO and MERRA and ocean-atmospheric indices for the period August 2006 to December 2013. The values that are significant at 95% confidence level based on the reduced degree of freedom are bolded. *Source* Khandu et al. [2]

| Data | COSMIC RO | | MERRA | |
|---|---|---|---|---|
| | Temperature | Height | Temperature | Height |
| Nino3.4 & PC 1 | **0.77** | **−0.74** | **0.78** | **−0.75** |
| IOD & PC 1 | 0.35 | 0.37 | 0.35 | 0.38 |
| QBO & PC 2 | 0.36 | 0.36 | **0.53** | **0.54** |

regional scale, e.g., [22, 59, 60], which is evidently in response to enhanced warming in the upper troposphere and substantial cooling in the lower stratosphere.

Next, PCA was applied on the deseasonalized time-series of tropopause temperatures and heights in order to study the spatio-temporal characteristics of tropopause over the GBM River Basin. PCA is particularly relevant here because tropopause is a transitional layer that responds to perturbations from both the troposphere and stratosphere, which makes it difficult to understand their variability modes. Figure 12.11 shows the EOFs (or spatial maps) for the first three leading modes of variability. The first EOF accounts for a variability of ∼73% (COSMIC RO) and 63∼% (MERRA) indicating positive anomalies (up to 1.1 °C) across the GBM River Basin. EOF 1 appears to be rather symmetric around 29°N in COSMIC RO but seems to be shifted slightly southwards in MERRA (Fig. 12.11a, d). Their corresponding PCs are shown in Fig. 12.12. PC 1 (Fig. 12.12a) is found to be highly correlated with Niño3.4 index with a correlation of 0.77 (COSMIC RO) and 0.78 (MERRA) with a time-lag of one month indicating that ENSO dominates tropopause variability over the region (see, Table 12.4. DMI is also moderately correlated (0.35) with PC 1 of both COSMIC RO and MERRA (with a lag of 2 months) indicating that warmer SSTs in the equatorial Indian ocean might be having some influence on the tropopause variability.

The second EOF shown in Fig. 12.11b, e indicate a diagonal (dipole) pattern with positive (negative) anomalies in the northwest (southeast) accounting for variance of ∼10% (COSMIC) and ∼18% (MERRA). Its corresponding PC is found to be significantly correlated with the QBO index with a correlation coefficient of 0.40 (COSMIC RO) and 0.53 (MERRA) (at zero lag). It is not surprising that the relationship between PC 2 and QBO is relatively low compared to the equatorial

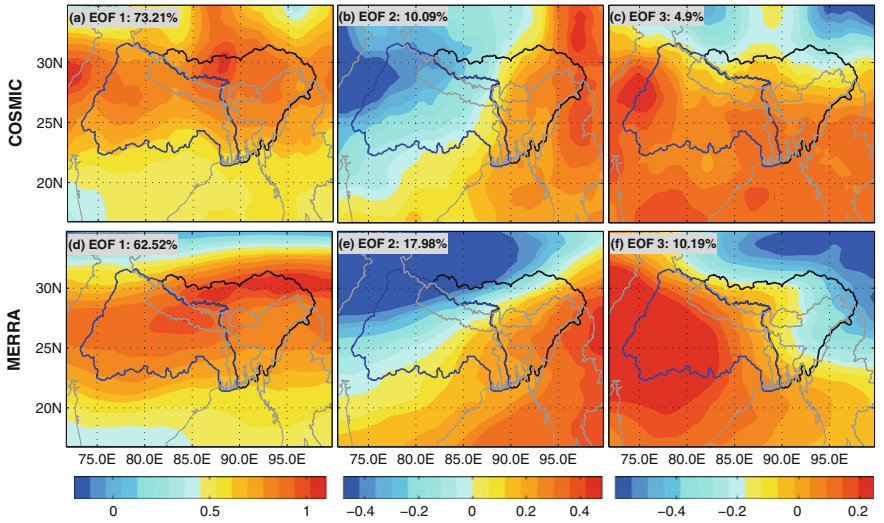


**Fig. 12.11** The first three leading EOFs of tropopause temperature (°C) based on MERRA data and COSMIC RO data for the period August 2006 to December 2013. *Source* Khandu et al. [2]

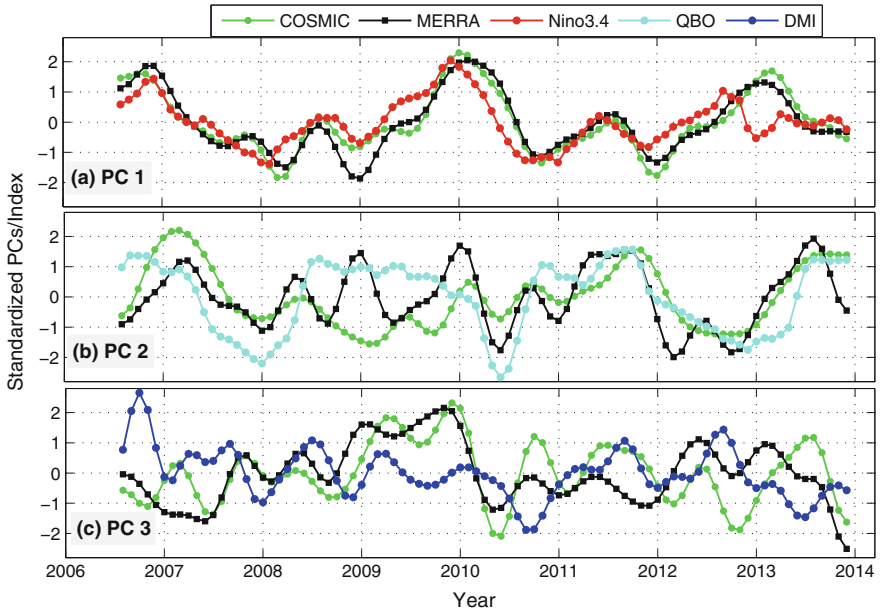


**Fig. 12.12** The corresponding PCs (temporal components) based on the three leading orthogonal modes shown in Fig. 12.11. *Source* Khandu et al. [2]

(or tropical) tropopause since QBO is much of tropical phenomenon, e.g., [3, 4, 11, 53]. It also stems from the fact that QBO westerly phase prolonged for an extended period of 21 months before changing to a westerly phase in January 2010. The third EOF (Fig. 12.11c, f) explains about 5% (COSMIC RO) and 10% (MERRA) of the variability and shows positive (negative) anomalies below (above) 30 °N, although MERRA shows a diagonal dipole pattern similar to EOF 2. Their corresponding PCs were found to be moderately correlated with ENSO and IOD. The tropopause heights are negatively correlated with their temperatures and therefore, vary inversely with its temperature, i.e., increase in tropopause height with decrease in temperature (figures not shown). The correlation coefficient between the PCs of three leading modes of tropopause heights and the ocean-atmospheric indices indicate similar magnitudes of correlations but with opposite signs (see, Table 12.4).

To show the influence of ENSO mode on the tropopause, the seasonal mean area-averaged anomalies of tropopause temperatures and heights are plotted in Fig. 12.13. Seasonal mean anomalies were obtained averaging the products of EOF 1 and PC 1 (of the COSMIC RO data). The ENSO effect is found to be maximum during the winter (e.g., 2009–2010, 2012–2013) when ENSO was at its peak. Its effects are also felt during autumn (in 2007 and 2011) and spring (in 2008), and during the El Niño and La Niña periods. The largest tropopause anomaly occurred during the major El Niño event of 2009/2010 when tropopause temperature (height) increased (decreased) by about 1.5 °C (300 m) in the winter (Fig. 12.13a, b). La Niña periods (e.g., 2007/2008, 2010/2011) are mainly associated with deep convections in the troposphere leading to a wider troposphere or higher tropopause height (see, Fig. 12.13b).

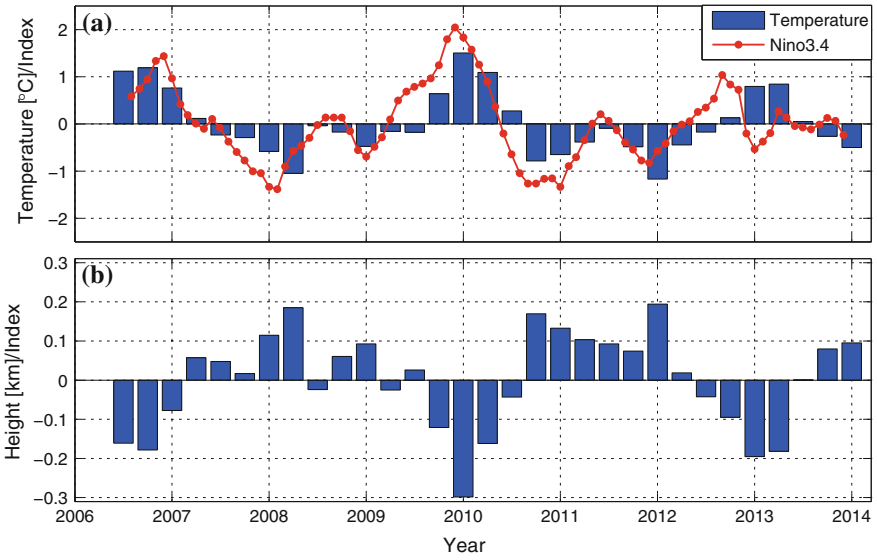


**Fig. 12.13** Seasonal mean tropopause temperature and height anomalies due to ENSO mode together with the Niño3.4 index. The area-averaged time series were obtained by multiplying EOF 1 and PC 1, i.e., basically showed the replication of ENSO mode. *Source* Khandu et al. [2]

## 12.7 Concluding Remarks

This chapter examined the inter-annual variability of temperature in the UTLS including tropopause temperatures and heights over the GBM River Basin in South Asia using 89 months (August 2006 to December 2013) of COSMIC RO data and two global reanalyses (MERRA and ERA-Interim). The GBM River Basin received an average of ∼576 well-distributed COSMIC RO profiles/month during the period with more than 56% of the profiles reaching at least 1.5 km above the mean sea level height. Even though the reanalysis products such as MERRA and ERA-Interim are significantly warmer (by up to 2 °C) than COSMIC RO data at 200–50 hPa level, the warm bias is found to be consistent over time. The UTLS temperature showed considerable inter-annual variability during the past 8 years (2006–2013) with modest trends in the troposphere and stratosphere. ENSO is found to have the largest effect at the 100 hPa level with a correlation of 0.82 (at 1 month lag) while SSW signals tend to dominate the lower stratospheric temperature anomalies (e.g., at 50 hPa level). The temperature at 200 hPa level decreased by ∼1.5 °C during the last major El Niño event of 2009/2010. The SSW events that occurred in 2008/2009 and 2010/2011 winters are marked by pronounced cooling at 50 hPa level.

The relationship between ENSO and QBO has been reported to be strong between 2004 and 2008, see, [53], but has weakened substantially over the years due to a persistent westerly phase that lasted for 21 months from June 2008 to January 2010. The IOD mode plays a significant role on the tropospheric temperature warming over the GBM River Basin as enhanced upwellings in the equatorial Indian ocean drives more convection in the region. However, their role seems to be limited within the troposphere as the magnitude of correlation between DMI and temperature decreases from −0.53 at 400 hPa level to −0.42 hPa at 200 hPa level. Consistent with the previous studies, there is a warming (cooling) trend in the upper troposphere (lower stratosphere), which are consistent with other estimated global warming trends, see, e.g., [61, 62, and references therein].

The tropopause temperatures and heights derived from COSMIC RO and MERRA were investigated in detail due to their importance in climate change and attribution studies, see, e.g., [8, 9, 61]. The interannual variability of tropopause temperatures and heights over the GBM River Basin was studied by applying the PCA method. The results indicate a dominant effect of ENSO, accounting for a variance of about 73% (COSMIC RO) and 63% (MERRA) of the first variability mode. PC 1 shows a near-accurate representation of the ENSO mode (represented by the Niño3.4 index) with a correlation of 0.77 (COSMIC RO) and 0.78 (MERRA). The QBO accounts for ∼10% (COSMIC RO) and ∼18% (MERRA) of the variability, as indicated by the correlation between PC 2 and the QBO index. The largest temperature anomaly was recorded in 2009/2010 winter corresponding to a major El Niño event. The tropopause temperatures (heights) increased (decreased in heights) by about 1.5 °C (300 m) during this period. Because IOD effects are generally found to be concentrated within

the troposphere, the correlations between and DMI and tropopause (temperature and height) are found to be low but nevertheless, requires further examination using longer time-series.

## References


1. Hammond WC, Brooks BA, Bürgmann R, Heaton T, Jackson M, Lowry AR, Anandakrishnan S (2011) Scientific value of real-time global positioning system data. Eos 92(15):125–126. doi:10.1029/2011EO150001
2. Khandu Awange J, Forootan E (2016) Interannual variability of upper tropospheric and lower stratospheric (UTLS) temperature over Ganges-Brahmaputra-Meghna basin based on COSMIC GNSS RO data. Atmos Meas Tech 9(4):1685–1699. doi:10.5194/amt-9-1-2016
3. Reid GC, Gage KS (1985) Interannual variations in the height of the tropical tropopause. J Geophys Res 90:5629–5635. doi:10.1029/JD090iD03p05629
4. Randel WJ, Wu F, Gaffen DJ (2000) Interannual variability of the tropical tropopause derived from radiosonde data and NCEP reanalyses. J Geophys Res 105(D12):15509–15523. doi:10.1029/2000JD900155
5. Karl TR, Hassol SJ, Miller CD, Miller WL (eds) (2006) Temperature trends in the lower atmosphere: steps for understanding and reconciling differences. Technical report, U.S, Climate Change Science Program, Washington, DC
6. Lott FC, Stott PA, Mitchell DM, Christidis N, Gillett NP, Haimberger L, Perlwitz J, Thorne PW (2013) Models versus radiosondes in the free atmosphere: a new detection and attribution analysis of temperature. J Geophys Res 118:2609–2619. doi:10.1002/jgrd.50255
7. Thorne PW, Brohan P, Titchner HA, McCarthy MP, Sherwood SC, Peterson TC, Haimberger L, Parker DE, Tett SFB, Santer BD, Fereday DR, Kennedy JJ (2013) A quantification of uncertainties in historical tropical tropospheric temperature trends from radiosondes. J Geophys Res 116: doi:10.1029/2010JD015487
8. Santer BD, Thorne PW, Haimberger L, Taylor KE, Wigley TML, Lanzante JR, Solomon S, Free M, Gleckler PJ, Jones PD, Karl TR, Klein SA, Mears C, Nychka D, Schmidt GA, Sherwood SC, Wentz FJ (2008) Consistency of modelled and observed temperature trends in the tropical troposphere. Int J Clim 13:1703–1722. doi:10.1002/joc.1756
9. Santer BD, Wehner MF, Wigley TML, Sausen R, Meehl GA, Taylor KE, Ammann C, Arblaster J, Washington WM, Boyle JS, Bruggemann W (2003) Contributions of anthropogenic and natural forcing to recent tropopause height changes. Science 301:479–483. doi:10.1126/science.1084123
10. Santer BD, Sausen R, Wigley TML, Boyle JS, Doutriaux KA, Hansen JE, Meehl GA, Roeckner E, Ruedy R, Schmidt G, Taylor KE (2003b) Behavior of tropopause height and atmospheric temperature in models, reanalyses, and observations: decadal changes. J Geophys Res 108:ACL 1-1–ACL 1-22. doi:10.1029/2002JD00225
11. Gettelman A, Randel WJ, Massie S, Wu F, Read WG, Russell JM (2001) El Nino as a natural experiment for studying the tropical tropopause region. J Climate 14(16):3375–3392. http://journals.ametsoc.org/doi/abs/10.1175/1520-0442(2001)014<3375:ENOAAN>2.0.CO;2
12. Wilcox LJ, Hoskins BJ, Shine KP (2011) A global blended tropopause based on ERA data. part II: trends and tropical broadening. J Geophys Res 138:576–584. doi:10.1002/qj.910
13. Trenberth KE (1990) Recent observed interdecadal climate changes in the Northern hemisphere. Bull Am Meteorol Soc 71:988–993. doi:10.1175/1520-0477(1990)071<0988:ROICCI>2.0.CO;2
14. Baldwin MP, Gray LJ, Dunkerton TJ, Hamilton K, Haynes PH, Randel WJ, Holton JR, Alexander MJ, Hirota I, Horinouchi T, Jones DBA, Kinnersley JS, Marquardt C, Sato K, Takahashi M (2001) The quasi-biennial oscillation. Rev Geophys 39:179–229. doi:10.1029/1999RG000073

15. Ansari MI, Madan R, Bhaita S (2015) Verification of quality of GPS based radiosonde data. Mausam 66:367–374. metnet.imd.gov.in/mausamdocs/16632_F.pdf
16. Gupta MD, Das S, Prasanthi K, Pradhan PK (2005) Validation of upper-air observations taken during the ARMEX-I and its impact on the global analysis-forecast system. MAUSAM 56:139–146
17. Sun B, Reale A, Seidel JD, Hunt DC (2010) Comparing radiosonde and COSMIC atmospheric profile data to quantify differences among radiosonde types and the effects of imperfect collocation on comparison statistics. J Geophys Res 115:D23104. doi:10.1029/2010JD014457
18. Kumar G, Madan R, Saikrishnan K, Kundu SK, Jain PK (2011) Technical and operational characteristics of GPS sounding system in the upper air network of IMD. Mausam 62:403–416. metnet.imd.gov.in/mausamdocs/16632_>F.pdf
19. Anthes RA, Ector D et al (2008) The COSMIC/FORMOSAT-3 mission: early results. Bull Amer Meteor Soc 89:313–333. doi:10.1175/BAMS-89-3-313
20. Rocken C, Anthes R, Exner M, Hunt D, Sokolovski S, Ware R, Gorbunov M, Schreiner S, Feng D, Hermann B, Kuo Y-H, Zou X (1997) Analysis and validation of GPS/MET data in the neutral atmosphere. J Geophys Res 102(D25):29849–29866. doi:10.1029/97JD02400
21. Anthes RA (2011) Exploring Earths atmosphere with radio occultation: contributions to weather, climate and space weather. Atmos Meas Tech 4:1077–1103. doi:10.5194/amt-4-1077-2011
22. Schmidt T, Wickert J, Haser A (2010) Variability of the upper troposphere and lower stratosphere observed with GPS radio occultation bending angles and temperatures. Adv Space Res 46:150–161. doi:10.1016/j.asr.2010.01.021
23. Healy SB, Thépaut JN (2006) Assimilation experiment with CHAMP GPS radio occultation measurements. Q J R Meteorol Soc 132:605–623. doi:10.1256/qj.04.182
24. Cucurull L, Derber JC, Treadon R, Purser R (2007) Assimilation of global positioning system radio occultation observations into NCEPs global data assimilation system. Mon Weather Rev 35:3174–3193. doi:10.1175/MWR3461.1
25. Poli P, Healy SB, Rabier F, Pailleux J (2008) Preliminary assessment of the scalability of GPS radio occultations impact in numerical weather prediction. Geophys Res Lett 35:L23811. doi:10.1029/2008GL035873
26. Poli P, Healy SB, Dee DP (2010) Assimilation of global positioning system radio occultation data in the ECMWF ERA Interim reanalysis. Q J R Meteorol Soc 136:1972–1990. doi:10.1002/qj.722
27. Foelsche U, Borsche M, Steiner AK, Gobiet M, Pirscher B, Kirchengast G, Wickert J, Schmidt T (2008) Observing upper troposphere-lower stratosphere climate with radio occultation from the CHAMP satellite. Clim Dyn 31:49–65. doi:10.1007/s00382-007-0337-7
28. Steiner AK, Hunt D, Ho S-P, Kirchengast G, Mannucci AJ, Scherllin-Pirscher B, Gleisner H, von Engeln A, Schmidt T, Ao C, Leroy SS, Kursinski ER, Foelsche U, Gorbunov M, Heise S, Kuo Y-H, Lauritsen KB, Marquardt C, Rocken C, Schreiner W, Sokolovskiy S, Syndergaard S, Wickert J (2013) Quantification of structural uncertainty in climate data records from GPS radio occultation. Atmos Chem Phys 13:1469–1484. doi:10.5194/acp-13-1469-2013
29. Lee IT, Matsuo T, Richmon AD, Liu JY, Wang W, Lin CH, Anderson JL, Chen MQ (2012) Assimilation of FORMOSAT-3/COSMIC electron density profiles into a coupled thermosphere/ionosphere model using ensemble Kalman filtering. J Geophys Res 117:A10318. doi:10.1029/2012JA017700
30. Zhang ML, Liu L, Wan WBN (2014) An update global model of hmF2 from values estimated from ionosonde and COSMIC/FORMOSAT-3 radio occultation. Adv Space Res 53:395–402. doi:10.1016/j.asr.2013.11.053
31. Wickert J, Reigber C, Beyerle G, Knig R, Marquardt C, Schmidt T, Grunwaldt L, Galas R, Meehan TK, Melbourne WG, Hocke K (2001) Atmosphere sounding by GPS radio occultation: first results from CHAMP. Geophys Res Lett 28:3263–3266. doi:10.1029/2001GL013117
32. Wickert J, Michalak G, Schmidt T, Beyerle G, Cheng CZ, Healy SB, Heise S, Huang CY, Jakowski N, Kohler W, Mayer C, Offiler D, Ozawa E, Pavelyev AG, Rothacher M, Tapley B, Arras C (2009) GPS radio occultation: results from CHAMP, GRACE and FORMOSAT-3/COSMIC. Terr Atmos Ocean Sci 20:35–50. doi:10.3319/TAO.2007.12.26.01(F3C)

33. Dee DP, Uppala SM, Simmons AJ, Berrisford P, Poli P, Kobayashi S, Andrae U, Balmaseda MA, Balsamo G, Bauer P, Bechtold P, Beljaars ACM, van de Berg L, Bidlot J, Bormann N, Delsol C, Dragani R, Fuentes M, Geer AJ, Haimbergere L, Healy SB, Hersbach H, Holm EV, Isaksen L, Kllberg P, Khler M, Matricardi M, McNally AP, Monge-Sanz BM, Morcrette J-J, Park B-K, Peubey C, de Rosnay P, Tavolato C, Thpaut J-N, Vitarta F (2011) The ERA-Interim reanalysis: configuration and performance of the data assimilation system. Q J R Meteorol Soc 137:553–597. doi:10.1002/qj.828
34. Rienecker MM, Suarez MJ, Gelaro R, Todling R, Bacmeister J, Liu E, Bosilovich MG, Schubert SD, Takacs L, Kim GK, Bloom S, Chen J, Collins D, Conaty A, da Silva A, Gu W, Joiner J, Koster RD, Lucchesi R, Molod A, Owens T, Pawson S, Pegion P, Redder CR, Reichle R, Robertson FR, Ruddick AG, Sienkiewicz M, Woollen J (2011) MERRA: NASAs modern-era retrospective analysis for research and applications. J Climate 24:3624–3648. doi:10.1175/JCLI-D-11-00015.1
35. Chowdhury MDR, Ward N (2004) Hydro-meteorological variability in the greater Ganges Brahmaputra Meghna basins. Int J Climatol 24:1495–1508. doi:10.1002/joc.1076
36. Chowdhury MR (2003) The El Niño-Southern oscillation (ENSO) and seasonal flooding Bangladesh. Theor Appl Climatol 76:105–124. doi:10.1007/s00704-003-0001-z
37. Mirza MQ, Warrick R, Ericksen N, Kenny G (1998) Trends and persistence in precipitation in the Ganges, Brahmaputra and Meghna river basins. Hydrol Sci 43:845–858. doi:10.1080/02626669809492182
38. Ashok K, Saji NH (2007) On the impacts of ENSO and Indian Ocean dipole events on sub-regional Indian summer monsoon rainfall. Nat Hazards 42:273–285. doi:10.1007/s11069-006-9091-0
39. Gautam R, Hsu NC, Lau KM, Tsay SC, Kafatos M (2009) Enhanced Pre-monsoon warming over the Himalayan-gangetic region from 1979 to 2007. Geophys Res Lett 36:L07704. doi:10.1029/2009GL037641
40. Lau WKM, Kim KM, Hsu CN, Holben BN (2009) Possible influences of air pollution, dust- and sandstorms on the Indian monsoon. Bull - World Meteorol Organ 58:2230
41. Ho SP, Zhou X, Kuo YK, Hunt D, Wang JH (2010) Global evaluation of radiosonde water vapor systematic biases using GPS radio occultation from COSMIC and ECMWF analysis. Remote Sens 2(5):1320–1330. doi:10.3390/rs2051320
42. Melbourne WG, Davis ES, Duncan CB, Hajj GA, Hardy K, Kursinski R, Mechan TK, Young LE, Yunck TP (1994) The application of spaceborne GPS to atmospheric limb sounding and global change monitoring. JPL Publication, Pasadena, pp 18–94
43. Awange JL, Fukuda Y, Takemoto S, Wickert J, Aoyama A (2004) Analytic solution of GPS atmospheric sounding refraction angles. Earth, Planet and Space 56: 573–587. doi:10.1186/BF03352518
44. Rienecker MM, Suarez MJ, Todling R, Bacmeister J, Takacs L, Liu HC, Gu W, Sienkiewicz M, Koster RD, Gelaro R, Stajner I, Nielsen JE (2008) The GEOS-5 Data Assimilation SystemDocumentation of versions 5.0.1, 5.1.0, and 5.2.0, NASA Technical Report Series on Global Modeling and Data Assimilation Vol. 27, NASA/TM2008104606, NASA Center for AeroSpace Information, Maryland, US
45. Pan LL, Randel WJ, Gary BL, Mahony MJ, Hintsa EJ (2004) Definitions and sharpness of the extratropical tropopause: a trace gas perspective. J Geophys Res 109(D23):103. doi:10.1029/2004JD004982
46. Sausen R, Santer BD (2003) Use of changes in tropopause height to detect influences on climate. Meteorol Z 12(3):131–136. doi:10.1127/0941-2948/2003/0012-0131
47. WMO (1957) Definition of tropopause. World Meteorological Organisation, Geneva
48. PSAS (2004) A quick derivation relating altitude to air pressure, Portland State Aerospace Society, US. http://psas.pdx.edu/RocketScience/PressureAltitude_Derived.pdf
49. Goovaerts P (2000) Geostatistical approaches for incorporating elevation into the spatial interpolation of rainfall. J Hydrol 228:113–129. doi:10.1016/S0022-1694(00)00144-X
50. Preisendorfer RW (1988) Principal component analysis in meteorology and oceanography. Elsevier, Amsterdam

51. Forootan E (2014) Statistical signal decomposition techniques for analyzing time-variable Satellite gravimetry data. Ph.D. thesis, University of Bonn, Germany. http://hss.ulb.uni-bonn.de/2014/3766/3766.htm
52. Resmi E, Mohanakumar K, Appu K (2013) Effect of polar sudden stratospheric warming on the tropical stratosphere and troposphere and its surface signatures over the Indian region. J Atmos Sol-Terr Phys 105–106:15–29. doi:10.1016/j.jastp.2013.07.003
53. Liang CK, Eldering A, Gettelman A, Tian B, Wong S, Fetzer EJ, Liou KN (2011) Record of tropical interannual variability of temperature and water vapor from a combined AIRS-MLS data set. J Geophys Res 116:D06103. doi:10.1029/2010JD014841
54. Sen PK (1968) Estimates of the regression coefficient based on Kendalls Tau. J Amer Stat Assoc 63:1379–1389. doi:10.1080/01621459.1968.10480934
55. Mann HB (1945) Nonparametric tests against trend. Econometrica 13:245–259
56. Kendall MG (1962) Rank correlation methods. J Amer Stat Assoc 63:1379–1389. doi:10.1080/01621459.1968.10480934
57. Seidel DJ, Gillett NP, Lanzante JR, Shine KP, Thorne PW (2011) Stratospheric temperature trends: our evolving understanding. WIREs Clim Chang 2:592–616. doi:10.1002/wcc.125
58. Mehta SK, Ratnam MV, Murthy BVK (2010) Variability of the tropical tropopause over Indian monsoon region. J Geophys Res 115:D14120. doi:10.1029/2009JD012655
59. Schmidt T, Wickert J, Beyerle G, Heise S (2008) Global tropopause height trends estimated from GPS radio occultation data. Geophys Res Lett 35:L11806. doi:10.1029/2008GL034012
60. Khandu Awange JL, Wickert J, Schmidt T, Sharifi MA, Heck B, Fleming K (2011) GNSS remote sensing of the Australian tropopause. Clim Chang 105(3–4):597–618. doi:10.1007/s10584-010-9894-6
61. IPCC (2007) Summary for policymakers, In: Solomon S, Qin D, Manning M, Chen Z, Marquis M, Averyt K, Tignor M, Miller H (eds) Climate change 2007: the physical science basis. contribution of working group I to the fifth assessment report of the intergovernmental panel on climate change. Cambridge University Press, Cambridge
62. IPCC (2013) Summary for policymakers, In: Stocker TF, Qin D, Plattner GK, Tignor M, Allen SK, Boschung J, Nauels A, Xia Y, Bex V, Midgley P (eds) Climate change 2013: the physical science basis. contribution of working 725 group I to the fifth assessment report of the intergovernmental panel on climate change. Cambridge University Press, Cambridge

# Chapter 13
# Environmental Impact Assessment

*Distances and locations are the important determinants of many choices that economists study. Economists often rely on information about these variables that are self-reported by respondents in surveys, although information can sometimes be obtained from secondary sources. Self-reports are typically used for information on distances from households or community centers to roads, markets, schools, clinics, and other public services. There is growing evidence that self-reported distances are measured with errors and that these errors are correlated with the outcomes of interest. In contrast to self-reports, global positioning systems (GPS) can determine locations to within 15 m in most cases. The falling cost of GNSS receivers makes it increasingly feasible for field surveys to use GNSS to more accurately measure locations and distances.*

J. Gibson and D. MacKenzie [1]

## 13.1 GNSS Support of EIA, SEA, and SA

### *13.1.1 Impact Assessments and the Need for Monitoring*

Environmental Impact Assessment (EIA) is defined by Munn [2] as the need to *identify* and *predict* the impact on the environment and on man's health and well-being of legislative proposals, policies, programs, projects, and operational procedures, and to interpret and communicate information about the impact. EIA is thus a process, a systematic process that examines the environmental consequence of development actions in advance [3, p. 4]. Glasson et al. [3] have defined the purpose of EIA as an *aid to decision making*, *an aid to the formulation of the development actions*, and *an instrument to sustainable development*. In order to achieve these goals, EIA requires monitoring data that can be used to identify and predict impacts, and also to evaluate the impacts of a given project once approved. Whereas EIA has been traditionally restricted to projects that are deemed to have significant impacts on the environment, it has recently expanded to include *strategic environmental*



J. Awange, *GNSS Environmental Sensing*, Environmental Science and Engineering, DOI 10.1007/978-3-319-58418-8_13

*assessment* (SEA) discussed in Sect. 13.4 and *sustainability assessment* (SA) presented in Sect. 13.5.

*Monitoring* involves the measuring and recording of physical, social and economic variables associated with development impacts (see Chap. 1). The activities seek to provide information on the characteristics and functioning of variables in *time* and *space*, and in particular in the occurrence and magnitude of impacts [3, p. 185]. It offers the possibility of determining or assessing the extent of human impacts on the environment and also compares human impacts with natural variation in the environment. The advantages of monitoring following project implementations are that it can improve project management, it can be used as an early warning system to identify harmful trends in a locality before it is too late to take remedial action, it can help to identify and correct for unanticipated impacts, and it can also be used to provide acceptable data base, which can be used in mediation between interested parties [3, p. 185]. Glasson et al. [3, p. 186] defines environmental impact auditing as the comparison between the impacts predicted in *environmental impact statements (EIS)* and those occurring after implementation in order to assess whether the impact prediction performs satisfactorily. EIS is the document that contains the information and estimates of impacts derived from the various steps of the EIA process.

### *13.1.2 Applications of GNSS*

GNSS satellites could be used to support the processes of project-based EIA, SEA and SA in provision of location-based data that support *monitoring* and *auditing*. As an example, in March of 2009, Kelly Core Salmon (KCS) Ltd filed an application with the Noca Scotia Department of Fisheries and Aquaculture (NSDFA) to relocate and expand the boundaries of the existing three aquaculture sites (Sand Point, Boston Rock, and Hartz Point) located in Shelburne Harbour, Nova Scotia [4]. The desire to relocate and expand was motivated by the need to improve the environmental performance of the three sites by allowing a greater flow and depth on the sites, easier access to the sites, and increased production, ensuring greater economic stability for KCS production in Nova Scotia [4].

For the relocations and expansion to take place, EIA was undertaken in order to satisfy the criteria of the New Brunswick Department of Agriculture and Aquaculture (NBDAA), Nova Scotia Department of Agriculture and Aquaculture (NSDAA), and Fisheries & Oceans Canada (DFO) [4]. In support of provision of location-based data, GNSS-DGPS (see Sect. 5.4.4.1) was employed to provide the relocated boundary co-ordinates.

GNSS could also be useful in supporting impact assessments in the following ways:

(a) Provide location-based data useful in identification of features of interest, which could be impacted during the undertaking of the project-based EIA. For example, GNSS could be used to provide the locations of boreholes in a given region where a project that has the potential of contaminating groundwater has been proposed.
(b) Providing distance information that is useful in measuring access to infrastructure and social services such as health care. Gibson and McKenzie [1] discuss how GNSS-based information on spatial distribution of population and services can lead to improved understanding of access to services. Understanding access to services is essential in spatial multi-criteria selection (e.g., Sect. 13.3.2), where a decision to choose an option from various alternatives is to be made. For instance, Perry and Gessler [5] applies GNSS to measure access from communities to health-care facilities in Andean Bolivia, and used the results to propose an alternative model of health distribution in the study area.
(c) Its distance and travel time data can be useful in identifying barriers to the use of services [1]. Often, such hidden barriers can lead to poor decision leading to the selection of a given alternative at the expense of the other methods, which might be optional. Knowledge of these hidden barriers could thus enable policy and decision makers to make informed decisions.
(d) A combination of GNSS-based location data and GIS would be very effective in illustrating access to services in a form that would be easily understood by the community during participatory stage of discussing environmental impact statement (EIS), and also for policy and decision makers during the selection of an option from given alternatives.
(e) In support of collection of socio-economic data, e.g., household surveys. Here, GNSS could be useful in improving the quality and cost-effectiveness of the survey data. GNSS locations could for instance be used to provide sampling boundaries as opposed to cases where such boundaries are arbitrarily selected or regular grids used where they are not useful (e.g., in monitoring variable features irregularly distributed over space such as air pollution). For example, Kumar [6] show how a combination of GNSS and remote sensing was useful in drawing samples in a survey of 1,600 households spread across different air pollution zones in Delhi (India).
(f) For SEA and SA, GNSS can be of use in providing data for econometric modelling of casual impacts of policies [1]. In this regard, it could provide data that could enable practitioners to better control the geographical and regressional characteristic of their models, e.g., by comparing individuals who are subjected to a given policy and those who are not.
(g) Further, for SEA and SA, its integration with GIS can prove particularly useful in supporting the evaluation of cumulative impacts (see e.g., Sect. 13.4.1). This is achieved through the ability of GIS-GNSS to consider spatial component and allow the analysis of the temporal evolution, see, e.g., [7].

## 13.2 Impact Monitoring to Detect Change

In defining monitoring in Sect. 1.1, *impact monitoring* was noted to focus on identifying possible impacts of human activities on environment and to distinguish them from the non-human environmental processes, while *compliance monitoring* had the objective of supporting stipulated legislations that aim at protecting and conserving the environment. According to Downes et al. [8], both compliance and impact assessments have a key objective of detecting change in selected variables, with impact assessment relying on comparisons within the collected data to assess whether an impact has occurred and the magnitude of such impact. Because impact assessment monitoring tend to be defined relative to natural conditions rather than being pegged to external criteria, Downes et al. [8] propose a monitoring design model, which if properly implemented, could support *change detection*.

The model is location-based taking into consideration the fact that in most cases, variables are measured at a specific impact location or locations, i.e., the *impact location(s)*. They then argue that a change being monitored in a variable should be seen to have occurred by comparing the variable's status prior to the activity (baseline data) which they call "*Before*" and after or during the activity (operational data) which they call "*After*". This Before-After model takes place at the impact location. In order to distinguish between natural and impact induced changes, a location outside the activity (impact area) is suggested, i.e., the "*control*" upon which data is to be simultaneously sampled together with the impact location "before" and "after". This before and after, control and impact locations form the BACI (Before-After-Control-Impact) model. The model proceeds as follows [8]:

- Data are collected at some ***impact locations*** over some period ***before*** the activity starts.
- Data are collected at some ***impact locations*** over some period ***after*** the activity starts.
- Data are collected at some ***control locations*** over the same period ***before*** the activity starts.
- Data are collected at some ***control locations*** over the same period ***after*** the activity starts.

In the BACI model above, the control location provides proxy data that are used to remotely sense the impact locations in the absence of a triggering activity. The assumption of the model is that if similar changes occur at both the control and impact locations, then the trigger for this changes would be natural causes since the control location does not have the activity. On the contrary, if the changes are only noticeable at the impact's location and not at the control location, then the activity at the impact location would be the most likely suspect. Because of the varying dynamics of the impacts and control locations, Downes et al. [8] suggest that several control locations and possibly impact locations be used, thus extending the BACI model to MBACI model, where multiple locations are considered.

Within these BACI and MBACI models, GNSS could be useful in providing the positions of control and impact locations upon which environmental impact

assessment monitoring could be collected simultaneously before and after the activity. Besides providing the positions of the control and impacted locations, GNSS could also be used to collect variable data for detecting the change being monitored.

Example 13.1 (Illustration of tourism impact on groundwater).

Consider that a particular hotel utilizes groundwater and due to increased number of tourists, lots of water is used, and that the impact of groundwater abstraction on the hotel is to be monitored to avert the potential danger of the building collapsing. Using relative positioning technique discussed in Sect. 5.4.2, coordinates of the hotel being monitored could be measured *before* it started operating to provide base data. During the operational phase, GNSS could be used to provide continuous coordinates of the building *after* the groundwater abstraction started. These observations are simultaneously observed to an established GNSS control points on stable locations some distance far away from the hotel both before, and after the groundwater abstraction started. The *relative positions* obtained will indicate the spatial variation of the hotel's position relative to the GNSS control (reference) before-and-after-the-impact. If no variation is noticed at the control location, but visible at the hotel (impact) location, then the variation could be attributed to groundwater abstraction. In such case, GNSS would have played a double role of providing locations of both impact (hotel) area and the control area, and also provision of time-variable data useful in generating relative motion (both horizontal and vertical) of the hotel useful in assessing the impact of groundwater abstraction.

♣ End of Example 13.1.

## 13.3 Project EIA

### *13.3.1 GNSS in Support of EIA Process*

EIA generally undergoes various stages, see e.g., [3, pp. 88–184] and [9, p.8]. Some of these stages, and possible areas in which GNSS could be useful are discussed. The first of these stages is *screening*, where a project is assessed as to whether it requires EIA or not. GNSS satellites could find use in supporting screening in EIA when used in combination with GIS to supply the location (spatial) information. For example, in the work of Geneletti [10], Geographical Information System (GIS) was combined with a decision aiding tool known as Multi-criteria analysis (MCA) to produce thematic nature conservation layer maps used to support decisions on whether to undertake EIA for a proposed project and also to choose the most suitable locations for new projects in the alpine area located in Trentino (northern Italy). Antunes et al. [11] propose a GIS approach for computing scores for criteria for use

in MCA. Since GIS (enhanced by GNSS-derived location-based information) brings visual capability, its combination together with MCA analytical tools will play a significant role in screening EIA projects as discussed in the next section.

The next stage of EIA after screening is the *scoping* stage, where the impacts and issues to be considered are identified. The process of scoping is that of deciding, from all of a projects possible impacts, and from all the alternatives that could be addressed, which ones are the most significant [3, p. 91]. Identification of significant alternatives requires comparison to be made at the scoping phase. Usually, at the initial phase of scoping, a small number of alternatives will be selected for further analysis from many potential alternatives, and in the final evaluation, these alternatives are subjected to more detailed evaluation. An example is presented in the rare earth case where 15 sites were selected in the initial case from which 6 sites were chosen for further analysis [12].

In evaluating alternative locations, GNSS satellites could play a vital role of not only providing the coordinates (i.e., positions) of these locations but could be used to provide rapid field measurements of factors such as distances to environmental sensitive locations (e.g., groundwater or conservation parks), and the actual spatial coverage of areas of each alternative.

Example 13.2 (GNSS in support of choosing from alternative locations).

Consider Fig. 13.1 where three alternative perimeter locations are to be considered for the purpose of setting out a project such as sugar processing factory. *First*, the areas of these locations are to be established so that the smallest parcel of land is chosen to accommodate the factory and at the same time minimize on the land purchasing cost. *Second*, the distances of the sites to the nearest water source is required so as to asses the potential of the sugar factory contaminating the groundwater source. GNSS could be used to establish the corner positions of the various sites A, B, and C from which the perimeter and area of each parcel of the land could be rapidly calculated. Further, distances from each site to the nearest water source can rapidly be obtained in the field by measuring baselines of two receivers, one stationed at a given site and the other stationed at the water source as illustrated in Fig. 13.1.

♣ End of Example 13.2.

Another possibility would be to use a hand-held GNSS (e.g., Fig. 18.1 on p. 389) to obtain the direct distance measurements from each site to the water source using the navigation functions of these receivers.

Analysis stage of EIA consists of *identification*, *prediction* and *evaluation* [13]. Impact identification brings together project characteristics and baseline environmental characteristics with the aim of ensuring that all the potential significant environmental impacts (adverse or favourable) are identified and taken into account during EIA process [3, p. 107]. GNSS satellites could help in provision of environmental baseline data before the project is established. This could then be used in impact prediction, which requires that it be based on available environmental baseline data

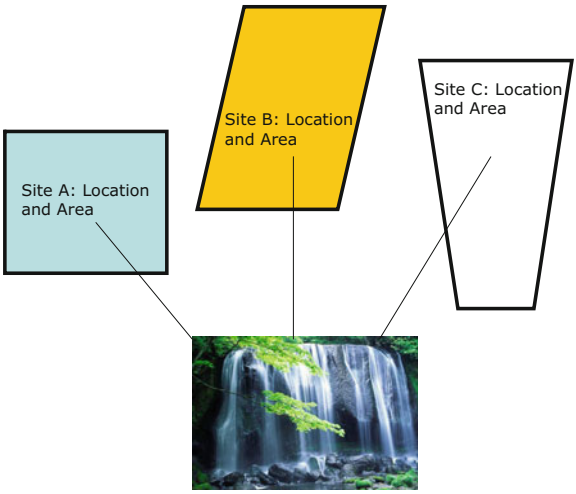


**Fig. 13.1** GNSS support of site selection from three different alternatives. GNSS could be useful in providing positions, distances, perimeters and areas of each site, information that could inform decision markers choice of the correct site

and proper use of technology to identify environmental modification, forecast the quantity and/or *spatial dimension of change* in the environment, and estimation of the probability that the impact will occur [13]. Techniques for impact identification and prediction are discussed, e.g., in Glasson et al., [3, pp. 88–184]. Several methods of impact identification exist and are generally divided into the following categories [3, p. 108]; *checklist*, *matrices*, *quantitative methods*, *networks* and *overlay maps*. These methods have been discussed in detail, e.g., by Shopley and Fuggle [14] and Westman [15]. Evaluation in EIA looks mostly at the cost and benefits of a proposed projects to the users, assesses the impact on environment and compares various alternatives that will yield benefit of the project with minimum environmental and social impacts. Such alternatives could be evaluated through methods such as Multi-criteria analysis (MCA; e.g., Sect. 13.3.2). GNSS satellites can play a vital role in this aspect of EIA with regard to identifying impacts associated with spatial changes. As illustrated in Fig. 13.1, GNSS could also assist in the determination of positions, distances, perimeters, and areas needed by decision makers to make informed choices.

## *13.3.2 GNSS in Support of Multi-criteria Analysis*

### 13.3.2.1 Spatial Multi-criteria Analysis (MCA)

The vast majority of environmental management decisions are guided by multiple stakeholders' interests. These decisions are often characterized by *multiple objectives*, *multiple alternatives* and *considerable uncertainties* [16]. Alternatives are means for accomplishing particular goals [17, pp. 109–110] and their evaluation

is a requirement in EIA of some countries. For example, the *National Environmental Policy Act* (NEPA) 1969 (US) requires that alternatives be considered while undertaking EIA. When multiple stakeholders with varied interests are involved, and multiple objectives and alternatives have to be considered, the situation often turns out to be very complex. In such cases, *Multi-criteria analysis* (MCA), a framework for evaluating decision alternatives against multiple objectives comes in handy. MCA is emerging as a popular approach for supporting multi-stakeholder environmental decisions as reported, e.g., in Regan et al. [18].

MCA are methods that seek to allow for a pluralist view of society, composed of diverse stakeholders with diverse goals and with differing values concerning environmental changes [3]. According to Munier [9, p.132], MCA are tools that are used for the analysis of projects, plans, programmes and options either with single objective or with several objectives with many different attributes or criteria. Besides being a tool for aiding the selection the best preferred alternative, Marttunen and Hamalainen [19] suggests that it could also be used to increase the understanding of the problem by value structuring (i.e., identification of the objective and the analysis of values). The components of MCA are listed by Annandale and Lantzke [20] as;

- a given set of alternatives,
- a set of criteria for comparing the alternatives, and
- a method for ranking the alternatives based on how well they satisfy the criteria.

Spatial multi-criteria decision problems typically involve a set of geographically-defined alternatives (events) from which a choice of one or more alternatives is made with respect to a given set of evaluation criteria [21, 22]. For spatial multi-criteria decision analysis, two considerations that are of utmost importance are [21, 23]:

(1) A GIS component such as data acquisition, storage, retrieval, manipulation, and analysis capability, where the location-based data can be obtained using GNSS.
(2) Spatial analysis component such as aggregation of spatial data and decision makers preferences into discrete decision alternatives.

MCA can help decision makers to choose between several alternatives by comparing the advantages and disadvantages of each alternative, one against the other, see e.g., [24]. The significant advantage of most MCA methods as stated by Annandale and Lantzke [20] is the capability to allow the evaluation criteria to be measured in either quantitative and/or qualitative terms, thus providing flexibility compared with other techniques such as cost-benefit analysis that require quantification of all values. Cost benefit analysis techniques are used, e.g., in economics to evaluate different alternatives, see e.g., [9, pp. 106–114].

There are several MCA techniques in operation in various countries, see e.g., [9, 25]. Examples of these techniques include Analytical Hierarchy Process (AHP), Mathematical Programming (MP), Additive Weighting and Concordance Analysis presented, e.g., in [9, 20, 26]. A principled problem in choosing a decision aid method for a real-life problem is that, for the same data, different methods may produce different results [25]. This problem is further compounded by the difficulty of objectively identifying the best alternative or method in view of these differing

results. In realization of this shortcoming, Lahdelma et al., [25] lists the requirements of MCA methods for use in environmental problems as:

1. Being well defined and easy to understand, particularly regarding the essential tasks such as setting of criteria and definition of weights.
2. Being able to support the necessary number of decision makers.
3. Being able to manage the necessary number of alternatives and criteria.
4. Being able to handle the inaccurate or uncertain criteria information.
5. Due to time and money constraints, the need of preference information from the decision makers should be as small as possible.

Clearly, it is difficult to have a method that satisfies all these requirements. All MCA methods have their strengths and weaknesses. The Additive weighting and Concordance analysis presented in the Example of Sect. 13.3.2.3 fulfil requirements 1, 2 and 3.

MCA does not actually provide an absolute answer by specifying a particular alternative, instead, it provides a process that ranks various alternatives and leaves the final decision to the policy makers. On the one hand, several studies indicate the success of MCA in ranking alternatives and therefore aiding in decision making, see e.g., [18]. On the other hand, researchers are still learning how it impacts on what could otherwise be an intuitive or ad-hoc group decision-making process [27]. As an example, Bojorquez-tapia et al., [28] report that some researchers have found out that MCA can alienate decision makers or experts in multi-stakeholder problems due to its complexity and 'black box' nature.

To address the shortcoming of alienating stakeholders, who most often comprise of the community (e.g., conservation groups and people likely to be directly affected by the project), CWP (community weighting process) in MCA is gaining momentum as a possible solution that attempts to carter for the community's interests. The increasing role played by CWP in environmental decision making with MCA as a processing tool is captured, e.g., by Hajikowicz [27] who states that the common reasons for applying MCA in multi-stakeholder decisions are to provide a transparent, structured, rigorous and objective evaluation of options.

***Some examples of applications of MCA in EIA***: As already discussed, EIA processes involve several stages, see, e.g., in [3, pp. 88–184], and [9, p. 8] many of which may utilize MCA.At the screening stage,for example,where a project is assessed whether or not it requires EIA,MCA could be used,e.g.,where one alternative location is to be chosen from several,see,e.g., [29]. The scoping stage of EIA is that of deciding, from all of a project possible impacts, and from all the alternatives that could be addressed,which are the significant ones [3, p. 91]. Identification of significant alternatives requires comparison to be made at the scoping phase. Usually, at the initial phase of scoping, a number of alternatives are selected for further analysis, and in the final stage, a small number of alternatives are chosen and subjected to more detailed evaluation. An example is provided by the EIA performed for Ashton Mining Ltd, which required a selection of the best location for iron ore processing from six possible locations [12]. MCA could be used in such scenario during scoping stage. This example is discussed further in Sect. 13.3.2.3.

*Evaluation* in EIA looks mostly at the cost and benefits of a proposed project to users, assesses the impacts on environment, and compares various alternatives that will yield benefits to the project while at the same time minimizes environmental and social impacts. MCA plays a vital role in evaluation in EIA as exemplified in the work of Janssen [24].

#### 13.3.2.2 Decision Making and Alternatives

Steinemann [30] considers alternatives as means to accomplish ends, and that from the perspective of EIA; these ends include not just a particular agency's goals, but also broader societal goals such as the *protection* and *promotion* of environmental quality. Steinemann [30] further opine that developing the set of alternatives that become the choice set and the center of analyzes is the most important part of the EIA process. Decision makers can then chose from these choice sets rather than simply having to rubber stamp a proposal. However, two problems that confront the development of alternatives are cited by Steinemann [30]. *First*, the public involvement often occurs too late to influence the development of the alternatives, and *second*, the alternatives are frequently eliminated from further consideration based on weak evaluations, which are not well-documented in the environmental impact statements (EISs). The first problem is associated with the very nature of project based EIA where the outcomes are almost always predetermined. In contrast to the project based EIA, SEA (Sect. 13.4) and SA (Sect. 13.5) enable earlier participation of the public. In evaluating alternatives, decision making is often based on some selected *criteria* and the desired objectives. Criteria are aggregate values computed from a much larger amount of so-called primary factors, which form the lowest level of information, also known as the assessment level [25].

The problems with environmental decision making, however, are that they are intrinsically complex because they almost always involve many alternatives and multiple attributes (e.g., biological, economical, and social), the relative importance of which has to be determined by subjective evaluations [19]. In an effective EIA process, alternatives will be sought that attempts to balance the data set with multiple attributes. The balancing act becomes even more crucial in SEA or SA where the desire is to balance the diverse ecological, social, and economic values over space and time. These values are usually represented in the form of multiple criteria and *indicators* that sometimes express conflicting management objectives [31].

In SEA or SA, complex projects are often involved which present many alternatives to choose from, necessitating the need for MCA for comparison. The situation is worsened when many stakeholders are involved and they conflict over the relative importance of the different comparison criteria. Annandale and Lantzke [20] state that "when decisions become this complex, there is a need for special tools or techniques to help in making sense of what can be a large amount of information". In addition, complex environmental planning problems will almost always include value judgements, public opinion, and controversies. So, the techniques need to deal with more than just technical information [20].

In such complex situations, MCA provides the means for comparing the advantages and disadvantages of each alternative, one against the other. By doing this, it provides decision makers with the means of choosing between several alternatives [24]. One of its advantages is that it permits public involvement in the process by allowing their voices to be heard through weighting of the criteria according to their preferences. Community weighting process (CWP) in MCA therefore leads to the community participating in decision making as already stated, and enhances public confidence in the final decision as opposed to where decisions are made using weak evaluation tools as already pointed out by Steinemann [30]. Its vital role is captured by Sheppard and Meitner [32] who state that "public involvement needs more effective, defensible techniques usable by managers at the sharp end of decision making, rather than just in the scoping of public concerns and in setting broad strategies".

*Specification of alternatives*: Alternatives are different ways of achieving an objective. For example, if the objective is to find a waste damping site, the alternatives would be the various possible locations that can serve as damping site at a minimal cost and minimize environmental and social impacts. In real life, there will be people with vested interest in these locations and thereby complicating the task of identifying a damping site. Specification of alternatives is helpful in such situations as they account for as many of the stakeholder opinions as possible. Annandale and Lantzke [20] suggest that the best approach in determining alternatives for a decision aiding exercise is the involvement of stakeholders and allowing them to offer as many alternatives as possible.

*Specification of comparison criteria*: In comparing alternatives, decision makers look for those alternatives that would be less costly in implementing but at the same time satisfy the environmental and social benefits. Criterion offers a possibility of comparing alternatives. Munier [9, p. 48] defines criteria as parameters used to evaluate the contribution of a project to meet the required objectives. Desirable properties for criteria are presented, e.g., in Annandale and Lantzke [20].

*Scoring the alternatives*: Annandale and Lantzke [20] discuss the three types of measurement scales; *ordinal*, *interval* and *ratio*. According to Annandale and Lantzke [20] ordinal scales provide information on order only and are unsuitable for mathematical manipulations (addition, subtraction, multiplication and division). It can only indicate that one alternative scores higher than another alternative, but does not indicate by how much (i.e., magnitude). Ordinal scales favour qualitative attributes and are often used interchangeably with quantitative reserved for ratio or interval scales [20]. The interval scale indicates the difference between two alternatives without giving the actual magnitude. Its advantage over the ordinal scale is that it permits addition and subtraction only. The ratio scale has a natural origin (zero value) and provides a measure of both difference and magnitude [20]. It permits the mathematical operations and as such, favours scores obtained when the attributes are directly measured. Glasson et al. [3] suggests that scoring may use qualitative or quantitative scales according to the availability of information. Both qualitative and quantitative scales could be used simultaneously as demonstrated in Annandale and Lantzke [20].

*Weighting the criteria*: Commonly, in MCA methods, a number is assigned to each criterion describing its importance. These numbers are called weights, and they model the decision makers' subjective preferences [25]. The interpretation of weights depends completely on the decision model used. Therefore, it is essential that the decision model be chosen prior to collecting weights, see e.g., [33]. The primary purpose of weighting the criteria is to develop a set of values, which indicate the relative importance of each criterion as valued by the community. These values are then used in ranking algorithms to determine the relative value of each alternative [34].

There are several ways of assigning weights. For example, weights could be assigned directly by the individuals undertaking the analysis to represent hypothetical point of view or they could be based on the data collected from opinion polls, focus groups, public meetings or workshops, or other direct forms of sampling public or expert opinion [20, 35]. Weights can also be assigned using some mathematical functions as indicated, e.g., in [9, p. 53]. It is therefore the portion of MCA, which takes into consideration divergent views of stakeholders to a project.

This is captured by Glasson et al. [3, p. 145] who states that MCA seeks to recognize plurality of views and their weights. Weights thus allow different views and their impacts on the final outcome to be expressed explicitly [20]. Several techniques for weighting are presented in literatures, e.g., direct assessment and pair-wise comparison methods such as AHP, see e.g., [36, 37]. In general, there exist no right weights that would allow comparisons between different alternatives. The weights obtained depend on the technique used [25].

#### 13.3.2.3 The Possibility of GNSS to Support MCA

In the following example, it is illustrated how GNSS could be used together with MCA to assist in the selection of alternatives for sitting of the secondary processing plant of a high-grade rare earths deposit at Mt Weld reported in Ashton Mining Ltd [12, 38]. This example uses both ratio and ordinal scales to score the alternatives relative to the criteria.

***Background of the Mt. Weld project***: In 1991, a two-year study programme was undertaken by Ashton Mining Ltd [12] to determine the feasibility of commercial development of a high-grade rare earths deposit at Mt Weld, near Laverton in the Eastern Goldfields in Western Australia. The project was to involve the mining and beneficiation of ores at Mt Weld and the secondary processing of rare earth concentrates to produce rare earth chemicals at a site that was to be determined [12]. The evaluation of the sites was undertaken in two stages. In the first stage, 15 sites assessed to have the potential for the sitting of the secondary processing plant were evaluated. These were [12]: Collie, East Rockingham, Esperance, Kalgoorlie, Karratha, Kemerton, Koolyanobbing, Kwinana, Moore River, Mt Weld, Muchea, Geraldton, Picton, Pinjarra and Northam in Western Australia.

Ashton Mining Ltd [12] adopted *qualitative* and *semi-quantitative* approaches to compare each of the sites. The *semi-quantitative* method focused on the economic considerations, i.e., capital and operating costs, while the qualitative assessments

included environmental considerations namely; public health, town planning, flora and fauna, and groundwater. It also included social considerations such as community infrastructure, availability of skilled labour, road and road-rail transport, and social acceptance.

Five appraisal categories adopted for each of the factors were; little or no constraint; manageable constraint, significant constraint, requiring detailed evaluation, and overriding constraint with the potential to preclude development. Out of the 15 sites, 6 (East Rockingharn, Collie, Kalgoorlie, Kemerton, Geraldton and Northam) were selected and subjected to further evaluation [12].

The results of the second evaluation stage indicated *Northam* as the preferred site. Five alternative sites in the Northam region were then evaluated, and the proposed Meenaar Industrial Park was assessed as being the site with the greatest potential [38]. Between road only and road-rail options considered for transporting the ore concentration, residues and chemicals, the road option was preferred. The proposal was then submitted for environmental impact assessment (EIA) and was subjected to a public environmental review (PER) in 1992, see [12].

Now, let us apply two multi-criteria analysis (MCA) methods (*Additive weighting* and *Concordance analysis*) together with GNSS to assist in the selection of alternatives and show that the same results, i.e., Northam could have been reached. Six alternative sites for the Mt Weld EIA case study are evaluated using these MCA methods. For each of the 6 alternatives, 11 criteria were compared and scored using ratio and ordinal scales and processed.

***Application of MCA***:

*Site Evaluation Criteria*: In the site evaluation by Ashton Mining Ltd, a number of general and specific site requirements were identified and used to develop appropriate criteria which were applied to each site, see e.g., [12, pp. 24–25]. The site evaluation criteria considered were those most suitable for the establishment of the secondary processing plant. Ashton Mining Ltd [12] adopted *economic*, *environmental* and *social* criteria to evaluate the sites. In these criteria, which we discuss below, GNSS could play the role of providing site locations and the distances of various environmental features, e.g., groundwater source or community infrastructure from a given site.

The main economic criteria considered were to minimize the capital and operating cost to establish and operate the plant. Capital cost was needed for the construction of the secondary processing plant and to establish infrastructure (i.e., supplying power, water, natural gas and housing). Operating cost was to cover the cost of power, water, natural gas, land rates, transport of concentrates, residues, chemicals and products. All the assumptions made in calculating capital and operating costs are presented in Ashton Mining Ltd [12, p. 52].

The environmental and social criteria adopted were those which minimized a site's potential for [12, p. 24]: Off-site effects on the public and to public health; conflict with surrounding (and future) land use, impact on the existing flora and fauna, impact on high-quality groundwater resources or other significant components of the physical environment, and inefficient utilization of land.

*Social criteria* were those which would ensure a site [12, p. 25]; is close to established and well developed community infrastructure, is near a suitably sized labour force with appropriate skills, minimizes the disruption and risks to the public from the transportation of materials, and is likely to be acceptable to the public. The assumptions made in deriving the environmental and social criteria are presented in [12, p. 25]. GNSS could be useful in providing positions of the sites, and the distances of these sites from infrastructure and labour force.

The results of the example when MCA was applied indicated both additive and concordance methods ranking Northam as the top site followed by East Rockingham, and demonstrated the suitability of Concordance analysis for evaluating alternatives when the criteria are scored using mixed ratio and ordinal scales, thus underscoring the usefulness of MCA in assisting decision makers to chose between alternatives during the evaluation process of environmental impact assessment (EIA). Care should however be taken to know the limitations of each method (e.g., Additive weighting), use proper weights, and agreeable threshold.

### *13.3.3 Example of Gnangara Mound Groundwater Resources*

During 1992–1995, a review was undertaken in Western Australia on the proposed changes to environmental conditions of Gnangara Mound groundwater resources under Sect. 46 of the *Environmental Protection Act (EPA)* 1986 (WA). Using it as an example, a theoretical examination of the possible areas of EIA process that could have benefited from using GNSS is presented.

#### 13.3.3.1 Background

The Gnangara Mound is Western Australias largest source of groundwater, supplying up to 60% of Perth's drinking water [39, 40]. Its area is estimated to be 2,356 $km^2$ and comprises Gnangara, Yanchep, Wanneroo, Mirrabooka, Gwelup, Perth and Swan Groundwater Management Units (GMUs). Gnangara Mound supports local wetlands and lake ecosystems and supplies irrigation for horticulture and agriculture [39]. It is also a major water source supporting a number of groundwater abstraction schemes operated by the Water Authority [41]. It is bounded to the north by Gingin Brook and Moore river, to the East by Ellen Brook, to the south by Swan River, and Indian Ocean to the West.[1]

***Physical environment***: Gnangara Mound is characterized by hot dry summers and mild wet winters with an average annual rainfall of about 800 mm [41]. Department

[1] See, e.g., http://www.water.wa.gov.au/sites/gss/ggs.html.

of Water [42] gives an average annual value of 814 mm. The hottest month of the year is reported as February with an average maximum temperature of 34°, while August is the coldest month with an average maximum of 18° [41]. Water Authority [41] state that the area does not have natural surface runoff due to the porous nature of soil in the area. Most of the water that falls as rainfall recharges the groundwater and that any surface water is due to discharge from groundwater. Recharge of groundwater depends largely on rainfall pattern, vegetation cover and the water table.

Groundwater flows westerly from the top of the Mound following the terrain slope. Wetlands are generally found in the low areas where the water table reaches above the ground surface much of the year. Due to the presence and absence of water above the ground in these wetlands, soil and vegetation have adopted to the pattern of groundwater. In general, groundwater quality is reported to be excellent [41]. It is however widely recognized that sustainability of the Mound as a water resource is under threat due to *climate change* and excessive drawing of water.

***Biological environment***: Water Authority [41] reported the dominant terrestrial vegetation as the candle Banksia (*Banksia attenuate*) and firewood Banksia (*B. Mennziesii*). Vegetation of high significant conservation value was also reported in the area [41]. Vegetation, soils and land forms of Gnangara have been mapped, e.g., in [43]. Fauna survey of 1977 and 1978 recorded 12 native mammals, 70 reptiles and amphibians and 223 bird species. Five caves out of the 273 documented caves in the Yanchep National Park were reported to be the most species rich subterranean ecosystem ever recorded, supporting 30 and 40 species compared to caves elsewhere in the world which rarely have five animal species [41]. GNSS can be been useful in providing the locations of these five caves.

***Social environment***: Water Authority [41] reported a general increase in urbanization in the Gnangara Mound area that led to incremental approach to planning, subsequently having significant implications for the future of the area. Increase in urbanization comes along with changes in land use, which in turn impact on the groundwater level. In the rural areas, common land uses reported at the time included market gardening and poultry farming. Specialized activities included flower, mushroom, and strawberry growing, and gourmet pheasant production, all of which required groundwater. Large areas of Gnangara Mound are State Forest under the management of Conservation and Land Management (CALM). Approximately 20,000 ha of this land was Pine plantation with the remainder of the State Forest being natural bushland [41].

Water Authority (ibid) further reported 14 archaeological sites registered with the Western Australian Museum. Specifically, McNess, Lake Mariginiup, Lake Joondalup, Lake Goollelal, and Lake Gnangara among others were said to be sites of Aboriginal mythology and/or historical Aboriginal use. According to Water Authority [41], it was also likely that most of the wetlands in the western linear wetland chain are potential areas of Aboriginal significance.

#### 13.3.3.2 Review of Allocation and Management of Groundwater Resource

Under the guidance of the Environmental Protection Authority (EPA), Water Authority manages groundwater resources of the Mound. Private groundwater abstraction is managed through area allocation and licensing of users [41]. Water Resource Authority, therefore, has the task of ensuring that the environmental impacts from users and its own activities are minimized. This is achieved, e.g., through assessing the impacts of proposed land use changes on groundwater levels and in providing advice to land management and planning organizations. In 1986, Water Authority submitted the Gnangara Mound Water Resources Environmental Review and Management Program (ERMP) to Environmental Protection Authority (EPA) for;

1. approval to develop the Pinjar Groundwater Scheme, and
2. approval for changes to private groundwater allocations.

In 1988, the Minister of Environment approved development of Pinjar Stage 1 Groundwater Scheme and the changed private groundwater allocation quotas, subject to a number of environmental conditions [41]. The approval allowed for increased abstraction of groundwater by the Water Authority and other users. The conditions to be met included measures to protect the environment through; *Maintenance of water level in the wetlands*, *limits on private groundwater allocations*, *establishment of a management and monitoring program*, and *setting in place a range of administrative mechanism regarding inter agency interaction on groundwater management* [41]. In 1992, Water Authority identified the need to review the management of the southern portion of the Mound. Factors which necessitated the requirement for the review were [41]:

- Identification of other ecosystems, which had been, or had the potential of being affected by groundwater abstraction. These included shallow cave streams and phreatophytic vegetation.
- Rapid increase in knowledge of Environmental Water Requirements (EWR), which suggested that water levels set by EPA in 1988 should be reviewed.
- Increase in demand of groundwater by private users called for an assessment of the potential impacts that would result from further groundwater allocation.
- There was a need by Water Authority to further develop groundwater schemes (e.g., Pinjar Stages 2 and 3) on the Gnangara Mound and as such, a review of allocation and management was essential before development of the schemes could commence.
- The recognition that land use on the Mound could significantly affect groundwater availability required that the impacts of likely future land use scenarios be considered in allocating and managing groundwater.
- Since the outcome of the review was likely to involve changes in some of the environmental conditions which applied to the management of Gnangara Mound, notably wetland water levels, allocation quotas and land use issues, consideration of any changes required the review to take the form of Environmental Impact Assessment (EIA).

A formal referral was submitted by Water Authority to the EPA[2] in late 1992, and it was decided that the conditions should be reviewed under Section 46 of the *Environmental Protection Act (EPA)* 1986 (WA). This then led to the review of allocation and management of groundwater resource by Water Authority. EPA guidelines for this review are presented in Water Authority [41, Appendix 2].

***Focus of the environmental review***: Environmental conditions reviewed focused on three main areas; *wetland water level*, *allocation quotas* and *land use issues*. EPA acknowledged that little information was available to determine EWR[3] for the wetlands and that there maybe changes to the set levels in future and required the initiation of research to provide an improved understanding of wetland ecology, which could then be used as a basis to review the wetland water level criteria.

With the continuing urban development in the Wanneroo region, evolving patterns of land use led to considerable changes in the pattern for demand for private water. Water demand in some areas, e.g., Flynn Drive could not be met. There was need to review groundwater availability with the view of allocating further resources to high demand areas. This could be achieved through further development of groundwater schemes within Gnangara Mound comprising Pinjar Stage 2 Part 1 groundwater scheme which was scheduled for December 1996 and had been approved by EPA subject to the outcome of the allocation and management review.

Since also allocation of Pinjar Stage 2 Part 2 and Stage 3 groundwater schemes were being sought at the time, Water Authority believed in reviewing the allocation and management of water resource before further development of groundwater schemes so as to ensure equitable distribution between the public water supply and private use while minimizing environmental impacts.

#### 13.3.3.3 Possible Areas of GNSS Support to the Gnangara EIA

***Impacts identification***: Water Authority adopted the checklist method in identifying the impacts. This is the common procedure used in Western Australia where the proponent is required to complete a referral form [42]. In what follows, a network approach based on Sorensen [44] and a GIS methods are compared in order to illustrate how GNSS satellites could have been useful in enhancing impact identification.

*The Sorensen Network Approach*: Recreating the impacts in Water Authority [41], first the activities to be undertaken in the Gnangara Mound review are specified. In this case, three major activities are identified from Water Authority [41] as; *groundwater allocation*, *land use*, and *artificial maintenance of wetland's water levels*. Let us add rainfall to this list as a climate variable that has the potential of impacting on the water level. The causes of environmental changes associated with the activities above are then identified and a matrix format applied to trace its impact. In Fig. 13.2, use is made of the Sorensen [44] principles to identify the impacts.

[2]Environmental Protection Authority.

[3]Environmental water requirement.

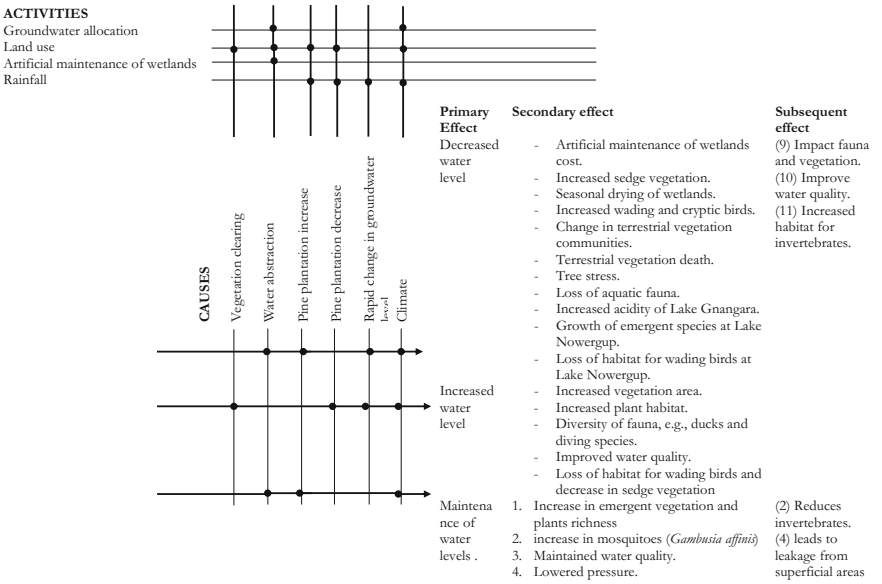


**Fig. 13.2** Sorensen Network for Gnangara Mound impact identification

For instance, land use activity potentially results in clearing of vegetation, water abstraction, increase and decrease in density of pine plants, and climate change. These environmental changes, in turn, results in increased water level (e.g., when vegetation is cleared) as the primary effect. Increased in water level in turn leads to increased wetland vegetation areas and plant habitats, diversity of fauna, e.g., ducks and diving species, and improved water quality all of which are positive secondary impacts. A negative secondary impact is the loss of habitat for wading bird species and sedge vegetation that rely on seasonal drying of the wetlands.

Water abstraction will occur when land use activities involve irrigation of farms, maintenance of golf course, and other uses which require water. This in turn leads to low wetland water levels as primary effects. Secondary effects as a result of the primary impact are presented in Fig. 13.2. All the potential impacts of land use can be traced in a similar way as demonstrated in Fig. 13.2. As demonstrated for the case of land use activity, the Sorensen network is used to identify the primary, secondary and subsequent impacts associated with the allocation of groundwater, artificial maintenance of wetlands and rainfall. Figure 13.2 summarizes the identified impacts using this method. It is evident that the identified impacts compare well with those reported in [41].

*GIS and Overlays*: For identification of environmental impacts having spatial distribution in nature, GIS with the assistance of GNSS satellites is an ideal tool. The potential of GIS in environmental impact assessments has been demonstrated, e.g., by Antunes et al. [11] who applied it to evaluate the impacts of a proposed highway in Central Portugal. Antunes et al. [11] suggested identification of environmental

components (e.g., ecosystem) and receptors (e.g., a particular species likely to be affected by the component) using GIS. Another example of application of GIS to EIA is presented by Haklay et al [45] who advances a GIS-based scoping method and discusses the conditions necessary for its utilization.

For the Gnangara Mound example, the environmental components that were likely to be affected by groundwater allocation and management were *pine trees*, *vegetation* and *wetlands*. Using Gnangara Mound Map of 1987 as a base for example, annual map layers of pine trees, vegetation, wetlands and urbanization can be overlaid on the base map in a GIS environment to produce a composite map, which can be used to identify hot spots (areas where land use are clearly identified to impact on wetland water levels and wetland vegetation). In this example, 1987 is selected as a base since environmental conditions issued by the Minister became operational in 1988. Annual groundwater level for specific wetlands are entered as attributes or produced in maps as contours. From the hot spots, areas and contours indicating water level changes and potential impacts can be identified. Where there is intense land use and sharp reduction in wetlands vegetation area, that specific land use could be said to impact on wetland water level, and subsequently vegetation. Linear trends can also be obtained on, e.g., the rate of pine growth/decline, vegetation clearing and urbanization by comparing annual values from 1997 to 1995. These could then be correlated with the groundwater levels to further identify the impacts. Negative linear trends will indicate adverse impact, while positive trend will indicate positive impact. Besides the trend analysis, visual examination of the layers could also indicate the spatial distribution. In this method, GNSS satellites provide location-based data to which the attributes, such as impacts on wetlands, are related.

Compared to the sorensen method, the GIS approach has the advantage of being able to identify pertinent environmental effects on the basis of readily available information under stringent time and budget constraints [45]. Since it is best suited for *spatially distributed impacts*, it can analyze cumulative impacts better than the checklist or Sorensen network approach. It also provides friendly visual presentations, which are easily understandable by non-experts. Its drawbacks, however, are that it does not consider the likelihood of an impact, secondary impacts of the difference between reversible and irreversible effects [3], and that it may require initial capital to establish.

***Impacts prediction***: Impact prediction requires that it be based on available environmental baseline data. In this example, the baseline data were readily available since regular water level monitoring had been taking place as part of the initial Ministerial conditions set out in 1988. GNSS satellites could have supported impact prediction of this EIA in two ways namely:

1. Provision of baseline data, and
2. Using the technique discussed in Chap. 8 to map boundaries of changing spatial features, e.g., wetland boundary changes as illustrated in Fig. 13.3.

By having permanent reference marks set around the wells, GNSS satellite could be used to provide continuous measurements of positions and elevations of these reference marks. The measured depths of the wells could then be referred to these

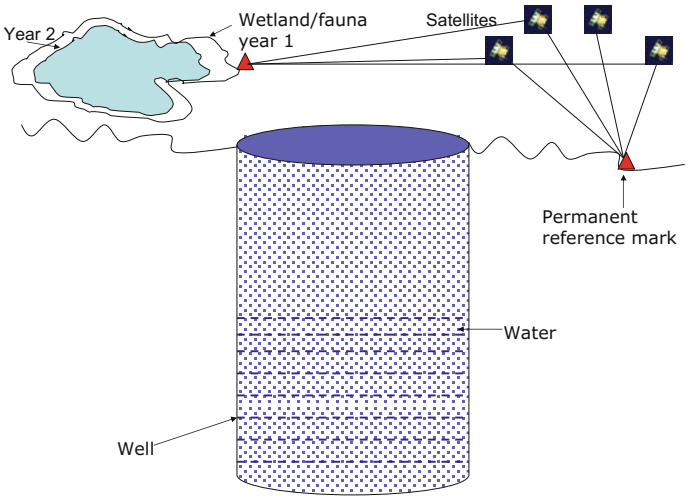


**Fig. 13.3** GNSS monitoring of the impacts of well water abstraction using, e.g., techniques discussed in Sect. 8.2.4 spatial changes maps of wetlands from years 1 to 2 (see e.g., Fig. 8.5) on p. 134. Also, GNSS provides reference points upon which measured groundwater levels can be referenced

reference marks and thus help in monitoring the state of the groundwater levels (Fig. 13.3). This can be related to the state of vegetation and fauna. To predict the impacts of groundwater abstraction on wetlands and other vegetation, similar techniques to those discussed in Sect. 8.2.4 (where GNSS is used to monitor Lake Finnery) could be used to provide changes in the wetlands' boundaries (i.e., perimeters and areas), as illustrated in Fig. 13.3 for years 1 and 2). By analyzing annual trend of these boundary changes, it is possible to predict the impacts of groundwater abstraction on e.g., wetlands, assuming that the changes are unrelated, e.g., to evaporation. This will require some control location (see e.g., discussions on BACI model in Sect. 13.2).

Impacts of groundwater variation on terrestrial vegetation were reported by Mattiske [46] as ranging from small change in community structure in favour of more drought tolerant species, through to deaths of Banksia woodland vegetation. Indeed, that the death of Banksia vegetation were triggered by groundwater variation was supported by the findings of Water Authority [47], which suggested that Banksia trees that occurred where depth to groundwater was less than 6 m were most vulnerable to groundwater reduction. The study further suggested a general stress on vegetation due to reduced groundwater level.

Groom et al. [48] deduced that a lowering of groundwater level by 2.2 m at a station P50 between the summers of 1990 and 1991, resulting from the cumulative effects of abstraction and below average annual rainfall (low groundwater recharge), coincided with a loss of between 20 and 80% of adults Banksia species within 200 m of the bore. Over a similar time period, no significant decreases in the abundance of species were recorded in the monitored site to have been influenced by groundwa-

ter abstraction. They concluded that negative impact of groundwater drawdown on Banksia populations made it an important indicator of decreasing groundwater levels on the Gnangara groundwater Mound. GNSS monitoring of groundwater abstraction (Fig. 13.3) therefore could be useful in predicting impact on Banksia trees if the proposed changes in environmental condition would impact on groundwater by similar level, i.e., lowering of groundwater level by more than 2.2 m.

Geneletti [10] demonstrates the capability of using GIS method to compute spatial indicators to predict and quantify critical impacts, such as ecosystem loss and fragmentation, soil erosion, geomorphologic hazards, interference with flora and fauna, and visibility. Since GIS has been successfully used by Geneletti [10], it could be applied together with GNSS to predict variation in spatial distribution of environmental components caused by groundwater level variation.

Once groundwater changes have been obtained using, e.g., piezometric readings, and boundaries of impacted features (e.g., wetland in Fig. 13.3) mapped using GNSS, overlaying the land use and vegetation cover maps could then be performed using GIS for the same time period. Correlation between the land use, terrestrial vegetation and groundwater level could then be developed and predictions made on the impact of land use and terrestrial vegetation on groundwater level, and impacts of groundwater level on wetland vegetation. Linear and cyclic trends analysis could then be developed to give predictions at various temporal resolutions.

To support the prediction of impact of groundwater abstraction on fauna in caves, hand-held GNSS receivers can be used to provide locations of these caves, which can be related to groundwater level. Jasinska and Knott [49] listed about 100 caves in Yanchep National Park and reported that little information was known about the biology of the aquatic fauna within these caves. They found aquatic species of high conservation value and concluded that one of the greatest threats to these species would be the permanent or temporary drying of the caves streams in which they occur. Since these aquatic fauna are of high conservation value, they could be seriously affected by drying of the streams within the cave to a point of extinction. GNSS could be useful in the prediction of the effect of regional warming on groundwater through the analysis of the GNSS derived tropopause heights as discussed in Chap. 11.

*Comparison of the prediction methods*: The model based approach adopted by the Water Authority [41] is the most commonly used method in most EIA of groundwater impacts. Models rely on the input data and the assumptions that are taken into consideration. The more they fit in the model, the more reliable are the output. The disadvantage of using models, however, is that they require some expert knowledge during their development and operation stages. Any wrong assumptions, input data, and usage can lead to false information and interpretation.

The field experiment using GNSS and GIS has the advantage of using real data in their predictions as opposed to simulated values as is the case of models. They also provide easy visual interpretation of the results. The disadvantage is that it comes at a cost. The initial cost of installing a GIS maybe high. Besides, there is the cost of validating the data using GNSS. Another disadvantage is the incapability to predict higher order impacts. In the Gnangara Mound example, it was difficult to use GNSS

and GIS to predict the impacts of variation of wetland vegetation to fauna, which may require other methods for enhancement.

In summarizing this example in identifying and predicting the impacts for Gnangara Mound using alternative GIS-based method to those adopted in the Water Authority [41], it has been pointed out that identification and prediction models are labour intensive and require knowledge of the system. More often, they are based on assumptions, which may not fit the model leading to delivery of meaningless results. Field experiments, though straight forward, requires some validation, which may increase the cost of EIA. Finally, baseline environmental parameters should be established upon which judgement of an impact can be made. Identification method should be a combination of methods that are simple to use, but which are capable of identifying higher order impacts and their inter-relations. Where models are adopted, they should be well understood by the analyst and assumptions must be clear and meaningful.

In particular, when used in conjunction with GIS and field data from the GNSS, a suitable approach for identifying and predicting impacts, which are spatially distributed could be obtained. This example indicates the possibilities of the GNSS assisted techniques to support identification and prediction of environmental impacts associated with the proposed change in environmental conditions of Gnangara Mound and highlight the limitations of the methods.

## 13.4 Strategic Environmental Assessment

SEA is the process that aims at integrating environmental and sustainability considerations in strategic decision-making [17]. In so doing, the goal is to protect the environment and promote sustainability. Sadler and Verheem [50] define SEA as a systematic process for evaluating the environmental consequences of a proposed policy, plan or programme initiative in order to ensure that they are fully included and appropriately addressed at the earliest appropriate stage of decision making at par with economic and social considerations. Wood and Djeddour [51] define a policy as inspirational and guidance for action, a plan as a set of coordinated and timed objectives for the implementation of the policy, and a programme as a set of projects in a given area, see also [17, p.12].

The basic principles of SEA have been presented, e.g., by Therivel [17] as being a tool for improving the strategic actions, promoting participation of stakeholders in decision making process, focusing on key environmental/sustainability constraints, identifying the best option; minimizing negative impacts, optimizing positive ones, and compensating for the loss of valuable features and benefits; and ensuring that strategic actions do not exceed limits beyond which irreversible damage from impacts may occur. Its advantages include [17]:

1. Being able to shape the projects at an earlier stage through the appraisal of strategic actions. This offers the chance to influence the kinds of projects that are going to happen, not just the details after the projects are already being considered.
2. SEA deals with impacts that are difficult to consider at project level. It deals with *cumulative* and *synergistic* impacts of multiple projects, e.g., cumulative impacts of various mining sites on the development of an entire area.
3. SEA can deal with large-scale environmental impact such as those of biodiversity or global warming more effectively than individual EIA.
4. Unlike project based EIA which formulate goals around an already selected approach, SEA promotes better consideration of alternatives, thereby ensuring a strategic approach to action.
5. It incorporates environmental and sustainability consideration in decision making thus adding an additional dimension to decision making.
6. It enables public participation in decision making thus making the whole process inclusive and transparent.
7. It has the potential to promote streamlined decision making.

SEA has also benefited from MCA as illustrated by Noble [52] who presents five scenarios that were evaluated within SEA to determine the most suitable option for power generation to be developed to cover the Canadian need up to the year 2050. The contribution of GNSS to support global warming monitoring is treated in Chaps. 11 and 12. In what follows, the cumulative impact aspect of SEA and the possible contribution of GNSS satellites is discussed.

### *13.4.1 GNSS Role in Supporting Cumulative Impacts Assessments*

Cumulative effects refer to the phenomenon of *temporal* and *spatial* accumulation of change in environmental systems in an additive or interactive manner and may originate from either an individual activity that recurs with time and is spatially dispersed, or *multiple activities* (independent or related) with sufficient spatial and temporal linkage for accumulation to result [53]. The attributes of cumulative effects are classified by Spaling and Smit [53] into three categories; *temporal accumulation*, which occurs if the interval between perturbation is less than the time required for an environmental system to recover from each perturbation, *spatial accumulation*, which results where spatial proximity between perturbation is smaller than the distance required to remove or disperse each perturbation, and the *nature of human induced activities or perturbations*, which also affect accumulation of environmental change provided the perturbations are sufficiently linked in time and space.

Cumulative impact assessment is thus defined by the Commonwealth Environmental Protection Agency [54] as predicting and assessing all other likely existing, past and reasonable foreseeable future effects on the environment arising from perturbations. In some legislations, e.g., in Canada, EIA regime has made it specific

and mandatory where consideration of cumulative effects assessment has been made explicit and mandatory both federally and in several provinces [3]. In USA, *National Environmental Policy Act* (1967) requires the assessment of cumulative impacts, while in Australia, assessments have largely been carried out by regulatory authorities, rather than project proponents. In Western Australia for example, the EIA process does not come out forcefully on cumulative impacts assessment.

Spaling and Smit [53] provide an in-depth look at the contributions and shortcomings of EIA to assessing cumulative impacts. Three key factors in favour of EIA are theoretical understanding of environmental change through empirical analysis and modelling of responses of environmental systems through human induced perturbations, the development of various analysis methods for projecting and assessing the various environmental changes associated with the proposed human activities, and regulatory and administrative mechanism contributed by EIA in the integration of environmental consideration in decision making. In EIA, cumulative impacts can be identified at the *scoping stage* where issues to be examined are pruned. It is at this stage where the spatial and temporal effects of cumulative impacts can be considered [55].

GNSS could be useful in *providing the locations of multiple activities*, *mapping the changes in spatial coverage* (see e.g., Fig. 8.5 on p. 134), and *monitoring variation in groundwater* as a results of cumulative impacts.

### *13.4.2 Example of Marillana Creek (Yandi) Mine*

***Background***: Marillana Creek (Yandi) Mine operated by BHP Billiton Ore Pty Ltd (BHPBIO) is located approximately 90 km north-west of Newman in the Pilbara region of Western Australia [56]. The mine is situated within lease ML 270SA, and is operated under the Iron Ore (Marilliana Creek) Agreement Act 1991 [56]. BHPBIO also has a smaller lease (M 47/292) located to the immediate north of ML 270SA. The Yandi orebody occurs within an ancient channel iron deposit (CID). This deposit is subdivided into a series of mine areas, i.e., central pits (C1 to C5), eastern pits (E1 to E8), and the western mesa pits (W1 to W6) [56]. The CID is about 80 m thick and the majority of mining is within the upper 60 m. BHPBIO (referred to as proponent in this example) operates dewatering bores that lower the water table in the vicinity of each pit by approximately 30 m [56].

In May 1988, an approval was granted by the Minister for Environment to mine E2 and C5 at a rate of 5 million tonnes per annum [57] and in 1991, mining commenced. In 1992, 1994 and 1995, EPA assessed modifications to the original proposal, which involved increased rates of production and mining of additional pits [58–60]. At the time of application for approval by the proponents, mining was taking place in the E2, C1/C2 and C5 areas. In 2004, the proponent sought approval under Part IV of the *Environmental Protection Act* (WA) 1986 to concurrently mine from pits across the leases (ML 270SA and M 47/292), and in addition update, assess, and agree on closure concepts for the whole of the deposit. During the mining of individual pits,

the proponents proposed to partially fill the voids with overburden (waste) material from other pits, and to use the same open cut mining techniques and ore processing methods over the remaining life of the mine [56]. The agreed concepts were to be documented through closure specific conditions that were issued by the Minister of Environment. The project was called the Marillana Creek (Yandi) Life of Mine and was expected to deliver 40 million tonnes per annum with a lifespan of 30 years [56].

The expansion of delivery capacity from an initial 5 million tonnes per annum to 40 million tonnes per annum resulting from concurrent pit mining had the potential to *significantly impact* on the environment. Besides, Hamersley Iron also held a mining lease (274SA) over the CID, east of BHPBIO's lease, and was mining up to 34 million tonnes per annum at the same time. The potential impact on the environment, therefore, was not only likely to come from the proposed project but also *cumulative* taking Hamersley into consideration. Thus, there existed a need for EIA under Part IV of the *Environmental Protection Act (EPA) 1986* (WA).

BHPBIO [56] produced an EIS[4] that documented the environmental objectives, potential impacts, proposed environmental management measures and predicted outcomes. Environmental Management Plan and Decommissioning and Final Rehabilitation Plan were also presented as key supportive documents to the Environmental Protection Statement (EPS). EPA was advised of the proposal in January 2004 and based on the information provided, considered that the proposal had the potential to impact on the environment, but could be managed to meet the EPA's environmental objectives [61]. Consequently, EPA determined, under Sect. 40(1) of the *EPA* 1986 (WA), that the level of assessment for the proposal was EPS.[5] EPA's advice and recommendations were then forwarded to the Minister of Environment in accordance with Sect. 44(1) of *EPA* 1986 (WA) [61]. The Minister of Environment granted approval with a set of conditions on 6th of July 2005.

***Cumulative impacts***: Since the EPS proposed to concurrently mine the pits within the leases as opposed to the previous pit by pit mining, there existed a potential to lead to *cumulative impacts* as discussed in Spaling and Smit [53]. Cumulative impacts were likely to be felt on the surface and groundwater. As part of the effort to manage cumulative effects accrued from surface water, the proponent proposed to integrate the surface water monitoring program to a wider monitoring initiative in the Marillana Creek catchment. This was to be achieved by adding flow gauge stations on the Marillana Creek and its tributaries within, upstream, and downstream of ML 270SA and 47/292 [56].

On groundwater resource, BHPBIO [56] identified the potential of cumulative impacts given the presence of Hamersly Iron operation in the neighbourhood. The proponents took into account the impacts in their regional groundwater model and dewatering licence. Both surface and groundwater monitoring to be undertaken by the proponents during mining was expected to provide a mechanism for monitoring cumulative impacts [56]. GNSS could play a role in providing location-based

[4]Environmental impact statements (EIA).

[5]Environmental protection statement.

information on test sites (flow-gauge stations) and also provide perimeter/area information that could help in monitoring of the cumulative impacts in the entire mining region (e.g., Fig. 13.3). This information could be integrated with a GIS system to provide an interactive system that could support management decisions.

## 13.5 Sustainability Assessment

Sustainability has been defined as meeting the needs of current and future generations through integration of environmental protection, social advancement and economic prosperity [62]. Sustainability assessment (SA) can be performed when a proponent requests a regulator to do so (external) for the purpose of approval or internally as a mechanism for improving internal decision-making and the overall sustainability of the final proposal, see e.g., [63, 64].

Pope et al. [65] classify SA into objective-led (strategic) and EIA based (narrow) approaches. Morrison-Saunders and Therivel [66] rank the various SA approaches with the EIA-led approach on bottom and the integrated (objective-led) approach at the top, see also [67]. Between them are various approaches, e.g., the win-win-win. Citing the dangers inherent in using the separate findings of the three sustainability pillars (environment, social, and economics) at the decision stage, Gibson [68] proposes adoption of an integrated approach. Caution should, however, be observed when using the term "integration" as it is used variedly by different authors, see e.g., [66, 69].

SA involves (i) *Sustainable decision making protocol*. A sustainable decision making protocol is a process of setting objectives, criteria and targets that underpin SA. Hacking and Guthrie [70] present several sources of sustainability development objectives and proposes the use of threshold as one of the means, (ii) *alternative approaches*, which are options, choices, or courses of action. They are means to accomplish particular goals [30]. Alternatives have been shown to be affected by the formulation of the decision question. SA, similar to SEA, has also benefited from MCA. In the province of Reggio Emilia (Northern Italy), Ferrarini et al. [71] used MCA to rank 45 municipalities based on 25 state of the environment indicators. Their results provided information on the state of sustainability in the province as a whole. GNSS could support SA in choosing the best alternative as already discussed in Sect. 13.3.2.2.

## 13.6 Concluding Remarks

The use of GIS to support impacts' assessment is still developing and certainly that of GNSS is a new concept. This Chapter attempted to motivate EIA, SEA and SA experts dealing with impact assessments to exploit the full potentials of GNSS especially with regard to its superb provision of location-based information and measurement of

spatial variations. GNSS satellites could for example be used to provide information related to distances, e.g., distances of the alternative sites from established and well developed community infrastructures. Using cheap hand-held receivers to obtain positions from two locations, one at the source (i.e., alternative sites) and the other at target (environmental sensitive site), the distances can readily be computed and incorporated into the MCA criteria and used to compute the desirable alternative that will inform decision making. GNSS could also be useful in providing information on spatial coverage of the proposed sites and also in environmental audit to evaluate compliance where location and spatial variation data are required (see e.g., Fig. 8.5 on p. 134). GNSS information can then be integrated with GIS to support the EIA process as discussed in this Chapter.

## References


1. Gibson J, MacKenzie D (2007) Using global positioning systems in household surveys for better economics and better policy. World Bank Res Obs 22(2):217–241. doi:10.1093/wbro/lkm009
2. Munn RE (1979) Environmental impact assessment: Principles and procedures, 2nd edn. Wiley, New York
3. Glasson J, Therivel R, Chadwick A (2005) Introduction to environmental impact assessment, 3rd edn. Routledge, New York
4. Sweeney International Management Corp (2009) Environmental Impact Assessment for Kelly Cove Salmon Ltd. proposed aquaculture site relocation for Sand Point, Boston Rock, and Hartz Point. Submitted to NS Department of Fisheries & Aquaculture. SIMCorp. File #SW2008-016, 017 & 018
5. Perry B, Gessler W (2000) Physical access to primary health care in Andean Bolivia. Soc Sci Med 50(9):1177–1188. doi:10.1016/S0277-9536(99)00364-0
6. Kumar N (2007) Spatial sampling for collecting demographic data. Paper presented at the annual meeting of the population association of America, 29-31 Mar, New York
7. Smit B, Spalding H (1995) Methods for cumulative effects assessment. Environ Impact Assess Rev 15(1):81–106. doi:10.1016/0195-9255(94)00027-X
8. Downes BJ, Barmuta LA, Fairweather PG, Faith DP, Keough MJ, Lake PS, Mapstone BD, Quinn GP (2002) Monitoring ecological impacts: Conceipts and practise in flowing waters. Cambridge University Press
9. Munier N (2004) Multicriteria environmental assessment. Kluwer Academic Publishers, Dordrecht, Netherlands, A practical guide
10. Geneletti D (2007) An approach based on spatial multicriteria analysis to map the nature conservation value of agricultural land. J Environ Manag 83:228–235. doi:10.1016/j.jenvman.2006.03.002
11. Antunes P, Santos R, Jordão L (2001) The application of geographical information systems to determine environmental impact significance. Environ Impact Assess Rev 21:511–535. doi:10.1016/S0195-9255(01)00090-7
12. Ashton Mining Ltd. (1991) Mt Weld rare earths project: sites evaluation study for a rare earths secondary processing plant, report prepared by Kinhill Engineers
13. Al-Rashdan D, Al-Kloub B, Dean A, Al-Shemmeri T (1999) Environmental impact assessment and ranking the environmental projects in Jordan. Eur J Oper Res 118:30–45. doi:10.1016/S0377-2217(97)00079-9
14. Shopley J, Fuggle R (1984) A comprehensive review of current EIA methods and techniques. J Environ Manag 18:25–47

15. Westman WE (1985) Ecology, impact assessment, and environmental planning. Wiley, New York
16. Gough JD, Ward JC (1996) Environmental decision making and land management. J Environ Manag 48(1):1–15
17. Therivel R (2004) Strategic environmental assessment in action. Earthscan, Sterling VA
18. Regan HM, Colyvan M, Markovchick-Nicholls L (2006) A formal model for consensus and negotiation in environmental management. J Environ Manag 80(2):167–176. doi:10.1016/j.jenvman.2005.09.004
19. Marttunen M, Haimailaiinen RP (1995) Decision analysis interviews in environmental impact assessment. Eur J Oper Res 87:551–563
20. Annandale D, Lantzke R (2000) Making good decisions: a guide to using decision-aiding techniques in waste facility siting. Murdoch University, Perth, Australia, Institute for Environmental Science
21. Jankowski P (1995) Integrating geographical information systems and multiple criteriadecision making methods. Int J Geogr Inf Syst 9(3):251–273
22. Malczewski J (1999) GIS and multicriteria decision analysis. Wiley, New York 392 pp
23. Carver SJ (1991) Integrating multi-criteria evaluation with geographical information systems. Int J Geogr Inf Syst 5(3):321–339. doi:10.1080/02693799108927858
24. Janssen R (2001) On the use of multi-criteria analysis in environmental impact assessment in the Netherlands. J Multi-Criteria Decis Anal 10:101–109. doi:10.1002/mcda.293
25. Lahdelma R, Salminen P, Hokkanen J (2000) Using multicriteria methods in environmental planning and management. Environ Manag 26:595–605
26. Ministry of Environment and Energy, Government of Ontarion (1990) Evaluation methods in environmental assessment, pp. 3-12, 33-51; 112-137
27. Hajikowicz SA (2007) Supporting multi-stakeholder environmental decisions. J Environ Manag 88(4):607–614. doi:10.1016/j.jenvman.2007.03.020
28. Bojórquez-tapia LA, Sanchez-colon S, Martinez AF (2005) Building consensus in environmental impact assessment through multicriteria modelling and sensitivity analysis. Environ Manag 36:469–481. doi:10.1007/s00267-004-0127-5
29. Kiker GA, Bridges TS, Varghese A, Seager TP, Linkov I (2005) Application of multicriteria decision analysis in environmental decision making. Integr Environ Assess Manag 1(2):95–108. doi:10.1897/IEAM_2004a-015.1
30. Steinemann A (2001) Improving alternatives for environmental impact assessment. Environ Impact Assess 21(1):3–21. doi:10.1016/S0195-9255(00)00075-5
31. Varma VK, Ferguson I, Wild I (2000) Decision support system for the sustainable forest management. Forest Ecol Manag 128(1–2):49–55. doi:10.1016/S0378-1127(99)00271-6
32. Sheppard SRJ, Meitner M (2005) Using multi-criteria analysis and visualisation for sustainable forest management planning with stakeholder groups. Forest Ecol Manag 207(1–2):171–187. doi:10.1016/j.foreco.2004.10.032
33. Vincke P (1992) Multicriteria decision-aid. Wiley, Chichester, UK
34. Hajikowicz SA, McDonald GT, Smith PN (2000) An evaluation of multiple objective decision support weighting technique in natural resource management. J Environ Plann Manag 43(4):505–518
35. Lantzke R (2006) MCA-the weighting process and overall comments on a weighting process. Environmental Science, Murdoch University. Unpublished. http://lms.murdoch.edu.au/webct/urw/lc152224987001.tp152225013001/RelativeResourceManager/Template/content/10_13evaluation/three-mca-wt-mthds.pdf. Accessed on15/4/2008
36. Saaty TL (1980) The analytic hierarchy process. McGraw-Hill, New York
37. Saaty TL (1987) Analytical hierarchy process - what it is and how it is used. Math Modell 9(3):161–176
38. Ashton Mining Ltd. (1992) Mt Weld rare earths project: Public environmental review, report prepared by Kinhill Engineers
39. Australian Water Resource (2005) Combined water management area: Gnangara Mound. http://www.water.gov.au/RegionalWaterResourcesAssessments/SpecificGeographicRegion/TabbedReports.aspx?PID=WA_GW_51x. Accessed on 8/3/2008

40. Department of Water (2008) Gnangara Mound - a unique water resource. http://portal.water.wa.gov.au/portal/page/portal/WaterManagement/Groundwater/Gnangara/. Accessed 14/03/08
41. Water Authority of WA (1995) Review of proposed changes to environmental conditions - Gnangara Mound groundwater resources (Section 46). Water Authority of WA
42. Department of Water (2007) Environmental management of groundwater abstraction from the Gnangara roundwater mound 2004–2005, annual compliance report to the Environmental Protection Authority, July 2004–2005
43. McArthur WM (1986) The Gnangara Mound landforms, soils and vegetation. Gnangara mound environmental review and management programme, Water Authority WA
44. Sorensen JC (1971) A framework for the identification and control of resource degradation and conflict in multiple use of the coastal zone. Department of Landscape Architecture, University of Carlifornia, Berkeley
45. Haklay M, Feitelson E, Doytsher Y (1998) The potential of a GIS-based scoping system: an isreali proposal and case study. Environ Impact Assess Rev 18:439–459
46. Mattiske EM (1994) Monitoring the effects of groundwater extraction on native vegetation on the Northern Swan Coastal Plain. EM Mattiske and associates
47. Water Authority of WA (1992) Gnangara Mound vegetation stress study - results of investigation. Report No WG 127, Water Authority of WA
48. Groom BPK, Froend RH, Mattiske EM (2000) Impact of groundwater abstraction on woodland, Swan Coastal Plain, WA. Ecolo Manag Restor 1:117–124. doi:10.1046/j.1442-8903.2000.00033.x
49. Jasinska EJ, Knott B (1991) Stability of root mat ecosystem in groundwater stream: Cabaret cave. WA, University of Western Australia, Yanchep National Park
50. Sadler B, Verheem R (1996) SEA: Status, challenges and future directions, Report 53. Ministry of housing, spatial planning and the environment, The Hague, Netherlands
51. Wood C, Djeddour M (1991) Strategic environmental assessment; EA of policies, plans and programmes. Impact Assess Bull 10(1):3–22
52. Noble B (2002) Strategic environmental assessment of Canadian energy policy. Impact Assess Proj Apprais 20(3):177–188. doi:10.3152/147154602781766681
53. Spaling H, Smit B (1993) Cumulative environmental change: conceptual frameworks, evaluation approaches, and institutional perspectives. Environ Manag 17(5):587–600. doi:10.1007/BF02393721
54. Commonwealth Environmental Protection Agency (1994) Review of Commonwealth environmental impact assessment. Canberra: CEPA 10
55. Scace R (2000) Vital Relationship: complementary responsibilities of government and proponent in scoping? In: Kennedy A (Ed) Cumulative environmental effects management: tools and approaches. Alberta Association of Professional Biologists, Edmonton, pp. 31–41
56. BHP Billiton Iron Ore Pty Ltd (2005) Marillana Creek (Yandi) mine - environmental management plan, Revision 3
57. EPA (1988) Yandicoogina (Marillana) iron ore project, Report and recommendations of the environmental protection authority, Bulletin 323. Environmental Protection Authority, Perth, Western Australia
58. EPA (1992) Yandicoogina (Marillana) iron ore project - change of ministerial condition due to increase in rate of production, Report and recommendations of the environmental protection authority, bulletin 622. Environmental Protection Authority, Perth, Western Australia
59. EPA (1994) Yandicoogina (Marillana) iron ore project - change of environmental conditions due to increase in rate of production, Report and recommendations of the environmental protection authority, bulletin 738. Environmental Protection Authority, Perth, Western Australia
60. EPA (1995) Duplication of iron ore mining operation, Yandi mine ML 270SA, Hamersley Range, 90 km north west of Newman, report and recommendations of the environmental protection authority, bulletin 802. Environmental Protection Authority, Perth, Western Australia
61. EPA (Environmental Protection Authority) (2005) Marillana Creek (Yandi) Mine Life of Mine proposal, mining leases 270SA and 47/292, 90 km north-west of Newman. Report and recommendation of the EPA, assessment no 1555, Bulletin 1166. Perth, WA

62. Government of Western Australia (2003), Hope for the future: the Western Australian State Sustainability Strategy. Department of the Premier and Cabinet Perth, Western Australia. http://www.sustainability.dpc.wa.gov.au/docs/Final%20Strategy/SSSFinal.pdf Accessed on 02/03/2008
63. Pope J (2006) What's so special about sustainability assessment? J. Environ. Assess. Policy Manag. 8: v–x. doi:10.1142/S1464333206002505
64. Pope J, Grace W (2006) Sustainability assessment in context: issues of process, policy, and governance. J Environ Assess Policy Manag 8:373–398. doi:10.1142/S1464333206002566
65. Pope J, Annandale D, Morrison-Saunders A (2004) Conceptualizing sustainability assessment. Environ Impact Assess Rev 24:595–616. doi:10.1016/j.eiar.2004.03.001
66. Morrison-Saunders A, Therivel R (2006) Sustainability integration and assessment. J Environ Assess Policy Manag 8(3):281–298. doi:10.1142/S1464333206002529
67. Hacking T, Guthrie P (2008) A framework for clarifying the meaning of triple bottom-line, integrated, and sustainability assessment. Environ Impact Assess Rev 28(2–3):73–89. doi:10.1016/j.eiar.2007.03.002
68. Gibson R (2006) Beyond the pillars: sustainability assessment as a framework for effective integration of social, economic and ecological considerations in significant decision-making. J Environ Assess Policy Manag 8(3):259–280. doi:10.1142/S1464333206002517
69. Lee M (2006) Bridging the gap between theory and practise in integrated assessment. Environ Impact Assess Rev 28:57–78. doi:10.1016/j.eiar.2005.01.001
70. Hacking T, Guthrie P (2006) Sustainable development objectives in impact assessment: why are they needed and where do they come from? J Environ Assess Policy Manag 8(3):341–371. doi:10.1142/S1464333206002554
71. Ferrarini A, Bodini A, Becchi M (2001) Environmental quality and sustainability in the province of Reggio Emilia (Italy): using multi-criteria analysis to assess and compare municipal performance. J Environ Manag 63:117–131. doi:10.1006/jema.2001.0465

# Chapter 14
# Water Resources

*With a growing population and a drying climate, Australia - like many rich nations - is running out of water. Solutions are not easy nor cheap ... and may require cities to tap their sewers*
S. Phillips [1]

## 14.1 Why Monitor Variation in Fresh Water Resources?

Essential for life, fresh water is one of the basic necessities without which human beings cannot live! Some of its uses include:

- Domestic, agricultural (including livestock) and industrial usage.
- Means of transportation.
- Home to various biodiversity, e.g., fish, birds, reptiles, and mammals.
- Recreational areas.
- Basis for ecosystems such as wetlands.

Although much of the Earth is covered by water, most of it is unsuitable for human consumption, since 96% of it is found in the saline oceans. According to the U.N., only 2.5% of the roughly 1.4 billion cubic kilometers of water on Earth is freshwater, and approximately 68.9% of the freshwater is trapped in glacial ice or permanent snow in mountainous regions, the Arctic and Antarctica regions. Roughly 30.8% is groundwater, much of which is inaccessible to humans, and the remainder 0.3% comprise surface waters in lakes and rivers [2]. Of these 0.3% available for human and animal consumption, much is inaccessible due to unreachable underground locations and depths [3].

This scarcity is such that it is estimated that by 2050, about two billion people will be short of water, a potential cause of conflict [4]. So vital are water resources that it is difficult to discuss any monitoring of the environment without it. The importance of water as a resource, therefore, calls for sound environmental conservation measures



J. Awange, *GNSS Environmental Sensing*, Environmental Science and Engineering, DOI 10.1007/978-3-319-58418-8_14

that enhance its protection and management. It is in relation to this that the World Bank, as an emerging priority of its lending, decided to broaden the development focus in its 1993 "Water resource management policy paper" to include the *protection* and *management* of water resources in an environmentally sustainable, socially acceptable, and economically efficient manner [5]. The protection and management of water resources calls for an elaborate and well established monitoring program.

Essential components of a water level monitoring program are presented, e.g., by Taylor and Alley [6] as; *selection of observation wells*, determination of the frequency of water level measurements, implementation of quality assurance, and establishment of effective practices for data reporting. In selecting the observation wells, they state that the decisions made about the number and locations of observation wells are crucial to any water-level data collection program [6]. In regard to locations, GNSS satellites could contribute in generating a fast and accurate survey of well location-based data. These data could then be integrated with other information such as water level in a GIS system to enhance the accessibility of water level data, where the GIS plays the role of depicting the locations of the observed wells relative to pertinent geographic, geologic, or hydrologic features, e.g., [6].

Taylor and Alley [6] present areas where the monitored groundwater levels could be used. Some of these include: determination of the hydraulic properties of aquifers (aquifer tests); mapping of the altitude of the water table or potentiometric surface; monitoring of the changes in groundwater recharge and storage; monitoring of the effects of climatic variability; monitoring of the regional effects of groundwater development; statistical analysis of the water level trends; monitoring of the changes in groundwater flow directions; monitoring of the groundwater and surface water interaction; and numerical (computer) modelling of groundwater flow or contaminant transport.

Information on the spatial and temporal behaviour of terrestrial water storage, therefore, is crucial for the management of local, regional and global water resources [7]. This information will:

- Enhance sustainable utilization of water resources by, e.g., farmers, urban consumers, miners, etc.
- Guide water resource managers and policy makers in the formulation of policies governing its sustainable use, conservation and management. In particular, state water managers are more informed in regulating the utilization of water, e.g., for industrial and irrigation purposes.
- Benefit local environmental monitoring, management policies and practices that ensures a balance between sustainable utilization and environmental conservation and protection. Changes in water availability impacts upon the environment in several ways, e.g., any significant imbalance in its level affects the ecological system by influencing salinity, land subsidence and the vulnerability of wetlands ecosystem among others.
- Benefit various government agencies at various levels (national, provincial, and local) by providing data that enhances and compliments their work. Such agencies include departments of *water*, *agriculture*, *weather forecasting* and *climate* studies, and so forth.

The conservation and management of water is of paramount importance in areas with arid or semiarid climates, which include many parts of Australia, especially in times of severe drought, as experienced in Murray Darling Basin [7]. In 2006, Australia faced its worst drought in a century as seen from daily reports that were emerging in both the local and international media, see also [8]. A more grim picture of the future of the water situation for Australia was to follow from the IPCC [9] report, which stated that Australia's water crisis will worsen in the coming years due to drought! There clearly exists an urgent need to have efficient monitoring technique(s). One such technique that monitors changes in stored water, is the use of GRACE satellites (Sect. 9.3.3), which is demonstrated in the examples to follow.

Timely and precise information on the changes in stored water at smaller (localized) scales of economical values, e.g., urban consumption, agriculture, industries, and mining to within 10–14 days, so far achievable by GRACE satellite through, e.g., the Mass Concentration (Mascon) technique discussed in Awange et al., [10], will enhance sustainable conservation and management of this precious *dwindling* resource.

The availability of techniques that delivers information on the changes in stored water at a more local scale, is the first step towards realizing an efficient water society. Water resource managers are able to make decisions based on timely and accurate knowledge; thereby saving considerable resources that are often spent as a penalty of inefficient decisions based on a lack of information. In the south-western wheat belt of Australia, for example, accurate knowledge of changes in stored water will be beneficial to the sustainable utilization of water, while at the same time realizing the economic contribution of wheat farming to the overall Gross Domestic Product (GDP). A blind focus on the GDP's growth without paying attention to the state of salient contributors such as water stored in aquifers is detrimental, since a fall in the amount of the available water in such areas would definitely mean reduced yields.

Since the entire system of stored water is coupled within the hydrological cycle (Fig. 14.1), hydrologists will be in a position to better understand their local hydrological cycle, thanks to information at localized levels. Hydrologists will also be able to use such information to refine and calibrate local-scale models, e.g., rainfall runoff models [11], for further improvement in their hydrological cycles. This will also contribute to our understanding of the impacts of climate change on regional and global hydrological cycles. For the geodetic community, knowledge of the changes in local stored water is vital for assessing the impact of groundwater on the stability of continuously operating GNSS monuments (e.g., Fig. 5.12 on p. 81), which in turn affects the overall accuracy of geodetic networks (see Sect. 5.5).

Environmental studies also have a chance of greatly benefiting from information about changes in stored water. It is widely acknowledged that stored water (surface and groundwater) plays a key role in sustaining natural biodiversity and the functioning of the environment as a whole. Knowledge of the changes in water level is therefore essential for the very survival of the entire ecosystem, which could be adversely affected by extreme change in stored water. In wetlands, for example, some vegetation and ecosystems have been known to respond to water level fluctuations [12].

Accurate monitoring of changes in stored water at smaller wetland scales will thus help in the preservation and conservation of such wetland ecosystems. Changes in water level also brings with it environmental phenomena such as salinity, compacting of aquifers due to the removal of water causing land subsidence, and changes in the properties of the top 5 cm of soil. Information on changes in stored water thus contributes enormously to the environmental conservation and protection.

## 14.2 Gravity Field and Changes in Stored Water

In Sect. 5.6.1 we introduced the concept of the *geoid* (Fig. 5.18 on p. 88) as a fundamental physical surface to which all observations are referred to if they depend on *gravity*, and whose shape is influenced by inhomogeneous mass distribution within the interior of the Earth [13, p. 29]. In the discussion that follows, the concept of *gravity field variations* discussed in Sect. 9.3 is related to hydrological processes. Measurements of the time-varying gravity field by LEO satellites, e.g., GRACE discussed in Sect. 9.3.3 are the key to the contribution of GNSS to space monitoring of changes in water levels at basin scales. Such techniques now enable the monitoring of groundwater recharge, which is the most important element in groundwater resources management and could also be applicable to monitoring salinity management measures at the catchment level (see Sect. 16.4.2). For example, in 2009, GRACE satellites showed that north-west of India's aquifers had fallen at a rate of 0.3048 m $yr^{-1}$ (a loss of about 109 $km^3$ per year) between 2002 and 2008.[1]

### *14.2.1 Gravity Field Changes and the Hydrological Processes*

The hydrological cycle (Fig. 14.1) refers to the pathway of water in nature, as it moves in its different phases through the atmosphere, down over and through land, to the ocean and back to the atmosphere [14]. The associated variations in gravity field are therefore caused, e.g., by

- the redistribution of water in the oceans, including e.g., El Niño and Southern Oscillation (ENSO) events,
- movement of water vapour and other components in the atmosphere,
- seasonal rainfall; snow and subsequent drying and melting,
- groundwater extraction, or
- drying and filling of lakes, rivers, and reservoirs.

[1] The Economist, September 12th 2009, pp. 27–29: Briefing India's water crisis.

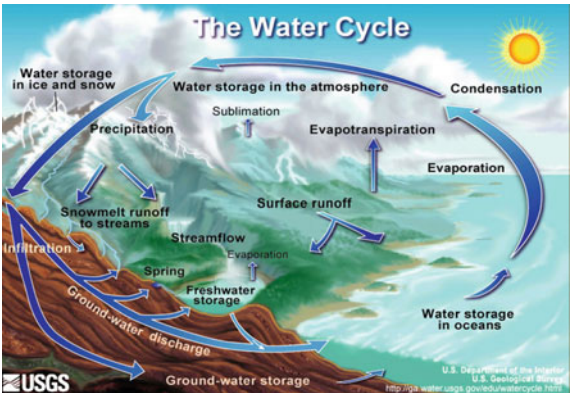


**Fig. 14.1** Components of hydrological cycle that lead to temporal variations in the gravity field. *Source* US Geological Survey (USGS)

### *14.2.2 Monitoring Variation in Stored Water Using Temporal Gravity Field*

The potential of using the relationship between temporal gravity changes and hydrology (Fig. 14.1) was first recognized by Montgomery [15] who estimated specific yield through a correlation between gravity and water-level changes [16]. In 1977, Lambert and Beaumont [17] used a gravity meter to correlate groundwater fluctuations and temporal changes in the Earth's gravity field. Goodkind [18] recorded observations from seven super conducting gravimetric stations to examine non-tidal variations in gravity and noted that at one of the stations (Geysers geothermal station), much of the variation could be correlated with rainfall and seismic activity. Such measurements had not been possible before the advent of super conducting gravimeters, thus providing evidence of the existence of temporal variation in gravity.

In 1995, while estimating the atmospheric effects on gravity observations around Kyoto, Mukai et al. [19] noted that changes in gravity around the station could have been caused by changes in underground water. In the same year, Pool and Eychaner [20] assessed the utility of temporal gravity-field surveys to directly measure *aquifer-storage* changes and reported gravity changes of around 100–134 μGal, equivalent to 2.4–3.2 m of water column, considering infinitely extended sheet approximation. Their results from the analysis of changes in stored water in the aquifer indicated an increase in the gravity field of 158 ± 6 μGal when the water table rose by about 17.7 m, providing further evidence of the possibility of using temporal gravity-field surveys to monitor changes in stored aquifer water. In fact, according to Bower and Courtier [21] who analyzed the effect of precipitation on gravity and well-levels at a Canadian absolute gravity site, 90% of the gravity variation was found to be due to the effects of precipitation, evapotranspiration and snow-melt.

The last decade has also recorded increased use of temporal gravity field studies in monitoring changes in stored water, see e.g., [22]. It saw the beginning of satellite missions dedicated to monitoring temporal variations in the gravity field. Smith

et al. [23] investigated the ability of ground-based gravity meters to monitor changes in soil moisture storage.

Moving from local tests to regional, a different application of gravity surveys was investigated by Damiata and Lee [24], who simulated the gravitational response to aquifer hydraulic testing. The synthetic system was composed of an unconfined shallow aquifer and the purpose of the investigation was to assess the potential of the gravity measurements for detecting groundwater extraction. Drawdown due to pumping causes a decrease in mass and consequently in gravity measured at the surface. The results showed that the gravitational response to aquifer testing could be used to monitor the spatial development of the drawdown cone. For the configuration considered in the investigation, the signal was of the order of tens of μGals and could be detected up to several hundred meters away from the pumping well.

Water storage changes, such as changes in soil moisture, snow and ice cover, surface and groundwater, including deep aquifers, can be monitored either by in-situ observations or indirectly through changes in gravity [25]. While in-situ observations provide valuable localized information, they suffer from limited spatial coverage for regional to continent-wide studies [26]. Any change in water storage also manifests itself in a change in the gravity field. This property can be used to infer water-storage changes from time-variable gravity observations as demonstrated by Rodell and Famiglietti [27] for 20 globally distributed drainage basins of sizes varying from 130,000 to 5,782,000 $km^2$ to assess the detectability of hydrological signals with respect to temporal and spatial variations. Space-borne techniques can provide time-variable gravity observations on a regional and global scale, thus allowing for large-scale water storage monitoring and the ability to close the 'gaps' between locally limited in-situ observations [11].

Since the launch of the GRACE satellite mission in 2002 (see Sect. 9.3.3), a new powerful tool for studying temporal gravity field changes has become available, and numerous articles assessing the potential of GRACE recovering hydrological signals have been published, see e.g., Awange et al. [28, and the references therein]. Tapley [25] provided early results of the application of the GRACE products for detecting hydrological signals in the Amazon-Orinoco basin. Following these results, numerous other authors have subsequently applied GRACE to detect hydrological signals in various situations and locations, see references in [28].

For instance, Ramillien et al. [29, 30] and Andersen et al. [31] investigated the potential of inferring inter-annual gravity field changes caused by continental water storage changes from GRACE observations between 2002 and 2003, and compared these changes to the output from four global hydrological models. It was possible to correlate large scale hydrologic events with the estimated change in the gravity field for certain areas of the world to an accuracy of 0.4 Gal, corresponding to 9 mm of water, see also [31–33].

Syed et al. [34] examined total basin discharge for the Amazon-Orinoco and Mississippi river basins from GRACE, while Rodell et al. [35] estimated groundwater storage changes in the Mississippi basin. Crowley et al. [36] estimated hydrological signals in the Congo basin, while Schmidt et al. [37] and Swenson et al. [38, 39] used GRACE to observe changes in continental water storage. Winsemius et al. [40]

compared hydrological model outputs for the Zambezi River Basin with estimates derived from GRACE. Monthly storage depths produced by the hydrological model displayed larger amplitudes and were partly out of phase compared to the estimates based on GRACE data. Likely reasons included leakage produced by the spatial filtering used in the GRACE data, and the difficulty to identify the time of satellite overpass as opposed to simply averaging over the whole period. Awange et al. [41, 42] used GRACE to study the fall of Lake Victoria's water level in Africa. This last example will be elaborated upon in more detail in Sect. 14.3.1.2.

As already discussed in Sect. 9.3.3, GRACE satellites detect changes in the Earth's gravity field by measuring changes in the distance between the two satellites at a 0.1 Hz sampling frequency. The variation in the distance between the two twin satellites caused by gravitational variations above, upon, and within the Earth all have an effect on the satellites. This variation in gravity could be due to *rapid* or *slow* changes caused, for example by the redistribution of water in the oceans, the movement of water vapor and other components in the atmosphere, the tidal effect of the Sun and Moon, and the displacement of the material by earthquakes and glacial isostatic adjustment. The data therefore must be processed to isolate these effects so as to retain only those which correspond to the process of interest, in this case, terrestrial water storage changes, see e.g., [43]. Equation (9.33) is used to compute changes in stored water. In the following examples, the application of GRACE satellites to monitor stored water resources are illustrated. It should be emphasized once more that GNSS do not directly measure changes in water storage but contributes as discussed in Sect. 9.3.3.

## 14.3 Examples of Space Monitoring of Changes in Stored Water

### *14.3.1 The Nile Basin*

The Nile Basin (Fig. 14.2) is one of the Earth's most impressive examples of the influence of topography and climate on the flow conditions of a water system. The Nile has two major tributaries, the White Nile and the Blue Nile, the latter being the source of most of the river's water. The White Nile rises in the Great Lakes region of Eastern Africa, and flows northwards through Uganda and the South Sudan. The Blue Nile starts at Lake Tana in the Ethiopian highlands, flowing into Sudan from the southeast and meets the White Nile at Khartoum in Sudan. From there, the Nile passes through Egypt and ends its journey by flowing into the Mediterranean Sea. A basin as large as the Nile, which crosses such a wide latitude range (from $\sim 5^{\circ}\mathrm{S}$ to *ca.* $31^{\circ}\mathrm{N}$) cannot be expected to experience homogeneous climatic and rainfall patterns over its extent. In addition, variations in the geology and soils of the basin

strongly influence groundwater availability. Significant rainwater deficits and the variable duration of the rainy seasons over yearly to decadal time scales results in hydrological deficits that are not necessarily reflected in a direct response of the base flow, e.g., [44].

*The East African lake region* includes the countries of Burundi, Rwanda, Uganda, Kenya and Tanzania, and is the home to Lake Victoria, the world's second largest freshwater lake, and the source of White Nile [45]. From Lake Victoria, the waters are discharged to Lake Kyoga, which also receives water from its surrounding 75,000 km$^2$ catchment before flowing on to Lake Albert. In addition to the waters received from Lake Kyoga, Lake Albert is supplied by its upstream Semiliki basin and the Lake Edward sub-basin (Fig. 14.2). Together, Lakes Edward, Albert, and George form the western edge of the Nile Basin, comprising an area of 48,000 km$^2$, of which 7,800 km$^2$ is open water [46]. In the Sudd swamp region, the supply to the Nile benefits from two other basins, the Bahr-El-Ghazal (500,000 km$^2$) to the west and the Sobat (150,000 km$^2$) to the east, before exiting at Malakal.

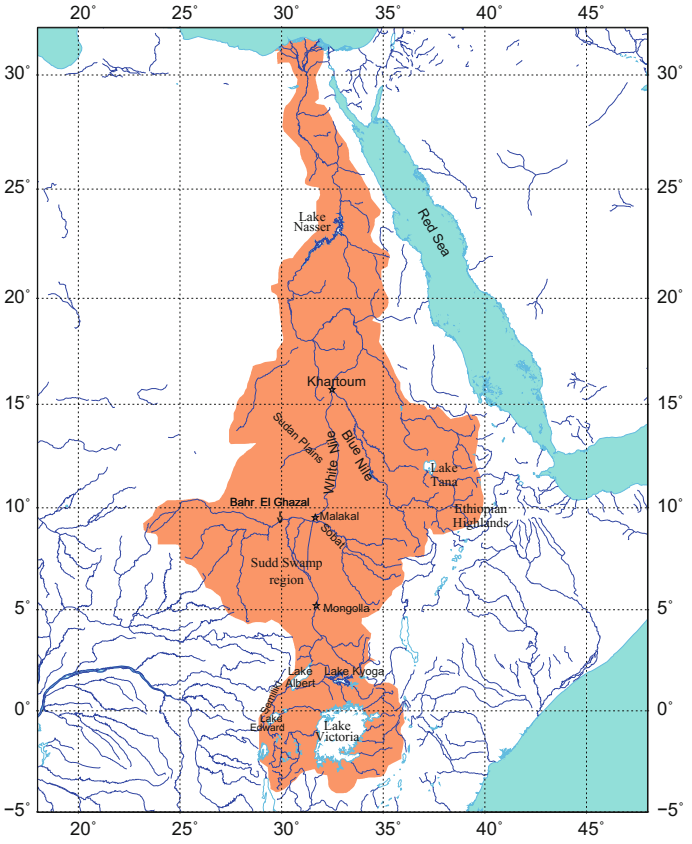


**Fig. 14.2** The Nile Basin (*brown shaded* region) with the major features and place names as discussed in the text

*The Ethiopian highlands* are comprised of twelve significant sub-basins aggregated into four primary basins; Lake Tana (200,000 $km^2$, the main headwaters of Blue Nile, although it contributes less than 10% of the total Blue Nile flow), the upper Blue (150,000 $km^2$), the lower Blue (60,000 $km^2$), and the Dinda-Raghad (70,000 $km^2$). All together, they cover almost 480,000 $km^2$ and contribute approximately 65% of the river Nile's total water [46].

*Lake Nasser region*: The Egyptian desert starts from Khartoum, where the Nile flows northward towards Egypt through Lake Nasser (formed by the Aswan dam) and then to the Mediterranean Sea. Yates and Strzepek [46] reported a net loss of water between the joining of the Atbara river with the Nile north of Khartoum, and Lake Nasser due to evaporation and seepage.

#### 14.3.1.1 Challenges Facing the Basin's Waters

The Nile river basin is one of the largest in the world, with an area of about 3,400,000 $km^2$ (almost one-tenth of Africa) and traversing some 6,500 km from south to north as it winds its way across the boundaries of eleven countries: Tanzania, Uganda, Kenya, Rwanda, Burundi, Democratic Republic of Congo (DRC), Eritera, Ethiopia, Sudan, South Sudan, and Egypt, e.g., [47]. As it flows through these countries, it supports a livelihoods of over 200 million people.

The Nile's water resources, however, have come under threat from both anthropogenic and natural factors, e.g., [48]. Anthropogenic influences have been fuelled by the increasing human population that has put pressure on domestic water needs, the supply of hydroelectric power, all coupled with the need to sustain economic growth. However, not only are the demands on water increasing, but the available water supplies appear to be decreasing, with environmental degradation of the upper Blue Nile catchment having increased throughout the 1980s [49]. Whittington and McClelland [49] found that about 86% of the annual Nile river flow into Egypt originates from Ethiopia, and warn of significant implications for Egypt and Sudan should Ethiopia undertake any potential extractions; this issue emphasizes the need for cooperation between the three Blue Nile riparian states.

Natural factors include the changing climate, which has been the subject of numerous studies, e.g., [46, and the references therein]. Therefore, a combination of human population growth, unsustainable water usage and development, and desertification are just some of the factors that threaten the Nile's ability to supply crucially needed water to the people of the basin.

The present-day state of the stored water variations and their relations to climate variability (e.g., El Niño and Southern Oscillation (ENSO) and the Indian Ocean Dipole (IOD)) in the Nile Basin are, however, also not well understood. Most studies dealing with the Nile Basin, however, have dealt mainly with modelling the impacts of climate change (e.g., [50, 51]), with very little being reported on how to monitor the spatial and temporal variations in the stored water (surface, groundwater and soil moisture) of the basin in a holistic manner, and linking them to climate variability. The reason for such few studies, e.g., [52–55] has been partly attributed to its large

size, as well as the lack of appropriate monitoring techniques that could cover such a vast spatial extent. For instance, the hydrological water balance involves the flow of surface water, the movement of deeper groundwater, and the coupling of the land, ocean and atmosphere through evaporation and precipitation. Monitoring these components requires an accuracy and completeness of geographical data coverage that challenges conventional measurement capabilities.

Using GRACE, GLDAS (Global Land Data Assimilation System),[2] and TRMM (Tropical Rainfall Measuring Mission)[3] data for the period 2002–2011, Independent Component Analysis ICA-method, e.g., [56], is applied in the examples below to localize the Nile Basin's hydrological signals into their respective sources. In Fig. 14.3, it is seen that the dominant signal associated with the Lake Victoria Basin is localized for all the three data set. This clearly shows the contribution of the Lake Victoria basin to the Nile waters. An analysis of the correlation between these signals and climate variability indicate a strong correlation (0.85) between the GRACE's total water storage and ENSO for the period 2006–2011. This confirms the known fact that climate variability, particularly ENSO, influences the changes in stored water of Lake Victoria Basin, and should be taken into consideration in evaluating the basin's hydrology. Section 14.3.1.2 discusses Lake Victoria Basin in more detail.

Figure 14.4 shows the localization of the signals within the Ethiopian highlands, thus indicating the importance of the region to the Nile basin. The Blue Nile receives its waters mainly from the heavy rainfall in the region as seen from the TRMM results (Fig. 14.4; IC5). Any land use patterns that could alter the use of water within the region would be capable of significantly impacting upon the entire Nile Basin. GRACE signals show a correlation of 0.52 with ENSO while GLDAS show 0.44 with ENSO and 0.4 with the Indian Ocean Dipole (IOD) index. Compared to Lake Victoria basin, the correlation to climate variability is not so strong, nonetheless, the fact that the changes in the stored water in the Ethiopian highlands is influenced by climate variability is noticeable. Figure 14.5 shows the localization of the signals within the Bahr-El-Ghazal region, which also contributes water to the River Nile by joining the tributaries from Sobat around Malakal (see Fig. 14.2). Both GRACE and GLDAS signals show a correlation of 0.68 with ENSO respectively, thus indicating that the variability of the stored water is influenced by climate variability. Finally, Fig. 14.6 shows the dynamics around Lake Nasser along the Red Sea. After removing this signal, Awange et al., [52] found a decline in stored water in the Western Plateau within the Nubian Aquifer covering Lake Nasser (see Fig. 14.7) at a rate of 2.6 mm/year (cf. 3.5 mm/year in Sultan et al., [57]). The loss of water in this region is attributed by Sultan et al. [57] to the fact that most of the water is extracted from the Nubian Aquifer and used for agricultural purposes that largely occur throughout the winter season, and also due to the fact that the UweinatAswan uplift prevents recharge of ground water flowing from the South to the North. To strengthen this argument is the fact that expansions of some large irrigation schemes such as East Uweinat project has seen heavy utilization of groundwater. In the East Uweinat project, for

[2] http://disc.sci.gsfc.nasa.gov/services/grads-gds/gldas.

[3] http://trmm.gsfc.nasa.gov/data_dir/data.html.

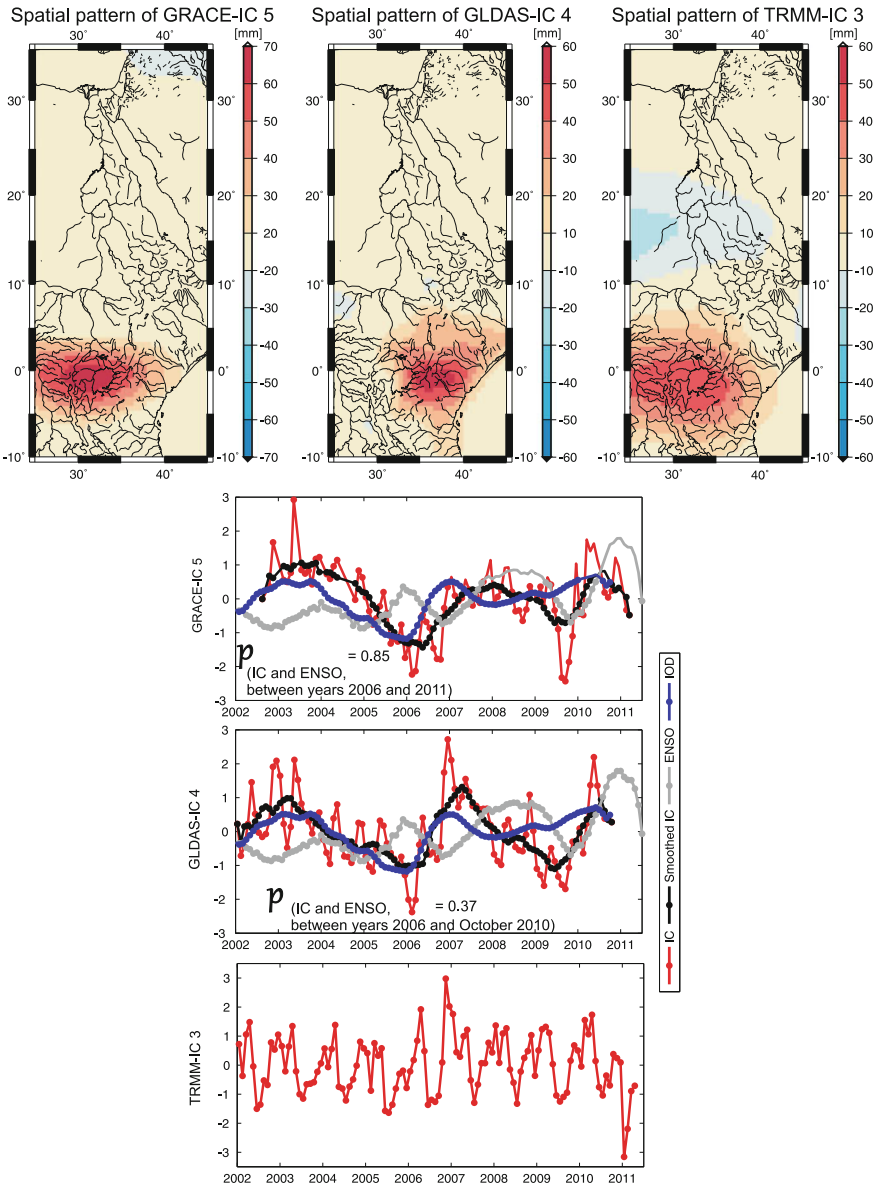


**Fig. 14.3** ICA analysis of the GRACE, GLDAS, and TRMM data for the Nile basin. In this figure the signals are localized within Lake Victoria basin in all the data set

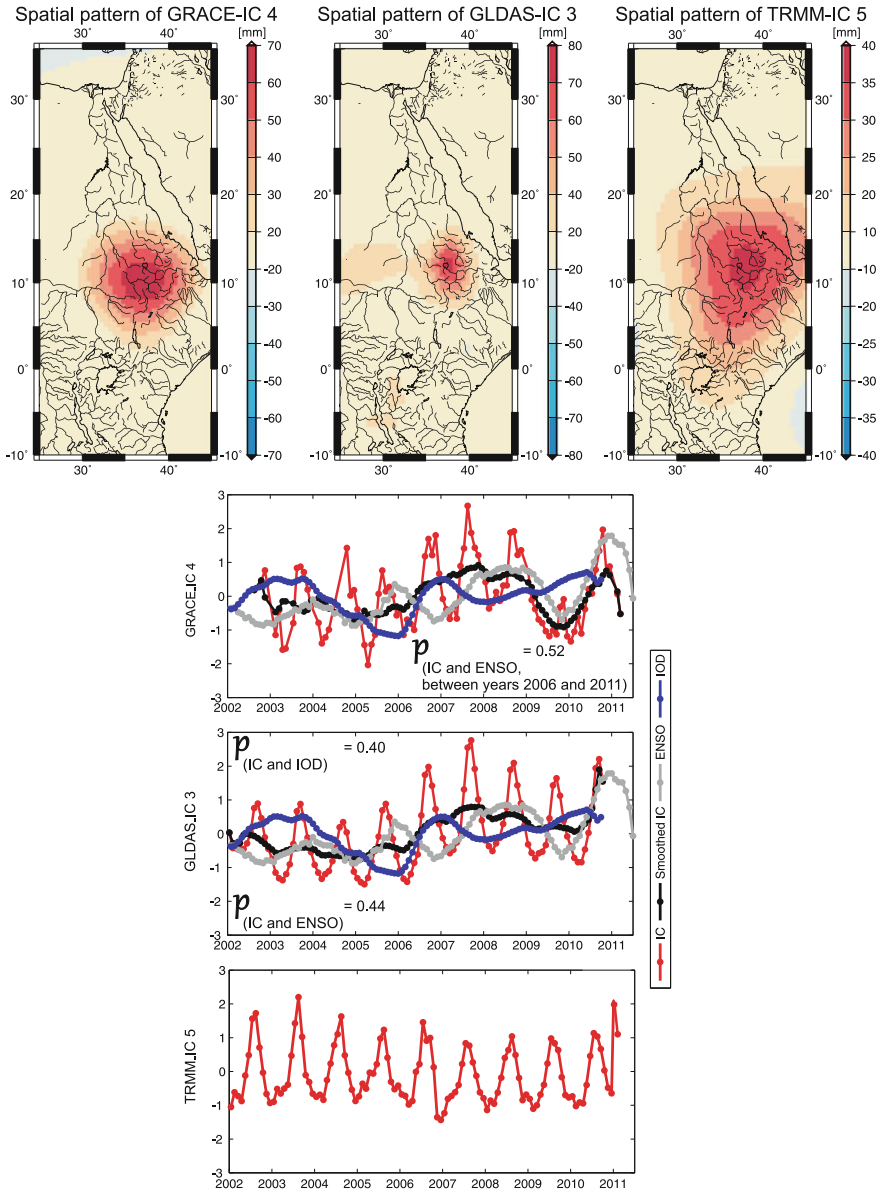


**Fig. 14.4** ICA analysis of the GRACE, GLDAS, and TRMM data for the Nile basin. In this figure the signals are localized within the Ethiopian highlands in all the data set

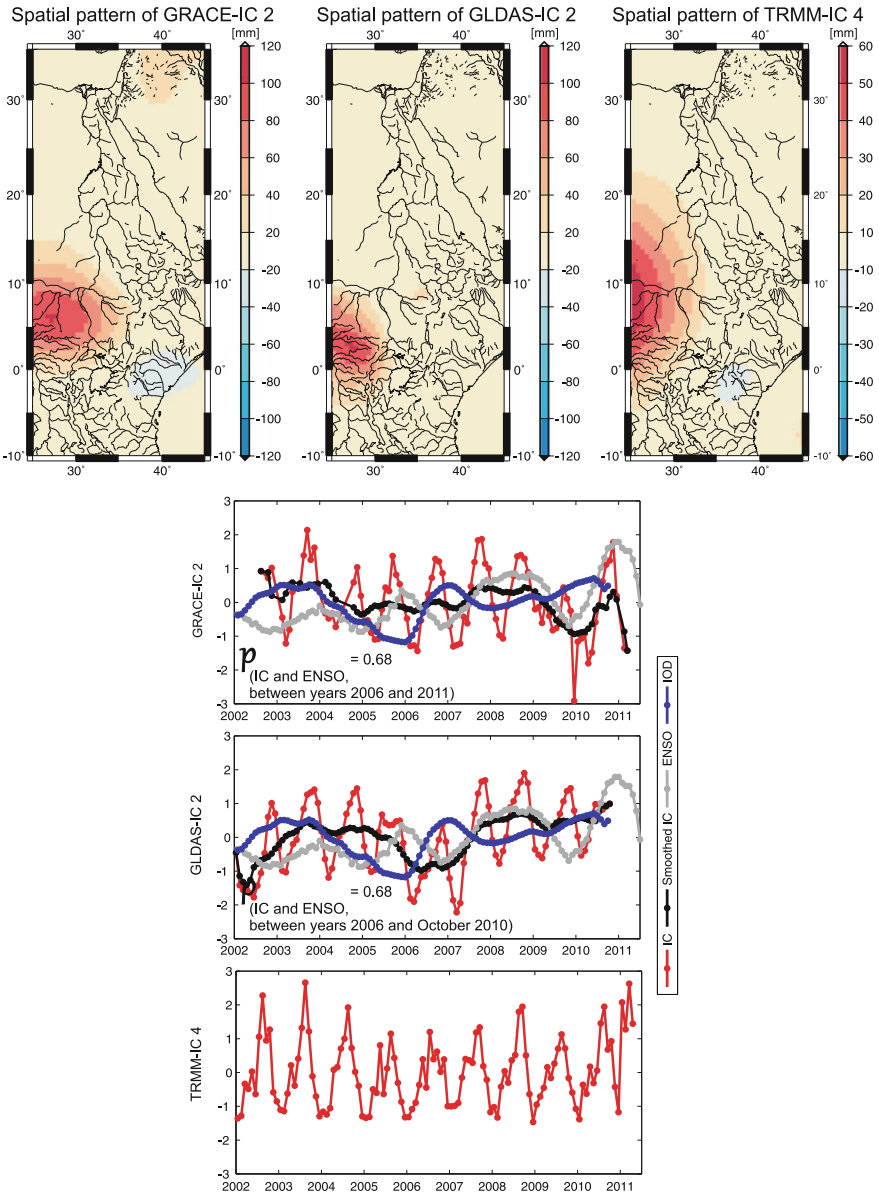


**Fig. 14.5** ICA analysis of the GRACE, GLDAS, and TRMM data for the Nile basin. In this figure the signals are localized within the Bahr-el-Ghazal region in all the data set

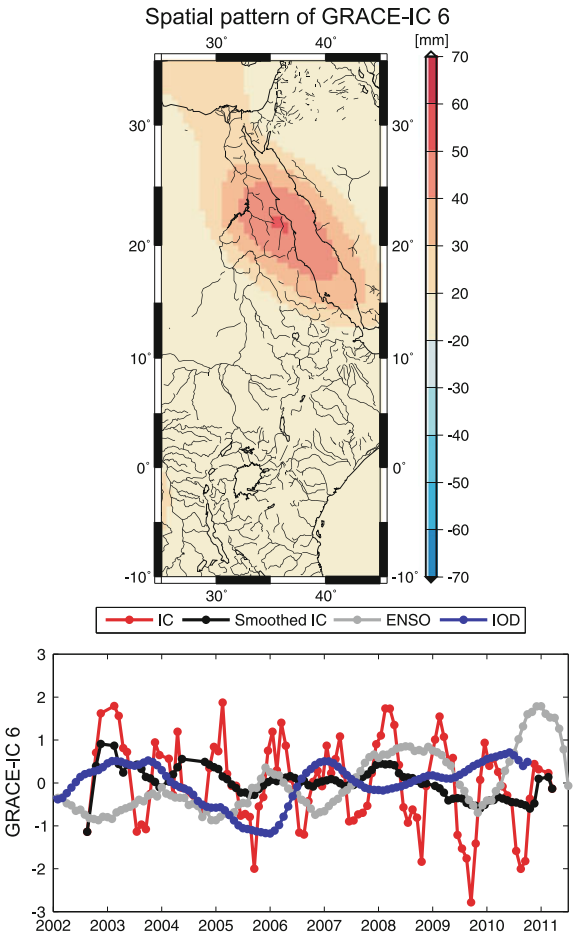


**Fig. 14.6** ICA analysis of the GRACE, GLDAS, and TRMM data for the Nile basin. In this figure the signals are localized within the Lake Nasser region in GRACE data set

example, the lands reclaimed amounted to 1200 ha in 1992 and 4200 ha in 2003, with the target of reclaiming a total of 75,000 ha by 2022, all of which will be irrigated using groundwater, [58, 59].

Positive correlations between the changes in total water storages and IOD corresponding to cool waters in the Indian Ocean associated with large scale circulation changes that leads to above average rainfall in East Africa leading to flooding, while Indonesia and several parts of Australia experience drought have been documented e.g., [60, 61]. This is true for the Lake Victoria Basin, the Ethiopian highlands and the Bar-El-Ghazal regions which are also related to ENSO. For the Lake Nasser region, the effect of climate variability is negligible. For the definitions and measured indices of ENSO and IOD, see Sect. 17.6.4.

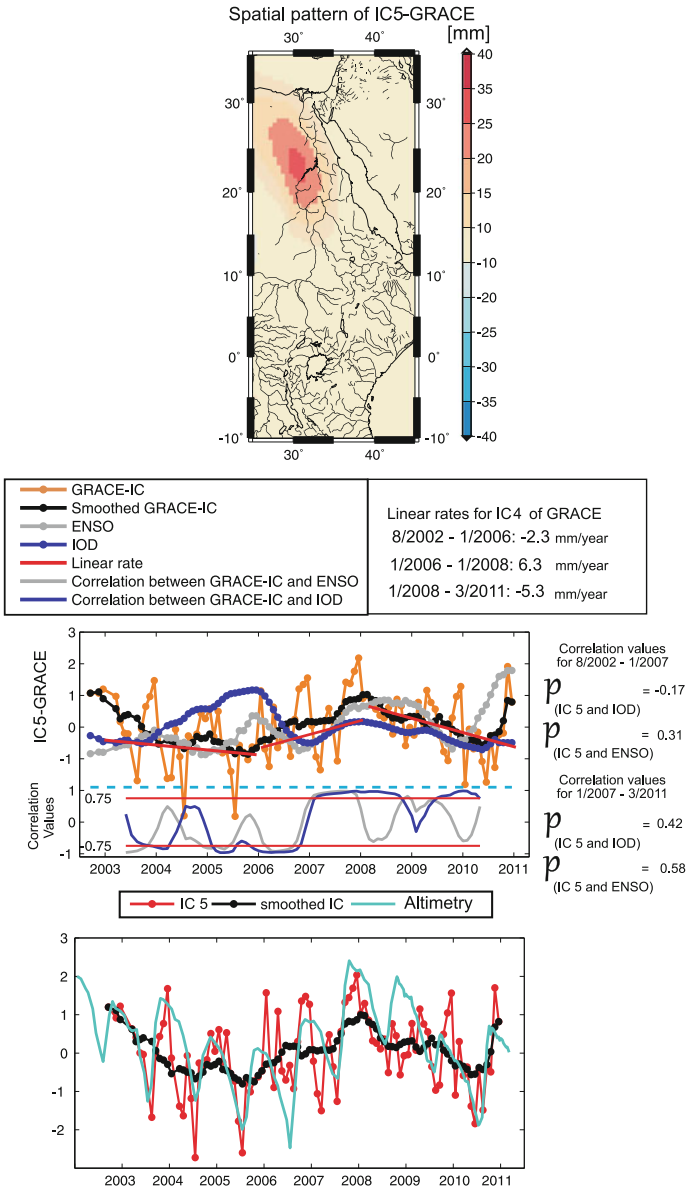


**Fig. 14.7** Dominant independent pattern of GRACE-TWS changes for the Nasser region derived from GRACE-TWS changes after correction for the water storage changes of the Red Sea (see Awange et al., [52] for more detail)


**Fig. 14.8** Lake Victoria basin. *Source* Kayombo and Jorgensen [65]

### 14.3.1.2 Lake Victoria Basin (LVB)

***Lake Victoria*** (Fig. 14.8), the world's third largest lake and the largest in the developing world, is a source of water for irrigation, transport, domestic and livestock uses, and supports the livelihood of more than 30 million people who live around it [45]. Nicholson [62, 63] documents its significance as an indicator of environmental and climate change over long-term scales. Since the 1960s, the lake level had experienced significant fluctuation, see e.g., [62, 63]. From 2001 to 2006, however, Lake Victoria's water level showed a dramatic fall that alarmed water resource managers as to whether the lake was actually drying up. Kull [64] reported that the lake's levels fell by more than 1.1 m below the 10 year average.

With the receding of the lake waters, acres of land that were lost to the floods of the 1960s were fast being reclaimed, creating sources of conflicts between man and wildlife. In some beaches, e.g., Usoma in Kenya, wetlands that were once breeding places for fish were dying up, leaving areas of land as playing fields for children and farmland. Ships were now forced to dock deep inside the lake, while the landing bays needed to be extended. Those who directly depended on the lake waters for domestic use were forced to go deeper into the lake to draw water, thus exposing women and children to water-borne diseases and risks of snakes and crocodiles. Water intakes that supplied major towns and cities had to be extended deeper into the lake, thus causing more financial burden to the municipalities that were already strained financially [42].

With 80% of Lake Victoria water coming from direct rainfall, changes in the lake level are directly related to the variation in the water stored in its basin, which contributes around 20% in the form of river discharge. A decrease in stored basin water was therefore suspected to contribute to the drop in the lake level. An analysis of the stored water in the Lake Victoria basin in relation to rainfall and evaporation was therefore necessary as a first diagnosis. This would provide water resource managers and planners with information on the state and changing trend of the stored water within the basin. Such basin scale observations could only be achieved through the use of satellites such as GRACE. Conventional methods for studying variations in stored water such as the Artificial Neural Network, GIS (Geographical Information System) and remote sensing could not diagnose the problem, see e.g., [42].

Having been motivated by the potential of the GRACE satellites, Awange et al. [41, 42] undertook a satellite analysis of the entire lake basin in an attempt to establish the cause of the decline in Lake Victoria's water levels. The GRACE and CHAMP satellites (Fig. 9.9 on p. 161) together with data from the TRMM satellite were employed in the analysis. Using 45 months of data spanning a period of 4 years (2002–2006), the GRACE satellite data were used to analyze the gravity field variation caused by changes in the stored waters within the lake basin. Figure 14.9 presents the annual variation of the geoid in the lake's basin during the high rain season months of March, April and May (MAM) for the period 2002–2006. The GRACE results indicated that the basin's total water storage dramatically decreased at a rate of 6.20 mm/month. These changes are expressed in equivalent water thickness (also known as total water storage (TWS)) in Fig. 14.10. For the period 2002–2006, the results indicate a general decline in the lake basin's water level at a rate of 1.83 km$^3$/month [42]).

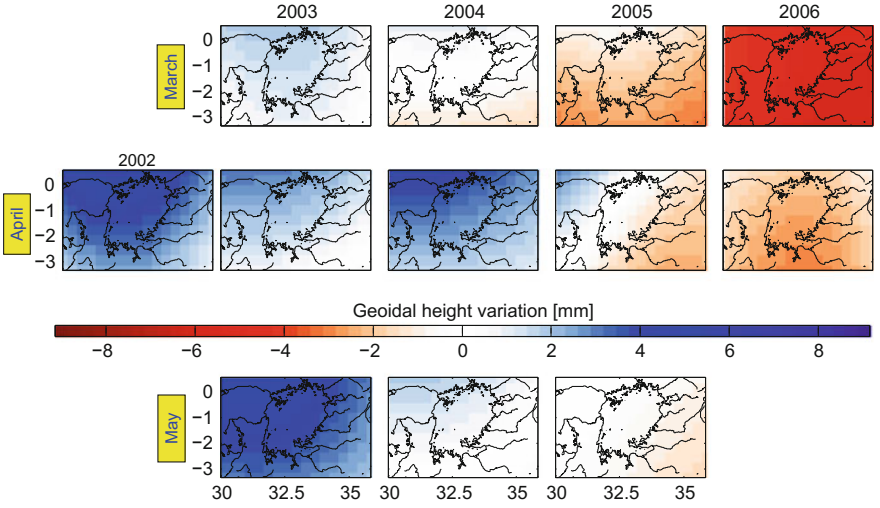


**Fig. 14.9** Inter-annual comparison in the geoid during the high rainy season of MAM from 2002–2006. The figure indicates a decline in total water storage in the Lake Victoria basin during this period. *Source* Awange et al. [42]

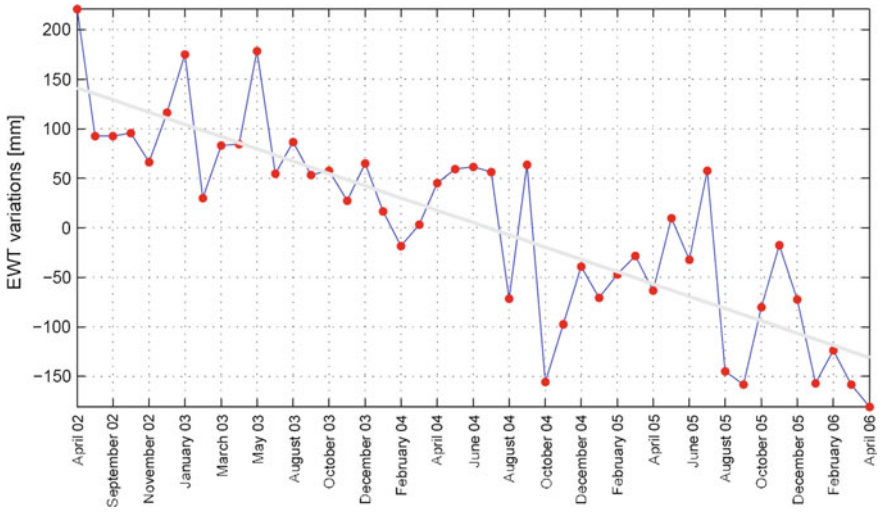


**Fig. 14.10** Lake Victoria basin total water storage (equivalent water *thickness*) changes between 2002–2006, as seen by the GRACE satellite. The figure indicates that the GRACE satellites observed a general decline in the lake's basin waters over this period (cf. Fig. 17.2 on p. 359 obtained from satellite altimetry). *Source* Awange et al. [42]

To validate the GRACE results, TRMM Level 3 monthly data for the same period of time were used to compute mean rainfall at a spatial resolution of $0.25° \times 0.25°$ ($25 \times 25$ km), as shown in Fig. 14.11, from which the rainfall trends were analyzed (Fig. 14.12). TRMM rainfall data over Africa has been validated, e.g., in Awange [66]. To assess the effect of evaporation, GNSS remote sensing data (59 CHAMP satellite occultations) for the period 2001–2006 were analyzed to define if tropopause warming took place (see the approach in Chap. 9). The results indicated that the tropopause temperature fell in 2002 by about 3.9 K and increased by 2.2 K in 2003 and remained above the 189.5 K value of 2002. The tropopause heights showed a steady increase from a height of 16.72 m in 2001 and remained above that value reaching a maximum of 17.59 km in 2005, an increase in height by 0.87 m. Temperatures did not, therefore, increase drastically to cause massive evaporation. TRMM results indicated the rainfall over the basin (and directly over the lake) to have been stable during this period (see Figs. 14.11 and 14.12). Since rainfall over the period remained stable, and temperatures did not increase drastically to cause increased evaporation, the remaining major contributor during the period 2002–2006 was suspected to be discharge from the expanded Owen Falls dam. Awange et al. [42] concluded, thanks to the GRACE and GNSS satellites, that the fall in Lake Victoria's water level between 2001 and 2006, also noted in Sect. 14.3.1, was due to human impact on the basin's environment (i.e., expanded dam) as opposed to natural factors.

In a related work, Swenson and Wahr [67] used satellite gravimetric and altimetric data to study trends in water storage and lake levels of multiple lakes in the Great Rift Valley region of East Africa for the years 2003–2008. GRACE total water storage

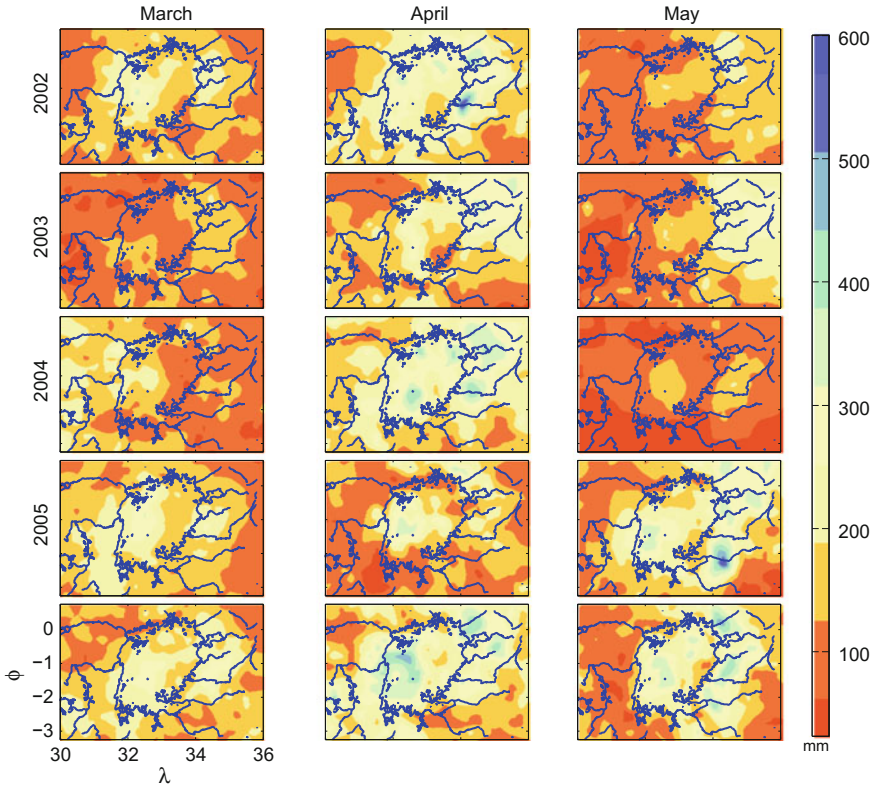


**Fig. 14.11** Inter-annual comparison of rainfall over the Lake Victoria basin during the high rainy season of MAM from 2002–2006 using TRMM results. *Source* Awange et al. [42]

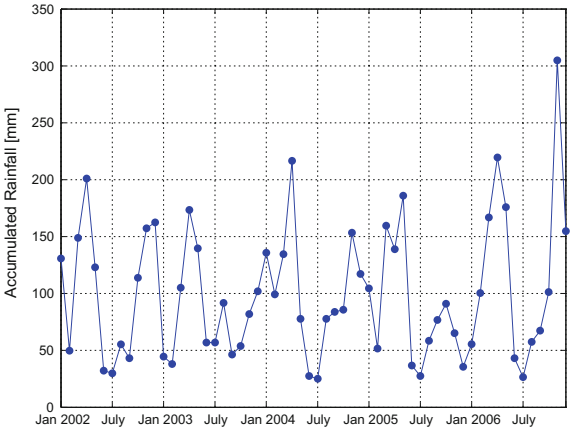


**Fig. 14.12** Time series of rainfall 2002–2006 for the lake Victoria basin as observed by the TRMM satellite. *Source* Awange et al. [42]

estimated by Swenson and Wahr [67] corroborated the findings of Awange et al. [42] that the lake's water level had declined by as much as 60 mm/year, while their altimetric data indicated that levels in some large lakes in the East African region dropped by as much as 1–2 m. Swenson and Wahr [67] concluded that the largest decline occurred in Lake Victoria and, like Awange et al. [42], attributed this to the role of human activities.

Both the findings of Awange et al. [42] and Swenson and Wahr [67] provide evidence that the GRACE satellites (supported by GNSS) could be used to provide independent means of assessing the relative impacts of climate and human activities on the balance of stored water that does not depend on in-situ observations, such as dam discharge values, which may not be available to the public domain.

#### 14.3.1.3 Application of GNSS to LVB Water Conflict Resolution

Let us revisit Fig. 2.1 on p. 19 where we have three boats with fishermen from each of the three East African countries that boarder Lake Victoria. If the three boats were in the middle of the Lake, with no visible land mark on the horizon, the fishermen would be at a loss to know which country owns that portion of the lake. In this case, they will not know whether they are in Kenyan, Ugandan or Tanzanian territory. Fishermen have frequently found themselves in this situation and the end result has often been conflict, leading to arrests and the confiscation of boats and fishing equipment. In such cases, hand-held GNSS receivers and a map could easily resolve such a dilemma. A real-case scenario is illustrated by Migingo Island in Fig. 14.13,[4] which is an island currently disputed between Kenya and Uganda due to it being home to the dwindling Nile Perch (*Lates niloticus*) fish. Owing to uncertainty about the boundary, GNSS receivers were used by a team of surveyors from both countries to mark the boundary and establish that the disputed island belongs to Kenya.

### *14.3.2 Understanding the Decline of Lake Naivasha*

#### 14.3.2.1 The Lake Naivasha Basin

Lake Naivasha (00° 40' S - 00° 53' S, 36° 15' E - 36° 30' E) is the second largest fresh water lake in Kenya with a maximum depth of 8 m. It is situated in the Central African Rift Valley at an altitude of 1890 m above sea level and is approximately 80 km northwest of the Kenyan capital, Nairobi. Its basin (Fig. 14.14) lies within the semi-arid belt of Kenya with mean annual rainfall varying from about 600 mm at the Naivasha township to some 1,700 mm along the slopes of the Nyandarua mountains, with open water evaporation estimated to be approximately 1,720 mm/year [68]. Mount Kenya and the Nyandarua Range capture moisture from the monsoon winds,

[4] Source: http://www.nation.co.ke.

**Fig. 14.13** The disputed Migingo Island in Lake Victoria (right). GNSS receivers were used to establish that the island belongs to Kenya, thus resolving a territorial dispute between Kenya and Uganda. *Source* Daily Nation, Kenya

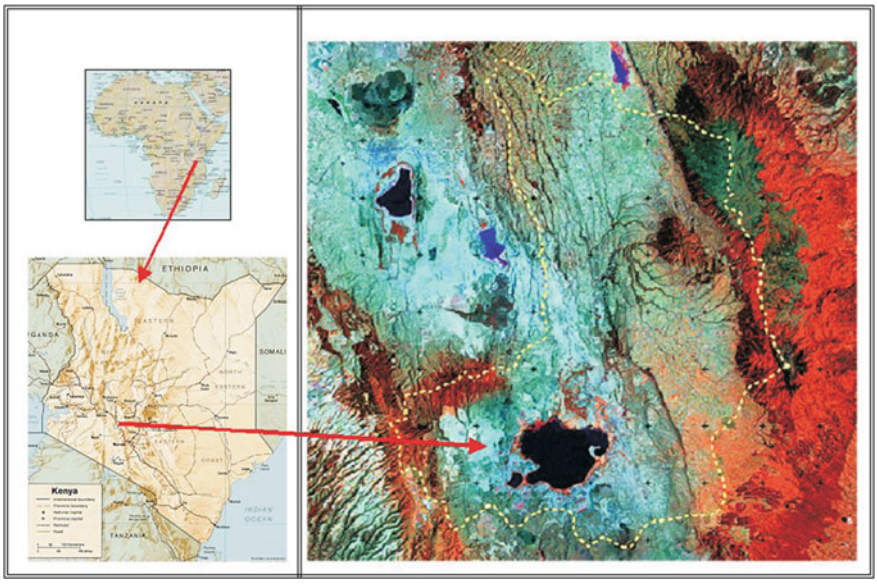


**Fig. 14.14** Location map of the Lake Naivasha Basin. *Source* Becht et al. [68]

thereby casting a significant rain shadow over the Lake Naivasha basin [68]. Unlike Lake Victoria, which has its highest rainfall during the March–April–May (MAM) wet season, e.g., [42, 69], Lake Naivasha basin experiences its highest rainfall period during April–May–June (AMJ). There is also a short rainy season from October to November. The lake's levels therefore follow this seasonal pattern of rainfall cycle, with changes of several meters possible over a few months. Imposed upon this seasonal behaviour are longer-term trends, for example, there has been a change in the lake's water level of 12 m over the past 100 years [68].

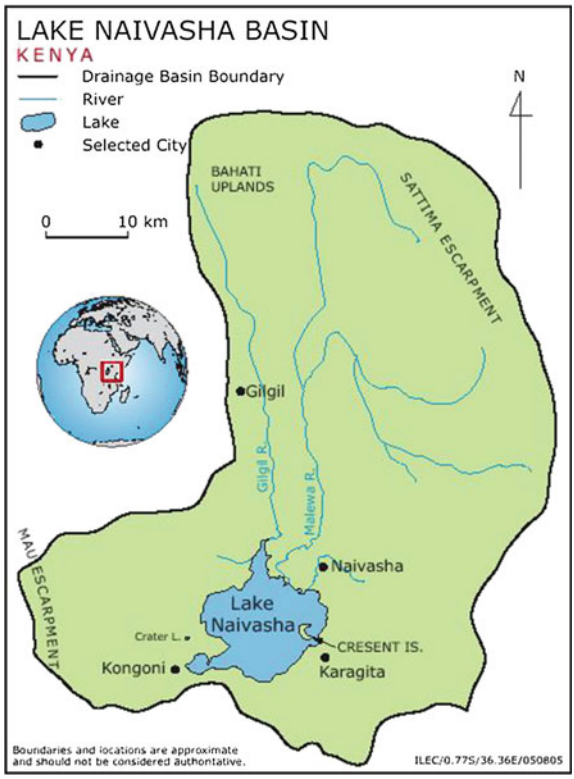


**Fig. 14.15** The Lake Naivasha drainage system. Three rivers flow into the Lake; Gilgil, Malewa, and Karati. The Lake's outlet is through an underground system to the south. *Source* Becht et al. [68]

The lake is fed by three main river systems: the Gilgil, the Malewa and the Karati, the last of which only flows during the wet season (see Fig. 14.15). There is also a groundwater inlet into the lake from the north, and an outlet to the south, which when combined with the river systems and the biochemical and geochemical sedimentation processes that remove ions such as sulphates and carbonates from the water, results in the freshness of the lake [70, 71]. Becht et al. [68] state that whereas a small portion of the groundwater evaporates and escapes in the form of fumaroles in the geothermal areas, the remaining water flows into Lakes Magadi and Elmentaita, taking thousands of years to reach them. The basin's water balance has been calculated from a model based upon long-term meteorological observations of rainfall, evaporation and river inflows [72]. This model reproduced the observed level from 1932 to 1982 with an accuracy of 95% of the observed monthly level, differing by 0.52 m or less [73]. This pattern was, however, noticed to deviate after 1982 and by 1997, the difference had reached 3–4 m [68]. In fact, the onset of this reduced ability to model the lake's level coincides with the increase in horticultural and floricultural activities.

In general, three contemporary global water issues can be identified as occurring in this region, namely *water scarcity/availability*, *water quality*, and *water security*. Several previous works have focused on the problem of water quality and competition

for water resources within the area. Water quality studies have endeavoured to analyze the physical, chemical and biological characteristics of the water, which represents a measure of the condition of water relative to the requirements of one or more biotic species and/or to any human need or purpose. Most studies have concluded that the main causative factors for the deterioration of the water quality of Lake Naivasha are the large quantities of sediment inflow from the catchments of the Malewa and Gilgil Rivers, polluting inflows from Naivasha town and the intensive floriculture enterprizes adjacent to the lake, see e.g., [74]. These pollutants include high levels of phosphates, nitrates, pesticide residues and other agro-chemicals.

The use of GNSS in monitoring water pollution discussed in Sect. 18.2 could also be applied to Lake Naivasha to map the sources of point pollutants. Although water security issues are a reality in the Lake Naivasha basin, few studies have been done to better understand the underlying issues. Carolina [75] asserts that the area of Lake Naivasha basin is of high economic and political importance to Kenya, which presents a wide variety of economic activities around the water resources with many different stakeholders often competing for the water resources.

The flower industry in Kenya has experienced a phenomenal growth, maintaining an average growth rate of 20% per year over the last decade. It is an industry that is the second largest export earner for Kenya, employing between 50,000 – 60,000 people directly and 500,000 others indirectly through affiliated services [76]. Although flowers are now grown in many areas with temperate climate and an altitude above 1,500 m in Kenya, the region around Lake Naivasha still remains the nation's main floriculture farming center. The foremost categories of cut flowers exported from Kenya include: roses, carnations, statice, alstromeria, lilies and hyperricum. Indeed, Kenya is arguably the largest exporter for flowers in the world, supplying over 35% of cut flowers to the world's largest market - the European Union [76].

#### 14.3.2.2 Impacts of Flower Farming

Lake Naivasha (Kenya) is the only freshwater lake in the Great Rift Valley of East Africa in an otherwise soda/saline lake series [77]. In fact, it is the freshness of the water of Lake Naivasha that is the basis for its diverse ecology [71]. However, recent years have seen a rapid decline in its extent to the point where questions are being raised in the local media as to whether the lake is actually dying.

So unique is Lake Naivasha in the chain of East African Rift Valley lakes that in 1995 it was declared a Ramsar site due to its importance as a wetland. Lake Naivasha and its basin supports a rich ecosystem, with hundreds of bird species, papyrus fringes filled with hippos, riparian grass lands where waterbuck, giraffe, zebra and antelopes graze, dense patches of riparian acacia forest with buffaloes, bushbuck and other species, swampy areas where waterfowl breed and feed and, at the same time, magnificent views of the nearby volcanoes [68]. The lake also supports local fishery and tourism, and is used for recreation, water sports, subsistence farming and hunting. The surrounding lands are dominated by the cultivation of flowers, vegetables, fruit and cereals, as well as power generation [72].

In fact, the *floriculture* industry in this area provides large quantities of flowers that are exported to Europe and other countries of the world. The growth in the flower industry has been favored by the permeable and fertile soils, low rainfall, reliable supply of good quality water, favourable climatic conditions, availability of cheap labour, and easy access to Nairobi airport [68]. Since much of the water used in the flower farms comes from irrigation, the only source, therefore, is the lake and its basin. The lake and basin also supply drinking water to Nakuru (of which Naivasha is part of, with a population of about 1.6 million as per the 2009 census) located 160 km north west of Nairobi.

The study of fluctuations in Lake Naivasha's water levels has been carried out, e.g., by [62, 78]. Richardson and Richardson [78], for instance, state that the lake was nearly twice as extensive in the 1920s as it was in 1960–61. Nicholson [62] noted trends of lower levels during the first half of the 19th century, very high levels during the last decades of the 19th century, with a rapid decrease occurring during the 20th century. He further points out that the lake returned to a relatively large extent during the 1960s, but this ended in the 1970s, a fact also stated by Richardson and Richardson [78] who point out that the wetter years beginning in 1961 saw a sharp rise in the levels of Lake Naivasha, as well as of Lakes Elmenteita and Nakuru. The decrease in the lake's water level between the 1920 to 1960s is attributed by Richardson and Richardson [78] to a slight trend of decreasing rainfall during this period, averaging 5 mm/year over the basin, between 1920 and 1949 (see also [79]), as well as an increase in human consumption from river influent and boreholes.

In the 1980s, the fall of the lake's level continued, with the local Olkaria geothermal power station and subsurface drainage thought to be the main culprits [80]. But then, there was little notice taken of the influence of the flower farms, since the first farms had just started in the early 1980s, see e.g., [68]. However, during the 1990s, over 100 $km^2$ of land around lake Naivasha was converted to floriculture for the European-cut flower trade, e.g., [73]. With this growth came an influx of workers leading to a greater extraction of water from the lake, local aquifers, and the inflowing rivers for the agriculture, floriculture and domestic use by the rapidly increasing population [73].

At this point, the impact of such development on the lake's resources begun to be felt, with its size shrinking due to this direct extraction from the lake and also indirectly from closely connected aquifers. In the work of Abiya [81], the exploitation of the resources of Lake Naivasha is said to pose serious threats to the fragile lake ecosystem and its biodiversity. Abiya [81] considered the dynamics of the changing lake ecosystem, the imminent threats to this system, and the community-based approach towards the sustainable utilization of the lake. Their study showed that the sustainable use of the lake was not going to be fully realized without a sound management plan, and recommended the enaction of consolidated environmental legislation in Kenya, which will enable the strengthening of environmental conservation and the protection of natural resources [81]. This in turn has led to other proposals for the sustainable use of the lake and basin, e.g., [70, 71].

In the last decade, the lake's level has continued to drop with floriculture being blamed for excessive water extraction from the lake and aquifers, and the small holder farms in the upper catchment being blamed for nutrient loadings, see e.g., [73, 82], leading to outcry in both the local and international media that this Ramsar site could be dying as a result of the very resource that it supports, see e.g., [82]. For example, Mekonnen and Hoekstra [82] observed that the total virtual water exported in relation to the cut flower industry from the Lake Naivasha basin was 16 $Mm^3$/yr during the period 1996–2005. Other factors that have also been proposed as influencing Lake Naivasha's water changes include irregular rainfall patterns [71], and trade winds [83]. All of these discussions therefore point to the need for the *reliable mapping* of the lake and its basin in order to properly understand the dynamics of this area. This need for accurately monitoring the lake was captured by Becht and Harper [72], who state that there is an urgent need to accurately measure all abstractions and provide consistent, reliable, hydrological and meteorological data from the catchment, so that a 'safe' yield may be agreed upon by all stakeholders and the sustainable use of the lake waters achieved.

However, lack of reliable basin mapping techniques hampered the proper mapping of changes in the lake basin, while also not allowing accurate predictions of the likely future situation, despite modelling methods being used to calculate its water balance, e.g., [72]. The situation is compounded by the fact that Lake Naivasha has no surface outlet that could assist in hydrological monitoring, and the fact that changes in its water level occur rapidly, over the order of several meters over just a few months, shifting the shoreline by several meters [68].

The emergence of satellite based methods offers the possibility of providing a broader and more integrated analysis of the lake and its basin. Using products from the GRACE gravity mission, changes in the stored water in the region extending from the Lake Naivasha basin to Lake Victoria may be assessed to determine whether the changes are climatic or human induced. Changes in precipitation can be examined by the analysis of products from the TRMM, allowing the determination of how much of the fluctuations in Lake Naivasha are related to changes in precipitation behaviour.

The fluctuations in the water level of Lake Naivasha can be determined using both ground-based tide gauge observations and satellite altimetry data (TOPEX/Poseidon and Jason-1; see Sect. 9.4 on the contribution of GNSS). These results may in turn be related to the use of satellite imagery (e.g., Landsat) and change detection techniques to map the shoreline changes of Lake Naivasha, analyzing the trend of changes over the period of interest, and correlating shoreline changes with proposed causes. In general, the combination of different data sets, both space-borne and ground based, provide a valuable contribution to understanding the hydrological behaviour of the East African Great Lakes region, e.g., [60].

Example 14.1 (Satellite-based monitoring [84]).

Several different types of space-borne observations were used in Awange et al. [84]:

(1) GRACE gravity-field products (2) precipitation records based on TRMM products (3) satellite remote sensing (Landsat) images (4) satellite altimetry data

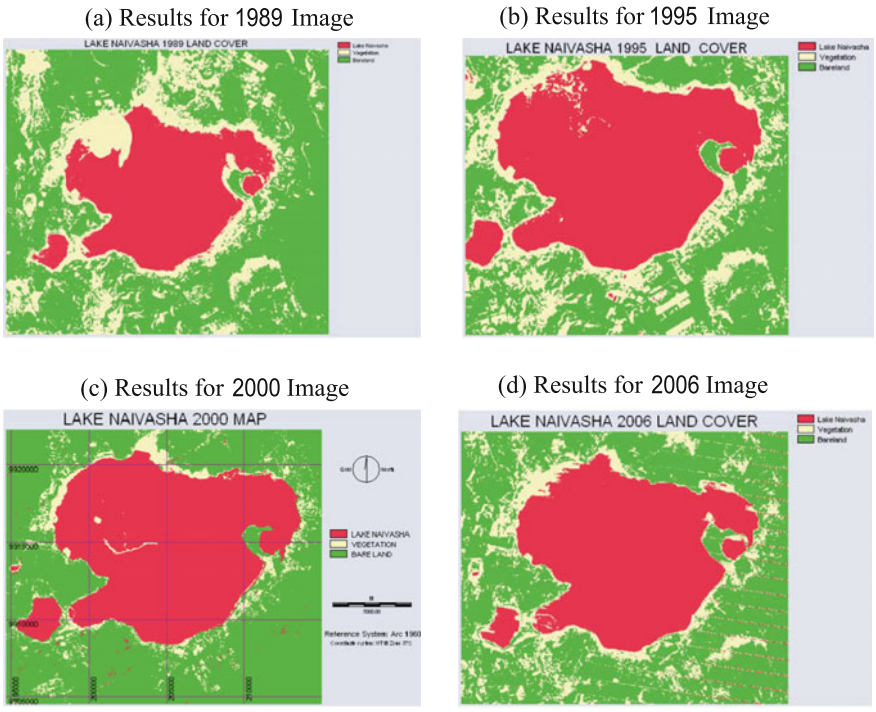


**Fig. 14.16** Surface-type classification results for the considered Landsat images. **a** 1989, **b** 1995, **c** 2000 and **d** 2006. GNSS satellites were used to georeference the satellite images. *Source* Awange et al. [84]

and (5) flower production data. In addition, data from an in-situ tide-gauge station were used. The results of Awange et al. [84] confirm that Lake Naivasha has been steadily declining with the situation being exacerbated from around the year 2000, e.g., Fig. 14.18, with water levels declining at a rate of –10.2 cm/yr and a shrinkage in area of –1.04 km$^2$/year (see e.g., Fig. 14.16 where GNSS was used to *georeference* the satellite imagery). This rapid decline can be traced largely to anthropogenic activities, a proposal supported by a coefficient of correlation $R^2$ value of 0.976 between the quantity of flower production and the lake's level for the period 2002–2010 (Fig. 14.17), a period during which such production doubled, see e.g., Fig. 14.19. These results, supported by the use of GNSS show that there is therefore a need for those different communities and interest groups that depend upon Lake Naivasha to better formulate their management plans, a need which can exploit results such as those presented in [84].

♣ End of Example 14.1.

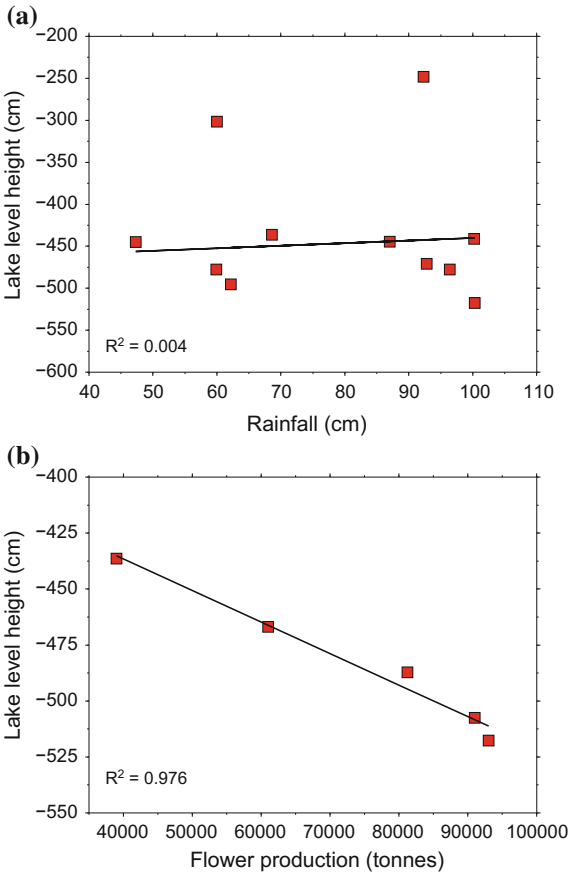


**Fig. 14.17** Comparing annual average lake levels with **a** TRMM rainfall and **b** flower exports. The solid lines are fitted linear trends, along with their correlation coefficient. A strong correlation coefficient (0.976) is noticed between the Lake's level and flower export between 2002–2010, the period when the flower export picked (see Fig. 14.19). *Source* Awange et al. [84]

### *14.3.3 Water, a Critical Dwindling Australian Resource*

Warning of Australia's acute water problem (see e.g., Fig. 14.20) had already been sounded by the National Land and Water Resource Audit (NLWRA [85]), which reported that Australian water resources were scarce and in high demand by agricultural, industrial and urban users. The alarming finding of the report was the fact that 26% of the river basins and 34% of the groundwater management units in Australia were approaching or beyond sustainable extraction limits.

The NLWRA highlighted the need for information that could assist in improving water resource management and conservation. Steffen et al. [86] issued a further alert that Australia would be faced with the impacts of climate change on its water quantity due to decrease in precipitation over parts of Australia.

Even though the need for up-to-date information on stored water resource to support policy formulation and management issues had already been realized, e.g., NLWRA [85], and specifically with the prevailing drought conditions in Australia,

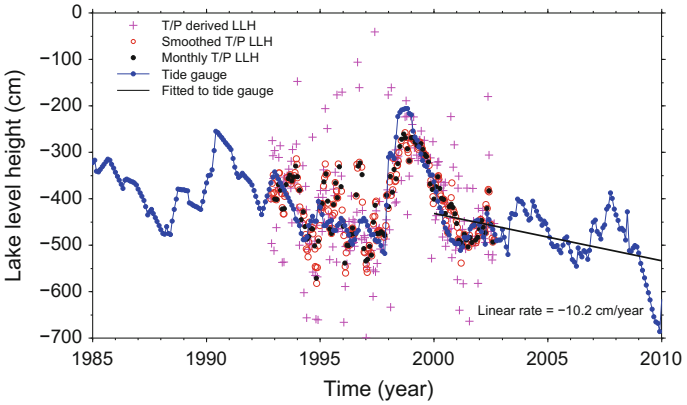


**Fig. 14.18** Time Series of lake level height (LLH) changes for Lake Naivasha as provided by satellite altimetry (T/P), and a tide gauge. GNSS satellites support the satellite altimetry as discussed in Sect. 9.4. *Source* Awange et al. [84]

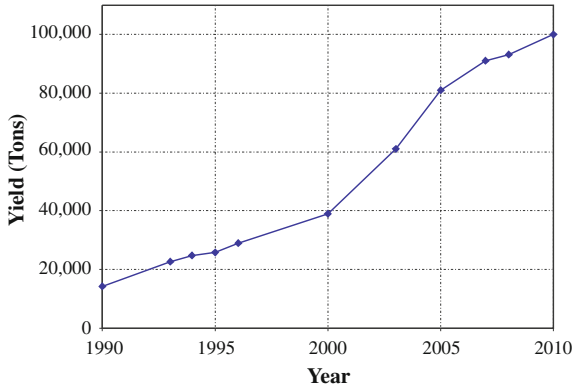


**Fig. 14.19** Annual flower exports from Kenya. *Source* Awange et al. [84]

the lack of appropriate techniques that offered high spatial and temporal resolution monitoring of changes in stored water remained a stumbling block [11]. The problem was further compounded by the fact that groundwater suitable for human consumption and utility is normally trapped inside aquifers (see Sect. 14.1) that are beyond reach of modern remote sensing methods. With the introduction of GRACE satellites (Sect. 9.3.3), however, the situation changed. In Awange et al., [28], its possibility to monitor changes in Australia's stored water was reported.

Example 14.2 (Monitoring changes in Australia's stored water [10]).

In order to use the GRACE satellite for monitoring the variation in Australia's stored water, Awange et al. [10] investigated the regional $4° \times 4°$ mascon (mass concentration) GRACE solutions provided by GSFC (Goddard Space Flight Center, NASA) for their suitability for monitoring Australian hydrology, with a particular focus on

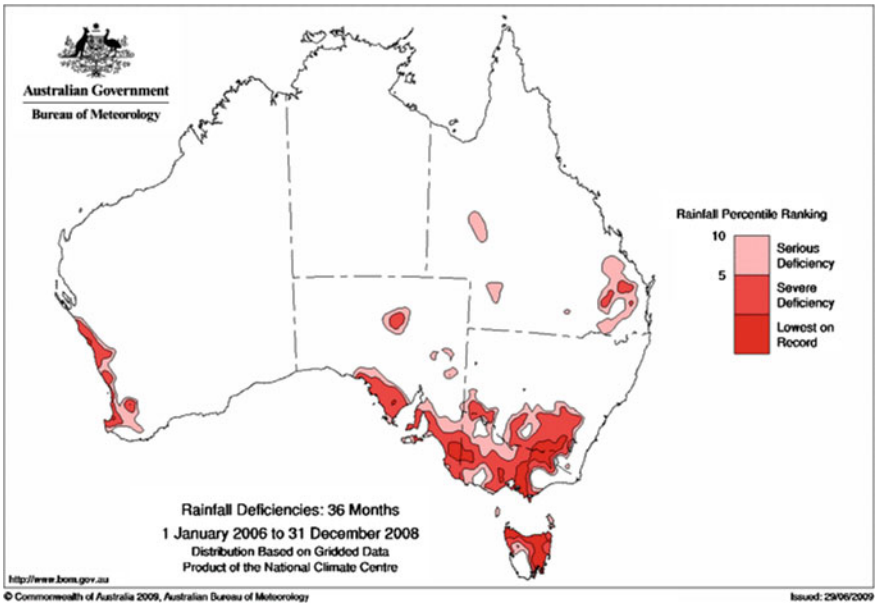


**Fig. 14.20** Rainfall deficiencies for the period 1st January 2006 to 31st December 2008 (3 years, Source: BOM)

the Murray-Darling Basin (MDB). Using principal component analysis (PCA) and multi-linear regression analysis (MLRA), the main components of the spatial and temporal variability in the mascon solutions over both the Australian continent as a whole and the MDB in particular were analysed and the results compared to those from global solutions provided by CSR (the Center for Space Research, University of Texas at Austin) and CNES/GRGS (Centre National d'Études Spatiales/Groupe de Recherche de Geodesie Spatiale, France) and validated using TRMM, water storage changes predicted by the WaterGap Global Hydrological Model (WGHM) and ground-truth (river-gauge) observations. The results of Awange et al. [10] indicated that for the challenging Australian case with weaker hydrological signals, all the solutions gave similar results.

For the PCA results in Fig. 14.21, the Australia-wide case was considered mainly to compare the different GRACE releases among themselves and with TRMM and WGHM time-series. The results of the PCA analysis for the first two modes are shown in Fig. 14.21. It was noticed that most of the variability were contained in the first mode (>50%), while considering the first 2 modes accommodates between 63% (for CNES/GRGS) and 81% (for mascon) of the total variability of each signal. The 1st mode (upper panel, Fig. 14.21) shows similar behaviour among all data sets, with all data displaying a general north-south varying empirical orthogonal function (EOF) pattern and strong annual signal in the principle components (PC), indicative of seasonal variations. The annual signal is also apparent in the 2nd PC mode (lower panel, Fig. 14.21), especially for the GRACE time-series, although less so for the filtered TRMM and WGHM results.

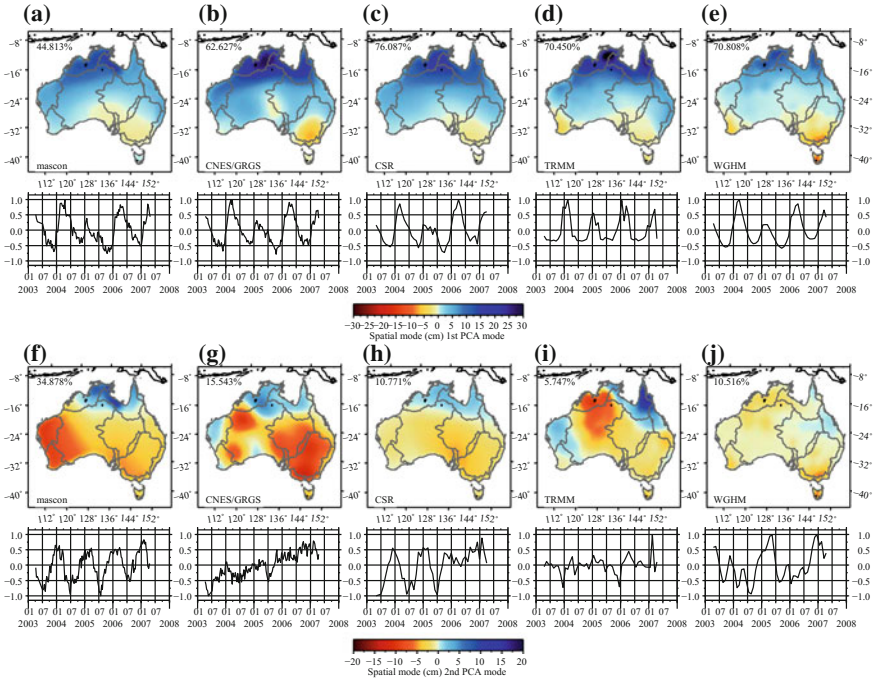


**Fig. 14.21** Results of the PCA applied to the whole of Australia for the 1st and 2nd modes. *Top rows* **a**–**e** the 1st mode results, *bottom rows* **f**–**j** the 2nd mode results. **a**, **f** mascon, **b**, **g** CNES/GRGS, **c**, **h** CSR, **d**, **i** TRMM and **e**, **j** WGHM. Australias drainage divisions (from the Australian Bureau of Meteorology, see the Acknowledgements) are marked by the *grey* boundaries (Lambert conformal conic projection). *Source* Awange et al. [10]

The dominant signal in northern Australia is a result of the annual monsoonal rains, and is much stronger than that in the southern part of the continent. Therefore, the 1st mode is dominated by changes in the north, which may lead to smaller hydrological changes in the south being excluded from this mode. The northern signal is very obvious in the 1st mode EOF patterns for all data sets examined, and also in the 2nd mode EOF for the mascon, CNES/GRGS, CSR and TRMM time-series. The PC of the 2nd modes also appears to show strong linear trends in the time-series, especially for the CNES/GRGS and CSR results. For both the 1st and 2nd modes, Central Australia shows a relatively low signal, a consequence of the aridity of this area having small hydrological changes. The shift in the seasons that receive the high rainfall (summer in the north, winter in the south) can be seen by the opposite signs in the signals given by the EOF (time-series in the upper panels, Fig. 14.21).

The Australia-wide results therefore show that all the GRACE solutions provided similar results and were able to identify the major climatological features of Australia, in particular the dominance of the monsoonal rainfall over northern Australia, and the offset (∼6 months) between the northern and southern wet seasons, as well

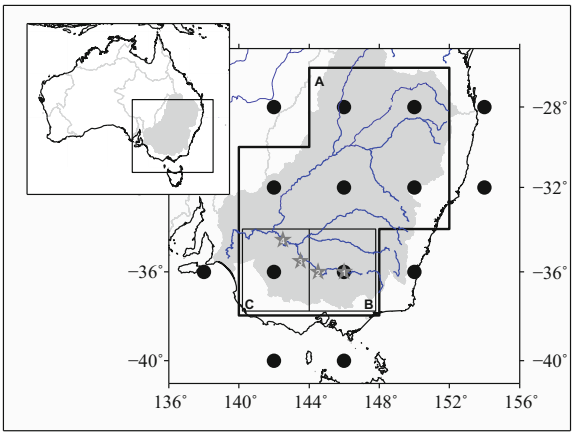


**Fig. 14.22** Location map of the Murray-Darling Basin (MDB). The *grey shading* marks the basins extent, with Australias other river basins also outlined in *grey*. Black filled circles are the centres of the mascon grid cells provided by GSFC (4° × 4° grid). The *thick black*-bounded area (A) covers most of the MDB, while the finer *black*-bounded areas (B and C) are examined with respect to ground-truth data in the form of river-gauge data (numbered stars). The river-gauges are at Yarrawonga (1), Swan Hill (2), Euston (3) and Torrumbarry (4). *Source* Awange et al. [10]

as the areas of mass gain (northern Australia) and loss (the MDB in the southeast and southwest Western Australia).

♣ End of Example 14.2.

Example 14.3 (Localised Murray-Darling Basin. Source: Awange et al. [10]).

Awange et al. [10] further examined the MDB to determine how the GRACE solutions performed for more localized areas, since the MDB is one of Australia's most important regions for agricultural production and is an area that has been severely affected by the recent drought conditions [87, 88]. First, they examined the area outlined in Fig. 14.22 denoted as A, which is defined by the mascon grid elements that cover much of the MDB. Figure 14.23 compared the inferred stored water variation from each data set.

Examining the three GRACE solutions in Fig. 14.23 over the time period covered by the mascon solutions (grey shaded area), Awange et al. [10] noted that the time-series generally follow each other reasonably well, as also shown by the resulting cross correlation values, i.e., CSR and CNE/GRGS, being global solutions, appear to be in closer agreement with each other ($R = 0.83$), than when compared to the mascon (mascon to CNES/GRGS, $R = 0.70$, and mascon to CSR, $R = 0.74$). The correlation between GRACE solutions is relatively high ($>0.7$), although much poorer when the GRACE solutions are compared to the TRMM and WGHM time-series ($<0.5$).

♣ End of Example 14.3.

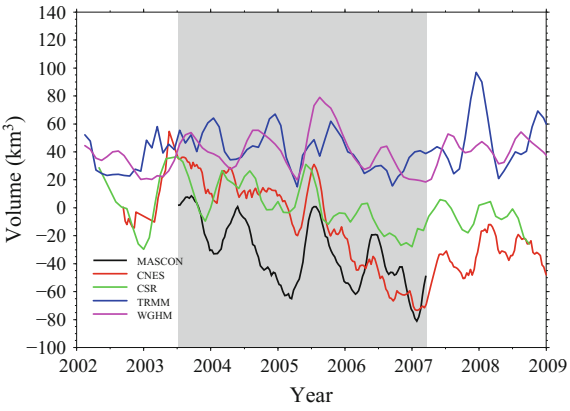


**Fig. 14.23** The change in water storage over the MDB, as outlined by sector A in Fig. 14.22 for the data sets used in this work. A three-month moving average has been applied to each time-series. The *gray shading* marks the time span over which the mascon solutions are available. Cross-correlations between pairs of data sets are listed in Awange et al. [10]

## 14.4 Concluding Remarks

The GRACE satellites had been recognized as having the potential to provide the first space-based estimate of changes in terrestrial water storage. In essence, it is a tool that will assist water managers in conserving and controlling the utilization of dwindling water resources in a sustainable way. Water is arguably one of the most precious resource in the world, therefore, it is logical to try to monitor its distribution as efficiently as possible, and GRACE offers one such opportunity, see e.g., [89]. This is because one of the environmentally important signals detected by GRACE is the temporal gravity field variation induced by changes in the distribution of water on and below the Earth's surface, i.e., hydrology, e.g., [28]. Satellite altimetry provides the possibility of monitoring sea or lake surface heights as was demonstrated for Lake Naivasha. GNSS plays a pivot role in supporting these satellites as discussed in Chap. 9. GNSS also plays a major role in providing location-based information for monitoring groundwater wells, and source of water pollutants as discussed in Chap. 18. Its application to coastal water resource are presented in the next chapter. Other studies undertaken with respect to use of GRACE to monitor hydrology include, e.g., [90–93].

## References

1. Phillips S (2006) Water crisis. COSMOS (9). http://www.cosmosmagazine.com/issues/2006/9/
2. UNEP (2002) A World of salt: total global saltwater and freshwater estimates. http://www.unep.org/dewa/assessments/ecosystems/water/vitalwater/freshwater.htm. Accessed 25 Aug 2010
3. Hofman AR (2004) The connection: water and energy security. http://www.iags.org/n0813043.htm. Accessed on 25 Aug 2010
4. IRIN humanitarian news and analysis, UN office for coordination of humanitarian affairs (2006). Global: The global water crisis: managing a dwindling resource. http://www.irinews.org. Accessed 25 Sep 2011

5. World Bank (2003) Water resource and environment. In: Davis R, Hirji R (eds). Technical note G.2, Lake Management
6. Taylor CJ, Alley WM (2001) Ground-water-level monitoring and the importance of long-term water-level data. U.S. Geological Survey Circular 1217, Denver, Colorado
7. Rieser D, Kuhn M, Pail1 R, Anjasmara IM, Awange J, (2010) Relation between GRACE-derived surface mass variations and precipitation over Australia. Aust J Earth Sci 57(7):887–900. doi:10.1080/08120099.2010.512645
8. van Dijk AIJM, Beck HE, Crosbie RS, de Jeu RAM, Liu YY, Podger GM, Timbal B, Viney NR (2013) The millennium drought in southeast Australia (2001–2009): natural and human causes and implications for water resources, ecosystems, economy, and society. In: Water resource research, vol 49, pp 1040–1057. doi:10.1002/wrcr.20123
9. IPCC (Intergovernmental Panel on Climate Change) (2007) Contribution of working group i to the fourth assessment report
10. Awange JL, Fleming KM, Kuhn M, Featherstone WE, Heck B, Anjasmara I (2011) On the suitability of the 4° × 4° GRACE mascon solutions for remote sensing Australian hydrology. Remote Sens Environ 115:864–875. doi:10.1016/j.rse.2010.11.014
11. Ellett KM, Walker JP, Rodell M, Chen JL, Western AW (2005) GRACE gravity fields as a new measure for assessing large-scale hydrological models. In: Zerger A, Argent RM (eds) MODSIM 2005 international congress on modelling and simulation. The Modelling and Simulation Society of Australia and New Zealand, December 2005, pp 2911–2917. ISBN: 0-9758400-2-9
12. Casanova MT (1994) Vegetative and reproductive responses of charophytes to water-level fluctuations in permanent and temporary wetlands in Australia. Aust J Mar Freshw Res 45:1409–1419
13. Leick A (2004) GPS satellite surveying, 3rd edn. Wiley, New York
14. Brutsaert W (2005) Hydrology. An introduction. 4th edn. Cambridge University Press, New York
15. Montgomery EL (1971) Determination of coefficient of storage by use of gravity measurements. PhD Thesis, University of Arizona, Tucson
16. Leirião S, He X, Christiansen L, Andersen OB, Bauer-Gottwein P (2009) Calculation of the temporal gravity variation from spatially variable water storage change in soils and aquifers. J Hydrol 365(3–4):302–309. doi:10.1016/j.jhydrol.2008.11.040
17. Lambert A, Beaumont C (1977) Nano variation in gravity due to seasonal groundwater movements: implications for the gravitational detection of tectonic movements. J Geophys Res 82(2):297–306. doi:10.1029/JB082i002p00297
18. Goodkind JM (1986) Continuous measurement of nontidal variations of gravity. J Geophys Res 91(B9):9125–9134
19. Mukai A, Higashi T, Takemoto S, Nakagawa I, Naito I (1995) Accurate estimation of atmospheric effects on gravity observations made with a superconducting gravity meter at Kyoto. Phys Earth Planet Inter 91(1–3):149–159
20. Pool DR, Eychaner JH (1995) Measurements of aquifer-storage change and specific yield using gravity surveys. Groundwater 33(3):425–432. doi:10.1111/j.1745-6584.1995.tb00299.x
21. Bower DR, Courtier N (1998) Precipitation effects on gravity measurements at the Canadian Absolute Gravity Site. Phys Earth Planet Inter 106:353–369. doi:10.1016/S0031-9201(97)00101-5
22. Ellett KM, Walker JP, Western AW, Rodell M (2006) A framework for assessing the potential of remote sensed gravity to provide new insight on the hydrology of the Murray-Darling Basin. Aust J Water Resour 10(2):89–101
23. Smith AB, Walker JP, Western AW, Ellett KM (2005) Using ground based measurements to monitor changes in terrestrial water storage. In: 29th Hydrology and water resources symposium (CD Rom), Institute of Engineers Australia
24. Damiata BN, Lee TC (2002) Gravitational attraction of solids of revolution - part 1: vertical circular cylinder with radial variation of density. J Appl Geophys 50(3):333–349. doi:10.1016/S0926-9851(02)00151-9

25. Tapley BD, Bettadpur S, Ries JC, Thompson PF, Watkins MM (2004) GRACE measurements of mass variability in the Earth system. Science 305:503–505. doi:10.1126/science.1099192
26. Rodell M, Famiglietti JS, Chen J, Seneviratne SI, Viterbo P, Holl S, Wilson CR (2004) Basin scale estimates of evapotranspiration using GRACE and other observations. Geophys Res Lett 31:L20504. doi:10.1029/2004GL020873
27. Rodell M, Famiglietti JS (1999) Detectability of variations in continental water storage from satellite observations of the time dependent gravity field. Water Resour Res 35(9):2705–2724. doi:10.1029/1999WR900141
28. Awange JL, Sharifi MA, Baur O, Keller W, Featherstone WE, Kuhn M (2009) GRACE hydrological monitoring of Australia. Current limitations and future prospects. J Spat Sci 54(1):23–36. doi:10.1080/14498596.2009.9635164
29. Ramillien G, Cazenave A, Brunau O (2004) Global time variations of hydrological signals from GRACE satellite gravimetry. Geophys J Int 158(3):813–826. doi:10.1111/j.1365-246X.2004.02328.x
30. Ramillien G, Frappart F, Cazenave A, Gutner A (2005) Time variations of land water storage from an inversion of two years of GRACE geoids [rapid communication]. Earth Planet Sci Lett 235(1–2):283–301. doi:10.1016/j.epsl.2005.04.005
31. Andersen OB, Seneviratne SI, Hinderer J, Viterbo P (2005) GRACE-derived terrestrial water storage depletion associated with the 2003 European heat wave. Geophys Res Lett 32(L18405):2–5. doi:10.1029/2005GL023574
32. Neumeyer J, Barthelmes F, Dierks O, Flechtner F, Harnisch M, Harnisch G, Hinderer J, Imanishi Y, Kroner C, Meurers B, Petrovic S, Reigber C, Schmidt R, Schwintzer P, Sun HP, Virtanen H (2006) Combination of temporal gravity variations resulting from superconducting gravimeter (SG) recordings, GRACE satellite observations and global hydrology models. J Geodesy 79(10–11):573–585. doi:10.1007/s00190-005-0014-8
33. Yan JP, Hinderer M, Einsele G (2002) Geochemical evolution of closed-basin lakes: general model and application to Lakes Qinghai and Turkana. Sediment Geol 148(1–2):105–122. doi:10.1016/S0037-0738(01)00212-3
34. Syed T, Famiglietti J, Rodell M, Chen J, Wilson C (2008) Total basin discharge for the Amazon and Mississippi River basins from GRACE and a land-atmosphere water balance. Water Resour Res 44:W02433. doi:10.1029/2006WR005779
35. Rodell M, Chen J, Kato H, Famiglietti JS, Nigro J, Wilson CR (2006) Estimating groundwater storage changes in the Mississippi River basin (USA) using GRACE. Hydrogeol J 15(1):159–166. doi:10.1007/s10040-006-0103-7
36. Crowley JW, Mitrovica JX, Bailey RC, Tamisiea ME, Davis JL (2006) Land water storage within the Congo Basin inferred from GRACE satellite gravity data. Geophys Res Lett 33:L19402. doi:10.1029/2006GL027070
37. Schmidt R, Schwintzer P, Flechtner F, Reigber C, Güntner A, Döll P, Ramillien G, Cazenave A, Petrovic S, Jochmann H, Wünsch J (2006b) GRACE observations of changes in continental water storage. Glob Planet Change 50(1–2):112–126. doi:10.1016/j.gloplacha.2004.11.018
38. Swenson S, Wahr J, Milly PCD (2003) Estimated accuracies of regional water storage variations inferred from the gravity recovery and climate experiment (GRACE). Water Resour Res 39(8):1223. doi:10.1029/2002WR001736
39. Swenson S, Yeh PJ-F, Wahr J, Famiglietti J (2006) A comparison of terrestrial water storage variations from GRACE with in situ measurements from Illinois. Geophys Res Lett 33:L16401. doi:10.1029/2006GL026962
40. Winsemius HC, Savenije HHG, van de Giesen NC, van den Hurk B, Zapreeva EA, Klees R (2006) Assessment of gravity recovery and climate experiment (GRACE) temporal signature over the upper Zambezi. Water Resour Res 42:W12201. doi:10.1029/2006WR005192
41. Awange JL, Anyah R, Agola N, Forootan E, Omondi P (2013) Potential impacts of climate and environmental change on the stored water of Lake Victoria Basin and economic implications. Water Resour Res 49:8160–8173
42. Awange JL, Sharifi M, Ogonda G, Wickert J, Grafarend EW, Omulo M (2008) The falling Lake Victoria water level: GRACE, TRIMM and CHAMP satellite analysis. Water Resour Manag 22:775–796. doi:10.1007/s11269-007-9191-y

43. Bettadpur S (2007) UTCSR level-2 processing standards document for level-2 product release 0004. Gravity recovery and climate experiment (GRACE) Rev 3.1, GRACE 327-742 (CSR-GR-03-03). Center for Space Research, The University of Texas at Austin
44. Owor M, Taylor RG, Tindimugaya C, Mwesigwa D (2009) Rainfall intensity and groundwater recharge: empirical evidence from the Upper Nile Basin. Environ Res Lett 4:035009. doi:10.1088/1748-9326/4/3/035009
45. Awange JL, Ong'ang'a O (2006) Lake Victoria-ecology resourcof the Lake basines and environment. Springer, Berlin
46. Yates DN, Strzepek KM (1998) Modelling the Nile Basin under climate change. J Hydrol Eng 3(2):98–108. doi:10.1061/(ASCE)1084-0699(1998)3:2(98)
47. Sahin M (1985) Hydrology of the Nile Basin. Developments in water Science, vol 21. Elsevier, New York, p 575
48. Hamouda MA, Nour El-Din MN, Moursy FI (2009) Vulnerability assessment of water resources systems in the Eastern Nile Basin. Water Resour Manag 23:2697–2725. doi:10.1007/s11269-009-9404-7
49. Whittington D, McClelland E (1992) Opportunities for regional and international cooperation in the Nile Basin. Water Int 17(3):144–154. doi:10.1080/02508069208686134
50. Beyene T, Lettenmaier DP, Kabat P (2010) Hydrologic impacts of climate change on the Nile River Basin: implications of the 2007 IPCC scenarios. Clim Change 100:433–461. doi:10.1007/s10584-009-9693-0
51. Conway D (2005) From headwater tributaries to international river: observing and adapting to climate variability and change in the Nile Basin. Glob Environ Change 15:99–114. doi:10.1016/j.gloenvcha.2005.01.003
52. Awange JL, Forootan E, Kuhn M, Kusche J, Heck B (2014) Water storage changes and climate variability within the Nile Basin between 2002 and 2011. Adv Water Resour 73:1–25. doi:10.1016/j.advwatres.2014.06.010
53. Awange J, Forootan E, Fleming K, Odhiambo G (2015) Dominant patterns of water storage changes in the Nile Basin during 2003–2013? In: Remote sensing of the terrestrial water cycle, Lakshmi V (ed), pp 367–382. Wiley, New Jersey
54. Bonsor HC, Mansour MM, MacDonald AM, Hughes AG, Hipkin RG, Bedada T (2010) Interpretation of GRACE data of the Nile Basin using a groundwater recharge model. Hydrol Earth Syst Sci Discuss 7:4501–4533. doi:10.5194/hessd-7-4501-2010
55. Senay GB, Asante K, Artan G (2009) Water balance dynamics in the Nile Basin. Hydrol Process 23:3675–3681. doi:10.1002/hyp.7364
56. Forootan E, Kusche J (2011) Separation of climate-driven signals in time-variable gravity using independent component analysis (ICA). J Geodesy, submitted
57. Sultan M, Ahmed M, Sturchio N, Yan YE, Milewski A, Becker R, et al. (2012) Assessment of the vulnerabilities of the Nubian sandstone fossil aquifer, North Africa (2012). Water Encyclopedia. In: Pielke RA (ed) Climate vulnerability: understanding and addressing threats to essential resources. Elsevier Inc. Academic Press (2012), pp 311–333. ISBN: 9780123847034
58. Salem OM, Pallas P (2002) The Nubian sandstone aquifer system, paper presented at Managing Shared Aquifer Resources in Africa ISARM-AFRICA, Tripoli, Libya, 2–4 June 2002
59. Salem OM (2007) Management of shared groundwater basins in Libya. African Water J 1(1):109. ISBN 92-1-125089-7
60. Becker M, Llowel W, Cazenave A, Güntner A, Crétaux J-F (2010) Recent hydrological behaviour of the East African Great Lakes region inferred from GRACE, satellite altimetry and rainfall observations. Comptes Rendus Geosci 342(3):223–233. doi:10.1016/j.crte.2009.12.010
61. Garcia-Garcia D, Ummenhofer CC, Zlotnicki V (2011) Australian water mass variations from GRACE data linked to Indo-Pacific climate variability. Remote Sens Environ 115:2175–2183. doi:10.1016/j.rse.2011.04.007
62. Nicholson SE (1998) Historical fluctuations of Lake Victoria and other lakes in the Northern Rift Valley of East Africa. In: Lehman JT (ed) Environmental change and response in East African lakes. Kluwer, Dordrecht, pp 7–35

63. Nicholson SE (1999) Historical and modern fluctuations of lakes Tanganyika and Rukwa and their relationship to rainfall variability. Clim Change 41:53–71. doi:10.1023/A:1005424619718
64. Kull D (2006) Connections between recent water level drops in Lake Victoria, dam operations and drought. http://www.irn.org/programs/nile/pdf/060208vic.pdf. Accessed 25 Sep 2011
65. Kayombo S, Jorgensen SE (2006) Lake Victoria: experience and lessons learned brief. International Lake Environment Committee, Lake Basin Management Initiative, Kusatsu, Japan. http://www.ilec.or.jp/eg/lbmi/reports/27_Lake_Victoria_27February2006.pdf. Accessed 25 Sep 2011
66. Awange JL, Ferreira VG, Forootan E, Khandu Andam-Akorful SA, Agutu NO, He XF (2016) Uncertainties in remotely sensed precipitation data over Africa. Int J Climatol 36(1):303–323. doi:10.1002/joc.4346
67. Swenson S, Wahr J (2009) Monitoring the water balance of Lake Victoria, East Africa, from space. J Hydrol 370:163–176. doi:10.1016/j.jhydrol.2009.03.008
68. Becht R, Odada EO, Higgins S (2005) Lake Naivasha : experience and lessons learned brief. In: Lake basin management initiative: experience and lessons learned briefs. including the final report: managing lakes and basins for sustainable use, a report for lake basin managers and stakeholders. Kusatsu: International Lake Environment Committe Foundation (ILEC) (2005). pp 277–298
69. Awange JL, Ogallo L, Kwang-Ho B, Were P, Omondi P, Omute P, Omulo M (2008) Falling Lake Victoria water levels: is climate a contribution factor? J Clim Change 89:287–297. doi:10.1007/s10584-008-9409-x
70. Everard M, Harper DM (2002) Towards the sustainability of the Lake Naivasha Ramsar site and its catchment. Hydrobiologia 488(1–3):191–203. doi:10.1023/A:1023390430571
71. Harper DM, Mavuti KM, Muchiri SM (1990) Ecology and management of Lake Naivasha, Kenya, in relation to climatic change, alien species' introductions, and agricultural development. Environ Conserv 17(04):328–336
72. Becht R, Haper DM (2002) Towards an understanding of human impact upon the hydrology of Lake Naivasha. Kenya. Hydrobiologia 488(1–3):1–11. doi:10.1023/A:1023318007715
73. ILEC (International Lake Environment Committee) (2005) Managing lakes and their basins for sustainable use. A report for the lake basin managers and stakeholders. In: International Lakes Environmental Committee Foundation: Kusatsu, Japan
74. Becht R (2007) Environmental effects of the floricultural industry on the Lake Naivasha Basin. ITC, Netherlands
75. Carolina BF (2002) Competition over water resources: analysis and mapping of water-related conflicts in the catchment of Lake Naivasha (Kenya). MSc Thesis, ITC
76. KFC (Kenya Flower Council) (2011). Kenya Flower Council. www.kenyaflowercouncil.org. Accessed 25 July 2010
77. Everard M, Vale JA, Harper DM, Tarras-Wahlberg H (2002) The physical attributes of the Lake Naivasha catchment rivers. Hydrobiologia 488(1–3):13–25. doi:10.1023/A:1023349724553
78. Richardson JL, Richardson AE (1972) History of an African rift lake and its climatic implications. Ecol Monogr 42(4):499–534. doi:10.2307/1942169
79. Sansome HW (1952) The trend of rainfall in East Africa. E Afr Meteorol Dep, Tech Mem 1. p 14
80. Darling W, Allen D, Armannsson H (1990) Indirect detection of subsurface outflow from a rift valley lake. J Hydrol 113(1–4):297–306
81. Abiya IO (1996) Towards sustainable utilization of lake Naivasha. Kenya. Lakes Reserv Res Manag 2(3–4):231–242. doi:10.1111/j.1440-1770.1996.tb00067.x
82. Mekonnen MM, Hoekstra AY (2010) Mitigating the water footprint of export cut flowers from the Lake Naivasha Basin, Kenya. In: Value of water research report series, vol 45, UNESCO-IHE, Delft, The Netherlands
83. Vincent CE, Davies TD, Beresford UC (1979) Recent changes in the level of Lake Naivasha, Kenya, as an indicator of equatorial westerlies over East Africa. Clim Change 2(2):175–189. doi:10.1007/BF00133223

84. Awange JL, Forootan E, Fleming KM, Kiema JBK, Ohanya S, Heck B (Submitted) Understanding the decline of Lake Naivasha using satellite-based methods. Water Resource Management
85. NLWRA (National Land and Water Resource Audit) (2001) Water resources in Australia. A summary of the National Land and Water Resource Audit's Australian water resources assessment 2000. Surface water and groundwater - availability and quality
86. Steffen W, Sanderson A, Tyson PD, Jäger J, Matson PA, Moore BIII, Oldfield F, Richardson K, Schellnhuber HJ, Turner BLII, Wasson RJ (2005) Global change and the earth system: a planet under pressure. Springer, Berlin
87. Leblanc M, Tregoning P, Ramillien G, Tweed S, Fakes A (2009) Basin-scale, integrated observations of the early 21st century multiyear drought in southeast Australia. Water resources research 45:W04408. doi:10.1029/2008WR007333
88. Ummenhofer C, England M, McIntosh P, Meyers G, Pook M, Risbey J, Gupta A, Taschetto A (2009) What causes southeast Australia worst droughts? Geophys Res Lett 36:L04706. doi:10.1029/2008GL036801
89. Khandu E, Forootan M, Awange Schumacher J, Miler Schmied H (2016) Exploring the influence of precipitation extremes and human water use on total water storage (TWS) changes in the Ganges-Brahmaputra-Meghna River Basin. Water Resour Res 52(3):2240–2258
90. Awange LJ, Gebremichael M, Forootan E, Wakbulcho G, Anyah R, Ferreira CG, Alemayehu T (2014) Characterization of Ethiopian mega hydrogeological regimes using GRACE, TRMM and GLDAS datasets. Advances in water resources 74:64–78. doi:10.1016/j.advwatres.2014.07.012
91. Forootan E, Khandu Awange J, Schumacher M, Anyah A, van Dijk A, Kusche J (2016) Quantifying the impacts of ENSO and IOD on rain gauge and remotely sensed precipitation products over Australia. Remote Sens Environ 172:50–66. doi:10.1016/j.rse.2015.10.027
92. Forootan E, Awange JL, Kusche J, Heck B, Eicker A (2012) Independent patterns of water mass anomalies over Australia from satellite data and models. Remote Sens Environ 124:427–443. doi:10.1016/j.rse.2012.05.023. (Data: The CHAMPCLIM Project. In: Foelsche U, Kirchengast G, Steiner A (eds) Atmosphere and climate studies by occultation methods. Springer, Berlin, pp 303–314)
93. Rieser D (2008) Comparison of GRACE-derived monthly surface mass variations with rainfall data in Australia. MSc Thesis. Graz University of Technology

# Chapter 15
# Coastal Resources

*Shoreline and beach surveys can today benefit from the state-of-the-art GNSS monitoring techniques, which directly offer both two- and three-dimensional data sets within a short period of time.*

Morton et al. [1]

## 15.1 Integrated Coastal Zone Management and Its Importance

The extreme importance of coastal zones for countries with highly-populated coastal areas has been discussed in Goncalves and Awange [2] who highlight the concerns about their future, particularly on the state of their natural resources that provide life support and opportunities for economic development and tourism for these countries [3]. However, one of the main environmental problems facing coastal areas the world over is that of coastal erosion, which includes, e.g., beach erosion and other natural and anthropogenic environmental factors that are present along the shoreline. Anthropogenic factors include, for example, settlement near the shore, which aggravates the situation as exemplified in the case of Brazil where hundreds of beaches are under severe erosion [4]. One way of efficiently accomplishing coastal management, therefore, is investing in monitoring of shorelines to support policy formulations.

Continuous monitoring of coastal zones is important for integrated coastal zone management (ICZM) in order to support informed decisions on policies governing coastal development [5–8]. For example, the State of Pernambuco in Brazil established a Coastal Management Policy through legislation (i.e., Law No. 14,258 December 23th, 2010, Pernambuco), which has an overarching policy of guiding the use of natural resources of Pernambuco State Coastal Zone. Among other things, this law aims at:

(i) promoting the development of monitoring activities of natural resources and settlement of the coastal zone,
(ii) promoting recovery actions and regeneration of beaches,



J. Awange, *GNSS Environmental Sensing*, Environmental Science and Engineering, DOI 10.1007/978-3-319-58418-8_15

(iii) promoting the integration of Coastal Management Information System with other State systems of environment, water resources and land use, and,
(iv) promoting and supporting training for coastal zone municipalities staff in order to strengthen the urban environmental control.

All the four itemised components of the legislation above require some sort of shoreline monitoring, which is essential to consistently organise the set of positional data that represents the evolution of a particular case.

Shoreline monitoring is, therefore, essential for integrated coastal zone management (ICZM) where it provides the necessary information needed to manage settlement of coastal areas, establish guidelines for management of social-economics activities within the coastal areas, provide information necessary for recovery actions of beach regeneration, and provides a reference baseline for studies related to climate change in coastal zones. Shoreline monitoring methods are largely dependent on the goals, costs, implementation, and applicability. For monitoring of short coastal shorelines (e.g., tens to hundreds of kilometers), Global Navigation Satellite Systems (GNSS)-based methods are emerging as low cost approaches that offer *rapid*, *weather-independent*, and *quickly updatable* products that could benefit policy makers where high costs of traditional methods such as photogrammetry and remote sensing are of concern. However, various GNSS methods applicable to shoreline monitoring exist, making it difficult for decision makers to choose a suitable approach. Using a case study of Pernambuco state ICZM in Brazil, Goncalves and Awange [2] evaluates three most commonly used GNSS-based shoreline monitoring methods; relative kinematic (RK), real-time kinematic (RTK) and precise point positioning (PPP), and provides a comprehensive analysis of their strengths and limitations. Their results highlight the issues and important considerations in choosing an economically viable GNSS method for mapping shoreline changes, particularly for supporting ICZM policies.

## 15.2 Marine Habitat

### *15.2.1 Background*

Marine habitats are comprised of zones termed *coastal terrestrial*, *open water*, and the *ocean bottom* until several meters deep. Several physical parameters, e.g., temperature, salinity, tides, currents, winds, etc., play a major role in defining the marine habitat. Malthus and Mumby [9] have listed marine ecosystem to comprise *mangroves, seagrasses, coral reefs, lagoonal microbial mats, shoreline features, sublittoral zone benthos* and *overlaying water column features*. The reflectance of these features can be measured by remote sensing methods to provide synoptic data at various scales. Such data are essential requirements for coastal managers to be able to address issues facing these diverse habitats. In most countries, these environments are either being degraded or not inventoried. This is due partly to inaccessibility and

partly due to large spatial coverage, leading to high costs when applying conventional methods.

Remote sensing and Geographical Information Systems (GIS) discussed in detail, e.g., in Awange and Kiema [10] offer possibilities of mapping and inventorying marine habitats, thus enhancing the understanding of the unique characteristic of marine habitats. Malthus and Mumby [9] have indicated that remote sensing could be used to reveal how patterns change across a near-continuum of spatial scales, details of which are useful in identifying the scale at which disturbance such as El Niño-Southern Oscillation (ENSO) causes changes in the marine environment. In what follows, we examine some of the ways in which remote sensing, GIS, and GNSS tools could be used to support mapping of marine habitats.

### *15.2.2 Satellites Monitoring of Marine Habitats*

The presentation in this section shows the complementary nature of remote sensing, GIS and GNSS methods in supporting monitoring of marine habitats. In general, GNSS play the following important roles; (i) that of validation of the remotely sensed data through georeferencing (i.e., the actual validation on the ground of what is seen on the photograph or any other remotely sensed images), (ii) georeferencing of the aerial photographs e.g., Fig. 16.3 on p. 337), and (iii) providing the sampling locations. Remote sensing techniques applicable to marine habitats include, e.g., aerial photography, airborne optical sensors, Synthetic Radar Aperture (SAR), and optical satellite-based sensors. Analysis tools include empirical models and multispectral classifications. Remote sensing and GIS techniques are useful in discriminating marine habitats as demonstrated, e.g., by Call et al. [11] who discriminates coral reef habitats. Held et al. [12] applied hyperspectral and radar techniques to map tropical mangroves. Discrimination of marine habitats requires that the radiative transfer properties of the marine environment be well understood. Effective use of remote sensing to monitor water quality will require an established relationship between water colour and constituent bio-optical water quality parameters such as suspended organic matter and dissolved organic matter [9]. Karpouzli et al. [13] have highlighted the need to understand the spatial and temporal variations in optical water quality parameters and their influence on inherent and apparent optical properties.

Due to the high spatial diversity of marine habitats, high spatial and spectral resolution data are required to discriminate between features. Moderate resolution sensors, e.g., Landsat ETM[1] and SPOT (approximately 10 m) are limited by poor spatial and temporal resolution, spectral capabilities, and important signatures falling outside visible bands. Held et al. [12] and Call et al. [11] demonstrate that sub-pixel-scale mixing prevent accurate identification of features leading to coarse descriptive levels of mapping. One possible way of improving the performance of moderate resolution sensors would be the combination of optical and SAR approaches as demonstrated by

[1] http://landsat.gsfc.nasa.gov/about/L7_td.html.

Held et al. [12], who combined these sensors for the case of mangroves. In this case, increased classification accuracies with the use of greater spatial data was possible.

Due to the optical similarity in the reflectance between the bottom marine features, leading to subsequent confusion during identification of remotely sensed data, care must be taken in distinguishing different classes (e.g., vegetation) on the basis of spectral reflectance, for instance, higher-spectral resolution reflectance are needed to perceive the subtle differences, see, e.g., [11]. Malthus and Mumby [9] point out that classification based on high-spectral resolution airborne data tends to provide the best results. They advocate the necessity to better understand the depth limits to which useful above surface spectral signatures can be derived, but still allow the discrimination of habitat types, as does the relationship to varying water column optical properties. For example, Call et al. [11] demonstrated that the point at which a signature begins to resemble a water column's optical properties rather than substrate for a coral reef system is 7 m. This applies for certain locations, in others, it is 15 or 20 m such as Ningaloo Marine Park in Australia.

As already pointed out, one of the shortcomings of remote sensing technique in mapping marine habitat is the poor spatial resolution (e.g., 30 x 30 m in a Landsat image). Call et al. [11] highlighted a critical resolution of 4 m for mapping seagrass in their littoral system. High-resolution sensors such as IKONOS and QuickBird could be of use. Mumby et al. [14] evaluated Landsat MSS,[2] Landsat TM,[3] SPOT XS, CASI (Compact Airborne Spectrographic Imager), SPOT pan and a combination of Landsat TM and SPOT-PAN to map Caribbean coral reefs. Landsat MSS was the least accurate sensor while CASI was found to be more accurate than satellites sensors and aerial photographs. They noted that maps with detailed habitat information had a maximum accuracy of 37% when based on satellite imagery, 67% based on aerial photography and 81% based on CASI. In tropical regions, characterized by prolonged cloud cover, low accessibility, high temperature and high humidity, digital airborne colour and infrared photography are useful [9].

Besides using optical remote sensing as a stand alone tool, a combination with other methods such as acoustic, SAR and LIDAR[4] could be useful. Optical, SAR and LIDAR will cover above surface, while acoustic could be used for sub-surface studies. In this combination, LIDAR would offer high data density for bathymetry, optical spectral information with degree of penetration into water column and wide spatial coverage, and SAR the structural components of the habitat (onshore and sub-surface) which are less visible in optical sensors. This could be enhanced by the incorporation of knowledge based processing packages such as ERDAS Images[5] to improve accuracies of classification [9].

To validate remotely sensed data, georeferencing is essential. This could be achieved through, e.g., matching signatures to defined biotopes; assessing changes between images; and applying the results in coastal zone management. Once the

[2] Multispectral Scanner.

[3] thematic mapper.

[4] Light Detection And Ranging.

[5] http://www.erdas.com/Homepage.aspx.

remote sensing data has been processed, they provide attributes to be used in a GIS system together with other data to generate a marine habitat georeferenced system that can be edited, updated, and queried, which greatly benefits marine habitat management. Ground truthing and georeferencing can also be achieved using GNSS, where positions of selected marked features on a remotely sensed image are determined, e.g., using hand-held GNSS receivers. Besides ground thruthing, GNSS is also useful in providing orientation to aerial photographs (e.g., Fig. 16.3 on p. 337.

Example 15.1 (Application to microbiology monitoring program).

Schiff and Weisberg [15] conducted an inventory to assess the number, type, spatial distribution, and costs of microbiological monitoring programs in southern California marine waters from Point Conception to the US/Mexico border. The location of each sampling site was determined using GNSS, while the estimates of geographic coverage were determined using GIS techniques. A list of organizations that conduct microbiological monitoring in marine waters was compiled by contacting all of the city and county public health agencies and regional water quality control boards in southern California. Monitoring organizations were then surveyed to ascertain the following information about each sampling site: station name, location (latitude/longitude, general description, water body type), depth of sampling, analytes measured, analytical methods, and sampling frequency by season. Where latitude and longitude data were unavailable, the sites were revisited and the position of the sampling sites found using DGPS (Sect. 5.4.4.1). The relative distribution of sampling effort among habitat types was assessed by differentiating sampling sites into offshore and shoreline strata. Shoreline sites were further differentiated into eight categories: (1) high-use sandy beaches, (2) low-use sandy beaches, (3) high-use rocky shoreline, (4) low-use rocky shoreline, (5) perennial freshwater input areas, (6) ephemeral freshwater input areas, (7) embayment, and (8) restricted access areas. This example show the role played by GNSS in providing sampled data locations and field validation through georeferencing.

♣ End of Example 15.1.

Next, another application of GNSS, that is, shoreline monitoring is presented.

## 15.3 Shoreline Monitoring and Prediction

### *15.3.1 Definition and Need for Monitoring*

A shoreline is defined as the boundary between the continent and the portion adjacent to the sea where there is no effective marine action beyond the maximum reach of the waves, and is identified by cliffs, the boundary between the vegetation and the seashore, by the rocks, or by any other feature that determines the beginning of

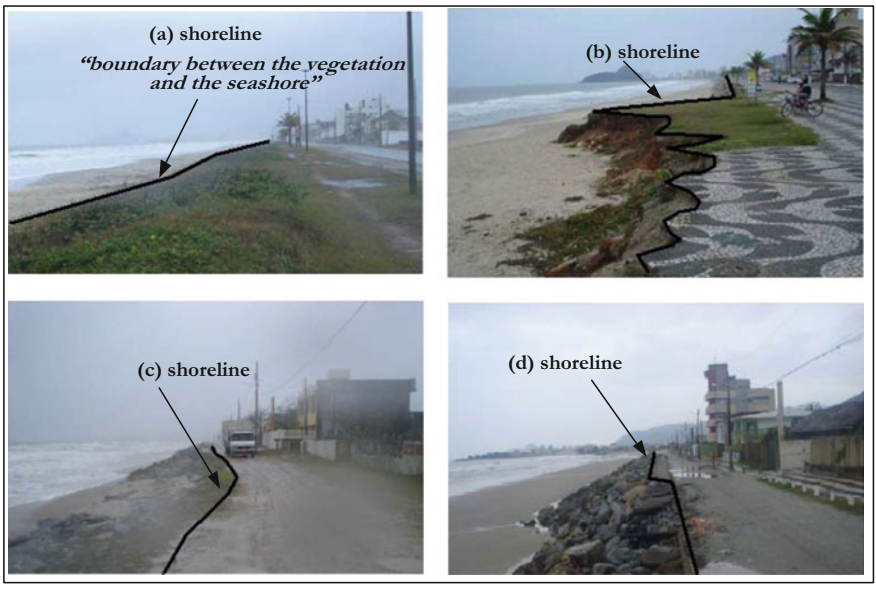


**Fig. 15.1** Examples of definition of a shoreline; **a** the shoreline is the boundary between the vegetation and the seashore while in **b, c, d**, the shoreline is the boundary between the continent and the portion adjacent to the sea where there is no effective marine action beyond the maximum reach of the waves, characterized by urban settlement and problems of coastal erosion. *Source* Goncalves [18]

the continental area [16, 17]. In Fig. 15.1, four examples of different scenarios that define the position of a shoreline are presented as follows; in (a), the shoreline is the boundary between the vegetation and the seashore while in (b), (c), and (d), the shoreline is the boundary between the continent and the portion adjacent to the sea where there is no effective marine action beyond the maximum reach of the waves, characterized by urban settlement and problems of coastal erosion.

Shorelines are known not to be stable and vary over time causing the effects of progradation (i.e., a shoreline moving towards the sea due to deposit) or retrogradation (i.e., a shoreline moving towards the land due to wave erosion). *Long-term changes* can be related to changes in sea level, sediment supply, wave energy, and geological controls (contemporary and antecedent), causing movements in the position of a shoreline over a period of centuries and millennia. *Short-term changes* on the other hand occur over time scales of 80 years or less and are related to daily, monthly, and seasonal variations in tides, currents, wave climate, episodic events and anthropogenic factors, see, e.g., [19–21]. Very rapid (episodic) changes in shoreline location can also occur as a result of (tropical) storms and hurricanes and can move a shoreline more than 30 m in a day [22]. Fenster and Dolan [23] describe shoreline movement as a complex phenomenon and the difficulties involved in distinguishing long-term shoreline movement (signal) from short-term changes (noise), although

for long-term analysis, the effect of storms are not treated as outliers, hence they are considered in the temporal data distribution, e.g., Fenster et al. [24]. The complexity of the definition of a shoreline, mapping, and subsequent utilization are discussed, e.g., in [6, 25].

Monitoring and prediction of shorelines is vital for environmental and resource management. Most coastal areas are known to experience soil erosion (see Fig. 15.2), which in some cases, lead to the disappearance of beaches, destruction of cliffs by gullies, or submersion of parts of the coast. Yet beaches have been known to be a source of revenue for those countries that attract tourism along their coasts. Environmental management is therefore essential in realizing the long term durability of such coastal areas. One way of realizing efficient management of beaches is through constant monitoring of the coastal shorelines. Through continuous monitoring, policy and decision makers are informed of the behavior of forcing and response parameters of shorelines. These forces are, e.g., changes in the forces that move the sand, namely wind, waves, and currents.

Monitoring is therefore essential in improving the database of information on shorelines evolution in an area, thereby indicating the trend in beach loses as demonstrated by Fig. 15.3. Metropolitan Borough of Sefton [26] have listed the benefits of shoreline evolution information as; *providing input to shoreline review plans*, *planned maintenance of coastal defenses*, *achievement of high government level targets*, *determination of appropriate design criteria for coastal works*, *biodiversity action plan*, *implementations of habitats directive*, and *leisure and amenity management of shoreline areas*. Shoreline information have also been used to support other monitoring studies, e.g., in microbiological monitoring of marine recreational waters, see e.g., [15], while accurate interpretation of its movement trends and precisely quantifying the rates of movement are necessary to accurately predict its future positions [1].

### *15.3.2 Monitoring*

Traditionally, monitoring of shorelines and beach dynamics has been undertaken using surveying techniques such as traversing and levelling where shoreline positions are determined in addition to the height information that are linked to a nearby monuments. To infer the rate of erosion, these positions and height information are compared to subsequent beach surveys to yield a two-dimensional cross-sectional area, which represents the amount of beach erosion and deposition that occurred between the surveys. A three-dimensional volumetric change in the beach is derived from the profiles by integrating between adjacent cross-sectional areas [1]. Morton et al. [1] lists the setback of these traditional approaches as (i) loss of the reference monument upon which the heights are referenced through, e.g., erosion (ii) errors in the generation of the cross-sections since subsequent surveys may not traverse the same course, (iii) amount of time required to undertake the extensive survey,

**Fig. 15.2** An example of environmental degradation of a coastal area in Brazil through erosion. *Source* Goncalves [18]

**Fig. 15.3** Impacts of shoreline erosion in Matinhos District in the coast of Paraná State, Brazil in 2007. *Source* Goncalves [18]

and (iv) the errors incurred in generating a three-dimensional volumetric data from a two-dimensional cross-sectional data.

To remedy these setbacks, shoreline and beach surveys can today benefit from the state-of-the-art GNSS monitoring techniques, which directly offer both two and three-dimensional data set within a short period of time, see e.g., [1]. Other mapping techniques that have benefited shoreline monitoring are photogrammetry, remote sensing, and LIDAR. These methods have been elaborately discussed, e.g., in Gorman et al. [27]. As discussed in details in Goncalves and Awange [2], starting in the 1920s, it was demonstrated that great efficiency gains in shoreline mapping could be realized by transitioning from ground-based methods (e.g., plane tables, alidades and stadia rods) to airborne methods (e.g., photogrammetry and aerial imagery interpretation), see e.g., [28–31]. Beginning in the 1970s, when earth observation satellite data became publicly available, further gains in shoreline mapping efficiency were enabled [32]. Today, photogrammetry, airborne lidar, and satellite imagery are well-established methods of mapping large stretches of shoreline in many areas around the world, see e.g., [29, 33–35]. Additionally, unmanned aerial vehicles (UAVs) (see Chap. 20) and structure from motion are also emerging as viable coastal mapping techniques, see e.g., [36, 37]. However, while the cost per linear kilometer of shoreline data acquisition will generally be lowest for satellites, followed by aircraft, there are a number of important benefits to ground-based shoreline mapping surveys. First, for very small project sites, the total acquisition cost can actually be lower using ground-based methods than for airborne methods. Second, ground-based shoreline surveys typically provide the highest accuracy, as well as the detailed knowledge obtained by "boots on the ground." Therefore, ground-based surveys can provide reference data for calibrating and validating airborne and space-borne shoreline mapping techniques. Third, when shoreline data with high temporal resolution (i.e., short repeat survey periods) are needed, ground-based methods may be the best option.

When and where ground-based survey methods are advantageous for shoreline mapping, GNSS is generally the technology of choice having the advantages of being quicker, all-weather, highly accurate, and capable of generating continuously updatable shoreline positional time series relevant for monitoring and management tasks undertaken by engineers and coastal authorities in cases of extremely small project sites that are located close to a field office and easily accessible. For such small projects, use of traditional remote sensing-based satellite techniques could be costly although this does not apply to all cases. Furthermore, as exemplified by the case of National Oceanic and Atmospheric Administration (NOAA)'s National Geodetic Survey, Coastal Mapping Program,[6] field-based GNSS shoreline surveys are sometimes performed to obtain high-accuracy reference data for evaluating airborne or space-borne shoreline mapping methods, see e.g., [30, 34].

GNSS comprising the use of the US-based GPS (Global Positioning System), Russian's GLONASS (GLObal NAvigation Satellite System), European's (GALILEO), and Chinese's Beidou (or Compass) discussed in Chap. 2 and also in [38] have already

[6] http://www.ngs.noaa.gov/RSD/cmp.shtml.

been proposed for shoreline monitoring, e.g., by [39]. However, with a large number of types of GNSS surveys, ranging from static surveys to Real Time Kinematic (RTK), Network Real Time Kinematic (NRTK), Post Processed Kinematic (PPK), and Precise Point Positioning (PPP), the Coastal Zone Management (CZM) community needs information on which types of GNSS surveys are most advantageous for shoreline mapping across a range of project types and coastal morphologies. To this end, Goncalves and Awange [2] empirically compared different GNSS survey methods in a study site along the coast of Pernambuco, in the northeast of Brazil. Three common types of GNSS surveys (PPK, RTK, and PPP; see Sect 5.4) were evaluated and the results compared. Their study concluded that the choice of a particular GNSS method is very important for an efficient and reliable shoreline monitoring. In their case study of Pernambuco state in Brazil, the PPP method was considered to be both economical and feasible for the case study and shown to be a reliable alternative for mapping and monitoring of shoreline that could be used to support the Pernambuco legislation presented in Article 10. They however recommend that, in general, other issues such as the use of a shoreline indicator and how to map and monitor it should be considered when choosing a method for mapping positional variations of shoreline to support ICZM policies. Furthermore, they point out other issues of concern such as the extent of the State's GNSS network configuration that does not provide ideal short baselines to support RTK and RK, and the lack of benchmarks in the survey area due to the low geographical density of stations belonging to the network.

White and El Asmar [40] provide an illustration where the Thematic Mapper (TM) imager is used to monitor the changing position of the Nile Delta coastline. To enhance these monitoring mapping tools, GIS techniques are now being used to analyze changes in natural phenomenon according to the evolution in time using spatio-temporal dynamic models in a Coastal Geographic Information System (CGIS). For example, CGIS has been used by Li et al. [25] to monitor the Malaysian shoreline. With respect to GNSS satellites, the following roles are foreseen:

1. Providing orientation to aerial photographs (e.g., Fig. 16.3) and ground truthing data for remote sensing satellites.
2. Provision of *real-time* monitoring of positional data of the shoreline that informs the decision making of environmental (coastal) managers (see, e.g., Fig. 15.4, right).
3. Provision of *historical data* needed for computing the parameters of the predictive models as discussed in the next section.

Example 15.2 (GNSS-based monitoring and mapping of shoreline position in support of planning and management of Matinhos/PR (Brazil) Goncalves et al. [41]).

Monitoring and mapping variations in shoreline location is an activity that can be undertaken using several different techniques of data collection, e.g., photogrammetric restitution, satellite images, LiDAR (Light Detection and Ranging) or classical topographical surveys to support coastal environmental protection such as identifying flood risk areas. The global navigation satellite system (GNSS) has been employed

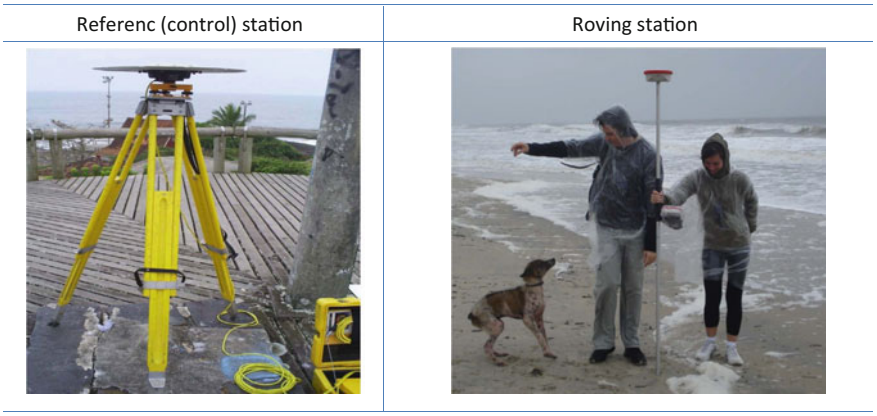


**Fig. 15.4** *Left* Base station in Matinhos. *Source* Goncalves [18]. *Right* Real-time GNSS shoreline monitoring. A roving GNSS receiver is used to provide shoreline's location-based data relative to the reference station whose position is known using one of the rapid positioning techniques discussed in Sect. 5.4.5. *Source* Goncalves [18]

by the Federal University of Parana (UFPR) as part of their research into the application of geodetic survey methods for shoreline mapping in coastal environments since 1996. The advantages of using GNSS are accuracy and productivity, given that a great number of points can be determined within a short period of time at decimeter-level accuracy. In this work, GNSS relative kinematic positioning approach was applied to monitor Matinhos coastal district of Brazil. Other important data, such as the high- and low-tide marks, all obtained using GNSS, and thematic maps were incorporated. Through the reanalysis of historical surveys, it was possible to make some conclusions about the shoreline dynamics and to use this information as material in support of the planning and management of the coastal environment, for example, when planning engineering works that set out to minimize coastal erosion and for urban planning. The results achieved in Goncalves et al. [41] include defining the position of the shoreline for 2008, developing the thematic map of the shoreline, the quantification of the advance and retreat of the shoreline between 2001 and 2008, and a map showing those critical areas where the shoreline position is equal to the high-tide water line. GNSS-based method offered quicker, all-weather, highly accurate and continuously updatable shoreline positional time series relevant for monitoring, thus enabling quicker management decisions to be undertaken, which may be of benefit to coastal engineering applications.

♣ End of Example 15.2.

### 15.3.3 Prediction

Whereas shoreline monitoring is essential as already discussed, predicting its future position is equally vital to support the *environmental impact assessment* and *management* of programs such as predicting increased shoreline erosion [42] and building setbacks to serve as protection for a time comparable to the expected lifetime of new coastal structures, usually 30 or 60 years [43]. According to Morton et al. [1], predicting future rates of coastal erosion and land loss progressed from a purely academic exercise to one of environmental importance since many coastal states and government agencies relied on technical data to determine construction setback lines and insurance hazard zones. This led to the establishment of elaborate networks of closely spaced beach profile monuments that were periodically revisited to assess magnitudes and rates of shoreline movement that were used to establish building zones and to create construction control lines [1]. Going back to Fig. 15.3 for example, if the shorelines had been predicted before the roads were developed, such environmental degradation could have been avoided by constructing the roads further inland.

Crowell et al. [43] states, however, that determining adequate setbacks requires estimating long-term shoreline changing trends from historical data. Fenster et al. [23] developed a predictive method that detects short-term changes in the long-term trend and identifies linear or high-order polynomial models that best fit the data according to the minimum description length (MDL) criterion. In this method, only linear models are extrapolated.

Douglas et al. [44] stressed the need to incorporate long-term erosion trends and historical records of storms, including their impact on shoreline position and beach recovery, in predictive models. Exploiting the relationship between shoreline and sea-level changes (i.e., using series of sparsely sampled sea level values as surrogate data for shoreline changes), they developed an algorithm to evaluate several predictive methods, such as the end-point method, linear regression, and minimum description length criterion. They evaluated several well-known shoreline prediction algorithms and established that linear regression gave superior results, see also [44]. Predictions shaped or influenced by higher-order polynomial schemes can sometimes be superior to those obtained from linear regressions, but they can also be extremely inaccurate [43]. Use of modern more accurate surveying measurement techniques such as photogrammetry and GNSS have also been shown to improve the quality of forecasts. Douglas and Crowell [45] demonstrated that this is achievable even if the inherent variability of shoreline position indicators remains at the level of many meters.

The linear regression models that are usually used to predict shoreline positions work well when the underlying linearity and normal distribution assumptions are fulfilled. In some cases, however, the sources of data, particularly photogrammetric data are of a poor quality. Indeed, this fact is acknowledged, e.g., by Douglas et al. [44] who point out that some data used in predicting shorelines are at times temporally poorly sampled historical shoreline positions, resulting in the violation of the linear

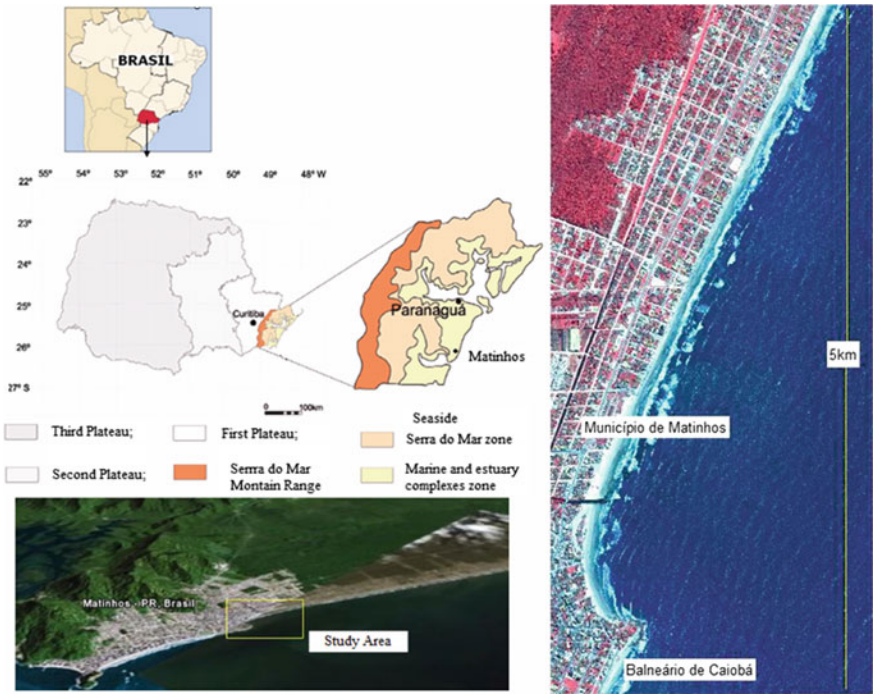


**Fig. 15.5** Matinhos District in the coast of Paraná State, Brazil. *Source* Goncalves [18]

regression assumptions. In others instances, the transformation process used to bring all the data into a common coordinate system (e.g., Sect. 5.6.2) may be poorly done, such that the resulting extracted shoreline positions used for predictive purposes are themselves inaccurate. In such cases, therefore, modern techniques such as GNSS provide *fast*, *efficient* and *accurate* means for data capture that support shoreline prediction. In the following example, the use of GNSS in supporting predictions of shoreline positions is illustrated.

Example 15.3 (Shoreline prediction of Matinhos Beaches in Paraná, Brazil) [18].

*Background of Matinhos*: Matinhos District is located along the coast of Paraná State, Brazil (Fig. 15.5). The coastal region of the State of Paraná, located between the 25–26° S and 48–49° W, is formed by the Serra do Mar mountain range, extensive coastal plains, and estuary complexes.

Exploitation of the Matinhos shoreline started as early as 1920, but the first settlement begun in the 1948 with a hotel built on the sandy shore. By 1949, a murram road had been constructed near the shore (see Fig. 15.6). The settlement in Matinhos occurred near the shore, whereby in some oceanic beaches, the settlement was characterize by constructions on the shoreline or over the sand, leading to the destruction of dunes, wetlands, and forcing rivers to change course. This was a result of unplanned


**Fig. 15.6** Photos of the Matinhos shore in 1920, 1948, and 1949. *Source* [47]


**Fig. 15.7** Vertical aerial photo taken in 1953. *Source* [46]

settlement that did not take the morphology and coastal dynamic environment into consideration, see e.g., Pierri et al. [46]. For instance, Fig. 15.7 indicates that the main road in front of the beach called Atlantic Avenue in Matinhos was planned to run alongside the shoreline in 1953, but has been faced with soil erosion problems.

Coastal erosion started in the 70s and to date, this environmental degradation continues to be fueled further by the expanding development as indicated in Fig. 15.7. Figure 15.8 shows the walls of concrete and rocks being used as protective tools against the encroaching ocean, but every year over the last decades, storms have destroyed them, exposing the coastal settlement to erosion. For the past 40 years, this beach has continued to languish under these problems. According to Pierri et al. [46], the process of coastal erosion once started has the tendency to grow and is


**Fig. 15.8** Photos of the Shore in 1981, 1994, and 1995. Walls of concrete were applied as protective tools against the encroaching ocean. *Source* [47]


**Fig. 15.9** Houses destroyed by an ocean storm in May 2000, and removal of the houses and dune reconstruction in 2004. *Source* [46]

often difficult to reverse thereby calling for prevention as the best cure. When the problems start, depending on the settlement of the shore, the best solution can be the removal of any structure.

In Matinhos, removal of houses was performed on an informal settlement in the central beach after the ocean storm of May 2000, which destroyed several houses. After four years there was a restoration of the beach and dune systems, as can be seen by comparing photographs taken at different times in Fig. 15.9. In May 2001, another storm struck the shore of Matinhos (Fig. 15.10), destroying sidewalks, much of the waterfront promenade, and some fishing families were displaced [48]. Figure 15.3 on p. 318 shows the situation at Matinhos in 2007, indicating that the problems of coastal erosion are still present.

**Fig. 15.10** Effects of an episodic event in Matinhos (May, 2001). *Source* [48]

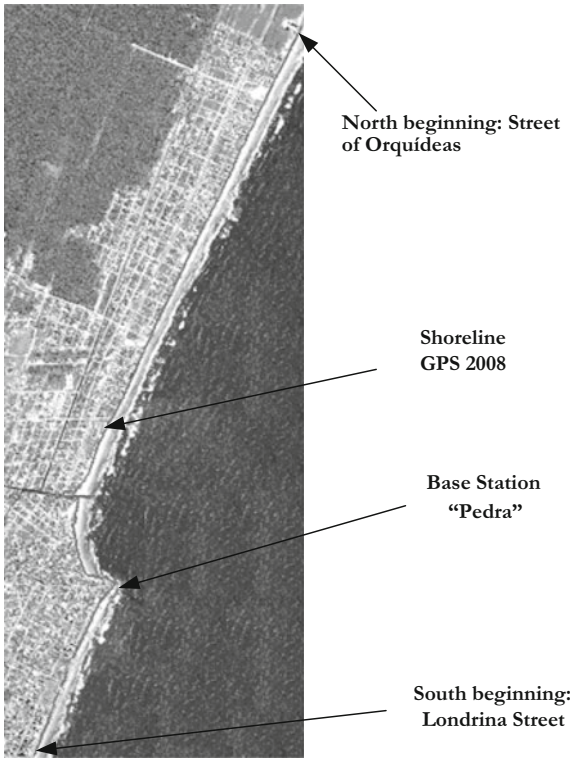


**Fig. 15.11** Location of the base station and the extent of the shoreline mapping. *Source* Goncalves [18]

*GNSS prediction of Matinhos' shoreline:* In order to monitor or predict shoreline position of Matinhos, a combination of various data sources are required. In this example, use was made of aerial photographs and GNSS (GPS) surveys for the years 2001, 2002, 2005 and 2008, to compare short-term prediction models (*robust parameter estimation*, *neural network* and *linear regression*). GNSS data from a geodetic survey of the shoreline in Matinhos was collected using the kinematic relative positioning method (e.g., Sect. 5.4.2). The reference (base) receiver was

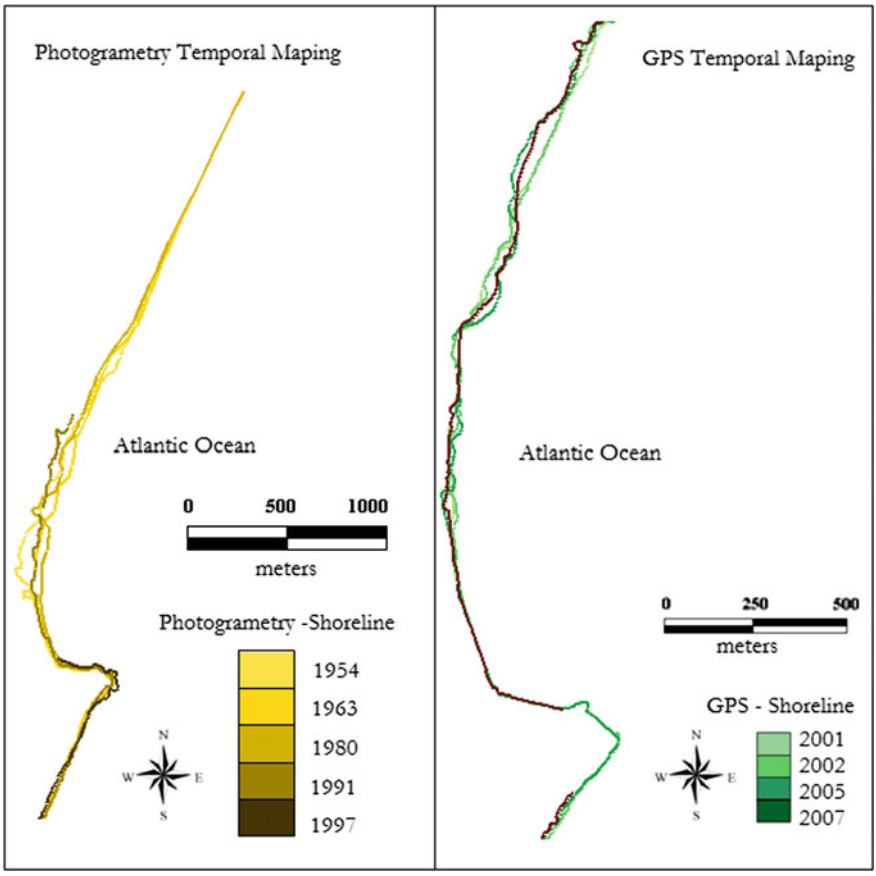


**Fig. 15.12** Temporal resolution of the GPS mapping. *Source* Goncalves [18]

stationed at Pedra (25° 49'05"S, 48° 31'49" W) as shown in Fig. (15.4, left). The southern GNSS survey began near Londrina Street, while the northern survey began near the Street of the Orqudeas (see Fig. 15.11). For this survey, dual frequency (L1 and L2) GNSS receivers were employed for the years 2001, 2002, 2005 and 2008 (see Fig. 15.12, right). Figure 15.13 indicate the residual between the predicted shoreline for 2007 compared to the actual shoreline position measured using GNSS.

The result of this comparison showed residuals of less than 8 meters between the predicted values for the year 2007 and the measured values using GNSS. The deviation was within the desired accuracy for predictive models of short-term shorelines, thus indicating the capability of GNSS to provide input data for predictive models and also in validating the shoreline prediction models.

♣ End of Example 15.3.

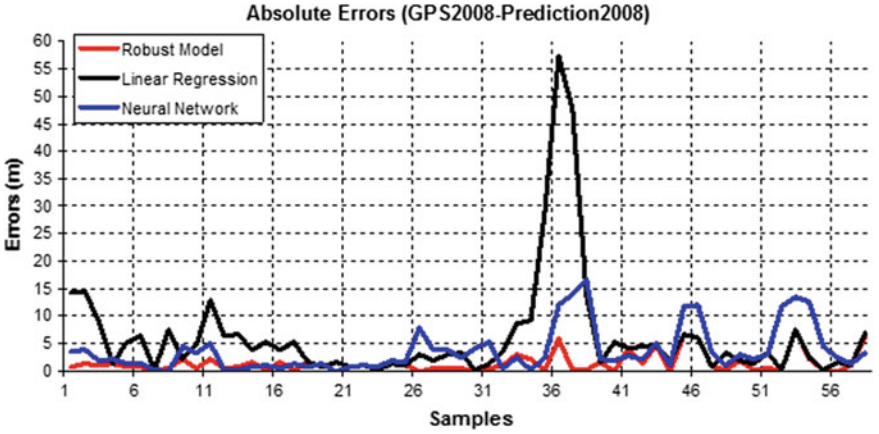


**Fig. 15.13** Predicted shoreline using linear regression, neural network and robust estimation models. *Source* Goncalves [18]

## 15.4 Concluding Remarks

This chapter has presented the applications of GNSS techniques to monitor the advance or retreat of coastal areas as well as marine habitats. GNSS-based methods offers quicker, all-weather, highly accurate and continuously updatable shoreline positional time series relevant for monitoring and management tasks undertaken by engineers and coastal authorities. Their disadvantages, however, are that they are only limited to small monitoring regions such as the case of Brazil considered in Sect. 15.3. For the countries such as Australia with very long coastal lines, the application of GNSS-based approach faces challenges of being time consuming and may require high manpower thus increasing the costs. Also, depending on coastal characteristics, e.g., of escarpment and mangrove trees, data collection using GNSS could be impracticable. In such cases, other techniques such as LIDAR come in handy. However, considering the case of Brazil where the cost of undertaking a GNSS shoreline monitoring is cost effective, the approach presented in this contribution suffices.

## References

1. Morton RA, Leach MP, Paine JG, Cardoza MA (1993) Monitoring beach changes using gps surveying techniques. J Coast Res 9(3):702–720
2. Goncalves R, Awange JL (2017) Evaluation of three mostly used GNSS-based shoreline monitoring methods to support Integrated Coastal Zone Management Policies. J Surv Eng. doi:10.1061/(ASCE)SU.1943-5428.0000219
3. Clarck, J.R. (1992). Integrated management of coastal zones. FAO Fisheries Technical Paper. No. 327. Rome, FAO. 167p. http://www.fao.org/docrep/003/T0708E/T0708E00.htm#TOC. Accessed 24 June 2013

4. Souza CRG (2009) Coastal erosion and the coastal zone management challenges in Brazil. J Integr Coast Zone Manag 9(1):17–37
5. Baldock J, Bancroft KP, Williams M, Shedrawi G, Field S (2014) Accurately estimating local water temperature from remotely sensed satellite sea surface temperature: A near real-time monitoring tool for marine protected areas. 96:73–81
6. Boak EH, Turner IL (2005) Shoreline definition and detection: a review. J Coast Res 21(4):688–703. doi:10.2112/03-0071.1
7. Botero C, Pereira C, Tosic M, Manjarrez G (2015) Design of an index for monitoring the environmental quality of tourist beaches from a holistic approach. Ocean Coast Manag 108:67–73
8. Jacobson C, Carter RW, Thomsen DC, Smith TF (2014) Monitoring and evaluation for adaptive coastal management. Ocean Coast Manag 89:51–57
9. Malthus TJ, Mumby PJ (2007) Remote sensing of the coastal zone: an overview and priorities for future research. Int J Remote Sens 24(13):2805–2815. doi:10.1080/0143116031000066954
10. Awange JL, Kiema JBK (2013) Environmental geoinformatics. Monitoring and management, Springer, Berlin
11. Call KA, Hardy JT, Wallin DO (2003) Coral reef habitat discrimination using multivariate spectral analysis and satellite remote sensing. Int J Remote Sens 24:2627–2639. doi:10.1080/0143116031000066990
12. Held A, Ticehurst C, Lymburner L, Williams N (2003) High resolution mapping of tropical mangrove ecosystems using hyperspectral and radar remote sensing. Int J Remote Sens 24:2739–2759. doi:10.1080/0143116031000066323
13. Karpouzli E, Malthus T, Place C, Chui MA, Garcia MI, Mair J (2003) Underwater light characterization for correction of remotely sensed images. Int J Remote Sens 24:2683–2702. doi:10.1080/0143116031000066972
14. Mumby PJ, Green EP, Edwards AJ, Clark CD (1997) Coral reef habitat mapping: how much details can remote sensing provide? Mar Biol 130:193–202
15. Schiff KC, Weisberg SB (2001) Microbiological monitoring of marine recreational waters in Southern California. Environ Manag 27(1):149–157. doi:10.1007/s002670010140
16. Soares CR, Vobel I, Paranhos Filho AC (1995) The marine erosion problem in Matinhos municipality. In: Land Ocean Interactions on the Coastal Zone, 1995, São Paulo. Boletim de Reumos do Land Ocean Interactions on the Coastal Zone, pp 48–50
17. Suguio K (1992) Dicionaário de geologia marinha. T.A, Queiroz, São Paulo, p 171
18. Goncalves RM (2010) Short-term trend modeling of the shoreline through geodetic data using linear regression, robust estimation and artificial neural networks. Ph D thesis, Geodetic sciences post-graduate program, Federal University of Parana (UFPR), Curitiba, Brazil, 152p
19. Demarest JM, Leatherman SP (1985) Mainland influence on coastal transgression: delmarva peninsula. Mar Geol 63:19–33
20. Galgano FA, Douglas BC, Leatherman SP (1998) Trends and variability of shoreline position. J Coast Res 26:282–291
21. Galgano FA, Douglas BC (2000) Shoreline position prediction: methods and errors. Environ Geosci 7(1):1–10. doi:10.1046/j.1526-0984.2000.71006.x
22. Gibeaut JC, Hepner T, Waldinger R, Andrews J, Gutierrez R, Tremblay TA, Smyth R, Xu L (2001) Changes in gulf shoreline position, Mustang, and North Padre Islands, Texas. A report of the Texas Coastal Coordination Council pursuant to National Oceanic and Atmospheric Administration. Bureau of Economic Geology, The University of Texas, Austin Texas
23. Fenster MS, Dolan R, Elder JF (1993) New method for predicting shoreline positions from historical data. J Coast Res 9(1):147–171
24. Fenster MS, Dolan R, Morton RA (2000) Coastal storms and shoreline change: signal or noise? J Coast Res 17(3):714–720
25. Li R, Di K, Ma R (2001) A comparative study of shoreline mapping techniques. In: The 4th international symposium on computer mapping and gis for coastal zone management, Nova Scotia, Canada, June 18–20

26. Metropolitan Borough of Sefton (2002) Shoreline monitoring annual report 2001/2002. http://www.sefton.gov.uk/pdf/TS_cdef_monitor_20012.pdf. Accessed 14 Nov 2008
27. Gorman L, Morang A, Larson R (1998) Monitoring the coastal environment; Part IV: mapping, shoreline changes, and bathymetric analysis. J Coast Res 14:61–92
28. Smith, JT, Jr. (1981). A History of Flying and Photography in the Photogrammetry Division of the National Ocean Survey, 1919–79. Silver Spring, Maryland: U.S. Department of Commerce, National Oceanic and Atmospheric Administration, National Ocean Service, p 486
29. Graham, D, Sault, M, Bailey, J(2003). National Ocean Service shoreline: past, present, and future. In: Byrnes, M, Crowell, M, Fowler, C (eds.), Shoreline mapping and change analysis: technical considerations and management implications, J Coastal Res , Special Issue No. 38, 14–32
30. Parrish, CE, Sault, M, White, SA, Sellars, J. (2005) Empirical analysis of aerial camera filters for shoreline mapping. In: Proceedings of the American society for photogrammetry and remote sensing annual conference, Baltimore, Maryland, p 1–11
31. Parrish, CE (2012). Shoreline Mapping in Advances in Mapping from Remote Sensor Imagery: Techniques and Applications (X. Yang and J. Li, eds.), CRC Press, Taylor and Francis Group, Boca Raton, Florida, p 145–168
32. Dolan R, Heywood J (1976) Landsat Application of Remote Sensing to Shoreline-Form Analysis. NASA Technical Report, NASA Goddard Space Flight Center, Greenbelt, Maryland, 33
33. Stockdon HF, Sallenger AH Jr, List JH, Holman RA (2002) Estimation of shoreline position and change using airborne topographic lidar data. J Coast Res 18(3):502–513
34. White SA, Parrish CE, Calder BR, Pe'eri S, Rzhanov Y (2011) Lidar-derived national shoreline: empirical and stochastic uncertainty analyses. J Coast Res. Special Issue 62:62–74
35. Yao F, Parrish CE, Pe'eri S, Calder BR, Rzhanov Y (2015) Modeling uncertainty in photogrammetry-derived national shoreline. Mar. Geod. 28:128–145
36. Westoby MJ, Brasington J, Glasser NF, Hambrey MJ, Reynolds JM (2012) Structure-from-motion'photogrammetry: a low-cost, effective tool for geoscience applications. Geomorphology 179:300–314
37. Mancini F, Dubbini M, Gattelli M, Stecchi F, Fabbri S, Gabbianelli G (2013) Using unmanned aerial vehicles (UAV) for high-resolution reconstruction of topography: the structure from motion approach on coastal environments. Remote Sens. 5(12):6880–6898
38. Awange JL (2012) Environmental monitoring using GNSS global navigations satellite systems. Springer, Berlin
39. Goncalves RM, Awange J, Krueger CP, Heck B, Coelho LS (2012) A comparison between three short-term shoreline prediction models. Ocean Coast Manag. 69:102–110
40. White K, Asmar EL (1999) Monitoring changing position of coastlines using thematic mapper imagery, an example from the Nile Delta. Geomorphology 29(1–2):93–105. doi:10.1016/S0169-555X(99)00008-2
41. Goncalves RM, Awange J, Krueger CP (2012) GNSS-based monitoring and mapping of shoreline position in support of planning and management of Matinhos/PR (Brazil). J Glob Position Syst 11(1):156–168. doi:10.5081/jgps.11.2.156
42. Hecky RE, Newbury RW, Bodaly RA, Patalas K, Rosenberg DM (1984) Environmental impact prediction and assessment: the southern Indian lake experience. Can J Fish Aquat Sci 41(4):720–732
43. Crowell M, Douglas BC, Leatherman SP (1997) On forecasting future U.S. shoreline positions: a test of algorithms. J Coast Res 13(4):1245–1255
44. Douglas BC, Crowell M, Leatherman SP (1998) Considerations for shoreline position prediction. J Coast Res 14(3):1025–1033
45. Douglas BC, Crowell M (2000) Long-term shoreline position prediction and error propagation. J Coast Res 16(1):145–152
46. Pierri N, Angulo RJ, Souza MC, Kim MK (2006). A ocupação e o uso do solo no litoral paranaense: condicionantes, conflitos e tendencias. Desenvolvimento e meio ambiente. Ocupação e uso do solo costeiro um mosaico de diversidade (13), editora UFPR, 137-167

47. Angulo RJ, Soares CR, Souza MC (2000) Excursion route along the state of Paraná (PR). In: 31st International geological congress. Rio de Janeiro, August 6–17, pp. 58–81
48. Krueger CP, Centeno JA, Mitishita EA, Veiga LAK, Zocolotti CAJ, Jubanski MJ (2002) Determinacao da linha de costa na regiao de Matinhos. Anais do Simposio Brasileiro de Geomatica, Presidente Prudente - SP, pp 206–211

# Chapter 16
# Land Management

*The Earth provides enough to satisfy every man's needs, but not every man's greed*

Mahatma Gandhi

## 16.1 Introductory Remarks

Land provides the base upon which *social*, *cultural* and *economic* activities are undertaken and as such is of significant importance in environmental monitoring. Social, cultural and economic activities have to be planned and managed in such a way that the sustainable use of land resources is enhanced. Sustainable land use ensures that economic and socio-cultural activities do not benefit at the expense of the environment (see Sect. 13.5). Monitoring of *changes* in land through indicators could help in policy formulation and management issues for the betterment of the environment. Some of the vital indicators for land management include vegetation, soil quality and health, biosolids and waste disposed on land, land evaluation, land use planning, contaminated land, integrity of the food supply chain, mine closure completion criteria, and catchment management, in particular water balance, salinity, eutrophication, and riparian/wetland vegetation. This chapter presents the possibility of using GNSS satellites to enhance the monitoring of some of these indicators.

## 16.2 GNSS for Reconnaissance and Validation

Before any field measuring campaign is undertaken, pre-field preparations are essential. *Topographical maps* (e.g., Chap. 8) and *aerial photographs* normally provide the main sources of information for determining land use capability. Maps and photographs of varying time span can be visually examined to identify any potential land use changes that has occurred during the time interval under consideration. *Relief changes* within the study area are identified and specific features, e.g., remnant vegetation (Fig. 16.1), identified for the purpose of georeferencing.



J. Awange, *GNSS Environmental Sensing*, Environmental Science and Engineering, DOI 10.1007/978-3-319-58418-8_16

**Fig. 16.1** Ground-truthing of aerial photos: Example of remnant vegetation at Mt. Kokeby, Australia

Hand-held GNSS receivers that position to within 5–15 m (see, e.g., Fig. 2.1 on p. 19) are useful for georeferencing tasks. This is because such features' spatial coverage are normally larger than the 15 m accuracy typical for positioning using single frequency hand-held receivers. It is worth pointing, as already done in the previous chapters, that during the actual undertaking of aerial photography, GNSS provide control points useful for orienting aerial cameras (Fig. 16.3).

Field reconnaissance entails the pre-visitation of a survey area before the actual survey. In this case, hand-held GNSS receivers are useful in providing navigation services. For example, if the crew members require to visit a specific location, they could easily use the navigation function of a hand-held GNSS to reach the desired location or to identify the derived feature.

## 16.3 Monitoring of Land Conditions

### *16.3.1 Soil Landscape Mapping*

GNSS satellites are also useful for mapping soil types. Conventionally, *soil maps* define mapping units where a particular soil type is believed to be. Verhagen et al. [1] demonstrated the usefulness of GNSS in georeferencing soil data and the sampling of soil fertility. The GNSS soil data information enabled them to perform dynamic simulation modelling to characterize soil water regimes and nutrient fluxes (e.g., of nitrate).

GNSS satellites could also provide the location-based data for soil landscape mapping. Soil-landscape mapping is a survey of land resources, which delineates repeating patterns of landscapes and associated soil types and differs from soil mapping in that the landscape component is an explicit part of the mapping [2]. Uses of land resource data collected during a soil-landscape mapping program include [2]; reducing the risk in decision-making (ensuring that changes in land management, are the result of land resource information that reduces the uncertainty about the impact of different strategies), improving our understanding of biophysical processes, designing large-scale land use changes (e.g., targeted revegetation to control dry land salinity), environmental regulation and trading systems, mapping and monitoring land conditions to support national policies on natural resource management support of international agreements (e.g., Kyoto Protocol demands for predictions of the distribution and dynamics of soil carbon over a range of scales), and support of environmental management systems. For example, Pieri [3] used GNSS to collect spatial data needed for planning sustainable land management. Using GNSS information, photographs and photomosaics, simple information such as field boundaries, farmers' appreciation of soil productivity or constraints (using, e.g., indigenous classification of soils), and land use rights were collected and registered. The report proposed the use of GNSS to spatially reference all physical and social information in land management planning.

Schoknecht et al. [2] divided the information about the soils and landscapes of Western Australia into point data stored in a soil profile database, which is comprised of site specific information such as soil profile descriptions, the results of laboratory analyzes and photographs, map unit polygons stored as digital lines, boundaries drawn around areas containing similar soil and landscape patterns, and a map unit database that contained descriptions of the map unit polygons and related them to broad areas rather than a specific point. In both point and polygon data, GNSS satellites played an important role during the data collection process.

### *16.3.2 Provision of Point Data*

Field surveys for soil landscape mapping involves occupying selected sites identified during a preliminary survey and reconnaissance. Factors influencing the selection of these sites include ease of access and the changing landscape. Representative soils from these selected sites are examined in soil pits with samples taken for chemical and physical analysis. Besides the examination of the soil, other physical description of the site, such as slope and vegetation, are also recorded.

The important contribution of GNSS satellites in this process would be the provision of the site locations, which can be achieved using a hand-held receiver as shown in Fig. 16.2. This allows point data information on which all the landscape information relating to a specific site, such as site *description*, *soil profile* description, *soil classification*, *soil profile's chemical*, and *physical properties* are related. The site description consists of information such as slopes measured using clinometers,

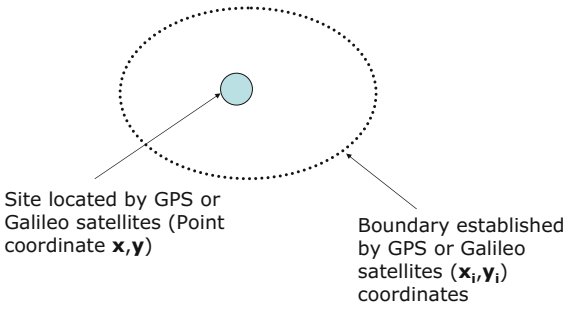


**Fig. 16.2** Schematic description of how GNSS can provide site and boundary locations. These values can easily be integrated in a GIS system to enhance analysis

landform patterns and elements of the survey area, the surrounding vegetation (e.g., Fig. 16.1), land surface and use. An example of mapping soil characteristics that significantly affects crop production, e.g., clay content, organic matter content, nutrient content, and plant available water, is illustrated, e.g., in the work of Brubaker et al. [4].

### *16.3.3 Provision of Polygon Data*

Since the aim is to produce the soil landscape maps, the boundary of the maps are traced on aerial photographs or satellite imagery and then captured digitally using computer-aided mapping systems (e.g., in a GIS). This is done by either scanning the photographs or by keying in directly the two dimensional $x$, $y$ coordinates. The boundary coordinates $\{x_i, y_i\}$ that form the map unit polygon are provided through satellites or ground surveying methods and are then mapped onto those of adjoining surveys. GNSS satellites provides control and tie points needed to match these boundaries (i.e., orienting the aerial photographs). For example, Fig. 16.3 indicate control points that are selected, marked, and accurately surveyed using GNSS positioning techniques discussed in Sect. 5.4.2. These points are then captured by aerial photographs and the GNSS positions compared with those of the photograph to control the quality of the maps derived from the photographs.

Alternatively, points could be located in older photographs and their positions established using GNSS receivers to control the quality of the digital maps derived from these photographs. Tie points on the other hand are common points that appear on different photographs (e.g., Fig. 16.3). They too could be located using GNSS satellites, and together with the control points provide the base upon which landscape maps could be prepared. Point data and map unit polygons form map unit databases that relate to the entire landscape. Use of such digital maps include precision farming discussed in Sect. 16.5.1. Details of the actual GNSS procedures needed to generate maps are discussed in Chap. 8.

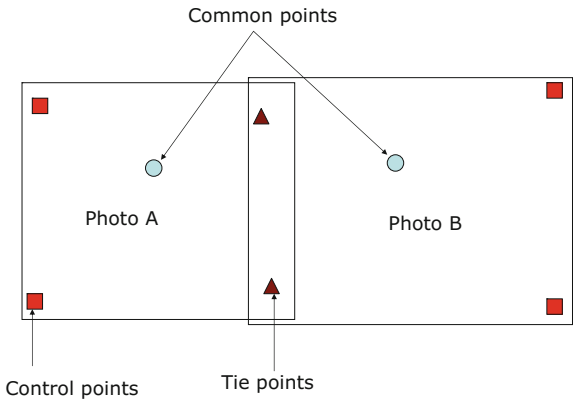


**Fig. 16.3** A schematic diagram of how GNSS satellite provide control and tie points, which are used to orient aerial photographs. These photographs provide the monitoring platform

## 16.4 Monitoring of Land Degradation

Bell [5] classifies land degradation as both a local and global problem. Locally, the individual land owners are faced with the problem of declining land productivity while globally, the increase in population poses a threat to the fertile land and decreasing resources. The demand for increased food production to feed the increasing population must increasingly be met from increased production per unit area [5]. Indeed, identifying the serious effects of land degradation on the environment leads to increased efforts in quantifying the problem, developing possible solutions, and engaging with the community to resolve these problems [5].

Land degradation can be seen through the effect of salinity, water erosion, wind erosion, waterlogging, remnant vegetation decline, sub-soil compaction, soil structure decline, structural decline, fertility decline, eutrophication, acidification and water repellence [6]. The main cause of these forms of land degradation has been attributed to water, which is often an off-farm impact as a result of water recharge, water discharge, water runoff and flooding, e.g., [5].

### *16.4.1 Soil Erosion Monitoring*

Soil erosion occurs through the process of detachment, transportation and the deposition of soil. The net effect is the loss of fertile top soil for agriculture, siltation of streams and lakes, eutrophication of surface water bodies, and the loss of aquatic biodiversity [7]. Mackenzie [8, p. 322] points out that an estimated 480 billion tons of topsoil have been lost to the world's farmers by erosion in the past few decades. Of this, 18 billion tons are said to be transported by rivers to oceans annually while the rest moves to other terrestrial ecosystem.

In order to minimize the impact of soil erosion, it is essential that management practices take into consideration the magnitude and *spatial distribution* of soil

erosion. Soil erosion models such as the Universal Soil Loss Equation (USLE) [9] and its modified version (Revised Universal Soil Loss Equation RUSLE, e.g., [7]) have been developed to estimate the rate of soil erosion. Determination of soil erosion, however, poses a challenge due to the contribution of biophysical factors (e.g., soil and climate) and the interactions between them. The limitation of these models is their inability to cope with the large amount of data that describes the heterogeneity of the natural system [10]. Within the scope of these models, remote sensing techniques find use in mapping and assessing the landscape attribute that control soil erosion such as land use/land cover, soil type, relief, slope, drainage etc.

Multi-temporal satellite images are useful in studying seasonal land use dynamics that contribute to soil erosion. Satellites also provide information on erosion features such as gullies and vegetation cover, and also contribute in the generation of Digital Elevation Models (DEM, e.g., Fig. 8.3 on p. 132), useful for soil erosion models. This is achieved through the analysis of stereoscopic and microwave (SAR) data. Lufafa et al. [11] combined aerial photo interpretation (API) and interpretation of Landsat TM images of 1994 to generate land use/land cover maps using the normalized digital vegetation index (NDVI). Parameters of the land use/land cover maps were then inserted in the USLE model to predict the rate of soil erosion. In Onyando et al. [7], multi-spectral image processing is used to extract thematic information from Landsat TM (bands 2, 3 and 4) data to generate land cover maps from which parameters for the USLE model are derived. Supervised classification using maximum likelihood is adopted. Other studies that have generated land cover maps useful for soil erosion include [10, 12, 13]. In [13], geometric rectification of the images was achieved using ground reference data collected from topographical maps. As was discussed e.g., in Chap. 8, GNSS-derived topographical maps could be useful. Besides, GNSS could also provide DEM (see e.g., Fig. 8.3), and also in providing location-based data for generating spatial distribution of soil erosion (as shown e.g., in Fig. 5.9 on p. 75).

### *16.4.2 Salinity Monitoring: The Catchment Approach*

Salinity can be classified into primary and secondary salinity. Over millions of years, salt from the ocean has been collected and deposited by wind and rain across landscape, with few rivers returning this salt to the sea. This led to a gradual accumulation of salt, which eventually became part of the natural landscape termed *primary salinity*.[1] *Secondary salinity* of soil, or 'salinisation', results from rise in water table, which is often caused by changing land use actions such as land clearing or irrigation, where the term 'water table' refers to undergroundwater (or groundwater), which may be very deep, but can be quite close to (or at) the surface (see footnote 1).

[1] http://www.environment.sa.gov.au/education/.

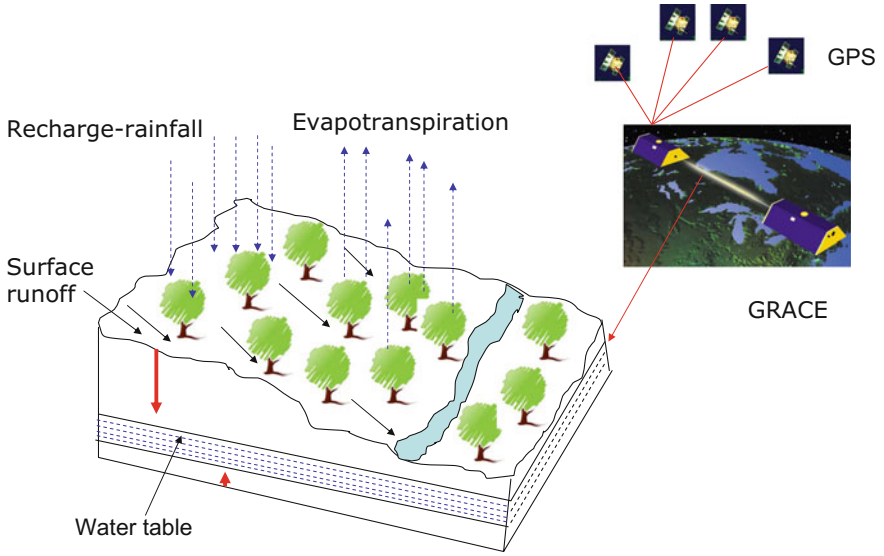


**Fig. 16.4** With natural vegetation, the water balance is maintained, groundwater levels are low, less recharge, less runoff and salinity is curbed

The major origin of salt causing secondary salinity is rainfall, which has deposited large amount of salt over ten thousands of years. Other contributors are weathering of minerals in the underlying bedrock and marine sediments. The processes leading to *secondary salinity* are traced to the altered water balance due to the fact that deeply rooted perennial native vegetation, which helped maintain the groundwater balance (e.g., Figs. 16.4 and 16.5) has been replaced by pastures and crops that do not use enough rainfall to lower water tables and significantly reduce salinity.

The clearing of such vegetation has seen increased recharge at a much faster rate than would otherwise occur naturally. The excess water not used by vegetation seeps into the soil, past the root zone, and contributes to increase in stored groundwater. With time, the groundwater water table rises and in the process dissolves the solid salt stored deep in the soil. When the water table reaches within 1–2 m of the soil surface, salt enters the plant root zone and growth is affected. This process is called *dryland salinisation* and has been reported, e.g., in [14] to affect a significant proportion of agricultural soils in south-western Australia.

Apart from the dryland salinity, there is also *irrigation salinity*, which is caused by the recharge of groundwater by excessive irrigation and leakage from irrigation channels. This again causes water tables to rise and in so doing brings salt to the root zones. Besides vegetation clearing and irrigation, the local landscape (i.e., geology and topography) and groundwater aquifer characteristics also play an important role in the susceptibility of land to salinization. In both dryland and irrigation salinity, saline groundwater near the soil surface kills native vegetation and reduces biodiversity, thus threatening the overall health of natural ecosystems (see Fig. 16.6). It also

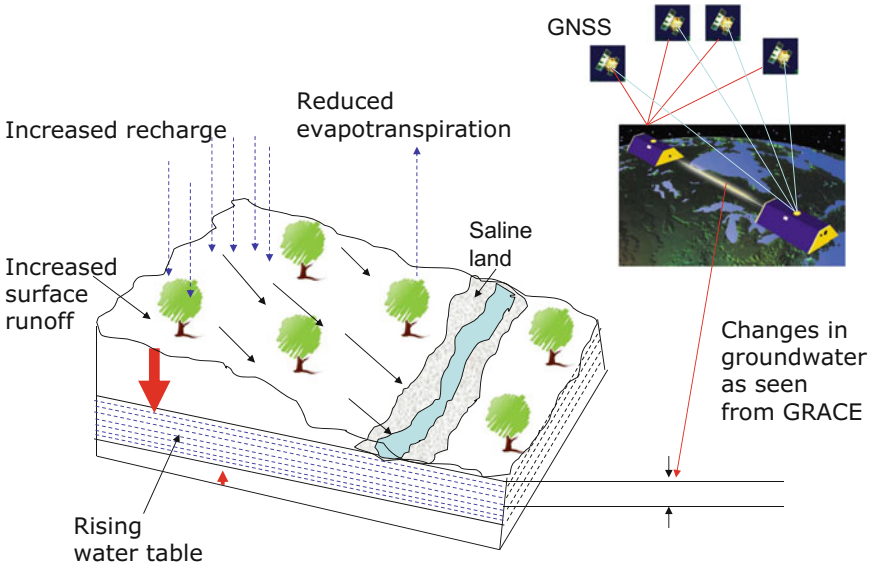


**Fig. 16.5** With vegetation cleared, the water balance is disturbed. Groundwater levels rise, recharge increases with increased runoff and salinity increases. GRACE satellites discussed in Sect. 9.3.3 could provide a possible means of measuring changes in water level at catchments having sufficient spatial resolution for its use

results in the loss of agricultural productivity, deteriorates the quality of drinking water, and damages infrastructure such as roads and buildings.

In the Murray-Darling Basin (MDB) in Australia for example, agricultural production is reported to account for approximately 40% of the total production in Australia [15]. This high level of agricultural production comes despite MDB's high aridity and low runoff compared to other major river basins [16]. This comes at the expense of irrigation, which uses about 75% of the total water used in Australia, and extensive clearing of native vegetation for cropping and pastoral land use [15].

As already illustrated in Fig. 16.5, vegetation clearing leads to salinity as does extensive irrigation. Since both irrigation and clearing of the MDB has occurred to sustain agricultural productivity, the landscape and river systems have been dramatically altered leading to several undesirable effects, including increased salinity, diminished biodiversity and ecosystem degradation [16]. The number of land parcels falling victims to salinity seems to be on the rise, calling for integrated catchment-based remedies. For instance in New South Wales (Australia), over 500,000 hectares of land were estimated to be impacted by salinity in the year 2000, with a projection of 2–4 million hectares by 2050 if changes in land use are not enacted [16].

*Management Options*: Management of salt-affected land (or potentially salt-affected land) must be based at least on a whole catchment approach, e.g., [17]. Catchment management involves all those activities related to the *capacity to produce* and *maintain* runoff and groundwater with desirable quality and quantity characteristics,

**Fig. 16.6** Impacts of salinity at Mt. Kokeby, Australia

and by reducing the undesirable consequences of land use on stream behaviour [5]. Catchment management should, therefore, be holistic in outlook, i.e., it should involve the consideration of all aspects of the physical and socio-economic environments that impinge on the catchment, its resources, and their use. Management of *discharge* areas will differ from the *recharge* areas. Discharges areas are part of the landscape where groundwater approaches or reaches the soil surface. Recharge areas on the other hand are part of the landscape where water passes below the root zone and adds to the groundwater (see Fig. 16.5).

*Management of discharge areas* aims at obtaining production (i.e., of salt tolerant shrubs or pasture) from the area while at the same time reducing the salt-affected land. Actions taken on, or immediately around, discharge areas can take the form of engineering remedies such as digging drains or banks, to biological methods such as planting shrubs, grasses or trees or a combination of both engineering and biological. Management of salt-affected areas to alleviate the problem uses four principles [5]; *increase water use*, *decrease surface evaporation*, *decrease waterlogging*, and *increase leaching* of salt.

*Management of recharge areas* essentially leads to the prevention of salinity with the objective being to reduce recharge water (Fig. 16.5) reaching groundwater. This can be achieved by increasing plant water use and by using engineering means to divert excess water from the saline areas to avert ponding and waterlogging. One approach for achieving this is to plant deep rooted plants with the ability to use water throughout the year. This approach has been found to yield fruit in some parts of Western Australia (WA). For instance, Greenwood [18] found that at North Bannister, the annual evaporation from trees (*Eucalyptus cladocalyx*, *E. globulus* and *E. maculata*) was some seven times the evaporation from grazed pasture [17]. Planting

trees and shrubs on recharge areas of agricultural catchments is also being advocated by the Department of Agriculture in WA. While it is not economic to indulge in large scale plantings, there are often areas in catchments which can be identified as "specific recharge areas" [19], which are small, make a major contribution to recharge, and do not produce economic crops or pastures, but can be used for planting trees or shrubs. Encouraging extensive planting, especially in high recharge zones, of deep-rooted perennial plants (trees, shrubs and pastures) is, therefore, one of the clearest mechanism to fight salination.

Plants such as barley and lupins are also known to have high water uptake owing to their deep roots and are encouraged for prevention. The difference in plant water usage is attributed to *rooting depth*, *leaf area index*, and *biomass*. For example, barley, and lupin have root penetration down to 2.5 m. Barley also has been shown to attain the highest leaf area index, followed by lupins, wheat and clover. Lupins have been shown to have higher transpiration rates than wheat and pasture in late winter due to greater biomass. The disadvantage with the plants approach is that they are not annual crops and are unable to utilize water throughout the year, thus rain which fall outside of the growing season still seep into the soil [5].

Example 16.1 (GNSS support of salinity management)

This can possibly be achieved in two ways:

(1) In the first instance, GNSS hand-held receivers could be useful in monitoring salt-tolerant pasture areas through the mapping of the boundary of salt-tolerant pasture species (e.g. barley) to assess the spread. This method could be augmented with photogrammetry and remote sensing where the positioning satellites could also be used to provide controls of reference features for the photographs and images (see Fig. 16.3).
(2) The second approach would be the monitoring of changes in groundwater as illustrated in Fig. 16.5. For large spatial coverage, use of piezometers may not suffice and hence the requirement of space techniques. The monitored variations in groundwater could then be correlated with the revegetation measures to assess the impacts of replanting of trees or retained native vegetation to curb salinity. In this particular scenario, GNSS plays the supportive role to GRACE remote sensing satellite (see, e.g., Chap. 9). It should be mentioned, however, that the resolution of the catchment area must be suitable for use of GRACE. Other components of the total water storage such as surface water and soil moisture need to be isolated to leave only the groundwater. This approach of using GRACE satellites, however, remains an ambitious proposal to be tested. With improved spatial resolution obtained from, e.g., Mascon solution, see Awange et al. [20], all possibilities exist.

♣ End of Example 16.1.

## 16.5 GNSS Support of Precise Farming

### *16.5.1 Precise Farming*

Traditionally, farming normally treats the "*whole field*" as a single (homogeneous) entity upon which decisions (based on field averages) have been made. Inputs (e.g., fertilizers) are then applied uniformly across the field. Modern farming methods (also known as precision farming or precision agriculture), however, divide large pieces of land into smaller segments that are managed separately to optimize productivity and reduce environmental impacts of excessive use of chemicals and fertilizers (see, e.g., Fig. 16.7) through the use of GNSS, in e.g., GPS guided (controlled) tractor. In Chap. 20, the use of unmanned aircraft vehicles (UAV)/drones will be discussed.

*Precision farming* is the gathering of information dealing with *spatial* and *temporal variation* within a field with the aim of using the information to manage inputs and practices. This is made possible by linking *computers*, *mobile sensors*, *GNSS*, and other devices [21]. It is a comprehensive approach to farm management and has the following goals and outcomes; *Increased profitability and sustainability*, *improved product quality*, *effective and efficient pest management*, *energy, water and soil conservation*, *surface and groundwater protection*, *yield rates*, *pest infestation* management, and *other factors that affect crop production* [22]. In addition to this, Verougstraete [23] states "*the future of durable global agriculture is not the general and sometimes unnecessary use of an agent as Roundup which should be greatly reduced or eliminated for use in any case. On the contrary, improved monitoring and management based on a big data approach will improve yield and imply a reduction of pesticide use as well as excessive fertilizer application. What is needed is fertilization in quantities optimal for the crop to deliver optimal harvests*". To achieve these outcomes, farm managers base their decisions on the requirements of each zone to control input resources. *GNSS and GIS can be used to control the input of these zones* as discussed, e.g., in [24, Chap. 9].

Precision farming allows the management of various zones, with the zone having a higher potential for economic return receiving more inputs, if needed, than less productive zones so as to achieve maximum economic return for each input [22]. Dobermann and White [25] refer to precision farming as site specific crop management and discuss how GNSS satellites are applicable to nutrient management.

Precise farming attempts to increase food production per unit area and as such, requires proper land utilization and management of the input resources, e.g., *fertilizers* to maximize the yield. When this is done in a manner such that the environment is protected and conserved, and social values also promoted, it can lead to *sustainable agriculture*, whose indicators are *state of resource*, *biophysical* and *economic* trends.

For instance, the application of GNSS to *precision farming* have been shown to include soil sample collection, chemical application controls, and harvest yield monitoring [26, p. 142]. The applications of GNSS for soil sampling was discussed in Sect. 16.3.1. Spraying of the field from aeroplanes could be integrated using aerial guidance systems in such a way that the field sprayer is guided using a moving

map display. Based on the sprayer's location, the system will apply the chemical at the correct locations, with minimal overlap, and automatically adjust the chemical's use rate, thus increasing the efficiency of chemical and fuel usage [26, p. 14] and in so doing minimize impacts on the environment. Veroustraete [23] puts it more candidly by comparing sick people to sick plants "*Though human medecine is in an advanced stage of development, plant 'medicine', has barely started in agriculture. Precision farming is a partial answer to lack of 'plant medicine'. When developed and implemented, yield will be increased, while environmental impacts will be reduced, e.g., precision farming is a transformation of classical 'chemically based' agriculture into durable agriculture*". The position of these field spots could be provided by GNSS as discussed in Sects. 16.3.3 and 17.1.2.

Example 16.2 (Trimble's AgGPS)

The Trimble group have developed the AgGPS system, which combines in-field guidance using GPS satellite receivers and intelligent farm management. The AgGPS field positioning systems enable field guidance at a higher accuracy, allowing farmers the possibility of collecting information on tillage, cultivation, irrigation, topography and infestations, which can then be mapped and analyzed to provide a better understanding of the elements affecting farm operations and management [27]. The system can be tailored for site specific applications such as yield mapping and variable rate management. Buick [27] lists the primary reasons why many farmers are considering (or reconsidering) numerous site-specific precision agriculture practices as the net gain in sustainable agriculture, i.e., *economic*, *environmental* and *sociological* paybacks from GNSS-guidance and automated steering systems, and the decrease in the cost of GNSS machine control systems. With more GNSS satellites on the way, this cost is expected to be even lower. Veroustraete [23] concludes "*Intensification based on monitoring, using modern techniques such as remote sensing, new agricultural techniques like GPS controlled tractors for fertilizing and carefully dosed disease treatments, fosters a reduction in environmental damage and a pathway to durable agriculture*".

♣ End of Example 16.2.

### *16.5.2 Farm Topographical Maps*

A farm topographical map is an example of maps (see Sect. 8.2.3) produced using either DGPS or RTK method of GNSS positioning discussed in Sects. 5.4.4.1 and 5.4.6 respectively. They are useful in depicting topographical features such as elevation, landscape, drainage, soil attributes, slopes etc. Since spatial yield variability is usually related to topographical features, see e.g., [28–33], the availability of high accurate GNSS *farm topographic maps* should enhance *operational efficiency* and lead to better, improved *agricultural and environmental management*. For instance, such maps should lead to improved management of agricultural inputs

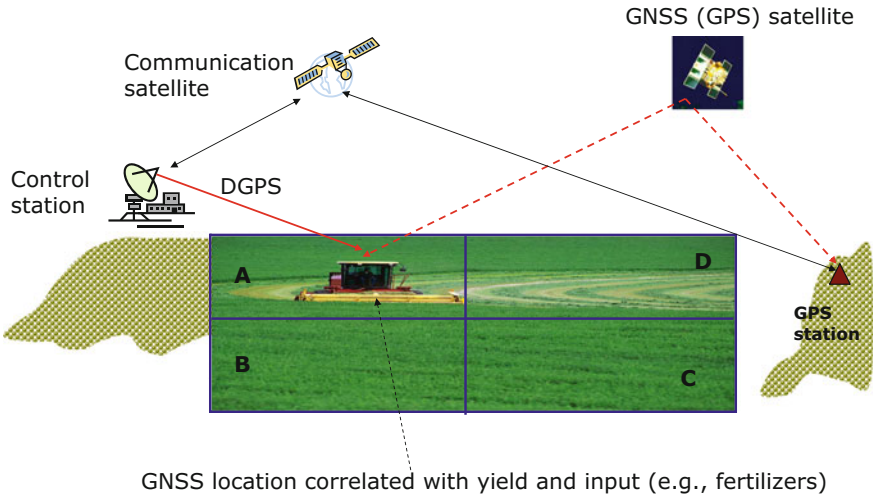


**Fig. 16.7** Application of GNSS to precision farming

such as fertilizers, and in water deficient countries such as Australia, contribute to better management of surface and groundwater.

Example 16.3 (Controlled Traffic Farming (CTF) Solutions)

Controlled Traffic Farming (CTF) Solutions is an Australian-based organization that seeks to provide solutions on focusing on efficient and effective use of *farm resources* to maximize production and minimize *environmental impacts* such as *soil erosion* and *waterlogging*.[2] CTF Solutions collects topographical data using a 2 cm auto steer operations during the period which the tractor is in the field undertaking farm operation or by using a vehicle with an antenna mounted on it. In order to collects gridded data for the purpose of generating elevations, the vehicle is driven at regular swath intervals (width of 20–40 m) with the GNSS receiver logging data at 5–10 m intervals. Besides these regular grids, data for other features of environmental interest, such as flood runners and erosion washers, are also collected. The data is then analyzed using a GIS system to generate topographic maps (see, e.g., Fig. 8.2 on p. 131).

An illustration of the CTF Solution's application of GNSS (RTK approach) is presented in Fig. 16.8, where CTF's RTK collected topographical data at 25 cm contour interval are overlayed on a high resolution IKONOS imagery.[3] The figure essentially shows that low lying areas of production have suffered significant crop loss due to waterlogging (Tim, pers. comm).

Following the results outlined in Fig. 16.8, drainage was undertaken on the paddock in 2005 and GNSS together with high resolution imagery once again applied to

[2] See http://www.ctfsolutions.com.au/ [Accessed on 8-09-2009].

[3] © Geoeye 2004 NIR band.

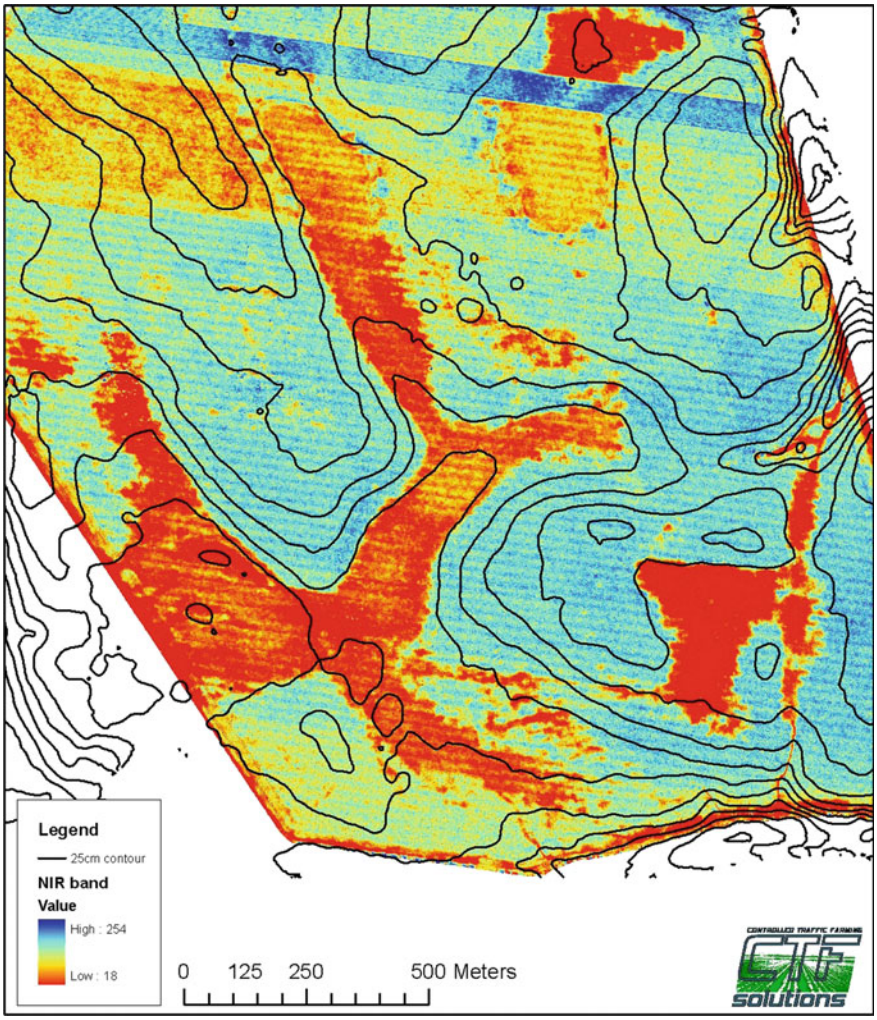


**Fig. 16.8** GNSS topographical map taken in 2004 by CTF overlayed on a high resolution IKONOS imagery. Dark red colours indicate areas of poor drainage affected by waterlogging. *Source* http://www.ctfsolutions.com.au

monitor the environmental impact of waterlogging in 2006 (Fig. 16.9). In 2004, this waterlogging cost the farmers in the order of Australian $50,000 in lost production (Tim, pers. comm). The combination of GNSS and high resolution imagery was the key to the success, otherwise each monitoring method on their own would not have told the whole story (Fig. 16.9). This example, therefore, provides a good illustration of the role played by GNSS in monitoring *environmental impacts* on farms.

♣ End of Example 16.3.


**Fig. 16.9** GNSS topographical map taken by CTF overlayed on a high resolution IKONOS imagery. The left figure was taken in April 2004 (see Fig. 16.8). The right figure indicates the same area in August 2006 after drainage was undertaken in 2005. *Source* http://www.ctfsolutions.com.au

## 16.6 Concluding Remarks

This chapter has presented the possibility of using GNSS satellites to support land management measures. It is clear from the discussion that the area of precision farming has received a greater share of GNSS application compared to other areas of land management. Moreover, Veroustraete [23] opines that with intensification, high productivity and good management on quality farmland more space for natural landscapes will likely be created. Therefore In general, however, the uses of GNSS satellites are more vital in areas of land management that requires information on positions and spatial coverage. With more GNSS satellites being launched, they are expected to become more useful to land management, particularly when coupled with GIS and/or Remote sensing methods. A point to note is the emergence of unmanned vehicles aircraft (UAV)/drones for agricultural monitoring. More on this will be covered in Chap. 20.

## References


1. Verhage A, Booltink HWG, Bouma J (1995) Site-specific management: balancing production and environmental requirements at farm level. Agric Syst 49:369–384
2. Schoknecht N, Tille P, Purdie B (2004) Soil landscape mapping in south-western Australia. Overview of methods and outputs. Resource management technical report 280, Department of Agriculture, Government of Western Australia
3. Pieri C (1997) Planning a sustainable land management: the hierarchy of user needs. ITC J 3(4):223–228
4. Brubaker SC, Jones AJ, Lewis DT, Frank K (1993) Soil properties associated with landscape position. Soil Sci Soc Am J 57(1):235–239
5. Bell RW (1997) Introduction. In: Bell RW (ed) Land management unit reader. Murdoch University, Perth, pp 3–7
6. Lantzke N, Fulton I (1993) Soils of the Northam advisory district. Volume 3 - The Darling Range and West Kokeby Zone. Agriculture WA Bulletin, pp 42–57
7. Onyando JO, Kisoyan P, Chemelil MC (2005) Estimating the potential of soil erosion for river Perkerra catchment in Kenya. Water Resour Manag 19(2):133–143. doi:10.1007/s11269-005-2706-5
8. Mackenzie FT (2003) Our changing planet; an introduction to Earth system science and global environmental change, 3rd edn. Prentice Hall, New Jersey
9. Hudson N (1985) Soil conservation. Batsford Academic and Educational, London
10. Pandey A, Chowdary VM, Mal BC (2007) Identification of critical erosion prone areas in the small agricultural watershed using USLE, GIS and remote sensing. Water Resour Manag 21(4):729–746. doi:10.1007/s11269-006-9061-z
11. Lufafa A, Tenywa MM, Isabirye M, Majaliwa MJG, Woomer PL (2003) Prediction of soil erosion in a Lake Victoria basin catchment using GIS-based Universal Soil Loss Model. Agric Syst 76(3):883–894. doi:10.1016/S0308-521X(02)00012-4
12. Ismail J, Ravichandran S (2007) RUSLE2 model application for soil erosion assessment using remote sensing and GIS. Water Resour Manag 22(1):83–102. doi:10.1007/s11269-006-9145-9
13. Lu D, Li G, Valladares GS, Batistella M (2004) Mapping soil erosion risk in Rondonia, Brazilian Amazonia: using RUSLE, remote sensing and GIS. Land Degrad Dev 15(5):499–512. doi:10.1002/ldr.634
14. NLWRA (National Land and Water Resource Audit) (2001) Water resources in Australia. A summary of the National Land and Water Resource Audit's Australian water resources assessment 2000. Surface water and groundwater - availability and quality
15. Ellett KM, Walker JP, Rodell M, Chen JL, Western AW (2005) GRACE gravity fields as a new measure for assessing large-scale hydrological models. In: Zerger A, Argent RM (eds) MODSIM 2005 international congress on modelling and simulation. Modelling and simulation society of Australia and New Zealand, December 2005, pp 2911–2917. ISBN: 0-9758400-2-9
16. Ellett KM, Walker JP, Western AW, Rodell M (2006) A framework for assessing the potential of remote sensed gravity to provide new insight on the hydrology of the Murray-Darling Basin. Aust J Water Resour 10(2):89–101
17. Read V (2001) Salinity in Western Australia a situation statement. Resource management technical report, No. 81. ISSN 0729-3135
18. Greenwood EAN, Klein JL, Beresford JD, Watson GD (1985) Differences in annual evaporation between grazed pasture and Eucalyptus species in plantations on a saline farm catchment. J Hydrol 78:261–278
19. Nulsen RA (1984) Saltland management - the catchment approach. Western Australia Department of Agriculture. Farmnote 133/84
20. Awange JL, Grafarend EW, Palancz B, Zaletnyik P (2010) Algebraic geodesy and geoinformatics. Springer, Berlin
21. Grisso RB, Alley MM, Heatwole C (2003) Precision Farming tools: global positioning system (GPS). Virginia Cooperative Extension (VCE) publication, pp 442–503

22. Grisso RB, Alley MM, McClellan P, Brann DE, Donohue SJ (2002) Precision farming: a comprehensive approach. Virginia Cooperative Extension (VCE) publication, pp 442–500
23. Veroustraete F (2016) Is there a future for precision farming with a smaller environmental impact? Adv Plants Agric Res 3(1):00080. doi:10.15406/apar.2016.03.00080
24. Steede-Terry K (2000) Integrating GIS and the global positioning system. ESRI Press, California
25. Dobermann A, White PF (1999) Strategies for nutrient management in irrigated and rainfed lowland rice systems. In: Balasubramanaian V, Ladha JK, Denning GL (eds) Nutrients. Resource managements in rice systems. Kluwer Academic Publishers
26. El-Rabbany A (2006) Introduction to GPS global positioning system, 2nd edn. Artech House, Boston
27. Buick R (2006) GPS guidance and automated steering renew interest in precision farming techniques. White paper, trimble agriculture division, 10355 Westmoor Drive, Suite #100, Westminster, CO 80021, USA
28. Cassel DK, Kamprath EJ, Simmons FW (1996) Nitrogen-sulfur relationships in corn as affected by landscape attributes and tillage. Soil Sci Soc Am J 88(2):133–140
29. Jones AJ, Mielke LN, Bartles CA, Miller CA (1989) Relationship of landscape position and properties to crop production. J Soil Water Conserv 44(4):328–332
30. Kravchenko AN, Bullock DG (2000) Correlation of corn and soybean grain yield with topography and soil properties. Agron J 92(1):75–83. doi:10.1007/s100870050010
31. Schmidt JP, Taylor RK, Gehl RJ (2003) Developing topographic maps using a sub-meter accuracy global positioning system. Appl Eng Agric 19(3):291–300
32. Timlin DJ, Pachepsky Y, Snyder VA, Bryant RB (1998) Spatial and temporal variability of corn grain yield on a hillslope. Soil Sci Soc Am J 62(3):764–773
33. Yang C, Peterson CL, Shropshire GJ, Otawa T (1998) Spatial variability of field topography and wheat yield in the Palouse region of the Pacific Northwest. Trans ASAE 41(1):17–27

# Chapter 17
# Disaster Management

*The greatest exploiter for all of us are floods today, droughts tomorrow, earthquake some times and all of these multiply our trauma of deprivation, pains of poverty and hunger. These disasters take away not only our crops, shelters, lives of our families, friends tattles, but also destroy our hopes and dreams of the future. Is there any event comparable to these, which causes so much human sufferings and injustice?—This is the cry in bewilderness of a common farmer of Koshi River basin, Bihar (India) in the midst of recurrent floods and droughts [1]. Indeed, the role pinpoint accuracy of positioning plays in the disaster discussed above may seem inconsequential at a first glance, but the truth is that GNSS and GIS are becoming more and more important - not just in the wake of disaster, when, for instance, relief efforts might call for quicker generated maps of flooded areas, for helicopters to navigate through thick smoke, or for the exact location of people buried alive - but in planning and preparatory phases of emergency management [2]. To this effect, the availability of real-time GNSS information will have important impacts on how scientists and societies prepare for and cope with natural disasters.*

Hammond et al. [3]

## 17.1 Geosensor Networks in Disaster Monitoring

### *17.1.1 Disasters and Their Impacts*

Natural disasters, whether of *meteorological* origin such as cyclones, floods, tornadoes and droughts or of having *geological* nature such as earthquakes and volcanoes, are well known for their devastating impacts on human life, economy and environment, and are also formidable physical constraints in our overall efforts to develop and utilize the natural resources on a sustainable basis [1]. Indeed, disasters have been known to hit hard as seen from the floods of 2010–2011 in Pakistan and Australia, the sludge flow in Hungary in 2010, and the landslide in Brazil in 2011,



J. Awange, *GNSS Environmental Sensing*, Environmental Science and Engineering, DOI 10.1007/978-3-319-58418-8_17

events which had environmental catastrophe. Disaster trends reveal that the most vulnerable and hardest hit are normally the poorest people, most of who live in developing countries. With tropical climate and unstable land forms, coupled with high population density, poverty, illiteracy and lack of infrastructure development, developing countries are more vulnerable to suffer from the damaging potential of such disasters [1]. For example, the year 2004 was witness to one of the greatest tragedies of humankind, the great tsunami that wiped out civilization in many parts of south-east Asia. Thousands were rendered homeless, and many lost their loved ones.

Though it is almost impossible to completely neutralize the damage due to these disasters, it is, however possible to [1];

1. minimize the potential risks by developing disaster early warning strategies,
2. prepare developmental plans to provide resilience to such disasters,
3. mobilize resources including communication and tele-medicinal services and,
4. to help in rehabilitation and post-disaster reconstruction.

Disasters, e.g., earthquakes, tsunamis and storm events are of short duration and require a fixed amount of consequence management. Others, e.g., outbreak of contagious diseases (e.g., bird flu and Ebola) and wild fires are more complex and unfold in a non-linear fashion over an extended period necessitating ongoing and adaptive consequence management [4]. Management plans should be put in place comprising three phases, which would address the issues related to *mitigation*, *preparedness*, *response and recovery*. The preparedness activities such as prediction and risk zone identification are taken up long before the event occurs; the prevention activities such as early warning/forecasting, monitoring and preparation of contingency plans are then taken up just before or during the event; and finally the response/mitigation phase where activities are undertaken just after the event which include damage assessment and relief management [5].

With regard to response, the concepts documented by Terhorst et al. [4, and reference therein] are *level of preparedness*, *response times*, *sustaining the response* and *coordinating the response*. Due to the fact that time is critical and the three primary challenges in the race against time are uncertainty, complexity and variability, Terhorst et al. [4] have proposed a *sensor web* (see Sect. 17.1.2 for discussion on geosensors) that can enhance the tempo of disaster response in context of vegetation fires.

To support these efforts, relevant information needed to undertake risk appraisal including vulnerability analysis of the terrain, prediction, warning, and prevention of a disastrous event need to be identified [1]. Disaster management measures also entail examination of the probability of occurrence and the consequences, understanding of the total processes in relation to the cause and effect, identification of preventive measures and implementation of rescue strategies [1].

Food security is dependent on social, economic as well as climatic factors. Climatic extremes, particularly droughts and floods, affect the state of food security in Africa [6–9]. Climatic extremes are normal occurrences and their impacts on society vary with respect to vulnerability and the success or failure of coping mechanisms

at both the household and national level. Absence of adaptation measures to climate variability results in negative impacts on food security, health, and ultimately, life.

The role pinpoint accuracy of positioning plays in the disaster discussed above may seem inconsequential at a first glance, but the truth is that GNSS and GIS are becoming more and more important - not just in the wake of disaster, when, for instance, relief efforts might call for quicker generated maps of flooded areas, for helicopters to navigate through thick smoke, or for the exact location of people buried alive - but in planning and preparatory phases of emergency management [2]. To support disaster management programs, GNSS could be used to provide support in pre-disaster preparedness programmes, in disaster response and monitoring activities, and post-disaster reconstruction, specifically in the provision of location-based information. Video cameras fitted with GNSS interface for instance could help in documenting the occurrences and locations of fire, insects, drought, flood, hail, and frost [10].

An example of the application of GNSS was during 11th March 2011 Tohoku-oki earthquake in Japan where a prototype GPS-based warning system, the NASA GPS Real-Time Earthquake and Tsunami GREAT Alert,[1] was operating in test mode. Once operational, systems such as GREAT should save on the time needed to recognize what has occurred, thus supporting quicker warnings that can save lives [3]. Other activities that could be supported by GNSS are [1];

- identification of hazard zones,
- risk assessment,
- creation of awareness at various levels,
- evolving systems for monitoring, prediction and warning,
- designing long-term preventive measures (structural and non-structural) and short-term protective measures and preparedness,
- early intervention measures,
- education, training, public information,
- transfer of technology, and
- research on improved technology and disaster management.

### *17.1.2 GNSS in Support of Geosensor Networks*

A geosensor network is a distributed ad-hoc wireless network of sensor-enabled miniature computing platforms (a sensor network) that monitors phenomena in geographic space [11, 12], and in which the *geospatial content* of the information collected, aggregated, analyzed and monitored is of fundamental importance [13]. Similar to the animal telemetry discussed in Sect. 19.2, geosensor networks consists of thousands of sensors (also called nodes, and maybe fixed or mobile) that monitor and process data, and are also capable of communicating to each other, and to

[1] See e.g., http://www.gdgps.net/products/great-alert.html.

transfer data to a central station via wireless communication, hence power consumption becomes a crucial issue [14]. Since these thousands of sensors are randomly deployed, GNSS plays a crucial role in providing their locations, to which the monitored environmental parameters (e.g., temperature and humidity) can be related.

Their environmental applications include the monitoring of drinking water quality [15], disasters (earthquakes, forest fires, volcanic eruptions, oil spill, movement of glaciers, deformations in wells and bridges, flood detection and prevention) [14, 16], wildlife habitat monitoring, watershed management, environmental pollution monitoring, deep sea explorations, to monitoring food safety, e.g., in South Africa and precision agriculture for large vineyards (e.g., in Southern Australia) [17]. They also offer the advantage of real-time environmental monitoring such as the progress of oil spill as was witnessed in the gulf of Mexico or real-time detection of toxic gas plumes in open public spaces [17].

The advantage of the GNSS technique is that they are unaffected by the actual impact since they are in space and in supporting the emerging geosensor environmental monitoring, particularly in disaster management, they contribute towards a shift from post-event, estimation based, historic data analysis to real-time, sensor-rich event detection and monitoring [17]. They are therefore useful in monitoring environmental disasters discussed in the coming sections and compliment ground based geodetic methods. In this regard, the main advantage of RTGPS data discussed in Sect. 5.4.3 would be the improved temporal resolution in observations of natural processes achieved through high-rate information. Real-time GPS (RTGPS) will likely demonstrate an impact similar to that of other high-rate geophysical observations (e.g., from seismological and meteorological networks) for monitoring and understanding earthquakes, seismic wave propagation, volcanic eruptions, magmatic intrusions, movements of ice, landslides, and structure and dynamics of the atmosphere [3].

The rest of this Chapter is organized as follows; In Sect. 17.2, the disasters related to the changing sea levels are addressed, while Sect. 17.3 presents Tsunami early warning systems. Section 17.4 presents land subsidence and slides, Sect. 17.5 looks at the earthquakes, and Sect. 17.6 treats the issue of floods. The Chapter then considers droughts in Sect. 17.7, disease outbreak in Sect. 17.8, before concluding in Sect. 17.9.

## 17.2 Changing Sea Levels

Sea levels have been known to change for a variety of reasons, with the changes varying in temporal and spatial scales, see e.g., [18]. In time scales, some changes occur rapidly, e.g., sea level change due to the effects of tsunami, while others take long. Spatially, the changes can be local or global. The average sea level about which these changes occur is generally known as the *mean sea level* [19]. Global warming, fuelled by the increase in greenhouse effect discussed in Chap. 11 is thought to be having an impact on the sea level rise around the world. This is in part due to the melting of the polar ice on the one hand, and the increase in water temperatures causing

expansion on the other hand. Today, one of the highest priorities is to understand and to reliably anticipate changes in the mean sea level and flood risks, particularly those that maybe due to global climate change [19]. In order to predict future changes of mean sea level, Pugh [19] suggests that it is necessary to have a full understanding of all the factors that influence sea levels at the coast and that the first step in realizing this is to measure the sea level over along period of time to provide a baseline data upon which scientific discussions could be made.

Measuring sea level entails the determination of the vertical height between the average surface of the sea and a fixed datum level (see Sect. 5.6.1), where the datum chosen depends on the application [19]. Some of the most commonly used datums such as tide gauge benchmark, chart datum, land survey datum (mean sea level), geocentric coordinates and geoid (Fig. 5.18, p. 88) are discussed in [19]. As was stated in Sect. 9.3.1, the GOCE (Gravity field and steady-state Ocean Circulation Explorer) satellite mission (Fig. 9.8 on p. 160) collected data that will significantly improve the accuracy of the static geoid, e.g., [20], and in so doing contribute to improved monitoring of changes in sea level. Methods of measuring sea levels are listed by Pugh [19] as:

1. Direct measurements by following the moving sea surface, e.g., using tide poles and float gauges. According to Pugh [19], for offshore, where there are no fixed structures, GNSS receivers have been placed on floating loosely moored buoys that measure sea levels to accuracies of few centimeters after averaging over along period of time to remove the effect of waves.
2. Use of fixed sensors (e.g., acoustic tide gauge and pressure measuring systems).
3. Use of satellite altimetry discussed in Sect. 9.4.

Precise measurements from GNSS combined with other methods are crucial in monitoring changing sea levels and provide early warning in case of evacuation. Since changes in sea level average about 1–3 mm per annum, any vertical motion of the crust must be monitored at this level of accuracy, and within short time spans of three to five years [21]. GNSS could also contribute indirectly to monitor changes in sea level through cryospheric measurements as discussed in Sect. 11.4.4.

### *17.2.1 Impacts of Rise in Sea Level*

For sea level changes, climate models used to study the effects of atmospheric greenhouse gases predict an overall increase in the global temperature during the current century to be in the range of 1–3.5 °C [22]. Though sea level rise could also be attributed to salinity changes, see e.g., [23], increase in magnitude in temperature to the level predicted by [22] could easily lead to rapid melting of ice sheets and glaciers that could lead to a sea-level change that departs dramatically from the assumption of a uniform redistribution of meltwater [24]. For instance, Bamber et al. [25] reassessed the potential of sea level rise resulting from a collapse of the West Antarctic ice sheet and obtained a value for the global, eustatic (changes due to addition or removal of

water mass) sea level rise contribution of about 3.3 m, with important regional variations. The maximum increase was found to be concentrated along the Pacific and Atlantic seaboard of the United States, where the value was about 25% greater than the global mean, even for the case of a partial collapse [25]. Although the eustatic sea-level rise contribution for West Antarctic ice sheet collapse is uncertain (e.g., IPCC estimates 5 m), Mitrovica et al. [24] show that, whatever the value, sea level changes at some coastal sites will be significantly higher or lower than the predicted eustatic value.

Temperature rise due to global change in climate will have several effects, notably the global rise in sea level, an undesirable scenario given that a large fraction of the Earth's total population resides close to the sea. Catastrophic impacts on agriculture, tourism, industries, etc., of 1 m global rise in sea level have already been pointed out, e.g., by [26] who note that low lying regions that slope gently such as Florida and Indonesia with 15% of the world's coastline or regions lying in the flood plains of large rivers such as Rhine, Nile, etc., are all in great risk, should the sea level rise by the predicted amount.

Titus et al. [27] estimated that in the United States, a global sea level rise by a similar magnitude would suffice to drown 20–85% of the coastal wetlands resulting in an encroachment of up to 7,000 square miles (about 18,130 $km^2$), an area the size of Massachusetts. The foregoing discussion therefore clearly indicates the necessity of monitoring of the changes in sea/lake levels in order to provide early warnings and enable formulation of policies that will provide remedial measures.

Although Warrick et al. [22] report that tide gauge data show the sea level to be already rising at a rate between 1.0 and 2.5 mm/yr averaged over the past century, understanding and characterizing the sources of the rise of sea level remains a problem. The two prominent source of rise in sea level are;

1. mass redistribution (from Antarctica, Greenland, and Glaciers and small ice caps), and
2. thermal expansion and salinity variation.

In both sources, as already pointed out, global warming contributes to the rise in sea level by melting of the ice and glaciers that find their way into the ocean during mass redistribution. In the latter case, global warming causes the warming and expansion of the water during thermal expansion. Existing methods for determining secular rise in sea level are based on the tide gauge approach, which as already mentioned has its own limitations. For rise in sea level therefore, it is vital for one to;

- characterize the sources of global rise in order to clearly distinguish between the thermal and mass redistribution contributions, and
- to relate the rise in sea level to global warming.

These can be done using remote sensing satellites discussed in Chap. 9, which are specifically designed to provide solutions to problems related to global warming and the changes in sea/lake levels.

### 17.2.2 Tide Gauge Monitoring

The traditional means of monitoring sea and lake levels has been based on tide gauges, which are normally sensitive to water level changes. Tide gauge records collected over long periods indicate a rise in global sea level of 10–30 cm over the past century (cf. 10–25 cm from [22] above), with a large discrepancies in the rates of change of sea level indicated by different tide gauges, or groups of tide gauges spanning particular regions [21]. These differences are considered to be largely caused by vertical land motion resulting from phenomena such as glacial rebound, subsurface fluid withdrawal and sediment consolidation [21].

In order to monitor absolute sea level changes, it is important to link the GNSS-measured heights and the those obtained from precise levelling to the relative measurements of the tide gauge.[2] GNSS are used to georeference these tide gauges.

### 17.2.3 GNSS Monitoring

*GNSS estimation of absolute and relative sea level changes*: Due to their capability to provide three-dimensional coordinates $\{\phi, \lambda, h\}$, GNSS satellites play a crucial role in:

1. the actual determination of the sea level changes by determining the phase center of the GNSS-equipped buoy receivers, and also through GNSS altimetry, see, e.g., [28, 29] discussed in Sect. 9.4, and
2. the realization of the reference frame upon which the tide gauges are referred.

For GNSS-equipped buoys capable of measuring dual frequency carrier-phases L1 and L2, their positions $\{\phi, \lambda, h\}$ relative to a fixed reference GNSS receiver can be computed as a function of time. The $h$ component can be used to provide a time-series measurement of sea level. If the buoy is horizontally constrained and measurements are made at appropriate frequency, the mean sea level, the sea level change due to tides, and the wave amplitudes and frequencies can be determined to cm-level accuracy using GNSS [30].

Using kinematic positioning approach (see Sect. 5.4.2), Kelecy et al. [31] demonstrated the applicability of GNSS by using two GPS-equipped buoys to collect data at two locations on two different days. Three-dimensional positions of the buoys were then computed using precise carrier-phase measurements relative to a GNSS reference station that was fixed 15 km away. From the derived positions, the height component $h$ corrected for tilt and vertical displacement were then used to compute two mean sea level measurements at the buoy locations to 6 cm-level accuracy when compared to altimetry readings. Kelecy et al. [31] thus succeeded in demonstrating that accurate GNSS buoy measurements could successfully be used to detect

[2] http://www.ga.gov.au/scientific-topics/positioning-navigation/geodesy/pacific-sea-level-monitoring-project.

changes in sea levels. They point out that such measurements could find use in complimenting altimetric data, e.g., in calibration of altimetric measurements, see e.g., [32–34], extending altimetric results to smaller scales by using an array of GNSS buoys for local studies, and enhancing the temporal resolution of altimetric data to resolve local uncertainties between satellite passes. Other application areas include measurement of absolute sea level, of temporal variations in sea level, and of sea level gradients (dominantly the geoid), while specific applications would include ocean altimetric calibration, monitoring of sea level in remote regions, and regional experiments requiring spatial and temporal resolution higher than that available from altimetric data [31].

The variations of vertical crustal velocities at CORS sites (e.g., Fig. 5.12 on p. 81) near tide gauge stations may also be used to determine the "absolute" sea level change with respect to the International Terrestrial Reference Frame, what previously was impossible to conduct before the proliferation of CORS in coastal areas [35]. In the realization of the reference frame upon which the tide gauges should be referred, measurements of vertical crustal movement together with tide gauges in a global geocentric reference system has been shown, e.g., by Snay et al. [36] to have the potential of estimating absolute sea level. Denoting $S(p)$ as the rate of relative sea level change at a point $p$ measured by a tide gauge and $U(q)$ the vertical velocity at a point $q$ in the ITRF2000 system, Snay et al. [36] indicate that the absolute sea level is given by

$$S(p) + U(q) = \xi + \epsilon, \tag{17.1}$$

where $\xi$ is the estimated absolute sea level rate for a sample of sites and $\epsilon$ the difference between the estimated values and the observations (i.e., the error vector). It is clear from the equation above that GNSS satellites will play a significant role in the determination of each ITRF2000 velocity $U(q)$ for each station using CORS observations (Sect. 5.5). The quantity $S(p) + U(q)$ provides an estimate of the absolute sea level rate at $p$, denoted $A(p)$, when the distance between $p$ and $q$ (see Fig. 17.1) is small [36]. In addition to provision of the velocity observations, GNSS contribute to monitoring absolute sea level changes through a regular re-survey of local networks of benchmarks and reference marks [21].

GNSS remote sensing techniques discussed in Sects. 9.3.3, 9.4, and 10.1 further provide means by which GNSS could be useful in measuring changes in sea level. As an example, Lake Victoria (Sect. 14.3.1.2) water levels for the period 1993 to 2006 are plotted for both TOPEX/Poseidon derived heights and tide gauge data in Fig. 17.2. The figure indicates a close relationship between the two data sets. Crétaux et al. [37] compares water levels of Lake Victoria from the Jinja tide gauge and those from Jason-1 altimetry satellite and obtains a coefficient of correlation value of 0.99 with a standard deviation of 2.7 cm for the period 2004–2007. This supports the fact that satellite altimetry provides useful information on changes in sea level, and further shows the significant contribution of GNSS to satellite altimetry used for monitoring changes in water levels. Indeed, by averaging the few-hundred thousand measurements collected by the satellite in the time it takes to cover the global oceans (i.e., 10 days for TOPEX/Poseidon), global mean sea level can be


**Fig. 17.1** GNSS absolute sea level monitoring

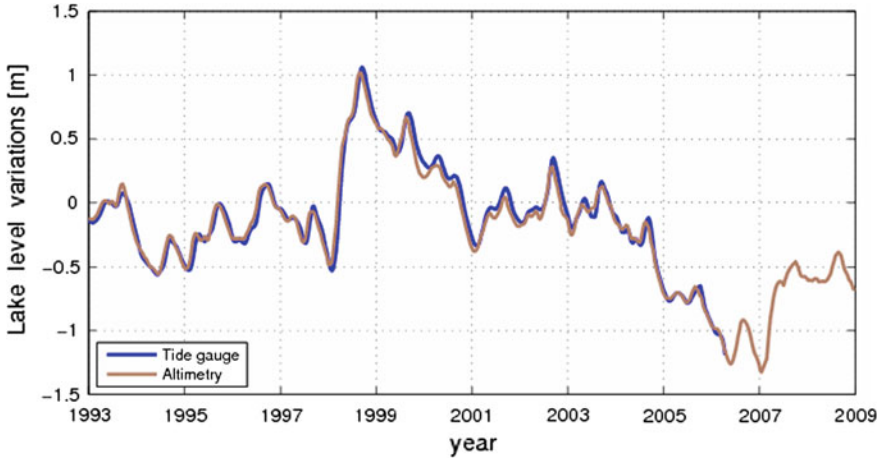


**Fig. 17.2** A comparison of water gauge readings at Jinja station in Uganda (near Lake Victoria's outlet, see Fig. 14.8) and water Levels from Topex/Poseidon and Jason-1 altimetry satellites. The figure shows a close match between the tide gauge and satellite altimetry data (cf. Fig. 14.10 on p. 290 obtained from GRACE)

determined with a precision of several millimeters [19]. Such information is vital for mitigation of disasters related to sea level changes. Detailed satellite altimetry study on East African lakes (e.g., Fig. 17.2) are given e.g., in [37, 38].

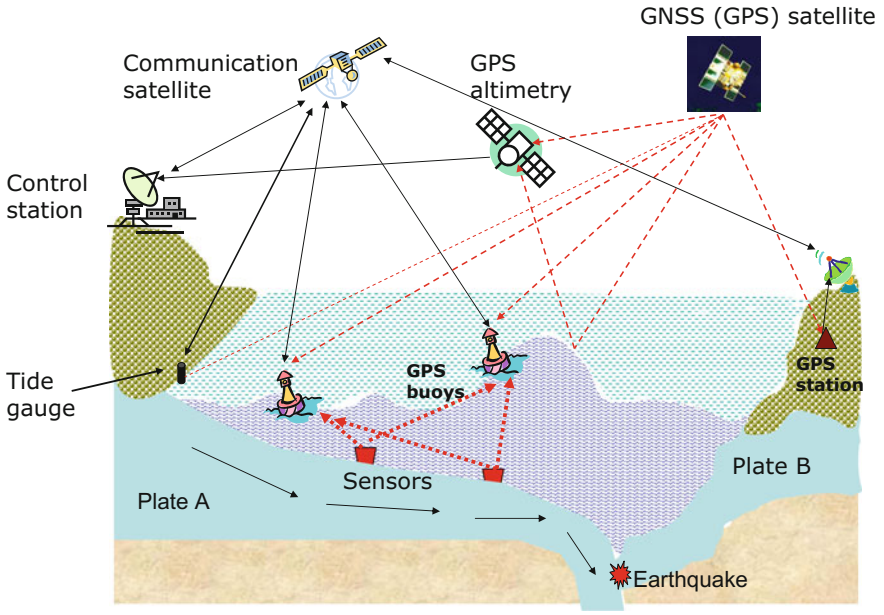


**Fig. 17.3** A schematic illustration of the possible application of GNSS to tsunami monitoring

## 17.3 Tsunami Early Warning System

Boxing day, the 26th of 2004 will be remembered as the day tsunami caused havoc in Asia and Africa killing more than 280,000 people[3] and destroying properties worth millions of dollars. In order to understand the cause of tsunami and how it could possibly be monitored using GNSS, use is made of Fig. 17.3. Tsunami is a series of waves created when a body of water such as ocean is rapidly displaced. Causes often range from land earthquakes, under ocean earthquakes, volcanic eruptions, under water explosions among others. In Fig. 17.3 for example, plate A is seen to move towards the right and as it does, it collides with plate B thereby causing under ocean earthquake with the epicenter at the point of collision as indicated in the figure. The effect of the earthquake immediately displaces the water mass causing rapid moving waves that rises to up to 30 m high [39]. As this approaches land, the rapid speed enables the waves to penetrate deep into land causing massive destruction as witnessed by the 11th March 2011 tsunami at Tohoku-Oki in Japan. Monitoring the onset of Tsunami enables early warning system that could at least minimize the cost of lives.

Tsunami warning has particular requirements for calculating accurate earthquake magnitude, propagation direction, and vertical and horizontal motion of the seafloor, with the goal of rapidly recognizing when a tsunami event is occurring and improving

[3] See e.g.,http://www.bom.gov.au/tsunami/about/atws.shtml.

predictions of where the wave will rise on near and distant coasts [3]. GNSS satellites are proving to be the key to such early warning systems in light of the fact that displacements at GNSS sites are useful in constraining a fault slip model, which predicts motion of the seafloor [3].

In the GITEWS (German Indonesian Tsunami Early Warning System),[4] which went into operation on 11th of November 2008 [39] with the ownership now in the hands of Indonesia, GNSS plays a leading role in key monitoring areas as demonstrated in Fig. 17.3. The indicators of this system are GNSS (GPS) instruments, seismometers, tide gauges and GPS-buoys, as well as, ocean bottom pressure sensors. The augmentation of all these sensors ensures a rapid locating and analysis of the tsunami information to inform warning decisions.

*Tide gauge sensors*: Tide gauges are used to measure changes in sea level and therefore indicate exceptionally rapid rise in sea level, which signals unusual event. To enhance the tide gauges, the GITEWS project has equipped them with GNSS receivers that enable them to measure vertical and horizontal land displacements in addition to sea levels. Measurement of GNSS velocities provide an indication of the direction of horizontal displacement. The actual vertical and horizontal displacement are deduced from the GNSS positional time-series measurements. Any unusual displacement can serve to indicate an oncoming tsunami. During the catastrophic earthquake of 2004, a horizontal and vertical displacement of several decimeters to meters was evident even at a distance of some hundred kilometers from the earthquake. The direction of this resulting shift gives reference to the mechanism of the earthquake break and thus to the possible tsunami potential and the expected hazard [39]. This information is transmitted towards the communication satellite, which relays it to the control station in Indonesia.

*GNSS Buoys*: These help to relay information received from the underwater pressure sensors, which detect the effect of the tsunami. Besides relaying the information, the incorporated GNSS antenna can act as a measuring device for sea motion (horizontal motion) and sea level (heights). The buoys therefore provide an independent indicator of the onset of a tsunami. For the GITEWS, the buoys also detect tsunami waves, which with speeds of up to 800 km/h and wavelengths of 200 km in the open sea, and through proper filtering, achieve cm-level accuracy detection of rise in the sea level thus also an early detection of a tsunami wave [39].

*Land based GNSS*: These are combined with seismometers to provide location-based mapping of the ground motion. Horizontal and vertical displacements together with velocities are delivered by GNSS. All these, plus ground motion from the seismometers are relayed to the communication satellites and further transmitted to the control center in Indonesia where warning decisions are made.

*GNSS altimetry*: Low flying satellites such as GRACE are able to measure reflected signals from GNSS satellites (see Sect. 10.1). They therefore would measure signals that hit the sea surface and are reflected to the low flying satellites. This helps in determining the sea levels and further provide more information on tsunami indicators. Besides, the GNSS satellites also help in positioning these low flying satellites

[4] See http://www.gtz.de/en/21020.htm.

in space. Studies have been initiated to test the feasibility of this concept, see e.g., Helm et al. [40].

An example of a tsunami early warning system that was in test mode during the Tohoku-Oki earthquake and tsunami of 11th March 2011 was the GREAT (GPS real-time Earthquake and Tsunami) Alert, see e.g., [3]. The GREAT Alert Project is a NASA-sponsored, multi-agency collaborative effort to develop an advanced Earthquake and Tsunami alert system that uses real-time GNSS discussed in Sect. 5.4.3) to enable more accurate and timely assessment of the *magnitude* and *mechanism* of large earthquakes, as well as the *magnitude* and *direction* of resulting tsunamis.[5]

Another example is the Australian Tsunami Warning System (ATWS), which is a national effort involving the Australian Bureau of Meteorology (Bureau), Geoscience Australia (GA) and Emergency Management Australia (EMA) to provide a comprehensive tsunami warning system capable of delivering timely and effective tsunami warnings to the Australian population, and also support international efforts to establish an Indian Ocean tsunami warning system and contribute to the facilitation of tsunami warnings for the South West Pacific.[6]

## 17.4 Land Subsidence and Landslides

Land-surface subsidence due to overextraction of groundwater has long been recognized as a potential problem in many areas that have undergone extensive groundwater development [41]. This is particularly significant in expanding metropolitan areas in arid and semi-arid areas as witnessed in most parts of Australia and Iran. Surface subsidence has been observed worldwide in areas where withdrawal exceeds natural recharge thereby depleting the volume of the stored water. This has been evidenced in cities such as Mexico where subsidence of land has reached almost 9 m, Bangkok (Thailand), Shangai, Tanjin, Xi'an (China), Osaka, Tokyo (Japan), and Las Vegas (USA) [42]. In 1991, the US National Research Council placed the annual costs from flooding and structural damage caused by land subsidence within the United States alone at over $125 million [41].

GNSS and other geodetic techniques, e.g., levelling and Interferometric Synthetic Aperture Radar (InSAR) have been widely used to detect the temporal and spatial pattern of surface deformation due to land subsidence. Of these methods, InSAR provides a unique tool for detecting and monitoring deformation over regions of ongoing groundwater development with the advantage of having wide spatial coverage (10,000 $km^2$), fine spatial resolution (100 $m^2$), and high accuracy ($\sim$1 cm), and as such, offers new capabilities to measure surface deformation caused by aquifer discharge and recharge at an unprecedented level of detail never before possible with techniques like GNSS and levelling [41]. For this reason, Motagh et al. [41] demonstrate in their study how spatially dense InSAR results complement sparse geodetic

[5] http://www.gdgps.net/products/great-alert.html. Accessed on 21/9/2011.

[6] http://www.bom.gov.au/tsunami/about/atws.shtml.

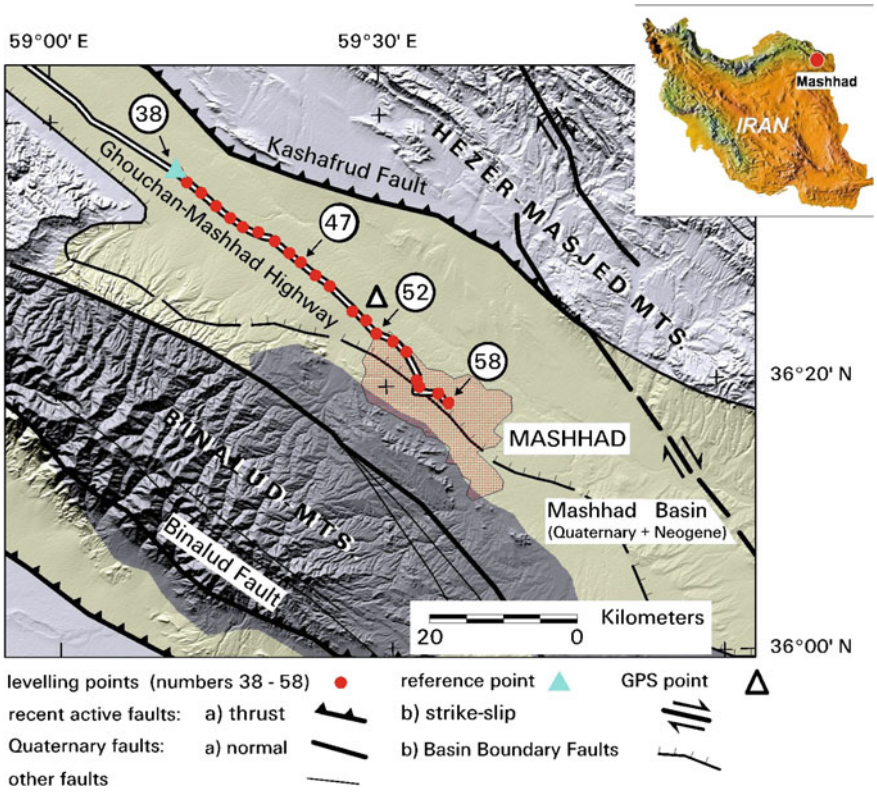


**Fig. 17.4** Generalized geologic map of the Mashhad region based on the published 1:2,500,000-scale geological map from National Iranian Oil Company (NIOC), and the map of major active faults in Iran from International Institute of Earthquake Engineering and Seismology (IIEES). The map is overlaid on a shaded-relief topographic image generated from the 3-arcsecond Shuttle Radar Topography Mission (SRTM) data. The inset shows the location of the figure within Iran. *Source* Motagh et al. [41]

measurements from GNSS and levelling, and thereby contributing to a better understanding of land subsidence associated with water extraction in the Mashhad area, northeast Iran (Fig. 17.4).

Example 17.1 (GNSS monitoring of subsidence in Mashhad [41]).

The Valley of Mashhad is a northwest-southeast (NW-SE) trending valley in northeast Iran and is bounded to the south by the Binalud Mountains and to the north by the Hezar-Masjed Mountains, see Fig. 17.4 [41]. The basin encompasses the city of Mashhad, a provincial capital inhabited by over 2 million people and visited annually by millions of tourists [41]. Mashhad extends over an area of more than 200 $km^2$ across the basin, is the second largest city in Iran, and is one of the fastest

**Fig. 17.5** An example of surface fissures in Mashhad Valley caused probably by excessive groundwater withdrawal and associated aquifer-system compaction. The fissure is located northwest of Mashhad City and to the east of the Tous. A GNSS station is marked by a triangle in Fig. 17.4 near the city of Tous. *Source* Motagh et al. [41]

growing metropolitan areas in Iran [41]. Water supply for the region mainly comes from groundwater, which is used for domestic, industrial and agricultural activities. However, substantial exploitation of this groundwater due to population growth, tourism and development, coupled with deficient natural recharge in recent decades, has resulted in severe depletion of the underground aquifer, leading to regional decline of water-table levels, lack of access to fresh water, and development of earth fissures and local sinking in many areas of the valley, see Fig. 17.5 [41]. From 2005 to 2006, a GNSS CORS station (refer to Sect. 5.5 for CORS) near the city of Tous provided continuous recordings that showed significant subsidence of approximately 22 cm at the station, e.g., Fig. 17.6 [41].

End of Example 17.1.

Landslide monitoring can be undertaken in two ways [43] (i) analyzing and comparing various spatial maps, e.g., topographic maps, aerial photographs, cadastral maps, and digital elevation maps, which represent instantaneous views of an unstable site on various dates, and (ii) carrying out in-situ measurements of the surface displacements by combining a space and time resolution adapted to the evolution speeds of the phenomena. In the context of the first approach, GNSS plays a pivotal role in map production (see, e.g., Figs. 8.2 and 8.3 in Chap. 8) that would aid in the analysis. With respect to the second approach, for example, GNSS has been applied to the case of monitoring the Vallcebre landslide in the Eastern Pyrenees, Spain

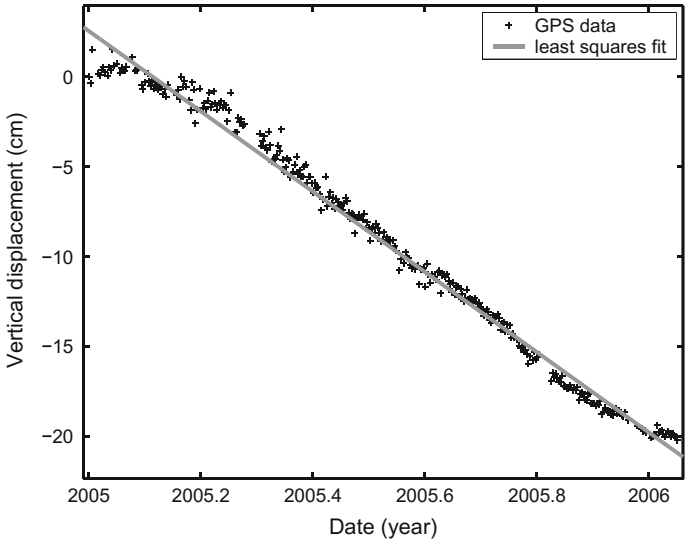


**Fig. 17.6** A plot of GNSS vertical components (in cm) for the Tous GPS station (triangle in Fig. 17.4) with least-squares linear trend (slope ∼22 cm yr.1) overlain. *Source* Motagh et al. [41]

[44]. This landslide had been periodically monitored since 1987 with terrestrial photogrammetry and total stations. The area of movement extended over 0.8 km$^2$ and showed displacements as large as 1.6 m during the period 1996–1997. Application of RTK discussed in Sect. 5.4.6 allowed greater coverage and productivity with similar accuracies (12 to 16 mm in the horizontal plane, and 18 to 24 mm in elevation) to classical surveying methods [44]. A general accuracy of GNSS monitoring of landslide is presented, e.g., in [43].

## 17.5 Earthquakes

The outer layer of the Earth is made up of large pieces known as tectonic plates which are in motion. When these plates collide, as indicate in Fig. 17.3, an earthquake occurs. Other factors that can lead to earthquakes include fault raptures or forces such as stress and strain. But most causes result from plate collision as they try to move past one another. There is also a tendency of earthquakes to occur in "gaps" that are in places along an earthquake belt where strong earthquake had not previously been observed [1]. Earthquake risk assessment involves identification of seismic zones through collection of geological/structural, geophysical (primarily seismological) and geomorphological data and mapping of known seismic phenomena in the region (mainly epicenters with magnitudes) [1]. Kamik and Algermissen [45] have pointed out that knowledge of trends in time or in space helps in defining the source regions

of future shocks, while Jayaraman et al. [1] point out that accurate mapping of geomorphological features adjoining lineaments reveal active movement or recent tectonic activities along faults.

GNSS satellites are emerging as a powerful geodetic tools for monitoring (geological) changes over time, which is the key for understanding the long-term geodynamical phenomena. They have been particularly useful in measuring the more complex deformation patterns across plate boundaries, where large and regional scale strain builds up, plate movements, and slips along faults, pre-seismic, co-seismic and post-seismic distortions [1, 46–48]. Indeed the GNSS through CORS (see Sect. 5.5) now enable detection of ground motion at the mm to cm-level accuracy before, during and after earthquakes [49], and have found use in seismological applications, see e.g., Larson [50].

Hammond et al. [3] point out that rapid detection and accurate characterization of earthquake related events can make a crucial difference during the minutes to hours that follow an earthquake event as was the case following the catastrophic 2004 Sumatra and 11th March 2011 Tohoku-oki earthquakes and tsunamis. In both of these events, the initial seismic notification of earthquake magnitude was available in minutes but was more than an order of magnitude smaller than the true event size, an uncertainty that can be addressed by GNSS in the rapid estimation of large earthquake magnitudes [3]. A review of the application of GNSS to geodynamics and earthquake studies is presented, e.g., in Segall and Davis [51]. Jia [49] documents three stages upon which measurements for the earthquake can be collected. These are pre-seismic, co-seismic and post-seismic defined as follows [49]:

*Pre-seismic*. These are measurements taken before the earthquake and normally serve as an early warning system of potential danger, especially when two plates indicate a possibility of collision (e.g., Fig. 17.3).

*Co-seismic*. These are measurements that provide direct information on the occurrence during an earthquake and are useful for providing data for estimating the likelihood of future earthquakes through, e.g., further investigations of fault slip models and of other seismic features of the earthquake.

*Post-seismic* monitoring entails using GNSS receivers to obtain time-series of location and plate movements long after the earthquake has occurred. Such post-seismic deformation information from all available GNSS sites in the earthquake region can help scientists analyze likely elastic, poroelastic and viscoelastic deformation, and plastic flow of the Earth's crust in the earthquake region, giving a better understanding of crustal relocation and redistribution after an earthquake.

By continuously sampling movements of permanent known GNSS locations, e.g., within a CORS network in a seismic area, accurate position differences between the stations (e.g., Fig. 5.12 on p. 81) can be established to an accuracy of a few millimeters in the horizontal and a centimeter in the vertical. These CORS networks (Sect. 5.5) are normally fitted with telemetry that relays the data to control stations for rapid processing (e.g., Fig. 17.3). The results are analyzed and used as monitoring data for possible future earthquakes. RTGPS presented in Sect. 5.4.3 are suggested by Hammond et al. [3] to be useful in earthquake monitoring. Its integration with seismic time-series are expected to enhance seismic source monitoring through monitoring

earthquake events occurring over very wide range of time scales. Its inclusion to extend measurements beyond typical seismic frequencies is essential to understanding the complete spectrum of fault slip behaviours associated with the earthquake cycle [3]. In what follows, two examples on the application of GNSS to monitor earthquakes is presented based on the works of Jia [49] and GEONET in Japan.

Example 17.2 (Sumatra-Andaman earthquake-Jia [49]).

Jia [49] assesses the Sumatra-Andaman earthquake by analyzing data from more than 250 GNSS (GPS) sites distributed through Australia, Malaysia, Thailand, Indonesia, the Philippines, China, India and the Maldives (Fig. 17.7). Co-seismic displacements from two combined seven-days' solutions, one before and one after the earthquake are computed. The displacements of the sites are calculated as the difference between

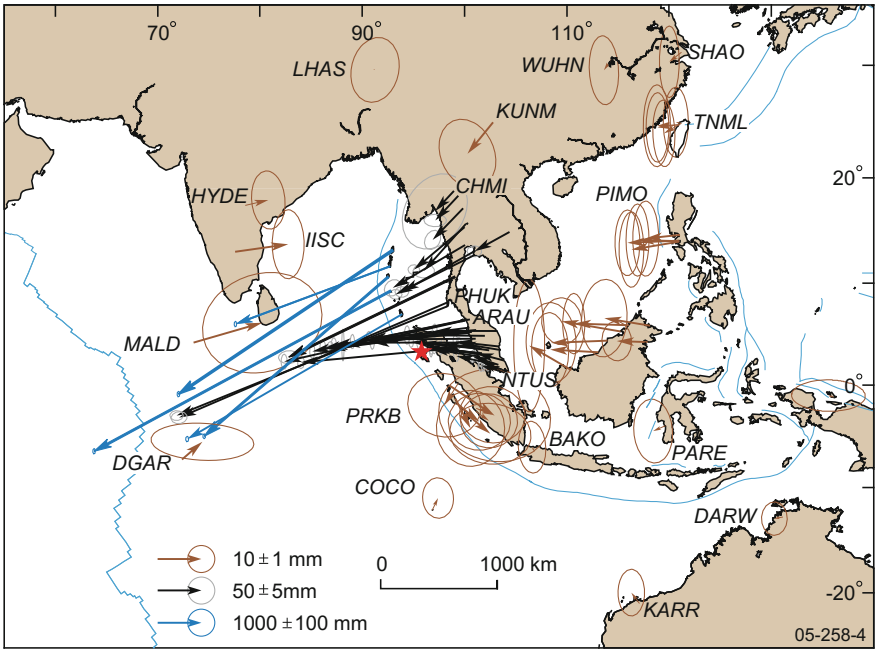


**Fig. 17.7** Displacement field for the earthquake region determined by GPS. The *red star* represents the epicentre, and the *blue lines* show plate and fault boundaries. The displacements vary from 3 to 6 m in the Andaman and Nicobar Islands, indicated by the *blue arrows* while the *black arrows* show displacements at sites in Thailand, Malaysia and Sumatra. Almost 28 cm displacement was detected at the GNSS site PHUK (Phuket Island, southern Thailand near northern Malaysia), decreasing gradually towards the north and south. Displacements reduced to 2 cm at the NTUS site (Singapore) and 3 cm at the CHMI site (northern Thailand). Deformation of around 10 mm was detected at large distances, indicated by *brown arrows*. Deformations from these sites, except for sites south-east from the epicentre, were also generally towards the epicentre or the great Sumatra fault, even though they were relatively small compared with their error ellipses. *Source* Jia [49]

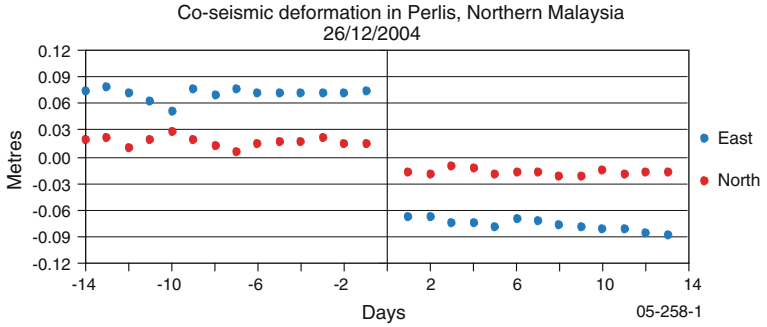


**Fig. 17.8** Co-seismic deformation before and after the earthquake at the GNSS site ARAU (Perlis, northern Malaysia). A displacement 15 cm in the east and 3 cm in the north was detected. *Source* Jia [49]

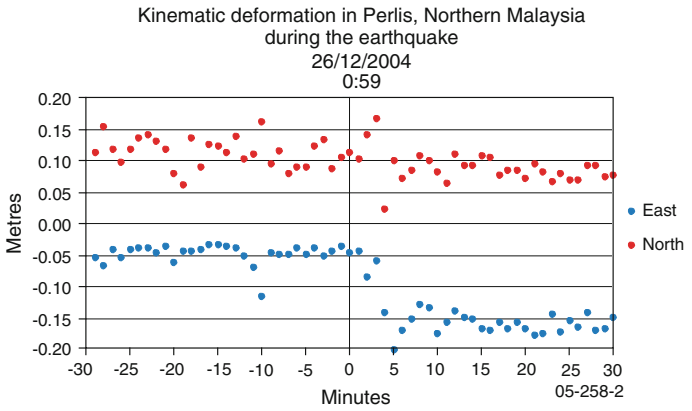


**Fig. 17.9** The progression of rapture at a GNSS site ARAU (Perlis, northern Malaysia) during the earthquake, which occurred at about 0:59 on 26 December 2004. Measurements were taken every 30 s for a period of 30 min before and after the earthquake. Two minutes after the earthquake waves hit the site, a deformation of about 10 cm was detected. *Source* Jia [49]

the two solutions and the results presented in Fig. 17.8 for the co-seismic deformation at the GNSS site ARAU (Perlis, northern Malaysia) where a displacements of 15 cm in the east and 3 cm in the north is reported. The results of Jia [49] indicate that the displacement detected by GNSS varies with location. Looking at the variation in GNSS coordinates computed by Jia [49] from stations near the earthquake every 30 s over 30-min periods before and after the earthquake (0:59, 26 December 2004) in Fig. 17.9, the progression of the rapture is noticed. Figure 17.9 indicates the deformation of 10 cm at a GNSS site of ARAU. In this particular case, Jia [49] point out that deformation was detected when the surface waves began to hit the site two minutes after the earthquake; four minutes later, positions at the site were relatively stable again.

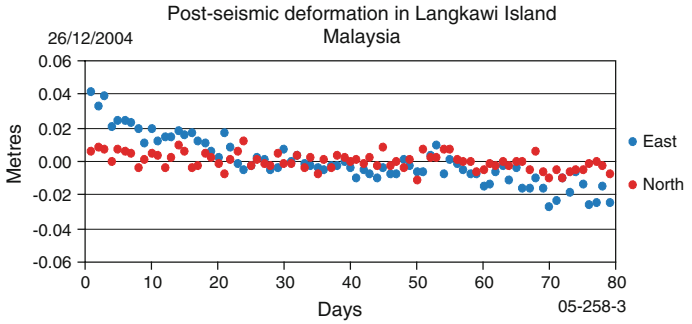


**Fig. 17.10** Post-seismic deformation at a GNSS site LGKW (Langkawi Island, northern Malaysia). *Source* Jia [49]

Using a long-term GNSS time-series after the earthquake, Jia [49] then examined the post-seismic deformation process in Fig. 17.10 and showed that the deformation at the GNSS site LGKW (Langkawi Island, Malaysia) declined continuously over time after the earthquake. An eastward deformation of more than 6 cm during the 80-day period after the earthquake is determined.

An example of such long-term GNSS time-series analysis in the work of Jia [49] shows that the Australian and Indian plates move towards Sumatra-Andaman at a rate of 5 cm and 4 cm per year, respectively (see Fig. 17.7) [49]. Jia [49] concludes that earthquake progressions of co-seismic type enable scientists to better understand the fault rupture process and that such studies could benefit tsunami early warning systems, such as the Australia Tsunami Warning System,[7] by allowing more reliable assessments of the likelihood of tsunami events to be made. For post seismic analysis, Jia [49] states that deformation information from all available GNSS sites in the earthquake region can help scientists analyze likely elastic, poroelastic and viscoelastic deformation, and plastic flow of the Earth's crust in the earthquake region, giving a better understanding of crustal relocation and redistribution after an earthquake.

End of Example 17.2.

In post-seismic activities, GNSS are also useful in monitoring deformation in structures such as dams. Other structures that could be monitored for deformation include buildings, bridges, etc. This could be done by installing GNSS equipments at strategic locations on these features and comparing the locations reading before and after the seismic activity. In built environment, Hammond et al. [52] state that through high-sample rate GNSS data, e.g., from RTGPS discussed in Sect. 5.4.3, the motion of large buildings and bridges in an inertial reference frame can be realized.

[7] http://www.bom.gov.au/tsunami/about/atws.shtml.

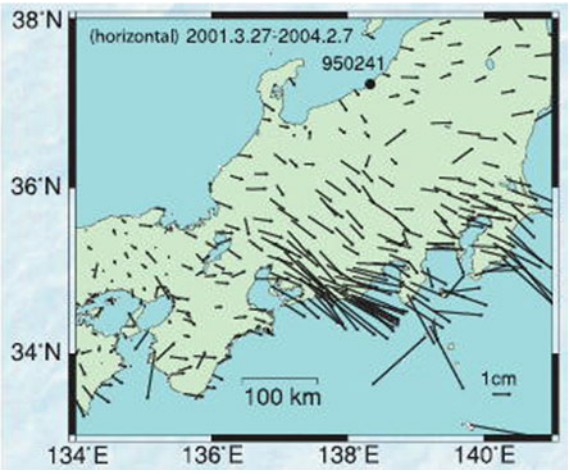


**Fig. 17.11** Horizontal displacement observed in the Tokai region due to crustal movements during the period of 27 March 2001 to 7 February 2004 with reference to the GPS station in Oogata, Niigata Prefecture(950241). *Source* (http://www.gsi.go.jp/ENGLISH/page_e30068.html)

Example 17.3 (GNSS monitoring of the Tokai crustal movement).

In Japan, GEONET (see Fig. 5.14, p. 85) has been used to monitor crustal activities by analyzing daily solutions of GNSS stations (e.g., Fig. 5.12 on p. 81) coordinates [53]. For example, when an extraordinary data are detected, or a big earthquake or volcanic eruption occurs, emergency analysis is performed to get the solutions every 3 h [53]. This enables the determination of displacement rates and strain rates throughout Japan [54]. Matsuzaka [53] points to the fact that the more than 1200 GEONET CORS stations provide data that are used in various disaster related meetings and geophysical model estimation of crustal activities, and thus reflect the decision making process to cope with disasters, as well as, scientific researches. GEONET is also quite useful in earthquake studies, precisely detecting co-seismic, post-seismic, and inter-seismic deformation signals, with these observations used to infer physical processes at the earthquake sources [54]. GEONET operates by having its stations, which are well distributed throughout the country relay real-time data by a dedicated line to the control and analysis center at the Geospatial Information Authority of Japan (GSI) in Tsukuba (Ibaraki Prefecture), thereby enabling a real-time monitoring of crustal movements.

The Tokai crustal movement has been monitored through such analysis (see, e.g., Fig. 17.11). Figure 17.11 shows the data of horizontal displacement observed in the Tokai region due to crustal movements during the period of 27 March 2001 to 7 February 2004 with reference to the GPS station in Oogata, Niigata Prefecture.[8] From the Tokai region to Nagoya, an area of displacement in the south-east direction is identified thus further indicating the possibility of using GNSS as a possible key to understanding a mechanism of the Tokai crustal movement.[9]

[8] http://www.gsi.go.jp/ENGLISH/page_e30068.html.

[9] http://www.gsi.go.jp/ENGLISH/page_e30068.html.

Slow slip events on plate boundaries as demonstrated above have been found from GNSS data, thus providing an important constraint on the mechanism of faulting [54]. Sagiya [54], however, pointed to the fact that there had been no success in detecting pre-seismic deformation but highlights the fact that GEONET enabled a good linkage between monitoring and modelling studies, opening a possibility of practical data assimilation. He suggests that for further contribution to earthquake studies, it is necessary to continue GEONET with high traceability on the details in observation and analysis [54].

End of Example 17.3.

## 17.6 Floods

In most countries that experiences frequent natural disasters, e.g., floods, droughts, earthquakes, forest fires, snow, and typhoons; floods could arguably be the most serious due to its recurrence. Almost every year, for example, Pakistan experiences severe floods caused by monsoon rains that cause considerable economic loss and serious damage to property. Another country that is perennially prone to floods is China, where the frequency of occurrence is higher than the world average, with the historical records showing more than 1000 floods [55]. Jeyaseelan [5] support the argument that floods are among the most devastating natural hazards in the world, claiming more lives and causing more property damage than any other natural phenomena, and as such is one of the greatest challenges to weather prediction.

A flood can be defined as any relatively high water flow that overtops a natural or artificial banks in any portion of a river or stream. When such a bank is overtopped, water spreads over the flood plain and generally becomes a hazard to society [5]. Jeyaseelan [5] classifies floods into:

- river floods formed from winter and spring rains, coupled with snow melt and torrential rains from decaying tropical storms and monsoons,
- coastal floods generated by winds from intense off-shore storms and tsunamis,
- urban floods, as urbanization increases runoff two to six times what would occur on natural terrain, and
- flash floods that can occur within minutes or hours of excessive rainfall or a dam or levee failure, or a sudden release of water.

For planning and undertaking of various management measures related to floods, information on watershed characteristics and river configuration and its behaviour to effectively utilize the same to understand flood situation is essential. To this extend, GNSS satellites could play a crucial role in providing information that could support *precipitation forecast* and warning (see Chap. 9), *inundation mapping* and *damage assessment*, and flood plain management, see, e.g., [1].

### 17.6.1 Flood Forecasting and Warning

Hydrologic models play a major role in assessing and forecasting flood risks. They require several types of data as input, e.g., land use, soil type, soil moisture, stream/river base flow, rainfall amount/intensity, snow pack characterization, digital elevation model (DEM) data, and static data (e.g., drainage basin size) [5]. Model predictions of potential flood extent can help emergency managers develop contingency plans well in advance of an actual event to help facilitate a more efficient and effective response [5]. In light of the above, GNSS could play a useful role of generating DEM (see Fig. 8.3 on p. 132). It could also find use in generating the drainage basin size through a similar approach to that used in obtaining the area of Jack Finney Lake discussed in Sect. 8.2.4 on p. 133. For example, GNSS was used to aid development of DEM of a flood prone area in Andhra Pradesh State that supported the assessment of spatial inundation at different water levels in the river [1]. When the satellite derived land cover/use and ancillary ground-based socio-economic data was draped over the DEM, flood vulnerability was assessed to provide location specific flood warnings [1].

As was discussed in Chap. 9, GNSS meteorology promises to be a real boost to atmospheric studies with expected improvements on weather forecasting and climatic change monitoring, which directly impact on our day to day lives. One such area is in the monitoring of flash floods. Flash floods are the floods that comes instantaneously following heavy rains. Factors that lead to flash flood producing rains are summarized in Fig. 17.12. In India for example, deforestation, extension of agricultural

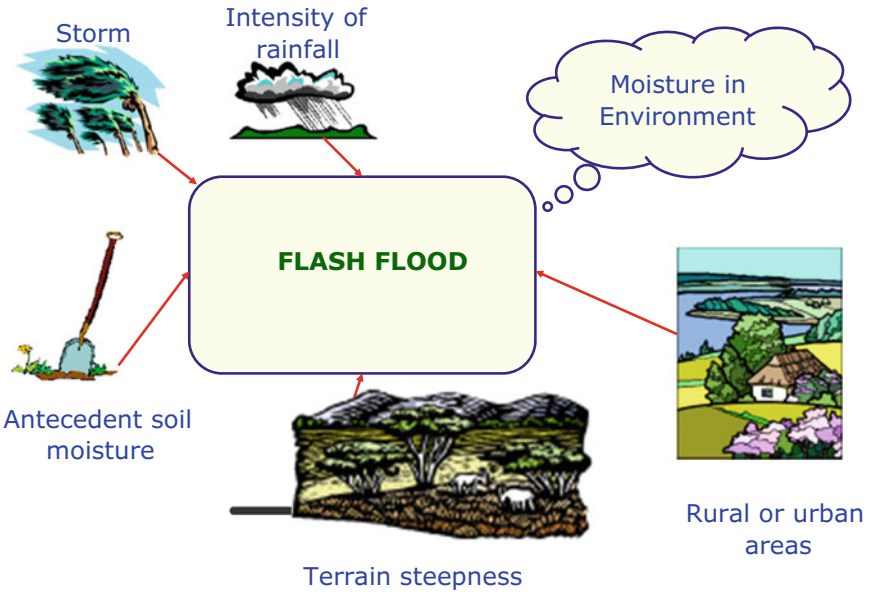


**Fig. 17.12** Factors causing flash flood

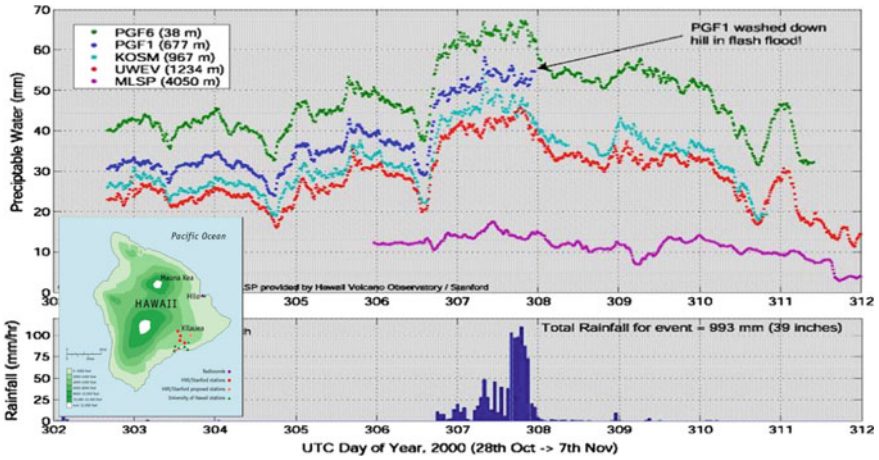


**Fig. 17.13** An example of flash flood monitoring using GNSS-derived IPWV

activities in vulnerable areas coupled with increased soil erosion and degradation of catchment areas have been mentioned as factors that have led to frequent flash floods through reduction in natural storage capacity [1]. In [56], the possible use of IPWV (see Sect. 9.2.2) for flash flood prediction is proposed, while [57] have outlined the potential of water vapour for meteorological forecasting.

Let us consider Fig. 17.13[10] as an example where GNSS-meteorology could have assisted in flash flood forecasting and warning. In the figure, the amount of integrated water vapour in the atmosphere is related to the rainfall and used to monitor flash flood in Hawaii (see the left bottom corner of the figure). One observes that as it was raining, if the Integrated Precipitate Water Vapour (IPWV) increased, more rain followed. By monitoring the intensity of water vapour, therefore, one can be able to predict the occurrence of flash flood. Station PGF1 and others were monitored and an increase noted after day 307. Shortly before day 308, the scientist reported the possibility of flash flood and indeed it occurred. Station PGF1 was washed away.[11]

### *17.6.2 Mapping of Flood Events and Damage Assessment*

During the preparedness period, flood disaster survey is necessary in order to provide information such as damage assessment of previous floods needed to generate risk zone maps that are used during the flood prevention stage. Jeyaseelan [5] groups flood risk zone maps into two categories (i) a detailed mapping approach, that is required for the production of hazard assessment useful in updating, and sometimes

[10] Source: Paroscientific Inc., http://www.paroscientific.com.

[11] More on information can be found by visiting http://www.paroscientific.com.

generating risk maps that contribute to the hazard and vulnerability aspects of flooding, and (ii) a larger scale approach that explores the general flood situation within a river catchment or coastal belt, with the aim of identifying areas that have greatest risk. In the first category, GNSS could be used to map location of features, e.g., water tanks or perimeters of areas of potential danger such as contaminated dams, while in the second case, they could be used in conjunction with remote sensing methods to map inundated areas at large spatial coverage. In mapping flood events and damaged areas, GNSS could also be used to provide both horizontal and vertical controls as exemplified, e.g., in [58], where a constrained adjustment of a static GNSS survey (e.g., Sects. 5.4.2 and 6.2.5) was performed to set basic horizontal and vertical controls for a flood control project near Guayama on the south coast of Puerto Rico. In this example, precise differential carrier-phase were applied and the end product was to obtain hydrographic and topographic data of project features to generate topographical maps (e.g., Fig. 8.2 on p. 131) for flood control.

During floods, timely and detailed situation reports are required by the authorities to *locate* and *identify* the affected areas, and to implement corresponding damage mitigation. It is essential that the location-based information be as accurate and timely as possible, in order to address emergency situations (e.g., in dealing with diversion of flood water, evacuation, rescue, resettlement, water pollution, health hazards, and handling the interruption of utilities) [5]. After the floods, follows the reconstruction of damaged or destroyed properties, where accurate information on the *locations* and the *extent of the damaged* properties is required. In both scenarios, during and after floods, location-based data and perimeter/area information could rapidly be provided by GNSS to assist in remedial measures.

Further, GNSS in conjunction with remote sensing satellite and Geographic Information System (GIS) could be integrated to provide a unified system of monitoring and evaluating flood disasters. For example, Zhanga et al. [55] discusses an airplane-satellite-ground system that arose from a research program on flood monitoring promoted by the Chinese government, which integrates remote sensing, GNSS, data transmission, and image processing. Another example is in Brahmaputra river basin in India, where GNSS was used to provide information on flooded areas and damage to croplands, roads and rail-tracks [1].

### *17.6.3 Flood Plain Management*

GNSS satellites together with remote sensing satellites could also be useful in identifying flood-prone river basins, assessment of expected risk levels, and selection of suitable land and water management measures to support management of flood plains. The application of these satellites is illustrated by Jayaraman et al. [1] who state that analyzing multidate satellite data can lead to flood risk zone maps, which are essential in regulating the use of flood plains in a planned manner. For example, in India, a satellite-derived input was used to develop an integrated river basin development plan for major river basins, which was used to identify and monitor

erosion-prone areas along river banks for the purpose of protecting land and habitat [1]. Maps prepared from remotely sensed data showing drainage congested areas could be used effectively to avoid flooding [1]. In these cases, GNSS data could provide location-based information for georeferencing of remote sensing images.

As an example, GNSS was used in conjunction with remote sensing satellites in flood management to map flood affected areas as demonstrated in the work of [59] who develop a method of wetland mapping and flood event monitoring based on a satellite multi-sensor data combination. Jayaraman et al. [1] state that because of the clear difference in the spectral signatures, it is quite possible to map areas under standing water, areas from where flood water had receded, submerged standing crop areas, sand casting of agricultural lands, breaches in the embankments, marooned villages and towns, etc., and that using multi-date satellite imageries enables the extent of damage due to crop loss, and the destruction of infra-structural facilities to be assessed. GNSS provide georeferencing of these remote sensing satellites.

Crétaux et al. [59] employed a series of airborne GNSS (GPS) measurements to map horizontal areas covered by open water, aquatic vegetation, vegetation on dry land and then detect the limit zone between each type of terrain, data which allowed the estimation of threshold values of the surface reflectance in different bands of frequency of the MODIS sensor that were used to characterize the land surface. Besides applying GNSS satellites for mapping purposes, they could be used to calibrate altimetry satellite (e.g., Fig. 9.10 on p. 165). For instance, GNSS data obtained during a field campaign carried out in Summer 2006 was used to calibrate the ICESat (Ice, Cloud, and land Elevation Satellite, e.g., Fig. 9.11 on p. 167)-derived topography on few points of control on the Goyder Lagoon [59].

### *17.6.4 GNSS Monitoring of ENSO and IOD*

The term "El Niño" originally applied to an annual weak warm ocean current that ran southward along the coast of Peru and Ecuador about Christmas time (hence Niño, Spanish for "the boy Christ-child") and only subsequently became associated with the unusually large warming that occur every few years and change the local and regional ecology [60]. The coastal warming, however, is often associated with a much more extensive anomalous ocean warming to the International Date Line (IDL), and it is this Pacific basin-wide phenomenon that forms the link with the anomalous global climate patterns [60]. The atmospheric component tied to El Niño is termed the "Southern Oscillation" forming El Niño-Southern Oscillation (ENSO), i.e., the phenomenon where the atmosphere and ocean collaborate together [61]. El Niño then corresponds to the warm phase of ENSO, while the opposite "La Niña" ("the girl" in Spanish) phase consists of a basin-wide cooling of the tropical Pacific and thus the cold phase of ENSO [60].

Satellite altimetry can play a crucial role in monitoring ENSO by observing the behaviour of the sea surface height (SSH). Through the observation of SSH (see Sect. 9.4), the 1997 – 1998 ENSO event, which was probably the biggest in recorded

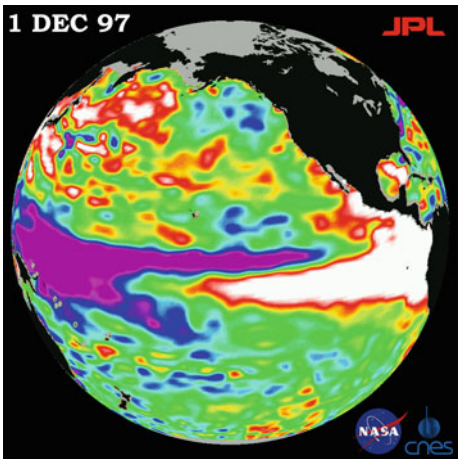


**Fig. 17.14** 1997–1998 ENSO monitored using TOPEX/Poseidon satellite. The *white-red* areas indicate unusual pattern of heat storage. *Source* http://en.wikipedia.org/wiki/File:1997_El_Nino_TOPEX.jpg

history, and whose socio-economic impacts were felt in most places around the world could be monitored. Figure 17.14 shows the image of the Pacific Ocean produced using SSH measurements taken by TOPEX/Poseidon satellite, where the image shows SSH relative to normal ocean conditions on Dec. 1, 1997.[12] In this image, the white and red areas indicate unusual patterns of heat storage; in the white areas, the sea surface is between 14 and 32 cm (6 to 13 in.) above normal while in the red areas, it is about 10 cm (4 in.) above normal. The green areas indicate normal conditions, while purple (the western Pacific) means at least 18 cm (7 in.) below normal sea level.[13]

The IOD (Indian Ocean Dipole) is an ocean-atmosphere interaction over the Indian Ocean, with alternative positive and negative sea surface height [38]. During positive events, anomalous cool (warm) waters appear in the eastern (western) Indian Ocean, associated with large-scale circulation changes that bring anomalous dry conditions to Indonesia and Australia, while East Africa experiences heavy rainfall [62]. By monitoring changes in stored water using GRACE (Sect. 9.3.3) and computing the correlation between these changes with ENSO-measured southern oscillation index (SOI) and the IOD-measured dipole mode index (DMI) as illustrated in Figs. 14.3, 14.4, 14.5 and 14.6 on pp. 283–286, it is possible to relate the effect of climate variability on water resources, see e.g., [38, 62, 63].

Garcia et al. [62] define SOI as being a measure of ENSO, which is based on the pressure difference between Tahiti and Darwin as provided by the Australian Bureau of Meteorology, while the DMI, a measure of IOD is estimated as the difference between the western and South-eastern tropical Indian Ocean sea surface temperature (SST) indices.

[12] http://en.wikipedia.org/wiki/File:1997_El_Nino_TOPEX.jpg.

[13] http://en.wikipedia.org/wiki/File:1997_El_Nino_TOPEX.jpg.

## 17.7 Droughts

Droughts are defined by WMO (World Meteorological Organization) through classification as a basis of [5] (i) rainfall, (ii) combinations of rainfall with temperature, humidity and or evaporation, (iii) soil moisture and crop parameter, (iv) climatic indices and estimates of evapotranspiration, and finally (v) the general definitions and statements. Through such a classification, drought can be grouped under *hydrological drought*, *agricultural drought*, and *meteorological drought*, whose sequence of impacts is shown in Fig. 17.15. Its impacts (direct or indirect) include, e.g., [5] reduced crop, rangeland, and forest productivity; increased fire hazard; reduced water levels; increased livestock and wildlife mortality rates; and damage to wildlife and fish habitat. Droughts occurrences are subject to extreme weather and climate similar to floods. As opposed to floods however, drought, which is a slow and progressive extreme climatic event last longer, and has been the least anticipated extreme in many regions. Drought is the single most important weather-related natural disaster often aggravated by human action since it affects very large areas for months and years

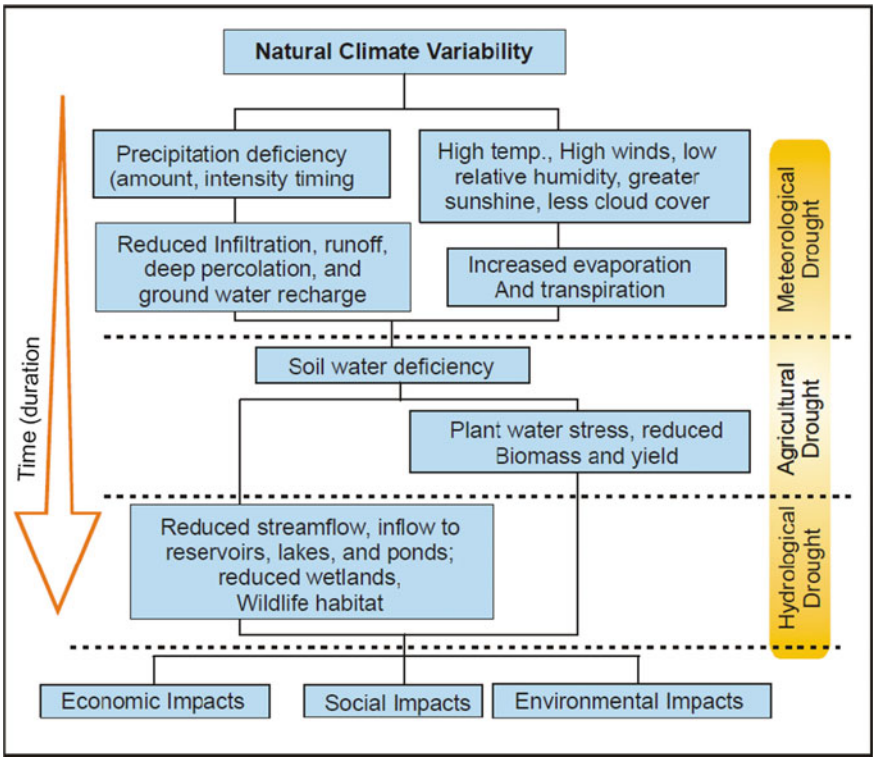


**Fig. 17.15** Sequence of hydrological, agricultural, and meteorological drought impacts as presented by Jeyaseelan [5]

and thus has a serious impact on regional food production, life expectancy for entire populations and economic performance of large regions or several countries [5]. As a result, its impacts are more adverse than those of floods because of the inadequacy of existing coping mechanisms. Although drought is a natural, recurring phenomenon which cannot be controlled, prediction of its frequency, see e.g., [7, and the references therein], severity and probability, e.g., Awange et al., [64] is essential for users such as top level policy makers at the national and international organizations, researchers, middle level policy makers at the state, province and local levels consultants, relief agencies and local producers including farmers, suppliers, traders and water managers interested in reliable and accurate drought and flood information for effective planning and management [5].

In the absence of such information, food security is threatened as exemplified in the 1999–2001 drought that affected most parts of Kenya, including some areas that normally receive high rainfall. At its peak, 4.5 million people in Kenya lost their livelihoods and ability to cope, and were subsequently entirely dependent on relief food provided jointly by the government and donors [65]. In 2011, drought affected Somalia, Ethiopia, and Northern Kenya. Adger et al. [66] discussed adaptation to climate change related phenomena in developing countries, Awange et al., [64] proposed the concept of living with drought while Barrett [8] described food assistance programs. The impacts of such extremes (in the context of climate change) on Lake Victoria Basin (LVB) has been assessed, e.g., in Phoon et al. [67]. On an average, statistics indicate that severe drought occurs once every five years in most of the tropical countries, though often they occur on successive years causing untold misery to human life and livestock [1]. For Lake Victoria basin, Awange et al. [7, 68] obtained a cycle of 5 to 8 years. With Brazil just coming out of a severe drought that has affected many areas of the country in 2015, Awange et al., [64] concluded that the probabilities of extreme droughts are 1 in 9 over northern Brazil, and 1 in 12 over southern Brazil, respectively. In general, no evidence of significant trend is detected in drought frequency, intensity, and duration over the last 11 decades at all four time-scales.

To manage effects of drought, therefore, measures should be taken, which involves both short term that includes, e.g., early warning, monitoring and assessment of droughts; and long-term strategies aimed at droughts mitigation measures through proper irrigation scheduling, soil and water conservation, and cropping pattern optimization [1]. Jeyaseelan [5] states that monitoring and assessment of drought using remote sensing and GIS dependent on the factors that cause drought, and the factors of drought impact.

### *17.7.1 Early Warning of Drought*

The first step in realizing a drought early warning system is to have a preparedness program, where drought-prone areas are identified well in advance, and drought-intensity and cycle predicted, e.g., [7]. Prediction is based on monitored parameters,

e.g., rainfall anomalies, crop conditions, weather, and vegetation. Jayaraman [1] list factors that can provide early indication of possible droughts as upper air winds, the development of hot low-pressure areas, ENSO phenomena, sea surface temperature, snow cover, cloud patterns, wind velocity and direction, and atmospheric temperature and humidity profiles.

GNSS-meteorology presented in Sect. 9.2 could be useful in providing temperature, pressure, and humidity profiles, see e.g., [69]. Section 11.4.3.2 discussed the possibility of using GNSS remote sensing techniques to monitor regional and global warming. Using the Australian example, Khandu et al. [70] showed how this technique, which has emerged over the past decade could prove to be an important tool for measuring global changes in tropopause's temperatures and heights, a valuable capacity given the tropopause's sensitivity to temperature variations. GNSS could also be useful in georeferencing satellite images that generate vegetation index, data that are useful in providing spatial information on drought-prone areas.

### *17.7.2 Monitoring and Assessment*

Monitoring and assessment of droughts are required for taking corrective measures at appropriate times in order to minimize the reduction in agricultural productivity in drought-prone areas, and also to provide objective information on the prevalence, severity level and persistence of drought conditions in a time-effective manner, which will be helpful to the resource managers in optimally allocating scarce resources to where and when they are most needed [1].

Normalized difference vegetation index (NDVI) has traditionally been used for vegetation cover modelling [71], and is a good summary overview of the prevailing plant water stress as a function of the prevailing weather conditions [72]. It measures the amount of radiation absorbed by plants, where this radiation is directly related to evapotranspiration, hence relating NDVI to rainfall. This relationship is already being exploited by the Famine Early Warning Systems Network (FEWS NET) to monitor crops and range lands in semi arid sub-Saharan Africa. In East Africa, there is a good correlation between NDVI and seasonal rainfall patterns [73], suggesting its possible use as a drought metric. In a recent study, Omute et al. [74] indicated that NDVI as a measure of vegetation vigour responded variably to *precipitation* and its *deficiency*. Its sensitive to vegetation stress enables drought conditions to be continuously monitored on a real-time basis, often helping the decision makers initiate strategies for recovery by changing cropping patterns and practices [1]. With Recently increased data availability from remote sensing (rainfall, vegetation condition index VCI, terrestrial water storage TWS), reanalysis (soil moisture and TWS), and land surface models (soil moisture), Agutu et al., [6] employed the products to characterise EA droughts between 1983 and 2013 in terms of severity, duration, and spatial extent. They further assessed capability of the products to capture agricultural drought impacts using maize and wheat production data. In Ndehedehe et al., [75], the utility of standardised indicators (standardised precipitation index (SPI),

standardised runoff index (SRI), standardised soil moisture index (SSI), and multivariate standardised drought index (MSDI)) and Gravity Recovery and Climate Experiment (GRACE) derived terrestrial water storage were employed to assess hydrological drought characteristics over the basin.

Remote sensing techniques that provide NDVI can be integrated with GIS and GNSS to effectively forecast and monitor drought where remote sensing will indicate areas of consistently healthy and vigorous vegetation, as well as stressed vegetation, while GNSS will provide location-based information that will enable these vegetation to be located, and play the role of georeferencing these remotely sensed satellite images.

The use of GRACE satellites discussed in Sect. 9.3 to provide spatial and temporal changes in terrestrial water storage, which could be used to monitor drought is emerging. For example, Chen et al. [76] used GRACE satellites to measures a significant decrease in terrestrial water storage (TWS) in the central Amazon basin in the summer of 2005, relative to the average of the 5 other summer periods in the GRACE era. Their results demonstrated the unique potential of GRACE satellites to remotely sense large-scale severe droughts and flooding events, and in evaluating advanced climate and land surface models. In Awange et al., [77], GRACE satellites have been employed to monitor hydrological drought over the greater horn of Africa, a region having hydrometeorological data deficiency.

### *17.7.3 Combating Drought*

Jayaraman et al. [1] indicate that while the construction of large reservoirs to ensure irrigation and drinking water contributed to a large extent towards mitigation of droughts in different countries, the poor and inefficient management of land and water resources in respective command areas have resulted in massive land degradation like salinity/alkalinity, waterlogging, etc., and thus causing serious concern to the conventional model of drought mitigation. In Chap. 16, ways in which GNSS satellites could be helpful in land management was presented. GNSS could also be useful in monitoring the large reservoirs. Finally, in Awange et al., [64], the concept of living with drought is emphasized.

## 17.8 Vector-Borne Diseases and Outbreak

Major epidemics of virulent disease have occurred with surprising frequency throughout human history, e.g., the numerous appearance of bubonic plaque in Europe in the late Middle Ages, the pandemic spread of influenza in the United States in 1918-19, and HIV-AIDS in our time [2]. Discovering and understanding the life cycle of a disease calls for painstaking research, literally years of trial and error, and for many biologists, GNSS and GIS could not have come at an opportune time [2]. In

general, where temporal and spatial information is required, GNSS techniques could be integrated with remote sensing and GIS to enhance optimality and provide useful information applicable, e.g., in monitoring emerging infectious diseases and to studies of global change effects on vector-borne diseases, see e.g., [78]. For example, an integration of GNSS with GIS, satellite imagery, and spatial statistics tools have been used to analyze and integrate the spatial component in epidemiology of vector-borne disease into research, surveillance, and control programs based on a landscape ecology approach [78].

Defining landscape ecology as dealing with the mosaic structure of landscapes and ecosystems by considering the spatial heterogeneity of biotic and abiotic components as the underlying mechanism which determines the structure of ecosystems, Uriel [78] describes how the integration of GNSS with the tools above, and the landscape ecology-epidemiology approach could be applicable to vector-borne diseases. They support their argument by presenting their work on malaria in Israel and tsetse flies in Kenya, and Lyme disease, LaCrosse encephalitis, and eastern equine encephalitis in the north-central United States as examples for application of the tools to research and disease surveillance [78].

On their part, Bonner et al. [79] consider the combination of GNSS and GIS geocoding in epidemiologic research, while Jayaraman et al. [1] indicate the possible application of remote sensing satellite to risk assessment from crop pest/diseases by using the temporal and spatial distribution of desert vegetation and rainfall derived from NOAA data to identify potential locust breeding grounds. Once these locations have been identified, GNSS could help by providing the actual coordinates of these positions.

Example 17.4 (Leishmaniasis research [2]).

Leishmaniasis is one of the infectious diseases causing significant health problems in Asia, Africa, India, North America, Latin America, and Europe, and is caused by a parasitic protozoan, which in turn can infect several hosts (i.e., an organism that harbors a parasite) and vectors (i.e., means of transmission, e.g., mosquitoes for malaria), making it difficult to control [2]. Researchers in Texas studied the relationship between the wood rats, which are the mammalian hosts for *Leishmania*, and the sand flies that act as vectors transmitting the disease from one host to another. To assist in their studies, the researchers employed GNSS (DGPS discussed in Sect. 5.4.4.1) to record the locations of the traps used to catch the rats, and also the locations of the Sand fly trapping stations used to catch and monitor the vector. GNSS also plays a subsidiary role of mapping roads and water features that are not found on a map, e.g., [2]. These information gathered from GNSS are integrated with other information in a GIS system through map overlaying to generate the information (maps) relating the trapping sites and the rats themselves, see e.g., [2, p. 46].

End of Example 17.4.

## 17.9 Concluding Remarks

What has been presented in this Chapter is by no means exhaustive on areas upon which GNSS satellites could contribute to management of disasters such as the 2011 landslide disaster in Brazil, where more than 1,000 people died and thousands displaced. It should be emphasized that no method can provide a full proof monitoring of a disaster. What is discussed in this Chapter are simply ways by which GNSS could contribute, albeit marginally, to monitoring disasters, which could lead to early warning and mitigation measures being taken. GNSS could also contribute towards preparedness measures and also during post-disaster periods as discussed in various sections of the Chapter. In general, GNSS complement other remote sensing satellites and where possibly, should be used in conjunction with those satellites to optimize the productivity of drought management.

## References

1. Jayaraman V, Chandrasekhar MG, Rao UR (1997) Managing the natural disasters from space technology inputs. Acra Astronaut 40(2–8):291–325
2. Steede-Terry K (2000) Integrating GIS and the global positioning system. ESRI Press, California
3. Hammond WC, Brooks BA, Bürgmann R, Heaton T, Jackson M, Lowry AR, Anandakrishnan S (2011) Scientific value of real-time global positioning system data. Eos 92(15):125–126. doi:10.1029/2011EO150001
4. Terhorst A, Moodley D, ISimonis I, Frost P, McFerren G, Roos S, van den Bergh F (2008) Using the sensor web to detect and monitor the spread of vegetation fires in Southern Africa. In: Nittel S, Labrinidis A, Stefanidis A (eds) GeoSensor networks, vol 4540. Lecture notes in computer science. Springer, Berlin, pp 239–251
5. Jeyaseelan AT (2003) Droughts & floods assessment and monitoring using remote sensing and GIS. In: Sivakumar MVK, Roy PS, Harmsen K, Saha SK (eds) Satellite remote sensing and GIS applications in agricultural meteorology. Proceedings of the training workshop, 7–11 July 2003, Dehra Dun, India, pp 291–313
6. Agutu N, Awange JL, Zerihun A, Ndehedehe C, Kuhn M, Fukuda Y (2017) Assessing multi-satellite remote sensing, reanalysis, and land surface models' products in characterizing agricultural drought in East Africa. Remote Sens Environ 194:287–302. doi:10.1016/j.rse.2017.03.041
7. Awange JL, Aluoch J, Ogallo L, Omulo M, Omondi P (2007) Frequency and severity of drought in the Lake Victoria region (Kenya) and its effects on food security. Clim Res 33:135–142. doi:10.3354/cr033135
8. Barrett CB (2002) Food security and food assistance programs. In: Gardner B, Rausser G (eds) Handbook of agricultural economics, vol 2. Elsevier Science, Amsterdam, pp 2103–2190
9. Kadomura H (1994) Climate changes, drought, desertification and land degradation in the Sudano-Sahelian region: a historic geographical perspective. In: Kadomura H (ed) Savannization process in tropical Africa II. Country briefs. Tokyo Metropolitan University, pp 203–228
10. James LF, Young JA, Sanders K (2003) A New approach to monitoring rangelands. Arid Land Res Manag 17:319–328. doi:10.1080/15324980390225467
11. Nittel S, Stefanidis A, Cruz I, Egenhofer M, Goldin D, Howard A, Labrinidis A, Madden S, Voisard A, Worboys M (2004) Report from the first workshop on geo sensor networks. In: ACM SIGMOD Rec 33(1)

12. Worboys M, Duckham M (2006) Monitoring qualitative spatiotemporal change for geosensor networks. Int J Geogr Inf Sci 20(10):1087–1108. doi:10.1080/13658810600852180
13. Stefanidis A (2006) The emergence of GeoSensor networks. Dir Mag. http://www.directionsmag.com/articles/the-emergence-of-geosensor-networks/123208. Accessed 22 Jan 2011
14. Bill R (2011) Precise positioning in ad hoc geosensor newtorks. http://www.ikg.uni-hannover.de/geosensor/Lecture/Wednesday/Session1/sess1_bill.pdf. Accessed 22 Jan 2011
15. Ailamaki A, Faloutsos C, Fischbeck P, Small M, VanBriesen J (2003) An environmental sensor network to determine drinking water quality and security. SIGMOD Rec 32(4):47–52. doi:10.1145/959060.959069
16. Brenner C (2011) Geo sensor networks-when and how?. http://dgk.auf.uni-rostock.de/uploads/media/2_2-Brenner.pdf. Accessed 22 Jan 2011
17. Nittel S, Labrinidis A, Stefanidis A (eds) (2008) GeoSensor networks, vol 4540. Lecture notes in computer science. Springer, Berlin, pp 1–6
18. Church JA, Gregory JM, Huybrechts P, Kuhn M, Lambeck K, Nhuan MT, Qin D, Woodworth PL (2001) Changes in sea level. In: Houghton JT, Ding Y, Griggs DJ, Noguer M, Van der Linden PJ, Dai X, Maskell K, Johnson CA (eds) Climate change 2001: the scientific basis: contribution of working group I to the third assessment report of the intergovernmental panel on climate change. Cambridge University Press, Cambridge, New York, pp 639–694
19. Pugh D (2004) Changing sea levels: effect of tides, weather and climate. Cambridge University Press, Cambridge
20. Hirt C, Gruber T, Featherstone WE (2011) Evaluation of the first GOCE static gravity field models using terrestrial gravity, vertical deflections and EGM2008 quasigeoid heights. J Geod 85:723–740. doi:10.1007/s00190-011-0482-y
21. Geoscience Australia (2008) Need for the geodetic component for absolute sea level monitoring. http://www.ga.gov.au/geodesy/slm/spslcmp/. Accessed 11 Dec 2008
22. Warrick RA, Le Provost C, Meier MF, Oerlemans J, Woodworth PL (1996) Changes in sea level. In: Houghton JT, Meira Filho LG, Callander BA, Harris N, Klattenberg A, Maskell K (eds) Climate change 1995. The science of climate change. Cambridge University Press, Cambridge, pp 359–405
23. Antonov JI, Levitus S, Boyer TP (2002) Steric sea level variations during 1957–1994: importance of salinity. J Geophys Res (Oceans) 107(C12):8013. doi:10.1029/2001JC000964
24. Mitrovica JX, Tamisiea ME, Davis JL, Milne GA (2001) Recent mass balance of polar ice sheets inferred from patterns of global sea-level change. Nature 409:1026. doi:10.1038/35059054
25. Bamber JL, Riva REM, Vermeersen BLA, LeBrocq AM (2009) Reassessment of the potential sea-level rise from a collapse of the West Antarctic ice sheet. Science 324:901. doi:10.1126/science.1169335
26. Dickey JO, Bentley CR, Bilham R, Carton JA, Eanes RJ, Herring TA, Kaula WM, Lagerloef GSE, Rojstaczer S, Smith WHF, Van Den Dool HM, Wahr JM, Zuber MT (1996) Satellite gravity and the geosphere. National Research Council Report, 112 pp, National Academies Press, Washington, D.C
27. Titus JG, Park RA, Leatherman SP, Weggel JR, Greene MS, Mausel PW, Brown S, Gaunt G, Trehan M, Yohe G (1991) Greenhouse effect and sea level rise: the cost of holding back the sea. Coast Manag 19:171–204
28. Lowe ST, LaBrecque JL, Zuffada C, Romans LJ, Young L, Hajj GA (2002) First spaceborne observation of an earth-reflected GPS signal
29. Rius A, Aparicio JM, Cardellach E, Martín-Neira M, Chapron B (2002) Sea surface state measured using GPS reflected signals. Geophys Res Lett 29(23):2122. doi:10.1029/2002GL015524
30. Rocken C, Kelecy TM, Born GH, Young LE, Purcell GH, Wolf SK (1990) Measuring precise sea level from a buoy using the global positioning system. Geophys Res Lett 17(12):2145–2148
31. Kelecy TM, Born GH, Parke ME, Rocken C (1994) Precise mean sea level measuring using global positioning system. J Geophys Res 99(c4):7951–7959
32. Born GH, Parke ME, Axelrad P, Gold KL, Johnson J, Key KW, Kubitschek DG, Christensen EJ (1994) Calibration of the TOPEX altimeter using a GPS buoy. J Geophys Res 99(C12):24517–24526

33. Leuliette EW, Nerem RS, Mitchum GT (2004) Calibration of TOPEX/Poseidon and Jason altimeter data to construct a continuous record of mean sea level change. Mar Geod 27(1):79–94. doi:10.1080/01490410490465193
34. Watson C, Coleman R, White N, Church J, Govind R (2003) Absolute calibration of TOPEX/Poseidon and Jason-1 using GPS buoys in bass strait. Australia. Mar Geod 26(3–4):285–304. doi:10.1080/01490410390256745
35. Snay R, Soler T (2008) Continuously operating reference station (CORS): history, applications, and future enhancements. J Surv Eng 134(4):95–104. doi:10.1061/(ASCE)0733-9453(2008)134:4(95)
36. Snay R, Cline M, Dillinger W, Foote R, Hilla S, Kass W, Ray J, Rohde J, Sella G, Soler T (2007) Using global positioning system-derived crustal velocities to estimate rates of absolute sea level change from North American tide gauge records. J Geophys Res 112:B04409. doi:10.1029/2006JB004606
37. Crétaux J-F, Jelinski W, Calmant S, Kouraev A, Vuglinski V, Bergé-Nguyen M, Gennero M-C, Nino F, Abarca Del Rio R, Cazenave A, Maisongrande P (2011) SOLS: a lake database to monitor in the near real-time water level and storage variations from remote sensing data. Adv Space Res 47:1497–1507. doi:10.1016/j.asr.2011.01.004
38. Becker M, Llowel W, Cazenave A, Güntner A, Crétaux J-F (2010) Recent hydrological behaviour of the East African great lakes region inferred from GRACE, satellite altimetry and rainfall observations. Comptes Rendus Geosci 342(3):223–233. doi:10.1016/j.crte.2009.12.010
39. GITEWS (German Indonesian Tsunami Early Warning System) (2008) A new approach in tsunami-early warning. Press-Information embargo: 11.11.2008, 10:00 CET. http://www.gitews.de/fileadmin/documents/content/press/GITEWS_operationell_eng_nov-2008.pdf. Accessed 10 Dec 2008
40. Helm A, Montenbruck O, Ashjaee J, Yudanov S, Beyerle G, Stosius R, Rothacher M (2007) GORS - A GNSS occultation, reflectometry and scatterometry space receiver. In: Proceedings of the 20th international technical meeting of the satellite division of the institute of navigation ION GNSS 2007, Fort Worth, Texas, 25–28 September, pp 2011–2021
41. Motagh M, Djamour Y, Walter TR, Wetze H, Zschau J, Arabi S (2007) Land subsidence in Mashhad Valley, Northeast Iran: results from InSAR, levelling and GPS. Geophys J Int 168:518–526. doi:10.1111/j.1365-246X.2006.03246.x
42. Schenk A (2006) Interpreting surface displacement in Tehran/Iran region observed by differential synthetic aperture radar interferometry (DINSAR). MSc thesis, Technical University of Berlin
43. Malet JP, Maquaire O, Calais E (2002) The use of global positioning system techniques for the continuous monitoring of landslides: application to the Super-Sauze earthflow (Alpes-de-Haute-Provence, France). Geomorphology 43(1–2):33–54. doi:10.1016/S0169-555X(01)00098-8
44. Gili JA, Corominas J, Rius J (2000) Using global positioning techniques in landslide monitoring. Eng Geol 155(3):167–192. doi:10.1016/S0013-7952(99)00127-1
45. Kamik V, Algermissen ST (1978) Seismic zoning- chapter in the assessment and mitigation of earthquake risk. In: UNESCO, Paris, pp 1–47
46. Dalton R (2007) GPS could offer better fault line mapping. Nat News. doi:10.1038/news070521-9. http://www.nature.com/news/2007/070521/full/news070521-9.html. Accessed 25 Sept 2011
47. Hofman-Wellenhof B, Lichtenegger H, Collins J (2001) Global positioning system: theory and practice, 5th edn. Springer, Wien
48. Hofman-Wellenhof B, Lichtenegger H, Wasle E (2008) GNSS global navigation satellite system: GPS. GLONASS; Galileo and more, Springer, Wien
49. Jia M (2005) Crustal deformation from the Sumatra-Andaman earthquake. Geoscience Australia's analysis of the largest earthquake since the beginning of modern space geodesy. Ausgeo News 80
50. Larson KM (2009) GPS seismology. J Geod 83:227–233. doi:10.1007/s00190-008-0233-x

51. Segall P, Davis JL (1997) GPS applications for geodynamics and earthquake studies. Annu Rev Earth Planet Sci 25:301–336. doi:10.1146/annurev.earth.25.1.301
52. Hammond WC, Brooks BA, Bürgmann R, Heaton T, Jackson M, Lowry AR, Anandakrishnan S (2010) The scientific value of high-rate, low-latency GPS data, a white paper. http://www.unavco.org/community_science/science_highlights/2010/realtimeGPSWhitePaper2010.pdf. Accessed 06 Jun 11
53. Matsuzaka S (2006) GPS network experience in Japan and its usefulness. In: Seventeenth united nations regional cartographic conference for Asia and the Pacific. Geographical Survey Institute, 18–22 September 2006, Bangkok, Thailand
54. Sagiya T (2005) A decade of GEONET: 1994–2003 The continuous GPS observation in Japan and its impact on earthquake studies? Earth Planets Space 56:xxiv–xli
55. Zhanga J, Zhoub C, Xua K, Watanabe M (2002) Flood disaster monitoring and evaluation in China. Environ Hazards 4:33–43. doi:10.1016/S1464-2867(03)00002-0
56. Awange JL, Fukuda Y (2003) On possible use of GPS-LEO satellite for flood forecasting. In: The International Civil Engineering Conference on Sustainable Development in the 21st Century "The Civil Engineer in Development" 12–16 August 2003, Nairobi, Kenya
57. Baker HC, Dodson AH, Penna NT, Higgins M, Offiler D (2001) Ground-based GPS water vapour estimation: potential for meteorological forecasting. J Atmos Solar-Terr Phys 63(12):1305–1314. doi:10.1016/S1364-6826(00)00249-2
58. US Army Corps of Engineers (2007) NAVSTAR global positioning system surveying. Engineering and Design Manual, EM 1110-1-1003
59. Crétaux J-F, Leblanc M, Tweed S, Calmant S and Ramillien G (2007) Combining of radar and laser altimetry, MODIS remote sensing and GPS for the monitoring of flood events: application to the flood plain of the Diamantina river. Geophys Res Abstr 9:07496. SRef-ID: 1607-7962/gra/EGU2007-A-07496
60. Trenberth KE (1997) The definition of El Niño. Bull Am Meteorol Soc 78:2771–2777
61. Trenberth K, Guillemot C (1996) Evaluation of the atmospheric moisture and hydrological cycle in the NCEP reanalyses. NCAR Technical Note TN-430, December
62. Garcia-Garcia D, Ummenhofer CC, Zlotnicki V (2011) Australian water mass variations from GRACE data linked to Indo-Pacific climate variability. Remote Sens Environ 115:2175–2183. doi:10.1016/j.rse.2011.04.007
63. Ummenhofer C, England M, McIntosh P, Meyers G, Pook M, Risbey J, Gupta A, Taschetto A (2009) What causes southeast Australia worst droughts? Geophys Res Lett 36:L04706. doi:10.1029/2008GL036801
64. Awange JL, Mpelasoka F, Goncalves R (2016) When every drop counts: analysis of droughts in Brazil for the 1901–2013 period. Sci Total Environ 566–567:1472–1488. doi:10.1016/j.scitotenv.2016.06.031
65. DMCN (Drought Monitoring Centre Nairobi) (2002) Factoring of weather and climate information and products into disaster management policy. UNDP, Government of Kenya, and WMO, Nairobi, A contribution to strategies for disaster reduction in Kenya
66. Adger WN, Huq S, Brown K, Conway D, Hulme M (2003) Adaptation to climate change in the developing world. Prog Dev Stud 3:179–195. doi:10.1191/1464993403ps060oa
67. Phoon SY, Shamseldin AY, Vairavamoorthy K (2004) Assessing impacts of climate change on Lake Victoria Basin, Africa: people-centered approaches to water and environmental sanitation. In: 30th International conference on water engineering and development centre (WEDC), Vientiane, Lao PDR, pp 392–397
68. Awange JL, Ogallo L, Kwang-Ho B, Were P, Omondi P, Omute P, Omulo M (2008) Falling Lake Victoria water levels: is climate a contribution factor? J Clim Chang 89:287–297. doi:10.1007/s10584-008-9409-x
69. Khandu Awange J, Forootan E (2016) Interannual variability of upper tropospheric and lower stratospheric (UTLS) temperature over Ganges-Brahmaputra-Meghna basin based on COSMIC GNSS RO data. Atmos Meas Tech. doi:10.5194/amt-9-1-2016
70. Khandu Awange JL, Wickert J, Schmidt T, Sharifi MA, Heck B, Fleming K (2011) GNSS remote sensing of the Australian tropopause. Clim Chang 105(3–4):597–618. doi:10.1007/s10584-010-9894-6

71. Privette JL, Fowler C, Wick GA, Baldwin D, Emery WJ (1995) Effects of orbital drift on advanced very high resolution radiometer products: normalized difference vegetation index and sea surface temperature. Remote Sens Environ 53(3):164–171. doi:10.1016/0034-4257(95)00083-D
72. Hatfield JL, Prueger JH, Kustas WP (2004) Remote sensing of dryland crops. In: Ustin S (ed) Remote sensing for natural resources and environmental monitoring: manual of remote sensing, vol 4, 3rd edn. Wiley, New Jersey, pp 531–568
73. Nicholson SE, Davenport ML, Malo AR (1990) A comparison of the vegetation response to rainfall in the Sahel and East Africa, using normalized difference vegetation index from NOAA AVHRR. Clim Chang 17(2–3):209–241. doi:10.1007/BF00138369
74. Omute P, Corner R, Awange J (submitted) NDVI monitoring of Lake Victoria water level and drought. Water Resource Management
75. Ndehedehe CE, Awange JL, Corner RJ, Kuhn M, Okwuashi O (2016) On the potentials of multiple climate variables in assessing the spatio-temporal characteristics of hydrological droughts over the Volta Basin. Sci Total Environ 557–558:819–837. doi:10.1016/j.scitotenv.2016.03.004
76. Chen JL, Wilson CR, Tapley BD, Yang ZL, Niu GY (2009) 2005 drought event in the amazon river basin as measured by GRACE and estimated by climate models. J Geophys Res 114:B05404. doi:10.1029/2008JB006056
77. Awange JL, Khandu Forootan E, Schumacher M, Heck B (2016) Exploring hydrometeorological drought patterns over the greater horn of Africa (1979–2014) using remote sensing and reanalysis products. Adv Water Resour. doi:10.1016/j.advwatres.2016.04.005
78. Kitron U (1998) Landscape ecology and epidemiology of vector-borne diseases: tools for spatial analysis. J Med Entomol 35(4):435–445
79. Bonner MR, Han D, Nie J, Rogerson P, Vena JE, Freudenheim Jo L (2003) Positional accuracy of geocoded addresses in epidemiologic research. Epidemiology 14:408–412. doi:10.1097/01.EDE.0000073121.63254.c5

# Chapter 18
# Environmental Pollution

*People blame their environment. There is only one person to blame – and only one – themselves.*

Robert Collier

## 18.1 The Concept of Pollution and Applications of GNSS

There exist various definitions to the word *pollution* depending on one's jurisdiction and the laws of a particular country. Springer [1, see references therein] looks at the meaningful concept of defining pollution in international law by posing the questions: "what are you talking about when you are talking about pollution? What is pollution? How would you define it if you are going to remove the concept of damage from it?" These questions are not easily answerable and as Springer [1] acknowledges, the term pollution is a word whose precise meaning in law, particularly international law, is not easily discerned [1]. It has been used in a wide variety of contexts, from international conventions to pessimistic speeches about the state of the environment, to describe different levels and kinds of man-induced changes in the natural world [1].

Within a particular context, pollution assumes a meaning, either explicitly stated or implicitly developed, which may bear little resemblance to its usage elsewhere. Springer [1] discusses the basic conceptual categories within which pollution has been approached in the past such as; pollution as an alteration of existing environment, pollution as a right to territorial sovereignty, pollution as a damage (to man and his property, and the environment), pollution as interference with other uses of environment, and pollution as exceeding assimilative capacity of environment.

Within this concept of environmental pollution, whether on land, water, or air, GNSS satellites could play an important role of providing maps indicating the *locations of the point sources of the pollutants*, and the *spatial changes* of areas impacted by the pollutants. It could also be useful in providing boundaries for sampling data for the purpose of pollution monitoring, e.g., air pollution monitoring that is irregular and cannot be represented by regular grids, see e.g., [2]. GNSS could also be used to



J. Awange, *GNSS Environmental Sensing*, Environmental Science and Engineering, DOI 10.1007/978-3-319-58418-8_18

support actions needed to be undertaken in order to curtail human exposure to *chemical pollution* within the framework of geosensor network monitoring discussed in Sect. 17.1.2. These includes:

(a) The monitoring of exposure of people and the environment to chemical pollutants. Here, GNSS could be used to provide location-based data indicating the physical location of sources of harmful chemical pollutants and the location of the households affected. Its distance-based data could be useful in knowing the measure of how far or close a chemical pollutant is.
(b) Institution of community-based education programmes to discuss the deleterious effects of industrial and agricultural pollutants on the environment and human health. This could be achieved through knowledge of point sources of the industrial and agricultural pollution, which could be derived from GNSS location-based data.

## 18.2 Water Pollution

That fresh water has played key roles in agriculture, industries, and municipalities, among others is highlighted for instance by [3, p. 314]. Whereas most of the world's fresh water lakes carry natural substances and nutrients, today, in addition to these natural materials, pollutants, e.g., chemicals and excess eroded soil also find their way into the lakes, e.g., [4].

Oceans, home to salt water marine, also face pollution from human-induced activities as witnessed by the BP oil leak at the Gulf of Mexico in 2010. There is need, therefore, to ensure that this vital source of life suffers minimum pollution as possible. Mackenzie [3, p. 314] defines water pollution as any physical or chemical change in water from both natural and anthropogenic sources that adversely affects the organisms living in it. Water resources undergoes pollution from both ***point*** and ***non-point*** sources discussed next.

### *18.2.1 Point and Non-point Sources*

*Points sources* are, e.g., factory outlet pipes and sewage treatment plant outlets whose positions can be accurately mapped using GNSS receivers. *Surface pollutants* include those produced from factories and industries, and agricultural activities. During rainy seasons, storm water carries with it chemicals from fertilizers and pesticides from farms, together with other nutrients from the neighbouring towns. These materials are either swept into water bodies (rivers, dams, boreholes, etc.) through surface runoffs or percolate into the ground to reach groundwater flows, and finally into the rivers. The rivers eventually pour their contents into the lakes and oceans. The consequence of sewage contamination of water quality include outbreak of human


**Fig. 18.1** Mobile hand-held GNSS

diseases and eutrophication problem, which result in the proliferation of algal blooms and undesirable aquatic macrophytes, e.g., water hyacinth, see e.g., [4]. In some countries such as Kenya, towns empty their sewage and other industrial effluent into the lakes. GNSS could be useful in mapping the locations and perimeters of these sources of sewage pollution, what could simply be achieved using a low cost hand-held GNSS receiver (Fig. 18.1[1]) in autonomous mode (see Sect. 5.4.1). This data can then be placed in a GIS system to inform decisions by the stakeholders.

An example of the effect of toxic chemical poisoning of water and its subsequent repercussion on human health was illustrated by the mercury poisoning of Minamata Bay in Japan [3, p. 324]. Around 1950s, mercury was discharged from a chemical plant located on a river flowing into the bay. The traces of this mercury found themselves in fish and were eventually consumed by people leading to the Mad Hatter's disease, a disease that affects the nervous system. Mackenzie [3, p. 324] report that older Japanese living around the bay today still exhibit evidence of the disease that has killed a number of people.

Another example of water pollution is presented by the case of Kisumu (Kenya) where pit latrines (Fig. 18.2) are in the same locality with boreholes supplying groundwater (Fig. 18.3) thus contaminating the water. GNSS could be useful in providing the locations and perimeters/areas data of these features (pit latrines and boreholes), which could be mapped in a GIS system to support waste management and policy formulations.

*Non-point sources* are those that are difficult to identify, e.g., pollution from transportation sector and wastes from mining operations, agricultural activities, and wastes carried by street runoffs and drainage. From the atmosphere, precipitation containing chemical such as *sulfur* and *nitrogen* oxides also contaminate water sources. Owing to their dispersive nature, non-point sources are difficult to control and also to map.

For Lake Victoria (East Africa), studies indicate that the high *phosphorous* and *nitrogen* loads choking it are attributed to several non-point sources. The most important of these are *agriculture*, *livestock*, *domestic* and *industrial effluents*. Most of these activities use large amounts of synthetic compounds including fertilizers and pesticides, see e.g., [6]. Although animal manure and domestic wastes contribute

[1] Source: © 1995–2010 Esri. http://www.esri.com/technology-topics/mobile-gis/graphics/geoxt-web-lg.jpg.

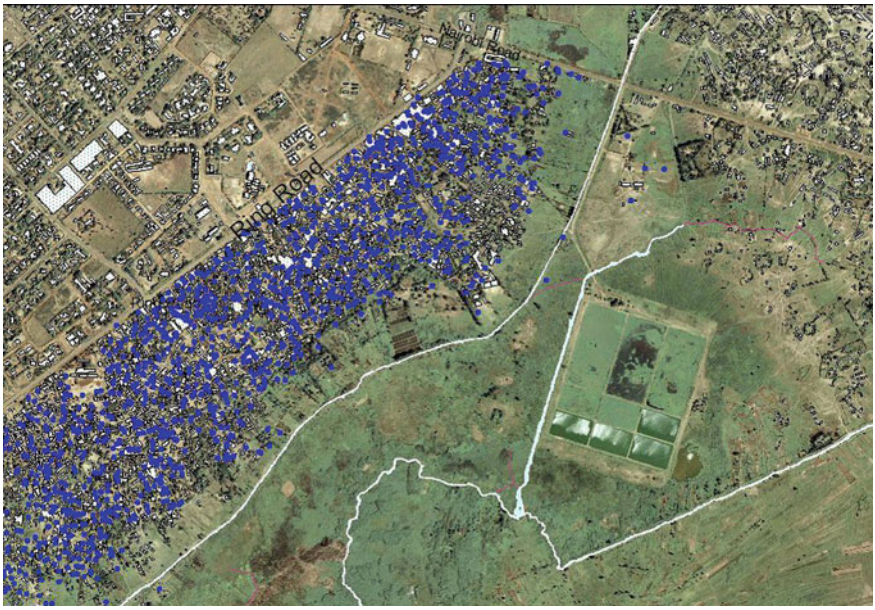


**Fig. 18.2** Pit latrine (*dotted blue*) plotted on a Map of Nyalenda (Kisumu, Kenya). GNSS could be useful in providing the perimeter/area covered by these pit latrines in addition to their actual locations. *Source* Department of Planning, MCK (Municipality of Kisumu, Kenya) and Regional Center for Mapping of Resources for Development (2006) in Opande [5]

about 3000 tons and 132 tons of the total, respectively, their nitrogen inputs are estimated at over 40,000 tons per year [7, p. 106]. This represents more than three times the amount contributed by synthetic fertilizers. GNSS could be useful in providing sampling boundaries for measuring the contributions of these pollutants, see e.g., [2].

### *18.2.2 Eutrophication of the Lakes*

Mackenzie [3, p. 318] defines eutrophication as the process of being fed too well. Eutrophication leads to water quality deterioration, taste and odour problems, oxygen depletion, reduced transparency, decline of fisheries, possible fish kills, clogging of waterways and toxic effects on animals and human beings. The phenomenon is a typical result of nutrient imbalances at several levels. The source of nutrients include agricultural activities, which produce nutrient rich runoffs resulting from the leaching of fertilizers and manure, garbage dumps, sewage, and industrial effluents. Odada et al. [8] listed three causes of eutrophication as:

(a) Enhanced effluent discharge.
(b) Runoff and storm water.
(c) Enhanced discharge of solids.

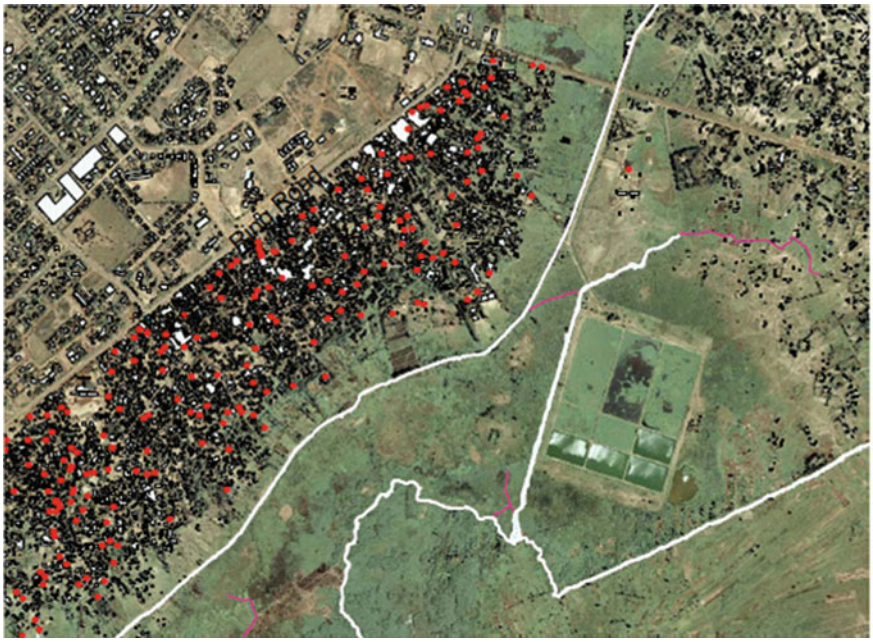

**Fig. 18.3** Well-water point locations (*dotted red*) plotted on a Map of Nyalenda (Kisumu, Kenya). GNSS could be useful in providing the positions of these wells. *Source* Department of Planning, MCK and Regional Center for Mapping of Resources for Development (2006) in Opande [5]

The first two are the most important causes of eutrophication. Sources of effluent discharge could be mapped using hand-held GNSS receivers (Fig. 18.1). In the US, the *Clean Water Act* 1972 focused on eliminating point source pollutants through regulating discharges from such point-sources. This was achieved by setting effluent limits by which business were required to adhere. By the 1980s, better control of point-source posed a minor threat to public waters and focus shifted to storm water management. The San Francisco Public Utilities Commission (SFPUC) in its attempt to reduce storm water pollution mapped the city's storm drain using a hand-held GNSS-based data collection device (e.g., Fig. 18.1) that captured the drain's precise locations and recorded digital notes on their conditions creating a GIS database [9].

## 18.3 Air Pollution

### *18.3.1 Background*

As stated in Chap. 1, environmental monitoring is concerned with monitoring the Earth's surface as well as the atmosphere. The Earth's atmosphere is known to be

sensitive to *global warming*, *ozone layer depletion*, and *air pollution*. Air pollution is the emitting of harmful substances into the air that are detrimental to the environment. These substances could include, e.g., harmful poisonous gases, volcanic eruptions, e.g., the Indonesian eruption of 2010, greenhouse gases such as $CO_2$ that contribute to global warming, just to list but a few. Perhaps, the most crucial, is the emission of greenhouse gases from transport sector. In both developed and developing nations, urban air pollution is increasingly being recognized as a major public health and environmental issue. In most developing countries, however, air quality monitoring is not routinely conducted and in some urban areas, such information does not even exist, though signs of deteriorating air quality and health problems related to air pollution are visible [10]. In Chap. 11, the possible contribution of GNSS satellites to global warming monitoring was discussed. In the next section, the possible contributions of GNSS satellites to monitor local pollution are presented. The benefits of local monitoring is that it supports environmental quality conservation.

At a local level, one major air pollutant is the transport sector that emits $CO_2$ gases to the atmosphere. Example of possible use of GNSS to monitor transport related pollution is presented in Sect. 18.3.2. Other source include industrial pollutants whose exact locations can readily be mapped using a hand-held GNSS receivers. These GNSS-based location data could then be integrated with other information such as the emission level per location in a GIS system to give a real-time air pollution monitoring capability.

For non-point sources, GNSS could play a role of mapping atmospheric quality parameters by being integrated with other devices in a geosensor network (e.g., Sect. 17.1.2), e.g., gas sensors, cell phones, and laptops in a mobile device such as that discussed, e.g., in Schreiner et al. [11]. In the work of Schreiner et al. [11], GNSS provided location-based data in terms of longitude, latitude, and altitude at points where the sensor recorded the pollution level. Both the sensor and GNSS transmitted their measured data to a laptop, which processed the information and relayed it to a mobile phone for remedial actions to be taken. In this example, GPS Map 196 receiver type was used.

### *18.3.2 Pollution from Transportation Sector*

Increased traffic volumes (see e.g., Fig. 18.4, right) in major towns such as Beijing, New York, etc., has potential for affecting ambient air. In most developing nations, such as Kenya, most of the vehicles are of the old generation (e.g., Fig. 18.4, left) and cannot sustainably run on unleaded fuel, as the conditions generated during combustion contribute to a rapid erosion of the valve seats, resulting in loss of engine performance through poor valve sealing.

The high lead content combined with the low combustion efficiency of the old type of engines lead to the emission of high volumes of exhaust gasses, which contain semi-combusted fuels combined with worn out engine parts and waste oils [12], hence high concentration of particulate matter in the air. From their study of air


**Fig. 18.4** Vehicle congestion and exhaust pollution

pollution in Beijing, Yang et al. [13] found that the relative particulate mass and the elemental concentrations of crustal and pollutant elements in the air particulate matter collected over the urban area was higher than rural areas.

The possible role that could be played by GNSS in supporting monitoring of transportation related emission and noise pollution is exemplified in the study of Taylor et al. [14] who discusses the Transportation System Center (TSC) developed at the University of South Australia based on the integration of GIS and GNSS systems. In this system, GIS played the role of data management, i.e., data entry and integration, data analysis and display, while GNSS had the role of determining the locations of both static observations and dynamic recordings of the vehicle positions over time. The GIS-GNSS system is further integrated with an engine management system of the vehicle to provide time-tagged data on GNSS position and speed, distance traveled, acceleration, fuel consumption, engine performance, and air pollution on a second-by-second basis [14].

Such data is vital not only for air pollution monitoring but also for *energy conservation* through monitoring of engine performance and fuel consumption. Acceleration data are useful in monitoring *noise pollution* level coming from the engine. An essential component of transportation that contributes to large fuel consumption and higher emission of greenhouse $CO_2$ gases is *traffic congestion*. In this GIS-GNSS system of [14], GNSS played a role of monitoring traffic congestion by measuring some component of total delay time, e.g., stopped time and acceleration noise (indicated by speed variation depending on the road condition). GNSS could also be useful in providing speed data, see e.g., [15, 16]. Further, congestion can be identified by the presence of queues, and as such, the knowledge of the incidence of queueing in any congestion monitoring system is essential [14]. As already stated, GNSS could help in measuring the proportion of stopped time (PST), which indicate the amount of time spent in queues during a journey [14].

## 18.4 Land Pollution

### *18.4.1 Solid Waste Collection and Management*

Natural resources on the fringes of urban areas always suffer severe depletion and degradation as urban centers create demand for goods and services thus exerting tremendous pressure on fragile ecosystems. The high rate of urbanization therefore rapidly increases the pressure on these ecosystems. The increasing population and economic growth of cities associated with urbanization create externalities due to the demand for resources and waste disposal [17].

Solid waste includes refuse from households, non-hazardous solid waste from industrial, commercial and institutional establishments (including hospitals and other health care facilities), market wastes, yard wastes and street sweepings. Solid Waste Management (SWM) encompasses the functions of storage, collection, transfer, treatment, recycling, resource recovery and disposal. Its first goal is to protect the health of the population. Other goals include promotion of *environmental quality* and *sustainability*, support of economic productivity and employment generation. Achievement of SWM goals requires sustainable systems, which are adapted to and carried out by the municipalities and their local partners including the communities within their jurisdictions.

In many cities of developing countries, private or public systems of SWM are inadequate, only able to achieve collection rates of between 30 and 50%. The uncollected wastes are often disposed off in ways detrimental to the environment such as open burning, burying, or dumping in rivers [18]. This problem is further compounded in low income areas where the authorities normally prioritize SWM lowly as compared to water supply, electricity, roads, drains, and sanitary services [19]. SWM is a major responsibility of local governments in developing countries consuming between 20 and 50% of their total budgets [20]. It is a complex supply driven task, which depends as much upon organization and cooperation between households, communities, private enterprizes, and government authorities, as it does upon the selection and application of appropriate technical solutions for collection, transfer, recycling and disposal [21]. It should therefore, be approached from the perspective of the entire cycle of material use with a broad scope encompassing planning and management, *waste generation* and waste handling processes [19].

### *18.4.2 GNSS Support of Solid Waste Management*

The functioning of solid waste management systems is influenced by the waste handling patterns and underlying attitudes of the urban population who are the waste generators; these factors are themselves, conditioned by the people's social and cultural context [19]. Fast growing low-income residential communities often comprise of a considerable social, religious and ethnic diversity, which strongly influences the

waste characteristics and socio-economic patterns thereby influencing the choice of SWM techniques to be applied.

In urban areas, the physical characteristics of a settlement such as the road conditions, topography, waste characteristics, etc., need to be considered when selecting and/or designing waste collection and transportation procedures and equipment. Use of GNSS and GIS technology could be valuable in visualizing this physical characteristic to improve on collection efficiency. More importantly, GNSS and GIS could be vital tools for urban planners in that they could enable them harmonize solid waste management and other services such as water, electricity, access roads, physical planning, and sanitation, all of which are associated with inadequate service delivery within a municipality. This technology would help in getting the exact location and properties of the containers, understanding the attributes of the infrastructure, and routing of the secondary collection vehicles.

At the level of natural systems, the interaction between waste handling procedures and public health conditions is influenced by climatic conditions such as seasonal weather variations and other ecological factors, e.g., the nature of animals reared within the homestead. In practical terms, climate determines the frequency by which waste collection points must be serviced in order to limit negative environmental consequences. The contribution of GNSS to weather and climate monitoring are presented in Chaps. 9 and 11.

The management methods and techniques employed in SWM should pay more attention to integrated approaches based on adequate information systems, e.g., GIS among other tools. With regard to operational planning and appropriate management methods, the approach should include among others, data collection techniques, analysis of waste composition, projecting waste amounts, scenario techniques and formulation of equipment specifications [22], all of which could be supported by GNSS as discussed above (Fig. 18.5).

### *18.4.3 Solid Waste from Transportation Sector*

Although pollution from industry, agrochemical factories and farmlands have been well documented (see, e.g., Sect. 18.2), the contribution of the transportation sector to the pollution of environment in terms of solid waste also deserve to be mentioned. Contribution of pollution from the vehicles takes the form of;

- litter generated at the termini and along the roads (e.g., Fig. 18.6),
- vehicle repair, service and maintenance yards and garages commonly known in Kenya as "Jua Kali" (i.e., open garages indicated by Figs. 18.7 and 18.8),
- exhaust fumes and oil spills on to the roads, which are washed into the water source (Figs. 18.9 and 18.10).

A hand-held GNSS receiver (e.g., Fig. 18.1) could be useful in providing locations of these sources, which could then be mapped and integrated with other data in a GIS to develop a real-time monitoring of system for decision makers in municipalities.


**Fig. 18.5** Informal waste dumping locations (*dotted red*) plotted on Map of Nyalenda (Kisumu, Kenya). GNSS could be useful in providing these locations. *Source* Opande [5]


**Fig. 18.6** Waste accumulation at bus termini in Kisumu (Kenya)

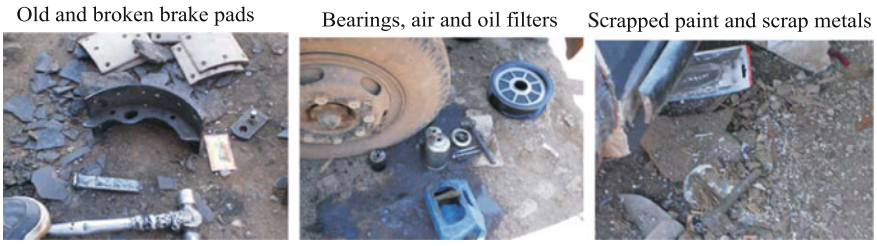


**Fig. 18.7** Wastes from vehicle repair known as Jua Kali in Kisumu (Kenya)


**Fig. 18.8** The spray painting process and wastes in Kisumu (Kenya)


**Fig. 18.9** Oil spills in Kisumu (Kenya)


**Fig. 18.10** Petrol station operations and the Caltex petrol depot at the Lake side in Kisumu (Kenya)

*Car Washing*: In East Africa, an increasingly popular practice at the beaches of Lake Victoria today is the car washing (Fig. 18.11) whose history stretches back to the late 1950s. The beach records very high turn over of vehicles of different classes that are washed at the Lake every day, see e.g., [4, 23]. Casual observations reveal that the shore waters are now dirtier and greasier. The waste oils from these vehicles, and dirt accumulated in transit are all washed into the Lake. Some of the vehicles


**Fig. 18.11** Washing of heavy petroleum vehicle in Lake Victoria in Kisumu (Kenya)

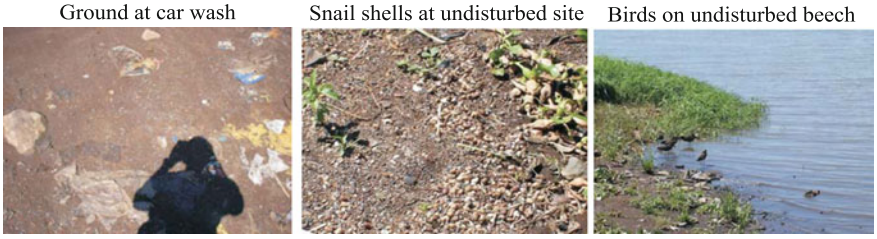


**Fig. 18.12** Environmental impacts of washing of heavy petroleum vehicles in Lake Victoria in Kisumu (Kenya). A hand-held GNSS could provide the location, perimeter, and area information of such impacted areas. This information could then be incorporated into a GIS system to support habitat conservation and management

have leaking systems hence the oils or the fuels drip into the Lake while they are being washed causing further problems.

As can be seen in Fig. 18.12, the shores are no longer supporting the original vegetation or other small life forms, due to the conscious removal by the car washers or possibly due to the decrease in the oxygen levels in the water occasioned by the oil covering the water surface. In Fig. 18.12, the floral and faunal composition has also changed as can be detected by the lack of shells at the car washing area. There has been a change in the trophic relations at the car washing area, which affects the entire Lake. It should be pointed out that Kichinjio beech in Kisumu (Kenya) is one of the breeding sites for some fish species and other aquatic life forms within the lake, a characteristic that is fast disappearing. The disturbance accompanied by oils

in the water could have adversely affected them. A hand-held GNSS receiver could play a vital role in providing locations, perimeters, and areas of such car washing impacted areas for the purposes of habitat conservation and management.

### *18.4.4 Acid Mine Deposit Sites*

Sulfide minerals occurring naturally are common minor constituents of the Earth's crust but occur in large quantities in some metallic ore deposits (e.g., Cu, Pb, Zn, Ni, U, Fe), phosphate ores, coal seams, oil shales and mineral sands [24, p. 29]. When not exposed to oxygen, sulphide are harmless. However, when exposed to oxygen through, e.g., mining, excavation, waste rock dams, etc., they become oxidized to produce sulphuric acid and high concentration of heavy metals such as Cu and Zn, see e.g., [25, p. 33]. Lottermoser [24, p. 29] point to the fact that the mineral pyrite ($FeS_2$) tend to be the most common sulphide mineral present whose weathering at mine sites cause the largest, and most testing, environmental problem facing the industry today - the acid mine drainage (AMD).

AMD generation can lead to the contamination of surface and groundwater resulting into expensive treatment. Johnson et al. [26] indicate that the cost of remediating impacts of AMD in Canada for example was in excess of $3 billion. In Australia, the environmental impact of AMD is most significant in the abandoned mines, e.g., Rum Jungle (NT), Mt Lyell (Tas) and Mt. Morgan (Qld) [25, p. 34]. The problem with AMD is that where it enters streams, there is a drop in pH leading to the disappearance of *aquatic ecosystems* and backside *plant communities*, soil contamination, the degradation of the food chain and contaminated groundwater [24, p. 69] and [27]. According to Lottermoser [24, p. 29], long-term exposure to contaminants in farmed food products may have the possibility of increasing health problems for humans. The extent to which extreme conditions of AMD develop depends on [25]:

- Water availability for oxidation and transportation.
- Oxygen availability.
- Physical characteristic of materials.
- Temperature, ferrous/ferric iron equilibrium, and microbial activity.

An effective approach for handling AMD entails managing of one of the factors above. Encapsulations of acid generating materials to prevent water leaching through the sulfidic materials and to limit oxygen contact with it are the two most important principles to apply [25]. The two steps above can only be applied once the materials on the mine sites, which have acid generating potential, have been identified [25].

GNSS could be useful in providing the locations of the materials once they have been identified and also in mapping sample sites for which tests such as net acid generation (NAG) are to be undertaken. These location-based data could support management measures by showing decision makers the exact places where the factors listed above have been implemented. A hand-held GNSS receiver would suffice for such a case.

## 18.5 Concluding Remarks

This chapter has outlined some examples of areas where GNSS could support pollution monitoring. The materials presented in this chapter are by no means exhaustive but a motivation for further research on how the application of GNSS and its integration with other technologies could contribute to enhancing pollution monitoring and management. This was shown, e.g., in the case of monitoring air pollution and storm water pollution where it was integrated with gas sensors and GIS respectively. It was also shown that GNSS will play a crucial role in transport pollution related monitoring through measurements, e.g., of stoppage time, and provision of location-based data.

## References

1. Springer AL (1977) Towards a meaningful concept of pollution in international law. Int Comp Law Q 26:531–557
2. Gibson J, MacKenzie D (2007) Using global positioning systems in household surveys for better economics and better policy. World Bank Res Obs 22(2):217–241. doi:10.1093/wbro/lkm009
3. Mackenzie FT (2003) Our changing planet; an introduction to Earth system science and global environmental change, 3rd edn. Prentice Hall, New Jersey
4. Awange JL, Ong'ang'a O (2006) Lake Victoria-ecology, resource of the Lake Basines and environment. Springer, Berlin
5. Opande T (2008) Planning solid waste collection in low income settlements of Nyalenda and Ondiek in Kisumu town, Kenya. MSc thesis, Maseno University, Kenya
6. Kairu JK (2001) Wetland-use and impact on Lake Victoria. Lakes Reserv: Resour Manag 6(2):117–125. doi:10.1046/j.1440-1770.2001.00135.x
7. Aseto O, Ong'ang'a O (2003) Lake Victoria (Kenya) and its environs: resource, opportunities and challenges. Africa Herald Publishing House, Kendu Bay
8. Odada EO, Olago DO, Kulindwa K, Ntiba M, Wandiga S (2004) Mitigation of environmental problems in Lake Victoria, East Africa: causal chain and policy options analyzes. R Swed Acad Sci 33(1):13–17
9. Corbley KP, Stauffer R (2006) Curbing water pollution with mobile GIS: mobile data collection with handheld GPS units facilitates a San Francisco utility's quest for cleaner water, enabling a two-pronged effort to build a storm drain GIS layer and educate citizens about pollution. Geospatial Solut. http://www.gpsworld.com/gis/local-government/curbing-water-pollution-with-mobile-gis-5361. Accessed 20 Jan 2011
10. Odhiambo GO, Kinyua AM, Gatebe CK, Awange JL (2010) Motor vehicles air pollution in Nairobi. Kenya. Res J Environ Earth Sci 2(4):178–187
11. Schreiner C, Branzila M, Trandabat A, Ciobanu RC (2006) Air quality and pollution mapping system, using remote measurements and GPS technology. Global NEST J 8(3):315–323
12. Municipal Council of Kisumu (2004) Kisumu City Environmental Profile. UN Habitat
13. Yang C, Peterson CL, Shropshire GJ, Otawa T (1998) Spatial variability of field topography and wheat yield in the Palouse region of the Pacific Northwest. Trans ASAE 41(1):17–27
14. Taylor MAP, Woolley JE, Zito R (2000) Integration of the global positioning system and geographical information systems for traffic congestion studies. Transp Res Part C 8(1–6):257–285. doi:10.1016/S0968-090X(00)00015-2
15. Zito R, D'Este GM, Taylor MAP (1995) Global positioning systems in the time domain: how useful a tool for intelligent vehicle-highway systems. Transp Res C 3(4):193–209

16. Zito R, Taylor MAP (1994) The use of GPS in travel time surveys. Traffic Eng Control 35(12):685–690
17. Leitman J (2000) Rapid environmental assessment: lessons from cities in the developing world, vol 1. Methodology and preliminary findings, Urban Management Programme, UNHCS, UNDP and the World Bank
18. Hoornweg D, Thomas L (1999) What a waste: solid waste management in Asia. Urban Development Sector Unit East Asia and Pacific Region, The International Bank for Reconstruction and Development/THE WORLD BANK, Washington
19. Schubeler P, Wehrle K, Christen J (1996) Conceptual framework for municipal solid waste management in low income countries. UMP working papers series no. 9, UNDP/SDC/UNCHS/World Bank, UMP/SKAT
20. Van Beukering P, Sekher M, Gerlagh R, Kumar V (1999) Analyzing urban solid waste in developing countries; a perspective on Bangalore, India. International Institute for Environment and Development (IIED), Working paper No. 24. CREED, London, UK
21. United Nations Centre for Human Settlement (UNCHS), Nairobi and United Nations Environmental Programme (UNEP) (1996) International source book on environmentally sound technologies for municipal solid waste management. IECT technical publication series, New York, USA
22. Senkwe B, Mwale A (2001) Solid waste in Kitwe, Zambia. A solid waste characterization study for the city of Kitwe, Zambia. Phase I. A consultancy report for SINPA, Zambia; Institute for Housing and Urban Development Studies, Netherlands; and the Copper Belt University, Kitwe, Zambia
23. Awange JL, Obera B (2007) Motor vehicles: are they emerging threats to Lake Victoria and its environment? Water Air Soil Pollut 182(1–4):43–56. doi:10.1007/s11270-006-9319-3
24. Lottermoser B (2003) Mine wastes. Characterization, treatment and environmental impacts. Springer, Berlin
25. Laboratory Manual (2008) ENV 310 land management practical manual. Learning materials: School of Environmental Science, Murdoch University
26. Johnson R, Wichern D (2007) Applied multivariate statistical analysis, 6th edn. Prentice Hall, Upper Saddle River
27. US-EPA (U.S. Environmental Protection Agency) (1994) Technical document. Acid mine drainage prediction. EPA 530-R-94-036; NTIS PB94-201829

# Chapter 19
# Animals and Vegetation Protection and Conservation

*During the past 35 years, new technologies have been developed for remotely tracking and studying free ranging animals [1], and advances in technology continue to increase opportunities for incorporating tracking and biotelemetry to study animal behaviour and ecology. Perhaps the most revolutionary advance in obtaining animal locations is the use of GNSS.*

Tomkiewicz et al. [2]

## 19.1 Introductory Remarks

This chapter presents ways in which the emerging GNSS methods could be useful in supporting management and conservation efforts of *animals* and *vegetation*. Ways in which animals and vegetation impact on the environment, and vice versa, i.e., the ways in which the environment impact, through human-induced anthropogenic activities, on the animals and vegetation are considered. Specific emphasis on how GNSS could support these efforts through monitoring, thereby enabling remedial measures to be undertaken are presented.

Section 19.2 introduces the concept of GNSS-based animal telemetry, which is an emerging powerful technology for wildlife studies that provides *continuous*, *high accurate* positional (time-series) data on animal locations, information which when combined with other data, such as very high frequency (VHF) radio tracking and/or remote sensing data (e.g., from MODIS - Moderate-resolution Imaging Spectro-radiometer) could lead to improved understanding of animal ecology, movement, foraging, and impact on the environment among other benefits. In overall, these benefits will enhance *conservation measures*.

The section starts by presenting the benefits (i.e., usefulness in *conservation* and *monitoring of the endangered species*) and background of animal tracking in Sect. 19.2.1, which highlights the advantages of GNSS-based animal telemetry approach over the conventional methods (e.g., VHF). Section 19.2.2 then looks at the observation and data management aspects, i.e., how the huge amount of data acquired can be managed. Finally, Sect. 19.2.3 concludes by presenting examples of



J. Awange, *GNSS Environmental Sensing*, Environmental Science and Engineering, DOI 10.1007/978-3-319-58418-8_19

real application areas where GNSS-based wildlife telemetry have been used. The materials presented in this section are largely adopted from the contributions of a theme issue "*Challenges and opportunities of using GPS-based location data in animal ecology*", which was held at Edmund Mach Foundation, Viote del Monte Bondone, Trento, Italy, in September 2008, see e.g., [3, and the contributions therein].

Section 19.3 then moves away from the animal world, to the plant kingdom and explores means by which GNSS could support management and conservation of vegetation. Vegetation itself comprises wide varieties of plant species, some of which are rear species such as those found in Australia. In this section, however, only forests and wetlands are discussed. The GNSS methods, nonetheless, are not limited to forests and wetlands, but could be useful to any other species of vegetation being monitored for conservation purposes. In Chap. 10 the possibility of using GNSS-R to remotely sense vegetation through the reflected signals was presented.

## 19.2 GNSS Animal Telemetry

### *19.2.1 Benefits and background*

#### 19.2.1.1 Benefits

Studying animal motion provides ecologist with the necessary location-based data for linking the animals (observed) to their environment (place or location, which they could impact or could inversely impact on them). This link opens the possibility of monitoring and studying how an individual animal interacts with its environment. This could lead to improved knowledge, for instance, on how an animal forages (i.e., what it likes and does not like), and how this impacts on the environment (see the example of giraffe in Fig. 19.3 on p. 410). This knowledge could in turn provide information to policy and decision makers on conservation measures required. Cagnacci et al. [3] discusses how knowing where animals go can help scientists in their search for understanding key concepts of ecology, e.g., resource use, home range and dispersal, and population dynamics. They postulate that intense sampling of movement, coupled with detailed information on habitat features at a variety of scales could enable the representation of animal's cognitive map of its environment and the intimate relationship between behaviour and fitness, data which when used over a long period of time could enhance monitoring of the impacts of climate change on *animal distribution* and *behaviour* [3, 4].

Hebblewhite and Haydon [4, Table 1] provide a nice and detailed summary of the potential advantages and disadvantages of a combined GNSS and Argos technology for supporting animal ecology and conservation issues such as resource selection and corridor mapping, behaviour, migration, home range, demographic studies (e.g., survival reproduction), movement ecology, human-wildlife conflicts, and climate change. Advantages are listed by Hebblewhite and Haydon [4, see references therein]

as improvements to habitat modelling conservation (e,g., identification of habitat corridors for trans-boundary conservation of Africa elephants, see e.g., [5, Chap. 8, p. 64]), mechanism of migrations (e.g., evidencing the main hypothesis for migration at scales and across system that had previously been unthinkable without GNSS technology), basic ecology and conservation of wide ranging species (e.g., advancement of basic ecology such as where animals forage, movement and distribution), conservation impacts (e.g., GNSS maps of wolf (*Canis lupus*), telemetry locations that clearly showed a dramatic avoidance of human activities), and projecting impacts of climate change (e.g., the effect of climate change on the predicted distribution of polar bears (*Ursus maritimus*) in the next 50 years).

The shortcoming of a GNSS-based animal telemetry are listed as costs, small sample size and poor population level inferences, overemphasis on the importance of fine-scale data, removing the need of actual human observation, and difficulty in relating fine-scale movements and coarse-scale evaluation of resource and behaviour [4]. It should be pointed out, however, that with the full realization of GNSS satellite constellation, e.g., with most of the satellites discussed in Chap. 2 now operational, receivers are being manufactured that integrate the full spectrum of GNSS lowering the cost. This has an added advantage for GNSS-based animal telemetry in terms of positional accuracy, which is now an order lower than the 15 m that has been achievable so far (see e.g., Fig. 5.7 on p. 69).

#### 19.2.1.2 Background

As early as 1960, the Craighead brothers realized the vast potentials inherent in locating animals within their environment without physically coming into contact with them when they radio-collared the first grizzly bears and elk as part of their ground breaking studies in Yellowstone National Park [4, 6, 7]. GNSS-based radio telemetry, therefore, could be traced back to the work of these scientists [4]. Since the pioneering work of the Craigheads, a fully functional GNSS tracking systems for wildlife, which is coupled with data transmission technologies has given birth to a new era of animal tracking as evidenced in literature that document numerous examples of successful studies using GNSS positioning, see, e.g., [2, and the references therein].

Conventional animal location tracking methods include, e.g., VHF-based telemetry, camera trapping, landscaping genetics, and Argos among others. GNSS-based telemetry provides systematic, highly accurate and relatively unbiased data compared to these conventional approaches, and enables the correction of bias in the GNSS fix-rate previously ignored in the VHF-based telemetry [4]. Though GNSS-based telemetry has the above mentioned advantages over the conventional methods, a combination with these methods, e.g., GNSS-Argos could offer significant improvements as opposed to a stand-alone approach. Hebblewhite and Haydon [4], for instance, report on the alleviation of substantial amount of time required to manually obtain location-based information brought about by the GPS-Argos combination. The positive outcome of this is the elimination of human bias that could be incurred from manual observation and significant saving of the resources that could have been

allocated for such manual observations [4]. It should also be noted that lessons and experiences learnt from the conventional approaches enhanced the advancement of GNSS-based approach.

This has resulted in a great potential of monitoring the impacts of domestic and wild animals on their habitats. This has come about due to the realization that these animals alter the biological equilibriums of their habitat as they roam about either to graze, look for water, or rest. In Fig. 19.3, for example, the impacts of giraffe on the vegetation of Ruma National park in Kenya can be seen. Such important alteration require an understanding of the impact of animals on their habitat.

One of the main objectives of ethologists and experts in landscape planning is to understand the factors influencing the movements, and therefore the distribution of animals over the land. The *acquisition of this information* is the only way animal populations, both wild and domestic, will be able to be managed in order to satisfy both the conservationist and the productive aims [8]. GNSS technology is fast becoming the preferred means of gathering of information related to animal movements and spatial distribution. GNSS data can be used to address animal ecology questions (e.g., resource selection, animal movement, and foraging behaviour) from a completely new perspective, i.e., closer to the animal point of view [9].

### *19.2.2 Observation and Data Management Techniques*

As opposed to traditional positioning procedures performed with the privilege of undertaking mission planning (e.g., Sect. 5.3) that enhances the achieved accuracies, animal tracking completely takes the GNSS receiver to the world of uncertainty as it becomes subject to the animal's mercy. The animal dictates where it goes based on factors such as food availability thereby seeing the receiver traverse terrains, some of which maybe hostile and others which may illicit blockage of the GNSS signals, especially when the animal moves under trees or inside forests. Two main features of the receiver that immediately comes to play are its size, i.e., depending on the animal to be tracked, and the durability of the receiver, i.e., how long is the animal to be observed?

The positional aspect of GNSS-based telemetry is presented, e.g., by Tomkiewicz et al. [2] who provide a chronological advancement of the animal based collar receivers. Just like the normal GNSS receivers used for positioning discussed in Chap. 5, a collar-based GNSS receiver also requires a period of initialization also known as initial fix. This is the period, which the receiver obtains its initial position when it is switched on by determining the satellites in view. At the period of infancy of GPS technology, receivers could take more than 30 min to determine their initial positions. Modernization of the receiver technology and increased availability of satellites, however, has reduced this period to less than a second. The maturity of the GNSS system now ensures availability of wide range of satellites. Receivers are now also being manufactured that can track multiple satellites from different GNSS constellations (see Chap. 2).

The basic operational principle involves a collar GNSS receiver that is tied around the animal's neck. The receiver measures positional pseudoranges and satellite ephemeris data (see Sect. 3) and stores them, while at the same time transmits the data to the control center. Besides size and durability, power consumption is also a major factor. In order to lower power consumption, the receiver can be set such that it measures only the pseudorange data and later uses precise ephemeris (see Sects. 3.4.1 and 5.4.2), in what is termed as 'rapid fix technology' by Tomkiewicz et al. [2]. Tomkiewicz et al. [2] presents two types of rapid fix (i) the quick fix pseudorange (QFP) and (ii) snapshot depending on whether land animals or marine animals are being monitored. Technological advances have now seen the emergence of smaller low voltage (3.0 Vdc) and low current that allow tracking of smaller mammal species and birds [2]. For animal collar receiver, this initial fix time is of great importance as marine animals, for example, surfaces for a shorter period of time, thus requiring a quick fix. The need to conserve receiver power consumption also dictates the operation as some receivers are turned on and off, thus also calling for quick fix.

In the QFP designed for marine mammals, a standard GNSS receiver that can collect data to 5 s of an animal surfacing is used, where pseudoranges are collected for post-processing and at the same time stored for later downloading if the receiver is recovered [2]. The snapshot receivers are specifically designed to digitize GNSS downlink signals in less than a second and either stores the digitized data in raw form thereby incurring huge files and low power consumption or extracts and calculates the pseudoranges thereby reducing the file sizes that are manageable (comparable to QFP) but using more power [2].

Due to the fact that GNSS-based radiotelemetry data are integrated with other forms of data (e.g., from remote sensing), a proper data management system is required. For instance, a micro-power data acquisition controller (MDAC) is used to manage the entire operation to achieve a functional system [2]. Urbano et al. [9] provide an evaluation of the requirement of a good management of GNSS-based animal tracking data and stress the need for a dedicated data management tool and expertise. They propose an example of such a spatial database model and how it operates in Fig. 19.1. In the next three subsections, examples of application areas; conservation of biodiversity, migratory/endangered species, and the mapping of the attacking Australian bears are presented.

### *19.2.3 Applications*

The use of GNSS-collar receivers to study the positions of animals is a common technique for studies on wild animal habitats (such as those of deer, bears, and wolves) [8]. Barbari et al. [8] provides an example on how GNSS is combined with GIS and used to track animal locations in the various grazing areas at the Animal Research Center of the University of Kentucky. In their study, 15 cows were individually equipped with GNSS collar receivers programmed to record positions

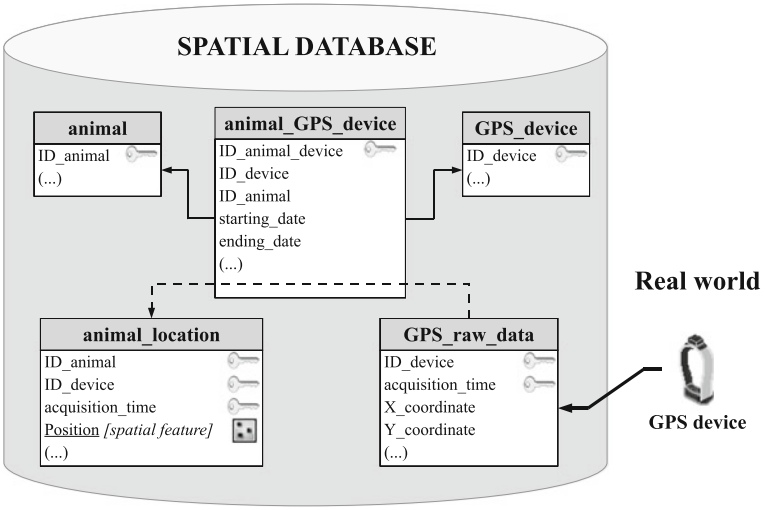


**Fig. 19.1** A general representation of a possible standard database data model for core wildlife GNSS (GPS) data by Urbano et al. [9]. When the GNSS device provides coordinates of a location at a specified time, they are uploaded in the database in a table (GPS_raw_data). A device is associated to an animal for a defined time range (table animal_GPS_device, connected to the tables animal and GPS_device with foreign keys, represented by *solid arrows* in the figure). According to the acquisition time, GNSS-based locations are therefore assigned to a specific animal (i.e. the animal wearing the device in that particular moment) using the information of the table animal_GPS_device. Thus, the spatial table animal_location is filled (*dashed arrow*) with the identifier of the individual, its position (as a spatial object), the acquisition time and the identifier of the GNSS device. *Source* Urbano et al. [9]

every 5 min in order to monitor their movements within the grazing area at regular time lags. The collected data were later downloaded into a GIS system and analyzed according to landscape features that were considered. Their results indicated the usefulness of GNSS in gathering location information with increased accuracy.

#### 19.2.3.1 Conservation of Biodiversity

In terms of conservation, Hebblewhite and Haydon [4] argue that it is the location-based information (i.e., where the animals move) as opposed to the mechanism of motion that have made substantial contribution to conservation. They present an example based on the Canadian Rockies' wolf that traveled over 100,000 $km^2$ area in Alberta, British Columbia, Montana, Idaho, and Washington in 1993 [4]. Argos collar was used and the results were reported to have given inspiration to the Yellowstone and Yukon conservation initiatives [4, 10]. Another example presented in [4] is the case where GNSS data from a pronghorn antelope in Wyoming revealed the movement corridors that were threatened by oil and gas development in a narrow migration pinch-point [4, 11].

The last example above indicate how GNSS-based animal telemetry supported one of the aims of conservation, i.e., identification of the type, nature, and extent of the main factors affecting the animals in order for intervention measures to be undertaken. Another aim of conservation is that of identifying human impacts on habitats. This, too, could benefit from GNSS-based animal telemetry in that it would yield habitat spatial data, which when combined with external data (e.g., from remote sensing) on the attributes of these habitats, such as human activities, could help identify human impacts on these animals and their environment. Examples are given, e.g., by [4, see reference therein] on how spatial data contributed to the understanding of the effect of energy development on Mule dear (*Odocoileus hemionus*) and Caribou (*Rangifer tarandus caribou*). Other examples include identification of habitat corridors for trans-boundary conservation of African elephants, see also [5, p. 64], and in understanding the impacts of human recreation on wide-ranging carnivores [4].

The examples above show how humans have impacted on the habitats, yet the reverse can also be said, i.e., the animals' impacts on habitats. As an example, let us consider the Rothschild (*Giraffa camelopardalis rothschildi*) species of giraffes that were relocated from Soi Ranch in the Rift Valley of Kenya to two national parks in the late 1970s and early 1980s in order to conserve the giraffes, which were then threatened by the spread of human settlements [12]. Twenty-seven (27; five males and 22 females) of these Rothschild giraffes were relocated to Ruma National Park (NP) that was established in 1966 and gazetted as Lambwe Valley Game Reserve in Kenya (Fig. 19.2), and 17 were relocated to Lake Nakuru NP.

A survey conducted in 2002 at Ruma NP to determine both the giraffe population and the impact of their introduction on the park's other animal species, on park's flora, and on human habitat found that the giraffes' population was approximately 75, and their presence had impacted on both the environment and the human communities that surround the park [12]. Here too, GNSS-based animal telemetry could provide useful information that could be used to study the impacts of giraffes on the environment, and could save resources incurred from undertaking a manual observation as was done in [12]. If these giraffes were collared with GNSS receivers, for example, it would be possible to relate their positions to the habitats as indicated in Fig. 19.3. These spatial information could then be integrated with the attributes of the Park's in a GIS system to enhance management and the study of the impacts of these giraffes on that habitat that are also home to other species.

#### 19.2.3.2 Monitoring Migratory and Endangered Species

Animals migrate to "follow food" and also for reproduction purposes among other reasons. For instance, herbivorous animals will tend to go to areas with greener pastures and water, and as they go, so follows the carnivores who hope to benefit. The Wildebeest migration of East Africa, for example, where millions of animals move across the Serengeti and Mara plains (e.g., about 800 km round trip during the migration) in search of food and water, and having to cross the jaws of the waiting crocodiles and other carnivores, has turned out to be one of the world's great wonders.

**Fig. 19.2** In 1983, 27 Rothschild giraffes (*Giraffa camelopardalis rothschildi*) were translocated from Kenya's Rift Valley to Ruma National Park (NP) as a conservation measure

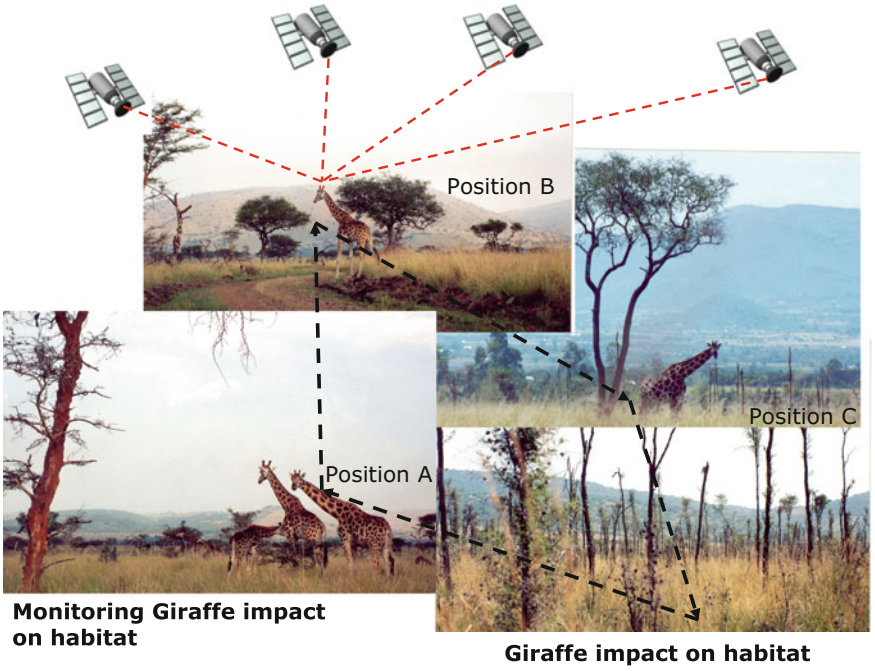


**Fig. 19.3** Monitoring the impact of giraffe on habitat at Ruma National Park, Kenya. From the figure, it is noticeable that the giraffes have left the shrub vegetation dilapidated. GNSS could provide the perimeters of such impacted environments, besides providing location-based data for the animal's movement

**Fig. 19.4** In Kenya, roan antelope (*Hippotragus equinus*) are found only in Ruma National Park. Their survival, however, is threatened by poaching and drought. GNSS could be used to provide location-based information on areas frequented by the roan antelope to inform conservation and protective measures

In Lake Victoria in East Africa, fishing birds such as gulls, terns, pelicans, kingfishers and cormorants are abundant in the river mouths of Sondu-Miriu, Kuja-Migori, Yala and Nzoia. Rocky beaches with clear sandy waters host plenty of cormorants, little egrets and African fish eagles. This can be attributed to the fact that the visibility allows the birds to capture prey with little effort.

Studying animal migration provides various examples where a combination of remotely sensed resource availability data together with GNSS movement (location-based data) have yielded definitive ecological insights [13]. For instance, Hebble-white and Haydon [4] indicate that by combining GNSS data on migratory movements with spatially matched resources available from remote sensing data such as MODIS[1] for terrestrial and aquatic forage resources, clear evidence has been generated for the main hypothesis for migration at scales and across systems that had previously been unthinkable without GNSS technology [4, see reference therein].

Besides monitoring of migratory species, GNSS-based animal telemetry could also be useful in monitoring endangered species. Let us consider an example of the roan antelope (*Hippotragus equinus*) at Ruma National Park (NP). The decision to make Ruma a national park was driven by the urgent need to conserve the roan antelope, locally known as "Omoro" (Fig. 19.4).

Roan antelopes are not endangered in the strict classification of endangered species, rather, they are classified as a low-risk, conservation-dependent species by the International Union for the Conservation of Nature and Natural Resources

[1] Moderate-resolution Imaging Spectroradiometer.

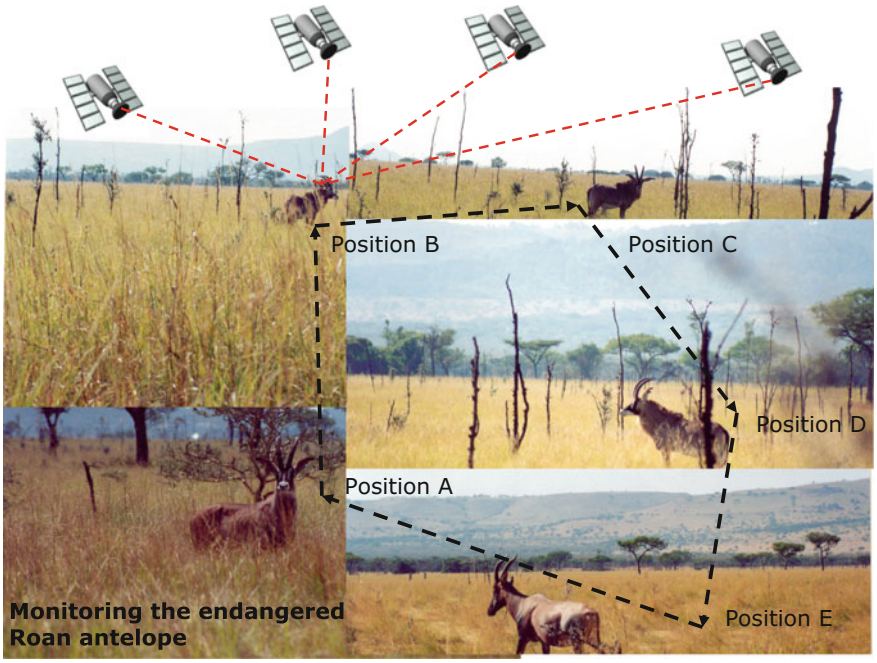


**Fig. 19.5** An example of how a GNSS receiver could be used to provide location-based information that could assist in monitoring of the endangered roan species at Ruma National Park, Kenya

(IUCN) or World Conservation Union [14]. They range across sub-Saharan central Africa from Guinea to Ethiopia, and south across Angola to South Africa.

In Kenya, roan antelope are only found in Ruma NP, where habitat factors could potentially enable them to thrive. However, poaching and drought have caused their population to dwindle in recent years. In 1994, research scientists from the Kenya Wildlife Society found only 34, and the census of September 1999 put the number at 25, see e.g., Awange et al. [12, Table 1].

Figure 19.5 demonstrates how a GNSS-based animal telemetry could be useful in monitoring the roan antelope as it moves from locations A, B, C, D, E, and finally back to A. Assuming these locations have known varying habitat characteristics, if these are coupled with the location-based data, conservationist could be able to study the behaviour of the roan antelope with regard to these habitats and thus take conservation measures. Examples of success of GNSS-based animal telemetry in monitoring endangered species are given, e.g., in [15], where environmental models for critical habitat identification was developed using data from 250 GNSS-radio collared endangered woodland Caribou (*Rangifer tarandus caribou*) across the entire boreal forest of Canada [4].

In Lake Victoria region (Kenya), which is habitat to 34 endemic waterfowl and migratory species, conservation activities have included direct protection of bird types and habitat. The location of these habitats can be mapped using a hand-held

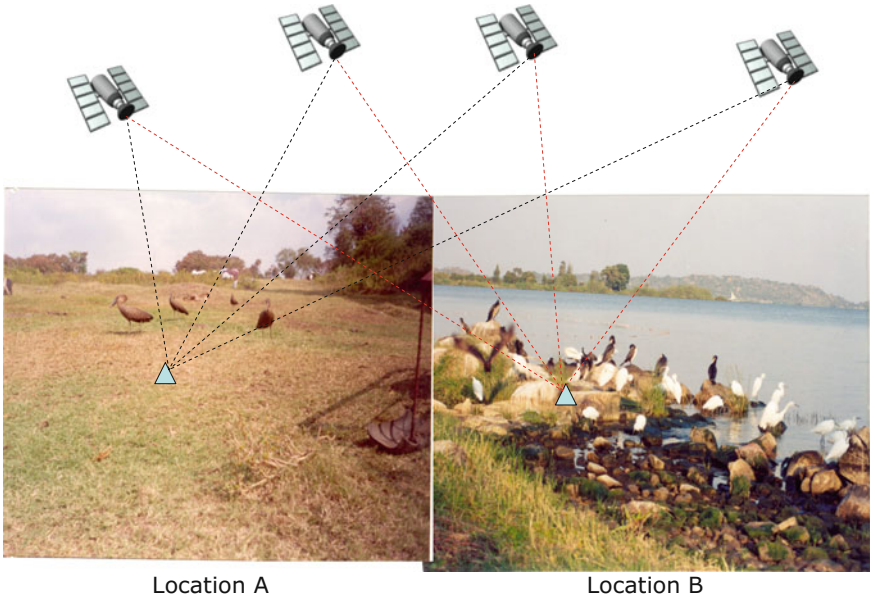


**Fig. 19.6** An example of possible use of hand-held GNSS receivers (e.g., Fig. 18.1 on p. 389) to provide location-based information on areas frequented by migratory birds

GNSS as illustrated in Fig. 19.6. Protected habitats include Important Bird Areas (IBAs) such as Lake Nyamboyo and Usenge. River Yala and Sondu-Miriu are home to some of the candidate species for conservation such as the papyrus gonolek (*Luniarus mufumbiri*), the papyrus yellow warbler (*Chloropeta gracilirostris*) and the Madagascar Squaco heron (*Ardea idea*). Plovers, sandpipers and stilts dominate the water edge community on sandy beaches along the Lake shores. Those dependent on emergent vegetation include herons, storks, cranes and passerines (warblers and weavers).

#### 19.2.3.3 Indirect Mapping of the Attacking Australian Drop Bears

In the preceding sections, we have treated the direct application of GNSS in animal telemetry, i.e., tagging the animal in question and monitoring its spatial and temporal evolutions. Whereas this is possible for animals that tend to forage in the open areas favouring the use of GNSS, the technique suffers when used for those animals that tend to stay in areas that do not favour GNSS. This is the case for the Australian drop bears (*Thylarctos plummetus*), predatory carnivals that resemble the Koala's (*Phascolarctos cinereus*). Unlike the Koalas, which stays on trees for food or rest, drop bears stay on trees to gain advantage upon which they can jump on their prey once they are within reach (see Fig. 19.7). Drop bears inhabit the densely forested


**Fig. 19.7** Drop bear **a** in its habitat and **b** attacking prey. *Source* Janssen [16]

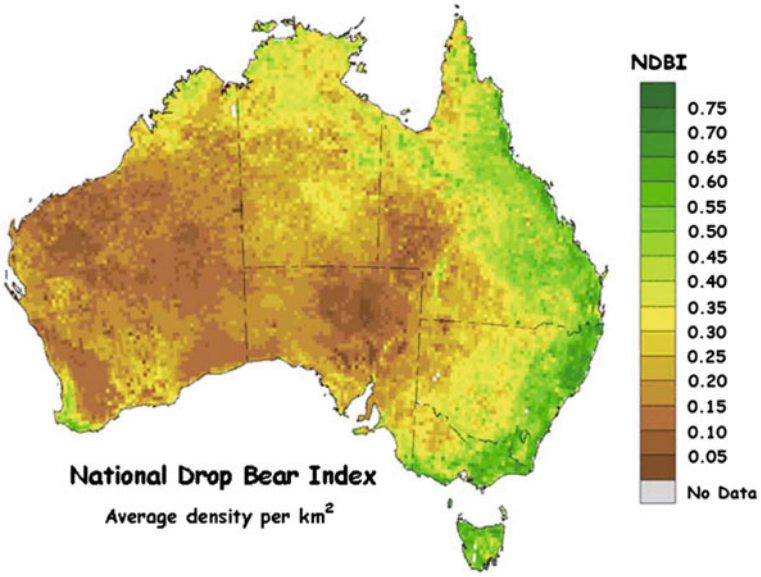


**Fig. 19.8** Distribution of drop bears in Australia, quantified by the National Drop Bear Index (NDBI). Janssen [16]

regions of the Great Dividing Range in South-eastern Australia and are also reported to be in south-east South Australia, Mount Lofty Ranges and Kangaroo Island.[2] The distribution of drop bear over Australia is shown in Fig. 19.8.

Although monitoring of the drop bears is essential for their conservation and to minimize human attacks, use of GNSS as discussed in the preceding sections is compounded by signal loss due to the long time spend by the animals on trees on the one hand, and severe damage and loss of the GNSS receiver during attacks on

[2] https://australianmuseum.net.au/drop-bear.

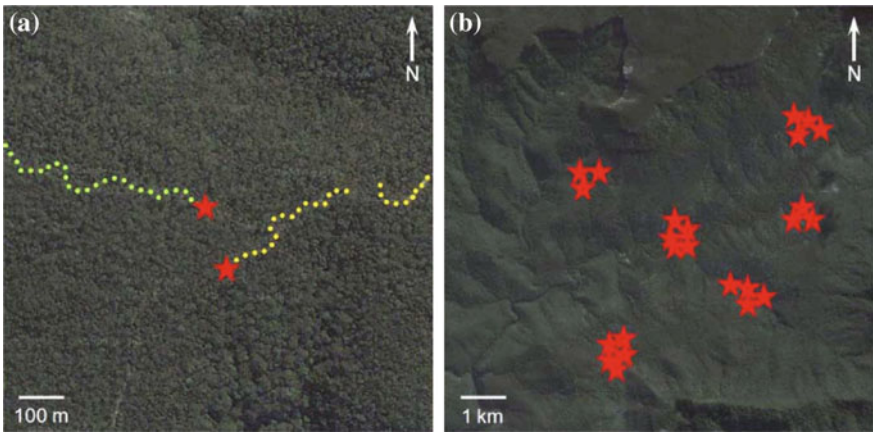


**Fig. 19.9** **a** Example of two GNSS tracks ending with a drop bear attack (denoted by *red stars*), and **b** summary of all drop bear attacks observed. Janssen [16]

their prey in addition to the animals rubbing their backs on the trees [16]. Janssen [16] proposed an indirect method of mapping these drop bears by tagging the prey instead. Using research assistants composed of international students tagged with GNSS receivers, a study was undertaken in the northern part of Morton National Park (about 120 km south-west of Sydney, Australia) over a period of a week from the 1st of April 2012, see [16].

The results of Janssen [16] (see Fig. 19.9) indicated that the attacks appeared in distinct cluster areas inhabited by the drop bears. This GNSS findings were vindicated by an independent research that examined the kill sites and scats in the study area a month before and after the use of GNSS. Janssen [16]'s indirect use of GNSS to track drop bears provides a method that is useful not only for mapping of the location and size of the drop bear populations but also of other rare and endangered animals that cannot be directly tagged.

## 19.3 Vegetation

Environmental monitoring of the *extent* and *quality* of vegetation plays a crucial role of indicating land condition. By monitoring the changes in vegetation colour, often as a results of stress, environmental impacts such as those arising from the exposure of plants to pollutants (e.g., air, acid rains, heavy metal contamination of the soil), insect infestation and disease can be deciphered [17]. Besides the stresses above, increase in population growth of urban cities lead to vegetation destruction to pave way to settlement or infrastructure. In this scenario, forests are cleared to provide timber for building and fuelwood. As a result, topsoil erosion and sedimentation are enhanced leading to increased suspended solid loads in the rivers that feed the

lakes. Monitoring of vegetation, therefore, provides information on the impacts on the environment as a result of human-induced activities or natural causes.

Remote sensing satellite provide means for detecting vegetation changes through monitoring of the changing vegetation colour, which occurs as a result of the stress stated above. This is achieved through monitoring of vegetation greeness/vigour quantified through the normalized difference vegetation index (NDVI) of Tucker [18]. Through integration with remote sensing satellites, GNSS provides location-based data and controls for vegetation mapping (e.g., Fig. 16.3 on p. 337). GNSS could also find use in monitoring of rangelands, and can also be indirectly used with altimetry satellites such as ICESat-2 (see Sect. 9.4.2) and GNSS-R (see Sect. 10.2) to map vegetation.

James et al. [19] defines rangelands as grasslands, shrublands, and open woodlands managed as natural ecosystems that are traditionally used by grazing animals. In this context, GNSS could be used in digital cameras to provide observations on amount and locations of poisonous, invading, or noxious plants; and threatened or endangered species [19]. The next two subsections examine forests and wetlands as examples of GNSS-based vegetation monitoring.

### *19.3.1 Forests*

Detailed and timely information on forests are required for traditional forest management, forest certification, and in monitoring forest health and biodiversity on the one hand, while on the other hand, there is an increasing need of having the information delivered at a lower cost [17]. Population increase has also put pressure on the available resources, e.g., land leading to increase in deforestation (e.g., Fig. 19.10).

Whereas remote sensing satellites detect damage on trees by monitoring colour changes from the leaves, which are indicative of the related stress, Holopainen et al. [17] discuss the role of GNSS as that of enhancing field work to achieve the required efficiency of acquiring spatial forest resource information at a lower cost.

GNSS applications to forest management span almost two decades. For example, Sirait et al. [20] pointed out that effective forest management requires balancing conservation and local economic-development objectives and demonstrated the capability of mapping customary land use systems using GNSS and GIS methods among other techniques. The derived maps by Sirait et al. [20] were then used in *forest protection* and *resource management*, with the limitations being accuracy of the base maps, ability of social scientists and map makers to accurately capture the complex relationships of traditional resource-management systems on maps, and the political will of the parties involved for recognizing different forms of land rights [20]. Part of the forest protection is in managing forest fires and vegetation health, an area where GIS has found wide use thanks to the capability of GNSS satellites to provide accurate positions. For example, GNSS has been in use at the Ventura County Sheriff's Office since the early 1990s to map wildfire perimeters [5]. James et al. [19]

**Fig. 19.10** Deforestation of the once densely forested Gwasi hills in Kisumu (Kenya) to pave way for farming. GNSS could be useful in providing the perimeter of the deforested region

point to the use of video cameras with GNSS interface to document occurrences and locations.

Raven Environmental Services [21] indicate the possibility of integrating GIS with GPS to produce maps that describe both the property and any underlying inventory data such as timber inventory for forest management units, the location and type of unique plant communities or any other type of special-use zone. From such maps, areas, lengths, distances to other features, and many other useful measures can also be calculated. The resulting underlying data associated with any management unit can then be exported as an Excel file, and used to periodically update a written management plan [21].

Integration of GNSS and GIS is exemplified in the work of Brondizio et al. [22] who produces a georeferenced map of land cover and land use for an area of the Amazon estuary inhabited by three populations of caboclos with distinct patterns of land use. The maps produced by Brondizio et al. [22] permitted measurements and differentiation of land uses and change detection between small areas of managed floodplain forests and unmanaged forests, and between three distinct age/growth classes of secondary succession following deforestation. Brondizio et al. [22] suggested means of balancing between use and conservation in Amazonian floodplain and estuarine areas, and the effectiveness of monitoring these types of land cover from satellite platforms (e.g., GNSS).

ICESat-2 will contribute to mapping of forest productivity by tracking the growth of individual forest stands, observations of tree phenology, forest diseases, and pest outbreaks through associated changes in canopy structures, and the mapping of forest

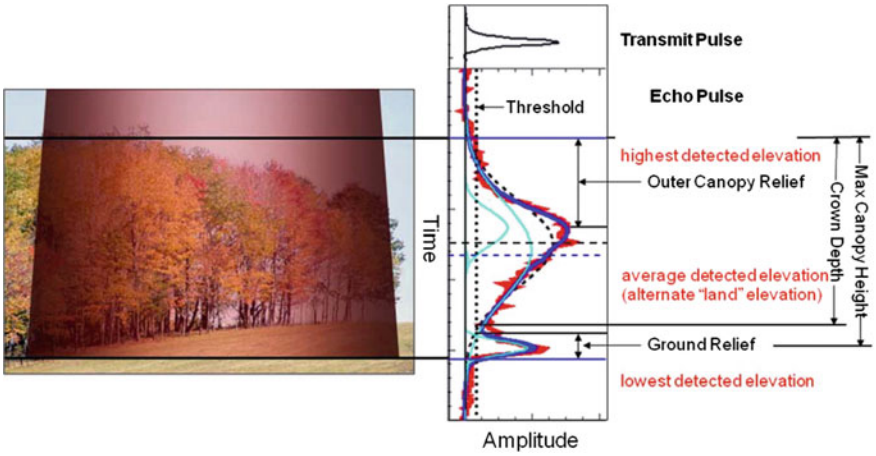


**Fig. 19.11** Application of ICESat or ICESat-2 to measure tree heights as presented by [24]

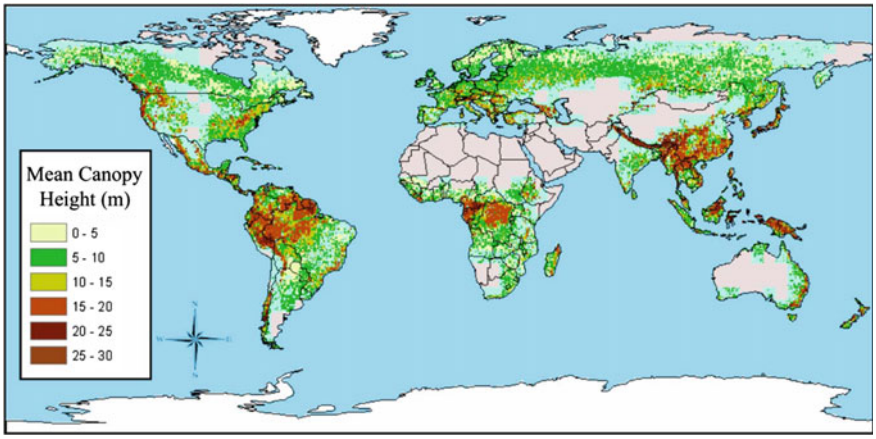


**Fig. 19.12** Global estimates of mean canopy heights derived from ICESat as presented by [23]. The capability of retrieving tree height with ICESat-2 will contribute to the large-scale biomass assessments

heights and above ground biomass at a scale that approaches one that is appropriate for forest carbon management, which would enable the global ecosystem community to further constrain the sources and sinks of carbon at regional to continental scales [23]. An illustration of ICESat-2's capability to map forest productivity is presented by [24], e.g., Fig. 19.11 that shows a clear ground return that is spread by the slope of the ground, the top of the canopy, and returns from within the canopy that are indicative of structure within the crown. Abdalati et al. [23] then provide a global estimate of mean canopy heights derived from ICESat in Fig. 19.12.

### *19.3.2 Wetlands*

The Ramsar International Convention on Wetlands of 1971 advocates for the wise use of wetlands by national actions and international co-operation as a means of achieving sustainable development throughout the world. Article 3.1 of the convention states that contracting parties shall formulate and implement their planning so as to promote the conservation of the wetlands, and as far as possible, the wise use of the wetlands in their territory.

Wetlands play a pivotal environmental role of providing sanctuary to biodiversity, store flood water, and improve water quality. It provides habitat for fish and wildlife, supporting a rich biodiversity that include many endangered and threatened species, see e.g., [14, 25]. Conservation of wetlands is necessary as they have the ability to sequester carbon and also tend to shift to net sources of greenhouse gases when perturbed by land use change such as drainage for agriculture or forestry. In this way, they help in preventing *global warming*, a consequence of *climate change* and its ecological effects on the environment. They have an inherent capacity for storage of carbon.

Ozesmi and Bauer [25] suggest the need for inventory and monitoring of wetlands and their adjacent uplands to assist in its conservation and management. Such inventory and monitoring can be achieved using remote sensing techniques, see e.g., [25–28]. Optical sensors that have been applied to wetlands include; Landsat Multi-spectral Scanner (MSS), Landsat Thematic Mapper (TM), SPOT (Système Probatoire d'Observation de la Terre)), NOAA AVHRR (Advanced Very High Resolution Radiometer), and radar system (JERS-1, ERS-1 and RADARSAT). Landsat MSS (bands 4 (0.5–0.6 m), 5 (0.6–0.7 m), 6 (0.7–0.8 m) and 7 (0.8–1.1 m) provide data that are useful in discriminating large vegetation wetlands [25]. Jensen et al. [29] indicate its possible use in change detection through multi-temporal analysis. Landsat TM (particularly band 5; 1.55–1.75 m) is useful in identification of wetlands and other land covers types, see, e.g., [30] and change [31]. In practice, a window of 9 pixels would be required to consistently identify an object [25]. Band 5 has the capability to discriminate between vegetation and soil moisture levels. Jensen et al. [29] add that the separability between wetlands types could be achieved using this band.

SPOT panchromatic (PAN) images have been used to provide reference data for registration and calibration purposes [32, 33], while [34] applied European Remote Sensing (ERS-1) synthetic aperture radar (SAR) to monitor the presence or absence of water in wetlands in south western Florida, USA. A combination of optical and radar sensors, where the two complement one another, is presented in the work of Townsend and Walsh [35] who combine Landsat TM and SAR to detect flooding in a forested wetland on the lower Roanoke River floodplain in North Carolina. Another sensor that has been used for wetland studies is the Indian Remote Sensing (IRS) satellite whose four bands are similar to those of Landsat TM (see, e.g., [36]).

Spectral reflections of wetlands provide the possibility of separating various types of wetland vegetation. Classification techniques used for wetlands include visual interpretation, unsupervised or clustering, and supervised. The importance of visual analysis in reconnaissance mapping of wetlands is demonstrated by Johnson and Wichern [37]. Unsupervised classification involve grouping together of pixels of similar spectral values, having the advantage of preserving spatial resolution of the images, see e.g., [29]. Supervised classification adopts statistical techniques such as the maximum likelihood. A hybrid system adopts a mixture of the two systems.

Vegetation indices find use in highlighting wetlands during classification methods above. Normalized Difference Vegetation Index (NDVI) and Transformed Vegetation Index (TVI) are some of the techniques used to enhance image identification. In addition, radar information is useful in wetland studies due to its capability to distinguish between flooded and non flooded areas. In all the remote sensing applications above, GNSS could be useful in georeferencing remotely sensed satellite data, providing orientation for aerial photographs, and providing sampled location-based and perimeter/area data. Furthermore, its application for sensing vegetation through the reflected signals (GNSS-R) is promising to enhance vegetation sensing (see Chap. 10).

## 19.4 Concluding Remarks

The chapter has outlined important functions of GNSS in support of animal and vegetation monitoring for conservation purposes. GNSS has brought with it a new horizon where animal conservation managers can make informed decisions based of simplified presentations (graphics and analysis) at no additional or sophisticated analysis [4]. Its challenges have also been presented and its role to support forest and wetlands also discussed. As already mentioned in Sect. 19.2.1.1, advantages of obtaining animal positions using GNSS tracking systems are its capability to record huge amounts of highly accurate animal locations with minimal work by the operators, thus allowing reduced sampling intervals, and increased accuracy and performance when compared with VHF radio-tracking systems [9]. The system also has the capability to position both on the surface of the Earth and in the air, are highly accurate and repeatable compared with ground-based conventional VHF triangulation techniques and VHF tracking from aircraft or Argos satellite Doppler-based positioning, offers the capability of 24-h coverage with position updates available in rapid succession (one location update per second is typical), the all weather positioning capability when other approaches can be restricted, and the additional accurate time stamping of a position that is delivered besides the actual positions, see [2, and the references therein].

## References


1. Fuller MR, Millspaugh JJ, Church KE, Kenward RE (2005) Wildlife radio telemetry. In: Braun CE (ed) Techniques for wildlife investigations and management, 6th edn. The Wildlife Society, Bethesda, pp 377–417
2. Tomkiewicz SM, Fuller MR, Kie JG, Bates KK (2010) Global positioning system and associated technologies in animal behaviour and ecological research. Philos Trans R Soc B 365:2163–2176. doi:10.1098/rstb.2010.0090
3. Cagnacci F, Boitani L, Powell PA, Boyce MS (eds) (2010) Challenges and opportunities of using GPS-based location data in animal ecology. Philos Trans R Soc B 365:2155. doi:10.1098/rstb.2010.0098
4. Hebblewhite M, Haydon DT (2010) Distinguishing technology from biology: a critical review of the use of GPS telemetry data in ecology. Philos Trans R Soc B 365:2303–2312. doi:10.1098/rstb.2010.0087
5. Steede-Terry K (2000) Integrating GIS and the global positioning system. ESRI Press, California
6. Craighead FC (1982) Track of the grizzly. Random House, New York
7. Craighead JJ, Sumner JS, Mitchell JA (1995) The grizzly bears of Yellowstone: their ecology in the Yellowstone ecosystem. Island Press, New York
8. Barbari M, Conti L, Koostra BK, Masi G, Sorbetti Guerri F, Workman SR (2006) The use of global positioning and geographical information systems in the management of extensive cattle grazing. Biosyst Eng 95(2):271–280. doi:10.1016/j.biosystemseng.2006.06.012
9. Urbano F, Cagnacci F, Clement C, Dettki H, Cameron A, Neteler M (2010) Wildlife tracking data management: a new vision. Philos Trans R Soc B 365:2177–2185. doi:10.1098/rstb.2010.0081
10. Chester CC (2006) Landscape vision and the Yellowstone to Yukon conservation initiative. In: Chester CC (ed) Conservation across borders: biodiversity in an interdependent world. Island Press, Washington, pp 134–157
11. Berger J (2004) The last mile: how to sustain long-distance migration in mammals. Conserv Biol 18:320–331. doi:10.1111/j.1523-1739.2004.00548.x
12. Awange JL, Aseto O, Ong'ang'a O (2004) A case study on the impact of Giraffes in Ruma National Park in Kenya. J Wildl Rehabil 27:16–21
13. Hebblewhite M (2009) Linking wildlife populations with ecosystem change: state-of-the-art satellite ecology for national-park science. ParkScience 26(1). http://www.nature.nps.gov/ParkScience/index.cfm?ArticleID=280. Accessed 25 Sept 2011
14. Awange JL, Ong'ang'a O (2006) Lake Victoria-ecology resource of the Lake Basines and environment. Springer, Berlin
15. Environment Canada (2008) Scientifi c Review for the Identifi cation of Critical Habitat for Woodland Caribou (*Rangifer tarandus caribou*), Boreal Population, in Canada. August 2008. Ottawa: Environment Canada. 72 pp. plus 180 pp Appendices
16. Janssen V (2012) Indirect tracking of drop bears using GNSS technology. Aust Geogr 43(4):445–452. doi:10.1080/00049182.2012.731307
17. Holopainen M, Leino O, Kämäri H, Talvitie M (2006) Drought damage in the park forests of the city of Helsinki. Urban For Urban Green 4:75–83. doi:10.1016/j.ufug.2005.11.002
18. Tucker CJ (1979) Red and photographic infrared linear combinations for monitoring vegetation. Remote Sens Environ 8(2):127–150. doi:10.1016/0034-4257(79)90013-0
19. James LF, Young JA, Sanders K (2003) A new approach to monitoring rangelands. Arid Land Res Manag 17:319–328. doi:10.1080/15324980390225467
20. Sirait M, Prasodjo S, Podger N, Flavelle A, Fox J (1994) Mapping customary land in East Kalimantan, Indonesia: a tool for forest management. Ambio 23(7):411–417
21. Raven Environmental Services (2008) Mapping and GIS/GPS Technology Services. http://www.ravenenvironmental.com/mapping.aspx. Accessed 06 Mar 2008
22. Brondizio ES, Moran EF, Mausel P, Wu Y (1994) Land use change in the Amazon estuary: patterns of caboclo settlement and landscape management. Hum Ecol 22(3):249–278

23. Abdalati W, Zwally HJ, Bindschadler B, Csatho B, Farrell SL, Fricker HA, Harding D, Kwok R, Lefsky M, Markus T, Marshak A, Neumann T, Palm S, Schutz B, Smith B, Spinhirne J, Webb C (2010) The ICESat-2 laser altimetry mission. Proc IEEE 98(5):735–751. doi:10.1109/JPROC.2009.2034765
24. Harding DJ, Carabajal CC (2005) ICESat waveform measurements of within-footprint topographic relief and vegetation vertical structure. Geophys Res Lett 32:L21S10. doi:10.1029/2005GL023471
25. Ozesmi SL, Bauer ME (2002) Satellite remote sensing of wetlands. Wetl Ecol Manag 10(5):381–402. doi:10.1023/A:1020908432489
26. Emerton L, Kekulandala LDCB (2003) Assessment of the economic value of Muthurajawela wetland. Occasional papers of IUCN Sri Lanka, vol 4 (2003)
27. Jonson RM, Barson MM (1993) Remote sensing of Australian wetlands: an evaluation of Landsat TM for inventory and classification. Aust J Mar Fresh Water Resour 44:235–252
28. Brooks RP, Wardrop DH, Cole CA (2006) Inventorying and monitoring wetland condition and restoration on a watershed basin with examples from Spring Creek Watershed, Pennsylvania. USA. Environ Manag 38(4):673–687. doi:10.1007/s00267-004-0389-y
29. Jensen JR, Christensen EJ, Sharitz R (1984) Nontidal wetland mapping in South Carolina using airborne multi-spectral scanner data. Remote Sens Environ 16:1–12
30. Han M, Sun Y, Xu S (2007) Characteristics and driving factors of marsh changes in Zhalong wetland of China. Environ Monit Assess 127:363–381. doi:10.1007/s10661-006-9286-6
31. Munyati C (2000) Wetland change detection on the Kafue Flats, Zambia, by classification of a multitemporal remote sensing image data set. Int J Remote Sens 21(9):1787–1806. doi:10.1080/014311600209742
32. Welch R, Remillard M, Doran RF (1995) GIS database development for South Florida's National Parks and Preserves. Photogramm Eng Remote Sens 61:1371–1381
33. Ausseil AE, Dymond JR, Shephard JD (2007) Rapid mapping and prioritisation of wetland sites in the Manawatu-Wanganui region, New Zealand. Environ Manag 39:316–325. doi:10.1007/s00267-005-0223-1
34. Kasischke ES, Bourgeau-Chavez LL (1997) Monitoring South Florida wetlands using ERS-1 SAR imagery. Photogramm Eng Remote Sens 63:281–291
35. Townsend PA, Walsh SJ (1998) Modelling floodplain inundation using an integrated GIS with radar and optical remote sensing. Geomorphology 21(3–4):295–312. doi:10.1016/S0169-555X(97)00069-X
36. Chopra R, Verma VK, Sharma PK (2001) Mapping, monitoring and conservation of Harike wetland ecosystem, Punjab India through remote sensing. Int J Remote Sens 22:89–98. doi:10.1080/014311601750038866
37. Johnson R, Wichern D (2007) Applied multivariate statistical analysis, 6th edn. Prentice Hall, Upper Saddle River

# Chapter 20
# Unmanned Aircraft Vehicles

*A lots is happening lately on the subject of drone applications in agriculture and precision farming. From the ability to image, recreate and analyze individual leaves on a corn plant from 120 meters height, to getting information on the water-holding capacity of soils to variable-rate water applications, agricultural practices are changing due to drones delivering agricultural intelligence for both armers and agricultural consultants.*

Frank Veroustraete [1]

## 20.1 Introductory Remarks

In recent decades, Unmanned Aircraft Vehicles (UAVs) became a popular household name that caught attentions over the world. With its continued development, its advantages are increasingly outstanding whether for military or civilian use. Compared to the manned aircrafts, UAVs are cheap, efficient, convenient, reduce casualty rates in the modern war and achieve complex goals when combined with other equipments (e.g., sensors, scanners) in the civil fields. Therefore, many countries, especially the developed countries, are already engaged in the research and development of UAVs. This chapter systematically introduces UAVs from perspectives of terminology and definitions, historical background, basics of unmanned aerial systems, GNSS in supporting UAVs, environment applications of UAVs, and finally discusses its future challenges.[1]

[1] Invited chapter from Hu Kexiang of Curtin University, Australia.



J. Awange, *GNSS Environmental Sensing*, Environmental Science and Engineering, DOI 10.1007/978-3-319-58418-8_20

## 20.2 Background to UAVs

### *20.2.1 Terminology and Definitions*

In literature and in practice, different terms have been used to describe unmanned aircrafts. Basically, three terms are used: Unmanned Aircraft Vehicles (UAVs) or Unmanned Aerial System (UAS), Drones, and Remotely Piloted Aircrafts (RPAs) or Remotely Piloted Vehicles (RPVs).

**UAVs or UAS**

Unmanned Aircraft Vehicles, also called Unmanned Aerial Vehicles (UAVs), is 'an aircraft piloted by remote control or onboard computers' or 'an aircraft without a human pilot aboard, flight can be remotely controlled or fully or intermittently autonomously controlled by onboard computers' (see [2] for more details). United States Department of Defence (U.S.DoD) [3] describes UAVs as: 'powered, aerial vehicles that do not carry a human operator, use aerodynamic forces to provide vehicle lift, can fly autonomously or be piloted remotely, can be expendable or recoverable, and can carry a lethal or nonlethal payload.' However, it does not include ballistic or semi-ballistic vehicles, cruise missiles, and artillery projectiles.

Unmanned Aerial System (UAS) is probably a less familiar term for the general public, which actually is an entire system of achieving operations of UAVs, therefore, UAVs are only a subset of UAS. The United Kingdom (UK) government [4] gives its official definition as 'a system, consisting of the unmanned aircrafts and all equipments (e.g., camera, GPS and software), data links and ground control stations'.

**Drone**

Drone might be a better well-known term among people compared to abbreviations such as UAVs or UAS. In English, drone originally stands for a male bee, its first use can be traced back to the 1930s, the inventions of 'Fairy Queen' (1931), 'Queen Bee' (1935), named by US Navy [5]. After that, the term 'drone' started to be used to describe pilotless aircrafts in relation to military context, especially for those aircrafts with weapons carriage capabilities. However, as time passed by, the term 'drone' slowly became a common word that designated any category of unmanned aircrafts in civil or in military. For now, 'drone' has exactly the same meaning as 'UAV', the only difference being that 'UAV' is more often used in official documents, including legislation, while drone is not used in any kind of legislation [6].

**RPAs and RPVs**

Although, 'UAV' and 'drone' already define the term unmanned aircraft, it sometimes still causes confusion to the general public, especially when one refers to the word 'unmanned'. Actually, some of UAVs are more or less human controlled, remotely. Therefore, pilots are physically necessary if it requires to be remotely controlled. The existence of pilots is the term 'Remotely Piloted Aircrafts (RPAs)' or 'Remotely Piloted Vehicles (RPVs)'. Hence, RPAs are only subset of UAVs and drones. Similar

to UAS, when RPAs combine with pilots, ground control station, data links and any other associated manpower systems and equipments, it forms Remotely Piloted Aircraft System (RPAS). Compared to the terms 'UAVs' and 'drones', 'RPAs' is less often used outside of Europe [6].

### *20.2.2 Historical Background of the UAV Development*

Unmanned Aircraft Vehicles (UAVs) were designed for military purposes in early development, although, its definition was not so clear as now, and simply interpreted as 'aircrafts without pilots on board or flying bombs' [7]. In 1849, the first conceptual UAV was recorded as balloons used by the Austrians, to attack city of Venice by carrying bombs [8]. However, they are barely considered as drones due to the fact that their flight could not be controlled. In 1883, Douglas Archibald, from England measured wind speed by putting an anemometer on line of a kite. Four years later, he tried to equip cameras on kites, which could be considered as one of the world's first reconnaissance UAVs used in combat [9].

In the beginning of the 20th century, aerial torpedoes and flying bombs were military conceptions that most countries wanted to achieve during World War I (1914–1918). These conceptions were not achieved until gyroscopes (flying stabilization devices) and radio techniques were applied to build UAVs. In 1917, Hewitt-Sperry Automatic Airplane (see Fig. 20.1), the first aircraft that demonstrated UAVs, was created by Elmer Sperry and Peter Cooper Hewitt of United States and successfully passed the test flight in Japan [7]. This product could fly to pre-set destination and drop bombs or dive to the target, which is the prototype of today's cruise missiles. However, due to the limitation of techniques, the requirement of target-hit accuracy could not be satisfied at that moment. The following inventions, 'Kettering Bug' and 'CurtissSperry Aerial Torpedo', made by the U.S. Army Air Force and Lawrence Sperry, respectively, could not be deployed and developed due to the fact that World War I ended before it [6, 9]. On the other hand, these aerial torpedoes or missiles could only be regarded as 'autonomously, pre-set flying bombs' according to the definition of UAVs in modern era. They did not have features of expendable, recoverable and remotely control.

Technically speaking, the world's first UAV that fits modern definition should be the 'DH.82B Queen Bee (see Fig. 20.2a)' [10], manufactured by the British, with the first test flight manned in 1935. It was an advanced version of 'De Havilland Tiger Moth' as target trainer aircraft. A total of 412 were built to serve Royal Air Force from 1933 to 1943. In 1937, a short time before World War II (1939–1945), Reginald Denny, an Englishman built a series of UAVs called RP1, 2, 3, 4 and successfully drew the attention of the US Army with his 'Radioplane Company'. After that, the RP4 was converted to 'Radioplane QQ-2' (target drones, see Fig. 20.2b), which was the first large-scale production of UAVs, around 15,000 were manufactured during World War II [6, 7, 9]. After World War II, the role of UAVs was not confined to drop bombs or be target drones. During Vietnam War (1955–1975), 'MQM-57 Falconers (see Fig. 20.2c)', the first unmanned reconnaissance aircrafts were made and used in

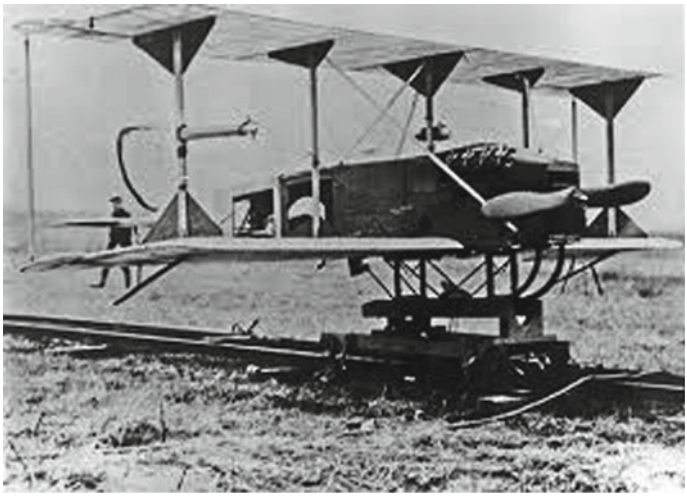

**Fig. 20.1** Hewitt-Sperry Automatic Airplane, prototype of today's cruise missiles. The first demonstration of the model of UAV, was created and passed the flight test in 1917

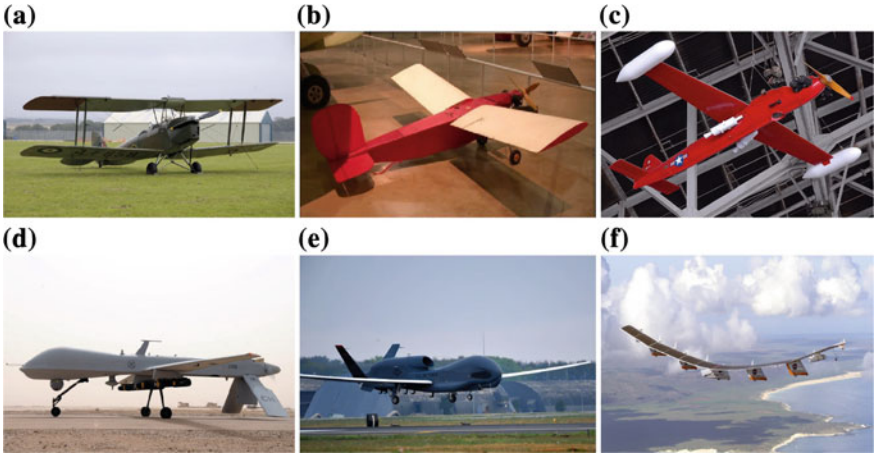


**Fig. 20.2** Background of UAV development. **a** De Havilland DH-82B Queen Bee; **b** Radioplane QQ-2; **c** MQM-57 Falconer; **d** MQ-1B Predator unmanned aircraft; **e** RQ-4 Global Hawk, **f** Helios made by NASA

1955. Until 1970s, 1,455 falconers were built for serving the U.S. Army and NATO (North Atlantic Treaty Organization) [11, 12]. Meanwhile, UAVs were also looking for direction of other applications, like weapons delivery platform, surveillance, and cargo transport. However, due to the limitation of techniques, most of researches in these applications failed [13]. Since then, UAVs became less attractive due to the fact that they could not show the outstanding advantages as expected in military forces and battlefields.

The low ebb of UAVs kept continuing until 1982, when reconnaissance, jamming and decoys drones were used against the Syrian air defence system in the Bekaa Valley by Israel. It proved the potential values of UAVs in real-time combat [9]. On the other hand, due to the end of cold war (1947–1991), most countries faced problems of military budget and member cuts, which forced them to seek cheaper ways of achieving strategic goals in battlefield. Therefore, the development of the UAVs climaxed in the 1990s.

After the Gulf War (1990–1991), over 30 countries forged ahead with their own UAVs. Representative models include, e.g., Scout, Pioneer and Searcher by Israel, Hunter and Outrider by the US, Mart by France, Brevel by German, CL-289 by Canada, Phoenix by UK, and so on. In 1993, prolonged flight became a main research point of reconnaissance drones in most countries, representative products include Predator (see Fig. 20.2d), Global Hawk (see Fig. 20.2e), Dark Star by the US, Heron, Hermes by Israel, Eagle by the French, etc. By the end of the 20th century, small fixed-wing, multi-rotor UAVs had features that were cheap, flexible, convenient to use and easy to combine with other military equipments, gradually becoming the first choice for most countries.

In regards to civilian applications, its history also began around 1990s. The most famous project was the 9-year ERAST (Environmental Research Aircrafts and Sensor Technology) ran by NASA (National Aeronautics and Space Administration). It included diverse development of techniques of UAVs, such as high elevation flight up to 30,000 m, engine improvement, sensor improvement, etc. The aircrafts that came out of this project were used in the fields of environmental measurement, including Helios (see Fig. 20.2f), Proteus, Altus, Pathfiner and so on [14]. At the start of the 21st century, civil use of UAVs became common and more often as we shall see in Sect. 20.5.

## 20.3 Basics of Unmanned Aerial System (UAS)

Unmanned Aerial System (UAS) basically consists of three parts, (i) the unmanned aircraft, (ii) the ground control station and (iii) data link. In addition, technology requirements and applications, features of payloads, launch and recovery equipments, and ground support equipments are also necessary.

### *20.3.1 Unmanned Aircrafts*

Unmanned aircraft is the basic component of UAS that carries payloads, data and communication terminals, remote flight control system, etc. Since the rise of UAVs in 1990s, various drones came out with different configurations for serving different goals. They can be generally classified based on two principles: the classification of flight platforms and the classification of aircraft size and weight [6].

#### 20.3.1.1 Classification Based on Flight Platforms

According to different flight platforms, UAVs can be divided into types of fixed-wing, rotary-wing, flapping-wing drones and blimps [15]. Also, there could be a hybrid UAV that contain multi-features above, but currently, the most common UAVs are fixed-wing and rotary-wing.

**Fixed-wing UAV**

Fixed-wing UAV refers to the unmanned aircraft by the power plant to produce the thrust or pull, by the fixed wing of the fuselage to produce lift, flying in the air. It has advantages of fast, wide flight range, long endurance and simple structure, which is usually used in surveying of large areas. However, most of the fixed-wing aircrafts require long runways for landing and lifting, only some very small size fixed-wing aircrafts can lift by simply 'throwing out'. In addition, its lifting and landing requires good weather conditions.

One of the examples is the 'Trimble Gatewing X100' (see Fig. 20.3a) that was designed for mapping and surveying purposes by 'Trimble' company in Belgium. It is capable of having maximum 45 min flight with a cruising speed of 80 km/h in good weather and 65 km/h in bad weather conditions (in light and rain). Maximum flight altitude reaches 2500 m, flight range at 53 km, basic land space requirement is 150 m × 30 m. In addition, this aircraft carries 3D laser scanner, which makes it able to capture digital surface models and orthophoto mosaics in either visible light or composite infrared, resolution can be at 3.3–25 cm, depending on range of altitude (100–750 m) [16].

**Rotary-wing UAV**

Rotary-wing UAV, also called rotor aircraft, refers to the aircrafts that have vertical take-off and landing capabilities. Usually, it has different setups with a minimum of one rotor (helicopter), 3 rotors (tricopter), 4 rotors (quadcopter), 6 rotors (hexacopter) as well as 8 rotors (octocopter), the blades can be even more depending on the purpose of use and requirement of operation accuracy [17]. Compared to fixed-wing UAV, rotary-wing UAV has lower speeds, shorter flight ranges, limited endurance and more complexity. However, it does not require a long runway to lift or land, which allows operations happening in small, narrow areas. The capabilities of hovering and flexible moveability could provide applications like small-area inspection, especially when precision movement and visual on a single target is required for an extended period of time. Meanwhile, a rotary-wing UAV is always the first choice of a learner, cheap and easy to handle, that is why it is so widespread [18]. Besides, rotary-wing UAVs are usually used to support search and rescue efforts. One typical example is that FUAV Seraphi Drone (see Fig. 20.3b), that was used to evaluate landslides and debris flow situations after China WenChuan earthquake in 2008 [19].

**Flapping-wing UAV**

Flapping-wing UAV, also named ornithopter, i.e., Greek ornithos 'bird' and pteron 'wing' (see Fig. 20.3c), refers to those aircrafts that fly by flapping their wings, like

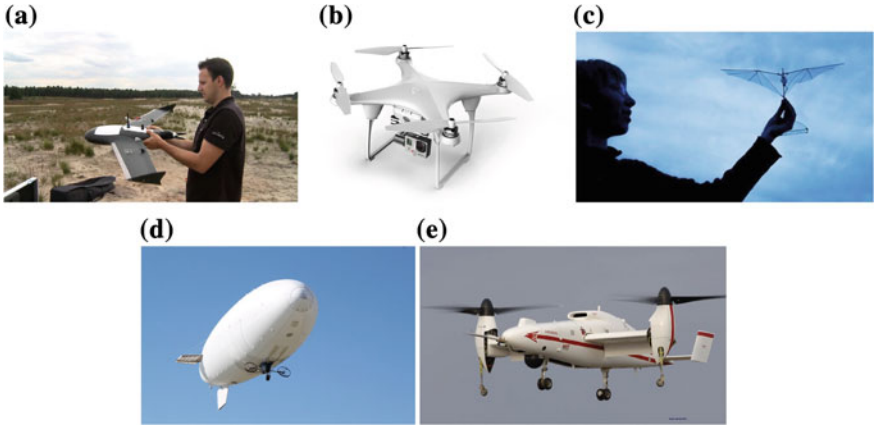


**Fig. 20.3** Types of UAVs classified based on flight platform. **a** Trimble Gatewing X100; **b** FUAV Seraphi drone; **b** A kind of flapping-wing UAV created by copying the wing anatomy of birds and bats; **d** RC blimp; **e** Bell Eagle Eye

birds or insects. It has advantages of low energy consumption, hovering flight, vertical take-off and landing as well as high maneuverability. However, its fuselage is usually very light and small, which can barely afford heavy payloads and cannot fly in bad weather conditions. Therefore, most of design purposes for flapping-wing UAVs are confined to reconnaissance in small areas [20, 21]. Also, due to the limitation of technologies, the flight system of this kind of UAVs is not mature and stable, which makes it less well-known and widely used compared to fixed-wing and rotary-wing UAVs.

**Blimp**

As Fig. 20.3d shows, blimp is a kind of aircraft that is made of balloon, which is lighter than air. It has features of long endurance, low speeds and generally large in size. The design purpose of unmanned blimps can be photography, surveillance, etc. [15].

**Hybrid UAV**

Hybrid UAV simply means that aircraft combines 2 or more types described above. There are various types of hybrid UAVs under developments, the most common type being the fixed-wing and rotary-wing such as Bell Eagle Eye shown in Fig. 20.3e. It has both advantages of fixed-wing and vertical take-off and landing.

#### 20.3.1.2 Classification Based on Size and Weight

As for drone's size and weight, there are various classification rules, which change based on different countries. Some of complex rules are even established on another classification rule, e.g., Clarke [5] adds weight indicators to the flight platforms,

**Table 20.1** Classification of UAS platforms based upon characteristics such as size, flight endurance, and capabilities [22]

| Classes | Description |
|---|---|
| MAV or NAV | Micro Air Vehicle (MAV) or Nano Air Vehicle (NAV), usually refers to the aircrafts with three dimensions smaller than 15 cm, which can easily be put into backpacks. Those MAV or NAVs can only fly at a very low elevation (< 300 m), and endurance have no more than 30min. |
| VTOL | VTOL refers to Vertical Take-Off and Landing, generally means rotary-wing UAVs or hybrid UAVs, include rotary-wing features, those aircrafts operate at varying altitudes depending on mission requirements as well as endurance. |
| LASE | LASE stands for Low Altitude, Short-Endurance, refers to those UAVs with wing span smaller than 3 m, endurance between 1 to 2 h, flight ranges only few km. |
| LASE Close | The advance on LASE, but have increased flight altitude up to 1500 m, endurance for few hours and larger size than LASE. |
| LALE | LALE means Low Altitude, Long Endurance, which has features of 5000 m operation altitude, and several kg payloads' carrying capacity. |
| MALE | Medium Altitude, Long Endurance, flight altitude and range increase to 9000 m and hundreds of km, endurance can be many hours. |
| HALE | High Altitude, Long Endurance, largest and with complex of the UAS, capable of flying at 20,000 m or more, flight range extends to thousands of km, endurance can be 30 h or more. |

which defines large drone as weight lighter than 150 kg for fixed-wing UAVs, but 100 kg for rotary-wing UAVs. Therefore, it is hard to build a universal classification rule for UAVs or UAS, due to the fact that they have totally different sizes, abilities, operating systems and applications. Some authors, e.g., Watts et al. [22] divided UAVs into 7 groups (see Table 20.1) in a very general way. Organizations, e.g., U.S.DoD [23], systematically established 5 groups of UAVs according to characteristics of maximum gross take-off weight (MGTW, UAV with payloads), operating altitude and air speed (see Table 20.2). Also, there are many other classification methods, which seem reasonable, such as the Indian UAS/RPV classifications and the Chinese fixed-wing UAVs classifications. Details can be found in e.g., Gupta et al. (2013) and Liping (2009) [15, 24].

### *20.3.2 Ground Control Station*

Ground control station (GCS), in some literature is also called MPCS (Mission Planning and Control Station). One traditional impression to general public, that GCS leaves, is like a hand controller, which only responses to the flight of UAVs. However, its functions are far more complex than a hand controller. Usually, depending on mission levels or requirements, GCS could be a simple computer, or several devices in a suitcase (see, e.g., Fig. 20.4a), or a large shelter with giant computers and other electrical equipments (see, e.g., Fig. 20.4b).

**Table 20.2** UAVs classification according to the U.S. Department of Defense (DoD). Note: (i) * AGL, Above Ground Level; (ii) # MSL, Mean Sea Level; (iii) If the UAS has even one characteristic of the next level, it is classified in that level; (iv) 1 lbs = 0.45 kg, 1 ft = 0.30 m and 1 knots = 1.85 km/h.) [23]

| Groups | MGTW (lbs) | Operating altitude (ft) | Airspeed (knots) | Size |
|---|---|---|---|---|
| Group 1 | 0–20 | <1,200 AGL* | <100 | Small |
| Group 2 | 21–55 | <3500 AGL | <250 | Medium |
| Group 3 | <1320 | <18,000 MSL# | <250 | Large |
| Group 4 | >1320 | <18,000 MSL | Any speed | Larger |
| Group 5 | >1320 | >18,000 MSL | Any speed | Largest |


**Fig. 20.4** **a** An example of transportable UAV ground control station; **b** An example of large Ground Control Station (GCS), the MQ-9 Reaper UAV GCS

Basically, it includes functions of the remote control of the unmanned aircraft, real-time data display, as the exchange platform of data relay and transmission, receiving commands from support headquarter, UAV payloads control, etc., which is a very important part among the UAS.

### *20.3.3 Data Link*

Both UAVs and GCS have setups of sensors, antennas and other devices that receive microwave, which is used to keep communication between UAVs, GCS as well as the GPS satellites. This communication is called data link system and is mainly responsible for controlling, tracking, locating and data transmitting of UAVs, which is a key subsystem in UAS. The links can be of two types; uplink and downlink, also called two-way communication. The function of uplink is for controlling the flight of UAVs, and downlink for sending the telemetry and video images from the payloads (e.g., cameras, laser sensors or radars) [25, 26].

There are two types of data link systems depending on flight control range, which is Line of Sight (LOS) and Beyond Line of Sight (BLOS), respectively. The LOS

is a case where UAVs and GCS have direct communication of uplink and downlink without the involvement of GPS satellites. On the contrary, BLOS is a communication system that uses geostationary satellites as relay, with the advantages of further communication distance than LOS (LOS communication distance only up to 200–250 km, while BLOS could be thousands kilometers) [25], which plays a very important role in UAVs with features of high altitude and long endurance flight.

### *20.3.4 Payload, Launch and Recovery Equipment and Ground Support Equipment*

Payload is the fundamental reason of existence of UAVs, which could be any equipments that the mission requires, e.g., camera, laser, sensor, radar, relay (communications, navigation signals), cargo, weapon, etc. Generally, it would not exceed 10–20% of gross weight [27].

Launch and recovery equipment is usually used for fixed-wing UAVs due to the limitation of terrain, there will not be always a long-run way to lift and land. Therefore, a launcher (see, e.g., Fig. 20.5) that contains a small launch track and a catapult will be necessary equipment in most time. Although, some small-scale UAVs could simply be launched by 'throwing out'. The rotary-wing UAVs or blimps usually do not need launch equipments due to the fact that they have vertical take-off and landing abilities, only the large-scale UAVs of this two types need a take-off and landing platform if the terrain is too sharp. As for recovery, the nets and parachutes are most common equipments for fixed-wing UAVs. Nets are easily used to capture multiple small air vehicles in small spaces, while the parachutes are mainly used for point recoveries [9].

Finally, ground support equipment becomes more and more important in modern era. Especially for those long endurance missions and UAS with mobility, which need plenty of maintenance equipments, supplies of spare parts, fuel backup, transportation vehicles for GCS, UAVs, antenna, etc.

## 20.4 GNSS in Supporting UAVs

### *20.4.1 Precise Hovering of Rotary-Wing UAVs*

For rotary-wing UAVs, hover is the most outstanding feature it has. However, it is hard to keep vehicles stable through operations of manual control. Hence, the UAS needs a fixed set of coordinate from GPS, which makes it hover accurately on the position of preset height and horizon. By continuously comparing the refreshed coordinates of real-time position and preset, the control unit on UAVs will adjust the motor power to perform a precise hover. Nevertheless, since the refresh rate of coordinates from

**Fig. 20.5** An example of large UAV launcher

GPS is slow for some low cost UAVs, the height is usually measured by using a barometer (most used on cheap, small UAVs) or ultrasonic sensor (less used, usually applies on very low altitude or indoor UAVs) instead of GPS to prevent the loss of height.

### *20.4.2 Automatic Return System and Autonomous Fly System*

The automatic return system allows UAVs to automatically return to the point where it took off in an emergency situations such as signal loss from the controller or low battery level. In the process of return, it requires the preset take off coordinates of which are compared to the current real-time location from GPS. The autonomous fly system has exactly the same work theory as automatic return system. The only difference is the existence of two manually preset coordinates, one start point and one destination point. After setting down, the UAVs could fly by itself without any controls.

### *20.4.3 Object Avoidance Program*

With rising of civilian UAVs, the frequency of using drones also increased quickly. Hence to prevent some dangerous situations happening, many laws already restrict airspace, e.g., near airports. The function of object avoidance program could keep UAVs only flying in areas legally permitted. The theory of this program is based on the pre-set database of local map and real-time location from GPS. By continuously comparing the current coordinates of UAV and coordinates on database of local map, UAVs would be able to 'know' where they are, so that they can avoid the areas that are not permitted.

### *20.4.4 GPS to Geo-Located Images Captured by UAVs*

High resolution of airborne images now are frequently used in aspects of land detections to generate maps of a whole city, such as mosaic imagery [28]. When sensors on UAVs capture images, the UAVs positions, elevations, distances between sensors to ground, and angle of cameras might keep changing, causing distortions and inconsistencies due to the fact that images are captured in different areas. The GPS can offer the real-time coordinates of UAVs, distances to ground, in order to combine with other sensor data sets to recover and adjust the pose of cameras so that all images will have correct and consistent geo-referenced coordinate systems.

## 20.5 Environment Application of UAVs

### *20.5.1 Agriculture Monitoring*

Precision agriculture, crop management that uses GPS and other big data is an efficient way to solve food crises [1]. In many developing countries, the technique of monitoring crop growth is still limited to 'walking in field' due to the high cost of modern technology [29]. As a result, crops are usually damaged by pests or diseases before the farmers can react. However, the rising use of drones brings the possibility to popularize the precision farming. For example, in vegetation health assessments and growth/coverage monitoring using NDVI [1, 30, 31], healthy plants reflect both green and infrared wavelengths of light. Using NDVI (Eq. 20.1) therefore, we could be able to tell if the corps or other plants are stressed from pest, nutrient, or water pressures.

$$NDVI = \frac{NIR - VIS}{NIR + VIS}. \tag{20.1}$$

In Eq. 20.1, NIR is the near-infrared light and VIS is the visible red light. To capture the images of fields, the drone, which carries multi-spectral sensor, just needs to hover above the study area with specific altitude and to capture photos (see, e.g., Fig. 20.6b).

Veroustraete [1] provides five applications of drones to agriculture; mid-season crop health monitoring, irrigation equipment monitoring, mid-field weed identification, variable-rate fertility, and cattle herd monitoring. In assessing mid-season crop health, the traditional method involved actual field visitations, an approach that is limited in spatial coverage and temporal resolutions. The use of drone-based NDVI, however, offers the advantages of covering more surface areas in a much shorter time, capturing data that cannot be seen by human eyes, thereby removing much of human errors associated with the traditional inventory work [1].

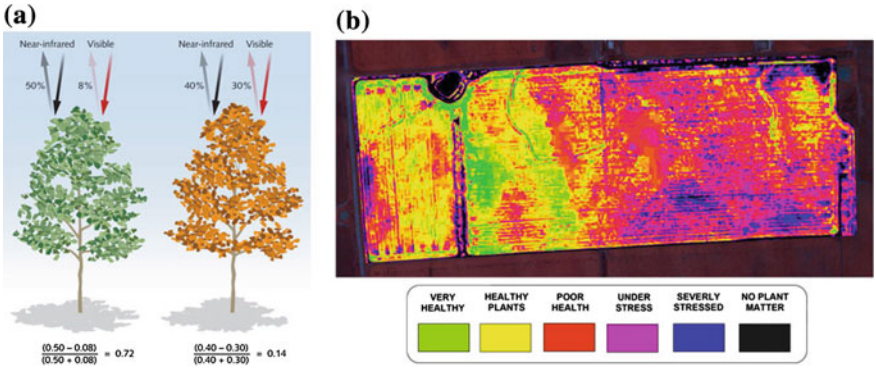


**Fig. 20.6** **a** Normalized difference vegetative index (NDVI), comparison of healthy plant and unhealthy plant. The more closer the NDVI value to 1, the more healthier the plant. **b** An example of normalized difference vegetative index (NDVI) image of crops' health monitoring on farm land (*Source* http://www.qlddrones.com.au/services/agriculture-drone-services/ndvi-crop-health-imaging/)

Drones are also useful in mid-season inspections of the nozzles and sprinklers on irrigation equipment, what is traditionally laborious especially for large growers with many fields that are widely spread, and when the crops reach certain heights. Moreover, drone-based NDVI data and post flight images could be used to generate weed maps that could help farmers and their agronomist to differentiate areas heavily infested with weeds from healthy growing areas [1]. Such differentiation lead to NDVI maps that could be used to regulate the amount of fertilizers, pesticides, etc. Thirdly, drone-based NDVI maps have been used to direct in-season fertilizer applications on corn and other crops using drone-generated variable-rate application (VRA) of fertilizers, see, e.g., [1]. On cattle herd monitoring, drones provide the capability for monitoring the herds from overhead tracking the quantity and activity of the animals, thereby being useful for night operations where human eyes are limited [1].

Other applications of drone to support agricultural activities have been reported, e.g., Leila et al. [32] who used high high-resolution multi-spectral images captured by drone to estimate soil moisture in large fields. Also, drones-based 2D and 3D digital models are used to quantify gully and bad land erosion in a large area [33]. Basically, drones-based products could save time, money, achieve real-time monitoring and satisfy multiple requirements of precision farming. Although, it might need to consider atmospheric impacts such as temperature and humidity when capturing images, it has no time and space constraints compared to 'walking in the fields' or using satellites remote sensing images.

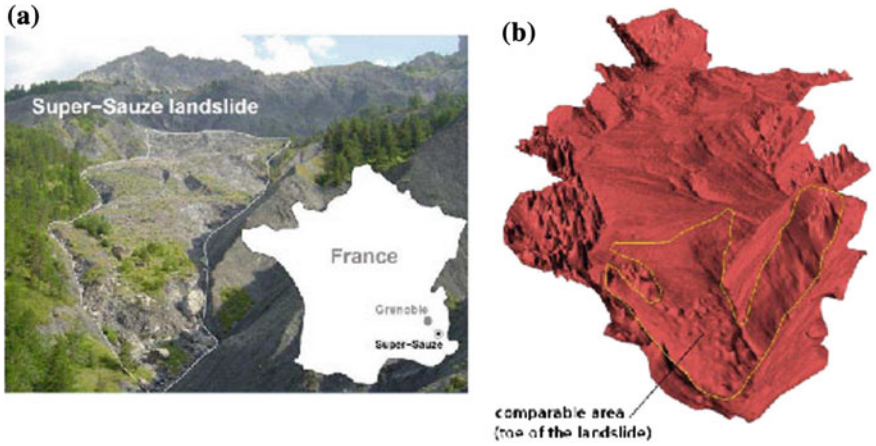


**Fig. 20.7** **a** Study area of Super-Sauze landslide captured by drones **b** Digital modeling of Super-Sauze landslide resulting from drone images [34]

### *20.5.2 DEM Models for Disaster Management and Reconstruction*

DEM (digital elevation model) is now a popular title, which is a kind of short-, close-range photogrammetry application. LiDAR (Light Detection and Ranging) sensor on the drone, consisting of a laser, a scanner, and a specialized GPS receiver are used to collect and provide data for Digital Surface Models (DSM) and Digital Elevation Models (DEM) [29], which could be applied in many disaster areas that humans can hardly reach. For example, The Super-Sauze landslide (see Fig. 20.7) is located on the north-facing slope of the Barcelonnette Basin (Southern French Alps). It is about 850 m long and located at an altitude of 1700–2100 m with an average slope of 25 degrees [34], which makes human monitoring or measuring almost impossible and dangerous. Therefore, high resolution, geo-referenced image monitoring by drone becomes a safe, quick and efficient alternative choice to assess this large landslide area. In Fig. 20.7a, drones was used to captured multiple high-resolution images from different distances (ground to drone) and angles for the whole study area, which generated Fig. 20.7b DSM (digital surface model) of the whole landslide. The DSM is then used to analysis and estimate the stability of landslide and identify dangerous areas.

Another example is the stability monitoring of coastal cliffs [35]. In this example, drones are used to keep continuously monitoring the surface of coastal cliff for several months to generate a DEM of cliff face with time series. Most of cliffs are high and steep that humans can hardly reach. Drones however can acquire the images without space constraints and give a close view of fractures on surface of cliff. Therefore, by analysing the direction, angle, number and length of fractures statistically, it is possible to assess the situation and predict the stability of cliff in future. Other

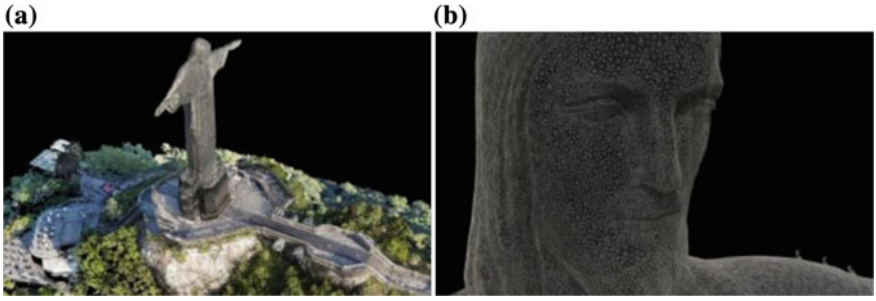


**Fig. 20.8** **a** Digital Map of statue of Christ the Redeemer in Rio de Janeiro **b** Face reconstruction from 3D point cloud data obtained from drones [39]

disasters monitoring and assessing applications include, e.g., flood assessment [36], storm monitoring [37], forest fire monitoring [38], etc.

Besides, digital 3D point cloud modeling is another technique that could also be applied in many other fields, such as architecture, e.g., the statue of Christ the Redeemer in Rio de Janeiro (Fig. 20.8a) has been reconstructed using 3D point cloud technique (see Fig. 20.8a) [39]. It is very challenging to acquire the data of the statue by humans considering bad weather conditions and huge size of the statue leading to difficulties in measuring and safety issues during the measuring process. Drones therefore, become a very ideal solution for reconstructing the statue, where thousands of pictures can be captured around the statue in a very short time. The data, after being processed, could create a large and accurate point cloud and a textured mesh to help in the reconstruction of the statue (see Fig. 20.8b). With respect to archeology, human touches and operations usually risk damaging the relics. Building the 3D point cloud from the data acquired by drone is therefore necessary, especially for large relics, e.g., the Neptune Temple in the archaeological area of Paestum is reconstructed from 3D point cloud data [40]. In addition, to generate DEM or 3D point cloud, high overlaps (60–80%) and low altitude flights of drones are usually required to obtain enough coverage area (see, e.g., Fig. 20.9), e.g., a longitudinal overlap of 70% and a transversal overlap of 60% is necessary. Drones, which fly at 50 m altitude could thus be useful.

### *20.5.3 Classification, Change Detection and Tracing*

By simply changing the types of sensor on drones, it could also achieve many other applications of environment monitoring. For example, high resolution of RGB camera can be applied to land use classification by using maximum likelihood classification algorithms [41, 42]. Also, by combining near-infrared sensor and RGB camera together, monitoring of construction areas is possible, which could be applied in studies, e.g., urban city sprawl [43], using time series images captured by drones

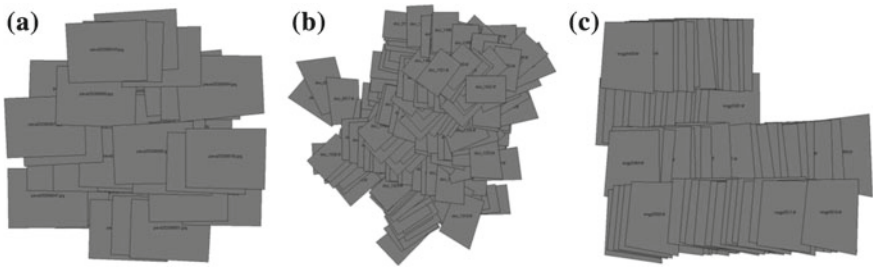


**Fig. 20.9** Three different overlap methods while drone captures images for 3D digital model and DEM: **a** manual mode and image acquisition with a scheduled interval, **b** low-cost navigation system with irregular image overlap; **c** automated flying and acquisition with a high quality navigation system [40]

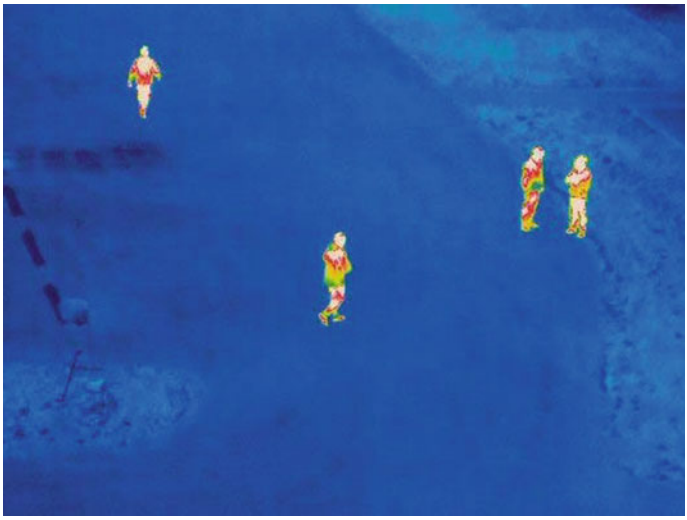

**Fig. 20.10** An image captured by thermal sensor to detect human activates

to detect city changes over years. Other change detection also include deforestation [44], soil erosion [33], etc. Although, these techniques are not very mature currently, they have advantages of being cheaper, having higher resolution, easier to use, and less constraint by space and time, compared to using satellite images. Advanced hyper-spectral sensor offers a broader spectrum, which could even characterize more objects such as temperature of oceans (inspections of El Niño), humans (for security issues), surface rocks (geology investigations), smoke (fire managements), etc. In addition, thermal sensor could enhance the visibility of objects in a dark environment by utilizing the infrared radiation. This could be used to trace animal, e.g., Fortuna et al. [45] indicated that low cost UAVs that carries thermal sensors could be used to inspect sharks' activities at coastal to avoid conflicts between them and

human. Human activities, e.g., Fig. 20.10 shows a clear view of human activities at night, this applications can also be used in searching and rescuing following disasters [19, 46].

## 20.6 Future Challenges of UAVs

### *20.6.1 Technology Aspect*

Although, UAVs seem to show great potentials to future market, there is still a long distance from drones replacing manned aircrafts. In aspect of UAS itself, there are three important challenges.

1. Sensor technology: This is a key part of the completion of unmanned aerial vehicles take off, landing, the implementation of tasks and return to the field. To achieve precise control, currently, technology requires radar, hyperspectral sensors, pressure sensors and so on, which is not the capability of small and micro unmanned aircrafts vehicles (MUAVs). In future, the sensor technology is going to be smaller, more accurate, and more functional.
2. Navigation technology: Provides the position, speed and flight attitude of the reference coordinate system to the UAV, and guides the UAV to fly according to the designated route, which is equivalent to the pilot in the man-machine system. GPS/INS(inertial navigation system) is the most commonly used system, but it has shortcoming of weak GPS signal, low accuracy, which usually cause crashes and accidents. The future development of UAV requires obstacles to avoid, high-precision, high reliability and high anti-jamming performance. Therefore, the combination of 'inertial + multi-sensor + GPS + photoelectric navigation system' will be the future development direction.
3. Engine technology: Various uses of UAVs on the power plant requirements are different, but all need small size, low cost, reliable engines. UAV is currently widely used in the power unit for the piston engine, but the piston is only suitable for low-speed low-altitude small UAV. Low-altitude unmanned helicopter generally use turboshaft engine while high-altitude long-range large unmanned aerial vehicles generally use turbofan engine (weight around tons). Multi-rotor drones generally use the battery-driven motor, take off the quality of less than 100 g, endurance is less than one hour. In future, turbines are expected to replace the piston as the main power of UAV models, solar energy, hydrogen, and other new energy motors are also possible for small unmanned aerial vehicles to provide more lasting viability.
4. Data links technology: Data link transmission system is an important technology of UAV, responsible for the completion of the UAV remote control, telemetry, tracking and positioning and sensor transmission. The development of modern data link technology will be toward high-speed, broadband, confidential, anti-jamming direction, and UAV practical ability will be more and more strong.

5. Artificial intelligence technology: Currently, the level of autonomous for UAV is very low, due to the fact artificial intelligence technology is far from mature, such as avoid technology, objects recognition system, intelligent decision and planning system, etc. However, with the advance technology in future, these functions will be expected to apply on most of UAV.

### *20.6.2 Legal Issue*

With rising civilian drones use, the privacy and ethical concerns become issues that people going to worry about. Mostly, these issues include the purpose which drones are used, as well as the extent and type of personal information that drones may capture, the type of operator, the context and location of the drones, and the type of technology equipments they carry. These issues have to be considered and regulated, if not, UAVs might become serious threats (causing accidents, criminal events) to general public, especially for small drones [47].

In 2007, Federal Aviation Administration (FAA) of U.S banned UAVs usage due to lack of regulations, which was quite a strike for drone market, considering over 70% percent of usage comes from the US. It was not open until 2015 when the US Federal Aviation Administration lifted the full ban on flying drones, by announcing the long-awaited management plans of UAVs. The new rules are mainly designed for small drones with weight under 25 kg, set the limitations of flight time, speed and carrying restrictions. Details include only flying during the day, and the whole flight process must be maintained in the operator's line of sight, the flight height of not more

**Table 20.3** Regulations for UAS use in several countries [40]

| Country | Laws and regulations |
|---|---|
| Australia | CASA (Civil Aviation Safety Authority) Circular, 2002 |
| Belgium | Certification Specification, Rev. 00, 24.01.07 |
| Canada | Approach to the Classification of Unmanned Aircraft, 19.10.10 |
| Denmark | Regulations on unmanned aircraft now weighing more than 25 kg, Edition 3, 09.01.04 |
| France | Decree concerning the design of civil aircraft fly without anyone on board, August 2010 |
| Great Britain | CAP 722, 06.04.10u. Joint Doctrin 2/11, 30.3.11 |
| Norway | Operation of unmanned aircraft in Norway, 29.06.09 |
| Sweden | Flying with UAVs in airspace involving civil aviation activity, 25.03.03 |
| Switzerland | Verordnung des UVEK über Luftfahrtzeuge besonderer Kategorien, 01.04.11 |
| Czech | Czech aviation regulation L2 - Rules of the air, 25.08.11 |
| USA | UAS Certification Status, 18.08.08; Fact Sheet- UAS, 15.7.10 and NJO7210.766, 28.3.11, 8.2.12 and FAA Bill |

than 150 m and the speed should not exceed 160 km, etc. Besides, drones should be at least eight kilometers away from a man-driven airplane airport, and operators must be older than 17 years old, and need to obtain the FAA UAV operator qualification certificate. On the other hand, due to the different environment conditions, UAV types, payloads, technology levels, different countries have their own regulations of civil use of drones, see Table 20.3. In future, a strong, clear, highly articulated and well-understood regulatory regime need to be established to prevent the illegal use of UAVs.

## 20.7 Concluding Remarks

UAV technology is a mechanical, aerodynamic, electronics, communications, software, highly integrated multi-disciplinary technology. In the past few decades, the huge application values and strong market demands for the UAV have been rapidly developed, which brings benefits to most fields, e.g., geophysics, meteorology, oceanography, public safety, and especially in agriculture where the European Union opened for certified drone equipped agricultural service providers [1]. Future developments of drone technology include the direction of becoming smaller, lighter, more efficient, accurate, and cheaper. Also, it would be expected that drones will gradually replace the use of manned aircrafts. However, the privacy and ethical issues need to be seriously considered to avoid illegal and unsafe use of UAVs.

## References

1. Veroustraete F (2015) The rise of the drones in agriculture. EC agriculture 325–327. https://www.researchgate.net/publication/282093589
2. Villasenor J (2012) What is a drone, anyway?. Scientific American. https://blogs.scientificamerican.com/guest-blog/what-is-a-drone-anyway/. Accesssed 6 Jan 2017
3. Gertler J (2012) U.S. unmanned aerial systems. Congressional research service. https://fas.org/sgp/crs/natsec/R42136.pdf. Accessed 8 Jan 2017
4. The Development, Concepts and Doctrine Centre (DCDC) (2011) Joint doctrine note 2/11. The UK approach to unmanned aircraft systems. Ministry of Defence. https://www.gov.uk/government/uploads/system/uploads/attachment_data/file/33711/20110505JDN_211_UAS_v2U.pdf. Accessed 8 Jan 2017
5. Clark R (2016) Understanding the drone epidemic. Comput Law Secur Rev 30(3):230–246. doi:10.1016/j.clsr.2014.03.002
6. Custers B (ed) (2016) The future of drone use - opportunities and threats from ethical and legal perspectives. Springer, Berlin. doi:10.1007/978-94-6265-132-6
7. Dalamagkidis K (2015) Handbook of unmanned aerial vehicles - chapter 4. Aviation history and unmanned flight. Springer, Netherlands, pp 57–81. doi:10.1007/978-90-481-9707-1_93
8. Renard JB, Dulac F, Berthet G et al (2015) LOAC: a small aerosol optical counter/sizer for ground-based and balloon measurements of the size distribution and nature of atmospheric particles - Part 2: first results from balloon and unmanned aerial vehicle flights. Atmos Meas Tech Discuss 27:1261–1299. doi:10.5194/amtd-8-1261-2015

9. Fahlstrom PG, Gleason TJ (2012) Introduction to UAV system, 4th edn. Wiley, New York
10. De Havilland Aircrafts Museum (2017) De Havilland DH82B queen bee. http://www.dehavillandmuseum.co.uk/aircraft/de-havilland-dh82b-queen-bee/. Accessed 9 Jan 2017
11. National museum of the US air force (2015) Radioplane/Northrop MQM-57 Falconer
12. Zaloga SJ (2011) Unmanned aerial vehicles: robotic air warfare 1917–2007. Bloomsbury Publishing, London
13. Keane JF, Carr SS (2013) A brief history of early unmanned aircraft. Johns Hopkins APL Tech Dig 32(3):558–571. https://pdfs.semanticscholar.org/ed38/531575cf6fce272fd3d88ebe06f9775b021f.pdf
14. Kenzo N (2007) Prospect and recent research and development for civil use autonomous unmanned aircraft as UAV and MAV. J Syst Des Dyn 1(2):120–128. doi:10.1299/jsdd.1.120
15. Gupta SG, Ghonge MM, Jawandhiya PM (2013) Review of unmanned aircraft system (UAS). Int J Adv. Res Comput Eng Technol 2(4):1646–1658. https://www.researchgate.net/profile/Mangesh_Ghonge/publication/249998592_Review_of_Unmanned_Aircraft_System_UAS/links/02e7e51e8ef1668ce8000000.pdf
16. UAV Insider (2013) Rotary wing vs fixed wing UAVs. http://www.uavinsider.com/rotary-wing-vs-fixed-wing-uavs/. Accessed 11 Jan 2017
17. QuestUAV (2015) Fixed wing vs rotary wing for UAV mapping applications. http://www.questuav.com/news/fixed-wing-versus-rotary-wing-for-uav-mapping-applications. Accessed 11 Jan 2017
18. Chapman A (2016) Types of drones: multi-rotor vs fixed-wing vs single rotor vs hybrid VTOL, DRONE, 3. http://www.auav.com.au/articles/drone-types/. Accessed 12 Jan 2017
19. Adams SM, Friedland CJ (2011) A survey of unmanned aerial vehicle (UAV) usage for imagery collection in disaster research and management. https://pdfs.semanticscholar.org/fd8e/960ca48e183452335743c273ea41c6930a75.pdf
20. Doncieux S, Mouret JB, Muratet L, Meyer JA (2004) The ROBUR project: towards an autonomous flapping-wing animat. In: Proceedings of the Journes MicroDrones. https://pdfs.semanticscholar.org/e993/f2787820f2684ca2a14271e065d817e329a7.pdf. Accessed 13 Jan 2017
21. Michelson RC, Reece S (1998) Update on flapping wing micro air vehicle research-ongoing work to develop a flapping wing, crawling entomopter. In: 13th Bristol international RPV/UAV systems conference proceedings, 30. http://edge.rit.edu/content/P06007/public/websites/senior%20design/MAVSD/shane/References/Bristol_MAV_ornithopter_Paper.pdf. Accessed 13 Jan 2017
22. Watts AC, Ambrosia VG, Hinkley EA (2012) Unmanned aircraft systems in remote sensing and scientific research: classification and considerations of use. Remote Sens 4:1671–1692. doi:10.3390/rs4061671
23. Winnefeld JA, Kendall F (2011) U.S. unmanned systems integrated roadmap FY2011-2036. Department of defence, United States of American. http://www.acq.osd.mil/sts/docs/Unmanned%20Systems%20Integrated%20Roadmap%20FY2011-2036.pdf. Accessed 13 Jan 2017
24. Liping O (2009) Brief introduction of UAVs. Bull Adv Technol Res 3(5):31–34. http://www.siat.cas.cn/xscbw/xsqk/200912/W020091208627529515062.pdf
25. Çuhadar İ, Dursun M (2016) Unmanned air vehicle systems data links. J Autom Control Eng 4(3):189–193. doi:10.18178/joace.4.3.189-193
26. Wolfgang WR (1999) UAV data-links: tasks, types, technologies and examples. Development and operation of UAVs for military and civil applications
27. Austin R (2011) Unmanned aircraft systems: UAVS design, development and deployment, vol 54. Wiley, New York
28. Xu Y, Ou J, He H, Zhang X, Mills J (2016) Mosaicking of unmanned aerial vehicle imagery in the absence of camera poses. Remote Sens 8:204. doi:10.3390/rs8030204
29. Tiwari A, Dixit A (2015) Unmanned aerial vehicle and geospatial technology pushing the limits of development. Am J Eng Res (AJER) 4(1):16–21. http://www.ajer.org/papers/v4(01)/C0401016021.pdf

30. Stehr NJ (2015) Drones: the newest technology for precision agriculture. Nat Sci Educ 44:89–91. doi:10.4195/nse2015.04.0772
31. Malveaux C, Hall S, Price RR (2014) Using drones in agriculture: unmanned aerial systems for agricultural remote sensing applications. 2014 ASABE and CSBE/SCGAB annual international meeting sponsored by ASABE
32. Leila HE, Alfonso TR, Austin J, Mac M (2015) Assessment of surface soil moisture using high-resolution multi-spectral imagery and artificial neural networks. Remote Sens 7:2627–2646. doi:10.3390/rs70302627
33. Sebastian O, Irene M, Klaus DP, Johannes BR (2012) Unmanned aerial vehicle (UAV) for monitoring soil erosion in Morocco. Remote Sens 4(11):3390–3416. doi:10.3390/rs4113390
34. Niethammer U, Rothmund S, Schwaderer U, Zeman J, Joswig W (2014) Open source image-processing tools for low-cost uav-based landslide investigations. Int Arch Photogramm remote Sens Spat Inf Sci 38(1):161–166
35. Barlow J, Gilham J, Cofrã II (2017) Kinematic analysis of sea cliff stability using UAV photogrammetry. Int J Remote Sens 38(8–10):2464–2479. doi:10.1080/01431161.2016.1275061
36. Feng Q, Liu J, Gong J (2015) Urban flood mapping based on unmanned aerial vehicle remote sensing and random forest classifier case of Yuyao, China. Water 7:1437–1455. doi:10.3390/w7041437
37. Zhang W, Wu J (2014) To explore the UAV application in disaster prevention and reduction. Mech Mater 590:609–612. doi:10.4028/www.scientific.net/AMM.590.609
38. Yuan C, Zhang Y, Liu Z (2015) A survey on technologies for automatic forest fire monitoring, detection, and fighting using unmanned aerial vehicles and remote sensing techniques. Can J For Res 45(7):783–792. doi:10.1139/cjfr-2014-0347
39. Lisa C, Betschart S (2015) Christ the redeemer reconstructed in 3D. GIM International Magazine. https://www.gim-international.com/content/article/christ-the-redeemer-reconstructed-in-3d
40. Nex F, Remondino F (2014) UAV for 3D mapping applications: a review. Appl Geomat 6(1):1–15
41. Marçal ARS, Borges JS, Gomes JA, Pinto Da Costa JF (2005) Land cover update by supervised classification of segmented ASTER images. Int J Remote Sens 26(7):1347–1362. http://www.fc.up.pt/pessoas/andre.marcal/papers/IJRS_26_1347.pdf
42. Movia A, Beinat A, Crosilla F (2015) Comparison of unsupervised vegetation classification methods from Vhr images after shadows removal by innovative algorithms. Int Archiv Photogramm Remote Sens Spat Inf Sci 40(7):1269–1276. doi:10.5194/isprsarchives-XL-7-W3-1269-2015
43. Moranduzzo T, Melgani F, Bazi Y, Alajlan N (2015) A fast object detector based on high-order gradients and Gaussian process regression for UAV images. Int J Remote Sens 36(10):2713–2733
44. Jaime P, Michael KM, Brian MN, Serge AW, Lian PK (2014) Small drones for community-based forest monitoring: an assessment of their feasibility and potential in tropical areas. Forests 5(6):1481–1507. doi:10.3390/f5061481
45. Fortuna J, Ferreira F, Gomes R, Ferreira S, Sousa J (2013) Using low cost open source UAVs for marine wild life monitoring - field report. IFAC Proc 46(30):291–295. doi:10.3182/20131120-3-FR-4045.00055
46. Rudol P, Doherty P (2008) Human body detection and geolocalization for UAV search and rescue missions using color and thermal imagery. In: Aerospace conference, 2008 IEEE pp 1–8. https://www.ida.liu.se/divisions/aiics/publications/AEROCONF-2008-Human-Body-Detection.pdf
47. Clarke R, Moses LB (2014) The regulation of civilian drones impacts on public safety. Comp Law Secur Rev 30:263–285. doi:10.1016/j.clsr.2014.03.007

# Index





J. Awange, *GNSS Environmental Sensing*, Environmental Science and Engineering, DOI 10.1007/978-3-319-58418-8